

UNIVERSITA' DEGLI STUDI DI PADOVA

Sede Amministrativa: Università degli Studi di Padova

Dipartimento di Scienze Chimiche

SCUOLA DI DOTTORATO DI RICERCA IN SCIENZE MOLECOLARI

INDIRIZZO SCIENZE CHIMICHE

CICLO XXII

***DESIGN, SYNTHESIS AND
CHARACTERISATION OF POLYFUNCTIONAL
COORDINATION POLYMERS***

Direttore della Scuola: Ch.mo Prof. Maurizio Casarin

Supervisore: Ch.mo Prof. Luciano Pandolfo

Dottoranda: Federica Garau

To my Grandmother

*“Experiments are the only means
of knowledge at our disposal;
the rest is poetry, imagination.”*

Max Planck

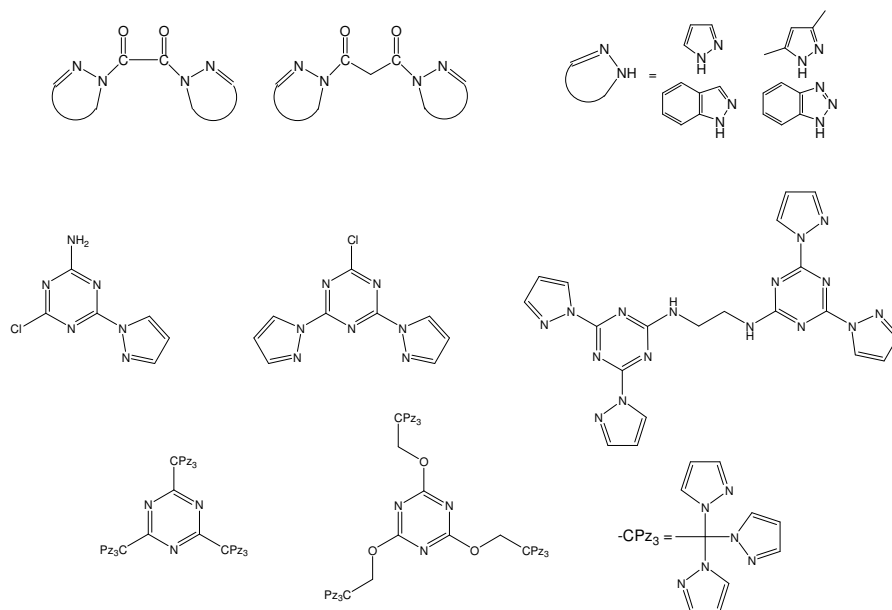
Index

Abstract	3
Sommario	5
Introduction	7
PhD Specific Work	17
Synthesis of Polynucleating Nitrogen Ligands	19
Ligands based on oxalate/malonate skeleton and azolate moieties	19
Ligands based on the 1,3,5-triazine spacer	19
Synthesis of new Trinuclear Triangular Cu(II) Coordination Polymers	25
Reactions of $[\text{Cu}_3(\mu_3\text{-OH})(\mu\text{-pz})_3(\text{CH}_3\text{COO})_2(\text{Hpz})]$ with strong acids	27
Reactions of trinuclear triangular Cu(II) clusters with dinucleating nitrogen ligands	39
Electrochemical Studies	55
Catalytic Activity Studies	59
Peroxidative oxidation of cyclohexane	59
Oxidation of methyl- <i>p</i> -tolyl-sulfide	69
Conclusions and Future Perspectives	71
Experimental Data	73
References	99
Participation to Congresses, Conferences, Schools and Meetings	107
Published Papers	109

Abstract

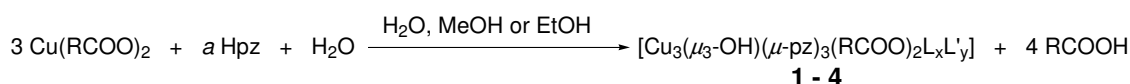
The research group where I performed my PhD researches is interested in the synthesis and characterisation of Coordination Polymers (CPs). CPs are infinite systems built up with metal ions (connectors) and organic ligands (linkers) as main elementary units, connected via coordination bonds and other weak interactions [Robin & Fromm (2006)]. One of the interests in building CPs is the creation of new tuneable functional materials, since CPs are promising materials for applications in gas storage, anion exchange, catalysis, conductivity, luminescence, chirality, magnetism, spin transition behaviour, NLO or deposition of thin films. CPs can be normally prepared by reacting a suitable polynucleating ligand with a transition metal ion, having at least two coordination sites available.

In order to obtain new CPs, during the first year of my PhD studies, two different classes (sketched below) of new potentially polynucleating nitrogen containing ligands were designed, synthesised and fully characterised.

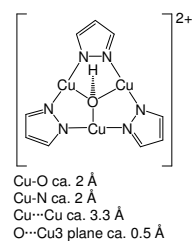


Unfortunately, some preliminary tests on the reactivity of these linkers with $\text{Cu}^{\text{(II)}}$, $\text{Ag}^{\text{(I)}}$, $\text{Zn}^{\text{(II)}}$ and $\text{Ru}^{\text{(II)}}$ in hydroalcoholic solvents evidenced the relatively easy hydrolysis of the ligands. For these reasons, at the moment, the study of the coordination properties of these ligands to transition metal ions has been set aside, and the attention has been focused on the understanding of the decomposition mechanism upon treatment with transition metal compounds [Casarin et al. (2009); Casarin et al. (2008) (b)].

Moreover, we continued some other studies, concerning the synthesis of trinuclear triangular $\text{Cu}^{\text{(II)}}$ clusters. The latter can be easily prepared by reacting copper(II) carboxylates with pyrazole (Hpz) in hydroalcoholic solvents, obtaining 1D, 2D or 3D CPs [Casarin et al. (2004); Casarin et al. (2005); Di Nicola et al. (2007) (a)].



- 1** R = -H, a = 5, L = Hpz, x = 2, y = 0;
- 2** R = -CH₃, a = 4, L = Hpz, x = 1, y = 0;
- 3** R = -CH₂CH₃, a = 3, L = EtOH, x = 1, y = 0;
- 4** R = -CH₂CH₂CH₃, a = 3, L = MeOH, L' = H₂O, x = y = 1.



Particularly, during my PhD studies some other trinuclear triangular Cu^(II) clusters (starting both from saturated and unsaturated Cu^(II) carboxylates) were synthesised and characterised [Di Nicola et al. (2009); Contaldi et al (2009)].

We started also to study the reactivity of the trinuclear triangular copper(II)/carboxylate/pyrazolate clusters towards substitution reactions. Particularly, we examined first the stability of the trinuclear triangular moiety by treating [Cu₃(μ₃-OH)(μ-pz)₃(CH₃COO)₂(Hpz)], **2**, with strong acids, observing that the trinuclear moiety was in a good extent maintained, and obtaining new hexanuclear and heptanuclear coordination polymers, in some cases porous [Casarin et al. (2007) (a); Zanforlin (2007); Di Nicola et al. (2007) (b); Di Nicola et al. (2008)].

Since the trinuclear moieties resulted to be quite stable towards decomposition, we decided to use them as starting material to synthesise new different CPs, having the trinuclear Cu^(II) clusters directly bridged by polynucleating ligands. We decided to follow two different approaches: i) substitution of the monocarboxylates with bicarboxylates; and ii) replacement of the neutral ligands coordinated to the Cu^(II) centres (pyrazole and/or solvent molecules) with neutral bidentate nitrogen-containing ligands. First attempts under bench-top conditions to replace the carboxylate ions by reacting the trinuclear compounds with dicarboxylic acids were not successful, leading to the isolation of the starting materials, while reactions carried out upon deprotonation of the acids led to the instantaneous precipitation of insoluble powders.

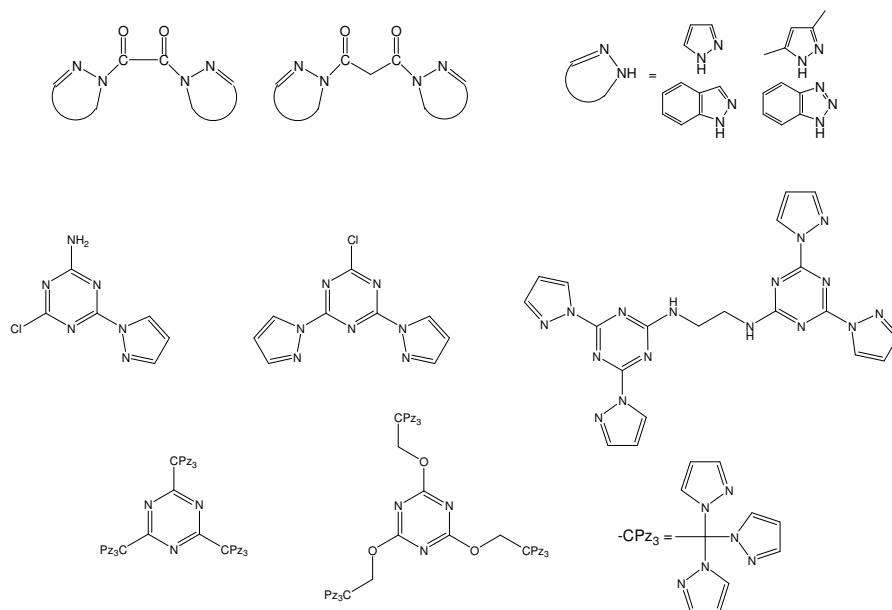
The reaction with bidentate nitrogen-containing ligands gave instead interesting results, and numerous new CPs were isolated and fully characterised. Noteworthy, upon reaction between [Cu₃(μ₃-OH)(μ-pz)₃(HCOO)₂(Hpz)₂(H₂O)], **1**, and an excess of 4,4'-bipyridine, a porous coordination polymer was obtained.

The electrochemical properties of some selected copper(II) CPs isolated by us were examined; we also investigated the catalytic activities of some of these compounds in the peroxidative oxidation of cyclohexane. Both of these researches were performed in prof. Armando J. L. Pombeiro laboratories, at the Centro de Química Estrutural of the Instituto Superior Técnico (Lisbon). Finally, more recently, we started to investigate the catalytic activity of **2** in the oxidation of methyl-*p*-tolyl sulfide to the corresponding sulfoxide. Preliminary results indicated that **2** is able to bind reversibly oxygen coming from H₂O₂ and transfer it to the sulfide.

Sommario

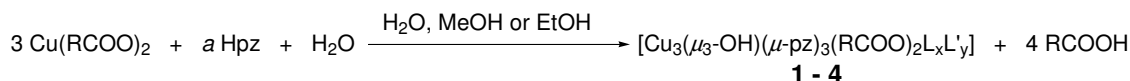
Il gruppo di ricerca presso cui ho svolto il Dottorato di Ricerca si occupa della sintesi e caratterizzazione di Polimeri di Coordinazione (CP). I CP sono dei sistemi polimerici infiniti, costruiti a partire da ioni metallici (connettori) e leganti organici (*linkers*) come principali unità di base, connessi tra loro attraverso legami di coordinazione e altre interazioni relativamente deboli [Robin & Fromm (2006)]. Uno dei principali interessi nella costruzione di CP è l'ottenimento di nuovi materiali funzionali, dotati di proprietà modulabili; i CP, infatti, presentano potenziali applicazioni in diversi settori, quali ad esempio immagazzinamento di gas, scambio ionico, catalisi, conduttività, luminescenza, chiralità, magnetismo, ottica non lineare o deposizione di strati sottili. I CP vengono generalmente sintetizzati per "copolimerizzazione" di un opportuno legante polinucleante con uno ione di un metallo di transizione avente almeno due siti di coordinazione disponibili.

Al fine di ottenere nuovi CP, durante il primo anno del Dottorato di Ricerca sono state progettate e sintetizzate due diverse classi di nuovi leganti azotati potenzialmente polinucleante, sotto riportati.

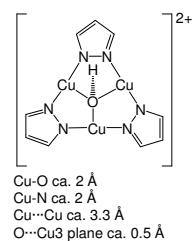


Test preliminari sulla reattività di questi composti con $\text{Cu}^{(II)}$, $\text{Ag}^{(I)}$, $\text{Zn}^{(II)}$ e $\text{Ru}^{(II)}$ in solventi protici hanno messo in evidenza la relativamente facile idrolisi dei leganti. Per questo motivo, lo studio delle loro proprietà coordinative a metalli di transizione è stato momentaneamente accantonato, e l'attenzione è stata focalizzata sulla comprensione del meccanismo della decomposizione in seguito al trattamento con metalli di transizione [Casarin et al. (2009); Casarin et al. (2008) (b)].

E' stato inoltre sviluppato un secondo progetto, riguardante la sintesi di *cluster* trinucleari triangolari di rame(II). Questi composti possono essere preparati facendo reagire carbossilati di $\text{Cu}^{(II)}$ con pirazolo (Hpz) in solvente protico (H_2O , MeOH o EtOH). L'autoassemblaggio dei *building blocks* porta alla formazione di CP di diversa dimensionalità (1D, 2D o 3D) [Casarin et al. (2004); Casarin et al. (2005); Di Nicola et al. (2007) (a)].



- 1** R = -H, a = 5, L = Hpz, x = 2, y = 0;
- 2** R = -CH₃, a = 4, L = Hpz, x = 1, y = 0;
- 3** R = -CH₂CH₃, a = 3, L = EtOH, x = 1, y = 0;
- 4** R = -CH₂CH₂CH₃, a = 3, L = MeOH, L' = H₂O, x = y = 1.



Sono stati quindi sintetizzati e caratterizzati nuovi *cluster* trinucleari triangolari di Cu^(II) (partendo sia da carbossilati di Cu^(II) saturi che insaturi) [Di Nicola et al. (2009); Contaldi et al (2009)].

Abbiamo inoltre esaminato la stabilità del frammento trinucleare $[\text{Cu}_3(\mu_3\text{-OH})(\mu\text{-pz})_3]^{2+}$ facendo reagire il composto $[\text{Cu}_3(\mu_3\text{-OH})(\mu\text{-pz})_3(\text{CH}_3\text{COO})_2(\text{Hpz})]$, **2**, con diversi acidi forti. Benché in tutti i casi siano stati isolati complessi mononucleari, derivanti dalla parziale decomposizione del *cluster* trinucleare, la contemporanea formazione di derivati tri-, esa- ed eptanucleari, in alcuni casi porosi [Casarin et al. (2007) (a); Zanforlin (2007); Di Nicola et al. (2007) (b); Di Nicola et al. (2008)], ha messo in evidenza la relativa stabilità del frammento $[\text{Cu}_3(\mu_3\text{-OH})(\mu\text{-pz})_3]^{2+}$.

Si è deciso quindi di utilizzare i differenti *cluster* trinucleari come materiale di partenza per la sintesi di nuovi CP, in cui più unità trinucleari fossero connesse tra loro tramite leganti polinucleanti. Abbiamo deciso di seguire due diversi approcci: i) sostituzione dei monocarbossilati con bicarbossilati; e ii) sostituzione dei leganti neutri coordinati ai centri di Cu^(II) (pirazolo e/o molecole di solvente) con leganti azotati neutri bidentati. I primi tentativi in condizioni *bench-top* di sostituire gli ioni carbossilato facendo reagire i composti trinucleari con acidi bicarbossilici non hanno avuto successo, portando all'isolamento dei composti di partenza, mentre le reazioni condotte utilizzando i bicarbossilati hanno portato all'istantanea precipitazione di polveri insolubili.

Le reazioni con leganti azotati neutri bidentati hanno invece portato all'ottenimento di risultati interessanti; infatti, sono stati isolati e caratterizzati numerosi nuovi CP. In particolare, dalla reazione di $[\text{Cu}_3(\mu_3\text{-OH})(\mu\text{-pz})_3(\text{HCOO})_2(\text{Hpz})_2(\text{H}_2\text{O})]$, **1**, con un largo eccesso di 4,4'-bipiridina, è stato isolato un polimero di coordinazione poroso.

Infine, sono state esaminate sia le proprietà elettrochimiche di alcuni CP di rame(II) da noi isolati che l'attività catalitica di alcuni di questi composti nella reazione di ossidazione perossidativa del cicloesano. Entrambi questi studi sono stati condotti nei laboratori del prof. Armando J. L. Pombeiro, presso il Centro de Química Estrutural dell'Instituto Superior Técnico (Lisbona). Più recentemente, abbiamo iniziato a studiare l'attività catalitica di **2** nell'ossidazione del metil-*p*-tolil solfuro al corrispondente solfossido. Risultati preliminari indicano che **2** è in grado di legare in modo reversibile l'ossigeno proveniente da H₂O₂ e di trasferirlo al solfuro.

Introduction

Over the past fifty years, research into porous materials resulted in a number of applications, with a direct impact on domestic life and large scale industrial processes [James (2003)]. Until the mid-1990s, basically two types of porous materials were known: inorganic solids and carbon-based materials. Zeolites are the best-known microporous inorganic solids and the term zeolite was coined by the Swedish mineralogist Axel Fredrik Cronstedt in 1756. He observed that upon rapidly heating the stilbite mineral, a large amount of steam was produced from the water adsorbed by the material. For this reason, he called the material zeolite, from the Greek ζέω (*zeō*), meaning “boil” and λίθος (*lithos*), meaning “stone”. Later, many natural zeolites were discovered, but the importance of this family increased when chemists were able to synthesise them; the first success dates back to 1862, and is due to Sainte Claire Deville. Most of the synthesis required organic molecules as templates [Férey (2001)]. Zeolites are crystalline, three-dimensional, hydrated alkaline or alkaline-earth aluminosilicates with the general formula $(M^I M^{II}_{1/2})_m (Al_m Si_n O_{2(m+n)}) \cdot xH_2O$ ($n \geq m$) (M = cation). Their frameworks are built from corner-sharing TO_4 tetrahedra ($T = Si, Al$) and may contain linked cages, cavities or channels, where H_2O molecules and metal ions are inserted. Porosity is obtained upon elimination of the water molecules, the structure usually remaining unaffected, since aluminosilicates usually form rigid frameworks [Noro et al. (2009)]. Because of their porosity, zeolites are employed in a variety of applications with a global market of several million tonnes per annum. The porosity of these materials allows guest molecules to diffuse into the bulk structure; the shape and size of the pores lead to shape- and size-selectivity over the guest which may be incorporated and, once incorporated, chemical transformations of the guests may take place. Large scale industrial examples of the latter applications are catalytic cracking and xylene isomerisation. Other uses are in ion exchange (which has led to zeolites application in detergents, water softening and purification), and in separation and removal of gases and solvents. Further applications are in agriculture, animal husbandry and construction. Although zeolites have high crystallinity, they are characterised by a relatively low porosity with respect to the whole solid volume. The principal limitation was the relatively small size of the pores in the crystallised solids, which were further shown to be quite disappointing concerning the applications [Férey (2008)].

On the contrary, activated carbons possess high open porosity and high specific surface area (up to $1200 \text{ m}^2\text{g}^{-1}$ in commercial active carbons) but have a disordered structure, whose essential feature is a twisted network of defective hexagonal carbon layers, cross-linked by aliphatic bridging groups. The width of the layer planes is typically about 5 nm, although it can vary. Activated carbons are largely used in many fields as efficient and versatile adsorbents (e.g. purification of water, air and many chemical and natural products) [Yenisoy-Karakaş et al. (2004)]. Simple functional groups and heteroelements are incorporated into the network and are bound to the periphery of the carbon layer planes. Activated carbons are characterised by a broad pore size distribution, so that many of the channels or cavities often are superfluous and unnecessary for the required porous functions, leading to poor storage/separation capacity for a specific guest. Moreover, because of their disordered microstructure, porous carbons cannot be tailored by control of the crystal structure, as in the case, for example, of zeolites [Barton et al. (1999)].

In 1989, Robson proposed that a new and potentially extensive class of solid polymeric materials with unprecedented and possibly useful properties can be obtained by connecting centres having either a tetrahedral or an octahedral array of valences with rod-like connecting units [Hoskins & Robson (1989)]. He described the synthesis and the X-ray crystal structure of the first example of a polymeric framework consisting of tetrahedral centres linked together by rod-like units, obtained through the substitution of the acetonitrile ligands in $[\text{Cu}(\text{CH}_3\text{CN})_4]^+$ by 4,4',4'',4'''-tetracyanotetraphenylmethane. Since the early 1990s, research into materials with polymeric, sometimes porous, structures based on metal ions and organic bridging ligands has increased greatly. Early papers by Robson [Hoskins & Robson (1989); Hoskins & Robson (1990); Abrahams et al. (1994)], Moore [Venkataraman et al. (1995); Gardner et al. (1995)], Yaghi [Yaghi et al. (1995)] and Zaworotko [Subramanian & Zaworotko (1995)] pointed out the rich possibilities for new material structures and properties offered by these coordination polymers.

Coordination Polymers (CPs), also known as Metal-Organic Coordination Networks (MOCNs) or Metal-Organic Frameworks (MOFs)*, are infinite systems built up with metal ions and organic ligands as main elementary units, connected via coordination bonds and other weak chemical bonds [Robin & Fromm (2006)].

The designed construction of extended porous frameworks from soluble molecular building blocks is one of the most challenging issues facing synthetic chemistry today [Yaghi et al. (1998)]. One of the interests in building CPs is the creation of new tuneable functional materials, since CPs are promising materials for applications in gas storage, anion exchange (due to the porosity and their zeolitic-like behaviour), catalysis, conductivity, luminescence, chirality, magnetism, spin transition behaviour, NLO or deposition of thin films.

CPs contain two central components, connectors and linkers, which are defined as the starting reagents from which the principal framework of the CP is constructed. In addition, there are other auxiliary components, such as counteranions, nonbonding guests (or template molecules) and blocking ligands. Metal ions are normally used as connectors in the construction of CPs. The choice of the metal is crucial, because it influences the properties of the product depending on its size, hardness/softness, ligand-field stabilisation energy and coordination geometries [Robin & Fromm (2006)]. Both transition metal and lanthanide ions have been studied, but transition metal ions are most widely used. Depending on the metal and its valence, different coordination geometries can arise (*i.e.* linear, tetrahedral, square planar, octahedral, and different distorted forms). For example, Ni(II) and Pt(II) are preferentially tetraordinated and square planar, Co(II) usually has an octahedral geometry, while Ag(I) normally has a linear geometry, etc.

On the other hand, the large coordination numbers from 7 to 10 and the polyhedral coordination geometry of the lanthanide ions should be useful for the generation of new and unusual network geometries; nevertheless, lanthanide ions are less used, because the high flexibility of their coordination numbers makes their behaviour very difficult to predict.

*Recently, a clear distinction has been proposed to distinguish MOFs from CPs, in terms of the bond strength between connectors and linkers. According to Yaghi et al., the term CP should be restricted to those materials in which metal centres are connected through "classical coordinative bonds", (as an example $\text{M-N}_{(\text{pyridine})}$) whose strength normally do not exceed ca. 100 kJ mol^{-1} , while in a MOF the energy of the metal-ligand bond acting as framework link (as an example the two Zn-O bonds present in MOF-5) is higher, ca. 350 kJ mol^{-1} , close to that of a typical C-C bond [Tranchemontagne et al. (2009)].

Generally speaking, to build CPs the linkers have to bridge metal ions, thus this requires multidentate ligands, with two or more donor atoms. Some important characteristics of the linkers are their shape (*i.e.* if the molecule is rigid or not), the length (*i.e.* the distance between the donor atoms) and the functionalities (*i.e.* further presence of heteroatoms, aromatic rings, alkyl chains, functional groups, etc.). In addition, ligands can be symmetric, asymmetric, chiral, or combining different functionalities on the same molecule. Particularly important are the rigid bridging ligands (having multiple bonds), since they allow for a certain control of the steric consequences in the assembly process.

Bridging ligands can be anionic or neutral. Di-, tri-, tetra- and hexacarboxylate molecules are typical anionic linkers, but also non-symmetric anionic ligands [such as pyridine-X-COO⁻ (X = spacer)] have been extensively studied. Among the neutral ligands, an important class is represented by aromatic molecules containing two or more 4-pyridyl donor units interconnected by chains or tether groups of different types, which can afford a variety of lengths, linear or non-linear geometries, and conformationally rigid or non-rigid molecular skeletons. Significantly, with one of the most used of these ligands, the simple 4,4'-bipyridine, a variety of architectures have been obtained over the past few years. The use of longer spacers between the two 4-pyridyl moieties has afforded very interesting structural motifs, such as double helices, multiple sheets, interpenetrated diamond nets, interpenetrated ladders, as a consequence of the different metal centres and counterions, and the nature of the groups joining the donor moieties [Banfi et al. (2002)]. Therefore, recent efforts have been devoted to the design and synthesis of long bridging ligands with appropriate spacers. By the accurate choice of the ligands, it is possible to tune the properties of the products. It is the bridging organic ligands which allow for the large diversity in the topologies and possible properties of the metal-organic frameworks. In principle, ligand design, together with the coordination properties of the transition metal centres, can be used to achieve control over the structure of the network and, thus, to tune the properties of the compounds.

Since transition metals normally are present as ions, giving a positive charge to the framework, an anionic source must be included to neutralise the overall charge, if neutral ligands are employed. Frequently used anionic sources are inorganic anions, such as ClO₄⁻, NO₃⁻, NCS⁻, CN⁻, CF₃SO₃⁻, SO₄²⁻, N₃⁻ and halides. These anions can influence the metal ion environment (more or less coordinating anions) and the overall structure, because they can be also involved in weak interactions with the framework.

In any case, as far as the crystal structures of CPs are concerned, it is to put in evidence that molecules in crystals tend to pack as close as possible, in order to maximise attractive intermolecular contacts. Therefore, it is quite rare to encounter molecular crystals with open channels or with discrete lattice voids larger than about 25 Å³ [Barbour (2006)]. Sometimes, CPs can be characterised by a more or less relevant porosity, but even in these cases, since nature avoids large empty spaces, the as-synthesised porous CPs (PCPs) normally have no void space, being all the cavities filled with guest, which may be solvent molecules, free ligands or counterions [Bureekaew et al. (2008)]. Therefore, crystal structures of PCPs may be controlled by a template effect of guest molecules, which often can be connected to the framework by weak interactions, such as hydrogen bonds, π - π , H- π interactions and so on. Finally, sometimes, solvent molecules can be removed under vacuum and/or upon heating, giving free channels or cavities.

Concerning this last point, the question of what porosity constitutes is open to a significant degree of interpretation [Barbour (2006)]. Pores, defined by Kitagawa as “minute openings through which fluids or gases can pass”, can be classified in two types: “rigid pores” and “dynamic (flexible) pores”. According to this definition, porous CPs (PCPs) can be divided into three categories, depending on their behaviour upon guest removal [Kitagawa & Kondo (1998); Kitagawa et al. (2004); Kitagawa & Uemura (2005)]. The 1st generation CPs contain cavities and/or channels, but these structures collapse losing their crystallinity after removal of the guest molecules, and are not useful for the required applications; sometimes, it is possible to talk about “recoverable frameworks”, because they collapse upon guest molecules removal, but regenerate under the initial conditions. The 2nd generation CPs have a zeolitic behaviour, remaining crystalline and stable as they are desolvated. Finally, the 3rd generation CPs have dynamic and flexible structure, which respond to external stimuli, such as light, electric field, magnetic field and guest molecules, changing their structures. Thus, an important criterion for a CP to be termed porous is that the framework structure is retained intact (2nd generation compounds) or changes dynamically in a well-defined way (3rd generation compounds) in the guest-free state and when exposed to a new guest species, as usually proven by X-ray powder diffraction (XRPD). This phenomenon is known as “crystal-to-crystal transformation”.

Some recent papers describe porous solids which, under an external stimulus, exhibit a very important flexibility, while retaining the same (or similar) topologies even though the atomic displacements reach sometimes several Å. This phenomenon is called “breathing”, and is associated with reversible movements between two states corresponding to expansion and contraction, respectively [Barthelet (2002); Serre et al. (2002); Loiseau et al. (2004); Barthelet et al. (2009)], normally induced by sorption/desorption of small molecules.

Two different strategies have been developed to build highly porous CPs. The first approach consists in the use of long linkers to increase the distance between the vertices in a net, yielding void space proportional to the length of the linker. In this case, a bond is replaced by a sequence of bonds, and this process is called *expansion*. Even if in principle such method should provide structure with large pores, actually the obtained frameworks are usually found to be interpenetrated, thus having low porosity [Eddaoudi et al. (2001)]. On the other hand, it is possible to replace a vertex of the framework with a group of vertices. This process is known as *decoration* [O’Keeffe (1991)], and usually affords rigid open structures without the tendency to interpenetrate.

In addition to the usual spectroscopic and analytical methods, such as elemental analysis, IR, UV-Vis, ESI-MS, multinuclear NMR and magnetic susceptibilities measurements, there are some specific important methods for the characterisation of CPs.

In particular, in order to interpret any observed property of a CP, it’s necessary to know its molecular structure. The most detailed information on the structure of CPs will be gained from single-crystal X-ray diffraction (XRD) measurements. In general, CPs are insoluble; for this reason, the most common crystallisation method, recrystallisation from a suitable solution, very often is not available [Noro et al. (2009)]. Moreover, even in the case of soluble CPs, since they normally degrade upon dissolution, any characterisation in solution (such as ESI-MS measurements) usually proves the existence of oligomeric fragments, from which the CP structure can only be inferred, but not proved. Therefore, improvement of the syntheses is essential in order to easily get good quality single-crystals.

Usually, CPs are synthesised at relatively low temperatures (*i.e.* < 250 °C). CPs can be prepared using solution methods under bench-top conditions (20-80 °C, 1 atm). In these conditions, the classical ways familiar to coordination chemistry are used. Two different solutions containing, respectively, the metal ions and the organic ligands, are mixed. Since crystals grow in saturated solutions, the ideal concentration can be achieved by slow evaporation of the mother liquors. Sometimes, the rapid mixing of the two solutions leads to the formation of microcrystals, which are not suitable for single-crystal XRD measurements. In this case, an alternative and useful approach is to slowly bring into contact the two solutions, instead of mixing them, by separating the two solutions with a solvent layer and/or a physical barrier (*i.e.* a septum).

An alternative synthetic approach for the obtaining of good quality single-crystals makes use of the solvothermal methods, which were originally developed for the synthesis of zeolites, and have been recently extended to the preparation of CPs. The solvothermal synthesis exploits the self-assembly of products from soluble precursors. The running temperature range is usually 120-260 °C and the reactions take place inside a closed space (autoclave) under autogenous pressure. In these conditions, solubility problems are minimised, and therefore a variety of precursors can be introduced, as well as a number of organic and/or inorganic structure-directing agents. Under such non-equilibrium crystallisation conditions, unprecedented CPs are most likely to be isolated, since in most cases the formation of kinetic phases is favoured with respect to the thermodynamic phase. On the other hand, the autoclave behaves very often as a sort of “black box”, being the obtained results not only unforeseeable in most cases, but, in some cases, it is also difficult to explain how an unexpected product formed.

Microwave irradiation has been developed as a novel heating technique either for the bench-top and, mainly, for the solvothermal synthesis of inorganic porous compounds. This technique attracted growing attention because it provides an efficient way to synthesise, with short crystallisation times, nanoporous inorganic materials, normally requiring several days to crystallise under solvothermal conditions. Other advantages provided by this method are narrow particle size distributions, facile morphology control and an efficient evaluation of the process parameters. The properties of the obtained crystals are of the same quality as those produced by the standard solvothermal process, but since the synthesis is much more rapid, small particles, on the order of 10-15 nm, are normally formed. Although the microwave method usually cannot yield crystals with a size suitable for single-crystal X-ray analysis, its homogeneous effects could create a uniform seeding condition; therefore the size and shape of the crystals can be well controlled and the synthesis cycle can be largely shortened for many practical applications [Ni & Masel (2006)]. For these reasons, microwave synthesis seems very promising for the preparation of CPs, but is so far the less used method.

The richness of the possibilities of isolating new CPs prompted some authors [Stock & Bein (2003); Stock & Bein (2004); Bauer et al. (2005); Serre et al. (2006); Forster et al. (2005)] to develop a dedicated application of high throughput synthesis to CPs systems. This method, already employed for zeolites, inorganic frameworks and polymers for applications in catalysis, implies four main steps: i) set-up of the experiment; ii) synthesis; iii) characterisation and iv) data evaluation. These steps have to be integrated in a workflow in order to reach a maximum of productivity and innovation. Since the HT-methods produce a big amount of data in a very short time, the design of the experiment is a step

of primary importance. The number of reactions must also be minimised, by including chemical knowledge into the set-up of the syntheses. Investigations are usually limited to some parameters, such as composition, temperature, time and pressure. For CPs, the applications of HT methods focus on the discovery of new compounds, the optimisation of reactions conditions (including the effect of dilution on crystal growth), as well as the identification of reaction trends with particular attention on the influence of pH and water content. In general, the large amount of data obtained in short time leads to an improvement towards the understanding of the role played by the chemical parameters in the formation of materials [Férey (2008)].

Single-crystal XRD determinations is the most suitable way to obtain information about CPs molecular structure, but CPs not always form well-shaped crystals, suitable for this kind of analysis. Recent advances in collimation techniques and detector technology enabled fast collection of highly redundant data, by which it is possible to easily measure very small or unstable single-crystals. Microcrystals can be analysed by synchrotron XRD measurements, since the synchrotron radiation light source provides much higher resolution and counting statistics diffraction data in comparison with the laboratory sources [Férey (2009)].

X-ray powder diffraction (XRPD), besides being widely employed in detecting and quantifying (down to a few percents level) different crystal phases (polymorphs, salts, solvates and co-crystals), represents nowadays a useful tool in molecular structure determination; in fact, in the last decade new experimental and computational methods appeared, raising the so-called *ab initio* structural characterisation from powder diffraction data [Masciocchi & Sironi (1997); Masciocchi & Sironi (2005)]. Moreover, using a high brilliance light source, such as the synchrotron radiation, small amounts of samples are required, and the diffraction experiment can be performed in a very short time. Such advantages enable the collection of good quality structural data that compare favourably with those obtained by single-crystal XRD analysis. In addition, powder diffraction methods avoid the difficulties related to the collapse of single crystals because of the volume change during guest adsorption and desorption [Kubota et al. (2007)].

A successful approach, developed by Férey group and others [Mellot-Draznieks et al. (2000); Mellot-Draznieks et al. (2002); Mellot-Draznieks & Férey (2003); Newsam et al. (1999); Schoen & Jansen (1999); Foster et al. (2003); Li et al. (2005); Mellot-Draznieks et al. (2004)], made it possible to predict the structures of CPs from Monte-Carlo computer simulations. This method requires the exact knowledge of the inorganic building block within the solvothermal solution during the reaction, which can only be obtained from *in situ* experiments in real time (NMR, EXAFS, synchrotron diffraction, etc.). Once the building block is known, and being the organic linker structurally inert, it is possible to examine all the possibilities of connection between them, rank them by decreasing energies and extract the thermodynamically viable candidates. Their theoretical XRPD pattern is then compared to the experimental one for identification [Férey (2009)].

Structural stability is an important factor in the evaluation of the microporous functions of CPs. There are two types of stability: i) whether or not a framework is maintained upon removal of the guest molecules from the micropores: ii) thermal stability - strong bonding between building blocks tends to give a framework stable at high temperatures. XRPD and thermogravimetric (TG) measurements are commonly used to investigate the structural stability of CPs. TG data provide information about the

temperatures T_1 and T_2 at which guest removal and framework collapse occur, respectively, but without giving any information on the stability of the framework upon guest removal. The XRPD pattern of a desolvated microporous framework, obtained by heating near T_1 but below T_2 under reduced pressure, provides information on the framework stability. Structural analysis indicates the rigidity or flexibility of the framework, the maintenance of the crystallinity or the formation of an amorphous phase. According to these analyses, microporous CPs are found to be thermally less stable than inorganic materials, because CPs' frameworks are normally built by coordination bonds, hydrogen bonds, and weaker aromatic interactions instead of covalent bonds. Typical T_2 values for this kind of framework are below 473 K, even if some CPs have a high thermal stability, where T_2 is above 573 K (for example, materials with strong $M^{n+}-O^-$ bonds) [Noro et al. (2009)].

A further relevant CPs' characterisation involves the adsorption of guest molecules. This adsorption is governed both by the interactions between guest molecules and the surface, and the size and shape of the pores, which are classified according to their size in macropores ($> 500 \text{ \AA}$), mesopores ($20\text{-}500 \text{ \AA}$) and micropores ($5\text{-}20 \text{ \AA}$). Essentially, there is no difference between adsorption by a macropore and adsorption on a single surface; both of them are governed by the Brunauer-Emmett-Teller (BET) equation. The adsorption by a mesopore is dominated by capillary condensation, which is responsible for a sharp adsorption rise around the mid-relative pressure region. This effect is not attributed to molecule-solid interactions, but to a purely geometrical requirement, illustrated by the Kelvin equation. Finally, the adsorption by micropores should be considered as the filling of molecules into a microspace, where a deep potential field is generated by the overlapping of the wall potentials [Radhakrishnan et al. (2000)]. In this case, the adsorption isotherm is characterised by a steep rise at very low relative pressure, reaching a *plateau* after saturation. There are six representative adsorption isotherms that reflect the relationship between porous structure and adsorption type [Brunauer et al. (1940); Gregg & Sing (1984)]; three of them are shown in Figure 1.

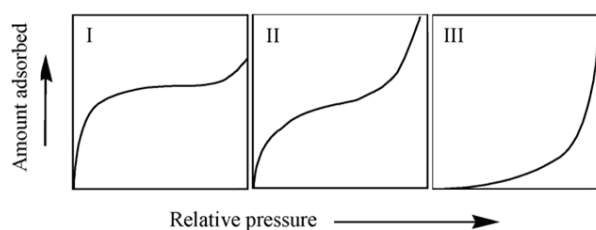


Figure 1.

Type I adsorption isotherm is characteristic of microporous adsorbents; types II and III of nonporous ones. The differences between types II and III result from the relative strength of fluid-solid and fluid-fluid attractive interactions. If the fluid-solid attractive interaction is stronger than that of fluid-fluid, the adsorption isotherm should be of type II, while the opposite situation leads to types III. When a structural transformation from nonporous to microporous, which is characteristic of CPs, occurs during the adsorption, the isotherm could be a combination of types I and II or III. If many structural transformations occur, a multistep adsorption profile would be observed.

The specific surface area is one of the most important factors for evaluating the pore capacity, and is associated with the number of guest molecules accommodated by direct contact. In general, BET

[Brunauer et al. (1983)] and Langmuir equations [Langmuir (1918)] are used to evaluate the specific surface area using N₂ adsorption isotherms measured at 77 K. Recently, the Langmuir surface areas attainable with CPs have increased from 500 m²g⁻¹, comparable to that of zeolites, to very large values, 4500 [Chae et al. (2004)] and 5900 m²g⁻¹ [Férey et al. (2005)]. These values are much higher than the ideal value of carbon materials, 2630 m²g⁻¹, which is calculated as the sum of two surfaces of graphite planes. In the case of inorganic zeolites, the pore walls are constructed with a thickness of several Si, O, and Al atoms; on the contrary, CPs can afford walls only one carbon atom thick, when the wall is of 4,4'-bpy, showing that almost all the atoms constructing the pore walls can be used as a surface [Noro et al. (2009)].

The increasing interest about CPs derives not only from their intrinsically intriguing and “beautiful” molecular and supramolecular architectures, but also from their possible industrial applications. It is to be pointed out that even though only a limited number of possible applications of CPs have been discussed and proposed so far, and none have been industrially realised yet [Mueller et al. (2006); Czaja et al. (2009)], nevertheless, CPs are out of their infancy and first products have been recently commercialised by BASF and Aldrich under the common name of Basolite™ [Czaja et al (2009); <http://www.sigmaaldrich.com/chemistry/chemical-synthesis/metal-organic-frameworks.html>].

On the other hand, a large number of academic studies have evidenced that PCPs have potential applications in the storage of different gases. Particularly, microporous CPs are good candidates for the storage of small molecules, such as energetically relevant gases (H₂, CH₄ and other small gaseous hydrocarbons, such as acetylene and ethylene). In the case of acetylene, exceptionally high uptakes were reported by Kitagawa [Matsuda et al. (2005)], in this case exceeding the packing density usually obtained in today's storage devices. Particularly important is the possible H₂ storage, because many governments throughout the world have the “hydrogen economy” as a stated aim for future energy needs [Dincă et al. (2007); Murray et al. (2009); DoE <http://www.eere.energy.gov/hydrogenandfuelcells/mypp/pdfs/storage.pdf>]. One of the challenges that needs to be overcome before the hydrogen economy becomes a reality is how to store hydrogen safely and economically, and CPs seem to be promising for this purpose. Actually, CP-storage for hydrogen works fully reversibly, avoids complicated heat treatments, and recharging proceeds within seconds or minutes [Férey et al. (2003); Férey et al. (2004); Serre et al (2004); Mueller et al. (2005); Matsuda et al. (2005); Rowsell & Yaghi (2005); Chen et al. (2005); Wong-Foy et al. (2006)].

In this context, it is noteworthy that inelastic neutron scattering studies are used to spectroscopically investigate the H₂-framework interaction. This technique provides a sensitive probe of the adsorption sites for molecular H₂. Neutrons are the ideal scattering probe for such experiments, because X-rays are not sensitive to the low electron density of hydrogen atoms. Based on the accumulated crystallographic and adsorption data of PCPs, computational modelling studies of small-molecule adsorption have been performed, an approach that is common in carbon and inorganic materials chemistry [Kaneko et al. (1994); Setoyama et al. (1998); Anderson et al. (1999); MacKinnon et al. (2001); Okhubo et al. (2002); Clark et al. (2005)].

PCPs can be potentially utilised in gas separation processes, and in this context an important application is the sorption of environmental important species (NO, CO and CO₂). The adsorption of

CO₂ by using PCPs is particularly interesting due to the awareness of global warming [Walton et al. (2008); Bae et al. (2008); Willans et al. (2009)].

PCPs are relevant also in the purification of gases, *i.e.* to remove ppm-traces of sulphur components from various gases. In particular, PCPs with accessible open metal sites are well suited to chemisorb, besides sulphur compounds, other electron-rich odour-generating molecules, such as amines and phosphines.

Finally, PCPs can be employed in heterogeneous catalysis. Their most remarkable characteristic is the lack of non-accessible bulk volume. Moreover, due to the very open architecture, the self diffusion coefficients of molecules in the pores are only slightly lower than in the bulk solvent. This means that mass transport in the pore system is not hindered. In addition, the ordered structure offers the opportunity to spatially separate active centres. As a result of their high surface areas, PCP-based catalysts contain a very high density of fully exposed active sites per volume. This characteristic results in enhanced activity, and thus a more effective catalytic system [Seo et al. (2000); Pan et al. (2003); Wu et al. (2005); Uemura et al. (2006); Uemura & Kitagawa (2009)].

PhD Specific Work

Synthesis of Polynucleating Nitrogen Ligands

As already mentioned in the **Introduction**, the use of suitably designed polytopic ligands may contribute to reduce the uncertainty intrinsically present in the obtaining of CPs having useful functional properties. For this reason, the preparation of such ligands continues to be an interesting challenge for chemists. During the first year of my PhD studies, two different families of new potentially polynucleating ligands were synthesised and fully characterised. Both classes possess nitrogen containing bonding moieties, such as pyrazole and its derivatives, connected to different spacers.

The first class is composed by ligands based on oxalate/malonate skeleton, while the second is formed by ligands based on the 1,3,5-triazine moiety.

Ligands based on oxalate/malonate skeleton and azolate moieties

We synthesised and characterised a series of diamidic ligands based on the rigid (oxalyl) or more flexible (malonyl) spacers and on different azolate moieties. These heteropolytopic oxalyl and malonyl diamidic ligands, derived from 1H-pyrazole, 3,5-dimethyl-1H-pyrazole, 1H-indazole and 1H-1,2,3-benzotriazole (see Chart 2), have been synthesised by reaction of the corresponding azole with oxalyldichloride and carbon suboxide, respectively, and fully characterised by elemental analyses, IR and NMR (^1H , ^{13}C). Moreover, for the pyrazole (**a** and **e**) and the benzotriazole (**c** and **g**) derivatives, it was also possible to get crystals suitable for an X-ray crystal structure determination.

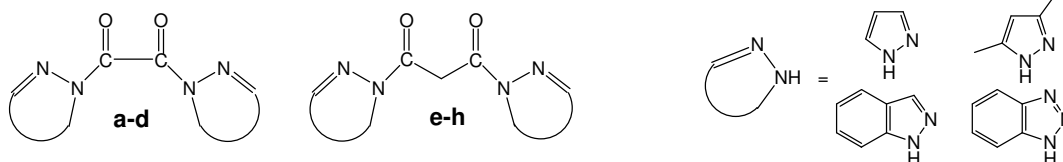


Chart 2.

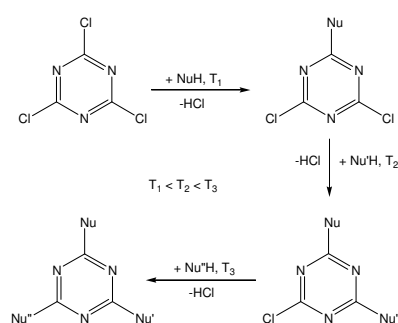
Compounds **a-h** were also tested in coordination reactions with $\text{Cu}^{(\text{II})}$ e $\text{Ag}^{(\text{I})}$ compounds in protic solvents (H_2O , EtOH), but preliminary results indicate that these ligands undergo relatively easy hydrolysis. All the obtained results have been published recently [Garau et al., in the press].

Ligands based on the 1,3,5-triazine spacer

The second class of ligands we synthesised is based on the 1,3,5-triazine (also known as *s*-triazine) spacer, which possesses interesting electronic and steric properties [Smolin & Rapoport (1959); Mooibroek & Gamez (2007)]. *s*-Triazine derivatives have found useful applications in disparate fields, from analytical chemistry [Brückner & Wachsmann (2003); Maekewa et al. (2004)] to electrochemistry [de la Hoz et al. (2001)]. Recently, *s*-triazine derivatives have been employed as templates in crystal engineering [Bernhardt & Hayes (1998); Prins et al. (2002)] and some ligands having the *s*-triazine ring as spacer have been synthesised in the last years [Gelling et al. (1997); Elguero et al. (2001); Milata et al. (2001); de Hoog et al. (2002); Gamez et al. (2002); Claramunt et al. (2003); Maekewa et al. (2004); Gamez & Reedijk (2006); Mooibroek & Gamez (2007)]. Furthermore, *s*-triazine ring is intrinsically able to form strong, directional H-bonds

[Zerkowski et al. (1994); Archer et al. (2000); Archer et al. (2001); Archer et al. (2002)], and this particularity has been exploited in the formation of numerous supramolecular networks, ranging from 1D or 2D polymers, to linear tapes, crinkled tapes, rosettes, etc [Kazuo et al. (1979); Whitesides et al. (1991); Prins et al. (2001); Glaser et al. (2005); Casarin et al. (2008) (a)].

Generally speaking, 2,4,6-trichloro-1,3,5-triazine, also known as cyanuric chloride, is largely used as starting material to easily synthesise important symmetrically or asymmetrically substituted derivatives, mainly thanks to the fact that chloride ions can be selectively substituted by almost any nucleophilic species, following the *Moffat's rule* [Cuthbertson & Moffat (1948)], sketched in Scheme 2.



Scheme 2.

Thus, we synthesised and characterised some potentially polynucleating ligands based on the s-triazine skeleton, bearing bonding fragments such as pyrazole, trispyrazolylmethane, and 1,2-diamine-ethane. Specifically, the compounds we prepared are 2-amino-4-chloro-6(1H-pyrazol-1-yl)-1,3,5-triazine, **i**, 2-chloro-4,6-di(1H-pyrazol-1-yl)-1,3,5-triazine, **j**, N,N'-bis(4,6-di(1H-pyrazol-1-yl)-1,3,5-triazin-2-yl)ethane-1,2-diamine, **k**, 2,4,6-tris(tri(1H-pyrazol-1-yl)methyl)-1,3,5-triazine, **l**, and 2,4,6-tris(2,2,2-tri(1H-pyrazol-1-yl)ethoxy)-1,3,5-triazine, **m** (see Chart 3).

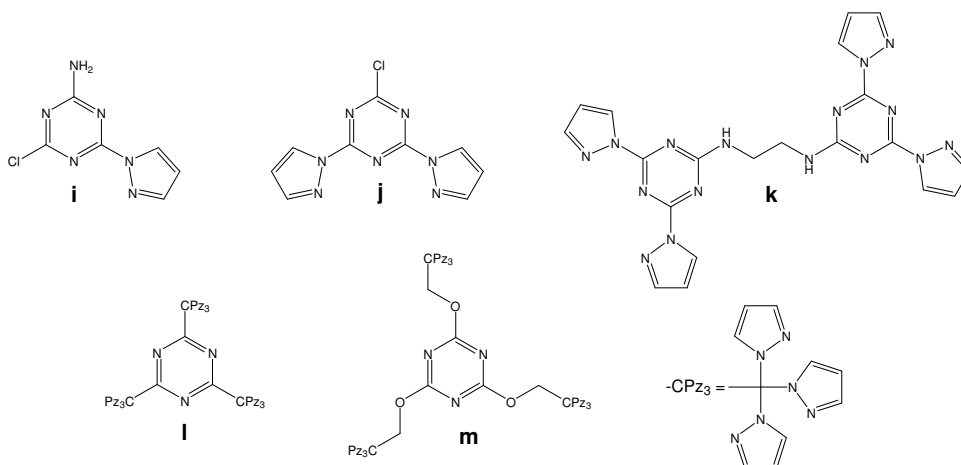


Chart 3.

Compound **i** has been prepared by refluxing 2-amino-4,6-dichloro-1,3,5-triazine with an excess of pyrazole in dioxane for 10 h. Workup of the obtained mixture gave ca. 20% of 2-amino-4,6-di(1H-pyrazol-1-yl)-1,3,5-triazine and ca. 80% of **i**. Recrystallisation from MeOH gave pure crystals of **i** which were used for a single crystal XRD structural determination and ^1H , ^{13}C and ^{15}N NMR measurements. The non-equivalence of the $-\text{NH}_2$ hydrogens evidences the iminium character of

this moiety. Compound **i**, exploiting strong H-bonds, self-assembles generating supramolecular linear tapes. Some theoretical DFT calculations at the PBE level were performed, and the results are in good agreement with experimental solid state and solution data. All the obtained results have been published [Casarin et al. (2008) (a)].

Compound **j**, 2-chloro-4,6-di(1H-pyrazol-1-yl)-1,3,5-triazine, has been obtained in a relatively high yield by reacting cyanuric chloride with two equivalents of pyrazole (and two equivalent of DIPEA) in toluene at rt. Standard analytical procedures have been used to characterise **j**, and all data validate the structure proposed in Chart 3. In particular, the most abundant signal of the ESI-MS spectrum corresponds to the protonated molecular fragment, and multinuclear NMR data fall in the range normally found for related derivatives [Casarin et al. (2008) (a)].

Compound **j** was employed as starting material in the synthesis of **k**, N,N'-bis(4,6-di(1H-pyrazol-1-yl)-1,3,5-triazin-2-yl)ethane-1,2-diamine, by reacting it with ethylenediamine in 2:1 ratio. Interestingly, compound **k** was also obtained by treating the product of the reaction between 2 moles of cyanuric chloride and one mole of ethylenediamine with four moles of sodium pyrazolate. We were unable to obtain crystals of **k** suitable for an X-ray crystal structure determination, but all the characterisations converge toward the structure shown in Chart 3. Particularly, the most intense ESI-MS signals correspond to the molecular ion or its dimer, being the positive charge supplied by H⁺ or Na⁺. Also multinuclear NMR data concerning the bis-pyrazolyl-triazine moieties give useful information on the structure. Particularly, the duplications of the signals of H₃, H₄, and H₅ indicate the non-equivalence of the two pyrazolyl moieties due to the hampered rotation around the C–NH bonds, analogously to what previously observed in the case of compound **i** [Casarin et al. (2008) (a)].

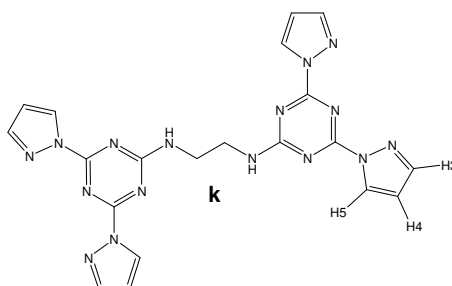


Chart 4.

Compound **I**, 2,4,6-tris(tri(1H-pyrazol-1-yl)methyl)-1,3,5-triazine, was synthesised by exploiting the acidity of the methyne hydrogen of trispyrazolylmethane (TPM). Specifically, three equivalents of the anion of TPM, obtained by deprotonation with *n*-BuLi, were reacted with cyanuric chloride, and workup gave **I**, which was recrystallised from acetone yielding crystal suitable for an X-ray crystal structure determination. In Figure 2 is reported the molecular structure of **I**.

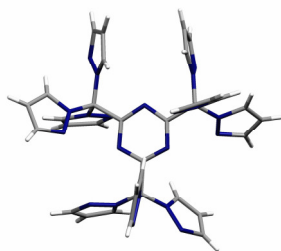


Figure 2. Molecular structure of **I**.

The crystal packing of **I** (Figure 3) shows how molecules fit together in the solid state, evidencing also that there are no relevant supramolecular interactions among different units, being the overall packing dictated only by dispersion forces.

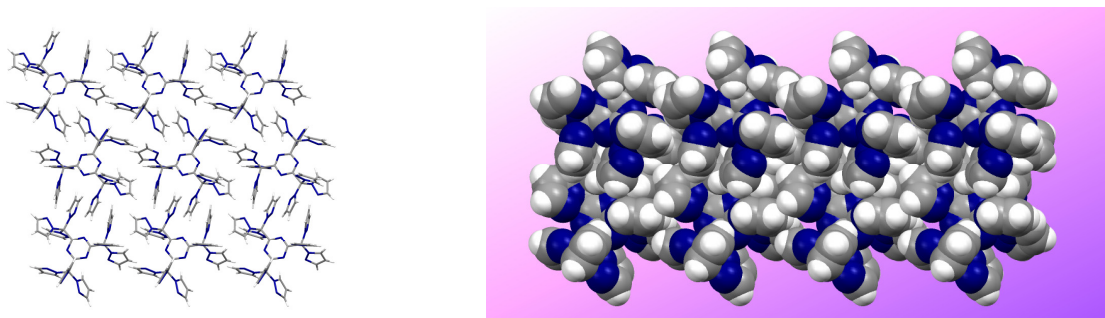


Figure 3. Capped stick representation of the crystal packing of **I** viewed along the crystallographic *a* axis (left) and space-filling view evidencing small, irregular, channels running parallel to the crystallographic *a* axis (right).

Spectroscopic data are in agreement with the above reported structural feature. Particularly, multinuclear NMR and IR spectra concerning the trispyrazolyl moieties of compound **I** show values falling in the ranges of trispyrazolylmethane [McLauchlan et al. (2004)].

Analogously to **I**, compound **m**, 2,4,6-tris(2,2,2-tri(1H-pyrazol-1-yl)ethoxy)-1,3,5-triazine, was obtained by exploiting the acidity of the hydroxylic hydrogen of 2,2,2-tris(1H-pyrazol-1-yl)ethanol (TPEtOH), which was first deprotonated with MeLi and then treated with cyanuric chloride. Unfortunately, we were unable to obtain crystals of **m** suitable for an XRD crystal structure determination, but elemental analysis, ESI-MS and multinuclear NMR data are in agreement with the structure proposed in Chart 3. In particular, NMR signals are very similar to the corresponding values of **I**, and signals due to the CH₂O fragments are also evident. Furthermore, the most relevant signal in the ESI-MS spectrum, at *m/z* 830.8, corresponds to the molecular fragment plus a sodium ion [C₃₆H₃₃N₂₁O₃ + Na]⁺. Another important signal at *m/z* 227.3 is due to the triply charged species [C₃₆H₃₃N₂₁O₃ + 2H + Na]³⁺, while the only signal coming from a decomposition process (*m/z* 740.8) is present in a quite low abundance (18%) and corresponds to the loss of a negative pyrazolate fragment from the molecular ion, [C₃₆H₃₃N₂₁O₃ - pz]⁺.

Structural and spectroscopic data suggest that compounds **I** and **m** exist in solution as isolated molecules, and we expected that their reactivity in solution towards metal centres was strictly related to that of TPM. In particular, compound **I** is quite stable (solutions in acetone or DCM remain unchanged for weeks) thus we reacted **I** with three equivalents of different metal ions, namely Cu^(II), Zn^(II), Ru^(III), and Ag^(I), and the reactions were carried out in the air using commercial,

not anhydrous, solvents. Quite surprisingly, in all the cases the ligand underwent C–C hydrolysis and the formation of metal complexes having coordinated TPM was observed. In detail, the reaction with $\text{Ag}(\text{CF}_3\text{SO}_3)$ and with $\text{Cu}(\text{NO}_3)_2 \cdot 2.5\text{H}_2\text{O}$ yielded the already known derivatives $\{[\text{Ag}(\text{TPM})_2](\text{CF}_3\text{SO}_3)_2$, **I_a** [Reger et al. (2006)], and $[\text{Cu}(\text{TPM})_2](\text{NO}_3)_2$, **I_b** [Astley et al. (1993)], respectively, while the reactions of $\text{Zn}(\text{CF}_3\text{SO}_3)_2$ and $[\{\text{RuCl}(\rho\text{-cymene})\}_2]$ with **I** led to the formation of the new compounds $[\text{Zn}(\text{TPM})_2](\text{CF}_3\text{SO}_3)_2$, **I_c**, and $[\text{Ru}(\rho\text{-cymene})(\text{TPM})](\text{Cl})(\text{OH}) \cdot 2\text{H}_2\text{O}$, **I_d**, respectively.

The IR spectra of compounds **I_c** and **I_d** show all the expected bands of the TPM ligand; also the ^1H NMR spectra confirm the breaking of **I** upon interaction with metals.

The structures of **I_a**-**I_d** were ascertained also through XRD determinations. Particularly, the X-ray crystal structure of compound **I_c**, $[\text{Zn}(\text{TPM})_2](\text{CF}_3\text{SO}_3)_2$, limited to the di-cationic moiety is shown in Figure 4.

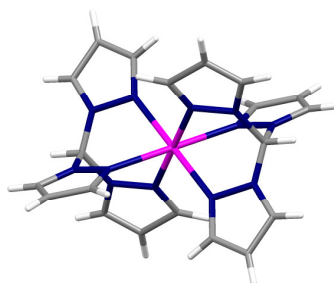


Figure 4. X-ray crystal structure of the di-cationic moiety $[\text{Zn}(\text{TPM})_2]^{2+}$.

Two TPM molecules are coordinated to the Zn ion, which seats in an inversion centre. Each TPM methyne carbon atom shows an almost regular tetrahedral environment, while the coordination around the metal ion is represented by a distorted octahedron. The triflate ions, omitted in Figure 4, have a quite regular geometry, and are not involved in the coordination to the metal. On the other hand, it is quite complicate to describe the position of these anions in the whole crystal structure. As a matter of fact, it appears that ten triflate anions surround the $[\text{Zn}(\text{TPM})_2]^{2+}$ moiety (see Figure 5) and are all involved in more or less weak “non-conventional” H-bonds, all of the type $\text{O} \cdots \text{H}-\text{C}$.

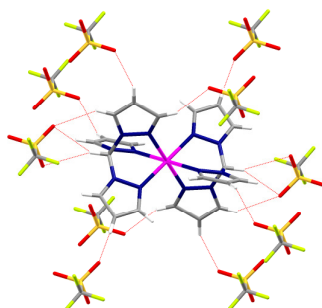


Figure 5. Arbitrary view of $[\text{Zn}(\text{TPM})_2]^{2+}$ of **I_c** surrounded by ten triflate ions interacting with it through H-bonds (red dotted lines).

The overall result of these interactions is the formation of a 3D supramolecular network that, as shown in Figure 6, presents small irregular channels having dimensions of about $2.7 \times 1 \text{ \AA}^2$ (taking into account the vdW radii), running parallel to the crystallographic *a* axis.

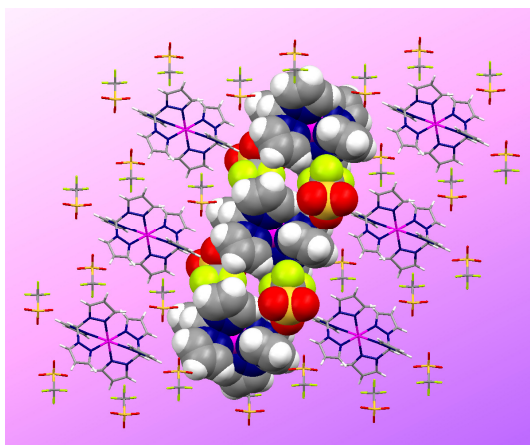


Figure 6. Crystal packing of **1c** viewed down the crystallographic *a* axis. The partial spacefill representation evidences the small channels running parallel to the same axis.

In Figure 7 is sketched the X-ray crystal structure of compound **1d**, [Ru(TPM)(cymene)](Cl)(OH)·2H₂O. The most evident feature in **1d** is that the double positive charge of Ru^(II) is balanced by a Cl⁻ and an OH⁻ ions, instead of the two chlorides as in the starting material. Moreover, both Cl⁻ and OH⁻ do not appear to be coordinated to the metal centre.

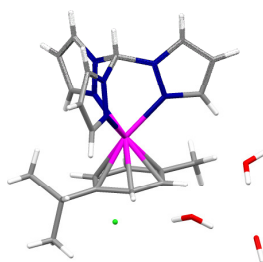


Figure 7. X-ray crystal structure of [Ru(TPM)(cymene)]Cl(OH)·2H₂O.

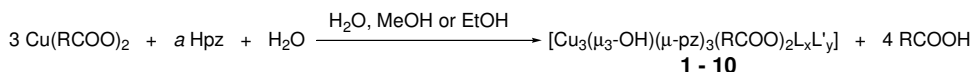
In the cationic fragment, TPM acts in a tridentate coordination and also the η^6 -cymene coordinates to Ru^(II) in an almost identical way as observed in other cases [Astley et al. (1993); Reger et al. (2006)], and these structural features do not deserve further particular description. At the moment we set aside the study of the coordination properties of our ligands to transition metal ions, and focused our attention on the understanding of the decomposition mechanism of **1** upon treatment with transition metal compounds. In order to achieve this goal, first of all we started studying the binding capability of TPM towards Cu^(I) and Ag^(I) ions. DFT has been used to look into the electronic structure of [M(TPM)]⁺ molecular ion conformers (M = Cu, Ag) and to study the energetics of their interconversion. Theoretical data pertaining to the free TPM state the intrinsic instability of its κ^3 -like conformation, thus indicating that, even though frequently observed, the κ^3 -tripodal coordinative mode is unlikely to be directly achieved through the interaction of M^(I) with the κ^3 -like TPM conformer. It was also found that the energy barrier for the κ^2 -[M(TPM)]⁺ \rightarrow κ^3 -[M(TPM)]⁺ conversion is negligible. As far as the bonding scheme is concerned, the TPM \rightarrow M^(I) donation, both σ and π in character, is the main source of the M^(I)-TPM bonding, whereas back-donation from completely occupied M^(I) d orbitals into TPM-based π^* levels plays a negligible role [Casarin et al. (2008) (b); Casarin et al. (2009)]. We recently adopted a similar theoretical approach to better understand the decomposition of the diamidic ligands **a-h** in protic conditions.

Synthesis of new Trinuclear Triangular Cu^(II) Coordination Polymers

The research group where I performed my PhD studies is interested in the synthesis and characterisation of CPs. As already mentioned in the **Introduction**, these compounds are infinite systems built up with metal ions and organic ligands as main elementary units, connected *via* coordination bonds and other relatively weak interactions. CPs are promising as materials for applications in gas storage and anion exchange, catalysis, conductivity, luminescence, chirality, magnetism, spin transition behaviour, NLO, deposition of thin films, etc.

As already discussed in the previous chapters, the synthetic approach for the preparation of CPs is the “copolymerisation” of transition metal ions and polytopic organic linkers. Sometimes, the assembly of these building blocks leads first to the formation of mono- or polynuclear metal-organic clusters, named SBU, which may assemble to give the polymeric structure.

In the laboratory where I performed my PhD studies, some new trinuclear triangular copper(II)/pyrazolate/carboxylate CPs (compounds **1-4** in Chart 5) were synthesised and fully characterised [Casarin et al. (2004); Casarin et al. (2005); Di Nicola et al. (2007) (a)]. These trinuclear complexes can be easily obtained by reacting copper(II) carboxylates with pyrazole (Hpz) in hydroalcoholic solvents*. The basic carboxylate ions deprotonate water and Hpz, producing OH⁻ and pz⁻ ions, which build, together with the Cu^(II) ions, the μ₃-OH capped nine-membered ring sketched in Chart 5. Following this protocol, we were able to synthesise new trinuclear triangular Cu^(II) CPs (both from saturated and unsaturated carboxylates), which were fully characterised, and the obtained data have been published recently [Garau et al. (2008); Di Nicola et al. (2009); Contaldi et al. (2009)].



- 1** R = -H, a = 5, L = Hpz, x = 2, y = 0;
- 2** R = -CH₃, a = 4, L = Hpz, x = 1, y = 0;
- 3** R = -CH₂CH₃, a = 3, L = EtOH, x = 1, y = 0;
- 4** R = -CH₂CH₂CH₃, a = 3, L = MeOH, L' = H₂O, x = y = 1;
- 5** R = -CH₂CH₂CH₂CH₃, a = 3, L = H₂O, x = 1, y = 0;
- 6** R = -CH₂CH₂CH₂CH₂CH₃, a = 3, L = EtOH, x = 1, y = 0;
- 7** R = -CH₂CH₂CH₂CH₂CH₂CH₃, a = 3, L = EtOH, x = 1, y = 0;
- 8** R = -CH=CH₂, a = 3, L = H₂O, L' = Hpz, x = 2, y = 1;
- 9** R = -CH=CH₂, a = 3, L = MeOH, x = 1, y = 0;
- 10** R = -C(CH₃)=CH₂, a = 3, x = y = 0.

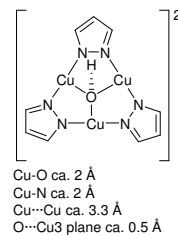


Chart 5.

These trinuclear compounds have the general formulation $[\text{Cu}_3(\mu_3\text{-OH})(\mu\text{-pz})_3(\text{RCOO})_2\text{L}_x\text{L}'_y]$ [R = -H, -CH₃, -CH₂CH₃, -(CH₂)₂CH₃, -(CH₂)₃CH₃, -CH₂CH(CH₃)CH₃, -(CH₂)₄CH₃, -(CH₂)₅CH₃, -CH=CH₂, -CH(CH₃)=CH₂; L, L' = Hpz, H₂O, MeOH, EtOH], and all of them are characterised by the presence of the $[\text{Cu}_3(\mu_3\text{-OH})(\mu\text{-pz})_3]^{2+}$ moiety, whose positive charge is balanced by two carboxylate ions coordinated to Cu^(II); most importantly, the trinuclear clusters **1-10** act as SBUs and self-assemble in the solid state leading to the formation of 1D, 2D or 3D CPs [Casarin et al. (2004); Casarin et al. (2005); Di Nicola et al. (2007) (a); Di Nicola et al. (2009); Contaldi et al. (2009)].

*Incidentally, the reaction conditions result of paramount importance to direct the synthesis toward the obtaining of the trinuclear derivatives, as proved by the fact that if the above indicated reactions are carried out in MeCN, instead of hydroalcoholic solvents, the 1D CP $[\text{Cu}(\mu\text{-pz})_2]_n$, presenting interesting solvatochromic properties was obtained [Cingolani et al. (2005); Bencini et al. (2009)].

The reactivity of the trinuclear moiety toward H^+ was checked by reacting the 2D CP $[Cu_3(\mu_3-OH)(\mu-pz)_3(CH_3COO)_2(Hpz)]$, **2**, with aqueous HCl. The reaction gave two hexanuclear and a heptanuclear cluster, the latter self-assembling through Cl^- bridges to form a PCP having hexagonal channels with a free diameter of *ca.* 4 Å [Casarin et al. (2007) (a); Di Nicola et al. (2007) (b); Di Nicola et al. (2008)].

These results prompted us to extend our studies to the reaction of **2** with other strong acidic species, namely H_2SO_4 , H_3PO_4 , $HClO_4$, HNO_3 , CF_3COOH and CF_3SO_3H . These reactions generated a wide variety of mono-, tri- and hexanuclear compounds, as well as some CPs.

Reactions of $[\text{Cu}_3(\mu_3\text{-OH})(\mu\text{-pz})_3(\text{CH}_3\text{COO})_2(\text{Hpz})]$, **2**, with strong acids

The reactions with strong acids broke the supramolecular assembly of **2**, most probably through the H^+ attack to the electrophilic acetate centres, yielding acetic acid. Moreover, analogously to what found in the reaction with HCl [Casarin et al. (2007) (a)] a partial breaking of the nine-membered ring, followed by rearrangements, was also observed. Actually, through fractional crystallisation of the obtained solutions, it was possible to isolate and characterise numerous different crystalline derivatives. Single crystal XRD determinations revealed that, in some cases, the trinuclear $[\text{Cu}_3(\mu_3\text{-OH})(\mu\text{-pz})_3]^{2+}$ fragment was maintained, but also mononuclear complexes formed. Moreover, supramolecular unprecedented assemblies were observed. The results obtained in the reactions of **2** with the above mentioned strong acids are summarised in Chart 6.

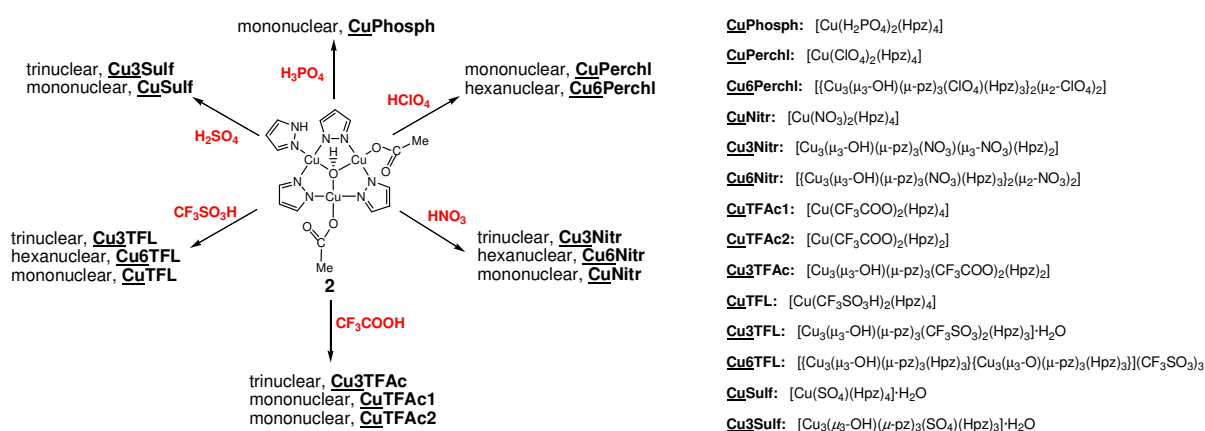


Chart 6.

Besides single-crystal XRD determinations, other characterisations were carried out on the obtained compounds, giving results in complete agreement with the XRD data. As an example, UV-Vis spectra of the mononuclear (**CuSulf**, **CuPhosph**, **CuPerchl**, **CuTFac1**, **CuTFac2** and **CuTFL**, Figure 8, left) and trinuclear or hexanuclear (**Cu3Sulf**, **Cu3TFac**, and **Cu3TFL**, **Cu6Perchl**, Figure 8, right) compounds have different typical patterns, which make it possible to distinguish between the two structural features.

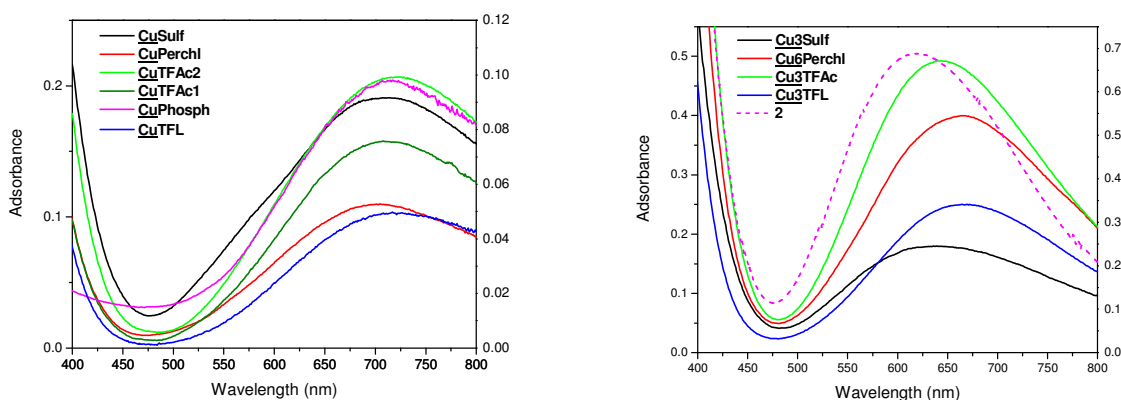


Figure 8. Solution electronic spectra of mononuclear (left) and trinuclear/hexanuclear (right) compounds.

In fact, while in the case of the mononuclear derivatives the maxima of the signals are in the range 708-720 nm, the spectra of the trinuclear triangular derivatives display a broad band having a maximum in the range *ca.* 630-670 nm.

Also the ESI-MS characterisations are in agreement with the trinuclear (**Cu3Sulf**, **Cu3TFac** and **Cu3TFL**) or mononuclear (**CuPhosph** and **CuTFac1**) structures. The most relevant signals are summarised in Table 1.

Table 1. Most relevant signals in ESI-MS spectra of compounds **Cu3Sulf**, **CuPhosph**, **Cu3TFac**, **CuTFac1** and **Cu3TFL**.

Compound	Signal ^a	R. A. ^b	Assignments
Cu3Sulf	199.0	50	[Cu ^{II} (Hpz) ₂] ⁺
	623.8	100	[Cu ₃ (OH)(pz) ₃ (SO ₄)(Hpz)(MeOH)(H ₂ O)+H] ⁺
CuPhosph^c	69.2	100	[Hpz+H] ⁺
	296.0	45	[Cu(H ₂ PO ₄)(Hpz) ₂] ⁺
Cu3TFac	604.2	73	[Cu ₃ (OH)(pz) ₃ (CF ₃ COO)(MeOH) ₂ (H ₂ O)] ⁺
	636.3	26	[Cu ₃ (OH)(pz) ₃ (CF ₃ COO) ₂ +H] ⁺
	672.3	100	[Cu ₃ (OH)(pz) ₃ (CF ₃ COO)(Hpz)(MeOH) ₂ (H ₂ O)] ⁺
CuTFac1	199.0	50	[Cu ^{II} (Hpz) ₂] ⁺
	312.0	100	[Cu(CF ₃ COO)(Hpz) ₂] ⁺
Cu3TFL	625.8	32	[Cu ₃ (OH)(pz) ₃ (CF ₃ SO ₃)(Hpz)] ⁺
	707.8	100	[Cu ₃ (OH)(pz) ₃ (CF ₃ SO ₃)(Hpz)(MeOH) ₂ (H ₂ O)] ⁺
	740.3	21	[Cu ₃ (OH)(pz) ₃ (CF ₃ SO ₃) ₂ (MeOH)+H] ⁺

^a Values corresponding to the higher signals of the isotopic clusters. All isotopic clusters fit satisfactorily with calculated ones [Senko (1994)].

^b Relative Abundance of the higher signal of the isotopic cluster.

^c Spectrum data obtained in water solution

The most intense signal of the ESI-MS spectra of **Cu3Sulf**, **Cu3TFac** and **Cu3TFL** corresponds to trinuclear clusters. Other trinuclear-based signals are also present, while no hexanuclear clusters have been found. Interestingly, signals suggesting the reduction of Cu^(II) to Cu^(I) in the employed condition are often detected. Even though the ESI-MS data cannot be considered an exhaustive proof of the presence of trinuclear clusters in the solid state, nevertheless they offer a great suggestion for this feature, also taking into account that the positive ESI-MS of the mononuclear species (**CuPhosph** and **CuTFac1**) show a completely different pattern.

The analysis of the room temperature magnetic susceptibility measurements shows some differences among the trinuclear-based derivatives. In compound **Cu3Sulf**, the 2.603 BM value, calculated for a trinuclear unit, is a little bit larger than that found in strictly related trinuclear-based polymeric species [Casarin et al. (2004); Casarin et al. (2005); Di Nicola et al. (2007) (a); Di Nicola et al. (2009); Contaldi et al. (2009)], but is smaller than the value expected for three independent Cu^(II) ions, thus indicating that some kind of exchange coupling operates. Analogously, this exchange is much more evident in the hexanuclear complex **Cu6Perchl**, being the room temperature magnetic susceptibility value of 3.18 BM, calculated for the hexanuclear formulation of **Cu6Perchl**, much smaller than that expected for six independent copper(II) moieties. The mononuclear complexes of formula [Cu(X)₂(Hpz)_n], **CuPhosph**, **CuPerchl** and **CuTFac1** have magnetic moments close to the spin-only value for an S = 1/2 system (1.73 BM at room temperature). On the other hand, it is interesting to evidence a significant difference between the first two mononuclear complexes (**CuPhosph** and **CuPerchl**) and the species **CuTFac1**. The observed value for **CuTFac1**, 1.63 BM, is somewhat less than the spin-

only value expected for a magnetically isolated Cu^{II} system [Hathaway (1984)], suggesting the presence of weak intermolecular interactions, possibly involving a H-bonding network [Hathaway (1973)].

The molecular structures of the obtained compounds, determined through single-crystal XRD measurements, revealed interesting features.

The reaction of **2** with H_2SO_4 produced the trinuclear derivative $[\text{Cu}_3(\mu_3\text{-OH})(\mu\text{-pz})_3(\text{SO}_4)(\text{Hpz})_3]\cdot\text{H}_2\text{O}$, **Cu3Sulf**, (Figure 9, left) which behaves as a SBU, forming a 1D CP running along the crystallographic *a* axis, where SO_4^{2-} bridges two trinuclear unit (Figure 9, right).

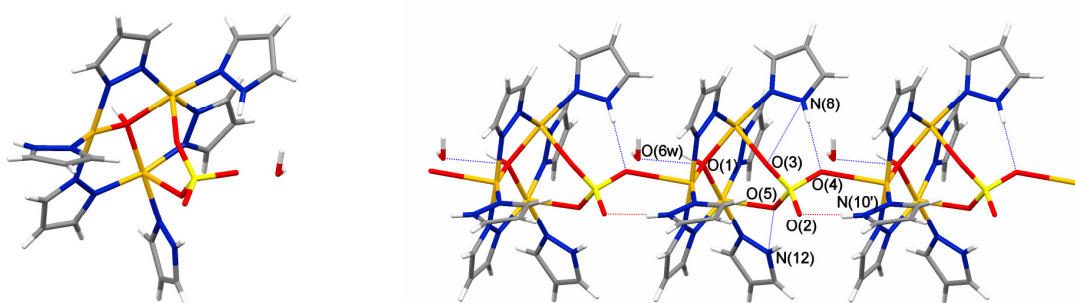


Figure 9. Asymmetric unit (left) of **Cu3Sulf**, assembling through SO_4^{2-} bridges, giving a 1D CP (right).

A series of H-bonds are also evident; besides the interaction between the $\mu_3\text{-OH}$ and the crystallisation water molecule, other three “intramolecular” interactions involving the NH groups of the coordinated pyrazoles with O(4), O(3) and O(5) (blue dotted lines in Figure 9, right) have to be mentioned. Moreover, the 1D CP is further stabilized by an “intermolecular” H-bond involving O(2) and N(10)H(10) of an adjacent trinuclear unit (red dotted lines in Figure 9, right).

Besides **Cu3Sulf**, from the reaction of **2** with H_2SO_4 it was possible to isolate also the mononuclear species $[\text{Cu}(\text{SO}_4)(\text{Hpz})_4]\cdot\text{H}_2\text{O}$, **CuSulf**, previously obtained through a completely different procedure [Shen et al. (2004)].

The reaction of **2** with H_3PO_4 produced, besides an unidentified light-blue solid (whose elemental analysis revealed the absence of organic fragments), the blue crystalline mononuclear complex $[\text{Cu}(\text{H}_2\text{PO}_4)_2(\text{Hpz})_4]$, **CuPhosph**, whose molecular structure is shown in Figure 10.

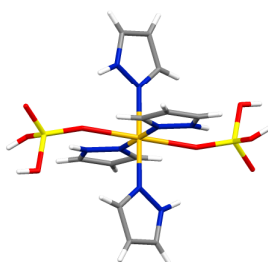


Figure 10. Molecular structure of **CuPhosph**.

The copper ion shows an almost regular octahedral coordination, where the dihydrogen phosphate ions occupy the axial sites. A strong “intramolecular” H-bond involves O(2) and N(2)H(2) (blue dotted

line in Figure 11). Each mononuclear unit is connected to other two identical units by two couples of identical H-bonds involving dihydrogen phosphate, forming 1D supramolecular networks, which then assemble in a 2D supramolecular network through quite strong “intermolecular” H-bonds (Figure 11).

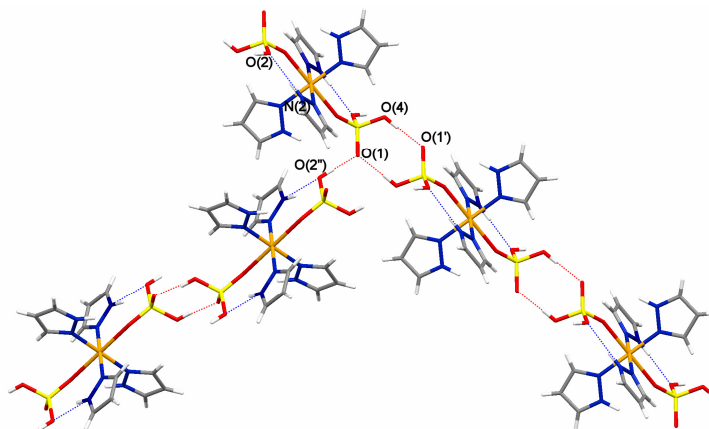


Figure 11. 2D supramolecular assembly of **CuPhosph**.

Another mononuclear complex, $[\text{Cu}(\text{ClO}_4)_2(\text{Hpz})_4]$, **CuPerchl**, has been obtained in the reaction of **2** with HClO_4 . Its molecular structure is reported in Figure 12, where the octahedral coordination is evident, being the perchlorate ions in the axial positions.

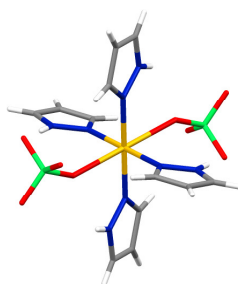


Figure 12. Molecular structure of **CuPerchl**.

The octahedral geometry is slightly distorted, and also the Cu-N distances are not identical, maybe due to the different kind of “intramolecular” H-bonds formed by NH with perchlorate oxygens, sketched in Figure 13. Actually, N(2)H(2) weakly interacts both with O(1) and with O(2), while N(4)H(4) interacts only with O(1).

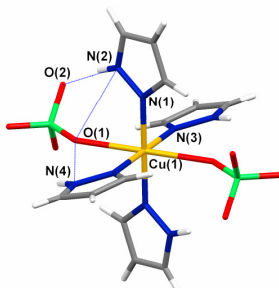


Figure 13. Schematic representation of the intramolecular H-bonds in **CuPerchl**.

The perchlorate oxygens O(3) are involved in weak “intermolecular” H-bonds with N(4)(H4A) of another adjacent molecules (red dotted lines in Figure 14, left), which generate a supramolecular 1D

network. Other weaker, non-conventional H-bonds contribute to assemble these linear polymers in an extended 2D network. A space-filling representation evidences, in the crystal packing, the presence of very small channels running along the crystallographic *b* axis (Figure 14, right).

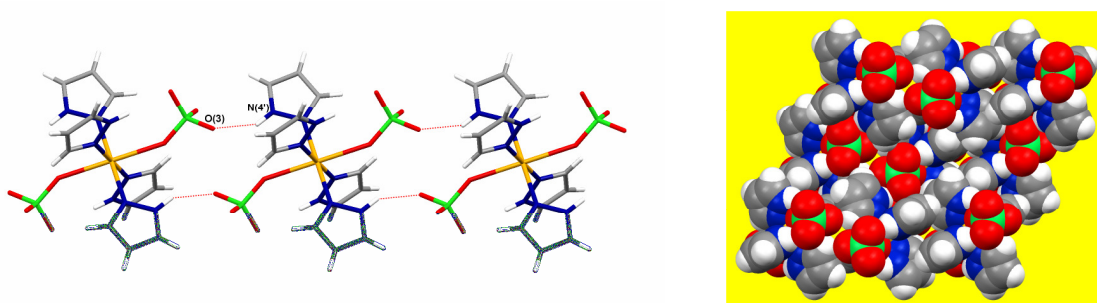


Figure 14. The asymmetric units of **CuPerchl** assemble through intermolecular H-bonds, leading to the formation of a 1D CP (left); space-filling representation of the crystal packing of **CuPerchl** evidencing the presence of very small channels running along the crystallographic *b* axis (right).

The reaction of **2** with HClO₄ generated also a hexanuclear derivative $[\{\text{Cu}_3(\mu_3\text{-OH})(\mu\text{-pz})_3(\text{ClO}_4)(\text{Hpz})_2(\mu_2\text{-ClO}_4)_2\}]_n$, **Cu6Perchl**, whose crystal structure is shown in Figure 15. Compound **Cu6Perchl** is formed by two trinuclear triangular $\{\text{Cu}_3(\mu_3\text{-OH})(\mu\text{-pz})_3(\text{ClO}_4)(\text{Hpz})_3\}$ units which are connected by two bridging perchlorates, with an inversion centre in the middle of the segment joining the hydrogens of the two $\mu_3\text{-OH}$ groups, which are faced each-other (Figure 15).

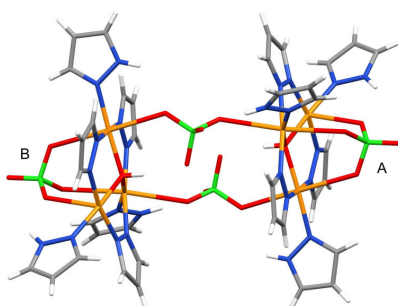


Figure 15. Molecular structure of **Cu6Perchl**.

Each trinuclear unit is capped, on the opposite side of $\mu_3\text{-OH}$, by a perchlorate ion which binds the three copper ions almost symmetrically, and each copper ion coordinates also a neutral pyrazole. The two trinuclear units are parallel (distance about 6.9 Å) and the bridging perchlorates act as bidentate ligands coordinating Cu(1) and Cu(2), thus forming a macrocycle. In **Cu6Perchl** it is possible to detect some “intramolecular” H-bonds, which contribute to reinforce the hexanuclear assembly. In particular, the oxygens of each bridging perchlorate are involved in two relatively strong interactions, between O(6) and $\mu_3\text{-OH}$ and O(9) with the NH of pyrazole coordinated to the Cu(1) of the other trinuclear unit, and in a weaker one between O(7) and the NH of pyrazole coordinated to the Cu(2) of the same trinuclear unit. Also the capping $\mu_3\text{-ClO}_4$ is involved in a H-bond between O(4) and NH of pyrazole coordinated to Cu(3) (Figure 16, right). The hexanuclear units also participate to “intermolecular” weak, non conventional, H-bonds, which generate 2D networks, parallel to the crystallographic *ac* plane (Figure 16, left).

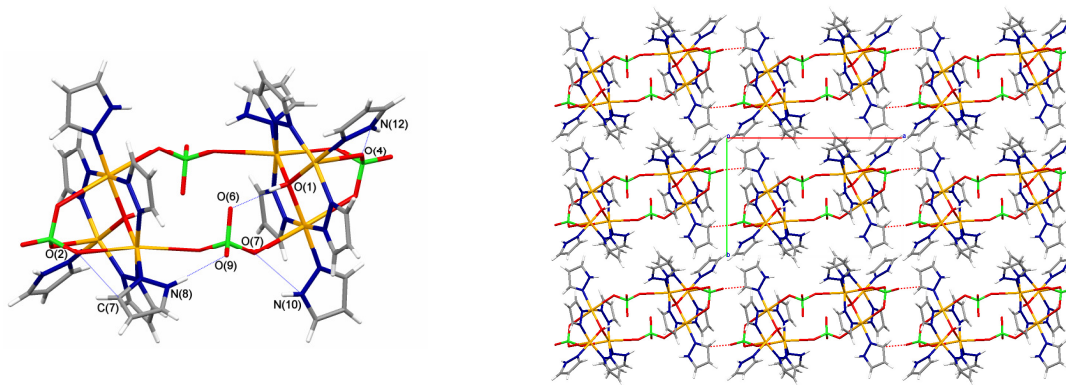


Figure 16. Schematic representation of the intramolecular H-bonds in **Cu6Perchl** (left); “intermolecular” weak, non conventional, H-bonds generating 2D networks, parallel to the crystallographic *ac* plane (right).

The reaction of **2** with HNO₃ yielded three different derivatives which were previously obtained, according to completely different procedures. In particular, it was possible to obtain the 1D CP [Cu₃(μ₃-OH)(μ-pz)₃(NO₃)(μ₃-NO₃)(Hpz)₂], **Cu3Nitr**, where a NO₃⁻ ion bridges two trinuclear SBUs [Hulsbergen et al. (1983)] and a hexanuclear assembly, [(Cu₃(μ₃-OH)(μ-pz)₃(NO₃)(Hpz)₃]₂(μ₂-NO₃)₂], **Cu6Nitr** [Sakai et al. (1996)], whose structure is closely related to that of another hexanuclear derivative, [(Cu₃(μ₃-OH)(μ-pz)₃(Cl)(Hpz)₃]₂(μ₂-Cl)₂·H₂O, previously obtained in the reaction of **2** with aqueous HCl [Casarin et al. (2007) (a)]. Finally, a mononuclear derivative, [Cu(NO₃)₂(Hpz)₄], **CuNitr** [Sakai et al. (1996)], was also obtained. **CuNitr** self-assembles in a 1D supramolecular network through H-bonds involving oxygens and NH pertaining to a different unit, while the crystal packing of **Cu6Nitr** reveals that this clusters assemble analogously to [(Cu₃(μ₃-OH)(μ-pz)₃(Cl)(Hpz)₃]₂(μ₂-Cl)₂·H₂O [Casarin et al. (2007) (a)] forming hexagonal free channels (1.33 x 1.9 Å², taking into account the vdW radii), running along the crystallographic *c* axis (Figure 17).

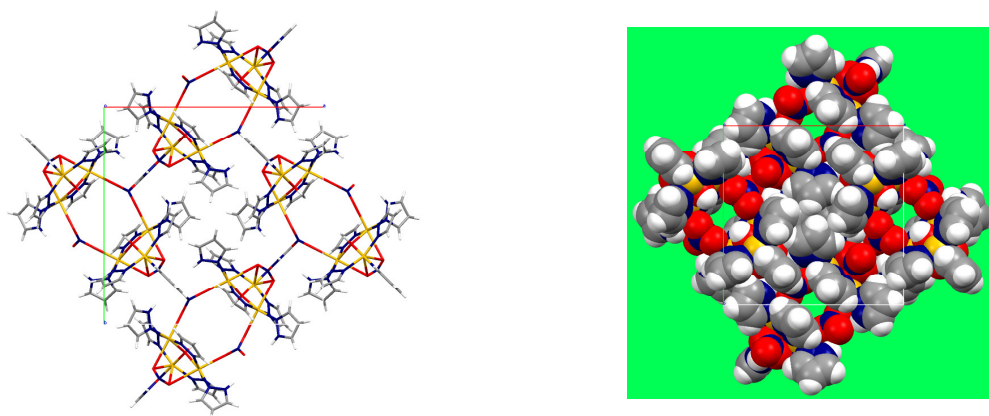


Figure 17. Capped-stick (left) and space-filling (right) representation of **Cu6Nitr** crystal packing evidencing small hexagonal channels running parallel to the *c* axis

The reaction of **2** with CF₃COOH led to the formation of one trinuclear and two mononuclear derivatives. The structure of the trinuclear compound [Cu₃(μ₃-OH)(μ-pz)₃(CF₃COO)₂(Hpz)₂], **Cu3TFac**, is shown in Figure 18.

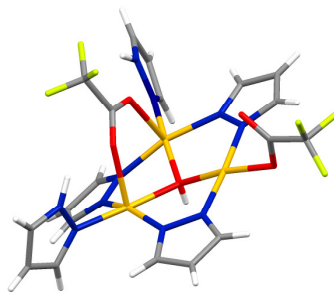


Figure 18. Molecular structure of **Cu₃TFac**.

The μ_3 -OH is placed on the opposite site with respect to one CF_3COO^- ion, which almost symmetrically caps Cu(1) and Cu(2). Each of the latter Cu ions coordinates also a neutral pyrazole, while Cu(3) coordinates the second CF_3COO^- ion in a monodentate fashion. In the trinuclear unit it is possible to distinguish two “intramolecular” H-bonds involving O(2) and O(3) of the capping CF_3COO^- ion and the NH of pyrazoles coordinated to Cu(2) and Cu(1), respectively (see Figure 19).

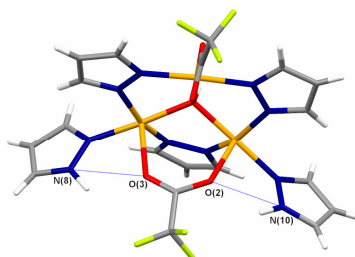


Figure 19. Schematic representation of the intramolecular H-bonds in **Cu₃TFac**.

Moreover, in **Cu₃TFac** also weak, non-conventional, “intermolecular” H-bonds can be detected, which are responsible for the formation of a supramolecular network, partly depicted in Figure 20 (left).

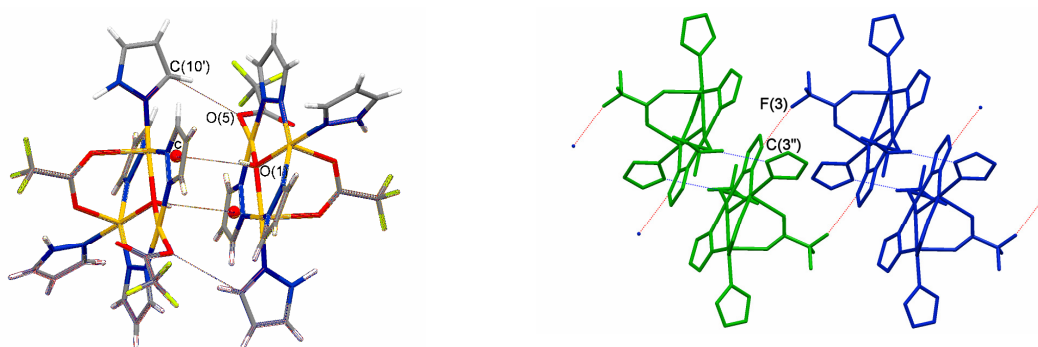


Figure 20. Schematic representation of the intermolecular H-bonds in **Cu₃TFac** (left); partial representation of the supramolecular network of **Cu₃TFac** (right).

In particular, each trinuclear unit weakly interacts symmetrically with another one in two different ways, involving O(5) and C(10)H(10) of another unit, while O(1)H(1) has a π -interaction with the aromatic pyrazolate ring of the other unit. These hexanuclear aggregates generate a 1D supramolecular network, running down the crystallographic *a* axis, thanks to weak H-bonds between F(3) and C(3)H(3) of other units (Figure 20, right). Moreover, the crystal packing evidences the formation of a 2D supramolecular network, developing down the crystallographic *a* axis and perpendicular to the *bc*

plane, which is sustained by weak H-bonds between F(2) and H(8''') of an adjacent unit of a parallel 1D chain and *viceversa*. Thus, in the crystal packing of **Cu₃TFac** it is possible to observe the presence of small, irregular channels having free dimension of about 2.4 x 1.6 Å² (Figure 21).

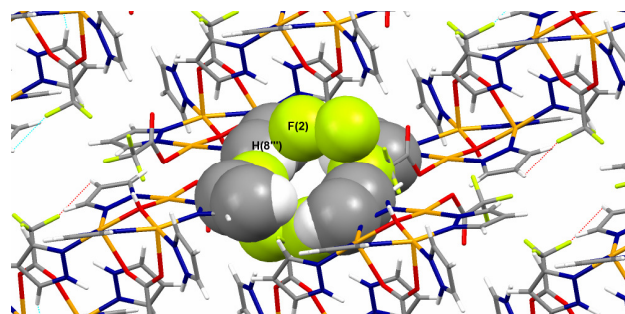


Figure 21. Space-filling representation of **Cu₃TFac** crystal packing, evidencing small channels.

From the mother liquors of compound **Cu₃TFac** it was possible to separate also two different mononuclear complexes. The first one, [Cu(CF₃COO)₂(Hpz)₄], **CuTFac1**, has been previously obtained through a completely different procedure, but it was only partly characterised [Kagane et al. (1992)]. Its crystal structure evidences that the Cu^(II) ion has a quite distorted octahedral coordination, with the four pyrazoles as equatorial ligands, as evidenced in Figure 22.

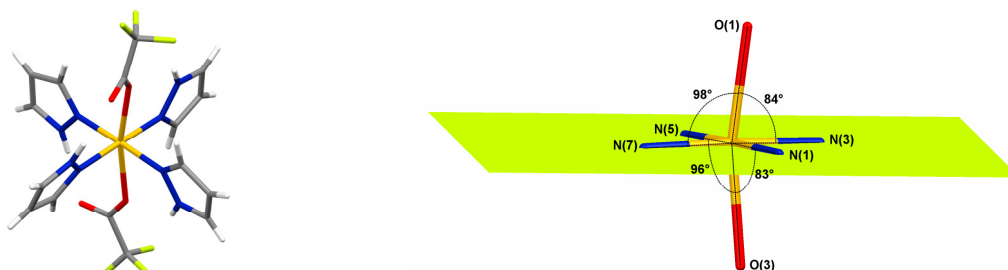


Figure 22. Molecular structure of **CuTFac1**.

Four “intramolecular” H-bonds, involving pyrazoles NH and carboxylates oxygens are present (Figure 23).

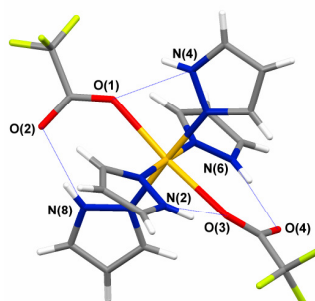


Figure 23. Schematic representation of the intramolecular H-bonds in **CuTFac1**.

Weak, non-conventional, “intermolecular” interactions involve O(4) and H(9)C(9) of a second unit generating dinuclear assemblies, (Figure 24, left), which further pack in parallel rows lying in the crystallographic *bc* plane (Figure 24, right).

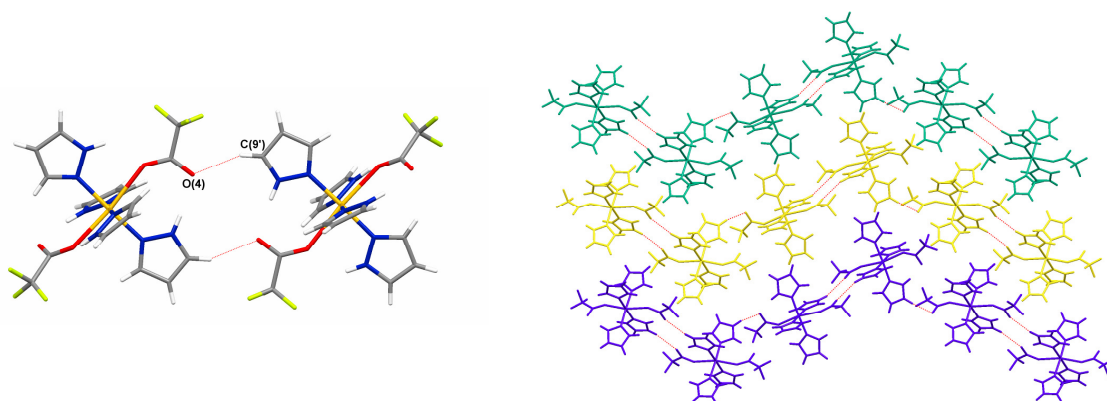


Figure 24. Schematic representation of the intermolecular H-bonds in **CuTFAc1** (left), leading to the formation of rows lying in the same plane (right).

From the reaction of **2** with CF_3COOH another mononuclear derivative $[\text{Cu}(\text{CF}_3\text{COO})_2(\text{Hpz})_2]$, **CuTFAc2**, was obtained. It is noteworthy that this latter compound was the only product obtained in the reaction between $\text{Cu}(\text{CF}_3\text{COO})_2$ and Hpz [Casarin et al. (2004)], which was carried out in different conditions with respect to those used by Kagane [Kagane et al. (1992)]. Its structure and supramolecular assembly, generating a 1D CP, have been previously reported [Casarin et al. (2004)]. From the reaction of **2** with $\text{CF}_3\text{SO}_3\text{H}$ we isolated, in low yields, three different crystalline derivatives. The first one has the trinuclear triangular structure $[\text{Cu}_3(\mu_3\text{-OH})(\mu\text{-pz})_3(\text{CF}_3\text{SO}_3)_2(\text{Hpz})_3]\cdot\text{H}_2\text{O}$, **Cu3TFL**, shown in Figure 25.

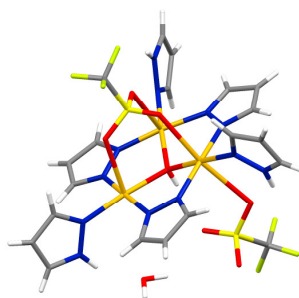


Figure 25. Molecular structure of **Cu3TFL**.

The $\mu_3\text{-OH}$ is on the opposite site with respect to one CF_3SO_3^- ion which caps, almost symmetrically, all the three $\text{Cu}^{\text{(II)}}$ ions. Each copper coordinates also a neutral pyrazole, while Cu(2) coordinate in a monodentate fashion the second triflate ion. A crystallisation water molecule is also present, and is involved in two “intramolecular” H-bonds, acting both as H-acceptor with NH of pyrazole coordinated to Cu(1), and as H-donor in the interaction with triflate O(5). Other two “intramolecular” H-bonds can be detected, the first one involving again O(5) and $\mu_3\text{-OH}$, while in the other one are interested the triflate O(6) and the NH of the pyrazole coordinated to Cu(2). Moreover, a weaker “intramolecular” interaction involves the triflate O(4) and the NH of the pyrazole coordinated to Cu(3).

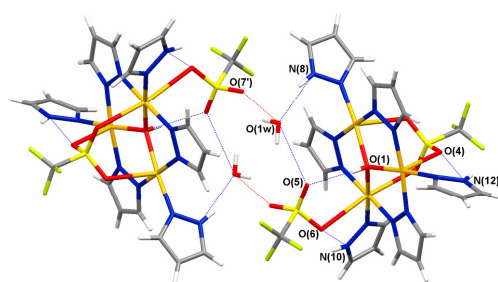


Figure 26. Supramolecular hexanuclear arrangement of **Cu₃TFL**.

The crystallisation water is involved also in an important “intermolecular” interaction with the triflate oxygen O(7) of another trinuclear unit, generating the supramolecular hexanuclear arrangement depicted in Figure 26.

From the reaction of **2** with triflic acid it was possible to obtain also a little crop of crystals having the very particular formulation $[\{\text{Cu}_3(\mu_3\text{-OH})(\mu\text{-pz})_3(\text{Hpz})_3\}\{\text{Cu}_3(\mu_3\text{-O})(\mu\text{-pz})_3(\text{Hpz})_3\}](\text{CF}_3\text{SO}_3)_3$, **Cu₆TFL**.

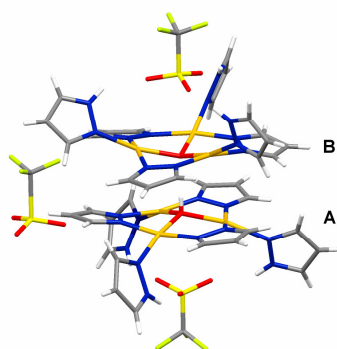


Figure 27. Molecular structure of **Cu₆TFL**.

As shown in Figure 27, compound **Cu₆TFL** consists of three not coordinated triflate anions and a trication which is made by two trinuclear triangular Cu^(II) clusters (A and B) faced each other with a distance between the respective Cu₃ planes of *ca.* 3.325 Å. In both the trinuclear units the nine-membered ring is not planar, being the pyrazolate bent toward the μ₃-OH (or μ₃-O) ion, while the neutral pyrazole coordinated to the copper ions are oriented in the opposite side. The two trinuclear units have very similar geometrical parameters and, most important, one triangular moiety (A) is capped by a μ₃-OH, while in the other one (B) a μ₃-O is present. In this context, the two triangular units are connected through the very particular, strong μ₃-O_A-H⋯O_B-μ₃ H-bond.

Both the oxygen of μ₃-OH and μ₃-O are out from the plane defined by the three respective Cu^(II) ions (*ca.* 0.43 Å for A and *ca.* 0.49 Å for B). Incidentally, these values are indicative of the fact that both oxygens share the H atom and that a “true” μ₃-O oxide is not present, being normally, in this case, the oxygen co-planar with its Cu^(II) ions [Angaridis et al. (2002); Boča et al. (2003)]. At the best of our knowledge, this particular feature has been previously reported only two times [Watson et al. (1984); Ferrer et al. (2007)] with almost identical O_A⋯O_B distances.

The three triflate ions, providing the electroneutrality to the whole system, are not coordinated at all, and are instead involved into a series of relevant non-covalent interactions. In particular, two triflate ions are placed up and down the tricationic fragment, being their C–S axes aligned and in the same line with the μ₃-O_A-H⋯O_B-μ₃ bridge. The third triflate is placed on one side of the cation and the C–S

axis is parallel to the other two triflates. As shown in Figure 28, the three triflate ions are involved in a series of “intramolecular” H-bonds. In particular, the three equivalent oxygens of the triflate near the trinuclear moiety B, O(4), are involved in three identical H-bonds with the NH of corresponding coordinated pyrazole, and a completely analogous feature is observed with the triflate near the trinuclear moiety A [O(10)].

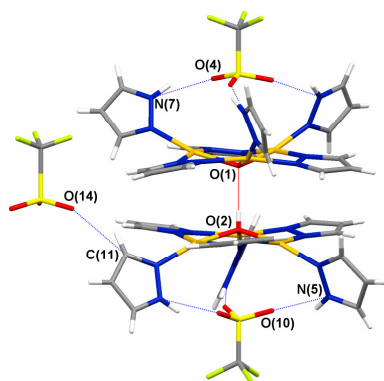


Figure 28. Schematic representation of the intramolecular H-bonds in **Cu₃TFL**.

The third, “equatorial”, triflate instead forms a weak, non-conventional, H-bond, involving a single oxygen [O(14)] and the C(11)H(11) of the A unit. Even though not very strong, these latter supramolecular interactions certainly contribute to generate a particular assembly in the plane *ab*. In fact, the “equatorial” triflate acts as a sort of μ_3 -bridge, connecting three cations of the *ab* layer, thus generating “true” empty pores, one of which is evidenced by a space filling representation in Figure 29 (left), alternated to other ones occupied by “equatorial” triflates. Since the different layers pack in a staggered way (60° rotation), the pores result not accessible, as evidenced in Figure 29 (right), where two layers are represented.

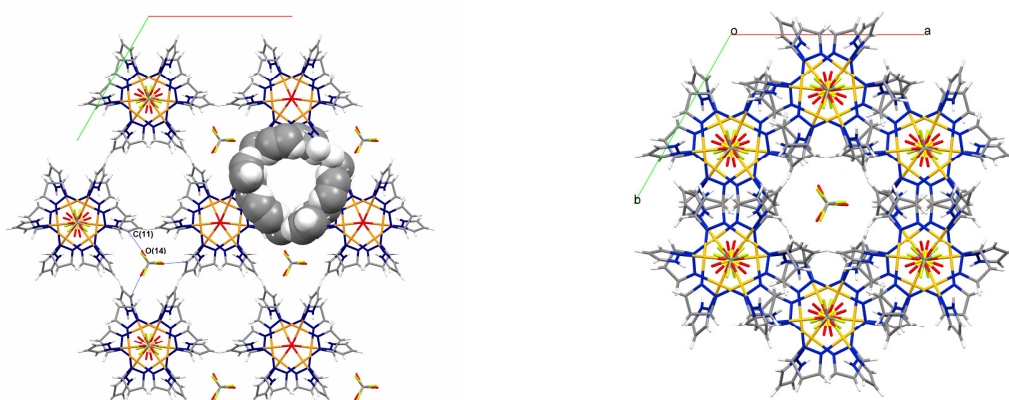


Figure 29. Space filling representation of one layer, evidencing the presence of “true” empty pores (left); since the different layers pack in a staggered way, (60° rotation) the pores result not accessible (right), where two layers are represented.

From the mother liquors of **Cu₆TFL** it was possible to crystallise the mononuclear complex [Cu(CF₃SO₃H)₂(Hpz)₄], **CuTFL**, whose molecular structure is shown in Figure 30.

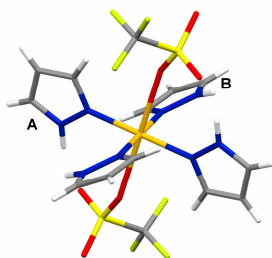


Figure 30. Molecular structure of **CuTFL**.

Cu is in the centre of a distorted octahedron where triflate ions occupy the axial positions. Pyrazoles are involved into two “intramolecular” H-bonds with triflate O(3) (Figure 31, left), and “intermolecular” H-bonds between triflate ions and NH of adjacent moieties generate the supramolecular 1D network running down the crystallographic *b* axis, sketched in Figure 31 (right).

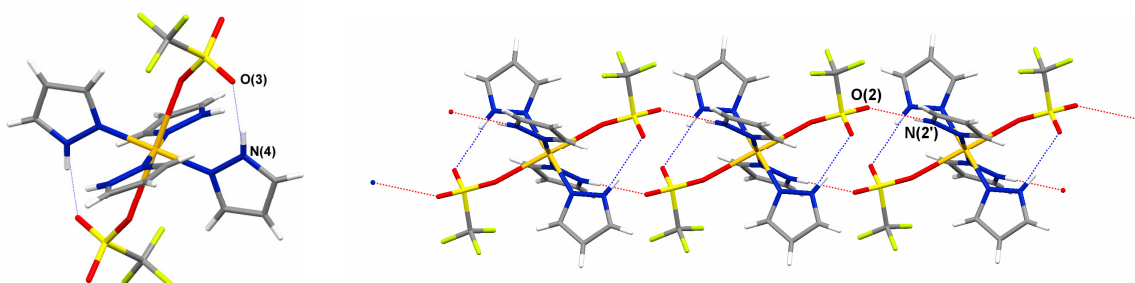


Figure 31. Schematic representation of the intramolecular (left) and of the intermolecular H-bonds (right), the latter generating a 1D network.

Reactions of trinuclear triangular Cu^(II) clusters with dinucleating nitrogen ligands

Even though upon reaction with strong acids in all the cases mononuclear complexes were isolated (indicating that, in some extent, the starting trinuclear cluster was destroyed), the concurrently formed tri-, hexa- and heptanuclear derivatives (sometimes assembled in CPs, PCPs or extended supramolecular networks) [Casarin et al. (2007) (a); Di Nicola et al. (2007) (b); Di Nicola et al. (2008)], evidenced that the trinuclear triangular $[\text{Cu}_3(\mu_3\text{-OH})(\mu\text{-pz})_3]^{2+}$ core is stable enough to be worthy of consideration as possible starting material to obtain different CPs. For this reason, we planned to synthesise novel materials having the trinuclear Cu^(II) clusters directly bridged by polynucleating ligands, and to do this two different approaches were available: i) substitution of the monocarboxylates with bicarboxylates; ii) substitution of the neutral ligands (pyrazole and/or solvent molecules) coordinated to the Cu^(II) centres with neutral bidentate ligands.

First attempts under bench-top conditions to replace the carboxylate ions by reacting the trinuclear compounds with dicarboxylic acids were not successful, leading to the isolation of the starting materials, while reactions carried out upon deprotonation of the acids led to the instantaneous precipitation of insoluble powders. For these reasons, the attention has been focused on the reactivity of compounds **1-10** with neutral polynucleating ligands, aiming to the displacement of neutral pyrazole and/or solvent molecules coordinated to the metal ions.

The reaction scheme we adopted to synthesise new coordination polymers exploits, besides the above mentioned stability of the trinuclear triangular $[\text{Cu}_3(\mu_3\text{-OH})(\mu\text{-pz})_3]^{2+}$ core, also the expected reactivity of the derivatives **1-10** towards the displacement of neutral molecules (pyrazole and/or solvent molecules) with different bridging ligands. In particular, we focused our attention on a family of ligands having two 4-pyridyl rings as donor units, connected by different spacers.



In details, compounds **1-10** have been employed in reaction with 4,4'-bipyridine (bpy), 1,2-bis(4-pyridyl)diazene (azopy), 1,2-bis(4-pyridyl)ethane (bpetha), 1,2-bis(4-pyridyl)ethylene (bpethy), 1,3-bis(4-pyridyl)propane (tmb), 1,2-bis(4-pyridyl)disulfane (bpsulf) and 1,5-naphthyridine (napht), whose structures are sketched in Chart 7.

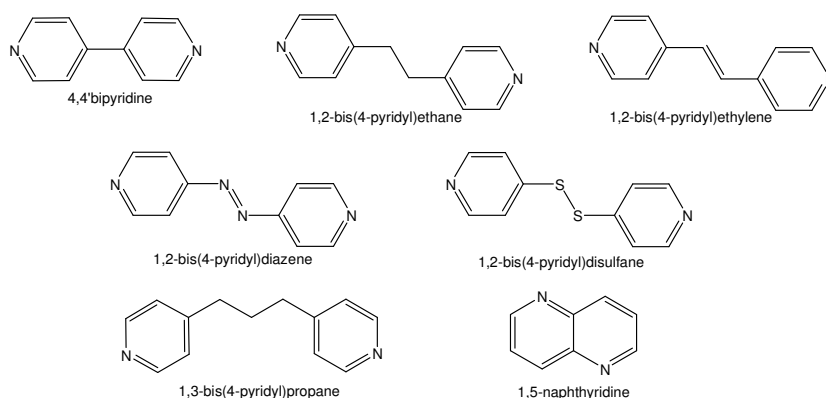


Chart 7.

Reactions with 4,4'-bipyridine

Reactions between compounds **1-10** and bpy led to the isolation of new trinuclear triangular Cu^(II) CPs, with different dimensionality. Most of them have been characterised by XRD analysis, confirming the presence of the trinuclear core, with the exception of compounds **Cu3AcryBpy** and **Cu3MethBpy**, whose formulae, reported in Table 2, have been proposed on the basis of the elemental analysis results.

Table 2. Formulae proposed on the basis of the elemental analysis results.

Compound	Formula
Cu3FormBpyL	$[[\text{Cu}_3(\mu_3\text{-OH})(\mu\text{-pz})_3(\text{HCOO})_2(\text{H}_2\text{O})][\text{Cu}_3(\mu_3\text{-OH})(\mu\text{-pz})_3(\text{HCOO})_2(\text{H}_2\text{O})(\text{MeOH})]]_2(\text{C}_{10}\text{H}_8\text{N}_2)$
Cu3FormBpyP	$[\text{Cu}_3(\mu_3\text{-OH})(\mu\text{-pz})_3(\text{HCOO})(\text{OH})(\text{C}_{10}\text{H}_8\text{N}_2)_3]_2(\text{H}_2\text{O})_x(\text{C}_{10}\text{H}_8\text{N}_2)_y$
Cu3AcBpy	$[\text{Cu}_3(\mu_3\text{-OH})(\mu\text{-pz})_3(\text{CH}_3\text{COO})(\text{OH})(\text{C}_{10}\text{H}_8\text{N}_2)_3]_2(\text{H}_2\text{O})_x(\text{C}_{10}\text{H}_8\text{N}_2)_y$
Cu3ProBpy	$[\text{Cu}_3(\mu_3\text{-OH})(\mu\text{-pz})_3(\text{C}_2\text{H}_5\text{COO})_2(\text{C}_{10}\text{H}_8\text{N}_2)(\text{H}_2\text{O})]$
Cu3*ButBpy	$[\text{Cu}_3(\mu_3\text{-OCH}_3)(\mu\text{-pz})_3(\text{C}_3\text{H}_7\text{COO})_2(\text{C}_{10}\text{H}_8\text{N}_2)]$
Cu3ValBpy	$[\text{Cu}_3(\mu_3\text{-OH})(\mu\text{-pz})_3(\text{C}_4\text{H}_9\text{COO})_2(\text{C}_{10}\text{H}_8\text{N}_2)(\text{MeOH})]$
Cu3HeptaBpy	$[\text{Cu}_3(\mu_3\text{-OH})(\mu\text{-pz})_3(\text{C}_6\text{H}_{13}\text{COO})_2(\text{C}_{10}\text{H}_8\text{N}_2)_{0.5}]$
Cu3AcryBpy	$[\text{Cu}_3(\mu_3\text{-OH})(\mu\text{-pz})_3(\text{CH}_2=\text{CHCOO})_2(\text{C}_{10}\text{H}_8\text{N}_2)(\text{H}_2\text{O})]$
Cu3MethBpy	$[\text{Cu}_3(\mu_3\text{-OH})(\mu\text{-pz})_3(\text{CH}_2=\text{C}(\text{CH}_3)\text{COO})_2(\text{C}_{10}\text{H}_8\text{N}_2)]$

Moreover, in all the cases, the ESI-MS characterisations are in agreement with the trinuclear structures. The most relevant signals are summarised in Table 3.

Table 3. Most relevant signals in the ESI-MS spectra of compounds **Cu3FormBpyL** – **Cu3MethBpy**.

Compound ^a	Signal ^b	R. A. ^c	Assignments
Cu3FormBpyL	258.0	100	$[\text{Cu}(\text{Hpz})(\text{HCOO})(\text{MeOH})_2(\text{H}_2\text{O})]^+$
	475.9	60	$[\text{Cu}_3(\text{OH})_2(\text{pz})_3(\text{MeOH})(\text{H}_2\text{O})]^+$
	549.8	50	$[\text{Cu}_3(\text{OH})(\text{pz})_2(\text{HCOO})_2(\text{MeOH})_2(\text{H}_2\text{O})_3]^+$
Cu3FormBpyP	624.3	80	$[\text{Cu}_3(\text{OCH}_3)(\text{pz})_3(\text{HCOO})(\text{bpy})]^+$
	785.3	100	$[\text{Cu}_3(\text{OH})(\text{pz})_2(\text{HCOO})_2(\text{bpy})_2(\text{MeCN})]^+$
	1303.4	60	$[\text{Cu}_6(\text{OH})_5(\text{pz})_6(\text{HCOO})(\text{bpy})_2(\text{H}_2\text{O})_3+\text{Na}]^+$
Cu3ProBpy	657.3	100	$[\text{Cu}_3(\text{OH})(\text{pz})_2(\text{C}_2\text{H}_5\text{COO})_2(\text{MeOH})_4(\text{MeCN})]^+$
	1029.3	80	$[\text{Cu}_6(\text{OH})_3(\text{pz})_7(\text{CH}_3\text{CH}_2\text{COO})(\text{H}_2\text{O})_3]^+$
	1065.3	77	$[\text{Cu}_6(\text{OH})_3(\text{pz})_7(\text{CH}_3\text{CH}_2\text{COO})(\text{H}_2\text{O})_5]^+$
Cu3*ButBpy	666.3	78	$[\text{Cu}_3(\text{OCH}_3)(\text{pz})_3(\text{CH}_3\text{CH}_2\text{CH}_2\text{COO})(\text{bpy})]^+$
	686.4	100	$[\text{Cu}_3(\text{OCH}_3)(\text{pz})_3(\text{CH}_3\text{CH}_2\text{CH}_2\text{COO})(\text{MeOH})(\text{H}_2\text{O})_8]^+$
	1071.4	90	$[\text{Cu}_6(\text{OH})_3(\text{pz})_7(\text{CH}_3\text{CH}_2\text{CH}_2\text{COO})(\text{MeOH})_2(\text{H}_2\text{O})]^+$
Cu3ValBpy	680.3	50	$[\text{Cu}_3(\text{OH})(\text{pz})_3(\text{C}_4\text{H}_9\text{COO})_2(\text{MeOH})(\text{H}_2\text{O})_2+\text{H}]^+$
	685.3	100	$[\text{Cu}_3(\text{OH})(\text{pz})_3(\text{C}_4\text{H}_9\text{COO})_2(\text{MeOH})(\text{MeCN})+\text{H}]^+$
	714.5	70	$[\text{Cu}_3(\text{OH})(\text{pz})_3(\text{C}_4\text{H}_9\text{COO})(\text{MeOH})_3(\text{H}_2\text{O})_6]^+$
	1113.6	60	$[\text{Cu}_6(\text{OH})_4(\text{pz})_6(\text{C}_4\text{H}_9\text{COO})(\text{MeOH})_5]^+$
	1149.6	65	$[\text{Cu}_6(\text{OH})_4(\text{pz})_6(\text{C}_4\text{H}_9\text{COO})(\text{MeOH})_5(\text{H}_2\text{O})_2]^+$
Cu3HeptaBpy	713.3	100	$[\text{Cu}_3(\text{OH})(\text{pz})_4(\text{Hpz})(\text{MeOH})_4(\text{MeCN})]^+$
	1197.7	85	$[\text{Cu}_6(\text{OH})_3(\text{pz})_6(\text{C}_6\text{H}_{13}\text{COO})_2(\text{MeOH})(\text{H}_2\text{O})_4]^+$
	1233.8	55	$[\text{Cu}_6(\text{OH})_3(\text{pz})_6(\text{C}_6\text{H}_{13}\text{COO})_2(\text{MeOH})(\text{H}_2\text{O})_8]^+$
Cu3AcryBpy	650.3	75	$[\text{Cu}_3(\text{OCH}_3)(\text{pz})_3(\text{CH}_2=\text{CHCOO})(\text{bpy})]^+$
	654.3	70	$[\text{Cu}_3(\text{OH})(\text{pz})_3(\text{CH}_2=\text{CHCOO})(\text{bpy})(\text{H}_2\text{O})]^+$
	655.3	100	$[\text{Cu}_3(\text{OH})(\text{pz})_3(\text{CH}_2=\text{CHCOO})_2(\text{MeOH})(\text{H}_2\text{O})_4+\text{H}]^+$
	1023.3	70	$[\text{Cu}_6(\text{OH})_4(\text{pz})_5(\text{CH}_2=\text{CHCOO})_2(\text{MeOH})_3]^+$
	1059.3	72	$[\text{Cu}_6(\text{OH})_3(\text{pz})_6(\text{CH}_2=\text{CHCOO})_2(\text{MeOH})_2(\text{H}_2\text{O})]^+$
Cu3MethBpy	664.3	75	$[\text{Cu}_3(\text{OCH}_3)(\text{pz})_3(\text{CH}_2=\text{C}(\text{CH}_3)\text{COO})(\text{bpy})]^+$
	669.2	90	$[\text{Cu}_3(\text{OH})(\text{pz})_3(\text{CH}_2=\text{C}(\text{CH}_3)\text{COO})_2(\text{H}_2\text{O})_5+\text{H}]^+$
	682.4	100	$[\text{Cu}_3(\text{OH})(\text{pz})_3(\text{CH}_2=\text{C}(\text{CH}_3)\text{COO})(\text{bpy})(\text{MeOH})]^+$
	1063.3	90	$[\text{Cu}_6(\text{OH})_3(\text{pz})_7(\text{CH}_2=\text{C}(\text{CH}_3)\text{COO})(\text{MeCN})(\text{H}_2\text{O})_2]^+$
	1101.4	75	$[\text{Cu}_6(\text{OH})_3(\text{pz})_7(\text{CH}_2=\text{C}(\text{CH}_3)\text{COO})(\text{MeCN})(\text{H}_2\text{O})_4]^+$

^a Cu₃: [Cu₃(OH)(pz)₃]²⁺; Cu₃*: [Cu₃(OCH₃)(pz)₃]²⁺

^b Values corresponding to the higher signals of the isotopic clusters. All isotopic clusters fit satisfactorily with calculated ones [Senko (1994)].

^c Relative Abundance of the higher signal of the isotopic cluster.

The most intense signals of the ESI-MS spectra correspond to trinuclear clusters. Only in the case of **Cu3FormBpyL**, the most intense signal corresponds to a mononuclear species, thus indicating that this CP is not particularly stable in ESI conditions. Other trinuclear and hexanuclear based signals are also present. Even though the ESI-MS data cannot be considered an exhaustive proof of the presence of trinuclear clusters in the solid state, nevertheless they offer a great suggestion for this feature. On the other hand, the preservation of trinuclear triangular structures is witnessed by XRD determinations, as will be shown in the following.

By reacting **1** with bpy in methanol, it was possible to isolate different CPs simply by changing the molar ratio between the reagents. In fact, using a 1:1 **1**/bpy molar ratio we obtained deep-blue crystals of compound $[[[Cu_3(\mu_3-OH)(\mu-pz)_3(HCOO)_2(H_2O)]-[Cu_3(\mu_3-OH)(\mu-pz)_3(HCOO)_2(H_2O)(MeOH)]]_2(C_{10}H_8N_2)]$, **Cu3FormBpyL_a**, while in a second preparation deep-blue crystals of compound $[[[Cu_3(\mu_3-OH)(\mu-pz)_3(HCOO)_2(H_2O)]-[Cu_3(\mu_3-OH)(\mu-pz)_3(HCOO)_2(H_2O)_2]]_2(C_{10}H_8N_2)]$, **Cu3FormBpyL_b**, were isolated. In both compounds, two hexanuclear moieties (in some extent reminiscent of the supramolecular structure of **1** [Casarin et al. (2005)]) are joined by a bpy molecule. The two products differ only for the presence of a coordinated MeOH molecule in **Cu3FormBpyL_a**, instead of a water molecule, difference which can be associated to fortuitously different crystallisation conditions. The two asymmetric units of compounds **Cu3FormBpyL_a** and **Cu3FormBpyL_b** are sketched in Figure 32.



Figure 32. Asymmetric unit of **Cu3FormBpyL_a** (left) and of **Cu3FormBpyL_b** (right). Hydrogens have been omitted for clarity.

The supramolecular assembly of the two compounds is the same, as it is possible to see by inspection of Figure 33, and generates almost identical CPs.

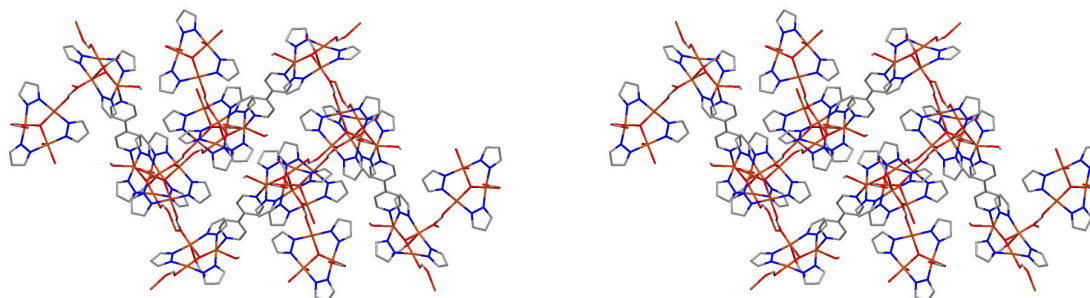


Figure 33. Crystal packing views of **Cu3FormBpyL_a** (left) and **Cu3FormBpyL_b** (right). Hydrogens have been omitted for clarity.

In both cases, the supramolecular assembly is originated by two different kinds of connections (Figure 34): connection 1→3 (*i.e.* an asymmetric unit is connected in its position 1 with the position 3 of another unit, and so on) leads to the formation of linear tapes, which are then covalently linked through connection 2→4. No interpenetration is observed between the tapes.

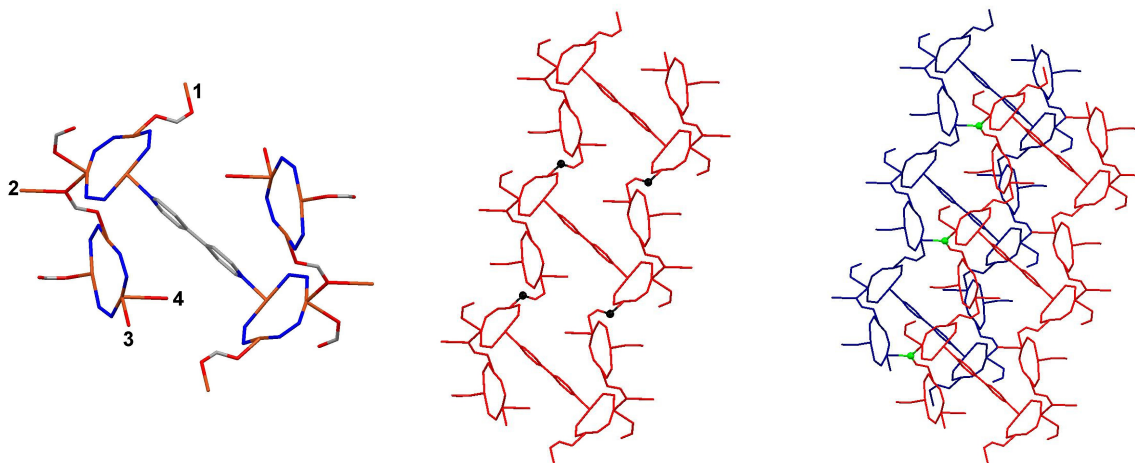


Figure 34. Schematic representation of the asymmetric unit of **Cu3FormBpyLa**; the numbers indicate the connection sites between the asymmetric unit and the others (left). Connection 1→3 (center, black dots) and connection 2→4 (right, green dots). Some atoms^{*} have been omitted for clarity.

A complete different behaviour was observed when compound **1** was reacted with a large excess of bpy, yielding quantitatively $[\text{Cu}_3(\mu_3\text{-OH})(\mu\text{-pz})_3(\text{HCOO})(\text{OH})(\text{C}_{10}\text{H}_8\text{N}_2)_3]_2(\text{H}_2\text{O})_2$, **Cu3FormBpyP**, whose asymmetric unit is reported in Figure 35.

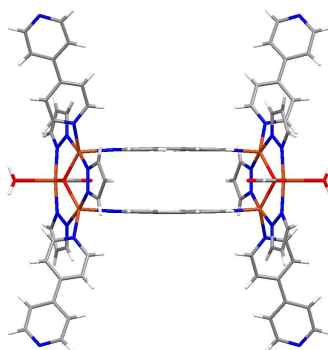


Figure 35. Asymmetric unit of **Cu3FormBpyP**.

Two trinuclear clusters are connected by two parallel bridging bipyridine ligands. Not only the neutral pyrazoles have been displaced; also a formate ion was replaced by an OH group.

The crystal packing evidences the formation of a porous solid, where two different kinds of channels, parallel to the *b* and *c* crystallographic axis respectively, are present (Figure 36).

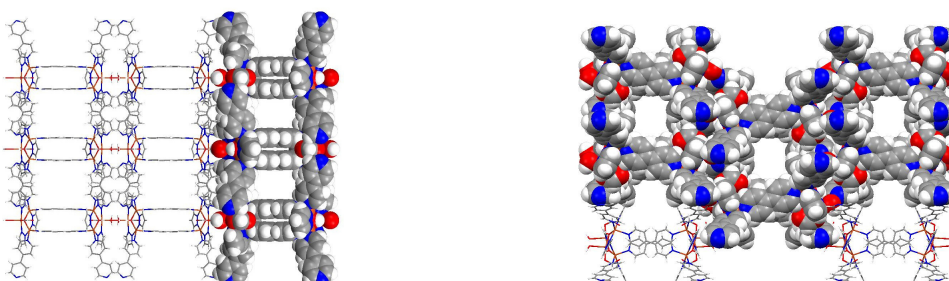


Figure 36. Crystal packing views of **Cu3FormBpyP** perpendicular to the *b* (left; pore dimensions: 4.83 x 5.86 Å²) and perpendicular to the *c* axis (right; pore dimensions: 4.99 x 4.79 Å²)

*In Figures 34, 39, 42, 45, 47, 49, 51, 52, 54 and 55, solvent molecules, hydrogen atoms, pyrazolate carbon atoms and $\mu_3\text{-OH}$ groups are omitted for clarity.

It is important to underline that these channels are not empty; in fact, they are partially filled with water molecules and free bpy, as confirmed also by the elemental analysis. A first attempt to remove the guest molecules, in order to obtain empty channels, was performed by drying a sample under vacuum at ca. 70 °C. The XRPD spectrum of the dried species evidences that crystallinity is maintained, but its pattern is different from that of compound **Cu3FormBpyP**.

It is noteworthy that an analogous compound, $[\text{Cu}_3(\mu_3\text{-OH})(\mu\text{-pz})_3(\text{CH}_3\text{COO})(\text{OH})(\text{C}_{10}\text{H}_8\text{N}_2)_3]_2(\text{H}_2\text{O})_2$, **Cu3AcBpy**, was obtained by prof. Pettinari research group in Camerino [Pettinari, C. personal communication], by reacting the acetate derivative, **2**, with an excess of bpy. Also in this case, a carboxylate was replaced by an OH group, and the obtained structure and crystal packing are very similar to the structure of **Cu3FormBpyP**, as evidenced in Figure 37.

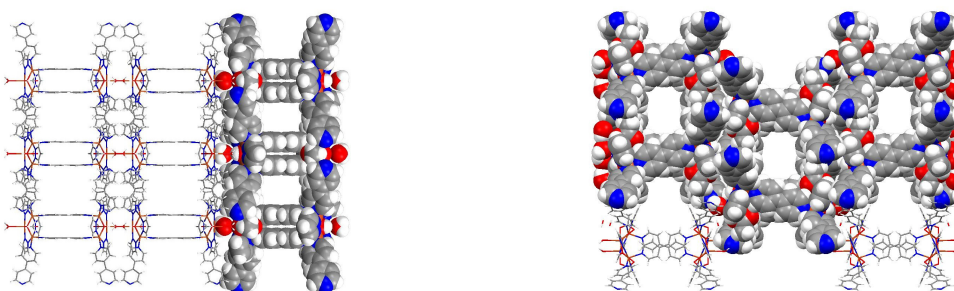


Figure 37. Crystal packing views of **Cu3AcBpy** perpendicular to the *b* axis (left; pore dimensions 4.73 x 5.94 Å²) and to the *c* axis (right; pore dimensions 5.21 x 5.85 Å²).

The reaction of the propionate derivative, **3**, with bpy led to the formation of a new 2D CP, $[\text{Cu}_3(\mu_3\text{-OH})(\mu\text{-pz})_3(\text{CH}_3\text{CH}_2\text{COO})_2(\text{C}_{10}\text{H}_8\text{N}_2)]$, **Cu3ProBpy**. This compound is characterised by the presence of carboxylate bridged hexanuclear clusters, connected by bpy, as evidenced in Figure 38.

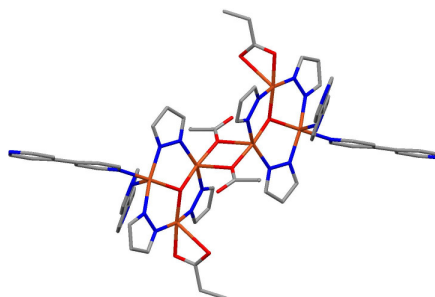


Figure 38. Hexanuclear clusters in **Cu3ProBpy**. Hydrogens have been omitted for clarity.

Two bpy are bonded to the same Cu^(II) ion, leading to the formation of sheets, *i.e.* a 2D CP. There is no covalent connection between the sheets; they are just pillared, as shown in Figure 39.

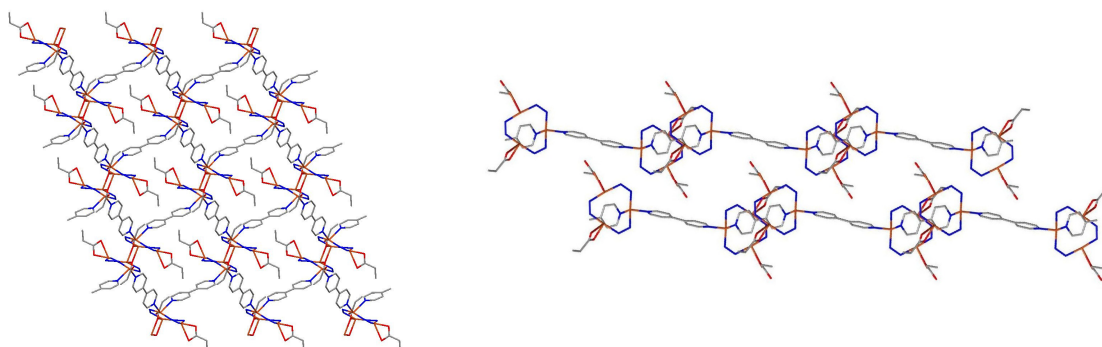


Figure 39. Schematic representation of the 2D nets (left) and of the crystal packing (right).

As highlighted in Figure 40, the supramolecular assembly of this compound is, to some extent, reminiscent of the supramolecular assembly of the starting material [Casarin et al. (2005)].

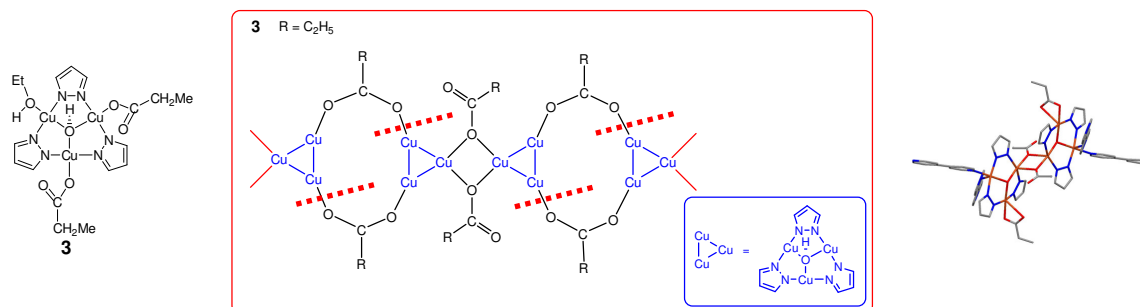


Figure 40. SBU of **3**, (left); schematic representation of the supramolecular assembly of **3** (centre) and of **Cu₃ProBpy** (right).

In fact, the hexanuclear clusters present in **3** are preserved, while bpy replaces the EtOH molecules, after breaking the rings formed by the bridging carboxylates, as shown by the red dotted lines in Figure 40.

The reaction of the butyrate derivative, **4**, with bpy, led to the formation of a new CP, [Cu₃(μ₃-OCH₃)(μ-pz)₃(CH₃(CH₂)₂COO)₂(C₁₀H₈N₂)], **Cu₃*ButBpy**, whose asymmetric unit is sketched in Figure 41.

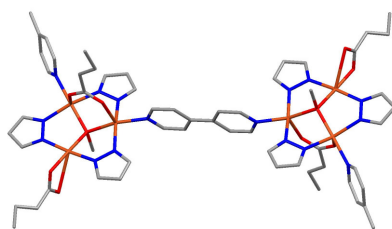


Figure 41. Asymmetric unit of **Cu₃*ButBpy**. Hydrogens have been omitted for clarity.

In this case, the stoichiometry between the trinuclear clusters and bpy is 1:1, leading to the formation of a 1D CP; parallel chains do not interact each other neither with covalent bonds, nor with supramolecular interactions, as represented in Figure 42.

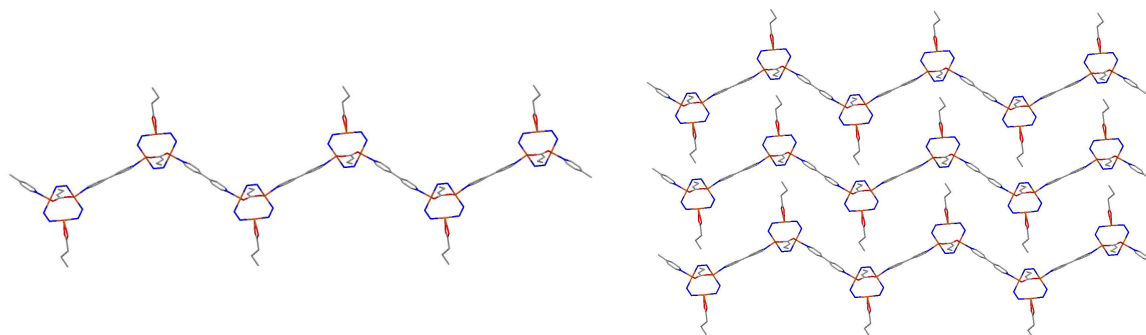


Figure 42. Schematic representation of the (left) and of the crystal packing (right).

It has to be underlined that even though carboxylate bridged hexanuclear clusters are present in compound **4**, we do not observe them, and the trinuclear units of **Cu₃*ButBpy** are connected only by bridging bpy, which evidently broke the carboxylate bridges. Moreover, the μ₃-OH group, which in all the previous reactions was stable towards substitution, in this case has been replaced by a methoxy

group. The substitution of the capping group is maybe due to the fact that bpy, besides acting as a ligand, can also behave as a base, favouring the deprotonation of the solvent, MeOH, and the substitution of μ_3 -OH with μ_3 -OCH₃.

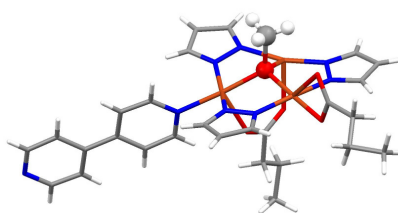


Figure 43. The μ_3 -OH group is substituted by a methoxy group.

The reaction of the valerate derivative, **5**, with bpy led to the formation of a new CP, [Cu₃(μ_3 -OH)(μ -pz)₃(CH₃(CH₂)₃COO)₂(C₁₀H₈N₂)(MeOH)], **Cu3ValBpy**, whose asymmetric unit is reported in Figure 44.

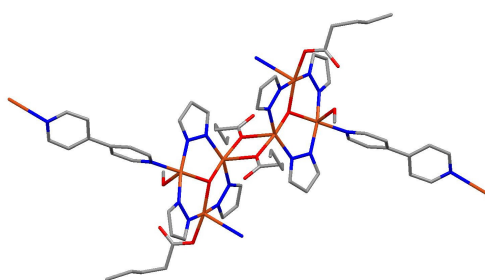


Figure 44. Asymmetric unit of **Cu3ValBpy**. Hydrogens have been omitted for clarity.

As in the case of **Cu3ProBpy**, hexanuclear clusters connected by bridging bpy are present, but in compound **Cu3ValBpy** we do not observe more than one bpy ligand bonded to the same copper ion. This leads to the formation of linear tapes (*i.e.* a 1D CP), instead of 2D nets. Parallel tapes stack one over the other, without any covalent connection, as schematically represented in Figure 45. It is noteworthy that the obtaining of **Cu3ValBpy** made it possible to evidence the very likely presence of hexanuclear clusters in compound **5**, for which we were unable to obtain a XRD structural determination. In fact, we inferred the presence of the trinuclear skeleton in **5** only on the bases of other physico-chemical determinations [Di Nicola et al. (2009)].

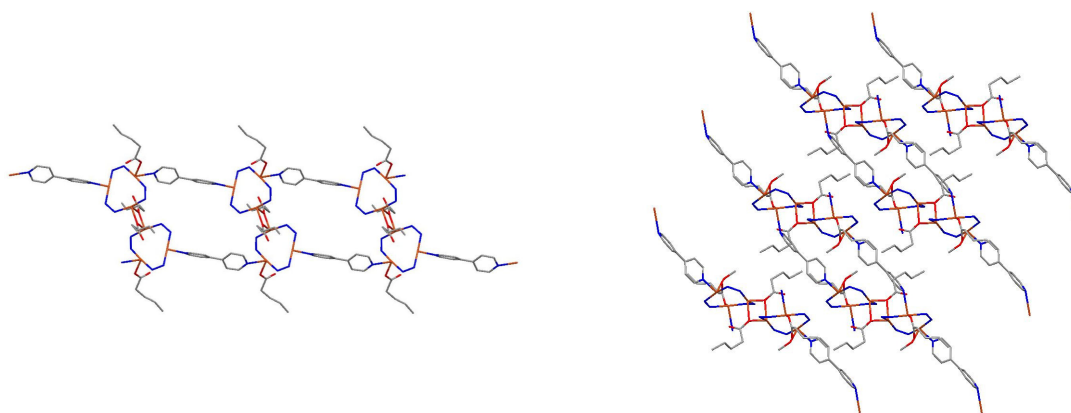


Figure 45. Schematic representation of the linear tapes formed by **Cu3ValBpy** (left) and of the crystal packing (right); views perpendicular to the *c* axis.

An analogous result was obtained in the reaction of the heptanoate derivative, **7**, with bpy, which led to the formation of a new CP, based on $[\{\text{Cu}_3(\mu_3\text{-OH})(\mu\text{-pz})_3(\text{CH}_3(\text{CH}_2)_5\text{COO})\}_2(\text{C}_{10}\text{H}_8\text{N}_2)]$, **Cu3HeptaBpy**, whose asymmetric unit is sketched in Figure 46.

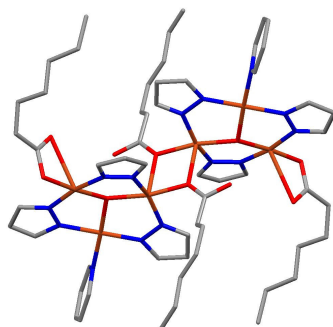


Figure 46. Asymmetric unit of **Cu3HeptaBpy**. Hydrogens have been omitted for clarity.

Bridging bpy ligands connect the hexanuclear clusters, generating linear tapes, *i.e.* a 1D CP. There is no covalent connection between parallel tapes, as represented in Figure 47.

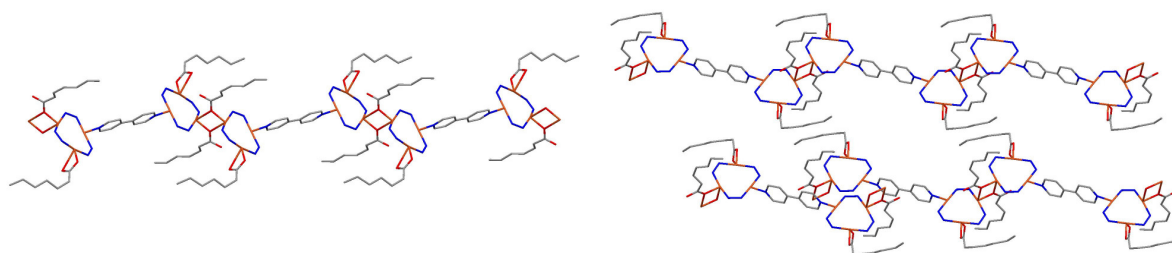


Figure 47. Schematic representation of the linear tapes formed by **Cu3HeptaBpy** (left) and of the crystal packing (right).

Analogously to the case of **Cu3ValBpy**, the obtaining of **Cu3HeptaBpy** made it possible to confirm the hexanuclear structure of compound **7**, for which we were unable to obtain a XRD structural determination [Di Nicola et al. (2009)].

The reaction of the two different acrylate derivatives, **8** and **9**, with bpy led to the obtaining of deep-blue crystals of a unique species, whose elemental analysis is consistent with the formula $[\text{Cu}_3(\mu_3\text{-OH})(\mu\text{-pz})_3(\text{CH}_2=\text{CHCOO})_2(\text{C}_{10}\text{H}_8\text{N}_2)(\text{H}_2\text{O})]$, **Cu3AcryBpy**, but the crystal structure still has to be solved.

Finally, reaction of the methacrylate derivative, **10**, with bpy, led to isolation of a microcrystalline solid, whose elemental analysis is consistent with the formula $[\text{Cu}_3(\mu_3\text{-OH})(\mu\text{-pz})_3(\text{CH}_2=\text{C}(\text{CH}_3)\text{COO})_2(\text{C}_{10}\text{H}_8\text{N}_2)(\text{H}_2\text{O})]$, **Cu3MethBpy**, the dimensions of the crystals being too small for a single-crystal XRD analysis.

In any case, as shown previously, the ESI-MS data are consistent with the presence of trinuclear moieties both in **Cu3AcryBpy** and in **Cu3MethBpy**.

Reactions with 1,2-bis(4-pyridyl)diazene

Reactions between compounds **1-7** and azopy led to the isolation of new $\text{Cu}^{(II)}$ compounds. While in the case of compounds **Cu3FormAzopy** and **Cu3AcAzopy** dark-green crystals suitable for an XRD

characterisation were obtained, in all the other cases single-crystal XRD determinations were not possible. Only the structure of **Cu3FormAzopy** has been solved so far; concerning the other compounds, the formulae proposed on the bases of the elemental analysis results are reported in Table 4.

Table 4. Formulae proposed on the basis of the elemental analysis results.

Compound	Formula
Cu3FormAzopy	$[[\text{Cu}_3(\mu_3\text{-OH})(\mu\text{-pz})_3(\text{HCOO})_2(\text{EtOH})]-[\text{Cu}_3(\mu_3\text{-OH})(\mu\text{-pz})_3(\text{HCOO})_2(\text{EtOH})_2]_2(\text{azopy})]$
Cu3AcAzopy	$[\text{Cu}_3(\mu_3\text{-OH})(\mu\text{-pz})_3(\text{CH}_3\text{COO})_2(\text{azopy})_{1.5}(\text{H}_2\text{O})]$
Cu3ProAzopy	$[\text{Cu}_3(\mu_3\text{-OH})(\mu\text{-pz})_3(\text{CH}_3\text{CH}_2\text{COO})_2(\text{azopy})_{1.5}(\text{H}_2\text{O})]$
Cu3ButAzopy	$[\text{Cu}_3(\mu_3\text{-OH})(\mu\text{-pz})_3(\text{CH}_3(\text{CH}_2)_2\text{COO})_2(\text{azopy})(\text{H}_2\text{O})]$
Cu3ValAzopy	$[\text{Cu}_3(\mu_3\text{-OH})(\mu\text{-pz})_3(\text{CH}_3(\text{CH}_2)_3\text{COO})_2(\text{azopy})]$
Cu3HexaAzopy	$[\text{Cu}_3(\mu_3\text{-OH})(\mu\text{-pz})_3(\text{CH}_3(\text{CH}_2)_4\text{COO})_2(\text{azopy})_{0.5}]$
Cu3HeptaAzopy	$[\text{Cu}_3(\mu_3\text{-OH})(\mu\text{-pz})_3(\text{CH}_3(\text{CH}_2)_5\text{COO})_2(\text{azopy})_{1.5}]$

The ESI-MS characterisations are in agreement with the proposed trinuclear structures. The most relevant signals are summarised in Table 5.

Table 5. Most relevant signals in the ESI-MS spectra of compounds **Cu3FormAzopy** – **Cu3HeptaAzopy**.

Compound	Signal ^a	R. A. ^b	Assignments
Cu3FormAzopy	95.2	100	[4-aminopyridine+H] ⁺
	536.0	85	$[\text{Cu}_3(\text{OH})(\text{pz})_3(\text{HCOO})(\text{MeOH})_2(\text{H}_2\text{O})]^+$
	629.0	60	$[\text{Cu}_3(\text{OH})(\text{pz})_2(\text{HCOO})_2(\text{MeOH})_2(\text{MeCN})(\text{EtOH})_2]^+$
	652.0	55	$[\text{Cu}_3(\text{OH})(\text{pz})_2(\text{HCOO})_2(\text{MeOH})_4(\text{EtOH})_2]^+$
	697.0	50	$[\text{Cu}_3(\text{pz})_3(\text{HCOO})_2(\text{H}_2\text{O})(\text{MeOH})_2(\text{MeCN})(\text{EtOH})_2]^+$
Cu3AcAzopy	95.2	100	[4-aminopyridine+H] ⁺
	737.3	65	$[\text{Cu}_4(\text{OH})_2(\text{pz})_3(\text{CH}_3\text{COO})_2(\text{Aminopy})(\text{H}_2\text{O})_2]^+$
Cu3ProAzopy	95.2	100	[4-aminopyridine+H] ⁺
	751.3	58	$[\text{Cu}_4(\text{OH})_2(\text{pz})_4(\text{C}_2\text{H}_5\text{COO})(\text{MeOH})(\text{H}_2\text{O})_5]^+$
Cu3ButAzopy	671.3	98	$[\text{Cu}_4(\text{OH})_4(\text{pz})_2(\text{C}_3\text{H}_7\text{COO})(\text{MeOH})_4]^+$
	1071.4	100	$[\text{Cu}_6(\text{OH})_3(\text{pz})_7(\text{C}_3\text{H}_7\text{COO})(\text{MeOH})_2(\text{H}_2\text{O})]^+$
	1107.4	50	$[\text{Cu}_6(\text{OH})_3(\text{pz})_7(\text{C}_3\text{H}_7\text{COO})(\text{MeOH})_2(\text{H}_2\text{O})_3]^+$
Cu3ValAzopy	95.2	100	[4-aminopyridine+H] ⁺
	685.3	80	$[\text{Cu}_3(\text{OH})(\text{pz})_3(\text{C}_4\text{H}_9\text{COO})_2(\text{MeOH})(\text{MeCN})+H]^+$
	779.5	50	$[\text{Cu}_4(\text{OH})_2(\text{pz})_4(\text{C}_4\text{H}_9\text{COO})(\text{MeOH})(\text{H}_2\text{O})_5]^+$
	1113.6	80	$[\text{Cu}_6(\text{OH})_4(\text{pz})_6(\text{C}_4\text{H}_9\text{COO})(\text{MeOH})_5]^+$
Cu3HexaAzopy	699.3	100	$[\text{Cu}_3(\text{OH})(\text{pz})_3(\text{C}_5\text{H}_{11}\text{COO})_2(\text{MeCN})(\text{H}_2\text{O})+H]^+$
	1155.7	98	$[\text{Cu}_6(\text{OH})_3(\text{pz})_6(\text{C}_5\text{H}_{11}\text{COO})_2(\text{H}_2\text{O})_5]^+$
	1191.7	60	$[\text{Cu}_6(\text{OCH}_3)_2(\text{pz})_6(\text{C}_5\text{H}_{11}\text{COO})_3]^+$
Cu3HeptaAzopy	95.2	100	[4-aminopyridine+H] ⁺
	708.5	60	$[\text{Cu}_4(\text{OH})_3(\text{pz})_3(\text{C}_6\text{H}_{13}\text{COO})(\text{MeOH})(\text{MeCN})]^+$
	807.5	50	$[\text{Cu}_4(\text{OH})_3(\text{pz})_3(\text{C}_6\text{H}_{13}\text{COO})(\text{MeOH})_2(\text{H}_2\text{O})_6]^+$

^a Values corresponding to the higher signals of the isotopic clusters. All isotopic clusters fit satisfactorily with calculated ones [Senko (1994)].

^b Relative Abundance of the higher signal of the isotopic cluster.

The most intense signals in almost all the ESI-MS spectra are found at 95.2 m/z, [4-aminopyridine+H]⁺, due to the decomposition of the azopy ligand in ESI conditions; other relevant signals are due to trinuclear and hexanuclear clusters but, significantly also signals associated to tetranuclear species are present, indicating that some kind of rearrangements likely happens in ESI-MS conditions. On the other hand, as already mentioned, even if the ESI-MS data offer important suggestions about the solid state structure, nevertheless the gas phase data are not always a mirror of what is present in the solid.

The reaction of **1** with 1,2-bis(4-pyridyl)diazene yielded a new coordination polymer, $[[[\text{Cu}_3(\mu_3\text{-OH})(\mu\text{-pz})_3(\text{HCOO})_2(\text{EtOH})]-[\text{Cu}_3(\mu_3\text{-OH})(\mu\text{-pz})_3(\text{HCOO})_2(\text{EtOH})_2]\}_2(\text{C}_{10}\text{H}_8\text{N}_4)]$, **Cu3FormAzopy**, whose asymmetric unit is reported in Figure 48.

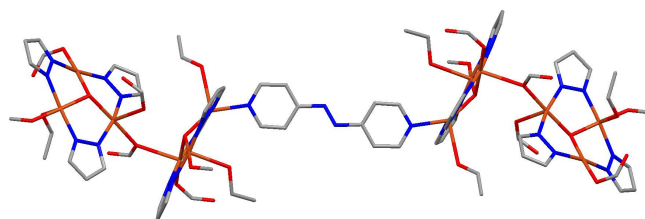


Figure 48. Asymmetric unit of **Cu3FormAzopy**. Hydrogens have been omitted for clarity.

The compound is characterised by the presence of hexanuclear clusters, also in this case reminiscent of the supramolecular assembly of **1** [Casarin et al. (2005)], which are connected by bridging azopy ligands. The supramolecular assembly is given by two different kinds of connections, with a behaviour which is, to some extent, similar to that of compound **Cu3FormBpyL**: connection 1→4 originates 2D nets, which are interconnected by connection 2→3. No interpenetration is observed between the nets.

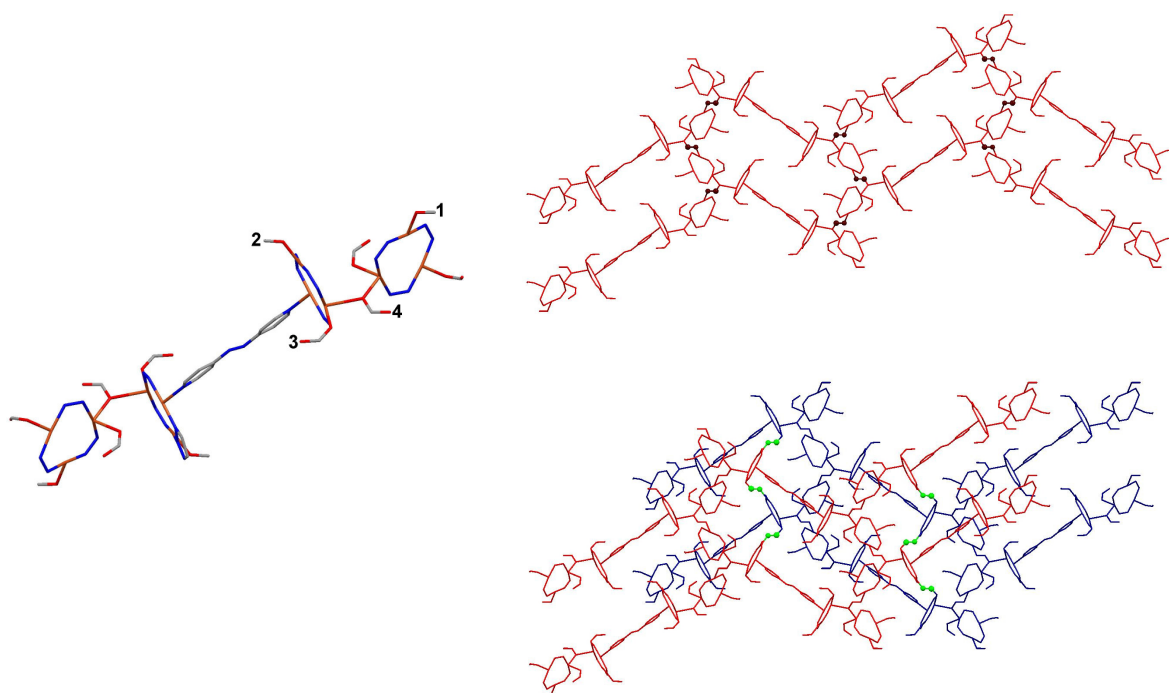


Figure 49. Schematic representation of the asymmetric unit of **Cu3FormAzopy**, the numbers indicate the connection sites between the asymmetric unit and the others (left); connection 1→4 (top, right; black dots) and connection 2→3 (down, right; green dots).

Reactions with 4,4'-dipyridylethane

Reactions between compounds **1-10** and bpetha led to the isolation of new $\text{Cu}^{(\text{II})}$ compounds. In most cases, well-shaped deep-blue crystals were isolated, but XRD analyses still have to be performed. In Table 6, the formulae proposed on the bases of the elemental analysis results are reported.

The ESI-MS characterisations are in agreement with the proposed trinuclear structures. The most relevant signals are summarised in Table 7.

Table 6. Formulae proposed on the bases of the elemental analysis results.

Compound	Formula
Cu3FormBpetha	$[\text{Cu}_3(\mu_3\text{-OH})(\mu\text{-pz})_3(\text{HCOO})_2(\text{bpetha})(\text{H}_2\text{O})_3]$
Cu3AcBpetha	$[\text{Cu}_3(\mu_3\text{-OH})(\mu\text{-pz})_3(\text{CH}_3\text{COO})_2(\text{bpetha})_2(\text{H}_2\text{O})_2]$
Cu3ProBpetha	$[\text{Cu}_3(\mu_3\text{-OH})(\mu\text{-pz})_3(\text{CH}_3\text{CH}_2\text{COO})_2(\text{bpetha})_{0.5}]$
Cu3ButBpetha	$[\text{Cu}_3(\mu_3\text{-OH})(\mu\text{-pz})_3(\text{CH}_3(\text{CH}_2)_2\text{COO})_2(\text{bpetha})_{0.5}]$
Cu3ValBpetha	$[\text{Cu}_3(\mu_3\text{-OH})(\mu\text{-pz})_3(\text{CH}_3(\text{CH}_2)_3\text{COO})_2(\text{bpetha})_{1.5}(\text{H}_2\text{O})]$
Cu3HexaBpetha	$[\text{Cu}_3(\mu_3\text{-OH})(\mu\text{-pz})_3(\text{CH}_3(\text{CH}_2)_4\text{COO})_2(\text{bpetha})]$
Cu3HeptaBpetha	$[\text{Cu}_3(\mu_3\text{-OH})(\mu\text{-pz})_3(\text{CH}_3(\text{CH}_2)_5\text{COO})_2(\text{bpetha})]$
Cu3AcryBpetha	$[\text{Cu}_3(\mu_3\text{-OH})(\mu\text{-pz})_3(\text{CH}_2=\text{CHCOO})_2(\text{bpetha})_{0.5}]$
Cu3MethBpetha1 (first crop)	$[\text{Cu}_3(\mu_3\text{-OH})(\mu\text{-pz})_3(\text{CH}_2=\text{C}(\text{CH}_3)\text{COO})_2(\text{bpetha})_{0.5}(\text{H}_2\text{O})]$
Cu3MethBpetha2 (second crop)	$[\text{Cu}_3(\mu_3\text{-OH})(\mu\text{-pz})_3(\text{CH}_2=\text{C}(\text{CH}_3)\text{COO})_2(\text{bpetha})_{1.5}]$

Table 7. Most relevant signals in the ESI-MS spectra of compounds **Cu3FormBpetha** - **Cu3MethBpetha2**.

Compound	Signal ^a	R. A. ^b	Assignments
Cu3FormBpetha	800.5	75	$[\text{Cu}_3(\text{OH})(\text{pz})_3(\text{HCOO})_2(\text{Hpz})_2(\text{MeCN})_2(\text{H}_2\text{O})(\text{MeOH})_2+\text{H}]^+$
	813.5	100	$[\text{Cu}_4(\text{OH})_2(\text{pz})_3(\text{HCOO})_2(\text{bpetha})(\text{H}_2\text{O})(\text{MeOH})]^+$
Cu3AcBpetha	568.3	65	$[\text{Cu}_3(\text{OH})(\text{pz})_3(\text{CH}_3\text{COO})(\text{H}_2\text{O})_2(\text{MeOH})_2]^+$
	666.5	85	$[\text{Cu}_3(\text{OCH}_3)(\text{pz})_3(\text{CH}_3\text{COO})(\text{bpetha})]^+$
	814.6	90	$[\text{Cu}_3(\text{OH})(\text{pz})_3(\text{CH}_3\text{COO})(\text{bpetha})(\text{H}_2\text{O})_9]^+$
	827.5	100	$[\text{Cu}_4(\text{OH})_2(\text{pz})_3(\text{CH}_3\text{COO})_2(\text{bpetha})(\text{H}_2\text{O})_2]^+$
Cu3ProBpetha	657.3	100	$[\text{Cu}_4(\text{OH})_3(\text{pz})_2(\text{C}_2\text{H}_5\text{COO})_2(\text{H}_2\text{O})_4]^+$
	680.5	95	$[\text{Cu}_3(\text{OCH}_3)(\text{pz})_3(\text{C}_2\text{H}_5\text{COO})(\text{bpetha})]^+$
	686.5	65	$[\text{Cu}_3(\text{OCH}_3)(\text{pz})_3(\text{C}_2\text{H}_5\text{COO})(\text{H}_2\text{O})_7(\text{MeOH})_2]^+$
	841.5	80	$[\text{Cu}_4(\text{OH})_3(\text{pz})_2(\text{C}_2\text{H}_5\text{COO})_2(\text{bpetha})(\text{H}_2\text{O})_4]^+$
	993.5	75	$[\text{Cu}_6(\text{OH})_3(\text{pz})_7(\text{C}_2\text{H}_5\text{COO})(\text{H}_2\text{O})]^+$
	1029.4	98	$[\text{Cu}_6(\text{OH})_3(\text{pz})_7(\text{C}_2\text{H}_5\text{COO})(\text{H}_2\text{O})_3]^+$
Cu3ButBpetha	671.3	80	$[\text{Cu}_4(\text{OH})_4(\text{pz})_2(\text{C}_3\text{H}_7\text{COO})(\text{MeOH})_4]^+$
	694.5	55	$[\text{Cu}_3(\text{OCH}_3)(\text{pz})_3(\text{C}_3\text{H}_7\text{COO})(\text{bpetha})]^+$
	855.5	60	$[\text{Cu}_4(\text{OH})_4(\text{pz})_2(\text{C}_3\text{H}_7\text{COO})(\text{bpetha})(\text{MeOH})_4]^+$
	1035.4	75	$[\text{Cu}_6(\text{OH})_4(\text{pz})_6(\text{C}_3\text{H}_7\text{COO})(\text{MeOH})_3]^+$
Cu3ValBpetha	1071.4	100	$[\text{Cu}_6(\text{OH})_3(\text{pz})_7(\text{C}_3\text{H}_7\text{COO})(\text{H}_2\text{O})(\text{MeOH})_2]^+$
	685.3	70	$[\text{Cu}_4(\text{OCH}_3)_2(\text{pz})_4(\text{C}_4\text{H}_9\text{COO})]^+$
	708.5	90	$[\text{Cu}_3(\text{OCH}_3)(\text{pz})_3(\text{C}_4\text{H}_9\text{COO})(\text{bpetha})]^+$
	742.5	82	$[\text{Cu}_3(\text{OH})(\text{pz})_3(\text{C}_4\text{H}_9\text{COO})_2(\text{H}_2\text{O})_6+\text{Na}]^+$
	856.7	85	$[\text{Cu}_3(\text{OH})(\text{pz})_3(\text{C}_4\text{H}_9\text{COO})(\text{bpetha})(\text{H}_2\text{O})_9]^+$
	869.5	100	$[\text{Cu}_3(\text{OH})(\text{pz})_3(\text{C}_4\text{H}_9\text{COO})_2(\text{bpetha})(\text{MeOH})(\text{MeCN})+\text{H}]^+$
	1113.6	90	$[\text{Cu}_6(\text{OCH}_3)_3(\text{pz})_7(\text{C}_4\text{H}_9\text{COO})(\text{MeOH})(\text{H}_2\text{O})_2]^+$
Cu3HexaBpetha	1149.6	50	$[\text{Cu}_6(\text{OCH}_3)_2(\text{pz})_6(\text{C}_4\text{H}_9\text{COO})_3]^+$
	699.3	70	$[\text{Cu}_3(\text{pz})_3(\text{C}_5\text{H}_{11}\text{COO})_2(\text{MeCN})(\text{H}_2\text{O})_2]^+$
	722.5	60	$[\text{Cu}_3(\text{OCH}_3)(\text{pz})_3(\text{C}_5\text{H}_{11}\text{COO})(\text{bpetha})]^+$
	770.5	100	$[\text{Cu}_3(\text{OH})(\text{pz})_3(\text{C}_5\text{H}_{11}\text{COO})(\text{H}_2\text{O})_6+\text{Na}]^+$
	870.7	58	$[\text{Cu}_3(\text{OCH}_3)(\text{pz})_3(\text{C}_5\text{H}_{11}\text{COO})(\text{bpetha})(\text{MeOH})+\text{H}]^+$
	883.5	87	$[\text{Cu}_4(\text{OH})_2(\text{pz})_3(\text{C}_5\text{H}_{11}\text{COO})_2(\text{MeOH})_4(\text{H}_2\text{O})_2]^+$
	1119.6	60	$[\text{Cu}_6(\text{OH})_3(\text{pz})_6(\text{C}_5\text{H}_{11}\text{COO})_2(\text{H}_2\text{O})_3]^+$
Cu3HeptaBpetha	1155.6	80	$[\text{Cu}_6(\text{OH})_3(\text{pz})_6(\text{C}_5\text{H}_{11}\text{COO})_2(\text{H}_2\text{O})_5]^+$
	713.3	68	$[\text{Cu}_4(\text{OCH}_3)_3(\text{pz})_3(\text{C}_6\text{H}_{13}\text{COO})(\text{H}_2\text{O})_2]^+$
	736.5	67	$[\text{Cu}_3(\text{OCH}_3)(\text{pz})_3(\text{C}_6\text{H}_{13}\text{COO})(\text{bpetha})]^+$
	798.5	75	$[\text{Cu}_3(\text{OH})(\text{pz})_3(\text{C}_6\text{H}_{13}\text{COO})_2(\text{H}_2\text{O})_6+\text{Na}]^+$
	884.7	50	$[\text{Cu}_3(\text{OH})(\text{pz})_3(\text{C}_6\text{H}_{13}\text{COO})_2(\text{H}_2\text{O})_9(\text{MeOH})+\text{Na}]^+$
	897.5	100	$[\text{Cu}_4(\text{OH})_2(\text{pz})_3(\text{C}_6\text{H}_{13}\text{COO})_2(\text{H}_2\text{O})_3(\text{MeOH})_3]^+$
	1197.7	86	$[\text{Cu}_6(\text{OH})_3(\text{pz})_6(\text{C}_6\text{H}_{13}\text{COO})_2(\text{MeOH})(\text{H}_2\text{O})_4]^+$
	1233.7	50	$[\text{Cu}_6(\text{OCH}_3)_2(\text{pz})_6(\text{C}_6\text{H}_{13}\text{COO})_3]^+$
Cu3AcryBpetha	839.5	68	$[\text{Cu}_4(\text{OCH}_3)_2(\text{pz})_4(\text{CH}_2=\text{CHCOO})(\text{bpetha})]^+$
	1023.3	100	$[\text{Cu}_6(\text{OCH}_3)_3(\text{pz})_5(\text{CH}_2=\text{CHCOO})_3]^+$
	1059.3	50	$[\text{Cu}_6(\text{OCH}_3)_2(\text{pz})_6(\text{CH}_2=\text{CHCOO})_3]^+$
Cu3MethBpetha1	1065.4	100	$[\text{Cu}_6(\text{OCH}_3)_3(\text{pz})_7(\text{CH}_2=\text{C}(\text{CH}_3)\text{COO})(\text{H}_2\text{O})_2]^+$
	1101.4	65	$[\text{Cu}_6(\text{OCH}_3)_2(\text{pz})_6(\text{CH}_2=\text{C}(\text{CH}_3)\text{COO})_3]^+$
Cu3MethBpetha2	692.4	58	$[\text{Cu}_3(\text{OH})(\text{pz})_3(\text{CH}_2=\text{C}(\text{CH}_3)\text{COO})_2(\text{H}_2\text{O})_5+\text{Na}]^+$
	840.5	100	$[\text{Cu}_3(\text{OH})(\text{pz})_3(\text{CH}_2=\text{C}(\text{CH}_3)\text{COO})(\text{bpetha})(\text{H}_2\text{O})_9]^+$
	853.5	75	$[\text{Cu}_4(\text{OCH}_3)_2(\text{pz})_4(\text{CH}_2=\text{C}(\text{CH}_3)\text{COO})(\text{bpetha})]^+$
	1065.4	70	$[\text{Cu}_6(\text{OCH}_3)_3(\text{pz})_7(\text{CH}_2=\text{C}(\text{CH}_3)\text{COO})(\text{H}_2\text{O})_2]^+$

^a Values corresponding to the higher signals of the isotopic clusters. All isotopic clusters fit satisfactorily with calculated ones [Senko (1994)].

^b Relative Abundance of the higher signal of the isotopic cluster.

ESI-MS spectra evidence, in most cases, signals correlated to tri- or hexanuclear clusters as the most intense ones, while in the cases of **Cu3FormBpetha**, **Cu3AcBpetha**, **Cu3ProBpetha** and **Cu3HeptaBpeta**, the higher signals correspond to tetranuclear clusters; analogously to what evidenced previously this can indicate the presence of hexanuclear clusters, which, in ESI conditions, may partly decompose, leaving one copper(II) of one of the trinuclear units attached on the second trinuclear unit. In this context, it is to be emphasized that numerous ESI fragments contain the OCH₃ moiety, instead of the “starting” OH. Even though the methoxy moiety may be present in obtained compounds, analogously to what observed in **Cu3*ButBpy**, its presence can be due, on the other hand, to extensive rearrangement processes which can happen in ESI conditions. Moreover, it is to be remembered that in the ESI-MS spectra of all compounds, even if of minor intensity, trinuclear and hexanuclear based signals are also present. Incidentally, it is noteworthy that signals associated to tetranuclear clusters are present as the most intense ESI signals also in spectra of compounds whose tri- or hexanuclear structure has been ascertained by XRD determinations (see data of compounds **Cu3FormBpethy** and **Cu3AcBpethy** reported below). Even though only XRD determinations, at the present in progress, will settle the question, we are confident that the trinuclear triangular structure is maintained also in these cases. Finally, XRD determination are hopefully expected to reveal also interesting supramolecular assemblies for the above indicated compounds.

Reactions with 1,2-bis(4-pyridyl)ethylene

Reactions of compounds **1** and **2** with bpethy led in both cases to the isolation of new trinuclear triangular Cu^(II) CPs, with different dimensionality. Both of them have been characterised by XRD analysis, confirming the presence of the trinuclear core.

Also the ESI-MS characterisations are in agreement with the trinuclear structures. The most relevant signals are summarised in Table 8.

Table 8. Most relevant signals in the ESI-MS spectra of compounds **Cu3FormBpethy** and **Cu3AcBpethy**.

Compound ^a	Signal ^b	R. A. ^c	Assignments
Cu3FormBpethy	183.3	50	[bpethy+H] ⁺
	811.3	100	[Cu ₄ (OH) ₂ (pz) ₃ (HCOO) ₂ (bpethy)(MeOH)(H ₂ O)] ⁺
Cu3AcBpethy	643.2	100	[Cu ₄ (OH) ₂ (pz) ₃ (CH ₃ COO) ₂ (H ₂ O) ₂] ⁺
	664.4	65	[Cu ₃ (OCH ₃)(pz) ₃ (CH ₃ COO)(bpethy)] ⁺
	825.5	75	[Cu ₄ (OH) ₂ (pz) ₃ (CH ₃ COO) ₂ (bpethy)(H ₂ O) ₂] ⁺
	987.3	60	[Cu ₆ (OH) ₄ (pz) ₆ (CH ₃ COO)(H ₂ O) ₂ (MeCN)] ⁺

^a Cu₃: [Cu₃(OH)(pz)₃]²⁺

^b Values corresponding to the higher signals of the isotopic clusters. All isotopic clusters fit satisfactorily with calculated ones [Senko (1994)].

^c Relative Abundance of the higher signal of the isotopic cluster.

As anticipated previously, the most intense signals of the ESI-MS spectra correspond in both cases to tetranuclear aggregates, while other less intense trinuclear and hexanuclear based signals are also present in the spectra of both compounds (see also the Experimental Section). As previously stated this can indicate the presence of hexanuclear clusters, which may partly decompose, in ESI conditions, leaving one copper(II) of one of the trinuclear units attached on the second trinuclear unit.

The reaction between **1** and bpethy generated a new 2D coordination polymer, based on $[(\text{Cu}_3(\mu_3\text{-OH})(\mu\text{-pz})_3(\text{HCOO})_2)_4(\text{C}_{12}\text{H}_{10}\text{N}_2)_5]$, **Cu3FormBPethy**, whose asymmetric unit is sketched in Figure 50.

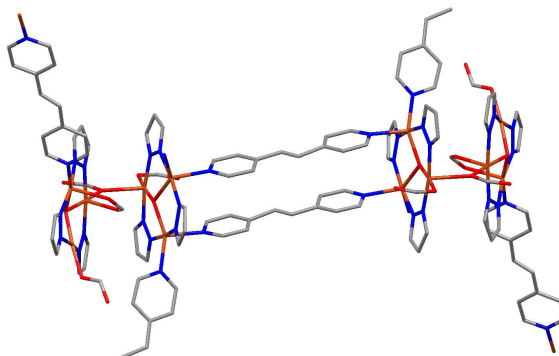


Figure 50. Asymmetric unit of **Cu3FormBPethy**. Hydrogen atoms have been omitted for clarity.

Two trinuclear triangular Cu^{II} units are linked through bridging formate ions, being the hexanuclear clusters reminiscent of the supramolecular structure of **1** [Casarin et al. (2005)]; they are connected by bpethy molecules, generating 2D nets, as schematically represented in Figure 51.

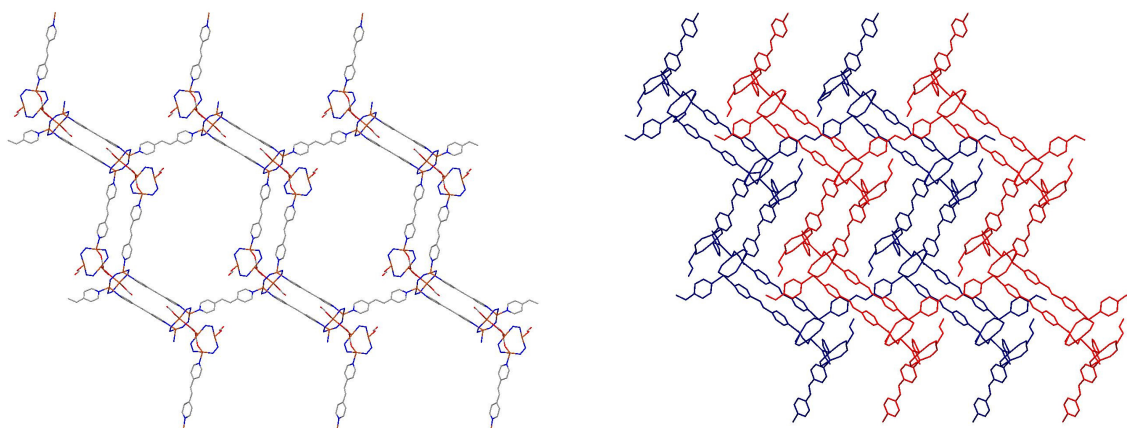


Figure 51. Schematic representation of the 2D nets of **Cu3FormBPethy**.

The crystal packing of **Cu3FormBPethy** evidences the pillaring of the 2D layers, as sketched in Figure 52. Any covalent interaction among the layers is absent.

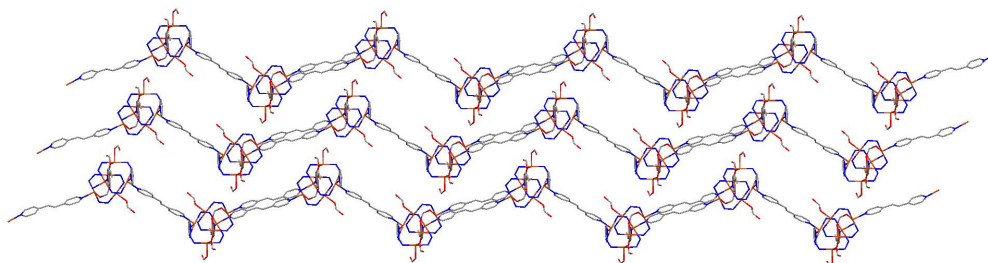


Figure 52. Schematic representation of the crystal packing of compound **Cu3FormBPethy**.

Reaction between **2**, and bpethy led to the formation of a new 1D CP, based on $[\text{Cu}_3(\mu_3\text{-OH})(\mu\text{-pz})_3(\text{CH}_3\text{COO})_2(\text{C}_{12}\text{H}_{10}\text{N}_2)(\text{H}_2\text{O})]$, **Cu3AcBPethy**, whose asymmetric unit is sketched in Figure 53.

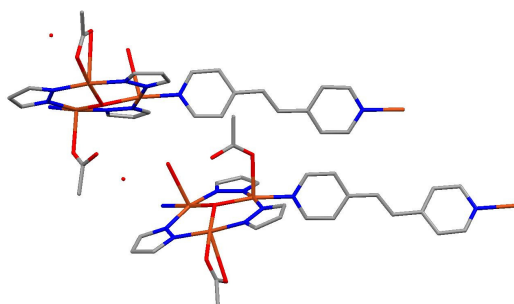


Figure 53. Asymmetric unit of **Cu3AcBpethy**. Hydrogen atoms have been omitted for clarity.

Cu3AcBpethy is characterised by the presence of trinuclear clusters, which are connected by bridging ligand molecules, generating zig-zag tapes, schematically represented in Figure 54.

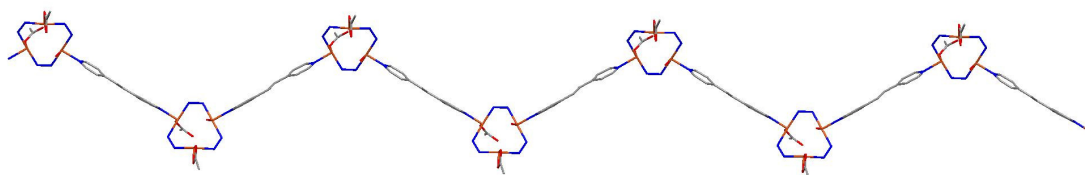


Figure 54. Schematic representation of the 1D chains of **Cu3AcBpethy**.

The different chains are not interconnected with covalent interactions; instead, they are just pillared one over the other. A schematic representation of the crystal packing of **Cu3AcBpethy** is sketched in Figure 55.

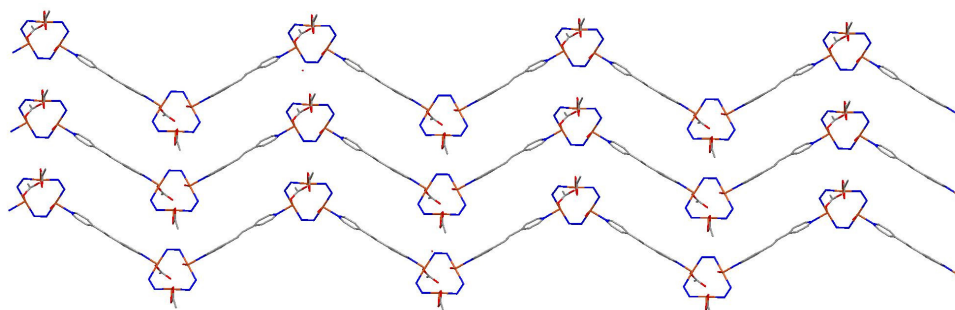


Figure 55. Schematic representation of the crystal packing of compound **Cu3AcBpethy**.

Reactions with 1,5-naphthyridine

Compounds **1**, **2**, **4** and **10** were reacted with 1,5-naphthyridine. While in the case of **2** and **4** no reactions takes place, being isolated only the starting materials, in the case of **1** and **10** we got blue well-formed crystals, suitable for an XRD characterisation. Only the structure of **1b** has been solved so far; concerning the other compound, the formula has been proposed on the bases of the elemental analysis results reported in Table 9 and on the ESI-MS data reported in Table 10.

Table 9. Formulae proposed on the bases of the elemental analysis results.

Compound	Formula
1b	$[\text{Cu}_3(\mu_3\text{-OCH}_3)(\mu\text{-pz})_3(\text{HCOO})_2(\text{Hpz})_2]$
Cu3AcryNapht	$[\text{Cu}_3(\mu_3\text{-OH})(\mu\text{-pz})_3(\text{CH}_2=\text{CHCOO})_2(\text{napht})]$

Table 10. Most relevant signals in the ESI-MS spectra of compounds **1b** and **Cu3AcryNapht**.

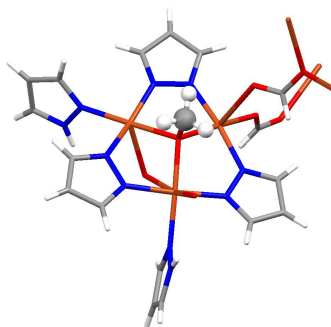
Compound ^a	Signal ^b	R. A. ^c	Assignments
1b	536.0	50	$[\text{Cu}_3(\text{OCH}_3)(\text{pz})_3(\text{HCOO})(\text{MeOH})(\text{H}_2\text{O})_2]^+$
	572.0	60	$[\text{Cu}_3(\text{OCH}_3)(\text{pz})_3(\text{HCOO})(\text{MeOH})(\text{H}_2\text{O})_4]^+$
	604.0	100	$[\text{Cu}_3(\text{OCH}_3)(\text{pz})_3(\text{HCOO})(\text{Hpz})_2]^+$
Cu3AcryNapht	602.0	95	$[\text{Cu}_3(\text{OH})(\text{pz})_3(\text{CH}_2=\text{CHCOO})_2(\text{MeOH})(\text{H}_2\text{O})+\text{H}]^+$
	624.0	60	$[\text{Cu}_3(\text{OCH}_3)(\text{pz})_3(\text{CH}_2=\text{CHCOO})(\text{Napht})]^+$
	1058.9	100	$[\text{Cu}_6(\text{OCH}_3)_2(\text{pz})_6(\text{CH}_2=\text{CHCOO})_3]^+$

^a Cu₃: $[\text{Cu}_3(\text{OH})(\text{pz})_3]^{2+}$

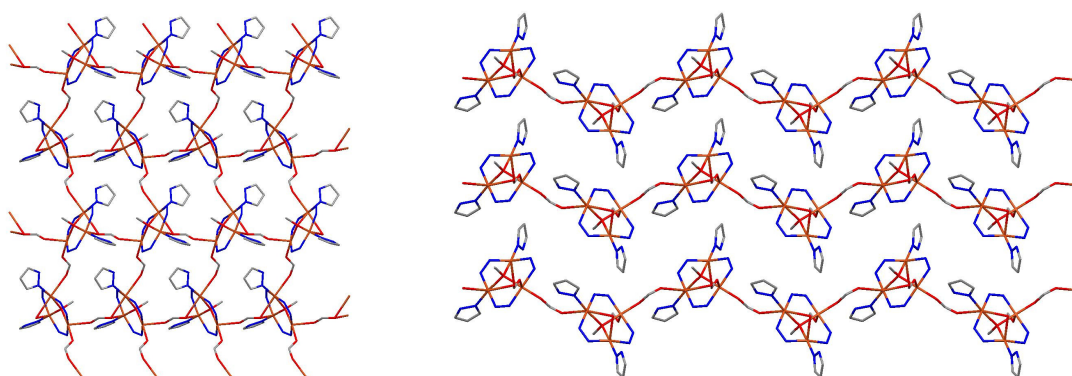
^b Values corresponding to the higher signals of the isotopic clusters. All isotopic clusters fit satisfactorily with calculated ones [Senko (1994)].

^c Relative Abundance of the higher signal of the isotopic cluster.

Curiously, the reaction of **1** with 1,5-naphthyridine led only to the replacement of the μ_3 -OH group with μ_3 -OCH₃, giving compound $[\text{Cu}_3(\mu_3\text{-OCH}_3)(\mu\text{-pz})_3(\text{HCOO})_2(\text{Hpz})_2]$, **1b**. In this case, 1,5-naphthyridine, instead of coordinating to the metal centres displacing neutral molecules, likely behaves as a base, favouring the deprotonation of the solvent, MeOH, and the substitution of μ_3 -OH with μ_3 -OCH₃, analogously to what observed in the case of **Cu3*ButBpy**. The asymmetric unit of compound **1b** is sketched in Figure 56.

**Figure 56.** Schematic representation of the asymmetric unit of **1b**. The μ_3 -OCH₃ group is evidenced in ball and stick style.

Analogously to compound **1**, **1b** is a CP. 2D nets are formed through bridging formate ions (Figure 57, left). The layers are then pillared one over the other, without any covalent interaction among them (Figure 57, right).

**Figure 57.** Schematic representation of the 2D nets (left) and of the crystal packing (right) of **1b**. Hydrogen atoms and pyrazolate carbon atoms are omitted for clarity.

Interestingly, the substitution of the μ_3 -OH group with μ_3 -OCH₃ does not affect the supramolecular assembly of **1**, which is preserved in compound **1b**, the supramolecular connections and the cell parameters remaining practically unchanged [Casarin et al. (2005)].

Reaction with 1,3-bis(4-pyridyl)propane and 1,2-bis(4-pyridyl)disulfane

Compound **1** was reacted with tmb and bpsulf. In both cases, microcrystalline products were obtained, the dimensions of the crystals being too small for an XRD analysis. The presence of the trinuclear cluster was inferred from elemental analysis results and ESI-MS characterisations, whose data are reported in Tables 11 and 12, analogously to previously discussed derivatives.

Table 11. Formulae proposed on the basis of elemental analysis results.

Compound	Formula
Cu3FormTmb	[Cu ₃ (μ_3 -OH)(μ -pz) ₃ (HCOO) ₂ (tmb)(H ₂ O)]
Cu3FormBpsulf	[Cu ₃ (μ_3 -OH)(μ -pz) ₃ (HCOO) ₂ (bpsulf)]

Table 12. Most relevant signals in the ESI-MS spectra of compounds **Cu3FormTmb** and **Cu3FormBpsulf**.

Compound ^a	Signal ^b	R. A. ^c	Assignments
Cu3FormTmb	666.5	90	[Cu ₃ (OH)(pz) ₂ (HCOO) ₂ (tmb)(H ₂ O) ₂] ⁺
	827.5	100	[Cu ₄ (OH) ₂ (pz) ₃ (HCOO) ₂ (tmb)(MeOH)(H ₂ O)] ⁺
Cu3FormBpsulf	221.1	85	[bpsulf+H] ⁺
	688.3	70	[Cu ₃ (OCH ₃)(pz) ₃ (HCOO)(bpsulf)] ⁺
	849.3	100	[Cu ₄ (OH) ₂ (pz) ₃ (HCOO) ₂ (bpsulf)(H ₂ O)(MeOH)] ⁺

^a Cu₃: [Cu₃(OH)(pz)₃]²⁺

^b Values corresponding to the higher signals of the isotopic clusters. All isotopic clusters fit satisfactorily with calculated ones [Senko (1994)].

^c Relative Abundance of the higher signal of the isotopic cluster.

Electrochemical Studies

The electrochemical behaviour of the trinuclear triangular Cu^(II) derivatives **1-10** was previously reported by us [Di Nicola et al. (2009); Contaldi et al. (2009)]. The redox properties of some of the above described new trinuclear Cu^(II) complexes (**Cu3Sulf**, **Cu3TFAc**, **Cu3ProBpy**, **Cu3*ButBpy**, **Cu3ValBpy**, **Cu3EptaBpy**) were also investigated by cyclic voltammetry (CV), at a Pt disc electrode, in a 0.2 M [ⁿBu₄N][BF₄]/DMSO solution, at room temperature. All the compounds exhibit (Figure 58 (left) for **Cu3TFAc** and Figure 58 (right) for **Cu3ProBpy**) two single-electron (per metal ion) irreversible reduction waves, assigned to the Cu^(II) → Cu^(I) and Cu^(I) → Cu⁽⁰⁾ reductions, at the reduction peak potential values given in Table 13 (^I*E*_p^{red} in the range from -0.35 to -0.45 V vs. SCE, and ^{II}*E*_p^{red} between -1.51 and -1.67 V vs. SCE). An irreversible anodic wave (^I*E*_p^{ox} in the range 0.26 – 0.44 V vs. SCE) is observed upon scan reversal after the first reduction wave (Figure 59 (left) for **Cu3TFAc** and Figure 59 (right) for **Cu3ProBpy**), corresponding to the oxidation of the Cu^(I) species formed at the first reduction process, while a second irreversible anodic wave (^{II}*E*_p^{ox} in the range from -0.03 to -0.21 V vs. SCE) is formed upon scan reversal after the second reduction wave in the case of compounds **Cu3Sulf**, **Cu3TFAc** and **Cu3ProBpy**. A reversible reduction wave is observed for **Cu3ProBpy**, **Cu3*ButBpy**, **Cu3ValBpy**, **Cu3EptaBpy**, assigned to the reversible reduction of bipyridine (^{III}*E*_{1/2}^{red} in the range from -1.75 to -1.77 V vs. SCE).

Table 13. Cyclic voltammetric data^a for trinuclear triangular complexes.

Complex ^b	CATHODIC WAVES			ANODIC WAVES	
	^I <i>E</i> _p ^{red}	^{II} <i>E</i> _p ^{red}	^{III} <i>E</i> _{1/2} ^{red}	^I <i>E</i> _p ^{ox,c}	^{II} <i>E</i> _p ^{ox,c}
Cu3Sulf [Cu ₃ (SO ₄)(Hpz)]	-0.35	-1.65	/	0.26	-0.03
Cu3TFAc [Cu ₃ (CF ₃ COO) ₂ (Hpz) ₂]	-0.38	-1.67	/	0.35	-0.05
Cu3ProBpy [Cu ₃ (CH ₃ CH ₂ COO) ₂ (C ₁₀ H ₈ N ₂)]	-0.43	-1.53	-1.77	0.36	-0.21
Cu3*ButBpy [Cu ₃ *(CH ₃ (CH ₂) ₂ COO) ₂ (C ₁₀ H ₈ N ₂)]	-0.45	-1.56	-1.76	0.37	/
Cu3ValBpy [Cu ₃ (CH ₃ (CH ₂) ₃ COO) ₂ (C ₁₀ H ₈ N ₂)(CH ₃ OH)]	-0.43	-1.51	-1.76	0.40	/
Cu3EptaBpy [Cu ₃ (CH ₃ (CH ₂) ₅ COO) ₂ (C ₁₀ H ₈ N ₂) _{0.5}]	-0.38	-1.51	-1.75	0.44	/

^a Potential values in Volt ± 0.02 vs. SCE, in a 0.2 M [ⁿBu₄N][BF₄]/DMSO solution, at a Pt disc working electrode, determined by using the [Fe(η⁵-C₅H₅)₂]^{0/+} redox couple (*E*_{1/2}^{ox} = 0.44 V vs. SCE) as internal standard at a scan rate of 200 mVs⁻¹.

^b Cu₃ = Cu₃(μ₃-OH)(μ-pz)₃; Cu₃* = Cu₃(μ₃-OCH₃)(μ-pz)₃

^c Only observed upon scan reversal following the corresponding reduction wave I^{red} or II^{red}.

No oxidation wave has been detected for any complex by a first anodic sweep without a previous reduction scan, indicating that neither a metal centered nor a ligand centered oxidation is observed. All these complexes are characterised by the same behaviour in CV, and the shape of their cyclic voltammograms is almost identical to that of other trinuclear triangular copper(II) compounds previously studied by us [Di Nicola et al. (2009); Contaldi et al. (2009)]. For this reason, it was not

necessary to run CPE experiments, but the occurrence of a single-electron reduction per Cu^(II) (or Cu^(I)) atom was confirmed by the similarity of the current functions ($i_p C^{-1} v^{-1/2}$) of the reduction waves of our complexes with those of other similar trinuclear complexes.

Any of the cathodic waves involves the reduction of the three metal ions, without any detected differentiation. In any case, it is not possible to rule out any metal-metal electronic communication because of the broadness of the reduction waves; this, in fact, can result from the overlap of distinct waves at close but distinct potentials, namely Cu^(II)Cu^(II)Cu^(II) → Cu^(I)Cu^(II)Cu^(II) → Cu^(I)Cu^(I)Cu^(II) → Cu^(I)Cu^(I)Cu^(I).

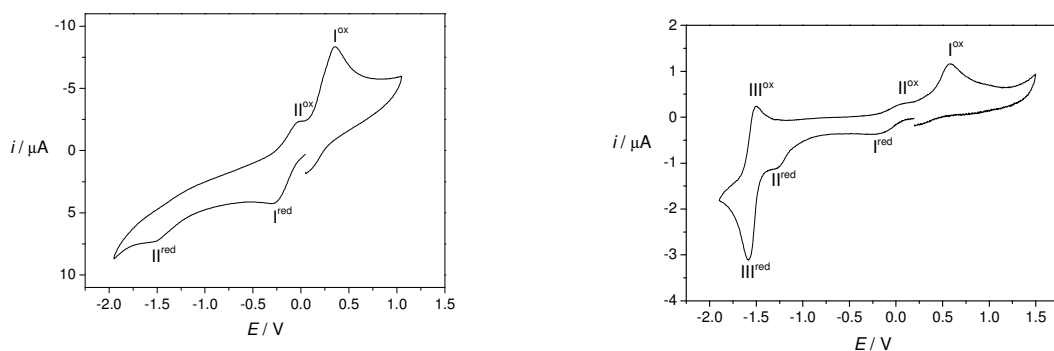


Figure 58. Cyclic voltammogram of **Cu3TFac** (left) and **Cu3ProBpy** (right) in a 0.2 M [ⁿBu₄N][BF₄]/DMSO solution, at a Pt disc working electrode ($d = 0.5$ mm), at a scan rate of 200 mVs⁻¹.

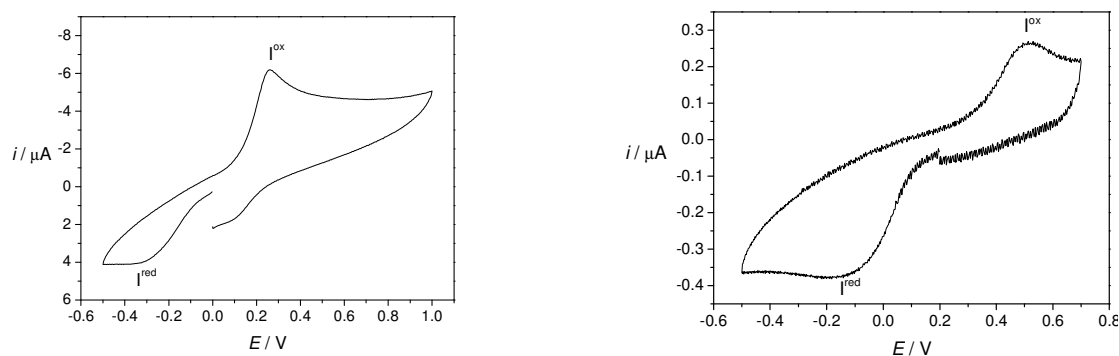


Figure 59. Cyclic voltammogram of **Cu3TFac** (left) and **Cu3ProBpy** (right) with scan reversal after the first reduction wave, in a 0.2 M [ⁿBu₄N][BF₄]/DMSO solution, at a Pt disc working electrode ($d = 0.5$ mm), at a scan rate of 200mVs⁻¹.

Besides the trinuclear derivatives, we also studied for the first time the electrochemical behaviour of some mononuclear Cu^(II) complexes (**CuTFac1**, **CuTFac2**, **CuSulf**, **CuPerchl**, **CuBenz**, **CuForm**, **CuTFL**). All the compounds exhibit, by CV at 200 mV/s, (Figure 60 (left) for complex **CuTFac2**) an irreversible reduction wave, assigned to the Cu^(II) → Cu⁽⁰⁾ reduction, at the reduction peak potential values given in Table 14 ($^I E_p^{red}$ in the range from -0.15 to -0.37 V vs. SCE). Two new irreversible anodic waves ($^I E_p^{ox,1}$ in the range -0.10 – 0.01 V vs. SCE and $^I E_p^{ox,2}$ between 0.22 and 0.38 V vs. SCE) are observed upon scan reversal after the reduction wave, corresponding to the Cu⁽⁰⁾ → Cu^(I) and Cu^(I) → Cu^(II) oxidations, respectively. The former (I^{ox,1}) has the typical shape associated to a desorption process. Compounds **CuBenz** and **CuForm** exhibit a second irreversible reduction wave II^{red} at the reduction peak potential values ($^{II} E_p^{red}$) given in Table 14. For these compounds, a new irreversible anodic wave (II^{ox}) is generated upon scan reversal after the second reduction wave (Figure 60 (right)

for complex **CuBenz**). By comparison with the CVs of the other mononuclear complexes, it can be inferred that II^{red} is possibly associated with a ligand-centred reduction process.

At the lowest scan rates (namely 20, 50 and 100 mV/s) for compounds **CuTFac1**, **CuTFac2** and **CuSulf** (Figure 61 (left) for **CuTFac2**) it is possible to see two distinct reduction waves $\text{I}^{\text{red},1}$ and $\text{I}^{\text{red},2}$, at close potentials; they are associated to the $\text{Cu}^{\text{(II)}} \rightarrow \text{Cu}^{\text{(I)}}$ and the $\text{Cu}^{\text{(I)}} \rightarrow \text{Cu}^{\text{(0)}}$ reductions, respectively (Figure 61 (right) for **CuTFac2**). In fact, upon scan reversal just after the first peak potential (I^{red}) only $\text{I}^{\text{ox},1}$ is observed (Figure 62 for **CuTFac2**). Upon further increase of the scan rate, the wave $\text{I}^{\text{red},2}$ displays a decreasing current intensity until it becomes undetectable at scan rates $\geq ca.$ 200 mV/s, when only the other reduction wave at I^{red} is visible.

Table 14. Cyclic voltammetric data^a for the mononuclear complexes.

Complex	CATHODIC WAVE		ANODIC WAVES ^b			
	$\text{I}^{\text{red},c}$	II^{red}	$\text{I}^{\text{ox},1}$	$\text{I}^{\text{ox},2}$	II^{ox}	
CuTFac1	[Cu(CF ₃ COO) ₂ (Hpz) ₄]	-0.15	-	-0.06	0.23	-
CuTFac2	[Cu(CF ₃ COO) ₂ (Hpz) ₂]	-0.20	-	0.01	0.27	-
CuSulf	[Cu(SO ₄)(Hpz) ₄]	-0.32	-	-0.10	0.28	-
CuPerchl	[Cu(ClO ₄) ₂ (Hpz) ₄]	-0.37	-	-0.07	0.32	-
CuBenz	[Cu(C ₇ H ₅ O ₂) ₂ (Hpz) ₂]	-0.26	-1.37	0.00	0.26	-0.18
CuForm	[Cu(HCOO) ₂ (Hpz) ₂]	-0.27	-1.82	0.01	0.31	-0.14
CuTFL	[Cu(CF ₃ SO ₃) ₂ (Hpz) ₄]	-0.16	-	-0.05	0.22	-

^a Potential values in Volt \pm 0.02 vs. SCE, in a 0.2 M [ⁿBu₄N][BF₄]/DMSO solution, at a Pt disc working electrode, determined by using the [Fe(η^5 -C₅H₅)₂]^{0/+} redox couple ($E_{1/2}^{\text{ox}} = 0.44$ V vs. SCE) as internal standard at a scan rate of 200 mVs⁻¹.

^b Only observed upon scan reversal following the reduction waves I^{red} and II^{red} .

^c Peak potential of the first reduction wave $\text{I}^{\text{red},1}$ (the reduction wave $\text{I}^{\text{red},2}$ at a close potential, is detected only at lower scan rates – see Figure 61)

No oxidation wave has been detected for any complex by a first anodic sweep without a previous reduction scan, indicating that neither a metal centered nor a ligand centered oxidation is observed.

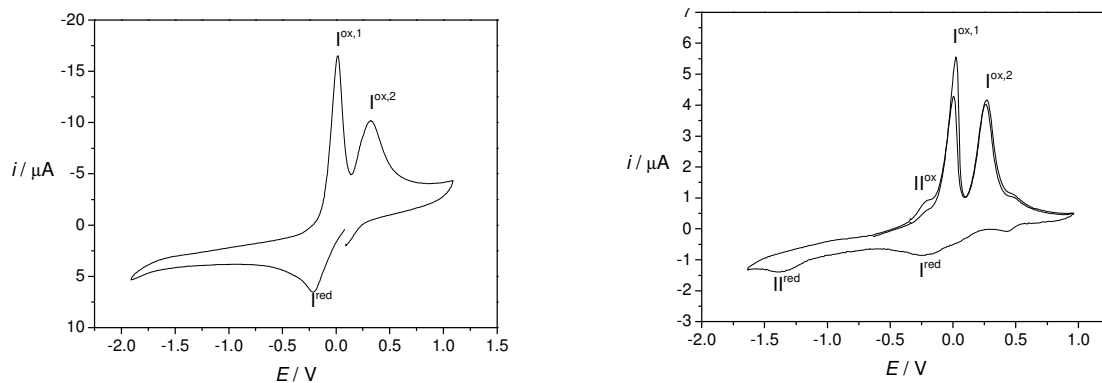


Figure 60. Cyclic voltammogram of **CuTFac2** (left), and of **CuBenz** (right, after the addition of ferrocene) in a 0.2 M [ⁿBu₄N][BF₄]/DMSO solution, at a Pt disc working electrode ($d = 0.5$ mm), at a scan rate of 200 mVs⁻¹.

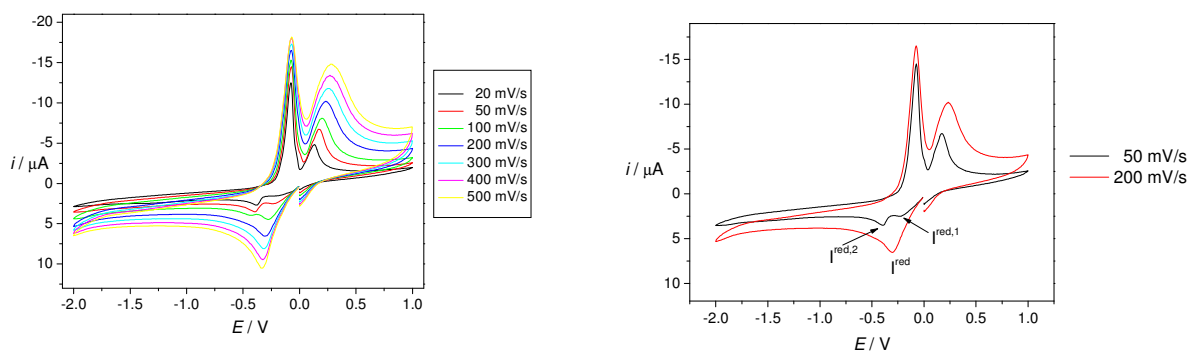


Figure 61. Cyclic voltammograms of **CuTFac2**, in a 0.2 M [ⁿBu₄N][BF₄]/DMSO solution, at a Pt disc working electrode (*d* = 0.5 mm).

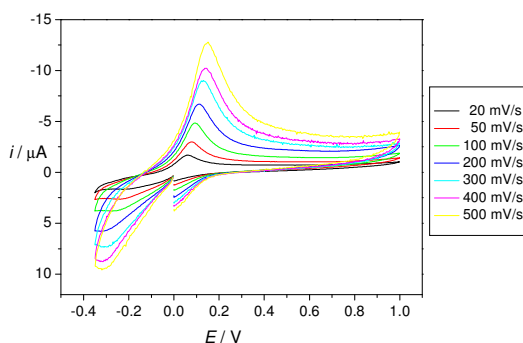


Figure 62. Cyclic voltammogram of **CuTFac2** with scan reversal just after the reduction wave $i^{red,1}$, in a 0.2 M [ⁿBu₄N][BF₄]/DMSO solution, at a Pt disc working electrode (*d* = 0.5 mm).

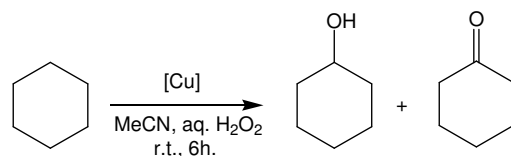
For the mononuclear complexes, the occurrence of a two-electron reduction per Cu^(II) atom was confirmed by exhaustive controlled potential electrolysis (CPE) at a Hg pool electrode at a potential slightly more cathodic than that of the reduction wave $i^{red,1}$ of **CuTFac2**. The CPE corresponds to a charge consumption of 2F/mol of complex, and leads to the deposition of metallic copper on the surface of the electrode.

Catalytic Activity Studies

Peroxidative oxidation of cyclohexane

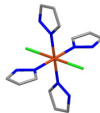
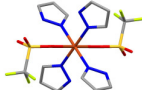
The strong interest about di-, tri- and polynuclear copper(II) complexes derives from the fact that copper has been recognised as a fundamental element in biological systems. As an example, copper species are present in numerous enzymes that selectively catalyse various oxidation reactions [Kaim et al. (1996); Holm et al. (1996); Klinman (1996); Cole et al. (1996); Elliot et al. (1997); Fraústo da Silva & Williams (2001); Itoh (2003); Lee (2003); Ayala & Torres (2004); Lieberman & Rozenweig (2004); Lieberman & Rozenweig (2005); Yoon & Solomon (2005)] including those performed by the still poorly characterized particulate methane monooxygenase (pMMO) present in methanotrophs, where a Cu cluster catalyses alkane hydroxylation and alkene epoxidation [Elliot et al. (1997); Lee (2003); Ayala & Torres (2004)]. Moreover, trinuclear arrays of copper(II) have been indicated as the essential functional units in numerous multicopper blue oxidases, such as laccase and ascorbate oxidases [Huber (1989)].

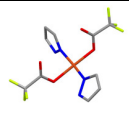




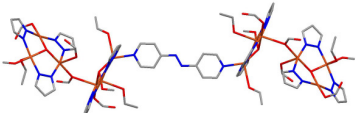
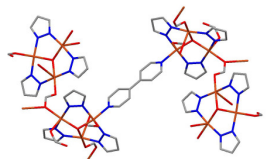
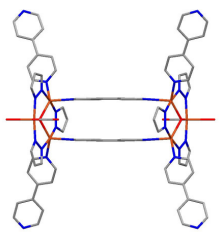
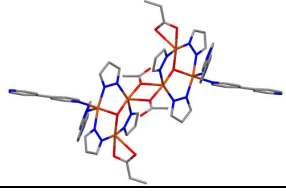
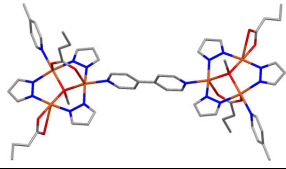
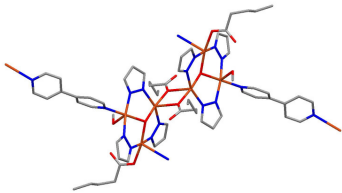
All the trinuclear triangular copper(II) complexes **1-10** have been tested, and behave as catalysts (or catalyst precursors) for the mild peroxidative oxidation of cyclohexane and cyclopentane with aqueous H₂O₂, at room temperature and atmospheric pressure, to the corresponding cyclic alcohols (*i.e.* cyclohexanol or cyclopentanol), and ketones (*i.e.* cyclohexanone or cyclopentanone), and the results have been previously reported [Di Nicola et al. (2007) (a); Di Nicola et al. (2009); Contaldi et al. (2009)].



During my PhD studies we also studied the catalytic activity in the peroxidative oxidation of cyclohexane of two coordination polymers obtained upon treatment of **2** with H₂SO₄ and CF₃COOH (**Cu3Sulf** and **Cu3TFAc**) and of some 4-pyridine-containing trinuclear derivatives described in the previous chapter (**Cu3FormAzopy**, **Cu3FormBpyL**, **Cu3FormBpyP**, **Cu3ProBpy**, **Cu3*ButBpy**, **Cu3ValBpy**). In Table 15 are shown all the above indicated compounds. Moreover, for comparative purposes, we also tested the activity of some Cu^(II)-pyrazole mononuclear derivatives in the same oxidation reaction. The complete list of the mono- and trinuclear Cu^(II) compounds employed is reported in Table 15.

Table 15. List of the catalyst precursors employed

Catalyst	Formula	Asymmetric unit
CuChl	[Cu(Cl) ₂ (Hpz) ₄]	
CuTFAc1	[Cu(CF ₃ COO) ₂ (Hpz) ₄]	

<u>CuTFAc2</u>	$[\text{Cu}(\text{CF}_3\text{COO})_2(\text{Hpz})_2]$	
<u>CuSulf</u>	$[\text{Cu}(\text{SO}_4)(\text{Hpz})_4]$	
<u>CuForm</u>	$[\text{Cu}(\text{HCOO})_2(\text{Hpz})_2]$	
<u>Cu3Sulf</u>	$[\text{Cu}_3(\mu_3\text{-OH})(\mu\text{-pz})_3(\text{SO}_4)(\text{Hpz})_3(\text{H}_2\text{O})]$	
<u>Cu3TFAc</u>	$[\text{Cu}_3(\mu_3\text{-OH})(\mu\text{-pz})_3(\text{CF}_3\text{COO})_2(\text{Hpz})_2]$	
<u>Cu3FormAzopy</u>	$[[\{\text{Cu}_3(\mu_3\text{-OH})(\mu\text{-pz})_3(\text{HCOO})_2(\text{EtOH})\} - [\text{Cu}_3(\mu_3\text{-OH})(\mu\text{-pz})_3(\text{HCOO})_2(\text{EtOH})_2]_2(\text{C}_{10}\text{H}_8\text{N}_4)]$	
<u>Cu3FormBpyL</u>	$[[\{\text{Cu}_3(\mu_3\text{-OH})(\mu\text{-pz})_3(\text{HCOO})_2(\text{H}_2\text{O})\} - [\text{Cu}_3(\mu_3\text{-OH})(\mu\text{-pz})_3(\text{HCOO})_2(\text{H}_2\text{O})(\text{MeOH})]_2(\text{C}_{10}\text{H}_8\text{N}_2)]$	
<u>Cu3FormBpyP</u>	$[\text{Cu}_3(\mu_3\text{-OH})(\mu\text{-pz})_3(\text{HCOO})(\text{OH})(\text{C}_{10}\text{H}_8\text{N}_2)_3]_2(\text{H}_2\text{O})]$	
<u>Cu3ProBpy</u>	$[\text{Cu}_3(\mu_3\text{-OH})(\mu\text{-pz})_3(\text{CH}_3\text{CH}_2\text{COO})_2(\text{C}_{10}\text{H}_8\text{N}_2)_2]$	
<u>Cu3*ButBpy</u>	$[\text{Cu}_3(\mu_3\text{-OCH}_3)(\mu\text{-pz})_3(\text{CH}_3(\text{CH}_2)_2\text{COO})_2(\text{C}_{10}\text{H}_8\text{N}_2)_2]$	
<u>Cu3ValBpy</u>	$[\text{Cu}_3(\mu_3\text{-OH})(\mu\text{-pz})_3(\text{CH}_3(\text{CH}_2)_3\text{COO})_2(\text{C}_{10}\text{H}_8\text{N}_2)(\text{CH}_3\text{OH})_2]$	

The activity and selectivity depend on different factors, such as the relative amounts of the reagents which can be varied in order to optimise the reaction conditions as reported for other catalytic systems employed in the functionalisation of alkanes [Kirillov et al. (2006); Kirillova et al. (2007); Kirillova et al. (2008); Kirillov et al. (2005); Karabach et al. (2006); Silva et al. (2008); Alegria et al. (2007); Kirillova et al. (2008); Mishra & Pombeiro (2005); Mishra & Pombeiro (2006); Mishra et al. (2007); Mishra et al. (2008)]. The obtained results are reported in the following paragraphs.

Effect of the Amount of Nitric Acid

The addition of acid to the system has been reported to increase the catalytic activity. This may be due to different reasons; for example, the acid can promote the unsaturation of the metal centre upon protonation of the ligands, and it can hamper the decomposition of hydrogen peroxide to give water and oxygen [Di Nicola et al. (2007); Di Nicola et al. (2009); Contaldi et al. (2009); Kirillov et al. (2006); Kirillov et al. (2005)].

Some selected data on the effect of the amount of HNO₃ on the catalytic activity of our Cu^(II) catalyst precursors are reported in Table 16, while in Figures 63 and 64 the behaviour of all the compounds is summarised. We observed that in the case of the mononuclear complexes (Figure 63) the highest yields were obtained without the addition of nitric acid, while in the case of the trinuclear derivatives the acid is required to maximise the yields. But, while in the case of **Cu3Sulf** and **Cu3TFAc** (Figure 64, left) the best yield was obtained with a 10:1 acid/catalyst molar ratio, in the case of **Cu3FormAzopy**, **Cu3FormBpyL**, **Cu3FormBpyP**, **Cu3ProBpy**, **Cu3*ButBpy**, **Cu3ValBpy**, increasing the molar ratio does not result in a general behaviour, maybe due to the complexity of our catalyst precursors (Figure 64, right). Since the addition of strong acids (nitric, hydrochloric, trifluoroacetic, sulfuric, trifluoromethanesulfonic, ...) to trinuclear copper(II) complexes can, to some extent, destroy the trinuclear triangular unit, leading to the formation of mononuclear species [Casarin et al. (2007) (a); Zanforlin (2007); Di Nicola et al. (2007) (b); Di Nicola et al. (2008)], it is possible that the observed results may be due to the fact that the effective catalyst of the oxidation reaction is a mononuclear species.

Table 16. Peroxidative oxidation of cyclohexane by some selected catalyst precursors. Effect of the amount of nitric acid.

entry	Catalyst ^a	<i>n</i> (HNO ₃)/ <i>n</i> (catalyst) ^b	Cyclohexanone		Cyclohexanol		Total	
			Yield (%)	TON	Yield (%)	TON	Yield (%)	TON
1	CuChI	0	4.2	4.2	15.6	15.6	19.8	19.8
2	CuChI	5	4.7	4.7	15.1	15.1	19.8	19.8
3	CuChI	10	2.5	2.5	14.4	14.4	16.6	16.6
4	CuChI	15	3.2	3.2	12.8	12.8	16.0	16.0
5	CuChI	20	3.0	3.0	11.0	11.0	14.0	14.0
6	Cu3Sulf	0	0.9	0.9	13.5	13.5	14.4	14.4
7	Cu3Sulf	5	1.0	1.0	12.0	12.0	13.0	13.0
8	Cu3Sulf	10	1.4	1.4	22.4	22.4	23.8	23.8
9	Cu3Sulf	15	1.1	1.1	19.5	19.5	20.6	20.6
10	Cu3Sulf	20	0.2	0.2	4.3	4.3	4.5	4.5
11	Cu3ValBpy	0	0.7	0.7	7.3	7.3	8.0	8.0
12	Cu3ValBpy	5	0.7	0.7	7.6	7.6	8.3	8.3
13	Cu3ValBpy	10	7.4	7.4	17.3	17.3	24.7	24.7
14	Cu3ValBpy	15	6.7	6.7	17.3	17.3	24.0	24.0
15	Cu3ValBpy	20	6.6	6.6	18.9	18.9	25.5	25.5
16	Cu3ValBpy	25	5.4	5.4	18.9	18.9	24.3	24.3
17	Cu3ValBpy	30	4.3	4.3	14.2	14.2	18.5	18.5

^a Reaction conditions: catalyst (10.0 μmol), C₆H₁₂ (1.0 mmol), MeCN (4 mL), HNO₃ (0-0.40 mmol), H₂O₂ (5.0 mmol).

^b *n*(HNO₃)/*n*(catalyst) has been calculated using the formulae given in Table 15.

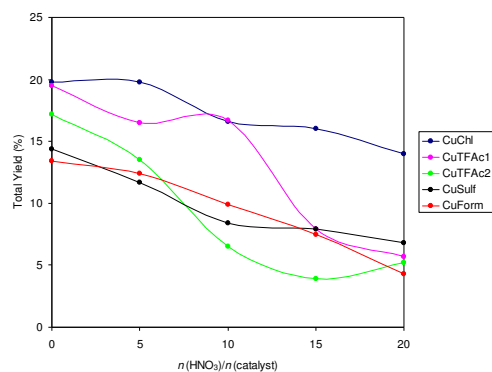


Figure 63. Peroxidative oxidation of cyclohexane. Effect of the amount of nitric acid in the case of the mononuclear complexes.

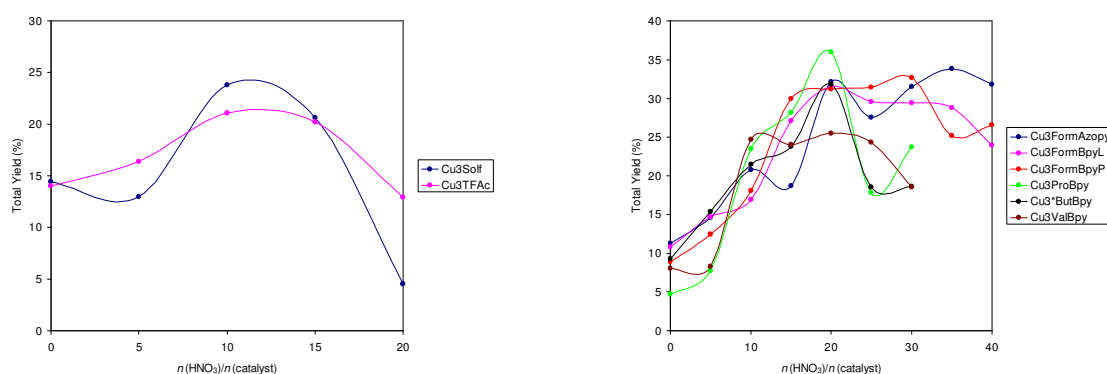


Figure 64. Peroxidative oxidation of cyclohexane. Effect of the amount of nitric acid in the case of trinuclear derivatives.

Effect of the Amount of Hydrogen Peroxide

The amount of hydrogen peroxide also has a pronounced effect on the yield of the reaction; the corresponding obtained data are summarised in Table 17 and in Figures 65 and 66, but it is to point out that it is very difficult to identify a general behaviour, likely due to the complexity of studied catalytic systems.

While increasing the $n(\text{H}_2\text{O}_2)/n(\text{substrate})$ ratio from 2.5 to 5 leads to the increase of the total yield for every catalyst, further increasing the $n(\text{H}_2\text{O}_2)/n(\text{substrate})$ ratio from 5 to 10 does not result in a general behaviour. In the case of complexes **CuTFac2**, **Cu3Sulf**, **Cu3FormAzopy**, **Cu3FormBpyL**, **Cu3FormBpyP**, **Cu3ProBpy** and **Cu3*ButBpy** an amount of 5 mmol of H_2O_2 [$n(\text{H}_2\text{O}_2)/n(\text{substrate}) = 5$] is required to maximize the yield of the reaction, but in the case of compounds **CuTFac1**, **CuSulf**, **CuChI**, **CuForm**, **Cu3TFac** and **Cu3ValBpy** it is necessary to use 10 mmol of oxidant [$n(\text{H}_2\text{O}_2)/n(\text{substrate}) = 10$]. Moreover, while in the case of catalysts **CuTFac1** and **CuTFac2** a plateau is reached, in the case of complexes **CuSulf**, **CuForm** and **Cu3TFac** the yield of the reaction continues to increase with the increase of $n(\text{H}_2\text{O}_2)/n(\text{substrate})$ ratio. Finally, in the case of compounds **Cu3Sulf**, **Cu3FormAzopy**, **Cu3FormBpyL**, **Cu3FormBpyP**, **Cu3ProBpy** and **Cu3*ButBpy** increasing the $n(\text{H}_2\text{O}_2)/n(\text{substrate})$ ratio from 5 to 10 leads to a drop of the reaction yield.

No oxidation products were detected in the absence of hydrogen peroxide. Since the reactions were performed under air, this means that molecular oxygen itself is not sufficient to oxidize the cyclohexane to the corresponding alcohol and ketone.

Table 17. Peroxidative oxidation of cyclohexane by some catalyst precursors. Effect of the amount of hydrogen peroxide.

entry	catalyst ^a	$n(\text{H}_2\text{O}_2)/n(\text{substrate})$	Cyclohexanone		Cyclohexanol		Total	
			Yield (%)	TON	Yield (%)	TON	Yield (%)	TON
1	CuChI	2.5	3.3	3.3	6.2	6.2	9.5	9.5
2	CuChI	5.0	4.2	4.2	15.6	15.6	19.8	19.8
3	CuChI	7.5	6.7	6.7	15.7	15.7	22.4	22.4
4	CuChI	10.0	8.0	8.0	16.4	16.4	24.4	24.4
5	Cu3TFac	2.5	0.8	0.8	12.3	12.3	13.1	13.1
6	Cu3TFac	5.0	1.7	1.7	19.4	19.4	21.1	21.1
7	Cu3TFac	7.5	1.6	1.6	19.0	19.0	20.6	20.6
8	Cu3TFac	10.0	4.7	4.7	19.2	19.2	23.9	23.9
9	Cu3FormBpyL	2.5	3.9	3.9	13.5	13.5	17.4	17.4
10	Cu3FormBpyL	5.0	7.0	7.0	24.5	24.5	31.5	31.5
11	Cu3FormBpyL	7.5	8.4	8.4	22.7	22.7	31.1	31.1
12	Cu3FormBpyL	10.0	5.2	5.2	10.0	10.0	15.2	15.2

^a Reaction conditions: catalyst (10.0 μmol), C_6H_{12} (1.0 mmol), MeCN (4 mL), HNO_3 (0 mmol for **CuChI**; 0.10 mmol for **Cu3TFac**; 0.20 mmol for **Cu3FormBpyL**, **Cu3ProBpy**, **Cu3*ButBpy** and **Cu3ValBpy**; 0.30 mmol for **Cu3FormBpyP**; 0.35 mmol for **Cu3FormAzopy**); H_2O_2 (2.5-10.0 mmol).

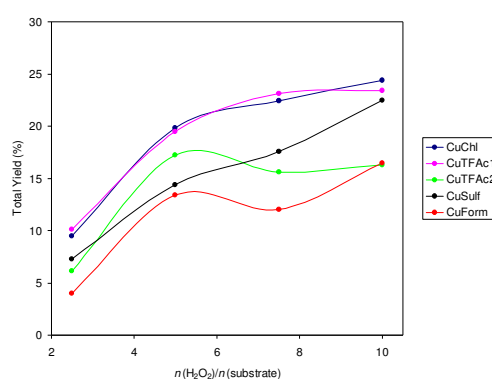


Figure 65. Peroxidative oxidation of cyclohexane. Effect of the amount of hydrogen peroxide in the case of the mononuclear complexes.

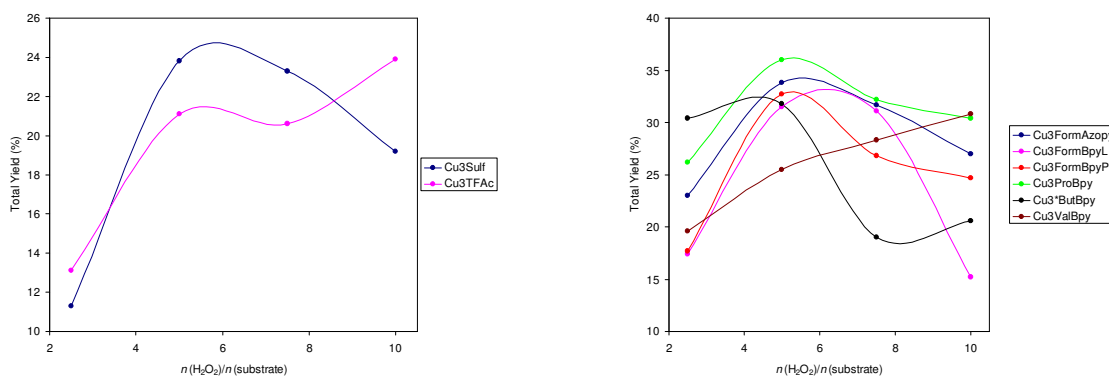


Figure 66. Peroxidative oxidation of cyclohexane. Effect of the amount of hydrogen peroxide in the case of trinuclear catalysts.

Effect of the catalyst amount

As evidenced in Table 18 and in Figure 67, decreasing the amount of catalyst leads to a decrease of the reaction yields. An enhancement of the overall TON is found for some of the complexes, reaching a maximum of 110 moles of oxidation products per mole of catalyst in the case of **Cu3ValBpy** (see Figure 68).

Table 18. Peroxidative oxidation of cyclohexane. Effect of the catalyst amount.

entry	catalyst ^a	catalyst amount, μmol	Cyclohexanone		Cyclohexanol		Total	
			Yield (%)	TON	Yield (%)	TON	Yield (%)	TON
1	CuChI	0.63	0.8	12.8	1.2	19.2	2.0	32.0
2	CuChI	1.25	1.7	13.6	3.5	28.0	5.2	41.6
3	CuChI	2.5	3.6	14.4	10.6	42.4	14.2	56.8
4	CuChI	5	6.2	12.4	14.7	29.4	20.9	41.8
5	CuChI	10	8.0	8.0	16.4	16.4	24.4	24.4
6	Cu3Sulf	0.63	0.2	3.1	0.0	0.0	0.2	3.1
7	Cu3Solf	1.25	0.4	3.2	0.6	4.8	1.0	8.0
8	Cu3Solf	2.5	0.4	1.5	6.4	25.6	6.8	27.1
9	Cu3Solf	5	1.0	2.0	14.1	28.2	15.1	30.2
10	Cu3Solf	10	1.4	1.4	22.4	22.4	23.8	23.8
11	Cu3ValBpy	0.63	1.5	24.0	5.2	83.2	6.7	107.2
12	Cu3ValBpy	1.25	2.1	16.8	11.7	93.6	13.8	110.4
13	Cu3ValBpy	2.5	3.6	14.4	22.7	90.8	26.3	105.2
14	Cu3ValBpy	5	6.9	13.8	20.5	41.0	27.4	54.8
15	Cu3ValBpy	10	9.9	9.9	20.9	20.9	30.8	30.8

^a Reaction conditions: catalyst (0.63-10.0 μmol); C_6H_{12} (1.0 mmol); MeCN (4 mL); HNO_3 (0 mmol for **CuChI**; 0.10 mmol for **Cu3Sulf**; 0.20 mmol for **Cu3ValBpy**); H_2O_2 (5 mmol for **Cu3Sulf**; 10mmol for **CuChI** and **Cu3ValBpy**).

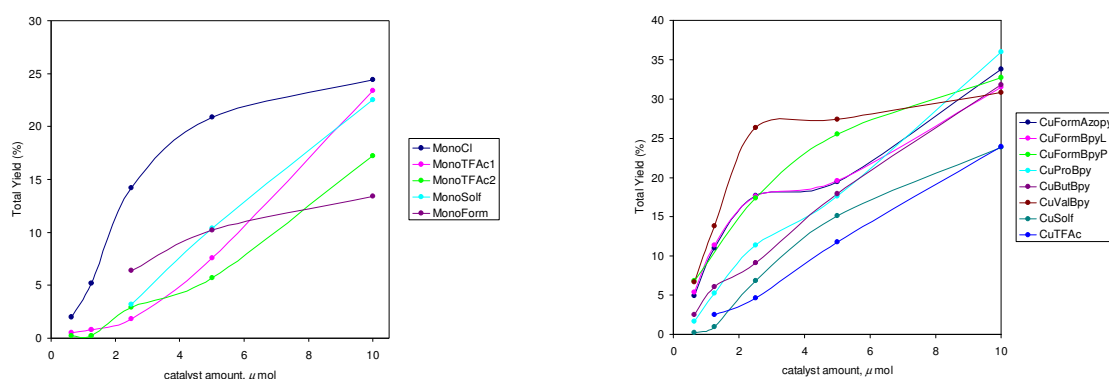


Figure 67. Peroxidative oxidation of cyclohexane. Effect of the catalyst amount on the total yield of the reaction.

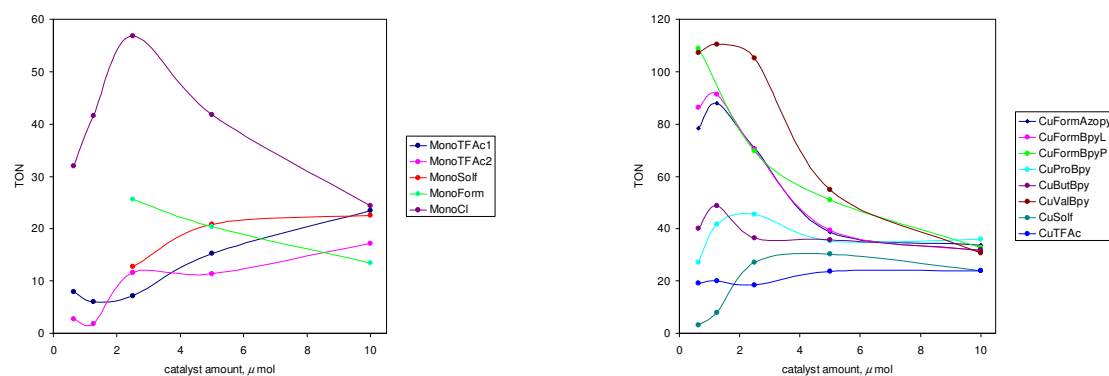


Figure 68. Peroxidative oxidation of cyclohexane. Effect of the catalyst amount on the total TON.

Effect of Radical Traps

The results obtained by using different radical trapping agents [CBrCl_3 (carbon radical trap), Ph_2NH (oxygen radical trap) and 2,6-di-*tert*-butyl-4-methyl-phenol (BHT) (radical trapping agent both for carbon and oxygen radicals)] evidence a radical pathway for the reaction, leading to a dramatic decrease of the yield of the oxidation products. In particular, the addition to the reaction mixture of CBrCl_3 essentially suppressed the formation of the products and cyclohexyl bromide was formed in the reaction mixture, thus showing that the cyclohexyl radical was generated and trapped. Data obtained for compound **Cu3ProBpy** are summarized in Table 19.

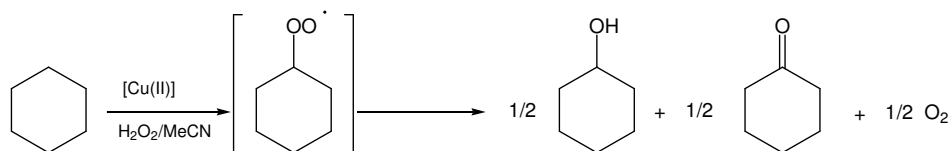
Table 19. Peroxidative oxidation of cyclohexane. Effect of radical traps.

catalyst ^a	radical trap	$n(\text{rad.trap})/$ $n(\text{C}_6\text{H}_{12})$	$n(\text{rad.trap})/n(\text{H}_2\text{O}_2)$	Yield of products (%)			Yield drop owing to rad. trap ^b (%)
				Cyclohexanone	Cyclohexanol	Total	
CuTFAc2	-	-	-	1.6	15.6	17.2	-
CuTFAc2	CBrCl ₃	1.0	0.2	0.4	1.2	1.6	91
CuTFAc2	BHT	1.0	0.2	2.1	3.7	5.8	66
CuTFAc2	Ph ₂ NH	5.0	1.0	0.2	1.4	1.6	91
1 Cu3ProBpy	-	-	-	5.5	30.5	36	-
2 Cu3ProBpy	CBrCl ₃	1.0	0.2	0	0	0	99
3 Cu3ProBpy	BHT	1.0	0.2	3.2	9.1	12.3	66
4 Cu3ProBpy	Ph ₂ NH	5.0	1.0	0.4	1.8	2.2	94

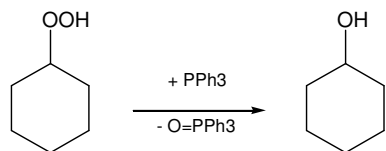
^a Reaction conditions: catalyst (10.0 μmol); C₆H₁₂ (1.0 mmol); MeCN (4 mL); HNO₃ (0 mmol for **CuTFAc2**; 0.20 mmol for **Cu3ProBpy**); H₂O₂ (5 mmol).

^b (1 – total yield with radical trap/total yield without radical trap) x 100.

It has been reported in the literature that the main product of the peroxidative oxidation of cyclohexane is cyclohexylhydroperoxyde, which, during the reaction partially decomposes to give the corresponding alcohol and ketone.

**Scheme 3.**

On the basis of the suggested radical pathway, an alkylperoxy radical is expected to be involved, according to Scheme 3 [Shul'pin et al. (2001); Shul'pin (2002); Shul'pin et al. (2003)]. This radical can disproportionate via the so-called Russel termination step, giving an approximate 1:1 alcohol/ketone molar ratio [Russel (1957); Kim et al. (1996)]. At the end of the reaction time, the reaction mixture will contain cyclohexylhydroperoxyde, cyclohexanol and cyclohexanone. Since the hydroperoxyde is not detectable by GC analysis (it decomposes in the chromatograph to give mainly a mixture of roughly 1:1 of cyclohexanol and cyclohexanone, apart from some other compounds not detectable in GC), samples are usually treated with an excess of PPh₃ prior the GC analysis in order to decompose quantitatively the cyclohexylhydroperoxyde to the corresponding alcohol, according to Scheme 4 [Shul'pin (2002)].

**Scheme 4.**

In order to confirm the formation of the hydroperoxyde as the main product of the reaction, some tests were run and the samples taken were analysed before and after the addition of PPh₃.

Table 20. Peroxidative oxidation of cyclohexane. Yields of oxigenates before and after treatment with PPh₃.

entry	Catalyst	Yield without PPh ₃ (%)			Yield with PPh ₃ (%)		
		Cyclohexanol	Cyclohexanone	Total	Cyclohexanol	Cyclohexanone	Total
1	CuTFac1	7.7	14.1	21.8	18.1	5.3	23.4
2	CuTFac2	3.7	7.6	11.3	15.6	1.6	17.2
3	CuSulf	7.2	13.0	20.2	16.4	6.1	22.5
4	Cu3TFac	10.4	12.3	22.7	19.2	4.7	23.9

^a Reaction conditions: catalyst (10.0 μmol); C₆H₁₂ (1.0 mmol); MeCN (4 mL); HNO₃ (0 mmol for **CuTFac1**, **CuTFac2** and **CuSulf**; 0.10 mmol for **Cu3TFac**); H₂O₂ (5 mmol for **CuTFac2**; 10 for **Cu3TFac**, **CuTFac1** and **CuSulf**.)

The total yield of the reaction is always higher after the addition of PPh₃, as summarised in Table 20, and this is because, as already mentioned, if a sample taken from the reaction mixture is injected in the GC as it is, the hydroperoxyde will be decomposed not only to the corresponding alcohol and ketone, but also to some other not detectable compounds, while the addition of the phosphine decomposes quantitatively the hydroperoxyde to the corresponding alcohol, which is detectable in GC. Treating the sample with the phosphine, it is possible to calculate the exact amount of ketone produced during the reaction (which, according to Scheme 3, is equal to the alcohol amount) and estimate the yield of the hydroperoxyde simply by subtracting the obtained amount of ketone from the total yield of the alcohol. The obtained data are summarised in Table 21.

Table 21. Peroxidative oxidation of cyclohexane. Estimated yields of the oxigenates after treatment with PPh₃.

entry	Catalyst	Total yield of	Yield of	Yield of	Yield of
		cyclohexanol (%)	cyclohexanone (%)	cyclohexanol (%)	cyclohexylhydroperoxyde (%)
1	CuTFac1	18.1	5.3	5.3	12.8
2	CuTFac2	15.6	1.6	1.6	14.0
3	CuSulf	16.4	6.1	6.1	10.3
4	Cu3TFac	19.2	4.7	4.7	14.5

^a Reaction conditions: catalyst (10.0 μmol); C₆H₁₂ (1.0 mmol); MeCN (4 mL); HNO₃ (0 mmol for **CuTFac1**, **CuTFac2** and **CuSulf**; 0.10 mmol for **Cu3TFac**); H₂O₂ (5 mmol for **CuTFac2**; 10 mmol for **Cu3TFac**, **CuTFac1** and **CuSulf**.)

In any case, it is important to notice that the mechanism reported in Scheme 3 is just a simplification of the real reaction mechanism. In fact, some tests were run using cyclohexanol as substrate, and they demonstrated that a small part of the cyclohexanone can derive not only from the decomposition of the alkylhydroperoxyde but also from the oxidation of the alcohol. The obtained data for catalysts **CuTFac2** and **Cu3TFac** are summarized in Table 22.

Table 22. Peroxidative oxidation of cyclohexanol.

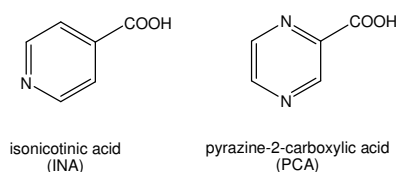
entry	Catalyst	Yield of cyclohexanone (%)
1	CuTFac2	5.1
2	Cu3TFac	3.3

^a Reaction conditions: catalyst (10.0 μmol); C₆H₁₁OH (1.0 mmol); MeCN (4 mL); HNO₃ (0 mmol for **CuTFac2**; 0.10 mmol for **Cu3TFac**); H₂O₂ (5 mmol for **CuTFac2**; 10 for **Cu3TFac**.)

Effect of different additives

A high promoting effect of heteroaromatic acids on the oxidation of alkanes (and other substrates) catalysed by various homogeneous vanadium species [Shul'pin et al. (1993); Shul'pin (2002)] and iron containing compounds [Nizova et al. (2002); Shul'pin et al (2004)] has previously been recognized by Shul'pin et al.; a similar co-catalytic effect on the oxyfunctionalisation of cyclic and linear alkanes with dioxygen catalyzed by oxovanadium or pyrazole-rhenium complexes supported on modified silica gel was also observed [Mishra & Pombeiro (2005); Mishra & Pombeiro (2006); Mishra et al. (2006); Shul'pin et al (2007); Mishra et al. (2008)].

We investigated the effect of different heteroaromatic additives, such as pyrazinecarboxylic acid (PCA) and isonicotinic acid (INA) on the catalytic activity of $[\text{Cu}_3(\mu_3\text{-OH})(\mu\text{-pz})_3(\text{CH}_3\text{COO})_2(\text{Hpz})]$, **2**; the influence of hydrochloric acid was tested as well for comparison purposes. The obtained data are reported in Table 23.



The catalytic activity of complex **2** in the peroxidative oxidation of cyclohexane in the presence of nitric acid was already reported [Di Nicola et al. (2009)]. In that case, the maximum total yield of oxidation products, obtained by using $n(\text{H}_2\text{O}_2)/n(\text{substrate}) = 5$ and $n(\text{HNO}_3)/n(\text{catalyst}) = 10$, was 31.0%. In the case of hydrochloric acid addition, the maximum total yield, in the same conditions, is 15.6%, which is more or less the half obtained using HNO_3 . In the case of pyrazinecarboxylic acid, the total yield is even lower (10.8%), while employing isonicotinic acid no oxidation products were detected.

Hydrochloric acid is a strong mineral acid, which differs from nitric acid by the better coordinating capability of the chloride ion compared to NO_3^- . Isonicotinic acid and pyrazinecarboxylic acid are heterocyclic nitrogen-containing compounds. It is possible that Cl^- ions and the heteroaromatic acids coordinate to the copper centres, saturating the coordination environment around the metal ions and thus decreasing the catalytic activity.

Table 23. Peroxidative oxidation of cyclohexane. Effect of different additives.

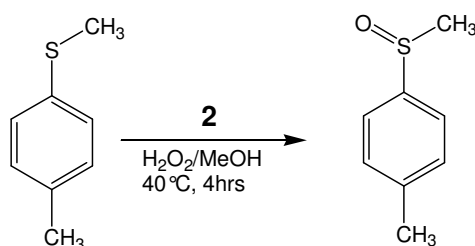
	catalyst ^a	additive	$n(\text{additive})/n(\text{catalyst})$	Cyclohexanone		Cyclohexanol		Total	
				Yield (%)	TON	Yield (%)	TON	Yield (%)	TON
1	2	HCl	0	0.6	0.6	3.0	3.0	3.6	3.6
2	2	HCl	5	1.9	1.9	3.3	3.3	5.2	5.2
3	2	HCl	10	5.1	5.1	10.5	10.5	15.6	15.6
4	2	HCl	15	3.3	3.3	10.1	10.1	13.4	13.4
5	2	HCl	20	2.4	2.4	8.6	8.6	11.0	11.0
6	2	PCA	0	2.8	2.8	8.0	8.0	10.8	10.8
7	2	PCA	5	0.2	0.2	0.1	0.1	0.3	0.3
8	2	PCA	10	-	-	-	-	-	-
9	2	PCA	15	-	-	-	-	-	-
10	2	PCA	20	-	-	-	-	-	-
11	2	INA	0	-	-	-	-	-	-
12	2	INA	5	-	-	-	-	-	-
13	2	INA	10	-	-	-	-	-	-
14	2	INA	15	-	-	-	-	-	-
15	2	INA	20	-	-	-	-	-	-

^a Reaction conditions: catalyst (10.0 μmol); C_6H_{12} (1.0 mmol); MeCN (4 mL); $n(\text{additive})/n(\text{catalyst})=0-20$; $n(\text{H}_2\text{O}_2)/n(\text{substrate})=5$.

Oxidation of methyl-*p*-tolyl-sulfide

Sulfoxides and other organosulfur compounds are important synthetic intermediates in organic chemistry, and are valuable in the preparation of biologically and pharmaceutically relevant materials [Carreño (1995); Fernández & Khiar (2003); Caron et al. (2006)]. An important oxidation reaction in pharmaceutical research and production is the oxidation of a sulfide to a sulfoxide, which is achieved with a large variety of reagents and catalysts [Caron et al. (2006)]. On the other hand, sulfoxides can undergo overoxidation to sulfones and therefore it is important that the catalyst has a low reactivity toward the sulfoxides [Dell'Anna et al. (2000); Venkataramanan et al. (2005)].

Due to the potentiality as oxidation catalyst of the trinuclear triangular Cu^{II} assembly above described, we started studying the catalytic activity of the trinuclear derivative $[\text{Cu}_3(\mu_3\text{-OH})(\mu\text{-pz})_3(\text{CH}_3\text{COO})_2(\text{Hpz})]$, **2**, in the oxidation of methyl-*p*-tolyl-sulfide to the corresponding sulfoxide.



The reaction was carried out in methanol, at 40 °C, using hydrogen peroxide as oxidant. Preliminary results showed that **2** is a catalyst precursor for the reaction. In fact, sulfide conversion is higher in the presence of **2** than in the blank experiments. It must be highlighted that at 40 °C the yield in sulfoxide is only 48.0%, probably due to partial decomposition of hydrogen peroxide. For limiting this competing path, further experiments will be performed at lower temperature.

Table 24. Oxidation of methyl-*p*-tolyl-sulfide. Preliminary results.

Catalyst	Reaction time	Yield (%)	
1	-	2 hours	7.5
2	2	2 hours	48.0
3	-	4 hours	16.0
4	2	4 hours	46.5

At the moment, the attention has been focused on the intermediates of **2** in the oxidation reaction. We observed that the solution of **2** in methanol, which is blue, turns green upon H_2O_2 addition. The change in the colour of the solution suggests that probably some Cu-based peroxo intermediate is formed. The change in the colour is evidenced by a shift in the absorption band in the UV-vis spectrum from 624 nm (which is characteristic for complex **2**) to 601 nm, as shown in Figure 69.

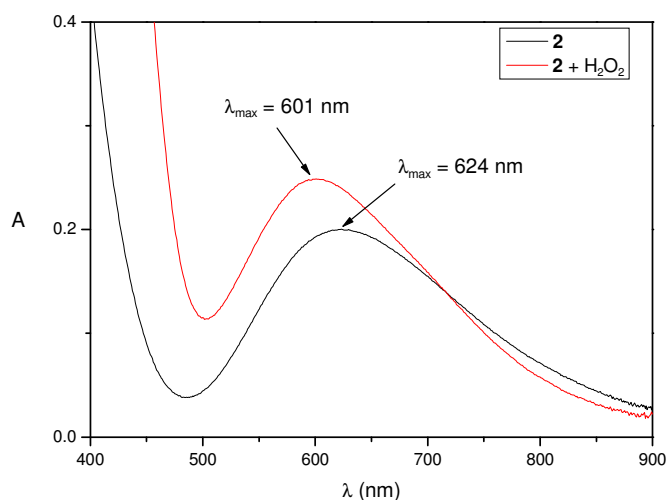


Figure 69. UV-vis spectrum of **2** in MeOH before the addition of H₂O₂ (black line) and after the addition of H₂O₂ (red line).

A titration, followed by UV-vis spectroscopy, was done to check the stoichiometry for the formation of the intermediate, and evidenced that 2 equivalents of H₂O₂ are required for the formation of the intermediate. Interestingly, in the absence of the sulphide substrate, the green solution then gradually turns again blue after more or less 12 hours, suggesting progressive decomposition of the intermediate formed upon H₂O₂ addition. The kinetic of decomposition of the intermediate was followed by UV-vis spectroscopy. Some of the recorded spectra are shown in Figure 70.

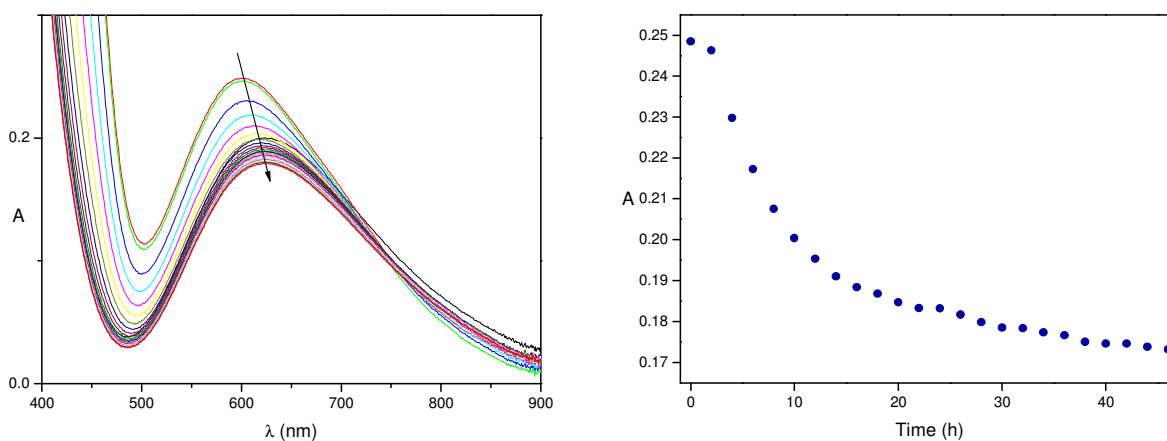


Figure 70. Left: selected UV-vis spectra of **2** + H₂O₂ in MeOH; the shift of the maximum position from 601 nm to 624 nm is shown. Right: plot of the adsorbance at 601 nm vs. time.

The solution was then let to slowly evaporate in the air, and after a couple of days some blue well-formed crystals were isolated. Their X-ray single crystal analysis confirmed that compound **2** was formed again. This evidence is quite interesting, because it suggests that in these conditions it may be possible to recover and recycle the catalyst precursor **2**. Most importantly, it also suggests that the trinuclear triangular moiety is very likely maintained in the structure of the effective catalyst.

Conclusions and future perspectives

During the three years of my PhD studies, the attention was focused on the design and synthesis of new coordination polymers. Among the possible strategies to make a CP, the easiest method is to react a potentially bridging ligand with a metal ion having more than one vacant or labile site [James (2003)]. This approach implies the use of accurately designed polynucleating ligands, having geometries capable to promote the assembly of more metal centres, thus directly generating polymeric systems.

During the first year, two different families of potentially polynucleating ligands were synthesised and characterised. These two classes are based on the *s*-triazine [Casarin et al. (2007) (b); Casarin et al. (2008) (a); Pettinari et al. (2009)] and on the oxalic and malonic skeletons [Garau et al. in the press], bearing in all the cases azolate fragments as coordinating nitrogen-based centres. Unfortunately, some preliminary tests on the reactivity of these ligands with Cu^(II), Ag^(I), Zn^(II) and Ru^(II) in hydroalcoholic solvents evidenced the relatively easy hydrolysis of the ligands. At the moment, the study of the coordination properties of these ligands to transition metal ions has been set aside, and the attention has been focused on the understanding of the decomposition mechanism upon treatment with transition metal compounds. Particularly, concerning the *s*-triazine derivative **1**, first studies on the binding properties of the TPM fragment towards Cu^(I) and Ag^(I) ions have been carried out. DFT has been used to look into the electronic structure of [M(TPM)]⁺ molecular ion conformers (M = Cu, Ag) and to study the energetics of their interconversion [Casarin et al. (2008) (b); Casarin et al. (2009)]. We recently started a similar theoretical study to better understand the decomposition of the oxalate and malonate based ligands in protic conditions. Moreover, from an experimental point of view, we are planning to study the reactivity of our ligands in aprotic conditions, with the aim to prevent their decomposition.

An alternative approach for the synthesis of CPs exploits the formation of small stable metal-clusters (SBUs), in which ligand coordination modes and metal coordination environments can be used to transform these fragments into extended porous networks by using polytopic linkers [Eddaoudi et al. (2001)]. In the case of the trinuclear Cu^(II) complexes, the spontaneous formation of stable triangular [Cu₃(μ₃-OH)(μ-pz)₃]²⁺ SBUs was observed upon reaction between Cu^(II) carboxylates and pyrazole in hydroalcoholic solvent. These trinuclear Cu^(II) clusters self assemble in the solid state through carboxylate bridges (in some cases assisted by hydrogen bonds), giving rise to different coordination polymers, in which the trinuclear triangular SBUs can be considered as a sort of monomers. In this context, a series of new trinuclear triangular Cu^(II) derivatives, both from saturated and unsaturated copper(II) carboxylates, were synthesised and characterised. Moreover, their electrochemical properties and catalytic activity in the peroxidative oxidation of cycloalkanes were investigated [Garau et al. (2008); Di Nicola et al. (2009); Contaldi et al. (2009)]. In the last months we started also a study about the catalytic activity of the acetate based trinuclear triangular derivative **2** in the oxidation of methyl-*p*-tolyl-sulfide to the corresponding sulfoxide. Preliminary results indicate that **2** is able to bind reversibly oxygen coming from H₂O₂ and transfer it to sulfides.

Some studies [Casarin et al. (2007) (a); Zanforlin (2007); Di Nicola et al. (2007) (b); Di Nicola et al. (2008)] proved that the trinuclear triangular [Cu₃(μ₃-OH)(μ-pz)₃]²⁺ core of our Cu^(II) CPs is quite stable

towards decomposition. Particularly, even though upon reaction of **2** with strong acids in all the cases mononuclear complexes were isolated (indicating that, in some extent, the starting trinuclear cluster was destroyed), the concurrently formed tri-, hexa- and heptanuclear derivatives (sometimes assembled in CPs, PCPs or extended supramolecular networks) evidenced that the trinuclear triangular core is stable enough to be worthy of consideration as possible starting material to obtain different CPs. On the bases of these results, we decided to exploit also their expected reactivity towards the displacement of neutral molecules (pyrazole and/or solvent molecules) with bridging neutral ligands, aiming to synthesise novel materials, having the trinuclear Cu^(II) clusters connected by polynucleating neutral ligands. In particular, we focused our attention on a family of ligands having two 4-pyridine rings (*i.e.* the donor units) connected by different spacers [*i.e.* 4,4'-bipyridine, 1,2-bis(4-pyridyl)ethane, 1,2-bis(4-pyridyl)ethylene, 1,3-bis(4-pyridyl)propane, 1,2-bis(4-pyridyl)diazene and 1,2-bis(4-pyridyl)disulfane]. New CPs were isolated and, in many cases, well-formed crystals were obtained, which let possible in some cases the determination of their XRD crystal structure, while in other cases XRD analysis is still in progress. Among the results obtained until now, and not yet published, it is noteworthy that, upon reaction between **1** and an excess of 4,4'-bipyridine, a porous coordination polymer, **Cu₃FormBpyP**, was obtained. All the new CPs were characterised and some of them were tested as catalyst precursors in the peroxidative oxidation of cyclohexane.

We are planning both to complete the characterisation of the obtained coordination polymers, paying special attention to the porous ones, and to synthesise new materials by using different nitrogen-based ligands, such as diamines. We also intend to synthesise new CPs by displacing the monocarboxylates with bicarboxylates (both saturated and unsaturated), in order to get more stable frameworks. Some preliminary tests were already performed, under bench-top conditions; reactions between compound **1** and the bicarboxylic acids lead to the isolation of the starting materials, while using sodium bicarboxylates, powders were formed. We are planning to repeat the reactions under solvothermal conditions, employing both conventional heating techniques and microwave radiation. We are planning to examine more in-depth the catalytic activity of our CPs in the oxidation of methyl-*p*-tolyl sulfide, and to extend the studies of the catalytic activity to other relevant oxidation reactions, both in homogeneous and in heterogeneous conditions. Finally, we will also test our CPs in gas sorption measurements.

Experimental Data

Materials and Methods. All the reactions and manipulations were carried out in air. Excluding formate and acetate (Aldrich), copper(II) carboxylates were prepared according to previously reported procedures [Martin & Waterman (1957)] which were in some cases slightly modified. Trinuclear triangular Cu(II) derivatives **1-4** were prepared as previously reported [Casarin et al. (2004); Casarin et al. (2005); Di Nicola et al. (2007)]. Trispyrazolylmethane (TPM) and trispyrazolyethanol (TPEtOH) were synthesised as described in the literature by Reger *et al.* [Reger et al. (2000)]. Elemental analyses (C, H, N) were performed with a Fisons Instruments 1108 CHNS-O elemental analyzer. Infrared spectra from 4000 to 600 cm^{-1} were recorded in a Perkin Elmer Spectrum One Model Fourier Transform Infrared (FTIR) spectrometer with ATR mode. Diamond type crystal in single bounce was used in the ATR. Approximately 30-35 mg of the sample was employed for each analysis. The electrical conductances of methanol or water solutions were measured with a Crison CDTM 522 conductimeter at room temperature. Positive electrospray mass spectra were obtained with a Series 1100 MSI detector HP spectrometer, using MeOH as mobile phase. Solutions for electrospray ionization mass spectrometry (ESI-MS) were prepared using reagent grade methanol, water and/or acetonitrile, and obtained data (masses and intensities) were compared with those calculated by using the IsoPro isotopic abundance simulator [Senko (1994)]. Peaks containing copper(II) ions are identified as the higher signal of isotopic clusters. The magnetic susceptibilities were measured at room temperature (20-28 °C) by the Gouy method with a Sherwood Scientific magnetic balance MSB-Auto, using $\text{HgCo}(\text{NCS})_4$ as calibrant and corrected for diamagnetism with the appropriate Pascal constants. The magnetic moments (in μB) were calculated from the equation $\mu_{\text{eff}} = 2.84(X_m^{\text{corr}} T)^{1/2}$. UV-Vis spectra were recorded on a Varian Cary 5E spectrophotometer. The electrochemical experiments were performed on an EG&G PAR 273A potentiostat/galvanostat connected to a computer through a GPIB interface. Cyclic voltammograms (CV) were obtained in 0.2 M solutions of $[\text{Bu}_4\text{N}][\text{BF}_4]$ in DMSO, at a platinum disc working electrode ($d = 0.5$ mm) and at 25 °C. The electrochemical experiments were performed on an EG&G PAR 273A potentiostat/galvanostat connected to a computer through a GPIB interface. Cyclic voltammograms (CV) were obtained in 0.2 M solutions of $[\text{Bu}_4\text{N}][\text{BF}_4]$ in DMSO, at a platinum disc working electrode ($d = 0.5$ mm) and at 25 °C. Controlled-potential electrolysis (CPE) was carried out in electrolyte solutions with the above-mentioned composition, in a three-electrode H-type cell, in which the two compartments were separated by a sintered glass frit and equipped with a mercury pool working electrode and a platinum-gauze counter electrode. For both CPE and CV experiments, a silver-wire pseudo-reference electrode was used. In the CV cell, a Pt wire was employed as counter-electrode. The CPE experiments were monitored regularly by CV, thus ensuring that no significant potential drift occurred along the electrolysis. The electrochemical experiments were performed under a N_2 atmosphere at room temperature. The potentials of the complexes were measured by CV in the presence of ferrocene as the internal standard, and the redox potential values are normally quoted relative to the SCE by using the $[\text{Fe}(\eta^5\text{-C}_6\text{H}_5)_2]^{0/+}$ redox couple ($E_{1/2}^{\text{ox}} = 0.44$ V vs SCE) in a 0.2 M $[\text{Bu}_4\text{N}][\text{BF}_4]$ /DMSO solution.

Crystallographic data collection and structure determination. The X-ray intensity data were measured on a Bruker Apex II CCD diffractometer. Cell dimensions and the orientation matrix were initially determined from a least-squares refinement on reflections measured in three sets of 20 exposures, collected in three different ω regions, and eventually refined against all data. A full sphere of reciprocal space was scanned by 0.3° ω steps. The software SMART [SMART & SAINT (1998)] was used for collecting frames of data, indexing reflections and determination of lattice parameters. The collected frames were then processed for integration by the SAINT program [SMART & SAINT (1998)], and an empirical absorption correction was applied using SADABS [Sheldrick (1996)]. The structures were solved by direct methods (SIR 97) [Altomare et al. (1999)] and subsequent Fourier syntheses and refined by full-matrix least-squares on F^2 (SHELXTL) [Sheldrick (1998)] using anisotropic thermal parameters for all non-hydrogen atoms. XRPD diffraction investigations were carried out by means of a PANalytical X'Pert Pro diffractometer equipped with an X'Celerator fast detector and using Cu/K α radiation. Molecular graphics were generated by using the program Mercury 1.4.2 [Macrae et al. (2006)]. Color codes for all molecular graphics: orange (Cu), blue (N), red (O), yellow (S, P), light green (F), green (Cl), grey (C), white (H).

NMR Experimental Section. ^1H , ^{13}C and ^{15}N NMR spectra were obtained as CDCl_3 or $\text{DMSO-}d_6$ solutions on a Bruker DRX-400 spectrometer operating at 400.13, 100.61 and 40.56 MHz, respectively, and equipped with a BVT2000 temperature controller. The chemical shift values are given in δ units with reference to Me_4Si for ^1H and ^{13}C , and MeNO_2 for ^{15}N . Suitable integral values for the proton spectra were obtained by a pre-scan delay of 10 s to ensure a complete relaxation for all the resonances. The proton assignments were performed by standard chemical shift correlations as well as by 2D *CORrelation SpectroscopY* (COSY), *TOTAL Correlation SpectroscopY* (TOCSY), and *Nuclear Overhauser Enhancement SpectroscopY* (NOESY) experiments. The ^{13}C and ^{15}N chemical shift values were obtained through 2D-heteronuclear correlation experiments (*Heteronuclear Multiple Quantum Correlation*, (HMQC), with *Bilinear Rotation-Decoupling*, BIRD, sequence [Bax & Subramian (1986); Drobny et al. (1979)] and quadrature along F1 achieved using the *Time-Proportional receiver Phase Incrementation*, TPPI, method [Otting & Wüthrich (1988)] for the H-bonded carbon and nitrogen atoms, and *Heteronuclear Multiple Bond Correlation*, HMBC, [Bax & Summers (1986)] for the other ^{13}C and ^{15}N nuclei).

Catalytic activity studies - Peroxidative oxidation of cyclohexane. To 0.63-10 μmol (typically 10 μmol) of catalyst contained in the reaction flask were added 4.0 mL of MeCN, 0.00 - 0.40 mmol of HNO_3 (65% in H_2O), 1.0 mmol of cyclohexane, and 2.50 - 10.00 mmol of H_2O_2 (30% in H_2O). The reaction mixture was stirred at room temperature for 6 h, whereafter 130 μL of nitromethane (as internal standard), 9.0 mL of diethyl ether (to extract the products and the substrate from the reaction mixture) and 1.0 g of PPh_3 (to reduce the organo-hydroperoxydes, if formed) were added. The resulting mixture was stirred for 15 min, and then a sample taken from the organic phase was analysed by GC using a Fisons Instrument GC 8000 series gas chromatograph with a DB-624 capillary column (P/N 124-1334) and the Jasco-Borwin v.1.50 software. In the experiments with radical

traps, the suitable compound, e.g. 2,6-di-*tert*-butyl-4-methyl-phenol (BHT), CBrCl₃ or Ph₂NH, was also added to the reaction mixture.

Catalytic activity studies - Oxidation of methyl-*p*-tolyl-sulfide. To 3 μmol of catalyst (complex **2**) contained in the reaction flask were added 3.0 mL of MeOH, 100 μmol of methyl-*p*-tolyl-sulfide and 0.6 mmol of H₂O₂. The reaction mixture was stirred at 40°C; a small sample was taken after 2 hours and 4 hours reaction time, and analysed by GC using a Shimadzu instrument GC-2010 gas chromatograph with a Supelco EquityTM-5 capillary column and the Shimadzu GC Solution software. Blank experiments were performed to check the oxidation properties of the system in the absence of the catalyst.

In the following are reported the experimental procedures and characterization data concerning only the until now unpublished compounds. For the other compounds synthesised during my PhD studies, please refer to specific, published, papers [Casarin et al. (2008); Contaldi et al. (2009); Di Nicola et al. (2009); Garau et al. (2010) in the press].

Synthesis of Polynucleating Nitrogen Ligands

Synthesis of 2-chloro-4,6-di(1H-pyrazol-1-yl)-1,3,5-triazine, j.

To a stirred solution of cyanuric chloride (540 mg, 2.9 mmol) and N,N-diisopropylethylamine (DIPEA) (0.98 mL, 766 mg, 5.8 mmol) in 20 mL of toluene, a solution of pyrazole (403 mg, 5.8 mmol) in 20 mL of toluene was added drop-wise, obtaining the immediately precipitation of a white solid. The mixture was stirred at 25°C for 24 h and the solvent was then removed under reduced pressure, leaving a white solid, which was vigorously stirred for 30 minutes with 25 mL of water, filtered, washed with further 20 mL of water and dried under vacuum.

j. Yield 582 mg, 81%. m.p. 161-163°C dec. Anal. Calcd for C₉H₆ClN₇: C 43.65; H 2.44; N 39.59. Found C 43.48; H 2.23; N 38.32. IR (KBr, cm⁻¹): 3436, 3174, 3150, 3129, 1563, 1522, 1445, 1396, 1306, 1265, 1027, 938, 830, 801, 770. ESI-MS (+) (MeOH, MeCN) (higher peaks, m/z; relative abundance, %): 248.1 (100) [C₉H₆N₇Cl+H]⁺, 270.0 (30) [C₉H₆N₇Cl+Na]⁺, 321.1 (50) [C₉H₆N₇Cl(MeOH)(MeCN)+H]⁺. ¹H NMR (δ, CDCl₃, 25°C): H₃ 7.97 (dd, ³J_{HH}, 1.2 Hz; ⁴J_{HH}, 0.6 Hz), H₄ 6.61 (dd, ³J_{HH}, 2.9 Hz; ³J_{HH}, 1.2 Hz), H₅ 8.68 (dd, ³J_{HH}, 2.9 Hz; ⁴J_{HH}, 0.6 Hz). ¹³C NMR (δ, CDCl₃, 25°C): C₃ 147.02, C₄ 111.17, C₅ 130.89, C' 173.68, C'' 162.98. ¹⁵N NMR (δ, CDCl₃, 25°C): N₁ -155, N₂ -75.

Synthesis of N,N'-bis(4,6-di(1H-pyrazol-1-yl)-1,3,5-triazin-2-yl)ethane-1,2-diamine, k.

A solution of j (626 mg, 2.5 mmol) and DIPEA (0.43 mL, 336 mg, 2.5 mmol) in 40 mL of toluene was heated to 80°C and ethylenediamine (86 μL, 77 mg, 1.3 mmol) was added drop-wise with stirring. Immediately upon addition a white solid formed and the mixture was stirred and maintained at 80°C for 48 h. The solvent was then removed under reduced pressure, leaving a pale orange solid which was stirred at r.t. for 30 minutes with 20 mL of water resulting in a white solid which was filtered, washed with water, diethyl ether and dried under vacuum.

k. Yield 377 mg, 63%. mp > 200°C. Anal. Calcd. for C₂₀H₁₈N₁₆: C 49.79; H 3.76; N 46.45. Found C 47.75; H 4.01; N 45.55. IR (KBr, cm⁻¹): 3423, 3285, 3153, 1593, 1553, 1527, 1448, 1396, 1344, 1078, 1040, 954, 806. ESI-MS (+) (MeOH, MeCN) (higher peaks, m/z; relative abundance, %): 483.3 (70) [C₂₀H₁₈N₁₆+H]⁺, 505.2 (45) [C₂₀H₁₈N₁₆+Na]⁺, 987.3 (100) [(C₂₀H₁₈N₁₆)₂+Na]⁺. ¹H NMR (δ, DMSO-*d*₆, 25 °C): CH₂ 3.72 (s), NH 8.84 (t, ³J_{HH}, 5 Hz), H₃ 7.85 (dd, ³J_{HH}, 1.5 Hz; ⁴J_{HH}, 0.7 Hz), H₃ 7.86 (dd, ³J_{HH}, 1.5 Hz; ⁴J_{HH}, 0.7 Hz), H₄ 6.55 (dd, ³J_{HH}, 1.5 Hz; ³J_{HH}, 2.7 Hz), H₄ 6.61 (dd, ³J_{HH}, 1.5 Hz; ³J_{HH}, 2.7 Hz), H₅ 8.69 (dd, ³J_{HH}, 2.8 Hz; ⁴J_{HH}, 0.7 Hz), H₅ 8.77 (dd, ³J_{HH}, 2.9 Hz; ⁴J_{HH}, 0.7 Hz). ¹³C NMR (δ, DMSO-*d*₆, 25 °C): CH₂ 40.61, C₃ 145.07, C₄ 109.99, C₅ 131.11. ¹⁵N NMR (δ, DMSO-*d*₆, 25 °C): N₁ -151.6, N₂ -69.4, N₃ -180.2, NH -273.3 (¹J_{NH}, 93 Hz).

Synthesis of 2,4,6-tris(tri(1H-pyrazol-1-yl)methyl)-1,3,5-triazine, l.

A solution of TPM, [Reger et al. (2000)] (502 mg, 2.3 mmol) in 30 mL of anhydrous THF was cooled to ca. -80°C and a solution of *n*-BuLi in hexane (1.5 mL, 1.6 M, 2.4 mmol) was added, drop-wise with stirring. Immediately upon the addition a white solid formed. The mixture was allowed to warm to r.t. and then solid cyanuric chloride (148 mg, 0.8 mmol) was cautiously added, obtaining a yellow solution. The mixture was refluxed for 3 days and then water (30 mL) and diethyl ether (20 mL) was added. The organic layer was collected and water solution was extracted with diethyl ether (3 x 15 mL). The

organic extracts were combined, dried over MgSO_4 and filtered. The solvent was removed under reduced pressure yielding a light-yellow solid which was vigorously shaken with 40 mL of a diethyl ether/hexane solution (1/7), filtered and dried under vacuum. Yield 342 mg, 60%. Compound **I** was recrystallised from acetone, yielding white crystal suitable for an X-ray crystal structure determination.

I. m.p. 177-179°C dec. Anal. Calcd for $\text{C}_{33}\text{H}_{27}\text{N}_{21}$: C 55.22; H 3.79; N 40.98. Found C 55.07; H 3.59; N 41.76. IR (KBr, cm^{-1}): 3417, 3137, 1556, 1523, 1421, 1358, 1331, 1261, 1196, 1100, 812, 751. ^1H NMR (δ , CDCl_3 , 25°C): $\text{H}_{3(5)}$ 7.59 (dd, $^3J_{\text{HH}}$, 1.8 Hz; $^4J_{\text{HH}}$, 0.7 Hz), H_4 6.27 (dd, $^3J_{\text{HH}}$, 1.8 Hz; $^3J_{\text{HH}}$, 2.6 Hz), $\text{H}_{5(3)}$ 7.57 (dd, $^3J_{\text{HH}}$, 2.6 Hz; $^4J_{\text{HH}}$, 0.7 Hz). ^{13}C NMR (δ , CDCl_3 , 25°C): C_3 141.54, C_4 107.11, C_5 132.51. ^{15}N NMR (δ , CDCl_3 , 25°C): N_1 -162.8, N_2 -69.1.

Synthesis of 2,4,6-tris(2,2,2-tri(1H-pyrazol-1-yl)ethoxy)-1,3,5-triazine, m.

To a solution of TPEtOH, [Reger et al. (2000)] (500 mg, 2.0 mmol) in 30 mL of anhydrous THF cooled to ca. -80°C a solution of MeLi in hexane (1.3 mL, 1.6 M, 2.1 mmol) was added, drop-wise with stirring. The mixture was allowed to warm to r.t. and then a solution of cyanuric chloride (126 mg, 0.7 mmol) in 10 mL of anhydrous THF was drop-wise added. The mixture was refluxed for 5 hours and then water (30 mL) and diethyl ether (20 mL) were added. The organic layer was collected and the water solution was extracted with diethyl ether (3 x 15 mL). The organic extracts were combined, dried over MgSO_4 and filtered. The solvent was removed under reduced pressure yielding a white solid which was vigorously shaken with 40 mL of a diethyl ether/hexane solution (10/1), filtered and dried under vacuum.

m. Yield 428 mg, 78%. m.p. 183-186°C dec. Anal. Calcd, for $\text{C}_{36}\text{H}_{33}\text{N}_{21}\text{O}_3$: C 53.53; H 4.12; N 36.41. Found C 53.40; H 4.00; N 36.43. IR (KBr, cm^{-1}): 3155, 1585, 1572, 1560, 1519, 1407, 1349, 1318, 1159, 1040, 947, 886, 865, 817, 791, 759, 743. ESI-MS (+) (MeOH, MeCN) [higher peaks, m/z; relative abundance, % (fragmentor 30)]: 227.3 (40) [$\text{C}_{36}\text{H}_{33}\text{N}_{21}\text{O}_3+2\text{H}+\text{Na}$] $^{3+}$, 740.8 (18) [$\text{C}_{36}\text{H}_{33}\text{N}_{21}\text{O}_3-\text{pz}$] $^+$, 830.8 (100) [$\text{C}_{36}\text{H}_{33}\text{N}_{21}\text{O}_3+\text{Na}$] $^+$. ESI-MS (+) (MeOH, MeCN) [higher peaks, m/z; relative abundance, % (fragmentor 300)]: 227.3 (100) [$\text{C}_{36}\text{H}_{33}\text{N}_{21}\text{O}_3+2\text{H}+\text{Na}$] $^{3+}$. ^1H NMR (δ , CDCl_3 , 25°C): $\text{H}_{3(5)}$ 7.65 ($^3J_{\text{HH}}$, 1.74 Hz; $^4J_{\text{HH}}$, 0.64 Hz), H_4 6.35 ($^3J_{\text{HH}}$, 1.74 Hz; $^3J_{\text{HH}}$, 2.66 Hz), $\text{H}_{5(3)}$ 7.31 ($^3J_{\text{HH}}$, 2.66 Hz; $^4J_{\text{HH}}$, 0.64 Hz), H_7 5.96. ^{13}C NMR (δ , CDCl_3 , 25°C): C_8 172.31, C_3 141.77, C_5 130.59, C_4 107.18, C_6 88.98, C_7 70.08. ^{15}N NMR; (δ , CDCl_3 , 25°C) N_3 -172.4, N_1 -161.4, N_2 -71.7.

Reactivity of Polynucleating Nitrogen Ligands with Some Transition Metal Ions

Reaction of I with $\text{Ag}(\text{CF}_3\text{SO}_3)$. Formation of $[\{\text{Ag}(\text{TPM})\}_2](\text{CF}_3\text{SO}_3)_2$, I_a .

A solution of I (172 mg, 0.2 mmol in 20 mL of MeOH) was added to a solution of $\text{Ag}(\text{CF}_3\text{SO}_3)$ (154 mg, 0.6 mmol) in 20 mL of MeOH. The colourless solution was stirred 4h at room temperature, then was evaporated under vacuum until a colourless, crystalline solid formed which was filtered off and identified as $[\{\text{Ag}(\text{tpm})\}_2](\text{CF}_3\text{SO}_3)_2$, I_a , [Reger et al. (2006)] through elemental analysis, ^1H NMR and XRD characterizations. Yield 65% with respect to starting silver triflate.

I_a . m.p. 170°C dec. Anal. Calcd. for $\text{C}_{11}\text{H}_{10}\text{AgF}_3\text{N}_6\text{O}_3\text{S}$: C 28.04; H 2.14; N 17.84; S 6.80. Found C 28.27; H 2.39; N 18.11; S = 6.76. IR (KBr, cm^{-1}): 3140, 3130, 1609, 1573, 1522, 1462, 1377, 1257, 1160, 1100, 1054, 1027, 979, 953, 916, 882, 859, 840, 811, 797, 762, 722, 636, 573, 517, 390, 371, 352. ^1H NMR (δ , CDCl_3 , 25°C): H_4 6.51 (dd, $^3J_{\text{HH}}$, 1.8 Hz; $^3J_{\text{HH}}$, 2.6 Hz), $\text{H}_{5(3)}$ 7.74 (d, $^3J_{\text{HH}}$, 1.8 Hz) $\text{H}_{3(5)}$ 8.06 (d, $^3J_{\text{HH}}$, 2.6 Hz).

Reaction of I with $\text{Cu}(\text{NO}_3)_2 \cdot 2.5\text{H}_2\text{O}$. Formation of $[\text{Cu}(\text{TPM})_2](\text{NO}_3)_2$, I_b .

A solution of I (87 mg, 0.1 mmol) in 20 mL MeOH was added drop-wise to a solution of $\text{Cu}(\text{NO}_3)_2 \cdot 2.5\text{H}_2\text{O}$ (33 mg, 0.1 mmol) in 20 mL MeOH. The resulting blue solution was allowed to evaporate in the air, yielding few blue crystals, that elemental analysis and XRD characterization revealed to be compound I_b [Astley et al. (1993)]. Yield 42% with respect to starting copper nitrate.

Reaction of I with $\text{Zn}(\text{CF}_3\text{SO}_3)_2$. Formation of $[\text{Zn}(\text{TPM})_2](\text{CF}_3\text{SO}_3)_2$, I_c .

A solution of I (172 mg, 0.2 mmol) in 20 mL of MeOH was added to a solution of $\text{Zn}(\text{O}_3\text{SCF}_3)_2 \cdot \text{H}_2\text{O}$ (229 mg, 0.6 mmol) in 20 mL of MeOH. The colorless solution was stirred 4h at room temperature, then stored at 0°C overnight. Pale-yellow crystals, suitable for an XRD determination formed which were filtered off, washed with Et_2O and identified as $[\text{Zn}(\text{tpm})_2](\text{CF}_3\text{SO}_3)_2$, I_c , in 35% yield with respect to starting zinc triflate.

I_c . m.p. 186°C dec. Anal. Calcd. for $\text{C}_{22}\text{H}_{20}\text{F}_6\text{N}_{12}\text{O}_6\text{S}_2\text{Zn}$: C 33.37; H 2.55; N 21.22; S 8.10. Found C 33.12; H 2.28; N 20.93; S 7.91. IR (KBr, cm^{-1}): 3140, 3130, 1578, 1549, 1527, 1409, 1292, 1200, 1166, 1110, 1094, 1029, 960, 920, 889, 857, 824, 810, 755, 722, 638, 597, 574, 517, 410, 389, 351. ^1H NMR (δ , CDCl_3 , 25°C): H_4 6.52 (dd, $^3J_{\text{HH}}$, 1.8 Hz; $^3J_{\text{HH}}$, 2.6 Hz), $\text{H}_{5(3)}$ 7.43 (d, $^3J_{\text{HH}}$, 1.8 Hz) $\text{H}_{3(5)}$ 8.74 (d, $^3J_{\text{HH}}$, 2.6 Hz), 10.46 (s, CH). Λ_m (DMSO, conc. = $0.95 \cdot 10^{-3}\text{M}$): $113 \Omega^{-1}\text{mol}^2\text{cm}^{-1}$.

Reaction of I with $[\{\text{RuCl}_2(\text{cymene})\}_2]$. Formation of $[\text{Ru}(\text{TPM})(\text{cymene})]\text{Cl}(\text{OH}) \cdot 2\text{H}_2\text{O}$, I_d .

A solution of I (172 mg, 0.2 mmol) in 20 mL of MeOH was added to a solution of $[\{\text{RuCl}_2(\text{cymene})\}_2]$ (186 mg, 0.3 mmol) in 20 mL of MeOH. The colourless solution was stirred 4h at room temperature, then was evaporated under vacuum until a colourless precipitate formed which was filtered off and identified as $[\text{Ru}(\text{tpm})(\text{cymene})]\text{Cl}(\text{OH}) \cdot 2\text{H}_2\text{O}$, I_d , in 50% yield with respect to the starting $[\{\text{RuCl}_2(\text{cymene})\}_2]$.

I_d . m.p. 200°C dec. Anal. Calcd. for $\text{C}_{20}\text{H}_{25}\text{ClN}_6\text{O}_3\text{Ru}$: C 44.65; H 5.43; N 15.62; Found C 44.33; H 5.49; N 15.61. IR (nujol, cm^{-1}): 3400, 3140, 3110, 1700, 1307, 1277, 1169, 1153, 1101, 105, 967, 860, 768, 722, 602, 549, 536, 447, 406, 386, 280. ^1H NMR (δ , CDCl_3 , 25°C): 1.24 (H_{CH_3} , d, 8.8 Hz), 2.49 (H_{CH_3} , s); 3.18 (H_{CH} , m, 8.8 Hz), 6.54 (CH_{cym} , dd), 6.77 (H_4 , dd, $^3J_{\text{HH}}$, 1.8 Hz; $^4J_{\text{HH}}$, 2.6 Hz), 8.45 ($\text{H}_{3(5)}$, dd, $^3J_{\text{HH}}$, 1.8 Hz; $^4J_{\text{HH}}$, 0.7 Hz), 8.86 ($\text{H}_{5(3)}$, dd, $^3J_{\text{HH}}$, 2.6 Hz; $^4J_{\text{HH}}$, 0.7 Hz), 9.62 (CH, s).

Reactivity of Trinuclear Triangular Cu^(II) Derivative

To facilitate the readers, here are reported the formulas and corresponding numbers of all the trinuclear triangular Cu^{II} compounds employed as starting materials in the following reactions.

- 1: [Cu₃(μ₃-OH)(μ-pz)₃(HCOO)₂(Hpz)₂(H₂O)]
- 2: [Cu₃(μ₃-OH)(μ-pz)₃(CH₃COO)₂(Hpz)]
- 3: [Cu₃(μ₃-OH)(μ-pz)₃(CH₃CH₂COO)₂(EtOH)]
- 4: [Cu₃(μ₃-OH)(μ-pz)₃(CH₃(CH₂)₂COO)₂(MeOH)(H₂O)]
- 5: [Cu₃(μ₃-OH)(μ-pz)₃(CH₃(CH₂)₃COO)₂(H₂O)]
- 6: [Cu₃(μ₃-OH)(μ-pz)₃(CH₃(CH₂)₄COO)₂(EtOH)]
- 7: [Cu₃(μ₃-OH)(μ-pz)₃(CH₃(CH₂)₅COO)₂(EtOH)]
- 8: [Cu₃(μ₃-OH)(μ-pz)₃(CH₂=CHCOO)₂(H₂O)₂(Hpz)]
- 9: [Cu₃(μ₃-OH)(μ-pz)₃(CH₂=CHCOO)₂(MeOH)]
- 10: [Cu₃(μ₃-OH)(μ-pz)₃(CH₂=C(CH₃)COO)₂]

Reactivity of the Trinuclear Triangular Cu^(II) Derivative **2** with Strong Acids

Reaction of **2** with H₂SO₄.

Synthesis of [Cu₃(μ₃-OH)(μ-pz)₃(SO₄)(Hpz)₃].H₂O, **Cu3Sulf**, and [Cu(SO₄)(Hpz)₄].H₂O, **CuSulf**.

To a suspension of 1.007 g of **2** (1.69 mmol) in 150 mL of deionised water, 21 mL of a 0.17 M water solution of H₂SO₄ (3.51 mmol) was added under stirring. The solid dissolved almost completely in ca. 30 min, a little insoluble material (ca. 50 mg) was filtered off and the solution was let to stay undisturbed at rt. In about 15 days two different, pure, crystal fractions (**Cu3Sulf** and **CuSulf**) were collected, dried in the air and examined.

Cu3Sulf. Yield: 231 mg, 41%. mp: >210 °C. Anal. Calcd for C₁₈H₂₄Cu₃N₁₂O₆S: C 29.73; H 3.33; N 23.11. Found: C 29.04; H 2.92; N 23.14. IR (KBr, cm⁻¹): 3450-3127, 1328, 1111, 766, 620. ESI-MS (+) (MeOH) (higher peaks, m/z; relative abundance, %) 69.2 (46) [Hpz+H]⁺, 199.0 (50) [Cu^(I)(Hpz)₂]⁺, 424.9 (28) [Cu₂(SO₄)(pz)₂(MeOH)(H₂O)₂+H]⁺, 623.8 (100) [Cu₃(OH)(pz)₃(SO₄)(Hpz)(MeOH)(H₂O)+H]⁺. μ_{eff} (295 K) = 2.603 BM. UV-Vis spectrum: λ_{max}/nm (MeOH solution 2.92·10⁻³ M) 639 (ε = 62).

CuSulf. Yield: 251 mg, 36%. Anal. Calcd for C₁₂H₁₈CuN₈O₄S: C 32.03; H 4.03; N 24.90. Found: C 31.29; H 4.49; N 24.94. UV-Vis spectra: λ_{max}/nm (MeOH solution 4.58·10⁻³ M) 713 (ε = 42). This compound has been previously reported. Its analytical and spectral data are in agreement with those already described in literature [Shen et al. (2004)].

Reaction of **2** with H₃PO₄.

Synthesis of [Cu(H₂PO₄)₂(Hpz)₄], **CuPhosph**.

To a suspension of 979 mg of **2** (1.64 mmol) in 20 mL of deionised water, 10.5 mL of a 0.354 M water solution of H₃PO₄ (3.72 mmol) was added under stirring. The solid dissolved almost completely in ca. 30 min, a little insoluble material (ca. 30 mg) was filtered off and the solution was let to stay undisturbed in the air at rt. In about a week a light blue, unidentified solid precipitated which was filtered off and eliminated. In about another week from mother liquors a dark blue crystalline fraction was obtained, which was filtered, dried in the air and identified as **CuPhosph**.

CuPhosph. Yield: 250 mg, 9%. mp.: 180 °C dec. Anal. Calcd. for C₁₂H₂₀CuN₈O₈P₂: C 27.20; H 3.80; N 21.15. Found: C 25.24, H 3.65, N 20.22. IR (KBr, cm⁻¹): 3277-3127, 1148, 1122, 1150, 906, 759, 606. ESI-MS (+) (MeOH) (higher peaks, m/z; relative abundance, %) 69.2 (85) [Hpz+H]⁺, 199.0 (100) [Cu^(I)(Hpz)₂]⁺; ESI-MS (+) (H₂O) (higher peaks, m/z; relative abundance, %) 69.2 (100) [Hpz+H]⁺, 198.0 (15) [Cu(pz)(Hpz)₂]⁺, 199.0 (5) [Cu^(I)(Hpz)₂]⁺, 216.1 (5) [Cu(pz)(Hpz)(H₂O)]⁺, 266.0 (15) [Cu(pz)(Hpz)₂]⁺, 296.0 (45) [Cu(H₂PO₄)(Hpz)₂]⁺. μ_{eff} (295 K) = 2.003 BM. UV-Vis spectra: λ_{max}/nm (H₂O solution 8.08·10⁻³ M) 715 (ε = 25).

Reaction of **2** with HClO₄.

Safety note – Even though we have never encountered problems (excluding in the execution of melting points), it is to be remembered that perchlorates should be handled with appropriate precaution, being known for their potential hazardous behavior.

Synthesis of $[\text{Cu}(\text{ClO}_4)_2(\text{Hpz})_4]$, CuPerchl, and $[\{\text{Cu}_3(\mu_3\text{-OH})(\mu\text{-pz})_3(\text{ClO}_4)(\text{Hpz})_3\}_2(\mu_2\text{-ClO}_4)_2]$, Cu6Perchl.

To a suspension of 100 mg of **2** (0.17 mmol) in 15 mL of deionised water, 1.8 mL of a 0.41 M water solution of HClO_4 (0.63 mmol) was slowly added under stirring. The solid dissolved almost completely in ca. 45 min, a little insoluble material (ca. 6 mg) was filtered off and the solution was let to stay undisturbed at rt. In about 15 days two crystalline fractions formed, which were collected, dried in the air and examined.

CuPerchl. Yield: 21 mg, 27%. m.p. 235-237°C (melts) and at 240°C bursts. Anal. Calcd for $\text{C}_{12}\text{H}_{16}\text{Cl}_2\text{CuN}_8\text{O}_8$: C 26.95; H 3.02; N 20.95. Found: C 26.73; H 2.95; N 21.40. IR (KBr, cm^{-1}): 3365-3136, 1408, 1382, 1357, 1144-1065, 775, 695, 624. μ_{eff} (295 K) = 2.014. UV-Vis spectra: $\lambda_{\text{max}}/\text{nm}$ (MeOH solution $4.26 \cdot 10^{-3}$ M) 705 ($\epsilon = 26$).

Cu6Perchl. Yield: 18 mg, 23%. mp: 245°C, bursts. Anal. Calcd for $\text{C}_{36}\text{H}_{44}\text{Cu}_6\text{Cl}_4\text{N}_{24}\text{O}_{18}$: C 26.63; H 2.73, N 20.70. Found: C 25.84; H 2.68; N 20.72. IR (KBr, cm^{-1}): 3362-3136, 1475, 1410, 1358, 1114-1048, 786, 763, 695, 626. μ_{eff} (295 K) = 3.18 BM. UV-Vis spectra: $\lambda_{\text{max}}/\text{nm}$ (MeOH solution $1.29 \cdot 10^{-3}$ M) 665 ($\epsilon = 309$). Λ_{M} (MeOH, $1 \cdot 10^{-3}$ M): $360 \Omega^{-1} \text{ mol}^2 \text{ cm}^{-1}$.

Reaction of 2 with HNO_3 .

Synthesis of $[\text{Cu}_3(\mu_3\text{-OH})(\mu\text{-pz})_3(\text{NO}_3)(\mu_3\text{-NO}_3)(\text{Hpz})_2]$, Cu3Nitr, $[\{\text{Cu}_3(\mu_3\text{-OH})(\mu\text{-pz})_3(\text{NO}_3)(\text{Hpz})_3\}_2(\mu_2\text{-NO}_3)_2]$, Cu6Nitr and $[\text{Cu}(\text{NO}_3)_2(\text{Hpz})_4]$, CuNitr.

To a suspension of 510 mg of **2** (0.86 mmol) in ca. 25 mL of deionized water, 8 mL of a 0.396 M water solution of HNO_3 (3.17 mmol) was added under stirring. The solid dissolved almost completely, a little insoluble material (ca. 20 mg) was filtered off and the solution was concentrated under vacuum to ca. 20 mL and then let to stay undisturbed at r.t. In about a week three pure crystalline fractions were obtained, which were collected, dried in the air and examined, yielding the results reported below.

Cu3Nitr. Yield 125 mg, 22%. Anal. Calcd. for $\text{Cu}_3\text{C}_{15}\text{H}_{18}\text{O}_7\text{N}_{12}$: C 26.93; H 2.71; N 25.12. Found: C 25.98; H 2.83; N 4.91. This compound has been previously reported. Its analytical and spectral data agree with those described in literature [Hulsbergen et al. (1983)].

Cu6Nitr. This compound, obtained in very low yield, has been previously described by Yamaguchi and coworkers [Sakai et al. (1996)]. Its analytical and spectral data agree with those reported in literature.

CuNitr. Also this compound, obtained in 19% yield (230 mg), has been previously described by Yamaguchi and coworkers [Sakai et al. (1996)]. Its analytical and spectral data agree with those reported in literature.

Reaction of 2 with CF_3COOH .

Synthesis of $[\text{Cu}_3(\mu_3\text{-OH})(\mu\text{-pz})_3(\text{CF}_3\text{COO})_2(\text{Hpz})_2]$, Cu3TFAc, $[\text{Cu}(\text{CF}_3\text{COO})_2(\text{Hpz})_4]$, CuTFAc1, and $[\text{Cu}(\text{CF}_3\text{COO})_2(\text{Hpz})_2]$, CuTFAc2.

To a suspension of 2.00 g of **2** (3.37 mmol) in ca. 100 mL of deionized water, 30 mL of a 0.41 M water solution of CF_3COOH (12.28 mmol) was slowly added under stirring. The solid dissolved almost completely, a little insoluble material (ca. 100 mg) was filtered off and the solution was let to stay

undisturbed at rt. In about 15 days three pure crystal fractions were collected, dried in the air and examined, yielding the results reported below.

Cu3TFac. Yield: 294 mg, 11%. m.p.: >210 °C. Anal. Calcd. for C₁₉H₁₈Cu₃F₆N₁₀O₅: C 29.60; H 2.35, N 18.17. Found: C 29.60; H 2.65; N 18.52. IR (KBr, cm⁻¹): 3450-3139, 1673, 1431, 1405, 1381, 1204, 1142, 768, 723, 626. ESI-MS (+) (MeOH) (higher peaks, *m/z*; relative abundance, %) 476.1 (10), [Cu₃(OH)₂(pz)₃(MeOH)(H₂O)]⁺, 555.2 (10), [Cu₂(OH)(CF₃COO)₂(Hpz)₂(MeOH)(H₂O)]⁺, 590.2 (10), [Cu₃(OH)(pz)₃(CF₃COO)(Hpz)]⁺, 604.2 (73), [Cu₃(OH)(pz)₃(CF₃COO)(MeOH)₂(H₂O)]⁺, 636.3 (26), [Cu₃(OH)(pz)₃(CF₃COO)(MeOH)₃(H₂O)]⁺ or [Cu₃(OH)(pz)₃(CF₃COO)₂+H]⁺, 672.3 (100), [Cu₃(OH)(pz)₃(CF₃COO)(Hpz)(MeOH)₂(H₂O)]⁺, 718.3 (20), [Cu₃(OH)(pz)₃(CF₃COO)(Hpz)(MeOH)₄]⁺. UV-Vis spectra: λ_{max}/nm (MeOH solution 2.85·10⁻³ M) 643 (ε = 173).

CuTFac1. Yield: 278 mg, 5%. m.p.: 168-170 °C. Anal. Calcd. for C₁₆H₁₆CuF₆N₈O₄: C 34.20; H 2.87; N 19.94. Found: C 33.85; H 3.12; N 20.17. IR (KBr, cm⁻¹): 3289-3061, 1669, 1463, 1406, 1376, 1358, 1206, 1128, 1067, 769, 722. ESI-MS (+) (MeOH) (higher peaks, *m/z*; relative abundance, %) 69.2 (18), [Hpz+H]⁺, 199.0 (50) [Cu^(II)(Hpz)₂]⁺, 312.0 (100) [Cu(CF₃COO)(Hpz)₂]⁺. μ_{eff} (295 K) = 1.63 BM. UV-Vis spectra: λ_{max}/nm (MeOH solution 3.9·10⁻³ M) 708 (ε = 40). Λ_M (MeOH, 1.37·10⁻³ M): 96 Ω⁻¹ mol² cm⁻¹; Λ_M (H₂O, 1.37·10⁻³ M): 203 Ω⁻¹ mol² cm⁻¹. This compound has been previously reported, but only partially characterized [Kagane et al. (1992)].

CuTFac2. Yield: 609 mg, 14%. m.p.: 159-162 °C. Anal. Calcd for C₁₀H₈CuF₆N₄O₄: C 28.21; H 1.89; N, 13.16. Found: C 27.81; H 2.09; N 12.87. UV-Vis spectra: λ_{max}/nm (MeOH solution 5.2·10⁻³ M) 720 (ε = 40). This compound has been previously reported. Its analytical and spectral data agree with those described in literature [Casarin et al. (2004)].

Reaction of 2 with CF₃SO₃H.

Synthesis of [Cu₃(μ₃-OH)(μ-pz)₃(CF₃SO₃)₂(Hpz)₃].H₂O, Cu3TFL, [(Cu₃(μ₃-OH)(μ-pz)₃(Hpz)₃]{Cu₃(μ₃-O)(μ-pz)₃(Hpz)₃](CF₃SO₃)₃, Cu6TFL, and [Cu(CF₃SO₃H)₂(Hpz)₄], CuTFL.

To a suspension of 1.01 g of **2** (1.7 mmol) in ca. 100 mL of deionized water, 17 mL of a 0.38 M water solution of CF₃SO₃H (6.38 mmol) was slowly added under stirring. The solid dissolved completely and the solution was let to stay undisturbed at r.t.. In about 15 days three pure crystal fractions were collected, dried in the air and examined, yielding the results reported below.

Cu3TFL. Yield: 168 mg, 21%. m.p. >210 °C. Anal. Calcd for C₂₀H₂₄Cu₃F₆N₁₂O₈S₂: C 25.85; H 2.60; N 18.09. Found: C 24.78; H 2.52; N 17.71. IR (KBr, cm⁻¹): 3497-3142, 1276, 1171, 1128, 1068, 1033, 765, 641. ESI-MS (+) (MeOH) (higher peaks, *m/z*; relative abundance, %) 475.9 (23), [Cu₃(OH)₂(pz)₃(MeOH)(H₂O)]⁺, 625.8 (32) [Cu₃(OH)(pz)₃(CF₃SO₃)(Hpz)]⁺, 672.3 (13), [Cu₃(OH)(pz)₃(CF₃SO₃)(MeOH)₃(H₂O)]⁺, 707.8 (100), [Cu₃(OH)(pz)₃(CF₃SO₃)(Hpz)(MeOH)₂(H₂O)]⁺, 740.3 (21), [Cu₃(OH)(pz)₃(CF₃SO₃)₂(MeOH)+H]⁺. UV-Vis spectra: λ_{max}/nm (MeOH solution 1.7·10⁻³ M) 672 (ε = 145).

Cu6TFL. Yield: 45 mg, 3%. m.p. 139-143 °C.

CuTFL. Yield: 259 mg, 8%. m.p. 182-186 °C. Anal. Calcd for C₁₄H₁₆CuF₆N₈O₆S₂: C 28.52; H 2.54; N 17.67. Found: C 29.01; H 2.82; N 17.37. IR (KBr, cm⁻¹): 3225-3103, 1250, 1166, 1127, 1066, 1049, 791, 775, 654. UV-Vis spectra: λ_{max}/nm (MeOH solution 2.3·10⁻³ M) 708 (ε = 21).

Reactions of Trinuclear Triangular Cu^(II) Derivatives with 4,4'-bipyridine

Reaction of **1** with 4,4'-bipyridine.

Synthesis of $[[\text{Cu}_3(\mu_3\text{-OH})(\mu\text{-pz})_3(\text{HCOO})_2(\text{H}_2\text{O})][\text{Cu}_3(\mu_3\text{-OH})(\mu\text{-pz})_3(\text{HCOO})_2(\text{H}_2\text{O})(\text{MeOH})]]_2(\text{C}_{10}\text{H}_8\text{N}_2)$, **Cu₃FormBpyL**.

To a solution of **1** (251 mg, 0.4 mmol) in 30 mL of MeOH a solution of 4,4'-bipyridine (64 mg, 0.4 mmol) in 5 mL of MeOH was added under stirring. The obtained solution was stirred for 5 minutes, and then let to slowly evaporate in the air, yielding well-formed blue crystals, whose XRD crystal structure was solved. **Cu₃FormBpyL**. Yield 150 mg, 66%. Anal. Calcd for $[[\text{Cu}_3(\mu_3\text{-OH})(\mu\text{-pz})_3(\text{HCOO})_2(\text{H}_2\text{O})][\text{Cu}_3(\mu_3\text{-OH})(\mu\text{-pz})_3(\text{HCOO})_2(\text{H}_2\text{O})(\text{MeOH})]]_2(\text{C}_{10}\text{H}_8\text{N}_2)$: C, 29.40; H, 3.17; N, 15.92. Found: C, 28.35; H, 3.36; N, 15.02.

IR (KBr, cm⁻¹): 3583, 3353, 3214, 3133, 2928, 2837, 1562, 1489, 1417, 1380, 1347, 1276, 1222, 1178, 1058, 1011, 967, 923, 882, 817, 751, 668. ESI-MS (+) (MeOH, MeCN) (higher peaks, m/z; relative abundance, %): 69.2 (22) [Hpz+H]⁺, 157.1 (55) [bpy+H]⁺, 199.0 (15) [Cu(pz)(Hpz)]⁺, 243.9 (25) [Cu(Hpz)₂(HCOO)]⁺, 258.0 (100) [Cu(Hpz)(HCOO)(MeOH)₂(H₂O)]⁺, 287.0 (10) [Cu(pz)(bpy)]⁺, 453.9 (18) [Cu₃(OH)(pz)₃(HCOO)]⁺, 467.9 (37) [Cu₃(OH)(pz)₂(HCOO)₂(H₂O)₂]⁺ or [Cu₃(OCH₃)(pz)₃(HCOO)]⁺, 475.9 (60) [Cu₃(OH)₂(pz)₃(MeOH)(H₂O)]⁺, 503.8 (15) [Cu₃(OH)(pz)₃(HCOO)(MeOH)(H₂O)]⁺, 517.8 (15) [Cu₃(OCH₃)(pz)₃(HCOO)(MeOH)(H₂O)]⁺, 525.8 (28) [Cu₃(OH)₂(pz)₃(MeOH)₂(H₂O)₂]⁺, 535.9 (30) [Cu₃(OH)(pz)₃(HCOO)(MeOH)₂(H₂O)]⁺ or [Cu₃(OCH₃)(pz)₃(HCOO)₂+Na]⁺, 549.8 (50) [Cu₃(OH)(pz)₂(HCOO)₂(MeOH)₂(H₂O)₃]⁺, 563.8 (37) [Cu₃(OH)(pz)₃(HCOO)₂(MeOH)₂+H]⁺, 577.8 (25) [Cu₃(OH)(pz)₃(HCOO)(MeCN)₃]⁺, 980.6 (18) [Cu₆(OH)(pz)₆(HCOO)₄]⁺. $\mu = 4.354$ BM (calculated for C₅₆H₇₂Cu₁₂N₂₆O₂₆).

Reaction of **1** with 4,4'-bipyridine.

Synthesis of $[\text{Cu}_3(\mu_3\text{-OH})(\mu\text{-pz})_3(\text{HCOO})(\text{OH})(\text{C}_{10}\text{H}_8\text{N}_2)_3]_2(\text{H}_2\text{O})_x(\text{C}_{10}\text{H}_8\text{N}_2)_y$, **Cu₃FormBpyP**.

To a solution of **1** (200 mg, 0.3 mmol) in 30 mL of MeOH a solution of 4,4'-bipyridine (191 mg, 1.2 mmol) in 5 mL of MeOH was added under stirring. The obtained solution was stirred for 5 minutes, and then let to slowly evaporate in the air, yielding green well-formed crystals, whose XRD crystal structure was determined.

Cu₃FormBpyP. Yield 322 mg, 95%. Anal. Calcd for $[\text{Cu}_3(\mu_3\text{-OH})(\mu\text{-pz})_3(\text{HCOO})(\text{OH})(\text{C}_{10}\text{H}_8\text{N}_2)_3]_2(\text{H}_2\text{O})_{17}(\text{C}_{10}\text{H}_8\text{N}_2)_{0.5}$: C, 45.47; H, 4.85; N, 15.59. Found: C, 45.21; H, 4.48; N, 15.09. IR (KBr, cm⁻¹): 3418, 3239, 3142, 2924, 2852, 2830, 1631, 1601, 1534, 1492, 1414, 1383, 1340, 1324, 1276, 1224, 1180, 1063, 1003, 877, 810, 761, 625, 483. ESI-MS (+) (MeOH, MeCN) (higher peaks, m/z; relative abundance, %): 157.2 (8) [bpy+H]⁺, 624.3 (80) [Cu₃(OCH₃)(pz)₃(HCOO)(bpy)]⁺, 744.5 (20) [Cu₃(OCH₃)₂(pz)₂(HCOO)(bpy)₂]⁺, 785.3 (100) [Cu₃(OH)(pz)₂(HCOO)₂(bpy)₂(MeCN)]⁺, 1303.4 (50) [Cu₆(OH)₅(pz)₆(HCOO)(bpy)₂(H₂O)₃+Na]⁺. $\mu = 2.972$ BM (calculated for C₈₀H₇₂Cu₆N₂₄O₈).

Reaction of **3** with 4,4'-bipyridine.

Synthesis of $[\text{Cu}_3(\mu_3\text{-OH})(\mu\text{-pz})_3(\text{C}_2\text{H}_5\text{COO})_2(\text{C}_{10}\text{H}_8\text{N}_2)(\text{H}_2\text{O})]$, **Cu3ProBpy**.

To a solution of **3** (252 mg, 0.4 mmol) in 30 mL of MeOH a solution of 4,4'-bipyridine (136 mg, 0.9 mmol) in 5 mL of MeOH was added under stirring. The obtained solution was stirred for 5 minutes, and then let to slowly evaporate in the air, yielding blue well-formed crystals, whose XRD crystal structure was determined.

Cu3ProBpy. Yield 140 mg, 48%. Anal. Calcd for $[\text{Cu}_3(\mu_3\text{-OH})(\mu\text{-pz})_3(\text{C}_2\text{H}_5\text{COO})_2(\text{C}_{10}\text{H}_8\text{N}_2)(\text{H}_2\text{O})]$: C, 41.18; H, 4.15; N, 15.37. Found: C, 41.17; H, 4.11; N, 15.50. IR (KBr, cm^{-1}): 3405, 3230, 3103, 2964, 2933, 1603, 1575, 1495, 1464, 1420, 1398, 1379, 1284, 1252, 1221, 1176, 1060, 886, 817, 767, 750, 645, 626, 495. ESI-MS (+) (MeOH, MeCN) (higher peaks, m/z; relative abundance, %): 532.3 (15) $[\text{Cu}_3(\text{OH})(\text{pz})_3(\text{C}_2\text{H}_5\text{COO})(\text{H}_2\text{O})(\text{MeOH})]^+$, 564.3 (30) $[\text{Cu}_3(\text{OH})(\text{pz})_3(\text{C}_2\text{H}_5\text{COO})(\text{H}_2\text{O})(\text{MeOH})_2]^+$, 606.3 (10) $[\text{Cu}_3(\text{pz})_3(\text{C}_2\text{H}_5\text{COO})_2(\text{H}_2\text{O})_2(\text{MeOH})]^+$, 657.3 (100) $[\text{Cu}_4(\text{OH})_3(\text{pz})_2(\text{C}_2\text{H}_5\text{COO})_2(\text{H}_2\text{O})_4]^+$, 1029.3 (80) $[\text{Cu}_6(\text{OH})_3(\text{pz})_7(\text{C}_2\text{H}_5\text{COO})(\text{H}_2\text{O})_3]^+$, 1065.3 (77) $[\text{Cu}_6(\text{OH})_3(\text{pz})_7(\text{C}_2\text{H}_5\text{COO})(\text{H}_2\text{O})_5]^+$. $\mu = 3.324$ BM (calculated for $\text{C}_{50}\text{H}_{60}\text{Cu}_6\text{N}_{16}\text{O}_{12}$).

Reaction of **4** with 4,4'-bipyridine.

Synthesis of $[\text{Cu}_3(\mu_3\text{-OCH}_3)(\mu\text{-pz})_3(\text{C}_3\text{H}_7\text{COO})_2(\text{C}_{10}\text{H}_8\text{N}_2)]$, **Cu3*ButBpy**.

To a solution of **4** (251 mg, 0.4 mmol) in 30 mL of MeOH a solution of 4,4'-bipyridine (133 mg, 0.9 mmol) in 5 mL of MeOH was added under stirring. The obtained solution was stirred for 5 minutes, and then let to slowly evaporate in the air, yielding blue well-formed crystals, whose XRD structure was determined.

Cu3*ButBpy. Yield 245 mg, 83%. Anal. Calcd for $[\text{Cu}_3(\mu_3\text{-OCH}_3)(\mu\text{-pz})_3(\text{C}_3\text{H}_7\text{COO})_2(\text{C}_{10}\text{H}_8\text{N}_2)]$: C, 43.87; H, 4.36; N, 15.16. Found: C, 44.22; H, 4.46; N, 14.81. IR (KBr, cm^{-1}): 3403, 3144, 3097, 3045, 3018, 2960, 2930, 2900, 2872, 2813, 1610, 1570, 1540, 1491, 1421, 1405, 1380, 1341, 1273, 1257, 1221, 1179, 1074, 1063, 1013, 990, 967, 891, 880, 845, 816, 757, 749, 640, 625. ESI-MS (+) (MeOH, MeCN) (higher peaks, m/z; relative abundance, %): 510.2 (12) $[\text{Cu}_3(\text{OCH}_3)(\text{pz})_3(\text{C}_3\text{H}_7\text{COO})]^+$, 598.5 (20) $[\text{Cu}_3(\text{OCH}_3)(\text{pz})_3(\text{C}_3\text{H}_7\text{COO})_2+\text{H}]^+$, 620.2 (15) $[\text{Cu}_3(\text{OCH}_3)(\text{pz})_3(\text{C}_3\text{H}_7\text{COO})_2+\text{Na}]^+$, 634.3 (15) $[\text{Cu}_3(\text{OCH}_3)(\text{pz})_3(\text{C}_3\text{H}_7\text{COO})_2(\text{H}_2\text{O})_2+\text{H}]^+$, 666.3 (78) $[\text{Cu}_3(\text{OCH}_3)(\text{pz})_3(\text{C}_3\text{H}_7\text{COO})(\text{bpy})]^+$, 686.4 (100) $[\text{Cu}_3(\text{OCH}_3)(\text{pz})_3(\text{C}_3\text{H}_7\text{COO})(\text{MeOH})(\text{H}_2\text{O})_8]^+$, 711.3 (22) $[\text{Cu}_3(\text{OCH}_3)(\text{pz})_3(\text{C}_3\text{H}_7\text{COO})_2(\text{MeCN})(\text{H}_2\text{O})_4+\text{H}]^+$, 722.4 (22) $[\text{Cu}_3(\text{OCH}_3)(\text{pz})_3(\text{C}_3\text{H}_7\text{COO})(\text{MeOH})(\text{H}_2\text{O})_{10}]^+$, 747.3 (10) $[\text{Cu}_3(\text{OCH}_3)(\text{pz})_3(\text{C}_3\text{H}_7\text{COO})_2(\text{MeCN})(\text{H}_2\text{O})_6+\text{H}]^+$, 1071.4 (90) $[\text{Cu}_6(\text{OH})_3(\text{pz})_7(\text{C}_3\text{H}_7\text{COO})(\text{MeOH})_2(\text{H}_2\text{O})]^+$, 1107.4 (20) $[\text{Cu}_6(\text{OCH}_3)_2(\text{pz})_6(\text{C}_3\text{H}_7\text{COO})_3]^+$, 1127.5 (15) $[\text{Cu}_6(\text{OCH}_3)_2(\text{pz})_5(\text{C}_3\text{H}_7\text{COO})_4]^+$. $\mu = 3.439$ BM (calculated for $\text{C}_{56}\text{H}_{68}\text{Cu}_6\text{N}_{16}\text{O}_{10}$).

Reaction of **5** with 4,4'-bipyridine.

Synthesis of $[\text{Cu}_3(\mu_3\text{-OH})(\mu\text{-pz})_3(\text{C}_4\text{H}_9\text{COO})_2(\text{C}_{10}\text{H}_8\text{N}_2)(\text{MeOH})]$, **Cu3ValBpy**.

To a solution of **5** (249 mg, 0.4 mmol) in 30 mL of MeOH a solution of 4,4'-bipyridine (251 mg, 1.6 mmol) in 10 mL of MeOH was added under stirring. The obtained solution was stirred for 5 minutes, and then let to slowly evaporate in the air, yielding blue well-formed crystals, whose XRD crystal structure was determined.

Cu3ValBpy. Yield 230 mg, 72%. Anal. Calcd for $[\text{Cu}_3(\mu_3\text{-OH})(\mu\text{-pz})_3(\text{C}_4\text{H}_9\text{COO})_2(\text{C}_{10}\text{H}_8\text{N}_2)(\text{MeOH})]$: C, 45.51; H, 5.06; N, 14.16. Found: C, 44.45; H, 4.71; N, 13.96. IR (KBr, cm^{-1}): 3377, 3222, 3131, 3104, 3063, 2954, 2931, 2871, 1615, 1598, 1562, 1533, 1488, 1451, 1415, 1379, 1345, 1319, 1292, 1277, 1220, 1177, 1165, 1098, 1059, 998, 930, 879, 858, 813, 760, 746, 662. ESI-MS (+) (MeOH, MeCN) (higher peaks, m/z; relative abundance, %): 157.1 (18) $[\text{bpy}+\text{H}]^+$, 524.3 (8) $[\text{Cu}_3(\text{OCH}_3)(\text{pz})_3(\text{C}_4\text{H}_9\text{COO})]^+$, 560.3 (20) $[\text{Cu}_3(\text{OH})(\text{pz})_3(\text{C}_4\text{H}_9\text{COO})(\text{MeOH})(\text{H}_2\text{O})]^+$, 592.3 (40) $[\text{Cu}_3(\text{OH})(\text{pz})_3(\text{C}_4\text{H}_9\text{COO})(\text{MeOH})_2(\text{H}_2\text{O})]^+$, 626.3 (15) $[\text{Cu}_3(\text{pz})_3(\text{C}_4\text{H}_9\text{COO})_2(\text{MeOH})]^+$, 648.2 (8) $[\text{Cu}_3(\text{OH})(\text{pz})_3(\text{C}_4\text{H}_9\text{COO})_2(\text{H}_2\text{O})_2+\text{H}]^+$, 662.5 (15) $[\text{Cu}_3(\text{OH})(\text{pz})_3(\text{C}_4\text{H}_9\text{COO})_2(\text{MeOH})(\text{H}_2\text{O})+\text{H}]^+$, 680.3 (50) $[\text{Cu}_3(\text{OH})(\text{pz})_3(\text{C}_4\text{H}_9\text{COO})_2(\text{MeOH})(\text{H}_2\text{O})_2+\text{H}]^+$, 685.3 (100) $[\text{Cu}_3(\text{OH})(\text{pz})_3(\text{C}_4\text{H}_9\text{COO})_2(\text{MeOH})(\text{MeCN})+\text{H}]^+$, 714.5 (70) $[\text{Cu}_3(\text{OH})(\text{pz})_3(\text{C}_4\text{H}_9\text{COO})(\text{MeOH})_3(\text{H}_2\text{O})_6]^+$, 750.5 (20) $[\text{Cu}_3(\text{pz})_3(\text{C}_4\text{H}_9\text{COO})_2(\text{bpy})]^+$, 800.5 (8) $[\text{Cu}_3(\text{OH})(\text{pz})_3(\text{C}_4\text{H}_9\text{COO})_2(\text{bpy})(\text{MeOH})+\text{H}]^+$, 1079.4 (20) $[\text{Cu}_6(\text{OH})_4(\text{pz})_6(\text{C}_4\text{H}_9\text{COO})(\text{H}_2\text{O})_7]^+$, 1113.6 (60) $[\text{Cu}_6(\text{OH})_4(\text{pz})_6(\text{C}_4\text{H}_9\text{COO})(\text{MeOH})_5]^+$, 1149.6 (65) $[\text{Cu}_6(\text{OH})_4(\text{pz})_6(\text{C}_4\text{H}_9\text{COO})(\text{MeOH})_5(\text{H}_2\text{O})_2]^+$, 1185.6 (15) $[\text{Cu}_6(\text{OH})_4(\text{pz})_6(\text{C}_4\text{H}_9\text{COO})(\text{MeOH})_5(\text{H}_2\text{O})_4]^+$. $\mu = 2.380$ BM (calculated for $\text{C}_{30}\text{H}_{40}\text{Cu}_3\text{N}_8\text{O}_6$).

Reaction of 7 with 4,4'-bipyridine.

Synthesis of $[\text{Cu}_3(\mu_3\text{-OH})(\mu\text{-pz})_3(\text{C}_6\text{H}_{13}\text{COO})_2(\text{C}_{10}\text{H}_8\text{N}_2)_{0.5}]$, **Cu3EptaBpy.**

To a solution of **7** (252 mg, 0.4 mmol) in 30 mL of MeOH a solution of 4,4'-bipyridine (110 mg, 0.7 mmol) in 5 mL of MeOH was added under stirring. The obtained solution was stirred for 5 minutes, and then let to slowly evaporate in the air, yielding well-formed blue crystals, whose XRD crystal structure was determined.

Cu3EptaBpy. Yield 238 mg, 80%. Anal. Calcd for $[\text{Cu}_3(\mu_3\text{-OH})(\mu\text{-pz})_3(\text{C}_6\text{H}_{13}\text{COO})_2(\text{C}_{10}\text{H}_8\text{N}_2)_{0.5}]$: C, 45.12; H, 5.41; N, 13.16. Found: C, 45.14; H, 5.69; N, 13.21. IR (KBr, cm^{-1}): 3440, 2955, 2927, 2858, 1568, 1490, 1400, 1377, 1277, 1178, 1110, 1060, 829, 766, 746, 627, 487. ESI-MS (+) (MeOH, MeCN) (higher peaks, m/z; relative abundance, %): 588.4 (12) $[\text{Cu}_3(\text{OH})(\text{pz})_3(\text{C}_6\text{H}_{13}\text{COO})(\text{MeOH})(\text{H}_2\text{O})]^+$, 620.4 (18) $[\text{Cu}_3(\text{OH})(\text{pz})_3(\text{C}_6\text{H}_{13}\text{COO})(\text{MeOH})_2(\text{H}_2\text{O})]^+$, 650.4 (10) $[\text{Cu}_3(\text{pz})_3(\text{C}_6\text{H}_{13}\text{COO})_2]^+$, 682.5 (8) $[\text{Cu}_3(\text{pz})_3(\text{C}_6\text{H}_{13}\text{COO})_2(\text{MeOH})]^+$, 713.3 (100) $[\text{Cu}_3(\text{OH})(\text{pz})_4(\text{Hpz})(\text{MeOH})_4(\text{MeCN})]^+$, 1161.7 (28) $[\text{Cu}_6(\text{OH})_3(\text{pz})_6(\text{C}_6\text{H}_{13}\text{COO})_2(\text{MeOH})(\text{H}_2\text{O})_2]^+$, 1197.7 (85) $[\text{Cu}_6(\text{OH})_3(\text{pz})_6(\text{C}_6\text{H}_{13}\text{COO})_2(\text{MeOH})(\text{H}_2\text{O})_4]^+$, 1233.8 (55) $[\text{Cu}_6(\text{OH})_3(\text{pz})_6(\text{C}_6\text{H}_{13}\text{COO})_2(\text{MeOH})(\text{H}_2\text{O})_6]^+$, 1295.8 (18) $[\text{Cu}_6(\text{OH})_2(\text{pz})_6(\text{C}_6\text{H}_{13}\text{COO})_3(\text{H}_2\text{O})_5]^+$. $\mu = 2.256$ BM (calculated for $\text{C}_{28}\text{H}_{40}\text{Cu}_3\text{N}_7\text{O}_5$).

Reaction of 8 with 4,4'-bipyridine.

Synthesis of $[\text{Cu}_3(\mu_3\text{-OH})(\mu\text{-pz})_3(\text{CH}_2=\text{CHCOO})_2(\text{C}_{10}\text{H}_8\text{N}_2)(\text{H}_2\text{O})]$, **Cu3AcryWBpy.**

To a solution of **8** (100 mg, 0.15 mmol) in 15 mL of MeOH a solution of 4,4'-bipyridine (48 mg, 0.3 mmol) in 5 mL of MeOH was added under stirring. The obtained solution was stirred for 5 minutes, and then let to slowly evaporate in the air, yielding blue well-formed crystals, suitable for an XRD crystal structure determination.

Cu3AcryWBpy. Yield 65 mg, 60%. Anal. Calcd for $[\text{Cu}_3(\mu_3\text{-OH})(\mu\text{-pz})_3(\text{CH}_2=\text{CHCOO})_2(\text{C}_{10}\text{H}_8\text{N}_2)(\text{H}_2\text{O})]$: C, 41.40; H, 3.61; N, 15.45. Found: C, 41.17; H, 3.53; N, 15.15. IR (KBr, cm^{-1}): 3397, 3237, 3099, 2927, 2853, 1638, 1620, 1604, 1563, 1647, 1491, 1426, 1413, 1382,

1364, 1338, 1279, 1220, 1181, 1163, 1062, 993, 964, 941, 895, 833, 815, 766, 748, 681, 629, 519. ESI-MS (+) (MeOH, MeCN) (higher peaks, m/z; relative abundance, %): 157.1 (20) [bpy+H]⁺, 530.2 (18) [Cu₃(OH)(pz)₃(CH₂=CHCOO)(MeOH)(H₂O)]⁺, 552.3 (18) [Cu₃(OH)(pz)₃(CH₂=CHCOO)₂+H]⁺, 562.3 (37) [Cu₃(OH)(pz)₃(CH₂=CHCOO)(MeOH)₂(H₂O)]⁺, 650.3 (75) [Cu₃(OCH₃)(pz)₃(CH₂=CHCOO)(bpy)]⁺, 654.3 (70) [Cu₃(OH)(pz)₃(CH₂=CHCOO)(bpy)(H₂O)]⁺, 655.3 (100) [Cu₃(OH)(pz)₃(CH₂=CHCOO)₂(MeOH)(H₂O)₄+H]⁺, 1023.3 (70) [Cu₆(OH)₄(pz)₅(CH₂=CHCOO)₂(MeOH)₃]⁺, 1059.3 (72) [Cu₆(OH)₃(pz)₆(CH₂=CHCOO)₂(MeOH)₂(H₂O)]⁺, 1383.5 (15) [Cu₆(OH)₂(pz)₆(CH₂=CHCOO)₃(bpy)₂(MeCN)]⁺.

Reaction of **9** with 4,4'-bipyridine.

Synthesis of [Cu₃(μ₃-OH)(μ-pz)₃(CH₂=CHCOO)₂(C₁₀H₈N₂)(H₂O)], **Cu3AcryMBpy**.

To a solution of [Cu₃(μ₃-OH)(μ-pz)₃(CH₂=CHCOO)₂(MeOH)] (100 mg, 0.17 mmol) in 20 mL of MeOH a solution of 4,4'-bipyridine (53 mg, 0.3 mmol) in 5 mL of MeOH was added under stirring. The obtained solution was stirred for 5 minutes, and then let to slowly evaporate in the air, yielding blue well-formed crystals, suitable for an XRD crystal structure determination.

Cu3AcryMBpy. Yield 49 mg, 40%. Anal. Calcd for [Cu₃(μ₃-OH)(μ-pz)₃(CH₂=CHCOO)₂(C₁₀H₈N₂)(H₂O)]: C, 41.40; H, 3.61; N, 15.45. Found: C, 41.23; H, 3.55; N, 15.35. IR (KBr, cm⁻¹): 3386, 3233, 3101, 2927, 1637, 1622, 1605, 1565, 1547, 1489, 1329, 1414, 1384, 1363, 1339, 1279, 1221, 1178, 1163, 1065, 993, 964, 943, 893, 830, 817, 764, 748, 682, 627, 579, 518. ESI-MS (+) (MeOH, MeCN) (higher peaks, m/z; relative abundance, %): 157.1 (20) [bpy+H]⁺, 530.2 (18) [Cu₃(OH)(pz)₃(CH₂=CHCOO)(MeOH)(H₂O)]⁺, 552.3 (18) [Cu₃(OH)(pz)₃(CH₂=CHCOO)₂+H]⁺, 562.3 (37) [Cu₃(OH)(pz)₃(CH₂=CHCOO)(MeOH)₂(H₂O)]⁺, 650.3 (75) [Cu₃(OCH₃)(pz)₃(CH₂=CHCOO)(bpy)]⁺, 654.3 (70) [Cu₃(OH)(pz)₃(CH₂=CHCOO)(bpy)(H₂O)]⁺, 655.3 (100) [Cu₃(OH)(pz)₃(CH₂=CHCOO)₂(MeOH)(H₂O)₄+H]⁺, 1023.3 (70) [Cu₆(OH)₄(pz)₅(CH₂=CHCOO)₂(MeOH)₃]⁺, 1059.3 (72) [Cu₆(OH)₃(pz)₆(CH₂=CHCOO)₂(MeOH)₂(H₂O)]⁺, 1383.5 (15) [Cu₆(OH)₂(pz)₆(CH₂=CHCOO)₃(bpy)₂(MeCN)]⁺.

Reaction of **10** with 4,4'-bipyridine.

Synthesis of [Cu₃(μ₃-OH)(μ-pz)₃(CH₂=C(CH₃)COO)₂(C₁₀H₈N₂)], **Cu3MethBpy**.

To a solution of **10** (100 mg, 0.17 mmol) in 50 mL of MeOH a solution of 4,4'-bipyridine (50 mg, 0.3 mmol) in 5 mL of MeOH was added under stirring. The obtained solution was stirred for 5 minutes, and then let to slowly evaporate in the air, yielding blue microcrystalline material.

Cu3MethBpy. Yield 71 mg, 58%. Anal. Calcd for [Cu₃(μ₃-OH)(μ-pz)₃(CH₂=C(CH₃)COO)₂(C₁₀H₈N₂)]: C, 44.11; H, 3.84; N, 15.24. Found: C, 44.61; H, 4.02; N, 16.40. IR (KBr, cm⁻¹): 3404, 3107, 2921, 1640, 1609, 1561, 1539, 1492, 1451, 1417, 1400, 1381, 1364, 1275, 1234, 1219, 1181, 1073, 1061, 1000, 938, 832, 816, 758, 747, 640, 626. ESI-MS (+) (MeOH, MeCN) (higher peaks, m/z; relative abundance, %): 157.1 (22) [Bipy+H]⁺, 544.2 (15) [Cu₃(OH)(pz)₃(CH₂=C(CH₃)COO)(MeOH)(H₂O)]⁺, 576.3 (22) [Cu₃(OH)(pz)₃(CH₂=C(CH₃)COO)(MeOH)₂(H₂O)]⁺, 630.2 (10) [Cu₃(OH)(pz)₃(CH₂=C(CH₃)COO)(MeOH)₂(H₂O)₄]⁺, 664.3 (75) [Cu₃(OCH₃)(pz)₃(CH₂=C(CH₃)COO)(bpy)]⁺, 669.2 (90) [Cu₃(OH)(pz)₃(CH₂=C(CH₃)COO)₂(H₂O)₅+H]⁺, 682.4 (100) [Cu₃(OH)(pz)₃(CH₂=C(CH₃)COO)(bpy)(MeOH)]⁺, 718.4 (15)

$[\text{Cu}_3(\text{OH})(\text{pz})_3(\text{CH}_2=\text{C}(\text{CH}_3)\text{COO})(\text{bpy})(\text{MeOH})(\text{H}_2\text{O})_2]^+$,	1027.4	(25)
$[\text{Cu}_6(\text{OH})_3(\text{pz})_7(\text{CH}_2=\text{C}(\text{CH}_3)\text{COO})(\text{MeCN})]^+$,	1063.3	(90)
$[\text{Cu}_6(\text{OH})_3(\text{pz})_7(\text{CH}_2=\text{C}(\text{CH}_3)\text{COO})(\text{MeCN})(\text{H}_2\text{O})_2]^+$,	1101.4	(75)
$[\text{Cu}_6(\text{OH})_3(\text{pz})_7(\text{CH}_2=\text{C}(\text{CH}_3)\text{COO})(\text{MeCN})(\text{H}_2\text{O})_4]^+$.		

Reactions of Trinuclear Triangular Cu^(II) Derivatives with 1,2-bis(4-pyridyl)diazene

Reaction of **1** with 1,2-bis(4-pyridyl)diazene.

Synthesis of **[[[Cu₃(μ₃-OH)(μ-pz)₃(HCOO)₂(EtOH)]-[Cu₃(μ₃-OH)(μ-pz)₃(HCOO)₂(EtOH)₂]]₂(C₁₀H₈N₄)], **Cu₃FormAzopy**.**

A solution of **1** (99 mg, 0.2 mmol) in 15 mL of EtOH was carefully layered over a solution of 1,2-bis(4-pyridyl)diazene (29 mg, 0.2 mmol) in 5 mL of CH₃Cl. The obtained system was let to slowly mix and evaporate in the air, yielding well-formed dark green crystals, whose XRD crystal structure was determined.

Cu₃FormAzopy. Yield 82 mg, 67%. Anal. Calcd for [[[Cu₃(μ₃-OH)(μ-pz)₃(HCOO)₂(EtOH)]-[Cu₃(μ₃-OH)(μ-pz)₃(HCOO)₂(EtOH)₂]]₂(C₁₀H₈N₄): C, 32.27; H, 3.78; N, 15.97. Found: C, 31.97; H, 3.71; N, 16.00. IR (KBr, cm⁻¹): 3412, 3254, 3123, 2969, 2923, 2848, 1589, 1565, 1489, 1422, 1381, 1350, 1281, 1181, 1064, 1037, 873, 767, 631, 483. ESI-MS (+) (MeOH, MeCN) (higher peaks, m/z; relative abundance, %): 95.2 (100) [4-aminopyridine+H]⁺, 185.1 (10) [azopy+H]⁺, 243.9 (10) [Cu(Hpz)₂(HCOO)]⁺, 475.9 (30) [Cu₃(OH)₂(pz)₃(MeOH)(H₂O)]⁺, 526.0 (20) [Cu₃(OH)₂(pz)₃(MeOH)₂(H₂O)₂]⁺, 536.0 (85) [Cu₃(OH)(pz)₃(HCOO)(MeOH)₂(H₂O)]⁺, 629.0 (60) [Cu₃(OH)(pz)₂(HCOO)₂(MeOH)₂(MeCN)(EtOH)₂]⁺, 652.0 (55) [Cu₃(OH)(pz)₂(HCOO)₂(MeOH)₄(EtOH)₂]⁺, 697.0 (50) [Cu₃(pz)₃(HCOO)₂(H₂O)(MeOH)₂(MeCN)(EtOH)₂]⁺, 944.8 (40) [Cu₃(OCH₃)(pz)₃(HCOO)₂-Cu₃(OH)(pz)₂(HCOO)₂]⁺, 980.6 (35) [Cu₃(OH)(pz)₃(HCOO)₂-Cu₃(pz)₃(HCOO)₂]⁺, 1302.4 (45) [Cu₃(OH)(pz)₃(HCOO)₂(EtOH)-Cu₃(pz)₃(HCOO)₂(EtOH)₂(azopy)]⁺. μ = 4.342 BM (calculated for C₆₆H₉₂Cu₁₂N₂₈O₂₆).

Reaction of **2** with 1,2-bis(4-pyridyl)diazene.

Synthesis of [Cu₃(μ₃-OH)(μ-pz)₃(CH₃COO)₂(C₁₀H₈N₄)_{1.5}(H₂O)], **Cu₃AcAzopy**

To a solution of **2** (100 mg, 0.17 mmol) in 40 mL of MeOH a solution of 1,2-bis(4-pyridyl)diazene (66 mg, 0.36 mmol) in 5 mL of CHCl₃ was added under stirring. The obtained solution was stirred for 5 minutes, and then let to slowly evaporate in the air, yielding dark green crystals, suitable for an XRD crystal structure determination.

Cu₃AcAzopy. Yield 44 mg, 32%. Anal. Calcd for [Cu₃(μ₃-OH)(μ-pz)₃(CH₃COO)₂(C₁₀H₈N₄)_{1.5}(H₂O)]: C, 40.95; H, 3.68; N, 20.47. Found: C, 40.34; H, 3.57; N, 21.06. IR (KBr, cm⁻¹): 3381, 3221, 2921, 2848, 1589, 1588, 1415, 1381, 1338, 1327, 1274, 1226, 1180, 1061, 1022, 1000, 966, 919, 844, 760, 672, 630, 619, 573, 526. ESI-MS (+) (MeOH, MeCN) (higher peaks, m/z; relative abundance, %): 95.2 (100) [4-aminopyridine+H]⁺, 550.3 (10) [Cu₃(OH)(pz)₃(CH₃COO)(MeOH)₂(H₂O)]⁺, 568.3 (30) [Cu₃(OH)(pz)₃(CH₃COO)(MeOH)₂(H₂O)₂]⁺, 576.3 (25) [Cu₃(OH)(pz)₃(CH₃COO)(H₂O)₆]⁺, 643.2 (40) [Cu₃(pz)₄(CH₃COO)(H₂O)₇]⁺, 666.5 (20) [Cu₃(OH)(pz)₃(CH₃COO)(4-aminopyridine)(MeOH)(H₂O)₄]⁺, 737.3 (65) [Cu₄(OH)₂(pz)₃(CH₃COO)₂(4-aminopyridine)(H₂O)₂]⁺, 987.3 (30) [Cu₆(OH)₂(pz)₅(CH₃COO)₄]⁺, 1023.3 (20) [Cu₆(OH)₂(pz)₅(CH₃COO)₄(H₂O)₂]⁺.

Reaction of 3 with 1,2-bis(4-pyridyl)diazene.

Synthesis of $[\text{Cu}_3(\mu_3\text{-OH})(\mu\text{-pz})_3(\text{C}_2\text{H}_5\text{COO})_2(\text{C}_{10}\text{H}_8\text{N}_4)_{1.5}(\text{H}_2\text{O})]$, Cu3ProAzopy.

To a solution of **3** (100 mg, 0.17 mmol) in 20 mL of MeOH a solution of 1,2-bis(4-pyridyl)diazene (65 mg, 0.35 mmol) in 5 mL of CHCl_3 was added under stirring. The obtained solution was stirred for 5 minutes, and then let to slowly evaporate in the air, yielding a dark green powder.

Cu3ProAzopy. Yield 138 mg, 96%. Anal. Calcd for $[\text{Cu}_3(\mu_3\text{-OH})(\mu\text{-pz})_3(\text{C}_2\text{H}_5\text{COO})_2(\text{C}_{10}\text{H}_8\text{N}_4)_{1.5}(\text{H}_2\text{O})]$: C, 42.42; H, 4.06; N, 19.79. Found: C, 42.47; H, 3.86; N, 20.27. IR (KBr, cm^{-1}): 3427, 3127, 2975, 2933, 2880, 2850, 1587, 1556, 1556, 1488, 1464, 1415, 1377, 1306, 1281, 1181, 1057, 881, 840, 755, 631, 566. ESI-MS (+) (MeOH, MeCN) (higher peaks, m/z; relative abundance, %): 95.2 (100) [4-aminopyridine+H]⁺, 590.3 (24) $[\text{Cu}_3(\text{OH})(\text{pz})_3(\text{C}_2\text{H}_5\text{COO})(\text{H}_2\text{O})_6]^+$, 596.3 (32) $[\text{Cu}_3(\text{OH})(\text{pz})_3(\text{C}_2\text{H}_5\text{COO})_2(\text{H}_2\text{O})+\text{Na}]^+$, 657.3 (32) $[\text{Cu}_4(\text{OH})_3(\text{pz})_2(\text{C}_2\text{H}_5\text{COO})_2(\text{H}_2\text{O})_4]^+$, 751.3 (58) $[\text{Cu}_4(\text{OH})_2(\text{pz})_4(\text{C}_2\text{H}_5\text{COO})(\text{MeOH})(\text{H}_2\text{O})_5]^+$, 1029.4 (25) $[\text{Cu}_6(\text{OH})_3(\text{pz})_7(\text{C}_2\text{H}_5\text{COO})(\text{H}_2\text{O})_3]^+$, 1065.4 (15) $[\text{Cu}_6(\text{OH})_3(\text{pz})_7(\text{C}_2\text{H}_5\text{COO})(\text{H}_2\text{O})_5]^+$, 1387.5 (10) $[\text{Cu}_6(\text{OH})_2(\text{pz})_6(\text{C}_2\text{H}_5\text{COO})_3(4\text{-aminopyridine})_2(\text{H}_2\text{O})_9]^+$.

Reaction of 4 with 1,2-bis(4-pyridyl)diazene.

Synthesis of $[\text{Cu}_3(\mu_3\text{-OH})(\mu\text{-pz})_3(\text{C}_3\text{H}_7\text{COO})_2(\text{C}_{10}\text{H}_8\text{N}_4)(\text{H}_2\text{O})]$, Cu3ButAzopy.

To a solution of **4** (50 mg, 0.08 mmol) in 20 mL of MeOH a solution of 1,2-bis(4-pyridyl)diazene (31 mg, 0.17 mmol) in 2 mL of CHCl_3 was added under stirring. The obtained solution was stirred for 5 minutes, and then let to slowly evaporate in the air, yielding a dark green powder.

Cu3ButAzopy. Yield 42 mg, 67%. Anal. Calcd for $[\text{Cu}_3(\mu_3\text{-OH})(\mu\text{-pz})_3(\text{C}_3\text{H}_7\text{COO})_2(\text{C}_{10}\text{H}_8\text{N}_4)(\text{H}_2\text{O})]$: C, 41.30; H, 4.36; N, 17.84. Found: C, 41.59; H, 4.47; N, 17.61. IR (KBr, cm^{-1}): 3374, 3231, 3106, 2969, 2927, 2874, 1609, 1559, 1488, 1421, 1408, 1381, 1341, 1319, 1280, 1225, 1180, 1061, 881, 846, 765, 746, 630, 569, 537, 485. ESI-MS (+) (MeOH, MeCN) (higher peaks, m/z; relative abundance, %): 95.2 (25) [4-aminopyridine+H]⁺, 546.3, 10, $[\text{Cu}_3(\text{OH})(\text{pz})_3(\text{C}_3\text{H}_7\text{COO})(\text{MeOH})(\text{H}_2\text{O})]^+$, 578.3 (23) $[\text{Cu}_3(\text{OH})(\text{pz})_3(\text{C}_3\text{H}_7\text{COO})(\text{MeOH})_2(\text{H}_2\text{O})]^+$, 598.3 (20) $[\text{Cu}_3(\text{pz})_3(\text{C}_3\text{H}_7\text{COO})_2(\text{MeOH})]^+$, 624.4 (15) $[\text{Cu}_3(\text{OH})(\text{pz})_3(\text{C}_3\text{H}_7\text{COO})(\text{MeOH})_4]^+$, 671.3 (98) $[\text{Cu}_4(\text{OH})_4(\text{pz})_2(\text{C}_3\text{H}_7\text{COO})(\text{MeOH})_4]^+$, 694.3 (45) $[\text{Cu}_3(\text{OCH}_3)(\text{pz})_3(\text{C}_3\text{H}_7\text{COO})(\text{azopy})]^+$, 714.5 (30) $[\text{Cu}_3(\text{OH})(\text{pz})_3(\text{C}_3\text{H}_7\text{COO})_2(\text{MeCN})(\text{H}_2\text{O})_5+\text{H}]^+$, 765.4 (20) $[\text{Cu}_4(\text{OH})_4(\text{pz})_2(\text{C}_3\text{H}_7\text{COO})(4\text{-aminopyridine})(\text{MeOH})_4]^+$, 1035.4 (35) $[\text{Cu}_6(\text{OH})_2(\text{OCH}_3)(\text{pz})_7(\text{C}_3\text{H}_7\text{COO})(\text{MeOH})]^+$, 1071.4 (100) $[\text{Cu}_6(\text{OH})_3(\text{pz})_7(\text{C}_3\text{H}_7\text{COO})(\text{MeOH})_2(\text{H}_2\text{O})]^+$, 1107.4 (50) $[\text{Cu}_6(\text{OH})_3(\text{pz})_7(\text{C}_3\text{H}_7\text{COO})(\text{MeOH})_2(\text{H}_2\text{O})_3]^+$, 1431.7 (20) $[\text{Cu}_6(\text{OH})_2(\text{pz})_6(\text{C}_3\text{H}_7\text{COO})_3(\text{azopy})(\text{MeOH})_3(\text{H}_2\text{O})_4]^+$.

Reaction of 5 with 1,2-bis(4-pyridyl)diazene.

Synthesis of $[\text{Cu}_3(\mu_3\text{-OH})(\mu\text{-pz})_3(\text{C}_4\text{H}_9\text{COO})_2(\text{C}_{10}\text{H}_8\text{N}_4)]$, Cu3ValAzopy.

To a solution of **5** (100 mg, 0.16 mmol) in 20 mL of MeOH a solution of 1,2-bis(4-pyridyl)diazene (58 mg, 0.31 mmol) in 5 mL of CHCl_3 was added under stirring. The obtained solution was stirred for 5 minutes, and then let to slowly evaporate in the air, yielding a dark green powder.

Cu3ValAzopy. Yield 117 mg, 92%. Anal. Calcd for $[\text{Cu}_3(\mu_3\text{-OH})(\mu\text{-pz})_3(\text{C}_4\text{H}_9\text{COO})_2(\text{C}_{10}\text{H}_8\text{N}_4)]$: C, 43.80; H, 4.56; N, 17.61. Found: C, 43.13; H, 4.54; N, 17.46. IR (KBr, cm^{-1}): 3439, 3338, 3129, 2963, 2933, 2872, 2856, 1626, 1583, 1550, 1521, 1491, 1414, 1395, 1382, 1279, 1208, 1178, 1061, 1017,

1001, 841, 756, 626, 571, 540, 526. ESI-MS (+) (MeOH, MeCN) (higher peaks, m/z; relative abundance, %): 95.2 (100) [4-aminopyridine+H]⁺, 560.3 (13) [Cu₃(OH)(pz)₃(C₄H₉COO)(MeOH)(H₂O)]⁺, 592.3 (20) [Cu₃(OH)(pz)₃(C₄H₉COO)(MeOH)₂(H₂O)]⁺, 618.3 (25) [Cu₃(OH)(pz)₃(C₄H₉COO)(H₂O)₆]⁺, 652.5 (40) [Cu₃(OH)(pz)₃(C₄H₉COO)₂(MeCN)+H]⁺, 685.3 (80) [Cu₃(OH)(pz)₃(C₄H₉COO)₂(MeOH)(MeCN)+H]⁺, 708.5 (25) [Cu₃(OH)(pz)₃(C₄H₉COO)(4-aminopyridine)(MeOH)(H₂O)₄]⁺, 742.5 (23) [Cu₃(pz)₃(C₄H₉COO)₂(4-aminopyridine)(H₂O)₃]⁺, 779.5 (50) [Cu₄(OH)₂(pz)₄(C₄H₉COO)(MeOH)(H₂O)₅]⁺, 1077.5 (35) [Cu₆(OH)₄(pz)₆(C₄H₉COO)₂+Na]⁺, 1113.6 (80) [Cu₆(OH)₄(pz)₆(C₄H₉COO)(MeOH)₅]⁺, 1149.6 (40) [Cu₆(OH)₄(pz)₆(C₄H₉COO)(MeOH)₅(H₂O)₂]⁺, 1471.7 (15) [Cu₆(OH)₂(pz)₆(C₄H₉COO)₄(azopy)(MeOH)₂+H]⁺.

Reaction of 6 with 1,2-bis(4-pyridyl)diazene.

Synthesis of [Cu₃(μ₃-OH)(μ-pz)₃(C₅H₁₁COO)₂(C₁₀H₈N₄)_{0.5}], Cu3HexaAzopy.

To a solution of **6** (101 mg, 0.15 mmol) in 20 mL of MeOH a solution of 1,2-bis(4-pyridyl)diazene (56 mg, 0.30 mmol) in 5 mL of CHCl₃ was added under stirring. The obtained solution was stirred for 5 minutes, and then let to slowly evaporate in the air, yielding a dark green powder.

Cu3HexaAzopy. Yield 104 mg, 95%. Anal. Calcd for [Cu₃(μ₃-OH)(μ-pz)₃(C₅H₁₁COO)₂(C₁₀H₈N₄)_{0.5}]: C, 42.71; H, 4.96; N, 15.32. Found: C, 43.09; H, 5.02; N, 15.66. IR (KBr, cm⁻¹): 3415, 3118, 2957, 2927, 2870, 2858, 1602, 1568, 1491, 1400, 1379, 1279, 1226, 1178, 1105, 1062, 852, 841, 754, 748, 626. ESI-MS (+) (MeOH, MeCN) (higher peaks, m/z; relative abundance, %): 95.2 (35) [4-aminopyridine+H]⁺, 606.3, 15, [Cu₃(OH)(pz)₃(C₅H₁₁COO)(MeOH)₂(H₂O)]⁺, 624.4 (15) [Cu₃(OH)(pz)₃(C₅H₁₁COO)(MeOH)₂(H₂O)₂]⁺, 690.5 (8) [Cu₃(OH)(pz)₃(C₅H₁₁COO)(4-aminopyridine)(H₂O)₄]⁺, 699.3 (100) [Cu₃(OH)(pz)₃(C₅H₁₁COO)₂(MeCN)(H₂O)+H]⁺, 722.5 (25) [Cu₃(OH)(pz)₃(C₅H₁₁COO)₂(MeOH)₂(H₂O)+H]⁺, 747.5 (23) [Cu₄(OCH₃)₂(pz)₃(C₅H₁₁COO)₂]⁺, 770.5 (23) [Cu₄(OH)₂(pz)₃(C₅H₁₁COO)₂(MeOH)(H₂O)]⁺, 793.5 (25) [Cu₄(OH)₂(pz)₄(C₅H₁₁COO)(MeOH)(H₂O)₅]⁺, 1119.7 (35) [Cu₆(OH)₃(pz)₆(C₅H₁₁COO)₂(H₂O)₃]⁺, 1155.7 (98) [Cu₆(OH)₃(pz)₆(C₅H₁₁COO)₂(H₂O)₅]⁺, 1191.7 (60) [Cu₆(OCH₃)₂(pz)₆(C₅H₁₁COO)₃]⁺.

Reaction of 7 with 1,2-bis(4-pyridyl)diazene.

Synthesis of [Cu₃(μ₃-OH)(μ-pz)₃(C₆H₁₃COO)₂(C₁₀H₈N₄)_{1.5}], Cu3HeptaAzopy.

To a solution of **7** (100 mg, 0.14 mmol) in 20 mL of MeOH a solution of 1,2-bis(4-pyridyl)diazene (53 mg, 0.29 mmol) in 5 mL of CHCl₃ was added under stirring. The obtained solution was stirred for 5 minutes, and then let to slowly evaporate in the air, yielding a dark green powder.

Cu3HeptaAzopy. Yield 118 mg, 89%. Anal. Calcd for [Cu₃(μ₃-OH)(μ-pz)₃(C₆H₁₃COO)₂(C₁₀H₈N₄)_{1.5}]: C, 48.37; H, 5.13; N, 17.81. Found: C, 48.17; H, 5.11; N, 17.82. IR (KBr, cm⁻¹): 3321, 3107, 2954, 2927, 2856, 1720, 1625, 1582, 1567, 1519, 1489, 1459, 1413, 1397, 1379, 1322, 1275, 1253, 1208, 1177, 1105, 1054, 1018, 1003, 963, 922, 880, 839, 753, 666. ESI-MS (+) (MeOH, MeCN) (higher peaks, m/z; relative abundance, %): 95.2 (100) [4-aminopyridine+H]⁺, 646.5 (18) [Cu₃(OH)(pz)₃(C₆H₁₃COO)(H₂O)₆]⁺, 708.5 (60) [Cu₄(OH)₃(pz)₃(C₆H₁₃COO)(MeOH)(MeCN)]⁺, 807.5 (50) [Cu₄(OH)₃(pz)₃(C₆H₁₃COO)(MeOH)₂(H₂O)₆]⁺, 1161.7 (10) [Cu₆(OH)₂(pz)₇(C₆H₁₃COO)₂(H₂O)]⁺, 1197.8 (15) [Cu₆(OH)₂(pz)₇(C₆H₁₃COO)₂(H₂O)₃]⁺, 1233.8 (8) [Cu₆(OH)₂(pz)₇(C₆H₁₃COO)₂(H₂O)₅]⁺.

Reactions of Trinuclear Triangular Cu^(II) Derivatives with 1,2-bis(4-pyridyl)ethane

Reaction of **1** with 1,2-bis(4-pyridyl)ethane.

Synthesis of [Cu₃(μ₃-OH)(μ-pz)₃(HCOO)₂(C₁₂H₁₂N₂)(H₂O)₃], **Cu3FormBpetha**.

To a solution of **1** (50 mg, 0.08 mmol) in 20 mL of EtOH a solution of 1,2-bis(4-pyridyl)ethane (115 mg, 0.62 mmol) in 5 mL of CH₂Cl₂ was added under stirring. The obtained solution was stirred for 5 minutes, and then let to slowly evaporate in the air, yielding green well-formed crystals, suitable for an XRD crystal structure determination.

Cu3FormBpetha. Yield 39 mg, 66%. Anal. Calcd for [Cu₃(μ₃-OH)(μ-pz)₃(HCOO)₂(C₁₂H₁₂N₂)(H₂O)₃]: C, 37.47; H, 4.10; N, 15.20. Found: C, 37.02; H, 4.19; N, 14.87. IR (KBr, cm⁻¹): 3571, 3192, 3091, 3015, 2952, 2931, 2865, 2800, 1606, 1570, 1490, 1455, 1423, 1382, 1370, 1334, 1280, 1251, 1223, 1211, 1179, 1059, 1027, 922, 874, 840, 818, 753. ESI-MS (+) (MeOH, MeCN) (higher peaks, m/z; relative abundance, %): 185.2 (20) [bpetha+H]⁺, 554.3 (35) [Cu₃(OH)(pz)₃(HCOO)(H₂O)₂(MeOH)₂]⁺, 616.3 (20) [Cu₃(OH)(pz)₃(HCOO)(H₂O)₉]⁺, 652.4 (45) [Cu₃(OH)(pz)₃(HCOO)(H₂O)₁₁]⁺, 684.3 (10) [Cu₃(OH)(pz)₃(HCOO)(H₂O)₁₁(MeOH)]⁺, 800.5 (75) [Cu₃(OH)(pz)₃(HCOO)₂(Hpz)₂(MeCN)₂(H₂O)(MeOH)₂+H]⁺, 813.5 (100) [Cu₄(OH)₂(pz)₃(HCOO)₂(bpetha)(H₂O)(MeOH)]⁺, 909.3 (15) [Cu₄(OH)₂(pz)₃(HCOO)₂(bpetha)(H₂O)(MeOH)₄]⁺, 1303.5 (5) [Cu₆(OH)₂(pz)₇(HCOO)₂(bpetha)(H₂O)₈]⁺.

Reaction of **2** with 1,2-bis(4-pyridyl)ethane.

Synthesis of [Cu₃(μ₃-OH)(μ-pz)₃(CH₃COO)₂(C₁₂H₁₂N₂)₂(H₂O)₂], **Cu3AcBpetha**.

To a solution of **2** (100 mg, 0.17 mmol) in 50 mL of MeOH a solution of 1,2-bis(4-pyridyl)ethane (64 mg, 0.35 mmol) in 5 mL of MeOH was added under stirring. The obtained solution was stirred for 5 minutes, and then let to slowly evaporate in the air, yielding blue crystals, suitable for an XRD crystal structure determination.

Cu3AcBpetha. Yield 113 mg, 71%. Anal. Calcd for [Cu₃(μ₃-OH)(μ-pz)₃(CH₃COO)₂(C₁₂H₁₂N₂)₂(H₂O)₂]: C, 47.71; H, 4.76; N, 15.04. Found: C, 47.42; H, 5.09; N, 15.01. IR (KBr, cm⁻¹): 3394, 3236, 2939, 2862, 1958, 1609, 1577, 1563, 1501, 1489, 1420, 1377, 1344, 1276, 1221, 1176, 1060, 1028, 1006, 822, 763, 680, 628, 551, 531. ESI-MS (+) (MeOH, MeCN) (higher peaks, m/z; relative abundance, %): 185.2 (15) [bpetha+H]⁺, 568.3 (65) [Cu₃(OH)(pz)₃(CH₃COO)(H₂O)₂(MeOH)₂]⁺, 643.3 (35) [Cu₄(OH)₂(pz)₃(CH₃COO)₂(H₂O)₂]⁺, 658.4 (38) [Cu₃(OH)(pz)₃(CH₃COO)(Hpz)(H₂O)₅(MeOH)]⁺, 666.5 (85) [Cu₃(OCH₃)(pz)₃(CH₃COO)(bpetha)]⁺, 814.6 (90) [Cu₃(OH)(pz)₃(CH₃COO)(bpetha)(H₂O)₉]⁺, 827.5 (100) [Cu₄(OH)₂(pz)₃(CH₃COO)₂(bpetha)(H₂O)₂]⁺, 951.3 (20) [Cu₆(OH)₄(pz)₆(CH₃COO)(MeCN)]⁺, 987.5 (30) [Cu₆(OH)₄(pz)₆(CH₃COO)(H₂O)₂(MeCN)]⁺, 1023.5 (10) [Cu₆(OH)₄(pz)₆(CH₃COO)(H₂O)₄(MeCN)]⁺, 1347.6 (18) [Cu₆(OH)₂(pz)₆(CH₃COO)₃(bpetha)(H₂O)₄(MeOH)₃]⁺.

Reaction of 3 with 1,2-bis(4-pyridyl)ethane.

Synthesis of $[\text{Cu}_3(\mu_3\text{-OH})(\mu\text{-pz})_3(\text{C}_2\text{H}_5\text{COO})_2(\text{C}_{12}\text{H}_{12}\text{N}_2)_{0.5}]$, **Cu3ProBpetha**.

To a solution of **3** (102 mg, 0.18 mmol) in 20 mL of MeOH a solution of 1,2-bis(4-pyridyl)ethane (64 mg, 0.35 mmol) in 5 mL of MeOH was added under stirring. The obtained solution was stirred for 5 minutes, and then let to slowly evaporate in the air, yielding blue crystals, suitable for an XRD crystal structure determination.

Cu3ProBpetha. Yield 91 mg, 78%. Anal. Calcd for $[\text{Cu}_3(\mu_3\text{-OH})(\mu\text{-pz})_3(\text{C}_2\text{H}_5\text{COO})_2(\text{C}_{12}\text{H}_{12}\text{N}_2)_{0.5}]$: C, 39.04; H, 3.90; N, 15.18. Found: C, 39.20; H, 3.98; N, 15.28. IR (KBr, cm^{-1}): 3421, 3129, 2975, 2933, 2873, 1614, 1578, 1488, 1460, 1432, 1401, 1382, 1362, 1304, 1291, 1276, 1177, 1066, 887, 834, 756, 744, 627, 557, 473. ESI-MS (+) (MeOH, MeCN) (higher peaks, m/z; relative abundance, %): 564.3 (22) $[\text{Cu}_3(\text{OH})(\text{pz})_3(\text{C}_2\text{H}_5\text{COO})(\text{H}_2\text{O})(\text{MeOH})_2]^+$, 582.3 (25) $[\text{Cu}_3(\text{OH})(\text{pz})_3(\text{C}_2\text{H}_5\text{COO})(\text{H}_2\text{O})_2(\text{MeOH})_2]^+$, 657.3 (100) $[\text{Cu}_4(\text{OH})_3(\text{pz})_2(\text{C}_2\text{H}_5\text{COO})_2(\text{H}_2\text{O})_4]^+$, 680.5 (95) $[\text{Cu}_3(\text{OCH}_3)(\text{pz})_3(\text{C}_2\text{H}_5\text{COO})(\text{bpetha})]^+$, 686.5 (65) $[\text{Cu}_3(\text{OCH}_3)(\text{pz})_3(\text{C}_2\text{H}_5\text{COO})(\text{H}_2\text{O})_7(\text{MeOH})_2]^+$, 753.3 (15) $[\text{Cu}_4(\text{OCH}_3)_2(\text{pz})_3(\text{C}_2\text{H}_5\text{COO})_2(\text{H}_2\text{O})_5]^+$, 828.6 (25) $[\text{Cu}_3(\text{OH})(\text{pz})_3(\text{C}_2\text{H}_5\text{COO})(\text{bpetha})(\text{H}_2\text{O})_9]^+$, 841.5 (80) $[\text{Cu}_4(\text{OH})_3(\text{pz})_2(\text{C}_2\text{H}_5\text{COO})_2(\text{bpetha})(\text{H}_2\text{O})_4]^+$, 993.5 (75) $[\text{Cu}_6(\text{OH})_3(\text{pz})_7(\text{C}_2\text{H}_5\text{COO})(\text{H}_2\text{O})]^+$, 1029.4 (98) $[\text{Cu}_6(\text{OH})_3(\text{pz})_7(\text{C}_2\text{H}_5\text{COO})(\text{H}_2\text{O})_3]^+$, 1065.4 (30) $[\text{Cu}_6(\text{OH})_3(\text{pz})_7(\text{C}_2\text{H}_5\text{COO})(\text{H}_2\text{O})_5]^+$.

Reaction of 4 with 1,2-bis(4-pyridyl)ethane.

Synthesis of $[\text{Cu}_3(\mu_3\text{-OH})(\mu\text{-pz})_3(\text{C}_3\text{H}_7\text{COO})_2(\text{C}_{12}\text{H}_{12}\text{N}_2)_{0.5}]$, **Cu3ButBpetha**.

To a solution of **4** (99 mg, 0.16 mmol) in 20 mL of MeOH a solution of 1,2-bis(4-pyridyl)ethane (63 mg, 0.34 mmol) in 5 mL of MeOH was added under stirring. The obtained solution was stirred for 5 minutes, and then let to slowly evaporate in the air, yielding blue microcrystals.

Cu3ButBpetha. Yield 105 mg, 97%. Anal. Calcd for $[\text{Cu}_3(\mu_3\text{-OH})(\mu\text{-pz})_3(\text{C}_3\text{H}_7\text{COO})_2(\text{C}_{12}\text{H}_{12}\text{N}_2)_{0.5}]$: C, 40.91; H, 4.48; N, 14.52. Found: C, 40.62; H, 4.52; N, 14.57. IR (KBr, cm^{-1}): 3424, 2961, 2936, 2879, 1614, 1583, 1575, 1492, 1430, 1403, 1382, 1338, 1298, 1279, 1253, 1226, 1177, 1062, 758, 625, 554. ESI-MS (+) (MeOH, MeCN) (higher peaks, m/z; relative abundance, %): 546.3 (5) $[\text{Cu}_3(\text{OH})(\text{pz})_3(\text{C}_3\text{H}_7\text{COO})(\text{H}_2\text{O})(\text{MeOH})]^+$, 578.3 (10) $[\text{Cu}_3(\text{OH})(\text{pz})_3(\text{C}_3\text{H}_7\text{COO})(\text{H}_2\text{O})(\text{MeOH})_2]^+$, 596.3 (15) $[\text{Cu}_3(\text{OH})(\text{pz})_3(\text{C}_3\text{H}_7\text{COO})(\text{H}_2\text{O})_2(\text{MeOH})_2]^+$, 671.3 (80) $[\text{Cu}_4(\text{OH})_4(\text{pz})_2(\text{C}_3\text{H}_7\text{COO})(\text{MeOH})_4]^+$, 694.5 (55) $[\text{Cu}_3(\text{OCH}_3)(\text{pz})_3(\text{C}_3\text{H}_7\text{COO})(\text{bpetha})]^+$, 714.5 (45) $[\text{Cu}_3(\text{OH})(\text{pz})_3(\text{C}_3\text{H}_7\text{COO})_2(\text{H}_2\text{O})_6+\text{Na}]^+$, 855.5 (60) $[\text{Cu}_4(\text{OH})_4(\text{pz})_2(\text{C}_3\text{H}_7\text{COO})(\text{bpetha})(\text{MeOH})_4]^+$, 1035.4 (75) $[\text{Cu}_6(\text{OH})_4(\text{pz})_6(\text{C}_3\text{H}_7\text{COO})(\text{MeOH})_3]^+$, 1071.4 (100) $[\text{Cu}_6(\text{OH})_3(\text{pz})_7(\text{C}_3\text{H}_7\text{COO})(\text{H}_2\text{O})(\text{MeOH})_2]^+$, 1107.5 (25) $[\text{Cu}_6(\text{OCH}_3)_2(\text{pz})_6(\text{C}_3\text{H}_7\text{COO})_3]^+$, 1429.5 (15) $[\text{Cu}_6(\text{OCH}_3)_2(\text{pz})_6(\text{C}_3\text{H}_7\text{COO})_4(\text{bpetha})(\text{H}_2\text{O})(\text{MeOH})+\text{H}]^+$.

Reaction of 5 with 1,2-bis(4-pyridyl)ethane.

Synthesis of $[\text{Cu}_3(\mu_3\text{-OH})(\mu\text{-pz})_3(\text{C}_4\text{H}_9\text{COO})_2(\text{C}_{12}\text{H}_{10}\text{N}_2)_{1.5}(\text{H}_2\text{O})]$, **Cu3ValBpetha**.

To a solution of **5** (103 mg, 0.16 mmol) in 20 mL of MeOH a solution of 1,2-bis(4-pyridyl)ethane (60 mg, 0.33 mmol) in 5 mL of MeOH was added under stirring. The obtained solution was stirred for 5 minutes, and then let to slowly evaporate in the air, yielding blue microcrystals.

Cu3ValBpetha. Yield 120 mg, 83%. Anal. Calcd for $[\text{Cu}_3(\mu_3\text{-OH})(\mu\text{-pz})_3(\text{C}_4\text{H}_9\text{COO})_2(\text{C}_{12}\text{H}_{10}\text{N}_2)_{1.5}(\text{H}_2\text{O})]$: C, 49.08; H, 5.34; N, 13.92. Found: C, 49.11; H, 5.17; N, 14.08. IR (KBr, cm^{-1}): 3427, 3070, 2965, 2930, 2868, 1615, 1604, 1580, 1559, 1507, 1488, 1431, 1419, 1401, 1379, 1342, 1309, 1275, 1225, 1177, 1061, 1028, 1004, 843, 824, 761, 745, 626, 543, 504. ESI-MS (+) (MeOH, MeCN) (higher peaks, m/z; relative abundance, %): 610.3 (40) $[\text{Cu}_3(\text{OH})(\text{pz})_3(\text{C}_4\text{H}_9\text{COO})(\text{MeOH})_2(\text{H}_2\text{O})_2]^+$, 685.3 (70) $[\text{Cu}_4(\text{OCH}_3)_2(\text{pz})_4(\text{C}_4\text{H}_9\text{COO})]^+$, 708.5 (90) $[\text{Cu}_3(\text{OCH}_3)(\text{pz})_3(\text{C}_4\text{H}_9\text{COO})(\text{bpetha})]^+$, 742.5 (82) $[\text{Cu}_3(\text{OH})(\text{pz})_3(\text{C}_4\text{H}_9\text{COO})_2(\text{H}_2\text{O})_6+\text{Na}]^+$, 856.7 (85) $[\text{Cu}_3(\text{OH})(\text{pz})_3(\text{C}_4\text{H}_9\text{COO})(\text{bpetha})(\text{H}_2\text{O})_9]^+$, 869.5 (100) $[\text{Cu}_3(\text{OH})(\text{pz})_3(\text{C}_4\text{H}_9\text{COO})_2(\text{bpetha})(\text{MeOH})(\text{MeCN})+\text{H}]^+$, 903.5 (30) $[\text{Cu}_4(\text{OCH}_3)_2(\text{pz})_3(\text{C}_4\text{H}_9\text{COO})_2(\text{bpetha})]^+$, 1077.5 (42) $[\text{Cu}_6(\text{OCH}_3)_3(\text{pz})_7(\text{C}_4\text{H}_9\text{COO})(\text{MeOH})]^+$, 1113.6 (90) $[\text{Cu}_6(\text{OCH}_3)_3(\text{pz})_7(\text{C}_4\text{H}_9\text{COO})(\text{MeOH})(\text{H}_2\text{O})_2]^+$, 1149.6 (50) $[\text{Cu}_6(\text{OCH}_3)_2(\text{pz})_6(\text{C}_4\text{H}_9\text{COO})_3]^+$, 1471.7 (17) $[\text{Cu}_6(\text{OH})_2(\text{pz})_6(\text{C}_4\text{H}_9\text{COO})_4(\text{bpetha})(\text{MeOH})+\text{H}]^+$.

Reaction of 6 with 1,2-bis(4-pyridyl)ethane.

Synthesis of $[\text{Cu}_3(\mu_3\text{-OH})(\mu\text{-pz})_3(\text{C}_5\text{H}_{11}\text{COO})_2(\text{C}_{12}\text{H}_{12}\text{N}_2)]$, **Cu3HexaBpetha.**

To a solution of **6** (101 mg, 0.15 mmol) in 20 mL of MeOH a solution of 1,2-bis(4-pyridyl)ethane (54 mg, 0.29 mmol) in 5 mL of MeOH was added under stirring. The obtained solution was stirred for 5 minutes, and then let to slowly evaporate in the air, yielding blue microcrystals.

Cu3HexaBpetha. Yield 80 mg, 65%. Anal. Calcd for $[\text{Cu}_3(\mu_3\text{-OH})(\mu\text{-pz})_3(\text{C}_5\text{H}_{11}\text{COO})_2(\text{C}_{12}\text{H}_{12}\text{N}_2)]$: C, 48.14; H, 5.39; N, 13.61. Found: C, 48.14; H, 5.48; N, 13.71. IR (KBr, cm^{-1}): 3415, 2957, 2930, 2871, 2858, 1587, 1490, 1433, 1417, 1392, 1384, 1302, 1276, 1227, 1178, 1062, 884, 830, 765, 748, 624, 551. ESI-MS (+) (MeOH, MeCN) (higher peaks, m/z; relative abundance, %): 624.5 (40) $[\text{Cu}_3(\text{OH})(\text{pz})_3(\text{C}_5\text{H}_{11}\text{COO})(\text{MeOH})_2(\text{H}_2\text{O})_2]^+$, 699.3 (70) $[\text{Cu}_3(\text{pz})_3(\text{C}_5\text{H}_{11}\text{COO})_2(\text{MeCN})(\text{H}_2\text{O})_2]^+$, 722.5 (60) $[\text{Cu}_3(\text{OCH}_3)(\text{pz})_3(\text{C}_5\text{H}_{11}\text{COO})(\text{bpetha})]^+$, 747.3 (20) $[\text{Cu}_4(\text{OCH}_3)_2(\text{pz})_3(\text{C}_5\text{H}_{11}\text{COO})_2]^+$, 770.5 (100) $[\text{Cu}_3(\text{OH})(\text{pz})_3(\text{C}_5\text{H}_{11}\text{COO})(\text{H}_2\text{O})_6+\text{Na}]^+$, 870.7 (58) $[\text{Cu}_3(\text{OCH}_3)(\text{pz})_3(\text{C}_5\text{H}_{11}\text{COO})(\text{bpetha})(\text{MeOH})+\text{H}]^+$, 883.5 (87) $[\text{Cu}_4(\text{OH})_2(\text{pz})_3(\text{C}_5\text{H}_{11}\text{COO})_2(\text{MeOH})_4(\text{H}_2\text{O})_2]^+$, 931.6 (28) $[\text{Cu}_4(\text{OCH}_3)_2(\text{pz})_3(\text{C}_5\text{H}_{11}\text{COO})_2(\text{bpetha})]^+$, 1119.6 (60) $[\text{Cu}_6(\text{OH})_3(\text{pz})_6(\text{C}_5\text{H}_{11}\text{COO})_2(\text{H}_2\text{O})_3]^+$, 1155.6 (80) $[\text{Cu}_6(\text{OH})_3(\text{pz})_6(\text{C}_5\text{H}_{11}\text{COO})_2(\text{H}_2\text{O})_5]^+$, 1191.7 (20) $[\text{Cu}_6(\text{OH})_3(\text{pz})_6(\text{C}_5\text{H}_{11}\text{COO})_2(\text{H}_2\text{O})_7]^+$.

Reaction of 7 with 1,2-bis(4-pyridyl)ethane.

Synthesis of $[\text{Cu}_3(\mu_3\text{-OH})(\mu\text{-pz})_3(\text{C}_6\text{H}_{13}\text{COO})_2(\text{C}_{12}\text{H}_{12}\text{N}_2)]$, **Cu3HeptaBpetha.**

To a solution of **7** (83 mg, 0.12 mmol) in 20 mL of MeOH a solution of 1,2-bis(4-pyridyl)ethane (43 mg, 0.23 mmol) in 5 mL of MeOH was added under stirring. The obtained solution was stirred for 5 minutes, and then let to slowly evaporate in the air, yielding blue microcrystals.

Cu3HeptaBpetha. Yield 85 mg, 83%. Anal. Calcd for $[\text{Cu}_3(\mu_3\text{-OH})(\mu\text{-pz})_3(\text{C}_6\text{H}_{13}\text{COO})_2(\text{C}_{12}\text{H}_{12}\text{N}_2)]$: C, 49.37; H, 5.68; N, 13.16. Found: C, 48.64; H, 5.77; N, 13.10. IR (KBr, cm^{-1}): 3415, 2952, 2927, 2856, 1586, 1490, 1433, 1395, 1379, 1307, 1288, 1275, 1177, 1107, 1063, 1029, 1003, 967, 843, 827, 764, 754, 747, 627, 554. ESI-MS (+) (MeOH, MeCN) (higher peaks, m/z; relative abundance, %): 713.3 (68) $[\text{Cu}_4(\text{OCH}_3)_3(\text{pz})_3(\text{C}_6\text{H}_{13}\text{COO})(\text{H}_2\text{O})_2]^+$, 736.5 (67) $[\text{Cu}_3(\text{OCH}_3)(\text{pz})_3(\text{C}_6\text{H}_{13}\text{COO})(\text{bpetha})]^+$, 775.5 (17) $[\text{Cu}_3(\text{OH})(\text{pz})_3(\text{C}_6\text{H}_{13}\text{COO})_2(\text{MeCN})(\text{MeOH})+\text{H}]^+$, 798.5 (75) $[\text{Cu}_3(\text{OH})(\text{pz})_3(\text{C}_6\text{H}_{13}\text{COO})_2(\text{H}_2\text{O})_6+\text{Na}]^+$, 884.7 (50) $[\text{Cu}_3(\text{OH})(\text{pz})_3(\text{C}_6\text{H}_{13}\text{COO})_2(\text{H}_2\text{O})_9(\text{MeOH})+\text{Na}]^+$,

897.5 (100) $[\text{Cu}_4(\text{OH})_2(\text{pz})_3(\text{C}_6\text{H}_{13}\text{COO})_2(\text{H}_2\text{O})_3(\text{MeOH})_3]^+$, 959.7 (28)
 $[\text{Cu}_4(\text{OCH}_3)_2(\text{pz})_3(\text{C}_6\text{H}_{13}\text{COO})_2(\text{bpetha})]^+$, 1135.6 (14) $[\text{Cu}_6(\text{OCH}_3)_3(\text{pz})_6(\text{C}_6\text{H}_{13}\text{COO})_2]^+$, 1161.7 (30)
 $[\text{Cu}_6(\text{OH})_3(\text{pz})_6(\text{C}_6\text{H}_{13}\text{COO})_2(\text{MeOH})(\text{H}_2\text{O})_2]^+$, 1197.7 (86) $[\text{Cu}_6(\text{OH})_3(\text{pz})_6(\text{C}_6\text{H}_{13}\text{COO})_2(\text{MeOH})(\text{H}_2\text{O})_4]^+$,
 1233.7 (50) $[\text{Cu}_6(\text{OCH}_3)_2(\text{pz})_6(\text{C}_6\text{H}_{13}\text{COO})_3]^+$, 1259.8 (15) $[\text{Cu}_6(\text{OH})_2(\text{pz})_6(\text{C}_6\text{H}_{13}\text{COO})_3(\text{H}_2\text{O})_3]^+$, 1295.8
 (14) $[\text{Cu}_6(\text{OH})_2(\text{pz})_6(\text{C}_6\text{H}_{13}\text{COO})_3(\text{H}_2\text{O})_5]^+$.

Reaction of 8 with 1,2-bis(4-pyridyl)ethane.

Synthesis of $[\text{Cu}_3(\mu_3\text{-OH})(\mu\text{-pz})_3(\text{CH}_2=\text{CHCOO})_2(\text{C}_{10}\text{H}_8\text{N}_2)_{0.5}]$, **Cu3AcryWBpetha**.

To a solution of **8** (101 mg, 0.15 mmol) in 20 mL of MeOH a solution of 1,2-bis(4-pyridyl)ethane (58 mg, 0.32 mmol) in 5 mL of MeOH was added under stirring. The obtained solution was stirred for 5 minutes, and then let to slowly evaporate in the air, yielding blue microcrystals.

Cu3AcryWBpetha. Yield 66 mg, 68%. Anal. Calcd for $[\text{Cu}_3(\mu_3\text{-OH})(\mu\text{-pz})_3(\text{CH}_2=\text{CHCOO})_2(\text{C}_{10}\text{H}_8\text{N}_2)_{0.5}]$: C, 39.22; H, 3.45; N, 15.25. Found: C, 39.69; H, 3.34; N, 15.05. IR (KBr, cm^{-1}): 3415, 3123, 2922, 2856, 1640, 1617, 1567, 1491, 1433, 1420, 1382, 1357, 1342, 1279, 1182, 1067, 950, 898, 827, 757, 744, 689, 681, 626, 556, 548, 483. ESI-MS (+) (MeOH, MeCN) (higher peaks, m/z; relative abundance, %): 580.3 (13) $[\text{Cu}_3(\text{OH})(\text{pz})_3(\text{CH}_2=\text{CHCOO})(\text{MeOH})_2(\text{H}_2\text{O})_2]^+$,
 655.2 (42) $[\text{Cu}_4(\text{OCH}_3)_2(\text{pz})_4(\text{CH}_2=\text{CHCOO})]^+$, 678.3 (40)
 $[\text{Cu}_4(\text{OCH}_3)_3(\text{pz})_3(\text{CH}_2=\text{CHCOO})(\text{MeCN})(\text{H}_2\text{O})]^+$, 826.5 (20)
 $[\text{Cu}_3(\text{OH})(\text{pz})_3(\text{CH}_2=\text{CHCOO})(\text{BPEta})(\text{MeCN})(\text{MeOH})(\text{H}_2\text{O})_5]^+$, 839.5 (68)
 $[\text{Cu}_4(\text{OCH}_3)_2(\text{pz})_4(\text{CH}_2=\text{CHCOO})(\text{BPEta})]^+$, 987.3 (42) $[\text{Cu}_6(\text{OH})_5(\text{pz})_5(\text{CH}_2=\text{CHCOO})(\text{MeOH})_3(\text{H}_2\text{O})]^+$,
 1023.3 (100) $[\text{Cu}_6(\text{OCH}_3)_3(\text{pz})_5(\text{CH}_2=\text{CHCOO})_3]^+$, 1059.3 (50) $[\text{Cu}_6(\text{OCH}_3)_2(\text{pz})_6(\text{CH}_2=\text{CHCOO})_3]^+$,
 1383.4 (29) $[\text{Cu}_6(\text{OH})_2(\text{pz})_6(\text{CH}_2=\text{CHCOO})_4(\text{BPEta})(\text{MeOH})_3+\text{H}]^+$.

Reaction of 9 with 1,2-bis(4-pyridyl)ethane.

Synthesis of $[\text{Cu}_3(\mu_3\text{-OH})(\mu\text{-pz})_3(\text{CH}_2=\text{CHCOO})_2(\text{C}_{12}\text{H}_{12}\text{N}_2)_{0.5}]$, **Cu3AcryMBpetha**.

To a solution of **9** (101 mg, 0.17 mmol) in 20 mL of MeOH a solution of 1,2-bis(4-pyridyl)ethane (64 mg, 0.35 mmol) in 5 mL of MeOH was added under stirring. The obtained solution was stirred for 5 minutes, and then let to slowly evaporate in the air, yielding blue well-formed crystals, suitable for an XRD crystal structure determination.

Cu3AcryMBpetha. Yield 13 mg, 12%. Anal. Calcd for $[\text{Cu}_3(\mu_3\text{-OH})(\mu\text{-pz})_3(\text{CH}_2=\text{CHCOO})_2(\text{C}_{12}\text{H}_{12}\text{N}_2)_{0.5}]$: C, 39.22; H, 3.45; N, 15.25. Found: C, 39.45; H, 3.24; N, 15.31. IR (KBr, cm^{-1}): 3415, 3123, 3233, 2856, 1639, 1616, 1568, 1491, 1430, 1417, 1384, 1359, 1344, 1278, 1178, 1068, 1029, 995, 978, 951, 901, 830, 759, 745, 689, 679, 625, 555, 483. ESI-MS (+) (MeOH, MeCN) (higher peaks, m/z; relative abundance, %): 580.3 (13)
 $[\text{Cu}_3(\text{OH})(\text{pz})_3(\text{CH}_2=\text{CHCOO})(\text{MeOH})_2(\text{H}_2\text{O})_2]^+$, 655.2 (42) $[\text{Cu}_4(\text{OCH}_3)_2(\text{pz})_4(\text{CH}_2=\text{CHCOO})]^+$, 678.3
 (40) $[\text{Cu}_4(\text{OCH}_3)_3(\text{pz})_3(\text{CH}_2=\text{CHCOO})(\text{MeCN})(\text{H}_2\text{O})]^+$, 826.5 (20)
 $[\text{Cu}_3(\text{OH})(\text{pz})_3(\text{CH}_2=\text{CHCOO})(\text{bpetha})(\text{MeCN})(\text{MeOH})(\text{H}_2\text{O})_5]^+$, 839.5 (68)
 $[\text{Cu}_4(\text{OCH}_3)_2(\text{pz})_4(\text{CH}_2=\text{CHCOO})(\text{bpetha})]^+$, 987.3 (42) $[\text{Cu}_6(\text{OH})_5(\text{pz})_5(\text{CH}_2=\text{CHCOO})(\text{MeOH})_3(\text{H}_2\text{O})]^+$,
 1023.3 (100) $[\text{Cu}_6(\text{OCH}_3)_3(\text{pz})_5(\text{CH}_2=\text{CHCOO})_3]^+$, 1059.3 (50) $[\text{Cu}_6(\text{OCH}_3)_2(\text{pz})_6(\text{CH}_2=\text{CHCOO})_3]^+$,
 1383.4 (29) $[\text{Cu}_6(\text{OH})_2(\text{pz})_6(\text{CH}_2=\text{CHCOO})_4(\text{bpetha})(\text{MeOH})_3+\text{H}]^+$.

Reaction of **10** with 1,2-bis(4-pyridyl)ethane.

Synthesis of $[\text{Cu}_3(\mu_3\text{-OH})(\mu\text{-pz})_3(\text{CH}_2=\text{C}(\text{CH}_3)\text{COO})_2(\text{C}_{12}\text{H}_{12}\text{N}_2)_{0.5}(\text{H}_2\text{O})]$, **Cu3MethBpetha1, and $[\text{Cu}_3(\mu_3\text{-OH})(\mu\text{-pz})_3(\text{CH}_2=\text{C}(\text{CH}_3)\text{COO})_2(\text{C}_{12}\text{H}_{12}\text{N}_2)_{1.5}]$, **Cu3MethBpetha2**.**

To a solution of **10** (102 mg, 0.18 mmol) in 20 mL of MeOH a solution of 1,2-bis(4-pyridyl)ethane (67 mg, 0.36 mmol) in 5 mL of MeOH was added under stirring. The obtained solution was stirred for 5 minutes, and then let to slowly evaporate in the air, yielding blue well-formed crystals, suitable for an XRD crystal structure determination.

Cu3MethBpetha1. Yield 55 mg. Anal. Calcd for $[\text{Cu}_3(\mu_3\text{-OH})(\mu\text{-pz})_3(\text{CH}_2=\text{C}(\text{CH}_3)\text{COO})_2(\text{C}_{12}\text{H}_{12}\text{N}_2)_{0.5}(\text{H}_2\text{O})]$: C, 40.10; H, 4.10; N, 14.23. Found: C, 40.36; H, 4.21; N, 14.43. IR (KBr, cm^{-1}): 3403, 3131, 2957, 2921, 1646, 1612, 1587, 1544, 1491, 1451, 1432, 1401, 1384, 1367, 1277, 1232, 1178, 1063, 1004, 936, 857, 829, 764, 747, 624, 550. ESI-MS (+) (MeOH, MeCN) (higher peaks, m/z; relative abundance, %): 594.3 (12) $[\text{Cu}_3(\text{OH})(\text{pz})_3(\text{CH}_2=\text{C}(\text{CH}_3)\text{COO})(\text{MeOH})_2(\text{H}_2\text{O})_2]^+$, 669.3 (42) $[\text{Cu}_4(\text{OCH}_3)_2(\text{pz})_4(\text{CH}_2=\text{C}(\text{CH}_3)\text{COO})]^+$, 692.5 (30) $[\text{Cu}_3(\text{OH})(\text{pz})_3(\text{CH}_2=\text{C}(\text{CH}_3)\text{COO})_2(\text{H}_2\text{O})_5+\text{Na}]^+$, 710.3 (25) $[\text{Cu}_3(\text{OH})(\text{pz})_3(\text{CH}_2=\text{C}(\text{CH}_3)\text{COO})_2(\text{H}_2\text{O})_6+\text{Na}]^+$, 840.5 (10) $[\text{Cu}_3(\text{OH})(\text{pz})_3(\text{CH}_2=\text{C}(\text{CH}_3)\text{COO})(\text{bpetha})(\text{H}_2\text{O})_9]^+$, 853.5 (39) $[\text{Cu}_4(\text{OCH}_3)_2(\text{pz})_4(\text{CH}_2=\text{C}(\text{CH}_3)\text{COO})(\text{bpetha})]^+$, 1029.4 (40) $[\text{Cu}_6(\text{OCH}_3)_3(\text{pz})_7(\text{CH}_2=\text{C}(\text{CH}_3)\text{COO})]^+$, 1065.4 (100) $[\text{Cu}_6(\text{OCH}_3)_3(\text{pz})_7(\text{CH}_2=\text{C}(\text{CH}_3)\text{COO})(\text{H}_2\text{O})_2]^+$, 1083.4 (10) $[\text{Cu}_6(\text{OCH}_3)_3(\text{pz})_7(\text{CH}_2=\text{C}(\text{CH}_3)\text{COO})(\text{H}_2\text{O})_3]^+$, 1101.4 (65) $[\text{Cu}_6(\text{OCH}_3)_2(\text{pz})_6(\text{CH}_2=\text{C}(\text{CH}_3)\text{COO})_3]^+$, 1425.4 (10) $[\text{Cu}_6(\text{OH})_2(\text{pz})_6(\text{CH}_2=\text{C}(\text{CH}_3)\text{COO})_4(\text{bpetha})(\text{MeOH})_2(\text{H}_2\text{O})+\text{H}]^+$.

Mother liquors were let to further evaporation, obtaining a second crop of crystals, suitable for an XRD crystal structure determination.

Cu3MethBpetha2. Yield 27 mg. Anal. Calcd. for $[\text{Cu}_3(\mu_3\text{-OH})(\mu\text{-pz})_3(\text{CH}_2=\text{C}(\text{CH}_3)\text{COO})_2(\text{C}_{12}\text{H}_{12}\text{N}_2)_{1.5}]$: C, 49.15; H, 4.48; N, 14.74. Found: C, 49.04; H, 4.53; N, 14.82. IR (KBr, cm^{-1}): 3421, 3088, 2921, 2850, 1616, 1569, 1502, 1489, 1455, 1429, 1403, 1382, 1273, 1221, 1179, 1072, 1059, 1026, 1009, 926, 843, 827, 813, 764, 755, 748, 627, 558, 546, 503. ESI-MS (+) (MeOH, MeCN) (higher peaks, m/z; relative abundance, %): 594.3 (37) $[\text{Cu}_3(\text{OH})(\text{pz})_3(\text{CH}_2=\text{C}(\text{CH}_3)\text{COO})(\text{MeOH})_2(\text{H}_2\text{O})_2]^+$, 669.3 (38) $[\text{Cu}_4(\text{OCH}_3)_2(\text{pz})_4(\text{CH}_2=\text{C}(\text{CH}_3)\text{COO})]^+$, 692.4 (58) $[\text{Cu}_3(\text{OH})(\text{pz})_3(\text{CH}_2=\text{C}(\text{CH}_3)\text{COO})_2(\text{H}_2\text{O})_5+\text{Na}]^+$, 710.5 (40) $[\text{Cu}_3(\text{OH})(\text{pz})_3(\text{CH}_2=\text{C}(\text{CH}_3)\text{COO})_2(\text{H}_2\text{O})_6+\text{Na}]^+$, 840.5 (100) $[\text{Cu}_3(\text{OH})(\text{pz})_3(\text{CH}_2=\text{C}(\text{CH}_3)\text{COO})(\text{bpetha})(\text{H}_2\text{O})_9]^+$, 853.5 (75) $[\text{Cu}_4(\text{OCH}_3)_2(\text{pz})_4(\text{CH}_2=\text{C}(\text{CH}_3)\text{COO})(\text{bpetha})]^+$, 1029.3 (35) $[\text{Cu}_6(\text{OCH}_3)_3(\text{pz})_7(\text{CH}_2=\text{C}(\text{CH}_3)\text{COO})]^+$, 1065.4 (70) $[\text{Cu}_6(\text{OCH}_3)_3(\text{pz})_7(\text{CH}_2=\text{C}(\text{CH}_3)\text{COO})(\text{H}_2\text{O})_2]^+$, 1101.4 (40) $[\text{Cu}_6(\text{OCH}_3)_2(\text{pz})_6(\text{CH}_2=\text{C}(\text{CH}_3)\text{COO})_3]^+$.

Reactions of Trinuclear Triangular Cu^(II) Derivatives with 1,2-bis(4-pyridyl)ethylene

Reaction of **1** with 1,2-bis(4-pyridyl)ethylene.

Synthesis of [(Cu₃(μ₃-OH)(μμ-pz)₃(HCOO)₂)₄(C₁₂H₁₀N₂)₅], **Cu₃FormBpethy**.

To a solution of **1** (50 mg, 0.08 mmol) in 20 mL of EtOH a solution of 1,2-bis(4-pyridyl)ethylene (120 mg, 0.66 mmol) in 5 mL of EtOH was added under stirring. The obtained solution was stirred for 5 minutes, and then let to slowly evaporate in the air, yielding well-formed blue crystals, whose XRD crystal structure was determined.

Cu₃FormBpethy. Yield 21 mg, 36%. Anal. Calcd for [(Cu₃(μ₃-OH)(μμ-pz)₃(HCOO)₂)₄(C₁₂H₁₀N₂)₅]: C, 42.97; H, 3.40; N, 16.38. Found: C, 42.69; H, 3.48; N, 15.88. IR (KBr, cm⁻¹): 3115, 3054, 2923, 2807, 2706, 1584, 1505, 1490, 1428, 1419, 1380, 1349, 1317, 1275, 1250, 1209, 1179, 1059, 1026, 1007, 991, 967, 922, 881, 837, 825, 750. ESI-MS (+) (MeOH, MeCN) (higher peaks, m/z; relative abundance, %): 183.3 (50) [bpethy+H]⁺, 629.2 (15) [Cu₃(OH)(pz)₂(HCOO)₂(MeOH)₂(MeCN)(EtOH)₂]⁺, 650.3 (35) [Cu₃(OH)(pz)₃(HCOO)₂(MeOH)₃(H₂O)₃+H]⁺, 664.3 (15) [Cu₃(OH)(pz)₃(HCOO)₂(MeOH)₄(H₂O)₂+H]⁺, 796.5 (35) [Cu₃(OH)(pz)₃(HCOO)₂(bpethy)(MeOH)₃(H₂O)+H]⁺, 811.3 (100) [Cu₄(OH)₂(pz)₃(HCOO)₂(bpethy)(MeOH)(H₂O)]⁺, 1305.3 (10) [Cu₆(OH)₃(pz)₇(HCOO)₂(bpethy)(H₂O)₆+Na]⁺.

Reaction of **2** with 1,2-bis(4-pyridyl)ethylene.

Synthesis of [Cu₃(μ₃-OH)(μ-pz)₃(CH₃COO)₂(C₁₂H₁₀N₂)(H₂O)], **Cu₃AcBpethy**.

To a solution of **2** (103 mg, 0.17 mmol) in 100 mL of MeOH a solution of 1,2-bis(4-pyridyl)ethylene (61 mg, 0.33 mmol) in 5 mL of MeOH was added under stirring. The obtained solution was stirred for 5 minutes, and then let to slowly evaporate in the air, yielding blue crystals, whose XRD crystal structure was determined.

Cu₃AcBpethy. Yield 39 mg, 32%. Anal. Calcd for [Cu₃(μ₃-OH)(μ-pz)₃(CH₃COO)₂(C₁₂H₁₀N₂)(H₂O)]: C, 41.29; H, 3.88; N, 15.41. Found: C, 41.43; H, 3.63; N, 14.86. IR (KBr, cm⁻¹): 3415, 3267, 3117, 3230, 2850, 1613, 1565, 1507, 1492, 1433, 1421, 1399, 1380, 1335, 1302, 1278, 1251, 1223, 1205, 1178, 1062, 1025, 984, 969, 836, 767, 628, 561, 482. ESI-MS (+) (MeOH, MeCN) (higher peaks, m/z; relative abundance, %): 183.2 (8) [bpethy+H]⁺, 566.2 (48) [Cu₃(OH)(pz)₄(H₂O)₅]⁺, 643.2 (100) [Cu₄(OH)₂(pz)₃(CH₃COO)₂(H₂O)₂]⁺, 656.3 (20) [Cu₃(OH)(pz)₄(H₂O)₁₀]⁺, 664.4 (65) [Cu₃(OCH₃)(pz)₃(CH₃COO)(bpethy)]⁺, 810.5 (30) [Cu₃(OH)(pz)₃(CH₃COO)₂(bpethy)(H₂O)₂(MeOH)₂+H]⁺, 817.3 (15) [Cu₄(OCH₃)₂(pz)₃(CH₃COO)₂(bpethy)]⁺, 825.5 (75) [Cu₄(OH)₂(pz)₃(CH₃COO)₂(bpethy)(H₂O)₂]⁺, 951.3 (40) [Cu₆(OH)₄(pz)₆(CH₃COO)(MeCN)]⁺, 987.3 (60) [Cu₆(OH)₄(pz)₆(CH₃COO)(H₂O)₂(MeCN)]⁺, 1023.3 (14) [Cu₆(OH)₄(pz)₆(CH₃COO)(H₂O)₄(MeCN)]⁺, 1347.4 (30) [Cu₆(OCH₃)₂(pz)₆(CH₃COO)₄(bpethy)(MeOH)₂(H₂O)+H]⁺.

Reaction of the Trinuclear Triangular Cu^(II) Derivatives **1** and **9** with 1,5-naphthyridine

Reaction of **1** with 1,5-naphthyridine.

Synthesis of [Cu₃(μ₃-OCH₃)(μ-pz)₃(HCOO)₂(Hpz)₂(H₂O)], **1b**.

To a solution of **1** (102 mg, 0.16 mmol) in 30 mL of MeOH a solution of 1,5-naphthyridine (43 mg, 0.33 mmol) in 5 mL of MeOH was added under stirring. The obtained solution was stirred for 5 minutes, and then let to slowly evaporate in the air, yielding well-formed blue crystals, whose XRD crystal structure was determined.

1b. Yield 82 mg, 77%. Anal. Calcd for [Cu₃(μ₃-OCH₃)(μ-pz)₃(HCOO)₂(Hpz)₂(H₂O)]: C, 32.41; H, 3.63; N, 21.00. Found: C, 32.05; H, 3.50; N, 21.51. IR (KBr, cm⁻¹): 3611, 3343, 3125, 2971, 2917, 2840, 2812, 2729, 1723, 1626, 1605, 1567, 1489, 1418, 1407, 1380, 1347, 1314, 1294, 1279, 1179, 1168, 1135, 1059, 1043, 972, 938, 911, 884, 845, 833, 789, 772, 765, 657. ESI-MS (+) (MeOH, MeCN) (higher peaks, m/z; relative abundance, %): 69.2 (15) [Hpz+H]⁺, 244.1 (10) [Cu(HCOO)(MeOH)₂(H₂O)₄]⁺, 453.9 (20) [Cu₃(OH)(pz)₃(HCOO)]⁺, 476.0 (40) [Cu₃(OCH₃)(pz)₃(OH)(H₂O)₂]⁺, 536.0 (50) [Cu₃(OCH₃)(pz)₃(HCOO)(MeOH)(H₂O)₂]⁺, 572.0 (60) [Cu₃(OCH₃)(pz)₃(HCOO)(MeOH)(H₂O)₄]⁺, 604.0 (100) [Cu₃(OCH₃)(pz)₃(HCOO)(Hpz)₂]⁺, 697.0 (40) [Cu₄(OCH₃)₂(pz)₃(HCOO)₂(H₂O)₅]⁺, 981.0 (15) [Cu₆(OCH₃)₂(pz)₆(HCOO)₃]⁺.

Reaction of **9** with 1,5-naphthyridine.

Synthesis of [Cu₃(μ₃-OH)(μ-pz)₃(CH₂=CHCOO)₂(C₈H₆N₂)(H₂O)], **Cu3AcryMNapht**.

To a solution of **9** (100 mg, 0.17 mmol) in 30 mL of MeOH a solution of 1,5-naphthyridine (45 mg, 0.35 mmol) in 5 mL of MeOH was added under stirring. The obtained solution was stirred for 5 minutes, and then let to slowly evaporate in the air, yielding blue well-formed crystals suitable for an XRD crystal structure determination.

Cu3AcryMNapht. Yield 42 mg, 35%. Anal. Calcd for [Cu₃(μ₃-OH)(μ-pz)₃(CH₂=CHCOO)₂(C₈H₆N₂)(H₂O)]: C, 39.51; H, 3.46; N, 16.03. Found: C, 39.55; H, 3.66; N, 16.22. IR (KBr, cm⁻¹): 3586, 3350, 3223, 3109, 3081, 3028, 2766, 1635, 1558, 1500, 1415, 1378, 1343, 1303, 1266, 1222, 1204, 1176, 1164, 1124, 1079, 1057, 1029, 981, 966, 921, 902, 836, 825, 816, 777, 753, 683, 667. ESI-MS (+) (MeOH, MeCN) (higher peaks, m/z; relative abundance, %): 131.1 (33) [napht+H]⁺, 494.0 (15) [Cu₃(OCH₃)(pz)₃(CH₂=CHCOO)]⁺, 525.9 (10) [Cu₃(OCH₃)(pz)₃(CH₂=CHCOO)(MeOH)]⁺, 530.0 (30) [Cu₃(OH)(pz)₃(CH₂=CHCOO)(MeOH)(H₂O)]⁺, 533.8 (35) [Cu₃(pz)₃(CH₂=CHCOO)₂]⁺, 602.0 (95) [Cu₃(OH)(pz)₃(CH₂=CHCOO)₂(MeOH)(H₂O)+H]⁺, 624.0 (60) [Cu₃(OCH₃)(pz)₃(CH₂=CHCOO)(napht)]⁺, 628.0 (45) [Cu₃(OH)(pz)₃(CH₂=CHCOO)(napht)(H₂O)]⁺, 655.0 (40) [Cu₄(OCH₃)₂(pz)₄(CH₂=CHCOO)]⁺, 1023.0 (35) [Cu₆(OCH₃)₂(pz)₅(CH₂=CHCOO)₃]⁺, 1058.9 (100) [Cu₆(OCH₃)₂(pz)₆(CH₂=CHCOO)₃]⁺.

Reaction of the Trinuclear Triangular Cu^(II) Derivative 1 with 1,3-bis(4-pyridyl)propane

Reaction of 1 with 1,3-bis(4-pyridyl)propane.

Synthesis of Cu₃(μ₃-OH)(μ-pz)₃(HCOO)₂(C₁₃H₁₄N₂)(H₂O)], Cu3FormTmb.

To a solution of **1** (101 mg, 0.16 mmol) in 20 mL of EtOH a solution of 1,3-bis(4-pyridyl)propane (65 mg, 0.33 mmol) in 5 mL of CHCl₃ was added under stirring. The obtained solution was stirred for 5 minutes, and then let to slowly evaporate in the air, yielding a blue powder.

Cu3FormTmb. Yield 87 mg, 76%. Anal. Calcd for [Cu₃(μ₃-OH)(μ-pz)₃(HCOO)₂(C₁₃H₁₄N₂)(H₂O)]: C, 40.31; H, 3.95; N, 15.67. Found: C, 40.87; H, 3.81; N, 15.35. IR (KBr, cm⁻¹): 3398, 3219, 3136, 2939, 2814, 2701, 1598, 1507, 1488, 1432, 1381, 1338, 1276, 1221, 1179, 1060, 758, 628. ESI-MS (+) (MeOH, MeCN) (higher peaks, m/z; relative abundance, %): 199.3 (40) [tmb+H]⁺, 568.3 (43) [Cu₃(OH)(pz)₃(HCOO)₂(Hpz)+H]⁺, 666.5 (90) [Cu₃(OH)(pz)₂(HCOO)₂(tmb)(H₂O)₂]⁺, 827.5 (100) [Cu₄(OH)₂(pz)₃(HCOO)₂(tmb)(MeOH)(H₂O)]⁺, 1305.4 (20) [Cu₆(OH)₂(pz)₆(HCOO)₃(tmb)(MeOH)₂(H₂O)₅]⁺.

Reaction of the Trinuclear Triangular Cu^(II) Derivative 1 with 1,2-bis(4-pyridyl)disulfane

Reaction of 1 with 1,2-bis(4-pyridyl)disulfane.

Synthesis of [Cu₃(μ₃-OH)(μ-pz)₃(HCOO)₂(C₁₀H₈N₂S₂)], Cu3FormBpsulf.

To a solution of **1** (103 mg, 0.16 mmol) in 20 mL of MeOH a solution of 1,2-bis(4-pyridyl)disulfane (71 mg, 0.32 mmol) in 5 mL of acetone was added under stirring. The obtained solution was stirred for 5 minutes, and then let to slowly evaporate in the air, yielding green microcrystals.

Cu3FormBpsulf. Yield 91 mg, 79%. Anal. Calcd for [Cu₃(μ₃-OH)(μ-pz)₃(HCOO)₂(C₁₀H₈N₂S₂)]: C, 35.15; H, 2.79; N, 15.62; S, 8.93. Found: C, 33.35; H, 2.91; N, 15.30; S, 9.65. IR (KBr, cm⁻¹): 3403, 3231, 3076, 2927, 2797, 1634, 1588, 1568, 1542, 1489, 1416, 1383, 1334, 1316, 1281, 1215, 1182, 1064, 1022, 871, 828, 753, 710, 625, 505. ESI-MS (+) (MeOH, MeCN) (higher peaks, m/z; relative abundance, %): 221.1 (85) [bpsulf+H]⁺, 476.2 (15) [Cu₃(OH)₂(pz)₃(MeOH)(H₂O)]⁺, 504.1 (14) [Cu₃(OH)(pz)₃(HCOO)(MeOH)(H₂O)]⁺, 526.2 (14) [Cu₃(OH)₂(pz)₃(MeOH)₂(H₂O)₂]⁺, 536.2 (30) [Cu₃(OH)(pz)₃(HCOO)(MeOH)₂(H₂O)]⁺, 550.2 (8) [Cu₃(OH)(pz)₂(HCOO)₂(MeOH)₂(H₂O)₃]⁺, 629.2 (45) [Cu₄(OH)₂(pz)₃(HCOO)₂(H₂O)(MeOH)]⁺, 688.3 (70) [Cu₃(OCH₃)(pz)₃(HCOO)(bpsulf)]⁺, 849.3 (100) [Cu₄(OH)₂(pz)₃(HCOO)₂(bpsulf)(H₂O)(MeOH)]⁺, 1303.4 (25) [Cu₆(OH)₂(pz)₆(HCOO)₃(bpsulf)(MeOH)₃(H₂O)₂]⁺.

REFERENCES

- Abrahams, B.F.; Hoskins, B.F.; Michail, D.M.; Robson, R. *Nature*, **1994**, *369*, 727.
- Alegria, E.C.B.; Kirillova, M.V.; Martins, L.R.; Pombeiro, A.J.L. *Appl. Catal. A: Gen.*, **2007**, *317*, 43.
- Altomare, A.; Burla, M.C.; Camalli, M.; Cascarano, G.L.; Giacovazzo, C.; Guagliardi, A.; Moliterni, A.G.G.; Polidori, G.; Spagna, R. *J. Appl. Cryst.*, **1999**, *32*, 115.
- Anderson, C.-R.; Coker, D.F.; Eckert, J.; Bug, A.L.R. *J. Chem. Phys.*, **1999**, *111*, 7599.
- Angaridis, P.A.; Baran, R.; Boča, R.; Cervantes-Lee, F.; Haase, W.; Mezei, G.; Raptis, R.G.; Werner, R. *Inorg. Chem.*, **2002**, *41*, 2219.
- Archer, E.A.; Golbderg, N.T.; Lynch, V.; Krische, M.J. *J. Am. Chem. Soc.*, **2000**, *122*, 5006.
- Archer, E.A.; Gong, H.G.; Krische, M.J. *Tetrahedron*, **2001**, *57*, 1139.
- Archer, E.A.; Krische, M.J. *J. Am. Chem. Soc.*, **2002**, *124*, 5074.
- Astley, T.; Gulbis, J.M.; Hitchman, M.A.; Tienkink, E.R. *J. Chem. Soc., Dalton Trans.*, **1993**, 509.
- Ayala, M.; Torres, E. *Appl. Catal. A*, **2004**, *272*, 1.
- Bae, Y.-S.; Mulfort, K.L.; Frost, H.; Ryan, P.; Punnathanam, S.; Broadbelt, L.J.; Hupp, J.T.; Snurr, R.Q. *Langmuir*, **2008**, *24*, 8592.
- Banfi, S.; Carlucci, L.; Caruso, E.; Ciani, G.; Proserpio, D.M. *Dalton Trans.*, **2002**, 2714.
- Barbour, J.L. *Chem. Commun.*, **2006**, 1163.
- Barthelet, K.; Marrot, J.; Riou, D.; Férey, G. *Angew. Chem. Int. Ed.*, **2002**, *41*, 281
- Barthelet, K.; Marrot, J.; Riou, D.; Férey, G. *Chem. Commun.*, **2004**, 520.
- Barton, T.J.; Bull, L.M.; Klemperer, W.G.; Loy, D.A.; McEnaney, B.; Misono, M.; Monson, P.A.; Pez, G.; Scherer, G.W.; Vartuli, J.C.; Yaghi, O.M. *Chem. Mater.*, **1999**, *11*, 2633.
- Bauer, S.; Bein, T.; Stock, N. *Inorg. Chem.*, **2005**, *44*, 5882.
- Bax, A.; Subramanian, S. *J. Magn. Reson.*, **1986**, *67*, 565.
- Bax, A.; Summers, M.F. *J. Am. Chem. Soc.*, **1986**, *108*, 2093.
- Bencini, A.; Casarin, M.; Forrer, D.; Franco, L.; Garau, F.; Masciocchi, N.; Pandolfo, L.; Pettinari, C.; Ruzzi, M.; Vittadini, A. *Inorg. Chem.*, **2009**, *48*, 4044.
- Bernhardt, P.V.; Hayes, E.J. *Inorg. Chem.*, **1998**, *37*, 4214.
- Boča, R.; Dlháň, L.; Mezei, G.; Ortiz-Pérez, T.; Raptis, R.G.; Telsler, J. *Inorg. Chem.*, **2003**, *42*, 5801.
- Brückner, H.; Wachsmann, M. *J. Chromatogr. A*, **2003**, *998*, 73.
- Brunauer, S.; Emmett, P.H.; Teller, E. *J. Am. Chem. Soc.*, **1938**, *60*, 309.
- Brunauer, S.; Deming, L.S.; Deming, W.E.; Teller, E. *J. Am. Chem. Soc.*, **1940**, *62*, 1723.
- Bureekaew, S.; Shimomura, S.; Kitagawa, S. *Sci. Technol. Adv. Mater.*, **2008**, *9*, 1.
- Caron, S.; Dugger, R.W.; Ruggeri, S.G.; Ragan, J.A.; Brow Ripin, D.H. *Chem. Rev.*, **2006**, *106*, 2943.
- Carreño, M.C. *Chem. Rev.*, **1995**, *95*, 1717.
- Casarin, M.; Corvaja, C.; Di Nicola, C.; Falcomer, D.; Franco, L.; Monari, M.; Pandolfo, L.; Pettinari, C.; Piccinelli, F.; Tagliatesta, P. *Inorg. Chem.*, **2004**, *43*, 5865.
- Casarin, M.; Corvaja, C.; Di Nicola, C.; Falcomer, D.; Franco, L.; Monari, M.; Pandolfo, L.; Pettinari, C.; Piccinelli, F. *Inorg. Chem.*, **2005**, *44*, 6265.

- Casarin, M.; Cingolani, A.; Di Nicola, C.; Falcomer, D.; Monari, M.; Pandolfo, L.; Pettinari, C. *Cryst. Growth Des.*, **2007** (a), 4, 676.
- Casarin, M.; Cerquetella, A.; Garau, F.; Monari, M.; Pandolfo, L.; Pettinari, C.; Venzo, A. *6th International School of Organometallic Chemistry*, Camerino, September 8-12, **2007** (b), P65.
- Casarin, M.; Garau, F.; Monari, M.; Pandolfo, L.; Pettinari, C.; Venzo, A. *Proceedings of VIII Congresso Nazionale di Chimica Supramolecolare*, Trieste, September 19-22, **2007** (c), P30.
- Casarin, M.; Garau, F.; Monari, M.; Pandolfo, L.; Pettinari, C.; Venzo, A. *New J. Chem.*, **2008** (a), 32, 358.
- Casarin, M.; Forrer, D.; Garau, F.; Pandolfo, L.; Pettinari, C.; Vittadini, A. *J. Phys. Chem. A*, **2008** (b), 112, 6723.
- Casarin, M.; Forrer, D.; Garau, F.; Pandolfo, L.; Pettinari, C.; Vittadini, A. *Inorg. Chim. Acta.*, **2009**, 362, 4358.
- Chae, H.K.; Siberio-Pérez, D.Y.; Kim, J.; Go, Y.; Eddaoudi, M.; Matzger, A.J., et al. *Nature*, **2004** 427 523.
- Chen, B.; Ockwig, N.W.; Millward, A.R.; Contreras, D.S.; Yaghi, O.M. *Angew. Chem. Int. Ed.*, **2005**, 117, 4823.
- Cingolani, A.; Galli, S.; Masciocchi, N.; Pandolfo, L.; Pettinari, C.; Sironi, A. *J. Am. Chem. Soc.*, **2005**, 127, 6144.
- Claramunt, R.M.; Cornago, P.; Cano, M.; Heras, J.V.; Gallego, M.L.; Pinilla, E.; Torres, M.R. *Eur. J. Inorg. Chem.*, **2003**, 2693.
- Clark, L.A.; Chempath, S.; Snurr, R.A. *Langmuir*, **2005**, 21, 2267.
- Cole, A.P.; Root, D.E.; Mukherjee, P.; Solomon, E.I.; Stack, T.D. P. *Science*, **1996**, 273, 1848.
- Contaldi, S.; Di Nicola, C.; Garau, F.; Karabach, Y.Yu.; Martins, L.M.D.R.S.; Monari, M.; Pandolfo, L.; Pettinari, C.; Pombeiro, A.J.L. *Dalton Trans.*, **2009**, 4928.
- Cuthbertson, W.W.; Moffat, J.S. *J. Chem. Soc.*, **1948**, 561.
- Czaja, A.U.; Trukhan, N.; Mueller, U. *Chem. Soc. Rev.*, **2009**, 38, 1284.
- de Hoog, P.; Gamez, P.; Driessen, W.L.; Reedijk, J. *Tetrahedron Lett.*, **2002**, 43, 6783.
- de la Hoz, A.; Díaz-Ortiz, A.; Elguero, J.; Martínez, L.J.; Moreno, A.; Sánchez-Migallón, A. *Tetrahedron*, **2001**, 57, 4397.
- Dell'Anna, M.M.; Mastroilli, P.; Nobile, C.F.; Taurino, M.R.; Calò, V.; Nacci, A. *J. Mol. Catal. A: Chem.*, **2000**, 151, 61.
- Dincă, M.; Seok Han, W.; Liu, Y.; Dailly, A.; Brown, C.M.; Long, J.R. *Angew. Chem. Int. Ed.*, **2007**, 46, 1419.
- Di Nicola, C.; Karabach, Y.Y.; Kirillov, A.M.; Monari, M.; Pandolfo, L.; Pettinari, C.; Pombeiro, A.J.L. *Inorg. Chem.*, **2007** (a), 46, 221.
- Di Nicola, C.; Garau, F.; Monari, M.; Pandolfo, L.; Pettinari, C. *Proceedings of VIII Congresso Nazionale di Chimica Supramolecolare*, Trieste, Settembre 19-22, **2007** (b), P53.
- Di Nicola, C.; Garau, F.; Monari, M.; Pandolfo, L.; Pettinari, C.; Pombeiro, A. J. L. *Proceedings of 4th EuChemMS Conference on Nitrogen Ligands*, Garmisch-Partenkirchen (Germania), Agosto 24-28, **2008**, P79.

- Di Nicola, C.; Garau, F.; Karabach, Y.Y.; Martins, L.M.D.R.S.; Monari, M.; Pandolfo, L.; Pettinari, C.; Pombeiro, A.J.L. *Eur. J. Inorg. Chem.*, **2009**, 666.
- Drobny, G.; Pines, A.; Sinton, S.; Weitekamp, D.; Wemmer, D. *Faraday Symp. Chem. Soc.*, **1979**, B33, 4912.
- Eddaoudi, M.; Moler, D.B.; Li, H.; Chen, B.; Reineke, T.M.; O'Keeffe, M.; Yaghi, O. *Acc. Chem. Res.*, **2001**, 34, 319.
- Elguero, J.; Guerriero, A.; de la Torre, G.F.; de la Hoz, A.; Jalón, F.A.; Manzano, A.B.; Rodríguez, A. *New J. Chem.*, **2001**, 25, 1050.
- Elliot, S.J.; Zhu, M.; Tso, L.; Nguyen, H.-H.T.; Yip, J.H.-K.; Chan, S.I. *J. Am. Chem. Soc.*, **1997**, 119, 9949.
- Férey, G. *Chem. Mater.*, **2001**, 13, 3084.
- Férey, G.; Latroche, M.; Serre, C.; Millange, F.; Loiseau, T.; Percheron-Guégan, A. *Chem. Commun.*, **2003**, 2976.
- Férey, G.; Serre, C.; Mellot-Draznieks, C.; Millange, F.; Surblé, S.; Dutour, J.; Margiolaki, I. *Angew. Chem. Int Ed.*, **2004**, 116, 6456.
- Férey, G.; Mallot-Draznieks, C.; Serre, C.; Millange, F.; Dutour, J.; Surblé, S. et al., *Science*, **2005**, 309, 2040.
- Férey, G. *Chem. Soc. Rev.*, **2008**, 37, 191.
- Férey, G.; Serre, C. *Chem. Soc. Rev.*, **2009**, 38, 1380.
- Férey, G. *Dalton. Trans.*, **2009**, 4400.
- Fernández, I.; Khair, N. *Chem. Rev.*, **2003**, 103, 3651.
- Ferrer, S.; Aznar, E.; Lloret, F.; Castiñeiras, A.; Liu-Gonzales, M.; Borrás, J. *Inorg. Chem.*, **2007**, 46, 372.
- Foster, M.D.; Delgado Friedrichs, O.; Bell, R.G.; Almeida Paz, F.A.; Klinowski, J. *Angew. Chem., Int. Ed.*, **2003**, 42, 3896.
- Forster, P.M.; Burbank, A.R.; O'Sullivan, M.C.; Guillou, N.; Livage, C.; Férey, G.; Stock, N.; Cheetham, A.K. *Solid State Sci.*, **2005**, 7, 1549.
- Fraústo da Silva, J.J.R. Williams, R.J.P. *The Biological Chemistry of the Elements*, Oxford University Press, Oxford, **2001**.
- Gamez, P.; de Hoog, P.; Roubeau, O.; Lutz, M.; Driessen, W.L.; Spek, A.L.; Reedijk, J. *Chem. Commun.*, **2002**, 1488.
- Gamez, P.; Reedijk, J. *Eur. J. Inorg. Chem.*, **2006**, 29.
- Garau, F.; Pandolfo, L.; Di Nicola, C.; Ngoune, J.; Pettinari, C.; Monari, M.; Pombeiro, A.J.L.; Martins, L.M.D.R.S.; Karabach, Y.Y. *1st International Conference on Metal-Organic Frameworks and Open Framework Compounds*, Augsburg (Germany), October 8-10, **2008**, P124.
- Garau, F.; Monari, M.; Pandolfo, L.; Pettinari, C.; Venzo, A. *Cryst. Eng. Comm.*, **2010**, in the press: DOI: 10.1039/b922874h.
- Gardner, G.B.; Venkataraman, D.; Moore, S.; Lee, S. *Nature*, **1995**, 374, 792.
- Gelling, A.; Olsen, M.D.; Orrel, K.G.; Osborne, A.G.; Šik, V. *Inorg. Chim. Acta*, **1997**, 264, 257.
- Glaser, J.; Tragl, S.; Meyer, H.J. *Z. Kristallogr.*, **2005**, 220, 214.
- Gregg, S.J.; Sing, K.S.W. *Adsorption, surface area, and porosity*. London: Academic Press; **1984**.

Hathaway, B.J. *Structure and Bonding*, **1984**, 57, 55.

Hathaway, B.J. *Structure and Bonding*, **1973**, 14, 49.

Holm, R.H.; Kennepohl, P.; Solomon, E.I. *Chem. Rev.*, **1996**, 96, 2239.

Hoskins, B.F.; Robson, R. *J. Am. Chem. Soc.*, **1989**, 111, 5962.

Hoskins, B.F.; Robson, R. *J. Am. Chem. Soc.*, **1990**, 112, 1546.

Huber, R. *Angew. Chem. Int. Ed.*, **1989**, 28, 848.

Hulsbergen, F.B.; ten Hoedt, R.W.M.; Verschoor, G.C.; Reedijk, J.; Spek, A.L. *J. Chem. Soc., Dalton Trans.*, **1983**, 539.

Itoh S. in *Comprehensive Coordination Chemistry*, Vol. 8 (Eds.: McCleverty, J.A.; Meyer, T.J.; Que, L.; Tolman W.B.), 2nd ed., Elsevier, Dordrecht, **2003**, chap. 8.15, pp. 369 – 393.

James, S.L. *Chem. Soc. Rev.*, **2003**, 32, 276.

Kagane, T.; Harada, K.; Umehara, M.; Hirota, R.; Nakahara, M. *Bull. Chem. Soc. Jpn.*, **1992**, 65, 2638.

Kaim, W.; Rall, J. *Angew. Chem. Int. Ed.*, **1996**, 35, 43.

Kaneko, K.; Cracknell, R.F.; Nicholson, D. *Langmuir*, **1994**, 10, 4606.

Karabach, Y.Y.; Kirillov, A. M.; Guedes da Silva, M.F.C.; Kopylovich, M.N.; Pombeiro, A. J. L.; *Cryst. Growth Des.*, **2006**, 6, 2200.

Kazuo, M.; Hironobu, K.; Koichiso, Y.; Junichi, N. *Jpn. Kokai Tokkyo Koho*, **1979**, 79, 588.

Kim, J.; Harrison, R. G.; Kim, C.; Que, L. Jr. *J. Am. Chem. Soc.*, **1996**, 118, 4373.

Kirillov, A.M.; Haukka, M.; Guedes da Silva M.F.C.; Pombeiro, A.J.L. *Eur. J. Inorg. Chem.*, **2005**, 2071.

Kirillov, A.M.; Kopylovich, M.N.; Kirillova, M.V.; Karabach, Y.Y.; Haukka, M.; Guedes da Silva, M.F.C.; Pombeiro, A.J.L. *Adv. Synth. Catal.*, **2006**, 348, 159, and references therein.

Kirillova, M.V.; Kuznetsov, M.L.; Reis, P.M.; da Silva, J.A.L.; Fraústo da Silva, J.J.R.; Pombeiro, A.J.L. *J. Am. Chem. Soc.*, **2007**, 129, 10531.

Kirillova, M.V.; Kirillov, A.M.; Guedes da Silva, M.F.C.; Pombeiro A.J.L. *Eur. J. Inorg. Chem.*, **2008**, 3423.

Kirillova, M.V.; Kuznetsov, M.L.; da Silva, J.A.L.; Guedes da Silva, M.F.C.; Fraústo da Silva, J.J.R.; Pombeiro, A.J.L. *Chem. Eur. J.*, **2008**, 14, 1828.

Kitagawa, S.; Kondo, M. *Bull. Chem. Soc. Jpn.*, **1998**, 71, 1739;

Kitagawa, S.; Kitaura, R.; Noro, S.-i. *Angew. Chem. Int. Ed.*, **2004**, 43, 2334.

Kitagawa, S.; Uemura, K. *Chem. Soc. Rev.*, **2005**, 34, 109.

Klinman, J.P. *Chem. Rev.*, **1996**, 96, 2541.

Kubota, Y.; Takata, M.; Kobayashi, T.C.; Kitagawa, S. *Coord. Chem. Rev.*, **2007** 251 2510.

Langmuir, I. *J. Am. Chem. Soc.*, **1918** 40 1361.

Lee D.H.; in *Comprehensive Coordination Chemistry*, Vol. 8 (Eds.: McCleverty, J.A.; Meyer, T.J.; Que, L.; Tolman W.B.), 2nd ed., Elsevier, Dordrecht, **2003**, chap. 8.17, pp. 437 – 457.

Li, Y.; Yu, J.; Jiang, J.; Wang, Z.; Zhang, J.; Xu, R. *Chem. Mater.*, **2005**, 17, 6086.

Lieberman, R.L.; Rosenzweig, A.C. *Crit. Rev. Biochem. Mol. Biol.*, **2004**, 39, 147.

Lieberman, A.C. Rosenzweig, R.L. *Nature*, **2005**, 434, 177.

Loiseau, T.; Serre, C.; Huguenard, C.; Fink, G.; Taulelle, F.; Henry, M.; Bataille, T.; Férey, G. *Chem. Eur. J.*, **2004**, 10, 1373.

MacKinnon, J.A.; Eckert, J.; Coker, D.F.; Bug, A.L.R. *J. Chem. Phys.*, **2001**, 114, 10137.

Macrae, C.F.; Edgington, P.R.; McCabe, P.; Pidcock, E.; Shields, G.P.; Taylor, R.; Towler, M.; van de Streek, J. *J. Appl. Crystallogr.*, **2006**, *39*, 453.

Maekewa, M.; Minematsu, T.; Konaka, H.; Sugimoto, K.; Kuroda-Sowa, T.; Suenaga, Y.; Munakata, M. *Inorg. Chim. Acta*, **2004**, *357*, 3456.

Martin, R.L.; Waterman, H. *J. Chem. Soc.*, **1957**, 2545.

Masciocchi, N.; Sironi, A. *J. Chem. Soc., Dalton Trans.*, **1997**, 4643.

Masciocchi, N.; Sironi, A. *C. R. Chimie*, **2005**, *8*, 1617 and references therein.

Matsuda, R.; Kitaura, R.; Kitagawa, S.; Kubota, Y.; Belosludov, R.V.; Kobayashi, T.C.; Sakamoto, H.; Chiba, T.; Takata, M.; Kawazoe, Y.; Mita, Y. *Nature*, **2005**, *436*, 238.

McLauchlan, C.C.; Varda, A.N.; Giles, J.R. *Acta Crystallogr. Sect. E: Struct. Rep. Online*, **2004**, *60*, o1419.

Mellot-Draznieks, C.; Newsam, J.M.; Gorman, A.M.; Freeman, C.M.; Férey, G. *Angew. Chem. Int. Ed.*, **2000**, *39*, 2270.

Mellot-Draznieks, C.; Girard, S.; Férey, G. *J. Am. Chem. Soc.*, **2002**, *124*, 15326.

Mellot-Draznieks, C.; Férey, G. *Curr. Opin. Solid. State Mat. Sci.*, **2003**, *7*, 13.

Mellot-Draznieks, C.; Dutour, J.; Férey, G. *Angew. Chem., Int. Ed.*, **2004**, *43*, 6291.

Milata, V.; Claramunt, R.M.; Cabildo, P.; Santa, M.D.; Cornago, P.; Infantes, L.; Cano, F.H.; Elguero, J. *Heterocycles*, **2001**, *55*, 905.

Mishra, G.S.; Pombeiro, A.J.L. *J. Mol. Cat. A: Chem.*, **2005**, *239*, 96.

Mishra, G.S.; Pombeiro, A.J.L. *Appl. Cat. A: Gen.*, **2006**, *304*, 185.

Mishra, G.S.; Fraústo da Silva, J.J.R.; Pombeiro, A.J.L. *J. Mol. Cat. A: Chem.*, **2007**, *265*, 59.

Mishra, G.S.; Alegria, E.C.B.; Martins, L.R.; Fraústo da Silva, J.J.R.; Pombeiro, A.J.L. *J. Mol. Cat. A: Chem.*, **2008**, *285*, 92.

Mooibroek, T.J.; Gamez, P. *Inorg. Chim. Acta*, **2007**, *360*, 381 and refs. therein.

Mueller, U.; Hesse, M.; Puetter, H.; Schubert, M.; Mirsch, D. *Patent*, EP, 1,674,555, **2005**.

Mueller, U.; Schubert, M.; Teich, F.; Puetter, H.; Schierle-Arndt K.; Pastré, J. *J. Mater. Chem.*, **2006**, *16*, 626.

Murray, L.J.; Dincă, M.; Long, J.R. *Chem. Soc. Rev.*, **2009**, *38*, 1294 and references therein.

Newsam, J.M.; Freeman, C.M.; Leusen, F.J.J. *Curr. Opin. Solid. State Mat. Sci.*, **1999**, *4*, 515.

Ni, Z.; Masel, R.I. *J. Am. Chem. Soc.*, **2006**, *128*, 12394.

Nizova, G.V.; Krebs, B.; Süß-Fink, G.; Schindler, S.; Westerheide, L.; Cuervo, L.G.; Shul'pin, G.B. *Tetrahedron*, **2002**, *58*, 9231.

Noro, S.-i.; Kitagawa, S.; Akutagawa, T.; Nakamura, T. *Progr. Polym. Sci.*, **2009**, *34*, 240.

O'Keeffe, M. *Z. Kristallogr.*, **1991**, *196*, 21.

Ohkubo, T.; Miyawaki, J.; Kaneko, K.; Ryoo, R.; Seaton, N.A. *J. Phys. Chem. B*, **2002**, *106*, 6523.

Otting, G.; Wüthrich, K. *J. Magn. Reson.*, **1988**, *76*, 569.

Pan, L.; Liu, H.; Lei, X.; Huang, X.; Olson, D.H.; Turro, N.J.; Li, J. *Angew. Chem. Int. Ed.*, **2003**, *42*, 542.

Pettinari, C.; Garau, F.; Monari, M.; Pandolfo, L.; Pettinari, R.; Marchetti, F. XIII *Congresso Nazionale della Società Chimica Italiana*, Sorrento, July 5-10, **2009**, INO-PO-35.

Prins, L.J.; Thalacker, C.; Würthner, F.; Timmerman, P.; Reinhoudt, D.N. *PNAS*, **2001**, *98*, 10042.

Prins, L.J.; Neuteboom, E.E.; Paraschiv, V.; Crego-Calama, M.; Timmerman, P.; Reichnoudt, D.N. *J. Org. Chem.*, **2002**, *68*, 4808.

Radhakrishnan, R.; Gubbins, K.E.; Sliwinska-Bartkowiak, M. *J. Chem. Phys.*, **2000**, *112*, 11048.

Reger, D.L.; Grattan, T.C.; Brown, K.J.; Little, C.A.; Lamba, J.J.S.; Rheingold, A.L.; Sommer, R. *J. Organomet. Chem.*, **2000**, *607*, 120.

Reger, D.L.; Semeniuc, R.F.; Little, C.A.; Smith, M.D. *Inorg. Chem.*, **2006**, *45*, 7758.

Robin, A.Y.; Fromm, K.M. *Coord. Chem. Rev.*, **2006**, *250*, 2127.

Rowell, J.L.C.; Yaghi, O.M. *Angew. Chem. Int. Ed.*, **2005**, *117*, 4748.

Russell, G. A. *J. Am. Chem. Soc.*, **1957**, *79*, 3871.

Sakai, K.; Yamada, Y.; Tsubomura, T.; Yabuki, M.; Yamaguchi, M. *Inorg. Chem.*, **1996**, *35*, 542.

Schoen, J.C.; Jansen, M. *J. Phys.: Condens. Matter*, **1999**, *11*, 6487.

Senko, M.W. *IsoPro Isotopic Abundance Simulator*, v. 2.1: National High Magnetic Field Laboratory, Los Alamos National Laboratory: Los Alamos, NM, **1994**.

Seo, J.S.; Whang, D.; Lee, H.; Jun, S.I.; Oh, J.; Jeon, Y.J.; Kim, K. *Nature*, **2000**, *404*, 982.

Serre, C.; Millange, F.; Thouvenot, C.; Nogues, M.; Marsolier, G.; Louer, D.; Férey, G. *J. Am. Chem. Soc.*, **2002**, *124*, 13519.

Serre, C.; Millange, F.; Surlé, S.; Férey, G. *Angew. Chem. Int. Ed.*, **2004**, *116*, 6446.

Serre, C.; Groves, J.A.; Lightfoot, P.; Slawin, A.M.Z.; Wright, P.A.; Stock, N.; Bein, T.; Haouas, M.; Taulelle, F.; Férey, G. *Chem. Mater.*, **2006**, *18*, 1451.

Setoyama, N.; Suzuki, T.; Kaneko, K. *Carbon*, **1998**, *36*, 1459.

Sheldrick, G.M. *SADABS, program for empirical absorption correction*, University of Göttingen, Germany, **1996**.

Sheldrick, G.M. *SHELXTLplus (Windows NT Version) Structure Determination Package*, Version 5.1. Bruker Analytical X-ray Instruments Inc.: Madison, WI, USA, **1998**.

Shen, W-Z.; Yi, L.; Chen, P.; Yan, S-P.; Liao, D-Z.; Jiang, Z-H. *Inorg. Chem. Commun.*, **2004**, *7*, 819.

Shul'pin, G.B.; Attanasio, D.; Suber, L. *J. Catal.*, **1993**, *142*, 147.

Shul'pin, G. B.; Kozlov, Y. N.; Nizova, G. V.; Suss-Fink, G.; Stanislas, S.; Kitaygorodskiy, A.; Kulikova, V. S. *J. Chem. Soc. Perkin Trans. 2*, **2001**, 1351.

Shul'pin, G. B. *J. Mol. Catal. A: Chem.*, **2002**, *189*, 39.

Shul'pin, G. B.; Gradinaru, J.; Kozlov, Y. N. *Org. Biomol. Chem.* **2003**, *1*, 3611.

Shul'pin, G.B.; Nizova, G.V.; Kozlov, Y.N.; Cuervo, L.G.; Süss-Fink, G. *Adv. Synth. Catal.*, **2004**, *346*, 317.

Shul'pin, G.B.; Mishra, G.S.; Shul'pina, L.S.; Strelkova, T.V.; Pombeiro, A.J.L. *Catal. Commun.*, **2007**, *8*, 1516.

Silva, T.F.S.; Alegria, E.C.B.; Martins, L.R.; Pombeiro, A.J.L. *Adv. Synth. Catal.*, **2008**, *350*, 706.

SMART & SAINT Software Reference Manuals, version 5.051 (Windows NT Version), Bruker Analytical X-ray Instruments Inc.: Madison, WI, **1998**.

Smolin, E.M.; Rapoport, L. *The Chemistry of Heterocyclic Compounds - s-Triazines and Derivatives*, Interscience Publisher Inc. New York, **1959**.

Stock, N.; Bein, T. *Solid State Sci.*, **2003**, *5*, 1207.

Stock, N.; Bein, T. *Angew. Chem. Int. Ed.*, **2004**, *43*, 749.

Subramanian, S.; Zaworotko, M.J. *Angew. Chem. Int. Ed.*, **1995**, *34*, 2127.

Tranchemontagne, D.J.; Mendoza-Cortés, J.L.; O'Keeffe, M.; Yaghi, O.M. *Chem. Soc. Rev.*, **2009**, *38*, 1257.

Uemura, T.; Kitaura, R.; Ohta, Y.; Nagaoka, M.; Kitagawa, S. *Angew. Chem. Int. Ed.*, **2006**, *45*, 4112.

Uemura, T.; Yanai, N.; Kitagawa, S. *Chem. Soc. Rev.*, **2009**, *38*, 1228.

Yenisoy-Karakaş, S.; Aygün, A.; Güneş, M.; Tahtasakal, E. *Carbon*, **2004**, *42*, 477.

Venkataraman, D.; Gardner, G.B.; Lee, S.; Moore, J.S. *J. Am. Chem. Soc.*, **1995**, *117*, 11600.

Venkataramanan, N.S.; Kuppuraj, G.; Rajagopal, S. *Coord. Chem. Rev.*, **2005**, *249*, 1249.

Walton, K.S.; Millward, A.R.; Dubbeldam, D.; Frost, H.; Low, J.J.; Yaghi, O.M.; Snurr, R.Q. *J. Am. Chem. Soc.*, **2008**, *130*, 406.

Watson, W.H.; Holley, W.W. *Croat. Chem. Acta*, **1984**, *57*, 467.

Whitesides, G.M.; Mathias, J.P.; Seto, C.T. *Science*, **1991**, *254*, 1312.

Willans, C.E.; French, S.; Barbour, L.J.; Gertenbach, J.-A.; Junk, P.C.; Lloyd, G.O.; Steed, J.W. *Dalton Trans.*, **2009**, 6480.

Wong-Foy, A.G.; Matzger, A.J.; Yaghi, O.M. *J. Am. Chem. Soc.*, **2006**, *128*, 3494.

Wu, C.-D.; Hu, A.; Zhang, L.; Lin, W. *J. Am. Chem. Soc.*, **2005**, *127*, 8940.

Yaghi, O.M.; Li, G.M.; Li, H.L. *Nature*, **1995**, *378*, 703.

Yaghi, O.M.; Li, H.; Davis, C.; Richardson, D.; Groy, T.L. *Acc. Chem. Res.*, **1998**, *31*, 474.

Yoon, L.; Solomon, E.I. *Inorg. Chem.*, **2005**, *44*, 8076.

Zanforlin, D.; MSc Thesis, University of Padova, Italy, 2007, http://tesi.cab.unipd.it/archive/00009432/01/Dario_Zanforlin_Tesi.pdf.

Zerkowski, J.A.; MacDonald, J.C.; Seto, C.T.; Wierda, D.A.; Whitesides, G.M. *J. Am. Chem. Soc.*, **1994**, *116*, 2382.

Participation to Congresses, Conferences, Schools and Meetings

Participation to the AIC International School "Scattering Techniques: From Microscopic To Atomic Structures.", Camerino (Italy), August 30th - September 4th, 2009.

Pettinari, C.; Garau, F.; Monari, M.; Pandolfo, L.; Pettinari, R.; Marchetti, F. "Synthesis and characterization of new polytopic ligands based on the 1,3,5 triazine spacer and pyrazolyl, tris-pyrazolylmethyl and tris-pyrazolylethoxy bonding fragments.", XXII Congresso Nazionale della Società Chimica Italiana, Sorrento (Italy) July 5-10, **2009**, INO-PO-35. (Poster)

Garau, F. "New coordination polymers based on the triangular $[Cu_3(\mu_3-OH)(\mu-pz)_3]^{2+}$ core and pyridine containing ligands.", 1st International Workshop on New Hybrid Metal-Organic Materials, Camerino (Italy), January 16-18, **2009**, OR-2. (Oral Communication)

Pandolfo, L.; Garau, F.; Casarin, M. "New di- and polynucleating ligands and their coordination behaviour.", 1st International Workshop on New Hybrid Metal-Organic Materials, Camerino (Italy), January 16-18, **2009**, OR-22. (Oral Communication)

Casarin, M.; Garau, F.; Pandolfo, L.; Masciocchi, N.; Pettinari, C.; Vittadini, A. "Reversible guest induced topochemical modifications in $[Cu(\mu-pz)_2]_n$. A DFT investigation.", 1st International Conference on Metal-Organic Frameworks and Open Framework Compounds, Augsburg (Germany), October 8-10, **2008**, P5. (Poster)

Garau, F.; Pandolfo, L.; Di Nicola, C.; Ngoune, J.; Pettinari, C.; Monari, M.; Pombeiro, A. J. L.; Martins, L. M. D. R. S.; Karabach, Y. Y. "Coordination polymers based on the triangular triangular $[Cu_3(\mu_3-OH)(\mu-pz)_3]^{2+}$ core and unsaturated carboxylates. Crystal structures, electrochemical behaviour and catalytic activity in peroxidative oxidation of cycloalkanes.", 1st International Conference on Metal-Organic Frameworks and Open Framework Compounds, Augsburg (Germany), October 8-10, **2008**, P124. (Poster)

Di Nicola, C.; Garau, F.; Guedes da Silva, M. F. C.; Ngoune, J.; Pandolfo, L.; Pettinari, C.; Pombeiro, A. J. L. "New porous coordination polymers based on the triangular $[Cu_3(\mu_3-OH)(\mu-pz)_3]^{2+}$ core and pyridine containing ligands.", 4th EuChemMS Conference on Nitrogen Ligands, Garmisch-Partenkirchen (Germany), August 24-28, **2008**, SL8. (Oral Communication)

Di Nicola, C.; Garau, F.; Monari, M.; Pandolfo, L.; Pettinari, C.; Pombeiro, A. J. L. "Coordination polymers based on the trinuclear triangular $[Cu_3(\mu_3-OH)(\mu-pz)_3]^{2+}$ SBU and strong acid anions. Synthesis, structural features and catalytic properties.", 4th EuChemMS Conference on Nitrogen Ligands, Garmisch-Partenkirchen (Germany), August 24-28, **2008**, P79. (Poster)

Di Nicola, C.; Garau, F.; Monari, M.; Pandolfo, L.; Pettinari, C. *“Trinuclear triangular secondary building units to build copper(II) metal organic frameworks.”*, VIII Congresso Nazionale di Chimica Supramolecolare, Trieste (Italy), September 19-22, **2007**, P53. (Poster)

Casarin, M.; Garau, F.; Monari, M.; Pandolfo, L.; Pettinari, C.; Venzo, A. *“An experimental and theoretical investigation on the structure of 2-amino-4-chloro-6-(pyrazol-1-yl)-[1,3,5]-triazine.”*, VIII Congresso Nazionale di Chimica Supramolecolare, Trieste (Italy), September 19-22, **2007**, P30. (Poster)

Casarin, M.; Cerquetella, A.; Garau, F.; Monari, M.; Pandolfo, L.; Pettinari, C.; Venzo, A. *“New ligands from old synthons. Synthesis and characterization of ligands based on the 1,3,5-triazine spacer and pyrazolyl or tris-pyrazolylmethyl bonding fragments. Preliminary results on reactivity with metal ions.”*, 6th International School of Organometallic Chemistry, Camerino (Italy), September 8-12, **2007**, P65. (Poster)

Published Papers

- Casarin, M.; Garau, F.; Monari, M.; Pandolfo, L.; Pettinari, C.; Venzo, A. *New J. Chem.*, **2008**, 32, 358.
- Casarin, M.; Forrer, D.; Garau, F.; Pandolfo, L.; Pettinari, C.; Vittadini, A. *J. Phys. Chem. A*, **2008**, 112, 6723.
- Bencini, A.; Casarin, M.; Forrer, D.; Franco, L.; Garau, F.; Masciocchi, N.; Pandolfo, L.; Pettinari, C.; Ruzzi, M.; Vittadini, A. *Inorg. Chem.*, **2009**, 48, 4044.
- Casarin, M.; Forrer, D.; Garau, F.; Pandolfo, L.; Pettinari, C.; Vittadini, A. *Inorg. Chim. Acta.*, **2009**, 362, 4358.
- Contaldi, S.; Di Nicola, C.; Garau, F.; Karabach, Y.Yu.; Martins, L.M.D.R.S.; Monari, M.; Pandolfo, L.; Pettinari, C.; Pombeiro, A.J.L. *Dalton Trans.*, **2009**, 4928.
- Di Nicola, C.; Garau, F.; Karabach, Y.Y.; Martins, L.M.D.R.S.; Monari, M.; Pandolfo, L.; Pettinari, C.; Pombeiro, A.J.L. *Eur. J. Inorg. Chem.*, **2009**, 666.
- Garau, F.; Monari, M.; Pandolfo, L.; Pettinari, C.; Venzo, A. *Cryst. Eng. Comm.*, **2010**, in the press: DOI: 10.1039/b922874h.

An experimental and theoretical investigation of the molecular and electronic structure of 2-amino-4-chloro-6-pyrazolyl-[1,3,5]triazine, forming supramolecular linear tapes in the solid state†‡

Maurizio Casarin,^a Federica Garau,^a Magda Monari,^{*b} Luciano Pandolfo,^{*a} Claudio Pettinari^{*c} and Alfonso Venzo^d

Received (in Montpellier, France) 20th July 2007, Accepted 25th October 2007

First published as an Advance Article on the web 7th November 2007

DOI: 10.1039/b711136c

The new derivative 2-amino-4-chloro-6-pyrazolyl-[1,3,5]triazine, **1**, prepared by reaction of 2-amino-4,6-dichloro-[1,3,5]triazine with an excess of pyrazole, has been characterized by ¹H, ¹³C and ¹⁵N NMR measurements and single crystal XRD structural determination.

The non-equivalence of the NH₂ hydrogens evidences the iminium character of this moiety.

Compound **1**, exploiting strong H-bonds, self-assembles generating supramolecular linear tapes.

Theoretical calculations are in good agreement with experimental solid state and solution data.

Electronic properties of **1** (lowest lying excitation energies and corresponding oscillator strength)

have also been determined by time dependent DFT at the PBE level.

Introduction

Supramolecular chemistry, the “chemistry of molecular assemblies and of the intermolecular bond”¹ is a vast interdisciplinary topical field of research and technology in contemporary chemistry. H-bonding, metal–ligand coordination, and π – π interactions are the noncovalent motifs mainly involved in the rational design of supramolecular assemblies.² The prevalent strategy for engineering the structures of crystals takes advantage of directional intermolecular interactions as the main way of controlling molecular assembly during crystallization.³ H-bonds exhibiting high directionality with respect to other noncovalent interactions,⁴ and being generally stronger than the strongest van der Waals (vdW) interaction,⁵ are largely employed to design and obtain self-assembled supramolecular organic structures.⁶

Besides carboxylic acids and amides, that easily form robust architectures via O–H...O=C,⁷ and N–H...O=C⁸ interactions, other H-bonding motifs, such as those involving the cyanuric acid–melamine system and, more generically, [1,3,5]triazine derivatives, have proven their great potential in crystal engineering,⁹ and *s*-triazine-containing molecules are involved in new developments in the field of functional

materials.¹⁰ As an example, by using substituted melamines and barbituric acids, Whitesides and coworkers created a variety of supramolecular motifs through intermolecular H-bonds, such as linear tapes, crinkled tapes and rosette motifs.¹¹ In linear tapes (infinite, quasi-1D arrangements of molecules held together by multiple noncovalent interactions) each molecule forms H-bonds with only two neighbouring molecules.¹² These tapes are expected to pack with their long axes parallel, further limiting possible orientations of molecules in the solids.¹³ These assemblies are expected to be quite stable, due to the high number of H-bonds involved and their relatively high strength.

Other “tapes”, based on [1,3,5]triazine derivatives have been reported,^{14,15} and also the simple 2-amine-4,6-dichloro-[1,3,5]triazine self-assembles through H-bonds forming in the solid state a series of intercalated tapes, all running along one crystallographic direction.^{16,17} Two examples are sketched in Chart 1.

In the synthesis of numerous compounds bearing the *s*-triazine core, 2,4,6-trichloro-[1,3,5]triazine has been largely

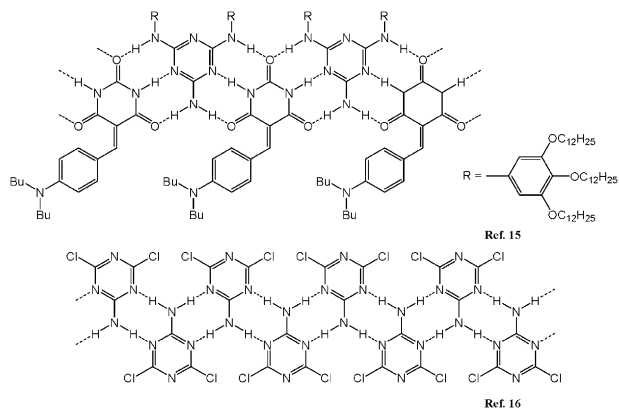


Chart 1

^a Dept. of Chemical Sciences, University of Padova, Via Marzolo, 1, I-35131 Padova, Italy. E-mail: luciano.pandolfo@unipd.it; Fax: +39 049 8275161; Tel: +39 049 8275157

^b Dept. of Chemistry “G. Ciamician”, University of Bologna, Via Selmi, 2, I-40126 Bologna, Italy. E-mail: magda.monari@unibo.it; Fax: +39 051 2099456; Tel: +39 051 2099559

^c Dept. of Chemical Sciences, Via S. Agostino, 1, University of Camerino, I-62032 Camerino (MC), Italy. E-mail: claudio.pettinari@unicam.it; Fax: +39 0737 637345; Tel: +39 0737 402234

^d CNR – ISTM University of Padova, Via Marzolo, 1, I-35131 Padova, Italy

† The HTML version of this article has been enhanced with colour images.

‡ Electronic supplementary information (ESI) available: Charts S1 and S2, Scheme S1, Table S1, Fig. S1–S8. See DOI: 10.1039/b711136c

used as a starting material, due to its particular reactivity. Selective syntheses of mono, di and trisubstituted *s*-triazine derivatives could generally be achieved by following *Moffat's rule*.¹⁸ the nucleophilic substitution of the first chloride can be carried out around 0 °C, while the second takes place at r.t., and the third requires temperatures higher than 60–80 °C (Scheme S1†). As far back as the 19th century^{19,20} to nowadays,²¹ numerous *s*-triazine containing compounds, having useful applications in disparate fields, have been obtained.^{22–25} More recently, *s*-triazine derivatives have been employed in combinatorial chemistry,²⁶ crystal engineering^{11,16,17,27–29} and as ligands.^{10,21b,22a,30} Here we report the synthesis of the asymmetric [1,3,5]triazine derivative, 2-amino-4-chloro-6-pyrazolyl-[1,3,5]triazine, **1**, as well as a combined experimental and theoretical study on its structure and solid state supramolecular self-assembly that generates linear tapes by exploiting strong H-bonds.

Experimental

Material and methods

All reactions and manipulations were carried out under an atmosphere of nitrogen with standard Schlenk or septum/cannula techniques. All solvents were purified by conventional methods³¹ and stored under nitrogen. Reagents (Aldrich) were used without further purification. Elemental analyses (C, H, N) were performed with a Fisons Instruments 1108 CHNS-O Elemental Analyser. IR spectra were recorded from 4000 to 400 cm⁻¹ with a Perkin-Elmer 983 instrument. UV-Vis spectra were recorded from 200 to 800 nm with a Varian Cary 5E instrument.

NMR experimental section

¹H, ¹³C and ¹⁵N NMR spectra were obtained as DMSO-*d*₆ solutions on a Bruker DRX-400 spectrometer operating at 400.13, 100.61 and 40.56 MHz, respectively, and equipped with a BVT2000 temperature controller. The chemical shift values are given in δ units with reference to Me₄Si for ¹H and ¹³C, and MeNO₂ for ¹⁵N. The assignments are according to the labelling scheme reported in Chart S1.† Suitable integral values for the proton spectra were obtained by a pre-scan delay of 10 s to ensure a complete relaxation for all the resonances. The proton assignments were performed by standard chemical shift correlations as well as by 2D correlation spectroscopy (COSY), total correlation spectroscopy (TOCSY), and nuclear Overhauser enhancement spectroscopy (NOESY) experiments. The ¹³C and ¹⁵N chemical shift values were obtained through 2D-heteronuclear correlation experiments (heteronuclear multiple quantum correlation, HMQC), with bilinear rotation-decoupling, BIRD, sequence³² and quadrature along F1 achieved using the time-proportional receiver phase incrementation, TPPI, method³³ for the H-bonded carbon and nitrogen atoms, and heteronuclear multiple bond correlation, HMBC,³⁴ for the other ¹³C and ¹⁵N nuclei.

Computational details

ADF calculations on **1** have been carried out by using the ADF 2006–2007 package.³⁵ Optimized geometries were obtained by employing generalized gradient (GGA) corrections

self-consistently included through the Perdew–Burke–Ernzerhof (PBE) formula.³⁶ A triple-ζ Slater-type basis set was used for all the atoms of the molecule. Inner cores of C(1s), N(1s) and Cl(1s2s2p) atoms have been kept frozen throughout the calculations. All the numerical experiments have been run without the assumption of any symmetry element (*C*₁ symmetry point group). The optimized structure was then used to calculate NMR isotropic shielding constants (σ). Chemical shifts were evaluated as δ = σ_{ref} – σ, where σ_{ref} is the shielding constant of ¹H in the reference compound (TMS). Finally, lowest lying excitation energies and corresponding oscillator strengths have been computed by employing time dependent density functional theory (TD-DFT).³⁷

Synthesis

2-Amino-4-chloro-6-pyrazolyl-[1,3,5]triazine, 1. To a stirred solution of 2-amino-4,6-dichloro-[1,3,5]triazine¹⁹ (301 mg, 1.8 mmol) and DIPEA (*N,N'*-diisopropylethylamine, 0.6 mL, 0.47 g, 3.6 mmol) in dioxane (10 mL) a solution of pyrazole (Hpz) (254 mg, 3.7 mmol) in dioxane (8 mL) was added dropwise. The mixture was refluxed for 10 h, obtaining an orange solution and the solvent was then removed under reduced pressure. The resulting orange solid was vigorously stirred with 20 mL of water at r.t. for 1 h giving a white solid that was filtered, washed with water and dried under vacuum. Yield 286 mg. ¹H NMR of the crude product indicated the presence of ca. 80% of **1**, that was recrystallized from MeOH, yielding a few white crystals suitable for X-ray crystal structure determination.

1: Mp > 200 °C. Anal.(%) Calcd. for C₆H₅N₆Cl: C, 36.66; H, 2.56; N, 42.75. Found: C, 36.82; H, 3.47; N, 37.78. IR (KBr) cm⁻¹: 3480; 3323; 3160; 1633; 1575; 1523; 1449; 1396; 1324; 1007. ¹H NMR (δ, DMSO-*d*₆, 25 °C): NH 8.30, 8.39, H₁ 7.87 (dd, ³J_{HH}, 1.4 Hz; ⁴J_{HH}, 0.7 Hz), H₂ 6.58 (dd, ³J_{HH}, 2.8 Hz; ³J_{HH}, 1.4 Hz), H₃ 8.48 (dd, ³J_{HH}, 2.8 Hz; ⁴J_{HH}, 0.7 Hz). ¹³C NMR (δ, DMSO-*d*₆, 25 °C) C₁ 145.11, C₂ 110.16, C₃ 130.51, C₅ 170.39, C₆ 161.98, C₄ 168.03. ¹⁵N NMR (δ, DMSO-*d*₆, 25 °C) N₆ –274.7, N₃₍₄₎ –175.6, N₁ –153.6, N₄₍₃₎ –148.0, N₂ –69.8.

Crystallographic data collection and structure determination.

The X-ray intensity data for **1** were measured on a Bruker Apex II CCD diffractometer. Cell dimensions and the orientation matrix were initially determined from a least-squares refinement on reflections measured in three sets of 20 exposures, collected in three different ω regions, and eventually refined against all data. A full sphere of reciprocal space was scanned by 0.3° ω steps. The software SMART³⁸ was used for collecting frames of data, indexing reflections and determination of lattice parameters. The collected frames were then processed for integration by the SAINT program,³⁸ and an empirical absorption correction was applied using SADABS.³⁹ The structure was solved by direct methods (SIR 97)⁴⁰ and subsequent Fourier syntheses and refined by full-matrix least-squares on F² (SHELXTL),⁴¹ using anisotropic thermal parameters for all non-hydrogen atoms. All hydrogen atoms were located in the Fourier map and, except the iminic hydrogens which were refined isotropically, added in calculated positions, included in the final stage of refinement with isotropic thermal

parameters, $U(H) = 1.2U_{eq}(C)$, and allowed to ride on their carrier carbons. The absolute structure was determined [Flack parameter $-0.03(4)$]. Crystal data and details of data collection for **1** are reported in Table 1. CCDC reference number 662889. For crystallographic data in CIF or other electronic format see DOI: 10.1039/b711136c

Molecular graphics were generated using Mercury⁴² and SCHAKAL⁴³ software.

Results and discussion

In the course of our search of polynucleating ligands able to generate metal–organic frameworks, we directed our attention to the potential of the [1,3,5]triazine supramolecular synthon and started our study from the relatively simple *s*-triazine derivative **1**. Actually, **1** was first obtained during an attempt to synthesize 2-amino-4,6-dipyrazolyl-[1,3,5]triazine. Workup of the mixture obtained by refluxing 2-amino-4,6-dichloro-[1,3,5]triazine with 2 equivalents of Hpz in dioxane for 10 h, yielded only *ca.* 20% of 2-amino-4,6-dipyrazolyl-[1,3,5]triazine and *ca.* 80% of **1**, as indicated by ¹H NMR spectroscopy and elemental analysis. Nevertheless, it was possible to recrystallize **1** from MeOH obtaining some crystals that were used for a single crystal XRD structural determination and ¹H, ¹³C and ¹⁵N NMR measurements.

The molecular structure of **1** is shown in Fig. 1 and relevant bond lengths and angles are reported in Table 2.

The molecule is almost completely planar, with the plane of the triazine ring forming a dihedral angle of *ca.* 9° with the plane of the pyrazolate ring. The [1,3,5]triazine ring shows

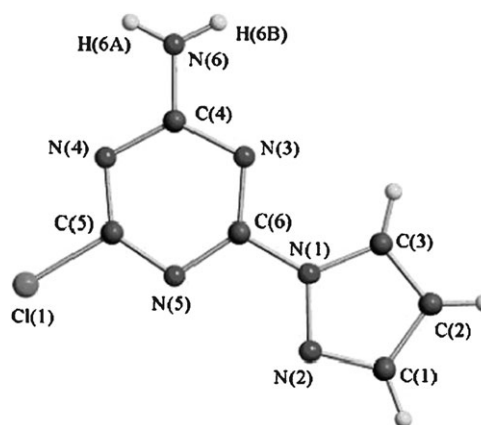


Fig. 1 Molecular structure of **1**.

significant distortions from regular hexagonal geometry due to the steric effects of the lone pair electrons as it has been found in the case of *s*-triazine.⁴⁴ The inner C–N–C angles are in the range 111.5–113.5(1)° (av. 112.7°) whereas the N–C–N angles fall in the range 124.6–129.3(1)° (av. 127.3°). These differences between C–N–C and N–C–N angles are even more marked than those found in the parent *s*-triazine [C–N–C 113.0(2)° and N–C–N 127.0(2)°].⁴⁴

The X-ray crystal structure shows that the geometry around N(6) is, in very good approximation, trigonal planar, with the nitrogen atom approximately lying in the plane formed by H(6A), H(6B) and C(4) (deviation from plane 0.06 Å). The C(4)–N(6) bond length [1.321(2) Å] well compares with the N(3)–C(6) and N(4)–C(5) distances [1.319(2) and 1.307(2) Å, respectively], while it is shorter than the C(4)–N(3) and C(4)–N(4) ones [1.351(2) and 1.357(2) Å, respectively]. These data, in very good agreement (Table S1†) with the optimized geometrical parameters of **1**, determined by DFT calculations at the PBE level, suggest a relevant iminium character of the NH₂ fragment (see also Chart S2†). Computed Hirshfeld charges of N(3) (−0.1836), N(4) (−0.1941), N(5) (−0.175) and N(6) (−0.144) further support this finding.

An inspection of the crystal packing reveals that each molecule of **1** is involved in infinite supramolecular linear tapes due to N–H⋯N and N–H⋯Cl hydrogen bonds established by the iminic hydrogens [H(6A), H(6B)] (Fig. 2). The

Table 1 Crystal data and details of data collection for compounds **1**

Compound	1
Formula	C ₆ H ₅ ClN ₆
Formula weight	196.61
<i>T</i> /K	293(2)
λ (MoK α)/Å	0.71073
Crystal symmetry	Monoclinic
Space group	<i>Pc</i>
<i>a</i> /Å	4.2896(5)
<i>b</i> /Å	5.4645(6)
<i>c</i> /Å	17.528(2)
α /°	90
β /°	91.449(2)
γ /°	90
<i>V</i> /Å ³	410.72(8)
<i>Z</i>	2
ρ_{calc} /Mg m ^{−3}	1.590
μ (Mo–K α)/mm ^{−1}	0.423
<i>F</i> (000)	186
Crystal size/mm	0.15 × 0.20 × 0.30
θ range/°	3.73–28.50
Reflections collected	3337(± <i>h</i> , ± <i>k</i> , ± <i>l</i>)
Unique observed reflections	1848 [<i>R</i> _{int} = 0.0153]
[<i>F</i> _o > 4 σ (<i>F</i> _o)]	
Goodness-of-fit-on <i>F</i> ²	1.094
Final <i>R</i> indices <i>I</i> > 2 σ (<i>I</i>)	<i>R</i> ₁ (<i>F</i>) ^{<i>a</i>} = 0.0261, w <i>R</i> ₂ (<i>F</i> ²) ^{<i>b</i>} = 0.0696
<i>R</i> indices (all data)	<i>R</i> ₁ (<i>F</i>) = 0.0270, w <i>R</i> ₂ = 0.0699
Largest diff. peak and hole/e Å ^{−3}	0.152 and −0.219
^{<i>a</i>} <i>R</i> ₁ = $\Sigma F_o - F_c /\Sigma F_o $. ^{<i>b</i>} w <i>R</i> ₂ = $[\Sigma w(F_o^2 - F_c^2)^2/\Sigma w(F_o^2)^2]^{1/2}$ where $w = 1/[\sigma^2(F_o^2) + (aP)^2 + bP]$ where $P = (F_o^2 + 2F_c^2)/3$.	

Table 2 Bond lengths (Å) and angles (deg) for **1**

Cl(1)–C(5)	1.736(1)	C(4)–N(6)	1.321(2)
N(5)–C(5)	1.323(2)	C(6)–N(1)	1.400(2)
N(5)–C(6)	1.336(2)	C(3)–C(2)	1.354(3)
N(4)–C(5)	1.307(2)	C(3)–N(1)	1.364(2)
N(4)–C(4)	1.357(2)	C(1)–N(2)	1.321(2)
N(3)–C(6)	1.319(2)	C(1)–C(2)	1.390(3)
N(3)–C(4)	1.351(2)	N(1)–N(2)	1.3560(2)
C(5)–N(5)–C(6)	111.5(1)	N(4)–C(5)–N(5)	129.3(1)
C(5)–N(4)–C(4)	113.1(1)	N(4)–C(5)–Cl(1)	116.5(1)
C(6)–N(3)–C(4)	113.5(1)	N(5)–C(5)–Cl(1)	114.3(1)
N(6)–C(4)–N(3)	117.8(2)	C(2)–C(3)–N(1)	106.3(2)
N(6)–C(4)–N(4)	117.6(2)	N(2)–C(1)–C(2)	112.5(2)
N(3)–C(4)–N(4)	124.6(1)	C(3)–C(2)–C(1)	105.4(2)
N(3)–C(6)–N(5)	128.0(1)	N(2)–N(1)–C(3)	112.0(1)
N(3)–C(6)–N(1)	116.4(1)	N(2)–N(1)–C(6)	121.0(1)
N(5)–C(6)–N(1)	115.6(1)	C(3)–N(1)–C(6)	126.9(1)
C(1)–N(2)–N(1)	103.7(2)		

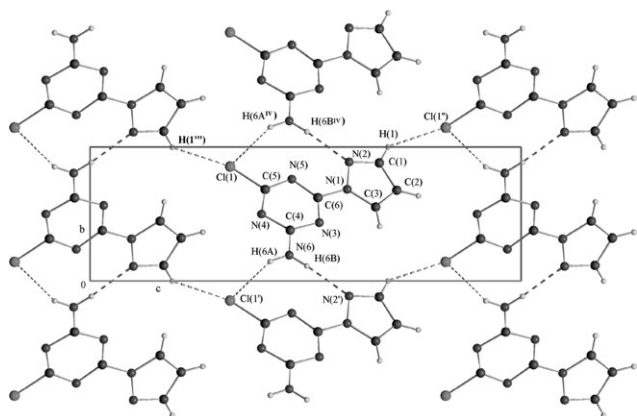


Fig. 2 View down the *a* axis of the crystal packing of **1** showing the intermolecular interactions. Symmetry codes: (I) $x, 1 - y, z - 0.5$, (II) $x, 2 - y, z + 0.5$; (III) $x, 2 - y, z - 0.5$, (IV) $x, 1 + y, z$.

H-bond involving H(6B) bound to N(6) of the substituted triazine ring is with the pyrazolate nitrogen N(2) of one neighbour molecule [$N(6) \cdots N(2')$ 3.012(2) Å, $N(6) - H(6B) \cdots N(2')$ 172(2)°], whereas the second iminic hydrogen H(6A) interacts with the chlorine atom of the same neighbour (Table 3).

These tapes are arranged in face-to-face π stackings with an interplanar distance of about 3.31 Å (Fig. 3), close to the graphitic one, but with a ring offset of 2.73 Å [centroid(triazine)–centroid(triazine) distance 4.29 Å]. As a consequence of this slippage the shorter interactions are between one nitrogen [N(5)] of the triazine and one nitrogen [N(1)] of the pyrazolate group of one molecule with the carbon [C(4)] bearing the NH₂ moiety and N(3) of the adjacent molecule, respectively [$N(5) \cdots C(4^a)$ 3.34 Å, $N(1) \cdots N(3^a)$ 3.32 Å, symmetry code: (a) $x + 1, y, z$].

In the overall crystal packing of **1** (Fig. 4) differently oriented columns arising by the π stacking of the molecules form dihedral angles of 75.25(3)°. The columns are mostly connected by van der Waals interactions between the chlorine atoms of one column and one hydrogen of the pyrazole ring [$Cl(1) \cdots H(1''')$ 2.94 Å, $Cl(1) \cdots H(1''') - C(1''')$ 145°, symmetry code as in Fig. 2] of the neighbour (sum of the vdW radii $Cl \cdots H = 2.95$ Å using the van der Waals radii according to Bondi).⁴⁵

Finally, the PLATON CALC SOLV routine⁴⁶ indicates that in solid **1** there are no solvent accessible areas, as suggested also by space-filling views (Fig. S1 and S2†).

Multinuclear NMR measurements have been carried out on DMSO-*d*₆ solutions of **1** (see Experimental) giving spectra in agreement with X-ray findings (Fig. S4–S6†). In particular, ¹H,^{30b} ¹³C,^{30b} and ¹⁵N⁴⁷ chemical shift values fall in the typical ranges reported for similar compounds.

Table 3 Hydrogen bonding interactions in **1**^a

D–H...A	D–H/Å	H...A/Å	D...A/Å	D...A/°
N(6)⋯N(2')	0.85(2)	2.17(2)	3.012(2)	172(2)
N(6)⋯Cl(1')	0.86(2)	2.89(2)	3.660(2)	150(2)

^a Symmetry transformations: (I) $x, 1 - y, z - 0.5$.

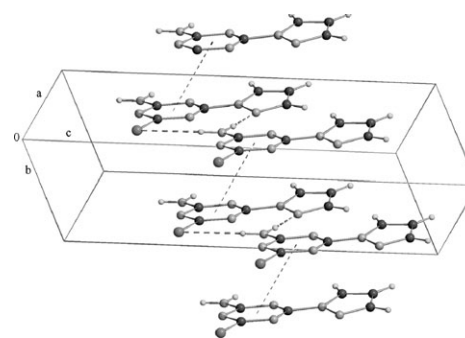


Fig. 3 Simplified crystal packing of **1** showing the offset π stacking of the triazine rings between pairs of molecules.

¹H NMR chemical shifts of **1** have also been estimated by carrying out numerical experiments at both the Becke–Perdew (BP) and PBE levels and the results are reported in Table 4.

Despite the fact that the calculated values pertinent to H(1), H(2) and H(3) for isolated **1** are in very good agreement with experimental data, those evaluated for H(6A) and H(6B) are rather poor. On the other hand, it is useful to keep in mind that the spectra were recorded in DMSO-*d*₆, and it is well known that this solvent breaks H-bonds and can form new ones involving the NH₂ moiety. On this basis, we decided to evaluate the ¹H chemical shifts of a hypothetical adduct formed by one molecule of **1** and two molecules of DMSO. The optimized geometry of the adduct (Fig. S3†) was obtained by using a triple- ζ Slater-type basis set for the O and S atoms and by freezing the inner cores of O(1s) and S(1s2s2p) throughout the calculations. The agreement between experiment and theory resulting was definitely better, particularly for the PBE functional.

The most relevant feature evidenced in the ¹H NMR spectrum of **1** (Fig. S4†) is the non equivalence of the two NH₂ hydrogens (two distinct signals at 8.30 and 8.39 ppm).⁴⁸ These data, supported also by theoretical results, indicate that the rotation around the C(4)–NH₂ bond is hindered, thus

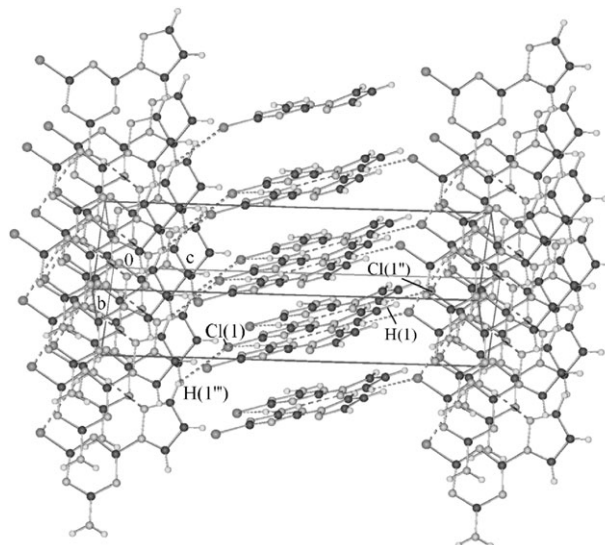


Fig. 4 Arbitrary view of the packing of **1** showing the differently oriented parallel rows of tapes. Symmetry codes as in Fig. 2.

Table 4 Calculated and experimental ^1H NMR chemical shifts of **1**. Atoms are labeled according to Chart S1†

	Isolated 1		1 -2DMSO adduct		Exp
	BP	PBE	BP	PBE	
H(1)	7.76	7.63	7.76	7.55	7.63
H(2)	6.72	6.53	6.60	6.42	6.53
H(3)	8.86	8.66	8.94	8.72	8.63
H(6A)	5.20	5.00	8.60	7.71	8.39
H(6B)	5.10	4.91	7.47	7.03	8.30

confirming the importance of the resonance iminium formula (Chart S2†) already evidenced by the X-ray crystal structure analysis. It is important to point out that the hindered rotation cannot be due to the participation of the NH_2 group to the intermolecular H-bonds (*vide supra*) that should be completely broken in $\text{DMSO}-d_6$ solution.

In order to obtain an evaluation of the rotational barrier around the C(4)–N(6) bond, we registered 1D ^1H NMR and 2D-EXSY (exchange spectroscopy) spectra at different temperatures, in the range 298–328 K. Qualitatively, we observed the beginning of the coalescence of the two N–H signals at 328 K, while the rate constant values for the exchange of H(6A) and H(6B) (Fig. 5) were evaluated by integrating the diagonal peaks and cross-peaks of the 2D-EXSY spectrum.⁴⁹

The activation energy (E_a) of the exchange process resulting from an Arrhenius plot⁵⁰ (Fig. 5) amounts to $E_a = 119 \text{ kJ mol}^{-1}$. The rotational barrier around the C(4)–N(6) bond was also theoretically estimated. We computed the binding energy (BE) of **1** as a function of torsion angle H(6B)–N(6)–C(4)–N(3) (θ) by scanning θ from 0° to 180° at 15° steps, without any geometrical optimization, obtaining a maximum for $\theta = 90^\circ$ (see Fig. S7†). The rotational barrier was evaluated as the difference between the maximum value of binding energy of the structure ($\theta = 90^\circ$) and that of the ground state ($\theta = 0^\circ$ or 180°), obtaining $E_a = 99 \text{ kJ mol}^{-1}$, in very good agreement with the value obtained from 2D-EXSY spectra.

From the synthetic point of view, it is also worth noting the lack of reactivity of the NH_2 moiety of **1** with C_3O_2 ,⁵¹ the anhydride of malonic acid,⁵² to give the corresponding diamidic derivative.⁵³ Such a behaviour, indicative of the unavail-

ability of the nitrogen lone pair on NH_2 , again confirms its iminium character.

A further point deserves to be mentioned. Compound **1** is almost completely insoluble in most organic solvents, showing a low solubility only in MeOH (from which it was recrystallized) and in DMSO. Since both solvents are known to break H-bonds, it is likely that insolubility is due to this kind of interaction, as suggested by the X-ray crystal structure determination (*vide supra*). To look into this point, a further series of numerical experiments have been carried out to get a semi-quantitative estimate of the intermolecular H-bond strength involving the N(6)–H(6B) moiety and the pyrazolate N atom of a second molecule.⁵⁴

We examined the dimeric assembly formed through the H-bond interaction between N(6)–H(6B) and N(2') of another molecule of **1**. This dimer was obtained by translating a single molecule along the axis defined by the C(4)–N(6) bond. The equilibrium distance between the two molecules was obtained by optimizing the structure of the dimeric assembly without any constraint. In this regard, it has to be remarked that calculations were limited to the PBE functional because it is well known that it provides quite good results when H-bonds are involved.^{55,56} The calculated equilibrium distance between the two monomers is in reasonable agreement with experimental data [N(5')–N(6): calcd. = 3.154 \AA , expt. = 2.945 \AA ; N(6)–N(2'): calcd. = 3.003 \AA , expt. = 3.013 \AA ; N(6)–H(6B)–N(2'): calcd. = 175.80° , expt. = 171.45°]. Furthermore, the ($E_D - 2E_M$) stabilization energy⁵⁷ corrected for the preparation energy (the energy required to relax the structure of the free monomers to the geometry they assumed in the dimer), and basis set superposition error (BSSE)⁵⁸ amounts to 34.3 kJ mol^{-1} . Strictly speaking, this stabilization derives also from the N(6)–H(6A)···Cl(1') weak interaction⁵⁴ but it is very likely that its contribution is negligible⁵⁹ with respect to the N(6)–H(6B)···N(2') H-bond. It is noteworthy that the calculated stabilization energy value is similar to that reported for $\text{O}=\text{C}-\text{OH}\cdots\text{O}=\text{C}-\text{OH}$ interactions in carboxylic acids.^{5a}

Finally, we evaluated the lowest lying excitation energies and corresponding oscillator strengths of **1** by employing time dependent DFT at the PBE level. Calculated transition energies are in good agreement with the experimental values

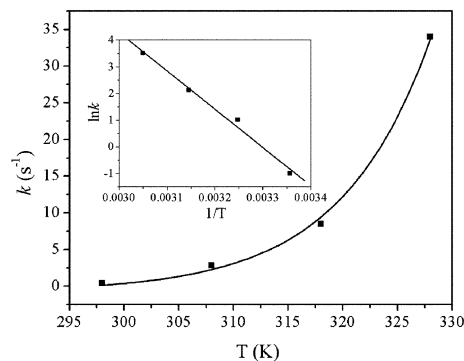


Fig. 5 Rate constant k for the exchange of H(6A) and H(6B) as a function of T . The inset accounts for the corresponding Arrhenius plot.

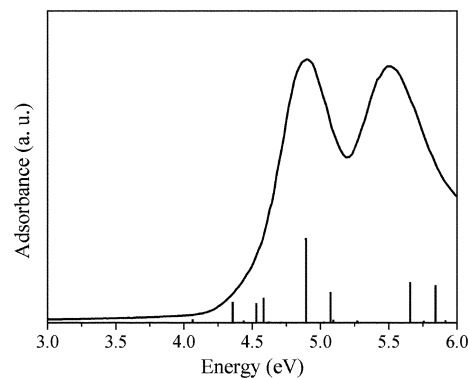


Fig. 6 Experimental UV-Vis spectrum of **1**. Vertical bars represent the theoretical oscillator strength values (f) obtained by TD-DFT calculations.

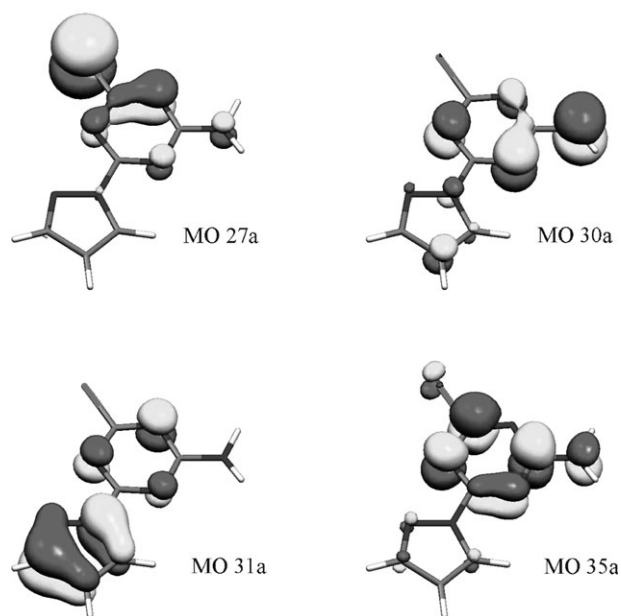


Fig. 7 3D contour plots of MO excited configurations generating UV-Vis spectrum of **1**.

obtained from UV-Vis spectrum in MeOH solution (see Fig. 6).

Both bands are generated by a significant mixing of excited configurations. In particular, to the lowest lying band, (4.89 eV, expt. 4.90 eV) the excited configurations 31a \rightarrow 35a, 31a \rightarrow 34a and 27a \rightarrow 34a contribute 57%, 24% and 11%, respectively, while, as far as the latter band (5.66 eV; expt. 5.51 eV) is concerned, the 30a \rightarrow 35a excited configuration contributes to it 68%. In Fig. 7 are shown the 3D contour plots of above indicated MOs.

Interestingly, transitions bearing a significant contribution from the HOMO \rightarrow LUMO (33a \rightarrow 34a) excited configuration (Fig. S8†) are all characterized by very low oscillator strength values.

Conclusions

We have reported that the reaction of 2-amino-4,6-dichloro-[1,3,5]triazine with 2 equivalents of Hpz at 100 °C yields a mixture containing only *ca.* 20% of the fully substituted product 2-amino-4,6-dipyrazolyl-[1,3,5]triazine and *ca.* 80% of the di-substituted 2-amino-4-chloro-6-pyrazolyl-[1,3,5]triazine, **1**. This finding indicates that the *Moffat's rule*¹⁸ is to be considered only as a qualitative indication, the reactivity of monosubstituted derivatives largely depending on the effect of the first introduced substituent. In our case, the presence of the NH₂ group strongly deactivates⁶⁰ the system towards the introduction of two pyrazolates, thus yielding prevalently **1** even in drastic reaction conditions.

In any case, compound **1** forms a new, robust supramolecular linear tape, whose formation is exclusively dictated by medium–strong H-bonds, as indicated not only by geometrical parameters but also by the calculated stabilization energy, of *ca.* 34.3 kJ mol⁻¹.

Even when the H-bonds are broken, as happens in DMSO solution, both experimental findings (¹H NMR, the unreactivity of **1** towards C₃O₂⁵¹) and DFT calculations provide evidence for the iminium character of the NH₂ moiety of **1** and the consequent unavailability of the nitrogen lone pair. This finding is particularly interesting, mainly in view of the possible use of **1** (and similar derivatives) in coordination chemistry. As a matter of fact, this means that the NH₂ of **1** cannot be involved into any metal coordination, analogously to what has been observed with melamine (2,4,6-triamine-[1,3,5]triazine). For the latter, only a few cases of structurally validated metal coordination compounds are reported⁶¹ and melamine always results in bonding like pyridine to the metal centres, with one nitrogen atom of the aromatic ring.⁶² On the other hand the NH₂ moiety might be involved in strong H-bonds, thus generating robust networks.

For these reasons our future researches in this field will be focused on the use of **1** (and related compounds) to coordinate metal ions through pyrazolate and/or endocyclic triazine nitrogen(s) while the NH₂ (iminic) moieties will be useful to form H-bonds, thus generating robust MOFs (metal–organic frameworks) by supramolecular interactions.

Acknowledgements

This work was supported by the Italian PRIN funding n. 2006038447. Computational resources and assistance were provided by the “Laboratorio Interdipartimentale di Chimica Computazionale” (LICC) at the Department of Chemical Sciences of the University of Padova. M. M. wishes to thank the University of Bologna for financial support.

References

- 1 J. M. Lehn, *Pure Appl. Chem.*, 1978, **50**, 871.
- 2 J. C. Noveron, M. S. Lah, R. E. Del Sesto, A. M. Arif, J. S. Miller and P. J. Stang, *J. Am. Chem. Soc.*, 2002, **124**, 6613.
- 3 J. C. MacDonald, P. C. Dorrestein, M. M. Pilley, M. M. Foote, J. L. Lundburg, R. W. Henning, A. J. Schultz and J. L. Manson, *J. Am. Chem. Soc.*, 2000, **122**, 11692.
- 4 K. Ariga and T. Kunitake, *Acc. Chem. Res.*, 1998, **31**, 371.
- 5 (a) T. Steiner, *Angew. Chem., Int. Ed.*, 2002, **41**, 48; (b) D. Braga and F. Grepioni, *Acc. Chem. Res.*, 2000, **33**, 601.
- 6 B. Gong, Y. Yan, H. Zeng, E. Skrzypczak-Jankunn, Y. W. Kim, J. Zhu and H. Ickes, *J. Am. Chem. Soc.*, 1999, **121**, 5607 and references therein.
- 7 J.-R. Li, Y. Tao, Q. Yu and X.-H. Bu, *Cryst. Growth Des.*, 2006, **6**, 2493.
- 8 G. Pavlović, V. Tralić-Kulenović, M. Vinković, D. Vikić-Topić, I. Matanović and Z. Popović, *Struct. Chem.*, 2006, **17**, 275.
- 9 R. Mondal, J. A. K. Howard, R. Banerjee and G. R. Desiraju, *Cryst. Growth Des.*, 2006, **6**, 2507.
- 10 P. Gamez and J. Reedijk, *Eur. J. Inorg. Chem.*, 2006, 29 and references therein.
- 11 (a) J. A. Zerkowski, J. C. MacDonald and G. M. Whitesides, *Chem. Mater.*, 1994, **6**, 1250; (b) J. A. Zerkowski and G. M. Whitesides, *J. Am. Chem. Soc.*, 1994, **116**, 4298; (c) J. A. Zerkowski, J. P. Mathias and G. M. Whitesides, *J. Am. Chem. Soc.*, 1994, **116**, 4305; (d) J. A. Zerkowski, C. T. Seto, D. A. Wierda and G. M. Whitesides, *J. Am. Chem. Soc.*, 1990, **112**, 9025.
- 12 (a) J. C. MacDonald and G. M. Whitesides, *Chem. Rev.*, 1994, **94**, 2383; (b) E. E. Simanek, A. Tsoi, C. C. Wang, G. M. Whitesides, M. T. McBride and G. T. R. Palmore, *Chem. Mater.*, 1997, **9**, 1954.

- 13 S. Palacin, D. N. Chin, E. E. Simanek, J. C. MacDonald, G. M. Whitesides, M. T. McBride and G. T. R. Palmore, *J. Am. Chem. Soc.*, 1997, **119**, 11807.
- 14 (a) Y. Z. Ren, S. G. Chen, X. D. Chai, Y. W. Cao, W. S. Yang, R. Lu, G. Li, A. D. Lu, M. X. Gong, Y. B. Bai, T. J. Li and J. M. Lehn, *Synth. Met.*, 1995, **71**, 1709; (b) W. S. Yang, S. G. Chen, X. D. Chai, Y. W. Cno, R. Lu, W. P. Chai, Y. S. Jiang, T. J. Li and J. M. Lehn, *Synth. Met.*, 1995, **71**, 2107.
- 15 F. Würthner, S. Yao, B. Heise and C. Tschierske, *Chem. Commun.*, 2001, 2260.
- 16 (a) E. A. Archer, N. T. Goldberg, V. Lynch and M. J. Krische, *J. Am. Chem. Soc.*, 2000, **122**, 5006; (b) E. A. Archer and M. J. Krische, *J. Am. Chem. Soc.*, 2002, **124**, 5074; (c) E. A. Archer, D. F. Cauble, V. Lynch and M. J. Krische, *Tetrahedron*, 2002, **58**, 721.
- 17 It is noteworthy that this compound exists in a second polymorphic crystal species having a slightly different molecular structure and forming similar tapes assembling in the lattice in a quite different fashion: J. Glaser, S. Tragl and H. J. Meyer, *Kristallogr.*, 2005, **220**, 214.
- 18 W. W. Cuthbertson and J. S. Moffat, *J. Chem. Soc.*, 1948, 561.
- 19 O. Diels, *Ber. Dtsch. Chem. Ges.*, 1899, **32**, 695.
- 20 A. Hofmann, *Ber. Dtsch. Chem. Ges.*, 1886, **19**, 2061.
- 21 (a) E. M. Smolin and L. Rapoport, *s-Triazines and Derivatives*, Interscience Publisher Inc., New York, 1959; (b) T. J. Mooibroek and P. Gamez, *Inorg. Chim. Acta*, 2007, **360**, 381 and references therein.
- 22 (a) M. Maekewa, T. Minematsu, H. Konaka, K. Sugimoto, T. Kuroda-Sowa, Y. Suenaga and M. Munakata, *Inorg. Chim. Acta*, 2004, **357**, 3456; (b) H. Brückner and M. Wachsmann, *J. Chromatogr., A*, 2003, **998**, 73.
- 23 A. de la Hoz, A. Díaz-Ortiz, J. Elguero, L. J. Martínez, A. Moreno and A. Sánchez-Migallón, *Tetrahedron*, 2001, **57**, 4397.
- 24 N. Lyapchenko, C. Eitner, G. Schroeder and B. Brzezinski, *J. Mol. Struct.*, 2004, **690**, 45.
- 25 G. Giacomelli, A. Porcheddu and L. D. Luca, *Curr. Org. Chem.*, 2004, **8**, 1497.
- 26 S. M. Kheronsky and Y. T. Chang, *J. Comb. Chem.*, 2004, **6**, 474.
- 27 (a) P. V. Bernhardt and E. J. Hayes, *Inorg. Chem.*, 1998, **37**, 4214; (b) L. J. Prins, E. E. Neuteboom, V. Paraschiv, M. Crego-Calama, P. Timmerman and D. N. Reinhoudt, *J. Org. Chem.*, 2002, **68**, 4808.
- 28 C. T. Seto and G. M. Whitesides, *J. Am. Chem. Soc.*, 1990, **112**, 6409.
- 29 L. J. Prins, C. Thalacker, F. Würthner, P. Timmerman and D. N. Reinhoudt, *Proc. Natl. Acad. Sci. U. S. A.*, 2001, **98**, 10042.
- 30 (a) A. Gelling, M. D. Olsen, K. G. Orrel, A. G. Osborne and V. Šik, *Inorg. Chim. Acta*, 1997, **264**, 257; (b) V. Milata, R. M. Claramunt, P. Cabildo, M. D. Santa, P. Cornago, L. Infantes, F. H. Cano and J. Elguero, *Heterocycles*, 2001, **55**, 905; (c) P. de Hoog, P. Gamez, W. L. Driessen and J. Reedijk, *Tetrahedron Lett.*, 2002, **43**, 6783; (d) P. Gamez, P. de Hoog, O. Roubeau, M. Lutz, W. L. Driessen, A. L. Spek and J. Reedijk, *Chem. Commun.*, 2002, 1488; (e) R. M. Claramunt, P. Cornago, M. Cano, J. V. Heras, M. L. Gallego, E. Pinilla and M. R. Torres, *Eur. J. Inorg. Chem.*, 2003, 2693.
- 31 D. D. Perrin, W. L. Armarego and D. R. Perrin, *Purification of Laboratory Chemicals*, 2nd edn, Pergamon Press, Oxford, 1980.
- 32 (a) A. Bax and S. Subramian, *J. Magn. Reson.*, 1986, **67**, 565; (b) G. Drobny, A. Pines, S. Sinton, D. Weitekamp and D. Wemmer, *Faraday Symp. Chem. Soc.*, 1979, **B33**, 4912.
- 33 G. Otting and K. Wüthrich, *J. Magn. Reson.*, 1988, **76**, 569.
- 34 A. Bax and M. F. Summers, *J. Am. Chem. Soc.*, 1986, **108**, 2093.
- 35 *Amsterdam Density Functional Package, Version 2006–2007*, Vrije Universiteit, Amsterdam, The Netherlands, 2007.
- 36 J. P. Perdew, K. Burke and M. Ernzerhof, *Phys. Rev. Lett.*, 1996, **77**, 3865.
- 37 (a) S. J. A. van Gisbergen, J. G. Snijders and E. J. Baerends, *Comput. Phys. Commun.*, 1999, **118**, 119; (b) S. J. A. van Gisbergen, *Molecular Response Property Calculations using Time Dependent Density Functional Theory in Chemistry*, Vrije Universiteit, Amsterdam, 1998, p. 190; (c) E. K. U. Gross, J. F. Dobson and M. Petersilka, in *Density Functional Theory*, ed. R. F. Nalewajski, Springer, Heidelberg, 1996.
- 38 *SMART & SAINT Software Reference Manuals, Version 5.051 (Windows NT Version)*, Bruker Analytical X-Ray Instruments Inc., Madison, WI, USA, 1998.
- 39 G. M. Sheldrick, *SADABS, Program for Empirical Absorption Correction*, University of Göttingen, Germany, 1996.
- 40 A. Altomare, G. Casciarano, C. Giacovazzo, A. Guagliardi, A. G. G. Moliterni, M. C. Burla, G. Polidori, M. Camalli and D. Siliqi, *Acta Crystallogr., Sect. A: Found. Crystallogr.*, 1996, **52**, C79.
- 41 G. M. Sheldrick, *SHELXTLplus Structure Determination Package, Version 5.1 (Windows NT Version)*, Bruker Analytical X-Ray Instruments Inc., Madison, WI, USA, 1998.
- 42 C. F. Macrae, P. R. Edgington, P. McCabe, E. Pidcock, G. P. Shields, R. Taylor, M. Towler and J. van de Streek, *Mercury: Visualization and Analysis of Crystal Structures*, *J. Appl. Crystallogr.*, 2006, **39**, 453.
- 43 E. Keller, *SCHAKAL A Computer Program for the Graphic Representation of Molecular and Crystallographic Models*, Institute for Crystallography of the University of Freiburg, Freiburg, Germany, 1997.
- 44 P. Coppens, *Science*, 1967, **158**, 1577.
- 45 A. Bondi, *J. Phys. Chem.*, 1964, **68**, 441.
- 46 A. L. Spek, *PLATON, A Multipurpose Crystallographic Tool*, Utrecht University, Utrecht, The Netherlands, 2003.
- 47 (a) M. Amm, N. Platzter, J. Guilhem, J. P. Bouchet and J. P. Volland, *Magn. Reson. Chem.*, 1998, **36**, 587; (b) W. von Philipsborn and R. Müller, *Angew. Chem., Int. Ed. Engl.*, 1986, **25**, 383.
- 48 The assignment of 8.39 and 8.30 ppm signals in the experimental spectrum to H(A) and H(B), respectively is made only by qualitative comparison with calculated values.
- 49 C. L. Perrin and T. J. Dwyer, *Chem. Rev.*, 1990, **90**, 935.
- 50 M. Umetsu, R. Seki, T. Kadota, Z. Y. Wang, T. Adshiri and T. Nozawa, *J. Phys. Chem. B*, 2003, **107**, 9876.
- 51 F. Garau and L. Pandolfo, unpublished results.
- 52 O. Diels and B. Wolf, *Ber. Dtsch. Chem. Ges.*, 1906, **39**, 689.
- 53 (a) T. Kappe and E. Ziegler, *Angew. Chem., Int. Ed. Engl.*, 1974, **13**, 491; (b) P. Ganis, G. Valle, L. Pandolfo, R. Bertani and F. Visentin, *Biopolymers*, 1999, **49**, 541.
- 54 XRD shows also that N(6)–H(6A) and chlorine of a second molecule are likely engaged in a very weak interaction [H(6A)⋯Cl(1') 2.90(2) Å, N6–H(6A)⋯Cl(1') 3.660(1) Å, N6–H(6A)⋯Cl(1') 150(2)°].
- 55 D. R. Hamann, *Phys. Rev. B: Condens. Matter Mater. Phys.*, 1997, **16**, R10157.
- 56 G. Rovira, J. J. Novoa and P. Ballone, *J. Chem. Phys.*, 2001, **115**, 6406.
- 57 E_D and E_M correspond to the binding energy of the dimeric assembly and of the isolated monomer, respectively.
- 58 BSSE was estimated through the use of reference energies computed with a ghost monomer. See: A. Rosa, A. W. Ehlers, E. J. Baerends, J. G. Snijders and G. te Velde, *J. Phys. Chem.*, 1996, **100**, 5690.
- 59 (a) G. Aullón, D. Bellamy, L. Brammer, E. A. Bruton and A. G. Orpen, *Chem. Commun.*, 1998, 653; (b) L. Brammer, E. A. Bruton and P. Sherwood, *Cryst. Growth Des.*, 2001, **1**, 277; (c) R. Banerjee, G. R. Desiraju, R. Mondal and J. A. K. Howard, *Chem.–Eur. J.*, 2004, **10**, 3373.
- 60 (a) V. I. Mur, *Russ. Chem. Rev.*, 1964, **33**, 92; (b) S. Samaritani, P. Peluso, C. Malanga and R. Menicagli, *Eur. J. Org. Chem.*, 2002, 1551.
- 61 (a) H. Zhu, Z. Yu, X. You, H. Hu and X. Huang, *J. Chem. Crystallogr.*, 1999, **29**, 239; (b) D. M. L. Goodgame, I. Hussain, A. J. P. White and D. J. Williams, *J. Chem. Soc., Dalton Trans.*, 1999, **29**, 2899; (c) K. Sivashankar, A. Ranganathan, V. R. Pedireddi and C. N. R. Rao, *J. Mol. Struct.*, 2001, **559**, 41; (d) J. Zhang, Z.-J. Li, Y.-H. Wen, Y. Kang, J.-K. Cheng and Y.-G. Yao, *J. Mol. Struct.*, 2004, **697**, 185; (e) Y.-Q. Yu, C.-Z. Lu, X. He, S.-M. Chen, Q.-Z. Zhang, L.-J. Chen and W.-B. Yang, *J. Chem. Crystallogr.*, 2004, **34**, 905; (f) C. Chen, C.-W. Yeh and J.-D. Chen, *Polyhedron*, 2006, **25**, 1307.
- 62 In ref. 61c is reported the formation of a coordination polymer where two endocyclic nitrogens of melamine bridge two Ag(I) ions.

Density Functional Theory Study of the Binding Capability of Tris(pyrazol-1-yl)methane toward Cu(I) and Ag(I) Cations

Maurizio Casarin,^{*,†,‡,§} Daniel Forrer,^{†,§} Federica Garau,[†] Luciano Pandolfo,^{†,§} Claudio Pettinari,^{||} and Andrea Vittadini^{‡,§}

Dipartimento di Scienze Chimiche, Università degli Studi di Padova, Padova 35131, Italy, Dipartimento di Scienze Chimiche, Università degli Studi di Camerino, Camerino (MC) 62032, Italy, Istituto di Scienze Molecolari del CNR, Padova 35131, Italy, and Consorzio Interuniversitario di Scienza e Tecnologia dei Materiali, Firenze 50121, Italy

Received: March 4, 2008; Revised Manuscript Received: April 28, 2008

Density functional theory (DFT) has been used to look into the electronic structure of $[M(\text{tpm})]^+$ molecular ion conformers ($M = \text{Cu}, \text{Ag}$; $\text{tpm} = \text{tris}(\text{pyrazol-1-yl})\text{methane}$) and to study the energetics of their interconversion. Theoretical data pertaining to the free tpm state the intrinsic instability of its κ^3 -like conformation, thus indicating that, even though frequently observed, the κ^3 -tripodal coordinative mode is unlikely to be directly achieved through the interaction of $M(\text{I})$ with the κ^3 -like tpm conformer. It is also found that the energy barrier for the κ^2 - $[M(\text{tpm})]^+ \rightarrow \kappa^3$ - $[M(\text{tpm})]^+$ conversion is negligible. As far as the bonding scheme is concerned, the $\text{tpm} \rightarrow M(\text{I})$ donation, both σ and π in character, is the main source of the $M(\text{I})$ - tpm bonding, whereas back-donation from completely occupied $M(\text{I})$ d orbitals into tpm -based π^* levels plays a negligible role.

1. Introduction

Tris(pyrazol-1-yl)borate (hereafter, tp) and tris(pyrazol-1-yl)methane (hereafter, tpm) are considered among the most useful ligands in modern coordination chemistry.¹ Substituted and unsubstituted tp and tpm supply in fact a significant steric shielding of the metal center serving, at the same time, as reliable spectator ligands. These peculiarities make them useful for the synthesis of complexes with virtually all metals in the periodic table, having thus applications in diverse and important fields ranging from catalysis to biomedicine, from metal extraction to biomimetic inorganic chemistry.^{1f,g,h,i} In general, tp and tpm behave as tripodal κ^3 -ligands through the lone pairs of the nitrogen heteroatoms $[N(\bullet)]$ of the three pyrazolyl fragments (see Figure 1d).² In this regard, these ligands are often labeled as scorpionates, a consequence of an oneiric description of their bonding capabilities where, like the pincers of a scorpion, the $N(\bullet)$ of two pyrazolyl moieties attached to B (tp) or C (tpm) bind a metal, and the third pyrazolyl attached to the central atom rotates forward like the scorpion's tail to "sting" the metal. Although such a picture is certainly attractive, crystallographic data pertaining to the free tp ^{3a} and tpm ,⁴ i.e., the simplest members of the scorpionate family, suggest alternative bonding mechanisms. In fact, both tp and tpm solid state structures are characterized by a single pyrazolyl group with $N(\bullet)$ in trans with respect to the H atom of the B–H (tp)/C–H (tpm) fragments (see Figure 1b).⁵

Theoretical work so far devoted to the study of tp and tpm ligands with metal ions is very limited. De Bari and Zimmer⁷ carried out a study of the conformational flexibility of tp and tpm behaving as κ^3 -tripodal ligands showing, through the use of molecular mechanics and database analysis, that "tripodal

scorpionate ligands can accommodate a variety of metal sizes by opening up the ligand".

In this paper we present and discuss the results of a series of first-principle numerical experiments devoted to the study of the electronic structure of κ^1 -monodentate, κ^2 -chelating, and κ^3 -tripodal $[M(\text{tpm})]^+$ molecular ions ($M = \text{Cu}, \text{Ag}$) as well as to the energetics of their interconversion.⁸ The first section of the contribution is dedicated to the theoretical analysis of the free pyrazole molecule (hereafter, Hpz)⁹ and its hypothetical $[M(\text{Hpz})]^+$ σ and π complexes with the aim of gaining quantitative information about the nature and the strength of the $M(\text{I})$ - Hpz interaction. The second part deals with the conformation flexibility of the free tpm ligand, leaving aside any problem concerning optical isomerism, and the third one is focused on binding energies and electronic properties of the $[M(\text{tpm})]^+$ molecular ions.

2. Computational Details

All the numerical experiments have been carried out by using the Amsterdam Density Functional (ADF) package¹² and adopting the scalar relativistic zeroth-order regular approximation (ZORA).¹³ Optimized geometries for ground and transition states (GS and TS, respectively) were obtained by employing generalized gradient (GGA) corrections self-consistently included through the Becke–Perdew formula,¹⁴ and without imposing any symmetry. All TS's have been estimated through the following procedure: (i) a linear transit (LT) calculation has been run by varying a dihedral angle¹⁵ (vide infra); (ii) from the TS guess provided by step (i), a stationary point on the energy surface has been searched; (iii) the adequacy of the TS estimate has been then checked by computing vibrational frequencies at the corresponding geometry and verifying that one of them is imaginary; (iv) the Hessian computed in the third step is employed for the final TS optimization.

TZP ZORA basis sets were adopted for all the atoms;¹⁶ inner cores of Cu (1s2s2p3s3p), Ag (1s2s2p3s3p3d), C (1s), and N

[†] Università degli Studi di Padova.

^{||} Università degli Studi di Camerino.

[‡] Istituto di Scienze Molecolari del CNR.

[§] Consorzio Interuniversitario di Scienza e Tecnologia dei Materiali.

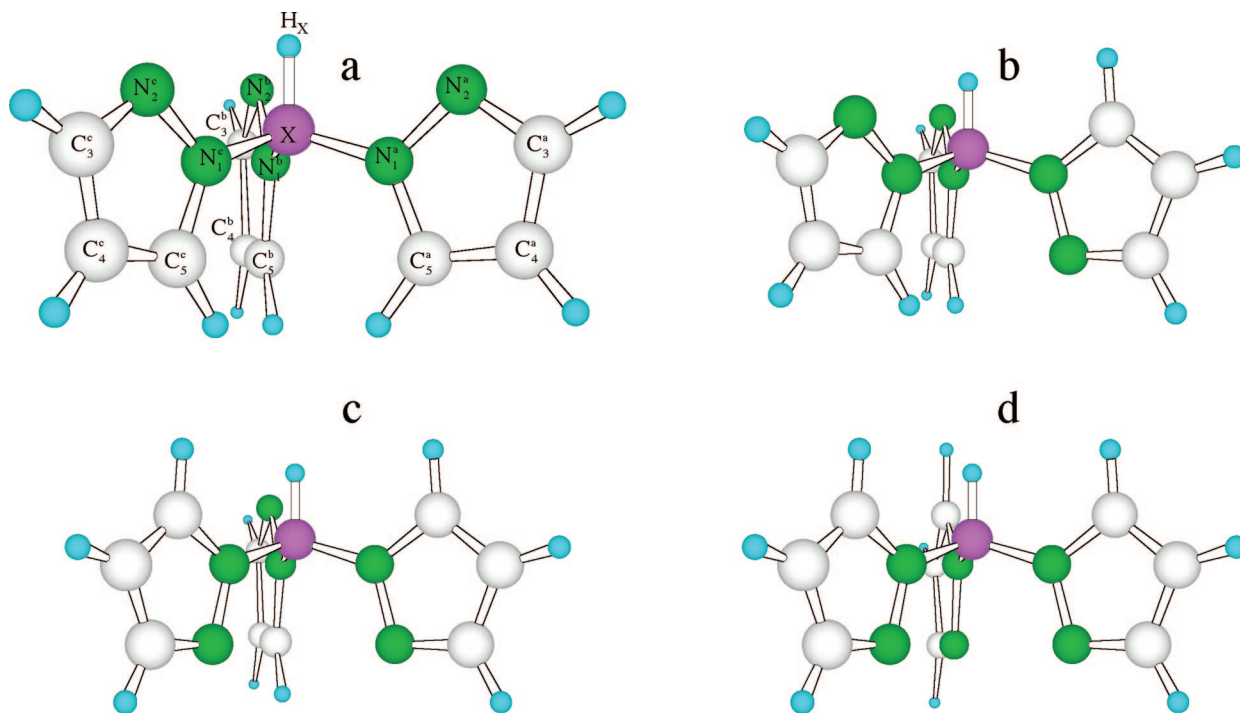


Figure 1. Schematic representation of possible relative arrangements of pyrazolyl fragments in tp ($X = B$) and tpm ($X = C$).

(1s) atoms were kept frozen throughout the calculations. Binding energies (BEs) were analyzed in terms of fragment molecular orbitals (FMO's) by applying the Ziegler's extended transition state method (ETS).¹⁷ According to the ETS scheme,

$$BE = \Delta E_{es} + \Delta E_{Pauli} + \Delta E_{int} + \Delta E_{prep} \quad (1)$$

where ΔE_{es} is the pure electrostatic interaction, ΔE_{Pauli} is the destabilizing two-orbital-four-electron interaction between the occupied orbitals of the interacting fragments ($(\Delta E_{es} + \Delta E_{Pauli})$ corresponds to the so called steric interaction (ΔE_{st}) contribution), ΔE_{int} derives from the stabilizing interaction between occupied and empty orbitals of the interacting fragments, and ΔE_{prep} provides information about the energy required to relax the structure of the free fragments to the geometry they assume in the final system. BE's were further corrected by taking into account the basis set superposition error (BSSE) which was estimated by making use of reference energies calculated with "ghost" fragments.¹⁸

Rather than displaying discrete eigenvalues along an energy axis, we preferred to plot the density of states (hereafter, DOS) as a function of energy by using a 0.25 eV Lorentzian broadening factor. These plots, based on Mulliken's prescription for partitioning the overlap density,¹⁹ have the advantage of providing insights into the atomic composition of MO's over a broad range of energy. Finally, information about the localization and the bonding/antibonding character of selected MO's was obtained by using crystal orbital overlap populations (COOP's)²⁰ computed by weighting one-electron energy levels by their basis orbital percentage.

3. Results and Discussion

As above mentioned, tpm is a potentially tripodal, neutral ligand characterized by the presence of three pyrazolyl moieties bonded to a central methine carbon atom (see Figure 1). Now, Hpz is planar, fully conjugated, and isoelectronic with the cyclopentadienyl anion, but the higher electronegativity of nitrogen (3.04)²¹ compared to that of carbon (2.55)²¹ determines

a higher electronic charge density on N atoms both in the molecular plane and out of it. In consequence of that, each tpm pyrazolyl group may be involved in two competitive metal–ligand bonding mechanisms: a σ -bonding implying the $N(\bullet)$ lone pair (hereafter, n_N) and a π -bonding involving the π electron density of the aromatic ring. An intimate comprehension of the tpm coordination capabilities necessarily passes through a deep understanding of the σ/π $[M(Hpz)]^+$ bonding scheme.

3.1. Hpz and σ/π $[M(Hpz)]^+$ Complexes. Optimized coordinates of Hpz are reported in Table S1, and selected geometrical parameters and Mulliken¹⁹ and Hirshfeld²² gross atomic charges are collected in Tables 1 and 2, respectively. The agreement with data obtained by accurate ab initio calculations (CBS-APNO QCISD/6-311G(d,p))²³ is remarkable; moreover, theoretical estimates of the Hpz dipole moment (μ), lowest ionization energies (IEs)²⁴ and VUV-absorption bands agree very well with experiment.²⁷

The Hpz valence manifold includes five π -like and the n_N MO's. Among them, the π_1 , π_2 , and π_3 ones (the 8a, 12a, and 13a levels, respectively) and n_N (the 11a MO) are occupied, whereas π_4 and π_5 (the 14a and 16a MO's, respectively) are empty; moreover, π_3 and π_4 correspond to the Hpz HOMO and LUMO, respectively. 3D-contour plots of the whole Hpz valence manifold are displayed in Figure 2.

The contemporary presence of the aromatic π system and of the n_N allows two competitive bonding mechanisms in $[M(Hpz)]^+$. With reference to the Hpz \rightarrow M(I) donation, a simple electron count coupled to symmetry arguments and overlap considerations indicate that (i) n_N will limit its involvement to the M(I)–Hpz σ bonding; (ii) the Hpz π system may contribute to both σ and π interactions; (iii) M(I) will participate with its s and p virtual atomic orbitals (AO's). As far as the M(I) \rightarrow Hpz back-donation is concerned, the charge transfer is possible between the fulfilled M(I) d AO's and the Hpz-based π_4 and π_5 virtual MO's.

A schematic representation of the optimized structure of σ/π $[M(Hpz)]^+$ complexes is displayed in Figure 3 (corresponding

TABLE 1: Selected Geometrical Parameters of the Free Hpz and σ/π [M(Hpz)]⁺ Complexes^a

Hpz	[Cu(Hpz)] ⁺		[Ag(Hpz)] ⁺	
	σ	π	σ	π
M–N(1)		3.205		3.412
M–N(2)	1.856	3.271	2.129	3.256
M–C(3)		2.593		2.548
M–C(4)		1.975		2.279
M–C(5)		2.565		2.972
N(1)–N(2)	1.356	1.366	1.363	1.358
N(2)–C(3)	1.340	1.353	1.351	1.335
C(3)–C(4)	1.415	1.398	1.400	1.454
C(4)–C(5)	1.386	1.389	1.435	1.387
C(5)–N(1)	1.361	1.350	1.335	1.342
N(1)N(2)C(3)	103.8	106.0	105.6	104.3
N(2)C(3)C(4)	112.0	110.0	111.9	110.4
C(3)C(4)C(5)	104.6	105.7	102.8	105.4
C(4)C(5)N(1)	106.0	107.5	106.0	107.3
C(5)N(1)N(2)	113.4	110.9	111.3	114.8

^a Bond lengths and bond angles in Å and deg, respectively.

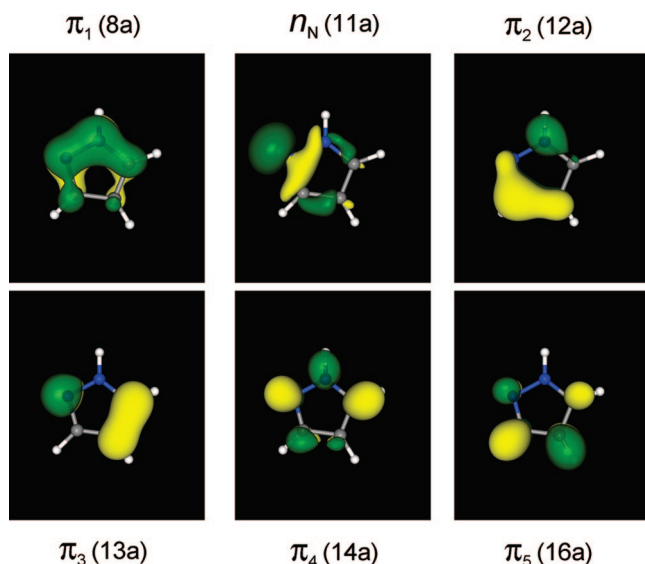


Figure 2. 3D contour plots of the Hpz π_1 – π_5 MO's. The 3D plot of the n_N is also included. Yellow (green) surfaces correspond to a constant positive (negative) value of $0.06 e^{1/2}/\text{Å}^{3/2}$.

optimized coordinates are reported in Tables S2–S5), and selected geometrical parameters, Mulliken/Hirshfeld gross atomic charges and ETS contributions to the metal-ligand BE's are collected in Tables 1, 2 and 3, respectively. Structural perturbations undergone by the C_3N_2 pyrazole ring are rather similar for the two coordinative modes, except for the significant rehybridization of C(4) in π -[M(Hpz)]⁺ (see Figure 3).²⁹ The analysis of COOP curves in Figure 4, and of gross atomic charge variations at C(4) on passing from the free ligand to the coordinated one (see Table 2) testifies that the C(4) rehybridization in π -[M(Hpz)]⁺ has to be ultimately traced back to the concomitant Hpz $\pi_3 \rightarrow M(I)$ sp donation and M(I) d $\rightarrow \pi_5$ back-donation, with the former much stronger than the latter.³⁰ According to that, a lengthening of the C(4)–C(5) and C(3)–C(4) bond distances is computed on passing from the free to the coordinated Hpz.

A further point to be emphasized concerns the relevance of π contributions to the metal-ligand bond in σ -[M(Hpz)]⁺ complexes. More specifically, the inspection of Figure 5 testifies that, besides the $n_M \rightarrow N(sp)$ donation, high lying Hpz π orbitals strongly localized on N(•) (π_3 and π_4 MO's, see Figure 2) significantly participate to the metal-ligand interaction.

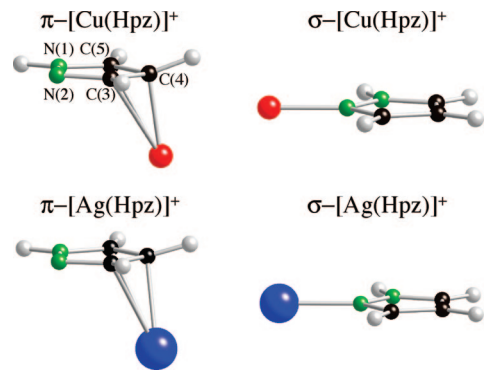


Figure 3. Schematic representations of the optimized structure of σ/π -[M(Hpz)]⁺ complexes.

As far as BE values are concerned, the examination of data reported in Table 3 is particularly intriguing. In fact, despite BE's of σ complexes being larger than those corresponding to the π ones and [Cu(Hpz)]⁺ BE's being larger than the [Ag(Hpz)]⁺ ones, ΔE_{int} contributions show an opposite trend, thus indicating that each BE value is the result of a subtle balance of different contributions, with ΔE_{st} playing a very important role.

3.2. tpm Conformational Flexibility. The tpm X-ray crystal structure is characterized by a single pyrazolyl group with N(•) (N_2^3 in Figure 1b) in trans with respect to the hydrogen of the C–H fragment. This conformer has been labeled tpm-1,³¹ and those corresponding to the κ^2 -chelating (Figure 1c) and κ^3 -tripodal (Figure 1d) coordinative modes have been tagged as tpm-2 and tpm-3, respectively. The tpm-0 conformer (see Figure 1a) is obviously the one with the three N(•) in cis with respect to the methine fragment. Relative BE's corresponding to tpm-0, tpm-1, and tpm-2 GS's as well as to relevant saddle points are displayed in Figure 6 where sketches of the corresponding optimized molecular structures are also reported.^{31,33} The tpm-3 conformer is not reported because it was found to be unstable.

Before going on, it deserves to be mentioned that the tpm-0 optimized structure is characterized by the presence of a C_3 axis with pyrazolyl fragments adopting a propeller-like orientation.³⁴ Such a result allowed us to label the linear combinations of Hpz-based frontier orbitals according to the $a + e$ irreducible representations of the C_3 point group (see Figure 7). Interestingly, even though BE(tpm-0) and BE(tpm-1) are very close ($\Delta BE_{0,1} = BE(tpm-0) - BE(tpm-1) = 0.88$ kcal/mol), tpm-1 corresponds to the absolute minimum not only in the solid state but also in the isolated molecule, thus confirming early semiempirical MNDO results of Claramunt et al.^{36,37} This rather small difference is the balance of opposite effects involving ΔE_{st} (positive) and ΔE_{int} (negative) contributions in eq 1: $\Delta E_{st}(tpm-0)$ is actually smaller than $\Delta E_{st}(tpm-1)$ by 18.88 kcal/mol, and $\Delta E_{int}(tpm-0)$ exceeds $\Delta E_{int}(tpm-1)$ by 19.76 kcal/mol. Furthermore, consistently with the free rotation around H_C-C-N bonds proved by NMR measurements at room temperature,³⁸ the energy barrier associated to the tpm-0 \rightarrow tpm-1 saddle point (TS1) is predicted very low (less than 2.5 kcal/mol).⁴⁰ We remark that, with the obvious exception of the LT parameter, all tpm internal coordinates are substantially unaffected by the tpm-0 \rightarrow tpm-1 conversion (see Figure 8).

For the tpm-1 \rightarrow tpm-2 conversion, two parameters can be chosen for the TS search, i.e., the rotations around either the $H_C-C-N_1^b$ bond (TS2b) or the $H_C-C-N_1^c$ one (TS2c, see Figure 1). The inspection of Figures 6 and 8 testifies that (i) TS2b and TS2c BE's are very similar and close to the TS1 one; (ii) $\Delta BE_{2,1} > \Delta BE_{0,1}$; and (iii) similarly to the tpm-0 \rightarrow tpm-1 conversion,

TABLE 2: Mulliken (Q^M) and Hirshfeld (Q^H) Charges of Selected Atoms of the Free Hpz and σ/π $[M(\text{Hpz})]^+$ Complexes

	Hpz	$[\text{Cu}(\text{Hpz})]^+$		$[\text{Ag}(\text{Hpz})]^+$	
		σ	π	σ	π
$Q_M^M (Q_M^H)$		0.79 (0.54)	0.51 (0.53)	0.83 (0.60)	0.63 (0.60)
$Q_{N(1)}^M (Q_{N(1)}^H)$	0.14 (-0.02)	0.18 (0.02)	0.17 (0.04)	0.17 (0.01)	0.17 (0.03)
$Q_{N(2)}^M (Q_{N(2)}^H)$	-0.28 (-0.15)	-0.45 (-0.07)	-0.20 (-0.07)	-0.42 (-0.08)	-0.20 (-0.09)
$Q_{C(3)}^M (Q_{C(3)}^H)$	0.28 (-0.03)	0.36 (0.03)	0.43 (0.03)	0.34 (0.02)	0.33 (0.01)
$Q_{C(4)}^M (Q_{C(4)}^H)$	0.10 (-0.09)	0.18 (-0.03)	-0.08 (-0.07)	0.17 (-0.04)	-0.02 (-0.06)
$Q_{C(5)}^M (Q_{C(5)}^H)$	0.25 (-0.02)	0.33 (0.05)	0.41 (0.05)	0.32 (0.04)	0.37 (0.04)

TABLE 3: Binding Energy Contributions in kcal/mol for σ/π $[M(\text{Hpz})]^+$ Complexes

	$[\text{Cu}(\text{Hpz})]^+$		$[\text{Ag}(\text{Hpz})]^+$	
	σ	π	σ	π
ΔE_{st}	-15.3	-1.2	26.1	43.2
ΔE_{int}	-59.5	-65.1	-79.4	-88.2
ΔE_{prep}	1.1	5.9	0.8	3.2
BSSE	1.2	1.7	0.3	0.4
BE	-72.5	-58.7	-52.2	-41.3

the tpm-1 \rightarrow tpm-2 one negligibly affects tpm internal coordinates (see Figure 8).

The $\Delta E_{\text{int}}(\text{tpm-1})$ and $\Delta E_{\text{int}}(\text{tpm-2})$ contributions are very similar (the latter is 0.25 kcal/mol larger than the former),

whereas $\Delta E_{\text{st}}(\text{tpm-2})$ exceeds $\Delta E_{\text{st}}(\text{tpm-1})$ by 2.75 kcal/mol. Such a result ultimately indicates that the lower stability of tpm-2 compared to tpm-1 has to be traced back to the repulsive

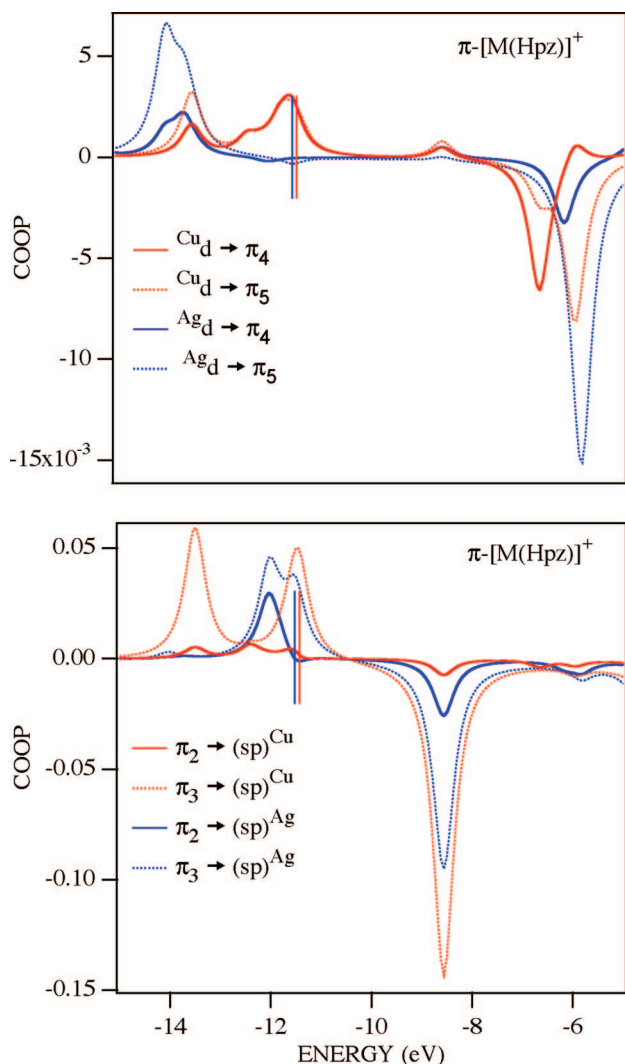


Figure 4. $M(\text{I}) d \rightarrow \pi^*$ Hpz (up) and Hpz $\pi \rightarrow sp M(\text{I})$ (down) COOP's in π - $[M(\text{Hpz})]^+$ complexes. Bonding (antibonding) states correspond to positive (negative) peaks. Vertical bars represent the HOMO energies.

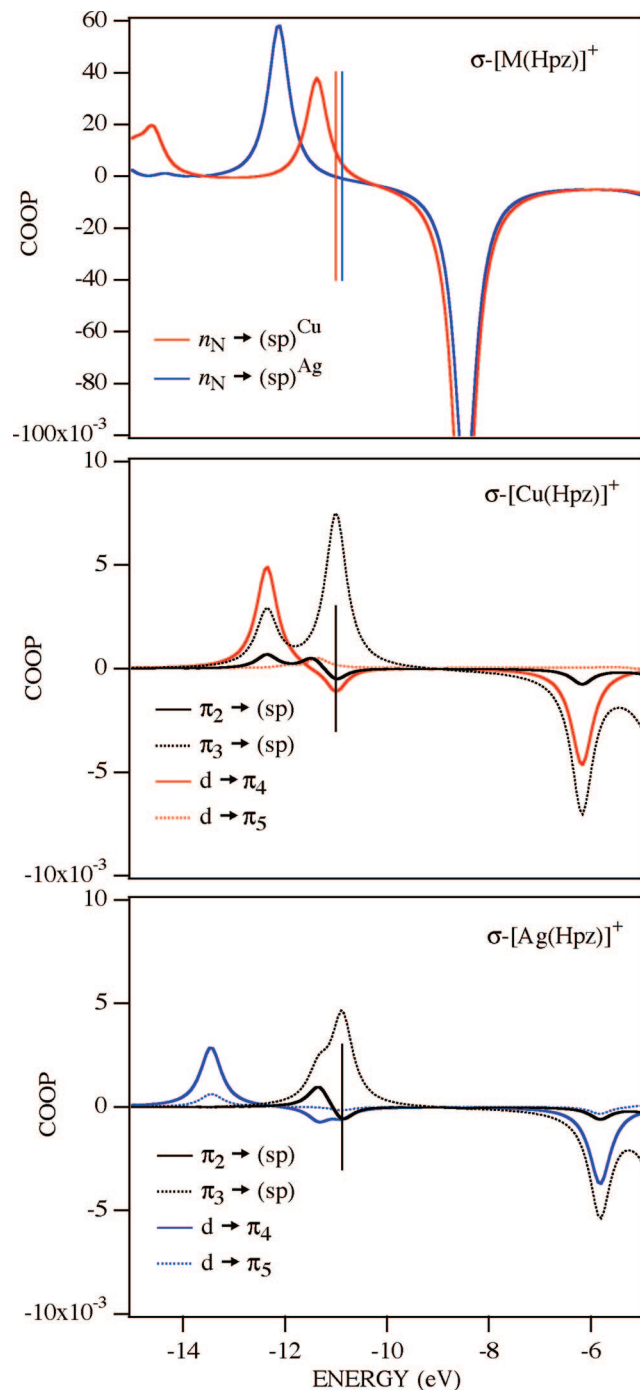


Figure 5. Hpz $n_N \rightarrow sp M(\text{I})$ (up) and $[\text{Hpz } \pi \rightarrow sp M(\text{I})]/[\text{M}(\text{I}) d \rightarrow \pi^* \text{Hpz}]$ (middle and down) COOP's in σ - $[M(\text{Hpz})]^+$ complexes.

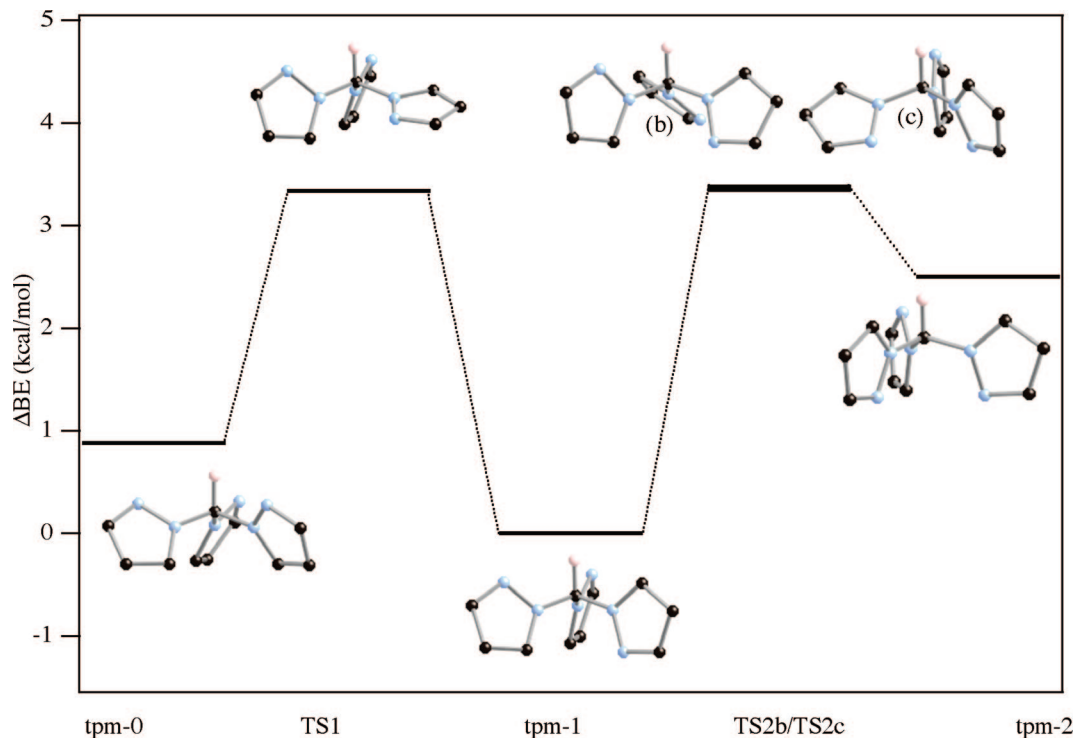


Figure 6. Relative BE values of tpm-0, TS1, tpm-1, TS2b/TS2c, tpm-2. The zero energy value corresponds to the tpm-1 BE. Schematic representations of the corresponding optimized structure are also displayed.

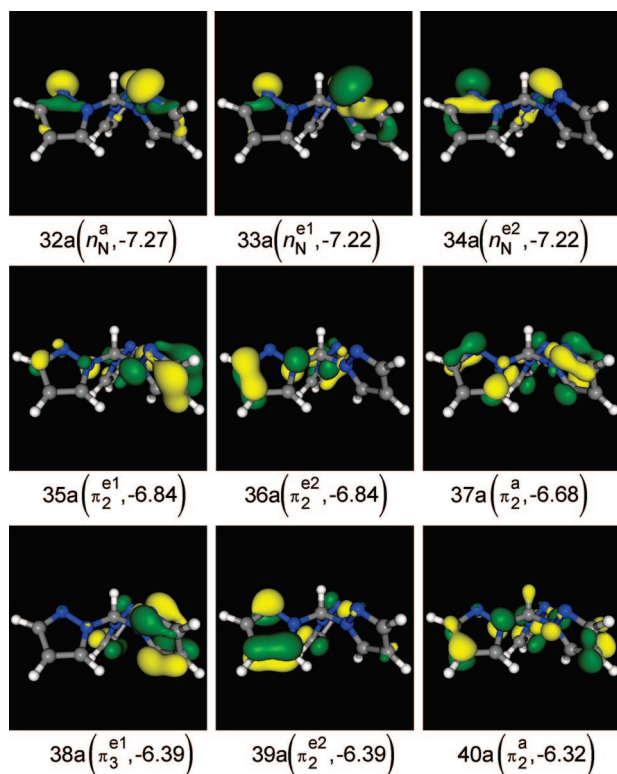


Figure 7. 3D contour plots of tpm-0 outermost occupied MO's. In parentheses is reported the energy in electronvolt of each level and its parenthood with the Hpz-based orbitals. Contour plot parameters are the same of Figure 2.

interaction between the two $N(\bullet)$ n_N in trans to the $H_C C$ fragment ($\Delta E_{\text{Pauli}}(\text{tpm-1})$ and $\Delta E_{\text{Pauli}}(\text{tpm-2})$ differ by 3.18 kcal/mol).

As a whole, the above described theoretical results outline that, though common, the tpm κ^3 -tripodal coordinative mode is unlikely to be achieved through the direct interaction of M(I) with tpm having a tpm-3 arrangement.

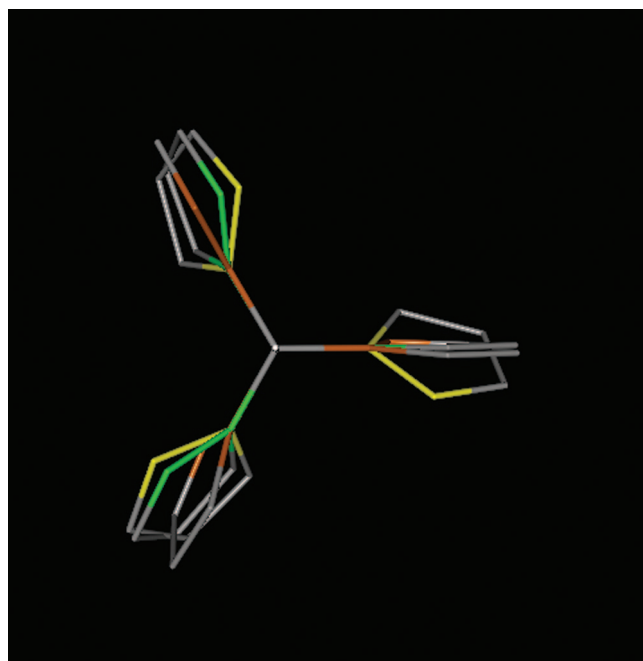


Figure 8. Superimposed licorice representation of tpm-0 (N atoms in yellow), tpm-1 (N atoms in light green), and tpm-2 (N atoms in orange) optimized structures. The view is along the C-H_c bond. Hydrogen atoms of pyrazolyl fragments are not displayed for the sake of clarity.

3.3. [Cu(tpm)]⁺ and [Ag(tpm)]⁺ Complexes. Reger and coworkers first reported the synthesis and characterization of cationic [tris(pyrazol-1-yl)methane]M(I) (M = Cu,^{41a} Ag^{41b}) complexes about ten years ago, and although a lot of chemistry has been published on this subject since then,⁴² not only are theoretical investigations devoted to tpm metal complexes very few in number,^{6e,32,43} but none of them has been specifically dedicated to the analysis of the metal–ligand bonding scheme.

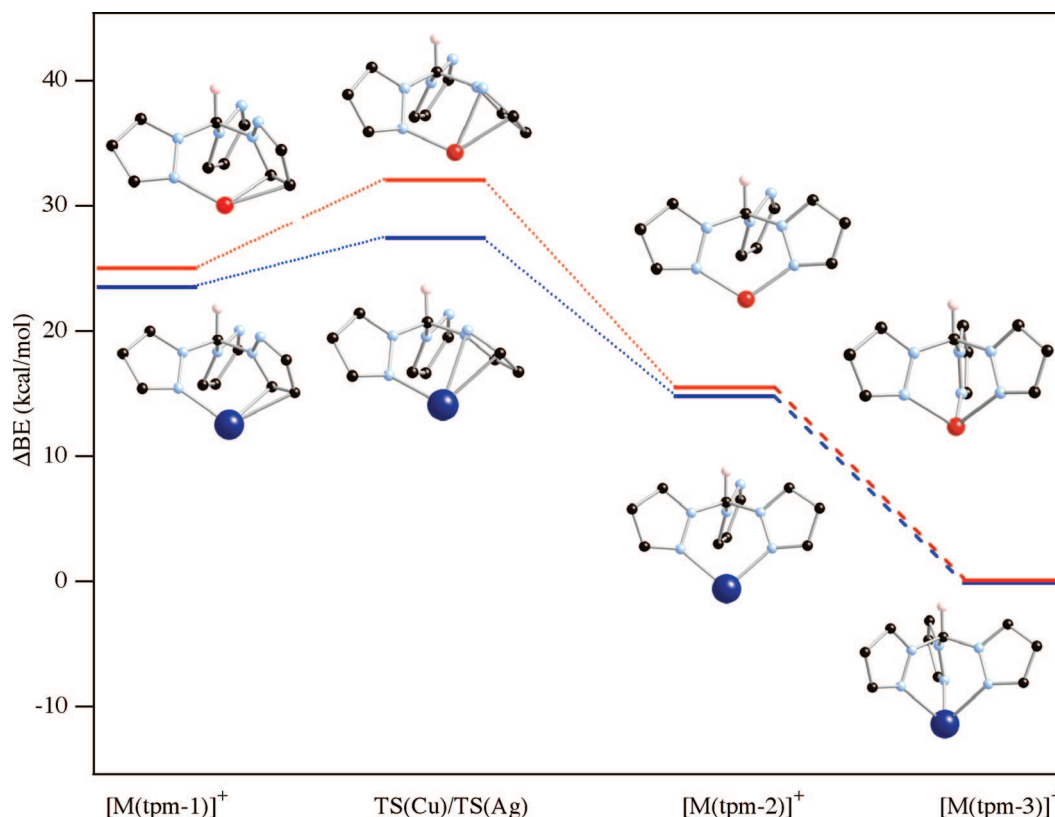


Figure 9. Relative BE values of $[M(\text{tpm-1})]^+$, $\text{TS}(M)$, $[M(\text{tpm-2})]^+$, and $[M(\text{tpm-3})]^+$. The zero energy value corresponds to the $[M(\text{tpm-3})]^+$ BE. Schematic representations of the corresponding optimized structure are also displayed. Red and blue spheres correspond to copper and Silver atoms, respectively.

TABLE 4: Binding Energy Contributions in kcal/mol for $[M(\text{tpm})]^+$ Complexes

	$[M(\text{tpm-1})]^+$	$\text{TS}(M)$	$M(\text{tpm-2})^+$	$M(\text{tpm-3})^+$
$\text{Cu} \Delta E_{\text{st}}$	-0.87	-4.97	-14.13	-30.14
$\text{Cu} \Delta E_{\text{int}}$	-97.18	-86.05	-93.47	-92.95
$\text{Cu} \Delta E_{\text{prep}}$	6.92		4.67	
CuBSSE	2.79		2.46	
CuBE	-88.34		-100.47	
$\text{Ag} \Delta E_{\text{st}}$	64.76	51.51	50.27	43.92
$\text{Ag} \Delta E_{\text{int}}$	-132.66	-115.46	-126.87	-135.32
$\text{Ag} \Delta E_{\text{prep}}$	4.50		3.91	
AgBSSE	0.66		0.52	
AgBE	-62.74		-72.17	

The strength and the nature of the $M(\text{I})\text{-tpm}$ bond in $[M(\text{tpm-}n)]^+$ ($n = 1, 2$, and 3) have been obtained through the ETS scheme by considering $M(\text{I})$ and tpm as interacting fragments.¹² Optimized coordinates of $[M(\text{tpm-}n)]^+$ species and of $\text{TS}(\text{Cu})$ and $\text{TS}(\text{Ag})$ saddle points corresponding to the $[M(\text{tpm-1})]^+ \rightarrow [M(\text{tpm-2})]^+$ conversions are collected in Tables S12–S19. Relative BE's are displayed in Figure 9 where sketches of the corresponding optimized molecular structures are also displayed.

The comparison between data of Figure 9 and Figure 6 reveals that, as a consequence of the $M(\text{I})\text{-tpm}$ interaction, the $[M(\text{tpm-2})]^+$ molecular ion is more stable than the $[M(\text{tpm-1})]^+$ one, reversing the energy order found for the free ligand. Quite unexpectedly, this is not due to covalent but to steric effects (see Table 4). In this regard, theoretical results pertaining to $[M(\text{tpm-}n)]^+$ molecular ions substantially mirror those already discussed for the $\sigma/\pi\text{-}[M(\text{Hpz})]^+$ species: despite the $\text{Ag}(\text{I})\text{-ligand}$ interaction being stronger than the $\text{Cu}(\text{I})\text{-ligand}$ one, ΔE_{st} contributions play a crucial role in determining final BE's values.

Interestingly, even though $[\text{Cu}(\text{tpm-2})]^+$ and $[\text{Ag}(\text{tpm-2})]^+$ correspond to local minima, we were unable to find the saddle point corresponding to the $[M(\text{tpm-2})]^+ \rightarrow [M(\text{tpm-3})]^+$ conversion because of the flatness of the potential energy surface in that region. This indicates that, when the $\kappa^2\text{-complex}$ is formed, either from the interaction of $M(\text{I})$ with tpm-2 or through the $[M(\text{tpm-1})]^+ \rightarrow [M(\text{tpm-2})]^+$ conversion, the $\kappa^3\text{-tripodal}$ species will be readily formed. However, the $[M(\text{tpm-2})]^+ \rightarrow [M(\text{tpm-3})]^+$ conversion could be hampered by several reasons such as (i) the coordinative saturation of the metal center by concurrent ligands; (ii) the coordination of the $\text{N}(\bullet)$ of the third pyrazolyl group to a different metal center; (iii) steric factors determined by bulky substituents of tpm.⁴⁴ In this regard, it has to be noted that, despite the $M(\text{I})$ coordinative unsaturation, the optimized geometrical parameters of $[\text{Ag}(\text{tpm-2})]^+$, $[\text{Cu}(\text{tpm-3})]^+$, and $[\text{Ag}(\text{tpm-3})]^+$ agree satisfactorily with those experimentally determined for $\text{Ag}(\text{I}) \kappa^2\text{-44i.1}$ and $M(\text{I}) \kappa^3\text{-complexes}$.^{41,44i.1,45} No X-ray data pertaining to $\text{Cu}(\text{I}) \kappa^2\text{-complexes}$ are available for comparison to our knowledge.

Further insights into the $M(\text{I})\text{-tpm}$ bonding scheme can be gained by referring to Figures 10 and 11 where $[M(\text{tpm-}n)]^+$ PDOS and COOP curves are displayed. The inspection of the two figures⁴⁶ testifies to (i) the leading role played by the tpm $\rightarrow M(\text{I})$ donation, mainly σ in character, (ii) the stronger involvement of the $M(\text{I})$ s AO compared to the one of the $M(\text{I})$ p AO's, and (iii) the negligible contribution provided by the $M(\text{I}) \rightarrow \text{tpm}$ back-donation.

4. Concluding Remarks

In this contribution we have presented and discussed the results of a series of first-principle numerical experiments

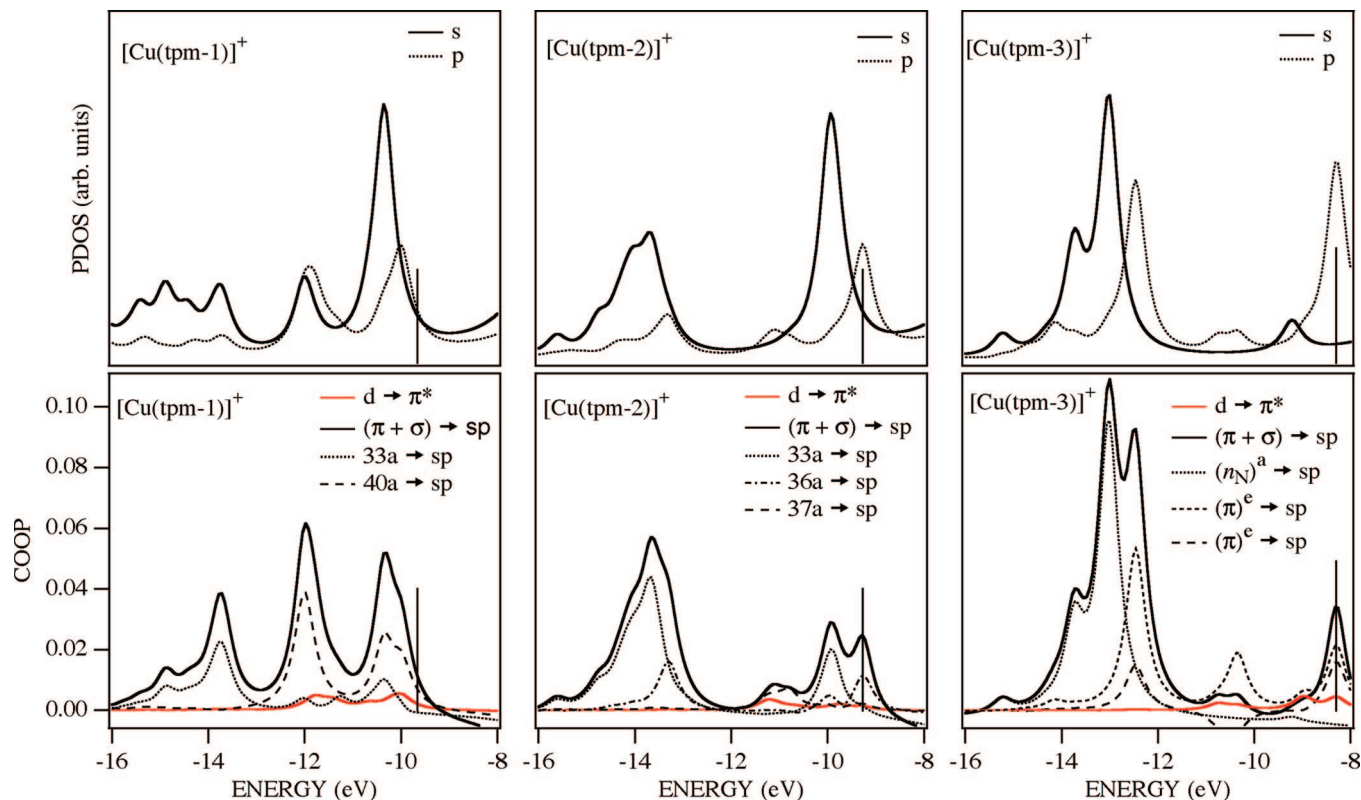


Figure 10. s and p PDOS (up) and major components of tpm $\sigma \rightarrow sp$ Cu(I), tpm $\pi \rightarrow sp$ Cu(I), and Cu(I) $d \rightarrow \pi^*$ tpm (down) for $[\text{Cu}(\text{tpm}-n)]^+$ ($n = 1, 2, \text{ and } 3$).

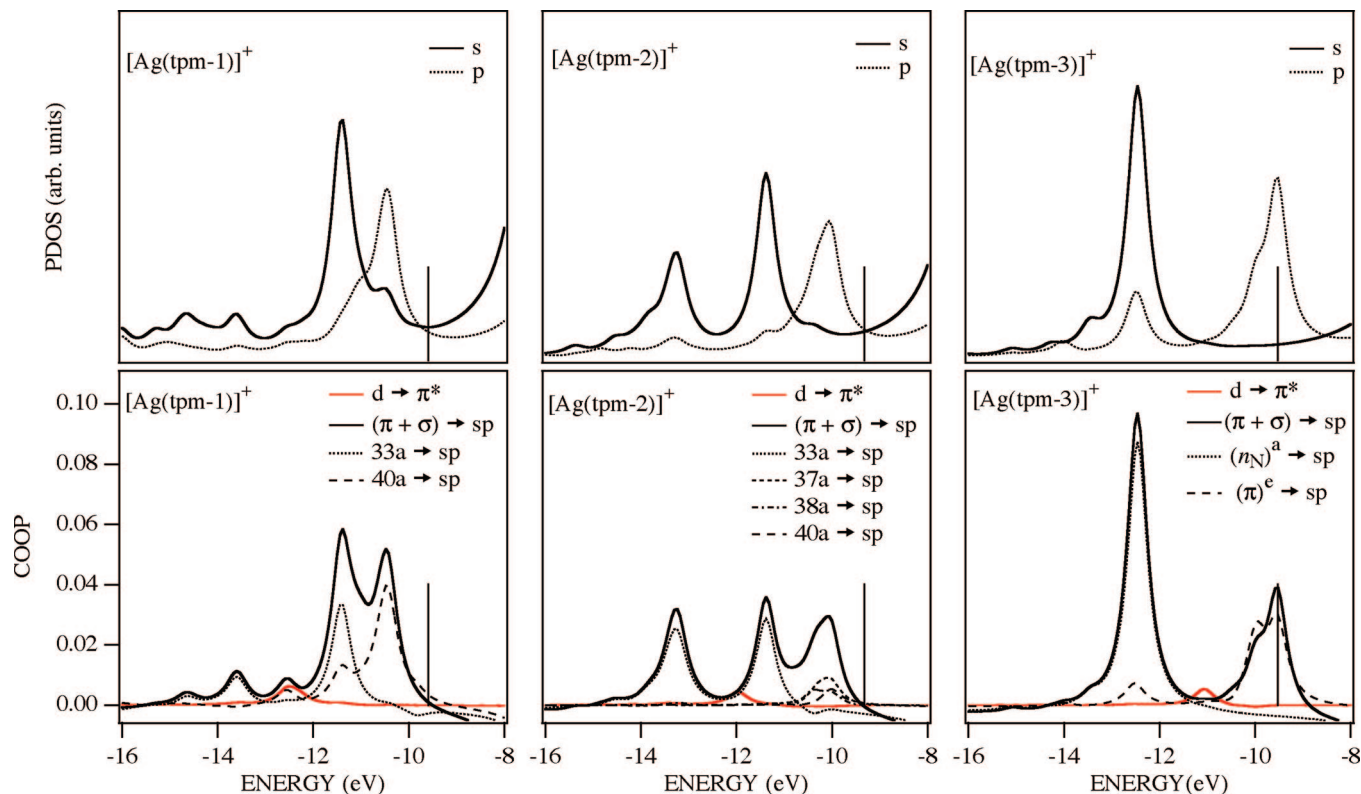


Figure 11. s and p PDOS (up) and major components of tpm $\sigma \rightarrow sp$ Ag(I), tpm $\pi \rightarrow sp$ Ag(I), and Ag(I) $d \rightarrow \pi^*$ tpm (down) for $[\text{Ag}(\text{tpm}-n)]^+$ ($n = 1, 2, \text{ and } 3$).

carried out on the free Hpz and tpm ligands, as well as on their Cu(I) and Ag(I) complexes. We gave detailed information about the energetics of interconversions among conformers, both for the free and for the coordinated ligands. Finally,

we analyzed the M–ligand interaction showing that, independently of the coordinative mode, this is dominated by the ligand \rightarrow M(I) σ donation with negligible contribution from back-donation.

Acknowledgment. This work was partially supported by the Italian PRIN founding n. 2006038447. The “Laboratorio Interdipartimentale di Chimica Computazionale” (LICC) at the Department of Chemistry of the University of Padova is acknowledged for support of the computer facilities.

Supporting Information Available: Optimized coordinates of Hpz, π -[Cu(Hpz)]⁺, σ -[Cu(Hpz)]⁺, π -[Ag(Hpz)]⁺, σ -[Ag(Hpz)]⁺, tpm-0, tpm-1, tpm-2, TS1, TS2b, TS2c, [Cu(tpm-1)]⁺, TS(Cu), [Cu(tpm-2)]⁺, [Cu(tpm-3)]⁺, [Ag(tpm-1)]⁺, TS(Ag), [Ag(tpm-2)]⁺, and [Ag(tpm-3)]⁺ are reported in Tables S1–S19, respectively. The comparison between the Hpz VUV-absorption spectrum and TD-DFT results is displayed in Figure S1. This material is available free of charge via the Internet at <http://pubs.acs.org>.

References and Notes

- (1) (a) Pettinari, C.; Pettinari, R. *Coord. Chem. Rev.* **2005**, *249*, 525, and references therein reported. (b) Pettinari, C.; Santini, C. *Compr. Coord. Chem. II* **2004**, *1*, 159. (c) Trofimenko, S. *Scorpionates, The coordination Chemistry of Polypyrazolylborate Ligands*; Imperial College Press: London, 1999. (d) Pettinari, C. *Scorpionates II: Chelating borate ligands*; World Scientific Publishing: New York, 2008. (e) Trofimenko, S. *J. Chem. Educ.* **2005**, *82*, 1715. (f) Murtuza, S.; Casagrande, O. L., Jr.; Jordan, R. F. *Polym. Mater. Sci. Eng.* **2001**, *84*, 109. (g) Santos, I.; Paulo, A.; Correia, J. D. *Top. Curr. Chem.* **2005**, *252*, 45. (h) Kitano, T.; Wada, H.; Mukai, H.; Ueda, K.; Sohrin, Y. *Anal. Sci.* **2001**, *17*, i1113. (i) de la Lande, A.; Gérard, H.; Moliner, V.; Izzet, G.; Reinaud, O.; Parisel, O. *J. Biol. Inorg. Chem.* **2006**, *11*, 593.
- (2) tp and tpm may also act as κ^2 -ligands bonded to a single metal (κ^2 -chelating), as κ^1 - κ^2 -ligands bridging two metals or, hardly ever, as κ^1 -ligands depending on the steric congestion around the metal center and the number of donor substituents on the central atom X, which may be P and Ga other than B and C (see refs 1 and 3).
- (3) (a) Paneque, M.; Sirol, S.; Trujillo, M.; Gutiérrez-Puebla, E.; Monge, M. A.; Carmona, E. *Angew. Chem. Int. Ed.* **2000**, *39*, 218. (b) Ellis, D. D.; Jeffery, J. C.; Jelliss, P. A.; Kautz, J. A.; Stone, F. G. A. *Inorg. Chem.* **2001**, *40*, 2041.
- (4) McLauchlan, C. C.; Varda, A. N.; Giles, J. R. *Acta Crystallogr. Sect. E: Struct. Rep. Online* **2004**, *60*, o1419.
- (5) The relative position of pyrazolyl fragments in substituted and unsubstituted tp and tpm is strongly influenced by the steric hindrance of substituents possibly present on the ring carbon atoms.⁶
- (6) (a) Dias, H. V. R.; Jin, W.; Kim, H.-J.; Lu, H.-L. *Inorg. Chem.* **1996**, *35*, 2317. (b) Reger, D. L.; Semeniac, R. F.; Smith, M. D. *Eur. J. Inorg. Chem.* **2003**, 3480. (c) Declercq, J. P.; van Meerssche, M. *Acta Crystallogr., Sect. C: Cryst. Struct. Commun.* **1984**, *40*, 1098. (d) Ochando, L. E.; Rius, J.; Louer, D.; Claramunt, R. M.; Lopez, C.; Elguero, J.; Amigo, J. M. *Acta Crystallogr., Sect. B: Struct. Sci.* **1997**, *53*, 939. (e) Fujisawa, K.; Ono, T.; Ishikawa, Y.; Amir, N.; Miyashita, Y.; Okamoto, K.; Lehnert, N. *Inorg. Chem.* **2006**, *45*, 1698. (f) Hammes, B. S.; Luo, X.; Carrano, M. W.; Carrano, C. J. *Angew. Chem. Int. Ed.* **2002**, *41*, 3259.
- (7) De Bari, H.; Zimmer, M. *Inorg. Chem.* **2004**, *43*, 3344 Database searches and analyses carried out by the authors were done by using the Conquest and Vista programs associated with Cambridge Structural Database13 (CSD) v5.24.
- (8) Here the negatively charged tp ligand is not taken into account to avoid the use of extended basis sets.
- (9) We are perfectly aware that Hpz electronic properties have been the subject of several theoretical¹⁰ and experimental¹¹ investigations, but we decided to extend our study to this molecule to compare homogeneous theoretical data.
- (10) (a) Kuznetsov, M. L.; Dementiev, A. I.; Krasnoshchoikov, S. V. *J. Mol. Struct. (THEOCHEM)* **1998**, *453*, 17. (b) da Silva, G.; Moore, E. E.; Bozzelli, J. W. *J. Phys. Chem. A* **2006**, *110*, 13979. (c) El-Azhary, A. A. *Spectrochim. Acta A* **2003**, *59*, 2009.
- (11) Walker, I. C.; Palmer, M. H.; Hubin-Franskin, M. -J.; Delwiche, J. *Chem. Phys. Lett.* **2003**, *367*, 517.
- (12) Amsterdam Density Functional (ADF) version 2007.01. <http://www.scm.com>.
- (13) (a) van Lenthe, E.; Baerends, E. J.; Snijders, J. G. *J. Chem. Phys.* **1993**, *99*, 4597. (b) van Lenthe, E.; Baerends, E. J.; Snijders, J. G. *J. Chem. Phys.* **1994**, *101*, 9783. (c) van Lenthe, E.; Ehlers, A. W.; Baerends, E. J.; Snijders, J. G. *J. Chem. Phys.* **1999**, *110*, 8543.
- (14) (a) Becke, A. D. *Phys. Rev. A* **1988**, *38*, 3098. (b) Perdew, J. P. *Phys. Rev. B* **1986**, *33*, 8822.
- (15) A LT calculation implies a linear change of a selected LT parameter from its initial to its final value through a specified number of equidistant steps.
- (16) van Lenthe, E.; Baerends, E. J. *J. Comput. Chem.* **2003**, *24*, 1142.
- (17) Ziegler, T.; Rauk, A. *Theor. Chim. Acta* **1977**, *46*, 1.
- (18) Rosa, A.; Ehlers, A. W.; Baerends, E. J.; Snijders, J. G.; te Velde, G. *J. Phys. Chem.* **1996**, *100*, 5690.
- (19) Mulliken, R. S. *J. Chem. Phys.* **1955**, *23*, 1833.
- (20) Hoffmann, R. *Solids and Surfaces: A Chemist's View of Bonding in Extended Structures*; VCH: New York, 1988.
- (21) Pauling electronegativity for most of the elements are reported in the following website <http://www.webelements.com/>.
- (22) Hirshfeld, F. L. *Theor. Chim. Acta* **1977**, *44*, 129.
- (23) Da Silva, G.; Moore, E. E.; Bozzelli, J. W. *J. Phys. Chem. A* **2006**, *110*, 13979.
- (24) IE's have been evaluated by using the Slater transition state procedure,²⁵ and lowest lying excitation energies and corresponding oscillator strengths were evaluated by employing the time dependent DFT (TD-DFT) approach.²⁶
- (25) Slater, J. C. *Quantum Theory of Molecules and Solids. The Self-Consistent Field For Molecules and Solids*; McGraw-Hill: New York, 1974, Vol. 4.
- (26) Gross, E. K. U.; Dobson, J. F.; Petersilka, M. In *Density Functional Theory*; Nalewajski, R. F., Ed.; Springer: Heidelberg, 1996.
- (27) The theoretical (experimental)²⁸ μ_{Hpz} value is 2.282 (2.214 \pm 0.015) D, theoretical (experimental)¹¹ IEs of n_{N} , π_2 , and π_3 frontier MO's are 10.68 (10.65), 9.74 (9.88), and 9.48 (9.15) eV, respectively. The comparison between theoretical and experimental¹¹ absorption spectrum in the 5–9 eV energy range is reported as Supporting Information.
- (28) Kirchnerhoff, W. H. *J. Am. Chem. Soc.* **1967**, *89*, 1312.
- (29) In the [Cu(Hpz)]⁺ ([Ag(Hpz)]⁺) π -complex the N(1)N(2)C(3)C(4) and N(2)N(1)C(5)C(4) dihedral angles are 1.5° (1.3°) and 0.1° (0.0°), respectively, and the N(2)C(3)C(4)H_{C(4)} and N(1)C(5)C(4)H_{C(4)} ones are 152.5° and 152.6° (both 160.9°), respectively. Moreover, the CuC(4)H_{C(4)} (AgC(4)H_{C(4)}) bond angle corresponds to 102.4° (99.7°).
- (30) Both π_3 and π_5 MO's are strongly localized on the C(4) atom (see Figure 2).
- (31) The tpm-1 conformer has not been associated to the κ^1 -mode because, to our knowledge, the only structurally ascertained compound with a scorpionate ligand truly κ^1 -monodentate is the Rh(I) complex reported by Paneque et al.^{3a} where the metal ion and the H atom of the B–H fragment of the hydrotris(3,5-dimethylpyrazolyl)borato are in a cis arrangement. Even if Reger et al.³² recently revealed an unprecedented coordination mode of a tpm analogue in {[Ph₂(O)POCH₂C(pz)₃Ag]₂(THF)₂}(BF₄)₂.
- (32) Reger, D. L.; Semeniac, R. F.; Captain, B.; Smith, M. D. *Inorg. Chem.* **2005**, *44*, 2995.
- (33) Optimized coordinates of tpm-0, tpm-1, tpm-2, TS1, and TS2 are reported in Tables S6–S11.
- (34) The propeller-like configuration is the same obtained, through molecular mechanics calculations, for the global minimum of free tp by Sohrin et al.³⁵
- (35) Sohrin, Y.; Kokusen, H.; Matsd, M. *Inorg. Chem.* **1995**, *34*, 3928.
- (36) Claramunt, R. M.; Elguero, J.; Fabre, M. J.; Foces-Foces, C.; Cano, F. H.; Fuentes, I. H.; Jaime, C.; López, C. *Tetrahedron* **1989**, *45*, 7805.
- (37) Even though MNDO calculations of Claramunt et al.³⁶ succeeded in foreseeing a tpm-1-like arrangement as the most stable conformation of the free ligand, they computed a $\Delta E_{0,1}$ (2.62 kcal/mol) value significantly higher than that herein reported (0.88 kcal/mol).
- (38) The ¹H NMR spectrum of tpm at room temperature shows a singlet for the CH methyne proton and two pseudodoublet and one pseudotriplet for the heterocyclic ring protons.^{39ab} The three pyrazolyl fragments are all equivalent likely as a consequence of the rapid rotation around the H–C axis. In this regard, Reger suggested that within each tpm unit, the orientation of the three pyrazolyl moieties has a propeller arrangement.^{39c}
- (39) (a) Elguero, J.; Claramunt, R. M.; Garcerán, R.; Julià, S.; Avila, L.; del Mazo, J. M. *Magn. Reson. Chem.* **1987**, *25*, 260. (b) Otting, G.; Messerle, B. A.; Soler, L. P. *J. Am. Chem. Soc.* **1996**, *118*, 5096. (c) Reger, D. L.; Grattan, T. C. *Synthesis* **2003**, *3*, 350.
- (40) The tpm-0 \rightarrow tpm-1 conversion has been evaluated by starting from tpm-0 and specifying, as single LT parameter, the rotation angle around a H_C–N bond.
- (41) (a) Reger, D. L.; Collins, J. E.; Rheingold, A. L.; Liable-Sands, L. M. *Organometallics* **1996**, *15*, 2029. (b) Reger, D. L.; Collins, J. E.; Rheingold, A. L.; Liable-Sands, L. M.; Yap, G. P. A. *Organometallics* **1997**, *16*, 349.
- (42) (a) Reger, D. L.; Watson, R. P.; Smith, M. D. *Inorg. Chem.* **2006**, *45*, 10077, and references therein reported. (b) Reger, D. L.; Semeniac, R. F.; Gardinier, J. R.; O'Neal, J.; Reinecke, B.; Smith, M. D. *Inorg. Chem.* **2006**, *45*, 4337, and references therein reported.
- (43) (a) Chu, H. S.; Xu, Z.; Ng, S. M.; Lau, C. P.; Lin, Z. *Eur. J. Inorg. Chem.* **2000**, 993. (b) Lehnert, N.; Cornelissen, U.; Neese, F.; Ono, T.; Noguchi, Y.; Okamoto, K.; Fujisawa, K. *Inorg. Chem.* **2007**, *46*, 3916.

(44) (a) Canty, A. J.; Minchin, N. J.; Patrick, J. M.; Healy, P. C.; White, A. H. *J. Chem. Soc., Dalton Trans.* **1982**, 1795. (b) Canty, A. J.; Minchin, N. J.; Patrick, J. M.; White, A. H. *J. Chem. Soc., Dalton Trans.* **1983**, 1253. (c) Canty, A. J.; Minchin, N. J.; Engelhardt, L. M.; Skelton, B. W. *J. Chem. Soc., Dalton Trans.* **1986**, 645. (d) Adams, C. J.; Connelly, N. G.; Emslie, D. J. H.; Hayward, O. D.; Manson, T.; Orpen, A. G.; Rieger, P. H. *Dalton Trans.* **2003**, 2835. (e) Bhambri, S.; Tocher, D. A. *J. Chem. Soc., Dalton Trans.* **1997**, 3367. (f) Iengo, E.; Zangrando, E.; Baiutti, E.; Munini, F.; Alessio, E. *Eur. J. Inorg. Chem.* **2005**, 1019. (g) Bellachioma, G.; Cardaci, G.; Gramlich, V.; Ruegger, H.; Terenzi, S.; Venanzi, L. M. *Organometallics* **1997**, *16*, 2139. (h) Titze, C.; Hermann, J.; Vahrenkamp, H. *Chem. Ber.* **1995**, *128*, 1095. (i) Reger, D. L.; Semeniuc, R. F.; Smith, M. D. *Eur. J. Inorg. Chem.* **2003**, 3480. (j) Reger, D. L.; Semeniuc, R. F.; Captain, B.; Smith, M. D. *Inorg. Chem.* **2005**, *44*, 2995. (k) Reger, D. L.; Semeniuc, R. F.; Little, C. A.; Smith, M. D. *Inorg. Chem.* **2006**, *45*, 7758. (l) Cingolani,

A.; Effendy; Martini, D.; Pellei, M.; Pettinari, C.; Skelton, B. W.; White, A. H. *Inorg. Chim. Acta* **2002**, 328, 87.

(45) (a) Cvetkovic, M.; Batten, S. R.; Moubaraki, B.; Murray, K. S.; Spiccia, L. *Inorg. Chim. Acta* **2001**, 324, 131. (b) Reger, D. L.; Semeniuc, R. F.; Smith, M. D. *Rev. Roum. Chim.* **2002**, *47*, 1037. (c) Choi, I. Y.; Ahn, S.; Seo, J.; Park, K.-M. *Bull. Korean Chem. Soc.* **2004**, *25*, 1065. (d) Fujisawa, K.; Ono, T.; Ishikawa, Y.; Amir, N.; Miyashita, Y.; Okamoto, K.; Lehnert, N. *Inorg. Chem.* **2006**, *45*, 1698. (e) Kaim, W.; Titze, C.; Schurr, T.; Sieger, M.; Lawson, M.; Jordanov, J.; Rojas, D.; Garcia, A. M.; Manzur, J. Z. *Anorg. Allg. Chem.* **2005**, 631, 2568.

(46) The absence of any local symmetry in $[M(\text{tpm-1})]^+$ and $[M(\text{tpm-2})]^+$ allows a quite extensive mixing among highest occupied tpm based MO's (n_N and π_2/π_3 linear combinations). MO's have been then labeled in Figures 10 and 11 by simply referring to their energy order in the free tpm fragment.

JP801902C

Magnetic Properties and Vapochromic Reversible Guest-Induced Transformation in a Bispyrazolato Copper(II) Polymer: an Experimental and Dispersion-Corrected Density Functional Theory Study

Alessandro Bencini,[†] Maurizio Casarin,^{*,§} Daniel Forrer,[‡] Lorenzo Franco,[‡] Federica Garau,[‡] Norberto Masciocchi,^{||} Luciano Pandolfo,^{*,‡} Claudio Pettinari,[⊥] Marco Ruzzi,[‡] and Andrea Vittadini^{*,‡,§}

Dipartimento di Chimica, Università di Firenze, via della Lastruccia 3, I-50019 Firenze, Italy, Dipartimento di Scienze Chimiche, Università di Padova, via Marzolo 1, I-35131 Padova, Italy, Istituto di Scienze e Tecnologie Molecolari del CNR (ISTM-CNR), via Marzolo 1, I-35131 Padova, Italy, Dipartimento di Scienze Chimiche e Ambientali, Università dell'Insubria, via Valleggio 11, I-22100 Como, Italy, and Dipartimento di Scienze Chimiche, Università di Camerino, via S. Agostino 1, I-62032 Camerino(MC), Italy

Received October 10, 2008

Dispersion-corrected density functional theory (DFT-D) calculations, Electron Spin Resonance spectroscopy (EPR), and variable temperature magnetic moment measurements were used to investigate the structure and the electronic/magnetic properties of bispyrazolato-copper(II) coordination polymer and of its hydration product. The Cu(II) ions are antiferromagnetically coupled through the σ system of the pyrazolate rings in both compounds. Theoretical electron density maps reveal that water molecules interact simultaneously and to a comparable extent with two Cu(II) centers (through the electronegative O end) and two pyrazolate rings (through the partly positively charged H atoms), which is compatible with the observed internuclear distances. DFT-D calculations indicate that low kinetic barriers are involved in the rearrangement of the host structure.

Introduction

The increasing demand for better materials for gas sensing and gas storage applications has stimulated the design of new porous materials based on molecular frameworks. This crystal engineering process is, however, hampered by the natural tendency of molecular systems to pack as close as possible, intrinsically limiting the number of porous compounds.¹ In this context, a promising class of materials is represented by systems which are able to reversibly change their crystal structure in the presence of guest molecules in such a way as to create otherwise absent pores or to modify their shapes, dimensions, and/or functional properties.²

In a recent communication,^{2a} some of us reported on the synthesis of a novel polymorph (the “ β ” phase) of copper(II) pyrazolate, β -[Cu(pz)₂]_n, a one-dimensional (1D) coordina-

tion polymer obtained by reacting Cu(II) carboxylates with pyrazole (Hpz) in MeCN. Remarkably, this compound is able, in the solid state, to absorb/desorb water and several other small guest molecules (viz. NH₃, MeNH₂, CH₃CN, pyridine, MeOH, and EtOH) through a reversible change of the mutual arrangement of the polymer chains, accompanied by significant color modifications. The crystal structure of the anhydrous and of the hydrated polymers were determined by X-ray powder diffraction (XRPD) methods: β -[Cu(pz)₂]_n, crystallizes in the monoclinic system (*P2₁/m* space group; *a* = 9.055 Å, *b* = 7.401 Å, *c* = 5.597 Å, β = 99.48°, see Figure 1a), whereas the hydrated phase [Cu(pz)₂·(H₂O)]_n, is orthorhombic (*Cmcm* space group; *a* = 16.960 Å, *b* = 6.236 Å, *c* = 7.283 Å, see Figure 1c).

In our preliminary communication,^{2a} the presence of a magnetic interaction coupling the Cu(II) ions was noted. In this work, we address in more detail these magnetic interactions from an experimental and computational point of view, and we obtain more detailed information on the bonding between the host and the guest water molecules, for which an approximate location was experimentally

* To whom correspondence should be addressed. E-mail: andrea.vittadini@unipd.it.

[†] Università di Firenze.

[‡] Università di Padova.

[§] Istituto di Scienze e Tecnologie Molecolari del CNR.

^{||} Università dell'Insubria.

[⊥] Università di Camerino.

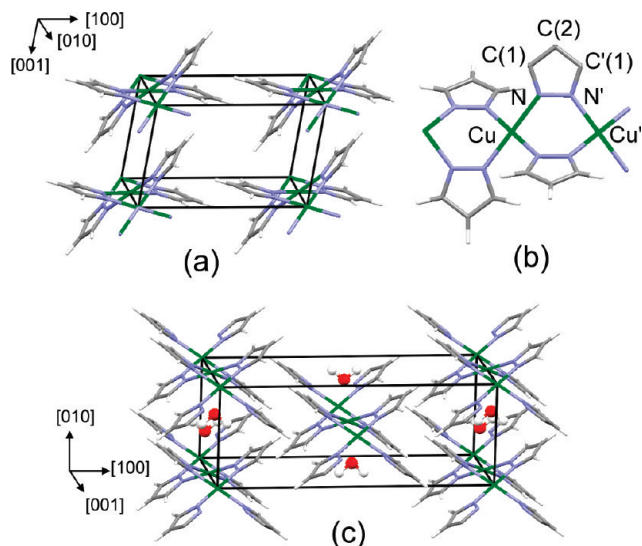


Figure 1. (a) Schematic drawings of: (a) β -[Cu(pz)₂]_n; (b) a portion of the Cu(pz)₂ chain running along [010]; (c) the unit cell of [Cu(pz)₂·(H₂O)]_n. The H₂O molecules, shown in a ball-and-stick representation, are in the equilibrium configuration as determined by the DFT calculations.

determined by XRPD. Furthermore, we investigate the mechanism of the structure transformations involved in the water sorption/desorption processes. Finally, we report also a new and more efficient synthetic procedure for the obtaining of β -[Cu(pz)₂]_n, that has also made possible its embedding into pumice sheets.

Material and Methods

Synthesis and Sample Manipulation. If not otherwise stated, reactions and manipulations were carried out in the air. Reagents (Aldrich) were used without further purification. Elemental analyses (C, H, N) were performed with a Fisons Instruments 1108 CHNS-O Elemental Analyzer. IR spectra were recorded from 4000 to 400 cm⁻¹ with a Perkin-Elmer 983 instrument. UV-vis spectra were recorded from 200 to 800 nm with a Varian Cary 5E instrument.

[Cu(pz)₂·(NH₃)]_n, **1**.

This species was obtained by slightly modifying a procedure reported by Inoue et al.³

A solution of Cu(NO₃)₂·2.5H₂O (1.823 g, 7.83 mmol) in 40 mL of 28% aqueous ammonia was added at room temperature (r.t.) under vigorous stirring to a solution of 1.088 g of Hpz (15.98 mmol) in 40 mL of 28% aqueous ammonia. The obtained dark-blue suspension was stirred for 20 min obtaining a blue precipitate that was filtered, washed with 28% aqueous ammonia, and dried under vacuum (0.1 mmHg) at r.t., obtaining 1.31 g of a blue solid (Yield 78%). Similar results were obtained by using copper(II) sulfate and copper(II) chloride.

1. Elem. Anal. Calcd for C₆H₉N₃Cu: C, 33.56; H, 4.22; N, 32.62. Found: C, 33.98; H, 3.91; N, 31.99.

Mp. At about 120 °C compound **1** turns into a light-brown solid (β -[Cu(pz)₂]_n, **2**, vide infra), stable up to about 300 °C, where decomposition begins.

β -[Cu(pz)₂]_n, **2**.

[Cu(pz)₂·(NH₃)]_n, **1**, (266.8 mg, 1.24 mmol) was heated (90 °C) under dynamic vacuum (0.1 mmHg) for 15 min observing a weight loss of 20.9 mg, corresponding to the elimination of 1.23 mmol of NH₃, and the simultaneous color change into beige.

2. Elem. Anal. Calcd for C₆H₆N₄Cu: C, 36.45; H, 3.06; N, 28.34. Found: C, 36.09; H, 3.30; N, 28.25.

[Cu(pz)₂·(H₂O)]_n, **3**.

Compound **2** at 25 °C easily absorbs water vapors from the air or from solvate moist environments and rapidly yields the pale-pink derivative [Cu(pz)₂·(H₂O)]_n, **3**.

3. Elem. Anal. Calcd for C₆H₈N₄OCu: C, 33.41; H, 3.74; N, 25.97. Found: C, 33.12; H, 3.85; N, 25.67.

The identity of **1**, **2**, and **3** was confirmed by their IR, UV-vis, and XRPD spectra that resulted identical to those previously reported.^{2a} Moreover, **2** adsorbs reversibly NH₃, H₂O, MeNH₂, and so forth, yielding the corresponding solvated derivatives previously reported.^{2a} Cycles of sorption/desorption of water and NH₃ were repeated on compound **2** 10 times without observing any degradation.

Embedding of 1, 2, and 3 into Pumice Sheets. Sheets of pumice (ca. 10 × 20 × 1 mm) were obtained by cutting a commercial pumice block obtained from a local hardware store. Subsequently, the sheets were accurately washed with water, maintained in *aqua regia* for 1 h, washed with running tap water for 2 h, with running deionized water for 1 h, put into 28% NH₃ aqueous solution for 2 h, rinsed with running deionized water for 20 min, and then dried by vacuum pumping (0.1 mmHg) for 8 h at r.t. The cleaned sheets of pumice were soaked for 2 h into a solution of Hpz (0.388 g, 5.7 mmol) in a 28% NH₃ aqueous solution and then dipped into a stirred solution of Cu(NO₃)₂·2.5H₂O (0.676 g, 2.9 mmol) in 10 mL of 28% NH₃ aqueous solution and here maintained overnight. Deep-blue colored sheets formed, which were washed with running deionized water for 20 min and finally dried under vacuum (0.1 mmHg) at rt, the blue color being practically unchanged. Upon heating (ca. 90 °C) under dynamic vacuum (0.1 mmHg) for 20 min, the blue sheets turned beige, indicating that the transformation of embedded **1** in **2** occurred. Moreover the beige sheets, changed color (pale pink) when put in contact with H₂O vapors (indicating the formation of embedded **3**) and became blue in the presence of NH₃, reversibly forming **1**, analogously to what was previously reported for pure bulk species.^{2a} The sorption/desorption cycles of water and NH₃ were repeated 10 times also on these sheets, obtaining analogous results with respect to pure compounds.

Electron Paramagnetic Resonance (EPR) Measurements. The EPR spectra were recorded on about 10 mg of powdered samples put into 4 mm diameter quartz tubes, using a Bruker ER200D X-band spectrometer equipped with a nitrogen-flow variable temperature system for measurements in the temperature range 100–400 K. Typical acquisition parameters were: microwave power 10 mW, modulation amplitude 5 G, sweep time 3 min. For g-factor determination, the microwave frequency was measured using a HP5342 frequency counter, and the magnetic field was calibrated using a DPPH standard.

Magnetic Susceptibility Measurements. The temperature dependence of the magnetic susceptibility of all the compounds was measured using a Cryogenic S600 SQUID magnetometer. The measurements were performed on polycrystalline powder samples

(1) Barbour, L. J. *Chem. Commun.* **2006**, 1163.

(2) (a) Cingolani, A.; Galli, S.; Masciocchi, N.; Pandolfo, L.; Pettinari, C.; Sironi, A. *J. Am. Chem. Soc.* **2005**, *127*, 6144. (b) Yamada, K.; Tanaka, H.; Yagishita, S.; Adachi, K.; Uemura, T.; Kitagawa, S.; Kawata, S. *Inorg. Chem.* **2006**, *45*, 4322. (c) Takamizawa, S.; Kojima, K.; Akatsuka, T. *Inorg. Chem.* **2006**, *45*, 4580. (d) Supriya, S.; Das, S. K. *J. Am. Chem. Soc.* **2007**, *129*, 3464. (e) Dobrzańska, L.; Gareth, O.; Lloyd, G. O.; Esterhuysen, C.; Barbour, L. J. *Angew. Chem., Int. Ed.* **2006**, *45*, 5856. (f) Nagarathinam, M.; Vittal, J. J. *Angew. Chem., Int. Ed.* **2006**, *45*, 4337. (g) Serre, C.; Millange, F.; Thouvenot, C.; Noguès, M.; Marsolier, G.; Louer, D.; Férey, G. *J. Am. Chem. Soc.* **2002**, *124*, 13519. (h) Serre, C.; Mellot-Draznieks, C.; Surlé, S.; Audebrand, N.; Filinchuk, Y.; Férey, G. *Science* **2007**, *315*, 1828.

(3) Inoue, M.; Kishita, M.; Kubo, M. *Inorg. Chem.* **1965**, *4*, 626.

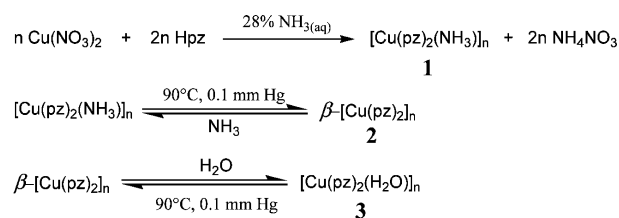
in an external magnetic field of 0.1 T varying the temperature between 2 and 300 K. β -[Cu(pz)₂]_n was kept in an oven at 80 °C under vacuum for 24 h and weighed in a glovebox. All the data were corrected for diamagnetism.⁴

Density Functional Calculations. Density functional (DF) calculations were performed using the Perdew–Burke–Ernzerhof exchange–correlation functional⁵ and Vanderbilt⁶ pseudopotentials. Because the polymer chains interact through dispersion forces, the dispersion-corrected DFT-D method by Grimme,⁷ recently implemented by some of us⁸ in the Quantum-ESPRESSO package,⁹ was adopted. A total of 11, 6, 5, 4, and 1 valence electrons were explicitly considered for Cu, O, N, C, and H, respectively. The smooth part of the wave function was expanded in plane waves, with a kinetic energy cutoff of 30 Ry, while the cutoff for the augmented electron density charge was 250 Ry. Plane wave calculations have been shown to be adequate for describing magnetic interactions in Cu(II) complexes.¹⁰ The Brillouin zone integration was performed using the Monkhorst–Pack scheme,¹¹ with 2 × 4 × 2 and a 1 × 2 × 4 meshes for β -[Cu(pz)₂]_n, **2** and [Cu(pz)₂·(H₂O)]_n, **3**, respectively. Both lattice constants and internal parameters were fully optimized with a BFGS algorithm. Finite-basis set effects were corrected following the procedure by Bernasconi et al.¹² with $A = 40$ Ry, $E_0 = 30$ Ry, and $\sigma = 4$ Ry. Calculations were performed for both the ferromagnetic (FM) and the antiferromagnetic (AFM) states. The energy difference was used to estimate the exchange coupling J by fitting to an Ising model.

Results and Discussion

In 1965 Inoue et al.³ in a study on the magnetic properties of a variety of copper(II) complexes with nitrogen heterocyclic ligands reported, inter alia, obtaining purple microcrystals of “bis(pyrazolato)copper(II) hemiammonia hemihydrate, Cu(C₃H₃N₂)₂·0.5NH₃·0.5H₂O” by reacting copper(II) sulfate with pyrazole in concentrated aqueous ammonia. They also observed that, on heating, the compound eliminated ammonia and water and the purple microcrystals turned brown, but this latter compound was not characterized further. Recently, we reported the synthesis and characterization of the β polymorph, β -[Cu(pz)₂]_n, **2**,^{2a} which is pale-brown and changes color on sorption of water and ammonia, giving [Cu(pz)₂·(H₂O)]_n, **3**, (pale pink) and [Cu(pz)₂·(NH₃)]_n, **1**, (blue), respectively. Suspecting that the brown compound observed by Inoue et al.³ was **2**, we repeated their procedures in slightly different conditions (see Materials and Methods section) and succeeded in obtaining [Cu(pz)₂·(NH₃)]_n, **1**, in about 78% yield, somewhat lower with respect to the almost quantitative yield of our previous synthesis.^{2a} On the other hand, this drawback is balanced by the possibility to use

Scheme 1



practically any copper(II) salt, and not only the more expensive carboxylates and, most important, to avoid the use of the organic solvents like MeCN. In this procedure MeCN is replaced by aqueous concentrated ammonia that acts also as deprotonating agent of Hpz, a role originally played by the carboxylate ions.^{2a} Thus, the deprotonated pyrazoles coordinated to cuproammoniacal species formed by Cu(II) salts are dissolved in aqueous ammonia yielding **1**. The accessibility of the cavities and the diffusion of the reactants within the pores of the bulk pumice make it possible to prepare solid, resistant sheets where **1** is permanently adsorbed.

Pure crystalline powders of **1** or even **1** adsorbed into pumice sheets show the reversible sorption/desorption behavior discussed in ref 2a, and schematically summarized in Scheme 1. This can be easily appreciated from Figure 2, where the different materials are collectively shown. This demonstrates that when suitably supported, the polymer could be in principle used to detect water or other small molecules.

Magnetic Susceptibility Results. The temperature dependence of χ of **2** and **3** is typical of an antiferromagnetic linear chain of $S = 1/2$ spins^{13,14} containing low amounts of paramagnetic impurities (Figure 3). Although much theoretical work has been done on low-dimensional magnetic systems in the last decades, there is still no exact closed-form equation for the temperature dependence of the magnetic susceptibility of a regular 1D chain of $1/2$ spins described by the Heisenberg isotropic exchange Hamiltonian, $H = -J\sum_i \mathbf{S}_i \cdot \mathbf{S}_{i+1}$ (J is the isotropic exchange coupling constants), which are valid for the whole temperature range. The magnetic susceptibility of these systems was originally solved by Bonner and Fisher,^{13,15} who computed the magnetic susceptibilities of ring chains of increasing size (up to 11 magnetic centers), and proposed an extrapolation for the infinite ring. Close equations exist for the low temperature limit¹⁵ when $J < 0$ (antiferromagnetic interaction), and for the high temperature region for both positive and negative J .¹⁶ An efficient way of measuring J is to use equations derived by fitting Bonner–Fisher’s numerical

(4) O’Connor, C. J. *Prog. Inorg. Chem.* **1982**, 29, 203.

(5) Perdew, J. P.; Burke, K.; Ernzerhof, M. *Phys. Rev. Lett.* **1996**, 77, 3865.

(6) Vanderbilt, D. *Phys. Rev. B* **1990**, 41, 7892.

(7) Grimme, S. *J. Comput. Chem.* **2006**, 27, 1787.

(8) Barone, V.; Casarin, M.; Forrer, D.; Pavone, M.; Sambi, M.; Vittadini, A. *J. Comput. Chem.* **2009**, 30, 934.

(9) Baroni, S.; dal Corso, A.; de Gironcoli, S.; Giannozzi, P.; Cavazzoni, C.; Ballabio, G.; Scandolo, S.; Chiarotti, G.; Focher, P.; Pasquarello, A.; Laasonen, K.; Trave, A.; Car, R.; Marzari, N.; Kokalj, A. <http://www.pwscf.org>.

(10) Massobrio, C.; Ruiz, E. *Monatsh. Chem.* **2003**, 134, 317.

(11) Monkhorst, H.; Pack, J. *Phys. Rev. B* **1976**, 13, 5188.

(12) Bernasconi, M.; Chiarotti, G. L.; Focher, P.; Scandolo, S.; Tosatti, E.; Parrinello, M. *J. Phys. Chem. Solids* **1995**, 56, 501.

(13) Kahn, O. *Molecular Magnetism*; VCH Publishers: New York, 1993.

(14) Jotham, R. W. *J. Chem. Soc., Dalton Trans.* **1977**, 266.

(15) Bonner, J. C.; Fisher, M. E. *Phys. Rev. A* **1964**, 135, 640.

(16) (a) Baker, G. A.; Rushbrooke, G. S.; Gilbert, H. E. *Phys. Rev.* **1964**, 135, A1272. (b) Baker, G. A.; Rushbrooke, G. S.; Gilbert, H. E. *Phys. Rev.* **1967**, 164, 800.



Figure 2. Pumice sheets embedding anhydrous β -[Cu(pz)₂]_n, **2**, (left), hydrated [Cu(pz)₂·(H₂O)]_n, **3**, (center), and ammonia complex [Cu(pz)₂·(NH₃)]_n, **1**, (right) together with corresponding microcrystalline powdered compounds.

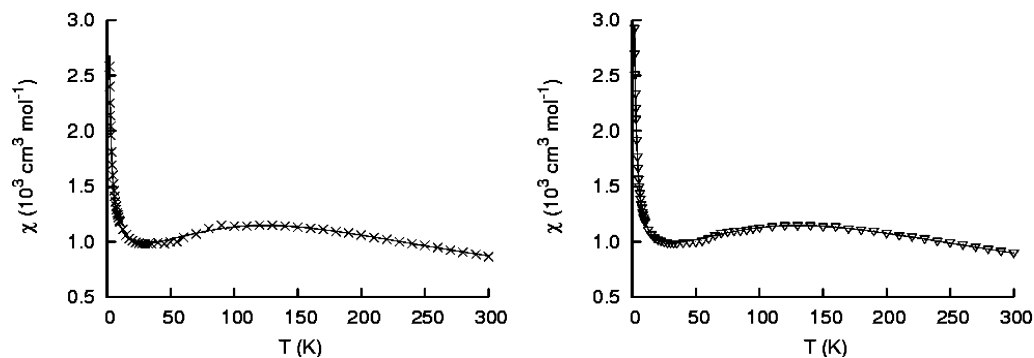


Figure 3. Temperature dependence of χ for [Cu(pz)₂]_n (left) and [Cu(pz)₂·(H₂O)]_n (right). Solid lines are the best fit curves (see text).

results with polynomial expressions by Jotham^{14,15} and Hall.¹⁷

We used here the Hall equation:

$$\chi_{\text{BF}}(T) = \frac{Ng^2\mu_{\text{B}}^2}{kT} \frac{0.25 + 0.074975x + 0.075235x^2}{1.0 + 0.9931x + 0.172135x^2 + 0.757825x^3} \quad (1)$$

where $x = |J|/kT$.

Including in eq 1 the effect of a paramagnetic impurity, we obtain the working equation expressing the magnetic susceptibility, χ_{c} , to be compared with the experimental values:

$$\chi_{\text{c}}(T) = \chi_{\text{BF}}(T)(1 - \rho) + \frac{Ng^2\mu_{\text{B}}^2}{3kT}\rho \quad (2)$$

where ρ is the molar fraction of the impurity assumed to have the same g of the Cu(II) ions in the chain. The magnetic data, $\chi_{\text{c}}(T)$, were fit using the MINUIT¹⁸ routine keeping J and ρ as free parameters. Since g and J were found to be strongly correlated, g was kept fixed at 2.07 (the value obtained from EPR spectra, vide infra). The experimental results are compared to the computed ones in Figure 3. The best fit curve (solid lines) were obtained with the parameters $J = -141.8(7) \text{ cm}^{-1}$, $\rho = 0.91(7)\%$ for β -[Cu(pz)₂]_n and $J = -145.5(3) \text{ cm}^{-1}$, $\rho = 0.97(6)\%$ for [Cu(pz)₂·(H₂O)]_n. The agreement factors were $R = 1.5\%$ and $R = 0.5\%$ in the two cases, respectively.

Antiferromagnetic interactions are commonly observed in bis-pyrazolato bridged dimers. Originally we reported a “weak

exchange interaction” on the basis of preliminary results. On repeating and better analysing the experiments, more accurate values of J (reported above) were determined, which can be considered rather high and in the range usually observed in dinuclear copper(II) complexes,¹⁹ and compare well with those of the α -[Cu(pz)₂]_n phase ($J = -156 \text{ cm}^{-1}$).^{16,20} Unexpectedly, these values indicate a scarce sensitivity on the stereochemical parameters. As a matter of fact, magnetostructural correlations, within the orbital model of the exchange interactions, showed that deviation from coplanarity of the two pyrazolato ligands could affect even the sign of the exchange coupling constant, apparently counter balanced by the non-co-planarity of the Cu(II) coordination planes.^{20,21}

EPR Results. EPR spectra of both β -[Cu(pz)₂]_n, **2**, and the hydrated compound [Cu(pz)₂·(H₂O)]_n, **3** at r.t., show a single isotropic resonance at $g = 2.07 \pm 0.01$. As a representative example, the polycrystalline EPR powder spectrum of β -[Cu(pz)₂]_n is shown in Figure 4. The line shape is almost purely Lorentzian and the peak-to-peak line width is 230 G for **2** and 250 G for **3**.

The Lorentzian line shape, maintained throughout the investigated temperature range (100–350 K), is due to the relatively strong spin exchange interaction between copper atoms, which averages out all the anisotropies from the g -factor and hyperfine interactions. Likely, this occurs because magnetic exchange overcomes other relaxation mechanisms, like spin–lattice relaxation.²² In the temperature

(17) (a) Hall, J. W. Ph.D. Dissertation, University of North Carolina, 1977. (b) Estes, W. E.; Gavel, D. P.; Hatfield, W. E.; Hodgson, D. *Inorg. Chem.* **1978**, *17*, 1415. (c) Estes, W. E.; Hatfield, W. E.; van Ooijen, J. A. C.; Reedijk, J. *J. Chem. Soc., Dalton Trans.* **1980**, 2121. (18) James, F. MINUIT, version 96.03; CERN program library: Geneva.

(19) Tanase, S.; Koval, I. A.; Bouwman, E.; de Gelder, R.; Reedijk, J. *Inorg. Chem.* **2005**, *44*, 7860.

(20) Ehlert, M. K.; Retting, S. J.; Storr, A.; Thompson, R. C.; Trotter, J. *Can. J. Chem.* **1989**, *67*, 1970.

(21) Ajò, D.; Bencini, A.; Mani, F. *Inorg. Chem.* **1988**, *27*, 2437.

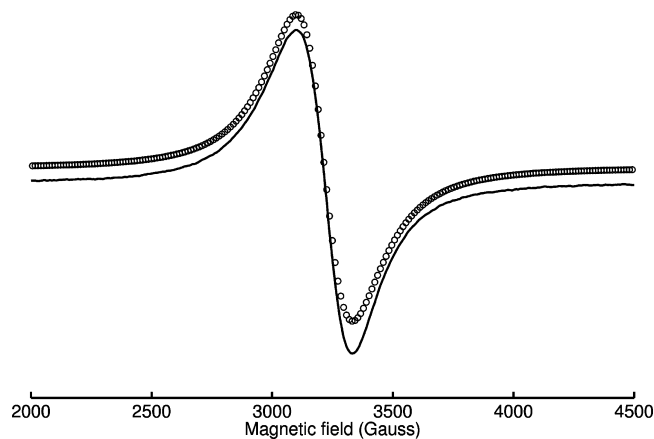


Figure 4. Room temperature polycrystalline powder EPR spectrum of β -[Cu(pz)₂]_n. Solid line: experimental spectrum. Circles: best fit Lorentzian line.

range 100–350 K, the doubly integrated EPR intensities show a maximum at about 160 K for **2** and at slightly higher temperature for **3** (data not shown).

The intensity of an EPR spectrum, when exchange interactions are dominating the relaxation mechanisms, is proportional to the magnetic susceptibility of the sample.¹⁹ Therefore an estimate of J can be obtained by fitting the EPR intensities with the polynomial expression of eq 2. The best fit values are $J = -168 \text{ cm}^{-1}$ for **2** and -190 cm^{-1} for **3**. Considering the larger uncertainties of the EPR results, these values are in fair agreement with magnetic susceptibility data.

Summarizing, magnetism and EPR measurements indicate that the presence of water molecules in the hydrated polymer is slightly increasing the superexchange interaction between the copper ions. This effect is, however, weak as a consequence of the relatively long Cu–OH₂ distance (as discussed below).

Theoretical Calculations. We first point out that this is, to our knowledge, the first application of the DFT-D method to coordination polymer systems. The DFT-D method allowed us to fully optimize the lattice structures, even though the polymer chains interact only through dispersion forces. The optimized cell constants are $a = 8.76 \text{ \AA}$ (-3.2%), $b = 7.52 \text{ \AA}$ ($+1.6\%$), $c = 5.20 \text{ \AA}$ (-7.1%), $\beta = 101^\circ$ β -[Cu(pz)₂]_n, **2**, and $a = 15.94 \text{ \AA}$ (-6.0%), $b = 6.08 \text{ \AA}$ (-2.6%), $c = 7.37 \text{ \AA}$ ($+1.3\%$) for [Cu(pz)₂·(H₂O)]_n, **3**. The underestimation of the lattice constants corresponding to the “soft” directions is similar to the one reported for DFT-D calculations on polyethylene.⁸ In this work, the aims of the theoretical calculations are the following: (i) understanding the mechanism of the Cu(II)–Cu(II) antiferromagnetic coupling; (ii) evaluating the water-host bonding interaction; (iii) obtaining insight into the mechanism of pore formation by water sorption. Whereas the inclusion of dispersion forces was found to be unimportant for the determination of the electronic and magnetic properties, significant improvements

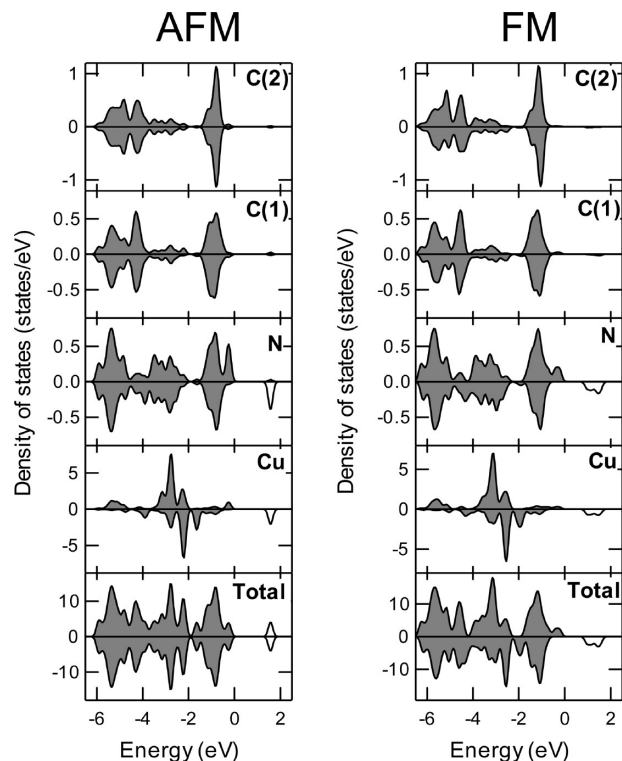


Figure 5. Spin-resolved density of states for β -[Cu(pz)₂]_n, **2**. Left: antiferromagnetic order; right: ferromagnetic order. Positive/negative values indicate spin up/down density of states. Filled areas indicate occupied states. Partial density of states are referred to single atoms. Atomic labels as indicated in Figure 1b.

were found in the estimate of the water sorption energy, and, most important, in the study of the energetics of the lattice transformation.

We start from the analysis of the magnetic interactions in β -[Cu(pz)₂]_n, **2**. Both the FM and the AFM phases were found to be insulating, with a large band gap (see Figure 5), the AFM system being more stable by 0.051 eV/cell. The superexchange coupling constant J can be evaluated from the total energies of the ferromagnetic, E^{FM} , and antiferromagnetic, E^{AFM} , phases through the formula:

$$E^{\text{AFM}} - E^{\text{FM}} = \frac{2zS^2J}{K} \quad (3)$$

where the z indicates the number of couplings per unit cell (2, in this case²³), and $K = 8065.6$ is the conversion factor from eV to cm^{-1} . This allows us to estimate that $J = -415 \text{ cm}^{-1}$. As found in similar calculations based on “pure” density functionals,²⁴ the coupling constant is significantly overestimated because of the excessively delocalized spin density.

More interesting is the information gained from local magnetic moments (M), which are obtained by projecting the wave functions into atomic functions (see Table 1), and from spin density maps (see Figure 6). As it clearly appears

(22) (a) Abragam, A.; Bleaney, B. *Electron Paramagnetic Resonance of Transition Ions*; Clarendon Press: Oxford, 1970. (b) Bencini, A.; Gatteschi, D. *Electron Paramagnetic Resonance of Exchange Coupled Systems*; Springer-Verlag: Berlin, 1990.

(23) In the case of [Cu(pz)₂·H₂O]_n the factor 2 should be replaced by a factor 4 to account for the presence of 4 chain interactions in the unit cell (see Figure 1c).

(24) (a) Ruiz, E.; Llunell, M.; Alemany, P. *J. Solid State Chem.* **2003**, *176*, 400. (b) Doll, K.; Wolter, A. U. B.; Klaus, H.-H. *Phys Rev. B* **2007**, *75*, 184433.

Table 1. Local Magnetic Moments (μ_B) Computed for Anhydrous and Hydrated Polymers in the AFM and FM States^a

	β -[Cu(pz) ₂] _n , 2		[Cu(pz) ₂ ·(H ₂ O)] _n , 3	
	AFM	FM	AFM	FM
Cu/Cu'	0.556/−0.556	0.574	0.573/−0.573	0.590
N/N'	0.090/−0.090	0.098	0.092/−0.092	0.096
C(1)/C'(1)	−0.005/0.005	−0.002	−0.006/0.006	−0.002
C(2)	0.000	0.007	0.000	0.006
O			0.000/0.000	−0.001

^a Atoms are labeled as in Figure 1b.

from Figure 6, the Cu magnetic orbital is the $d(x^2-y^2)$ one, while the superexchange interaction is mediated by the σ pyrazolate system. The spin density is largely carried by Cu and N atoms, only minor fractions of it being localized at the C(1) and C(2) sites (see Table 1). Local magnetic moments at the Cu ions are similar to those previously computed for other antiferromagnetic Cu polymers, Cu(thiazole)₂X₂, X = Cl, Br.²⁵

Turning now to [Cu(pz)₂·(H₂O)]_n, **3**, we first want to focus on the polymer-sorbate interaction. The equilibrium positions of water molecules were determined by performing several optimization runs, each started from different initial molecule orientations. In the most stable configuration, water molecules are oriented with the H atoms pointing toward the closest pyrazolate rings, as shown in Figure 7.

Optimized distances (in Å) are 0.98 (O–H); 2.85 (Cu···O); 3.34 (π ···O); and bond angles (in degrees) are 104.3 (H–O–H); 80.7 (Cu–O–Cu). The computed Cu–O distances fairly agree with the experiment (ca. 2.91 Å) and are rather long even for a weakly bound species as a μ -H₂O, being the usual Cu–O distance for a water molecule bridging Cu(II) ions below 2.4 Å.²⁶ This may be indicative that another species is competing in the interaction with the water molecules, as it occurs, for a lesser amount, for example, in the binuclear complex μ -acetato- μ -aqua- μ -hydroxo-bis[(1,4-dimethyl-1,4,7-triazacyclononane- κ N-3)-copper(II)] diperchlorate, where the electrostatic interaction between the μ -aquo ligand and the counteranions lengthens the Cu–OH₂ distance to 2.737 Å.²⁷ In the present case, the competing interaction may be the O–H··· π one, occurring between the water hydrogens and the pyrazolate rings of the nearest polymer chain. Interestingly, the computed O··· π distance is typical for OH··· π interactions for phenyl rings in neutral organometallic compounds.²⁸ Because, in contrast to that, the Cu–OH₂ bonds are unusually elongated, we infer that

the water-pyrazolate interaction is stronger than, or at least comparable to, the water-copper(II) one. This interpretation is supported by the electron difference density plots reported in Figure 8, which are obtained by computing the difference between the electron density of the *interacting* polymer–water system and that of a *non-interacting* system. The latter is obtained by summing the electron densities of the separated polymer and water moieties, each taken with the structure it assumes in the *interacting* system (i.e., the atomic positions are the same in both systems). These maps are useful to pinpoint the electron density rearrangements due to the formation of bonds and are particularly effective when dealing with molecular fragments. Looking at Figure 8, we can easily appreciate a considerable charge rearrangement in the Cu–O direction which is typical of weak electrostatic interactions:²⁹ the oxygen lone pairs are polarized toward the positive charged Cu atoms (see Figure 8b). In complete agreement with the previous discussion based on the simple inspection of interatomic distances, a *similar* and *comparable* charge rearrangement also occurs along the H···C directions (see Figure 8a). This similarity stems from the fact that also O–H··· π interactions are electrostatic in nature. On the other hand, the comparability of the charge rearrangements further confirms that the water-pyrazolate interactions are at least as strong as the water–Cu ones. Inter alia, this computational evidence may allow the comprehension of the “phase change” of **2** during water absorption (from a monoclinic to a orthorhombic lattice), likely driven by the formation of many (cooperative) OH··· π interactions in the lattice of **3**.

As far as the sorption energy is concerned, this can be straightforwardly computed from the total energies through the formula:

$$E_{\text{sorpt}}(\text{H}_2\text{O}) = E\{\text{[Cu(pz)}_2\text{(H}_2\text{O)]}\} - E\{\beta\text{-[Cu(pz)}_2\text{)]}\} - E\{\text{H}_2\text{O}\}$$

while the water/host interaction energy (E_{int}) can be computed by using an analogous formula where the β -[Cu(pz)₂] phase is replaced by an hypothetical relaxed “waterless” [Cu(pz)₂·(H₂O)] phase. The low (0.56 eV, 54 kJ/mol) computed E_{sorpt} value explains the facile dehydration of the compound, while the E_{int} value (0.71 eV, 69 kJ/mol) is well in tune with the electrostatic nature of the water-polymer interaction discussed above. Finally, magnetic moments (see Table 1) are scarcely affected by water sorption. Even lower is the effect on the relative energy of the FM and AFM phases (computed to be 0.050 eV/cell in favor of the latter), and, consequently, on J (computed to be -404 cm^{-1}).

We now turn our attention to the mechanism of the structural rearrangement occurring during the water sorption/desorption process. As pointed out in the Introduction, the β -[Cu(pz)₂]_n, **2**, \rightarrow [Cu(pz)₂·(H₂O)]_n, **3**, transformation (as well as [Cu(pz)₂·(NH₃)]_n, **1** \rightarrow β -[Cu(pz)₂]_n, **2**) is characterized by reversibility and easiness. Because a first-principle simulation of the transformation is obviously not feasible,

(25) Zhou, L.; Yao, K. L.; Liu, Z. L. *J. Phys.: Condens. Matter* **2006**, *18*, 3325.

(26) (a) Chaudhuri, P.; Ventur, D.; Wiegardt, K.; Peters, E.-M.; Peters, K.; Simon, A. *Angew. Chem., Int. Ed. Engl.* **1985**, *24*, 57. (b) Christou, G.; Perples, S. P.; Libby, E.; Foltling, K.; Huffman, J. C.; Webb, R.; Hendrickson, D. N. *Inorg. Chem.* **1990**, *29*, 3657. (c) Youngme, S.; van Albada, G. A.; Roubeau, O.; Pakawatchai, C.; Chaichit, N.; Reedijk, J. *Inorg. Chim. Acta* **2003**, *342*, 48. (d) He, H.-Y.; Zhou, Y.-L.; Zhu, L.-G. *Acta Crystallogr. C* **2004**, *60*, m569. (e) Barquin, M.; Gonzalez Garmendia, M. J.; Larrinaga, L.; Pinilla, E.; Torres, M. R. *Z. Anorg. Allg. Chem.* **2005**, *631*, 2151. (f) Gautier-Luneau, I.; Phanon, D.; Duboc, C.; Luneau, D.; Pierre, J.-L. *Dalton Trans.* **2005**, 3795. (g) Chailuecha, C.; Youngme, S.; Pakawatchai, C.; Chaichit, N.; van Albada, G. A.; Reedijk, J. *Inorg. Chim. Acta* **2006**, *359*, 4168.

(27) Elliot, D. J.; Martin, L. L.; Taylor, M. R. *Acta Crystallogr. C* **1998**, *54*, 1259.

(28) Braga, D.; Grepioni, F.; Tedesco, E. *Organometallics* **1998**, *17*, 2669.

(29) Casarin, M.; Maccato, C.; Vittadini, A. *J. Phys. Chem. B* **1998**, *102*, 10745.

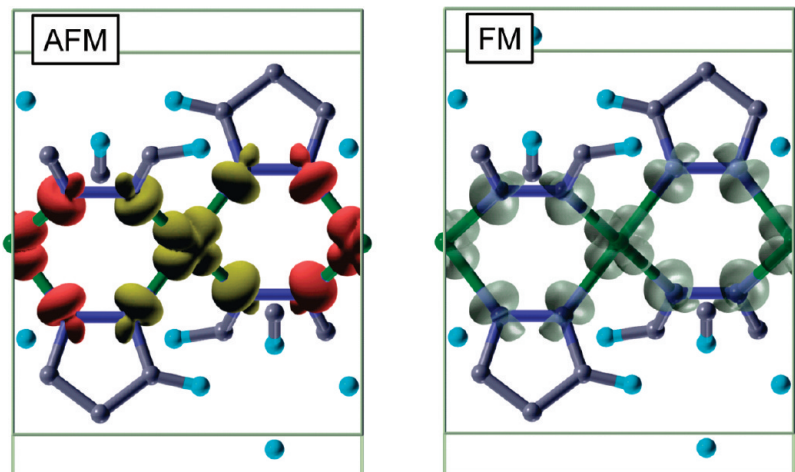


Figure 6. Three dimensional spin density maps for the AFM- (left) and the FM- (right) ordered phases β -[Cu(pz)₂]_n, **2** polymers. Displayed isosurfaces are $\pm 0.005 e/a_0^3$. For the AFM order, yellow/red color surfaces have been used to show regions with positive/negative spin density. For the FM phase, where negative spin density is negligible, a semitransparent surface has been adopted.

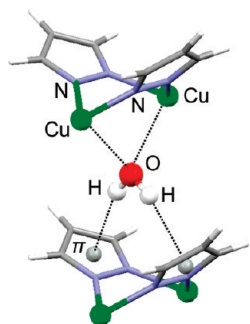


Figure 7. Local coordination of a water molecule to fragments of the nearest polymer chains in the AFM phase. Centroids of pyrazolate rings are displayed as gray balls and are marked by the π symbol.

we focus on an idealized model process where only the rearrangement of the host structure is considered, as described in the following. In Figure 9, where **2** and **3** are viewed down the (010) and the (001) planes, respectively, the close metric relationship between the two structures is evident. If we now consider for **3** the smaller oblique cell (indicated by the solid lines) instead of the more symmetric rectangular one, it turns out that the $2 \rightarrow 3$ transformation can be approximately described as a lowering of the monoclinic β angle from $\sim 100^\circ$ (the value of the anhydrous β phase) to $\sim 70^\circ$ (the angle corresponding to the hydrated phase). This can be easily done by shifting, in the horizontal direction, adjacent rows of 1D chains, and passing from a dense structure to a porous one, favored by new $\text{OH} \cdots \pi$ interactions with the guest molecules. Accordingly, this structure modification is somehow triggered by water molecules initially adsorbed at the surface of the polymer, and finds its driving force in the water sorption enthalpy. Considering that the latter has been computed to be rather small, the energy barrier for changing the polymer structure is probably low. To estimate this barrier, we performed “linear transit” (LT) calculations where the β parameter of the monoclinic structure of **2** was progressively lowered from 105° to 65° in 5° steps. Given the idealized nature of the investigated transformation, and the approximate nature of the LT approach, we avoided time-consuming variable cell calculations carrying out *two* sets

of runs, where the cell constants were kept fixed at the theoretical values of **2** and **3**, respectively (see Figure 10).

The total energy curve obtained for the denser structures corresponding to the β -[Cu(pz)₂]_n constants (Figure 10, squares) is characterized by a single, deep minimum at $\beta \sim 100^\circ$, characteristic of the dehydrated compound, and by an inflection point at $\beta \sim 85^\circ$. In contrast to that, two almost equivalent minima are found for the host structure when the constants of the more expanded [Cu(pz)₂·(H₂O)]_n phase are taken. The second minimum is found at $\beta \sim 75^\circ$, which is quite close to the value of the monoclinic cell of [Cu(pz)₂·(H₂O)]_n phase. An estimate of the activation energy involved in the pore opening transformation ($100^\circ \rightarrow 75^\circ$) is given by the energy of the crossing point between the two curves. The low resulting value (18 kJ/mol) explains the easiness of the water sorption process. On the other hand, the almost vanishing barrier for the backward ($75^\circ \rightarrow 100^\circ$) transformation indicates that the solvent-free porous structure is unlikely to be obtained. Overall, our approximated potential energy curve is quite well compatible with the reversibility of the water absorption/desorption process.

Conclusions

Solid microcrystalline coordination polymer β -[Cu(pz)₂]_n, **2**, can adsorb, reversibly, one molecule of water generating the hydrated species [Cu(pz)₂·(H₂O)]_n, **3**. In this solid state process, the monoclinic structure of **2** changes to the orthorhombic **3** and, being that the structure of **2** is compact, without pores or channels, water accommodates in voids that are “generated” in the adsorption process, a particular case of porosity “without pores”.¹ In the present paper we report, besides a new, more profitable synthetic procedure to obtain **2**, an experimental and theoretical study on the magnetic properties of **2** and of the hydrated phase **3**, carried out by magnetic susceptibility measurements, EPR spectroscopy, and DFT-D calculations.

Both theoretical and experimental evidence show that Cu(II) ions are antiferromagnetically coupled with a relatively strong exchange interaction. The additional water molecule in the hydrated phase slightly increases the interaction between copper ions. Inspection of the theoretical spin

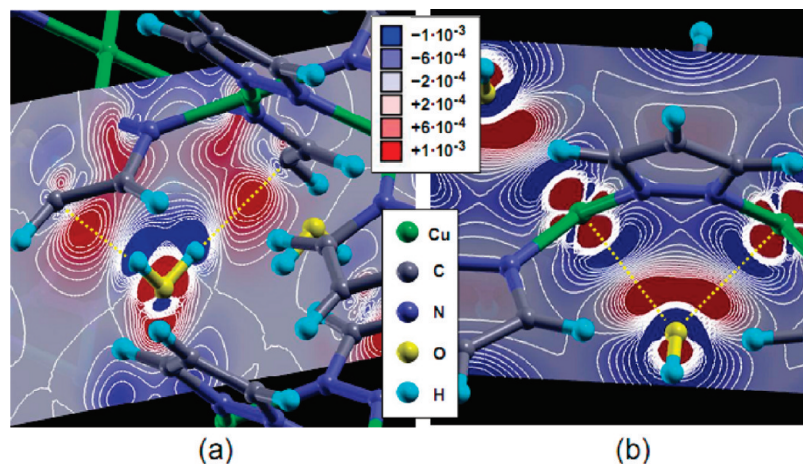


Figure 8. Electron difference density plots referring to the $\text{H}_2\text{O}-\text{Cu}(\text{pz})_2$ interaction (see text). Displayed sections are as follows: (a) a (100) plane bisecting two pyrazolate rings which bridge the same Cu atoms; (b) a (001) plane passing through the Cu atoms of a polymer chain.

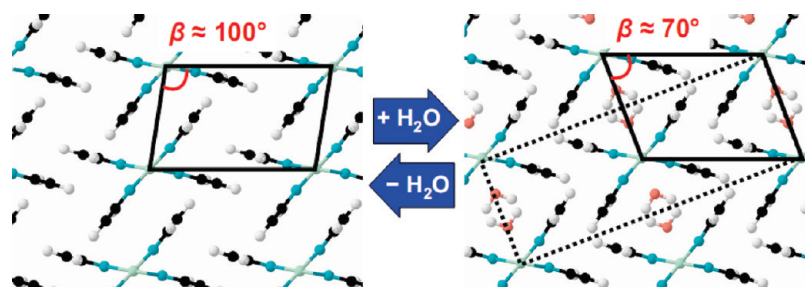


Figure 9. Left: view of the lattice structures of $\beta\text{-}[\text{Cu}(\text{pz})_2]_n$, **2**, down the (010) plane. Right: view of the lattice structure of $[\text{Cu}(\text{pz})_2 \cdot (\text{H}_2\text{O})]_n$, **3**, down the (001) plane. Solid lines show the monoclinic cells. The dashed line on the $[\text{Cu}(\text{pz})_2 \cdot (\text{H}_2\text{O})]_n$, **3** structure indicates the orthorhombic cell.

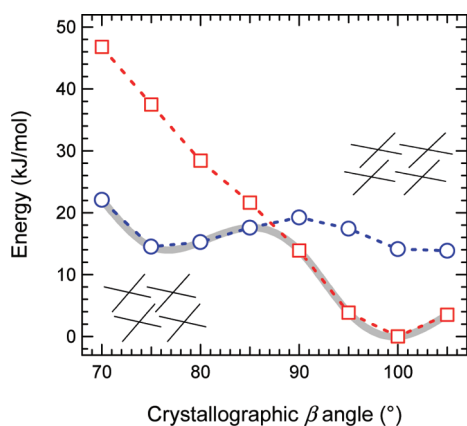


Figure 10. Total energy curves obtained by scanning the monoclinic β angle of the dehydrated phase over a 5° -spaced grid. The cell edges are kept fixed at the theoretical values corresponding to $\beta\text{-}[\text{Cu}(\text{pz})_2]_n$, **2** (squares) and to $[\text{Cu}(\text{pz})_2 \cdot (\text{H}_2\text{O})]_n$, **3**, (circles) experimental structures. Energies are referred to 1 mol of $\text{Cu}(\text{pz})_2$. The gray curve indicates the (approximate) path followed by the lattice transformation, schematically shown in the insets.

densities show that the dominant magnetic interactions involve the σ orbitals of the pyrazolate ligands. Furthermore,

calculations show that the long $\text{H}_2\text{O}-\text{Cu}(\text{II})$ distances are due to the concurrent interaction between the water protons and the pyrazolate rings of the neighboring chains. The energetics of the pore opening mechanism has also been studied, finding that the energy barriers for the pore formation are indeed low.

Acknowledgment. This work was supported by the Italian PRIN (n. 2006038447) and by FIRB 2003 (n. RBNE033KMA) funds. Computational resources and assistance were provided by the Laboratorio Interdipartimentale di Chimica Computazionale (LICC) at the Department of Chemistry of the University of Padova. Density functional calculations have been performed by using the Quantum-ESPRESSO package.⁹ Molecular graphics have been generated by XcrysDen³⁰ and Mercury.³¹

IC801928B

(30) Kokalj, A. *Comput. Mater. Sci.* **2003**, *28*, 155; Code available from <http://www.xcrysden.org/>.

(31) Bruno, I. J.; Cole, J. C.; Edgington, P. R.; Kessler, M.; Macrae, C. F.; McCabe, P.; Pearson, J.; Taylor, R. *Acta Crystallogr. B* **2002**, *58*, 389; Available from <http://www.ccdc.cam.ac.uk>.



Tris(pyrazol-1-yl)borate and tris(pyrazol-1-yl)methane: A DFT study of their different binding capability toward Ag(I) and Cu(I) cations

Maurizio Casarin^{a,c,d,*}, Daniel Forrer^{a,d}, Federica Garau^a, Luciano Pandolfo^{a,d}, Claudio Pettinari^b, Andrea Vittadini^{c,d}

^a Dipartimento di Scienze Chimiche, Università degli Studi di Padova, Via Marzolo 1, 35131 Padova, Italy

^b Dipartimento di Scienze Chimiche, Camerino, Italy

^c Istituto di Scienze Molecolari del CNR, Padova, Italy

^d Consorzio Interuniversitario di Scienza e Tecnologia dei Materiali, Firenze, Italy

ARTICLE INFO

Article history:

Received 1 November 2008

Accepted 5 February 2009

Available online 15 February 2009

Dedicated to the memory of Swiatoslaw ("Jerry") Trofimenko

Keywords:

Density functional theory

Scorpionates

Cu(I) and Ag(I) metal complexes

ABSTRACT

Density functional theory has been used to study the electronic structure of $[M(tp)]$ and $[M(tpm)]^+$ conformers ($M = Cu, Ag$; $tp = \text{tris(pyrazol-1-yl)borate anion}$, $tpm = \text{tris(pyrazol-1-yl)methane}$) and the energetics of their interconversions. Results for the free tp ligand are similar to those of tpm [M. Casarin, D. Forrer, F. Garau, L. Pandolfo, C. Pettinari, A. Vittadini, J. Phys. Chem. A 112 (2008) 6723], indicating an intrinsic instability of the tripodal conformation (κ^3 -like). This points out that, though frequently observed, the κ^3 -coordinative mode is unlikely to be directly achieved through the interaction of $M(I)$ with the κ^3 -like tp/tpm conformer. Analogously to the $[M(tpm)]^+$ molecular ions, the energy barrier for the κ^2 - $[M(tp)] \rightarrow \kappa^3$ - $[M(tp)]$ conversion is computed to be negligible. Though κ^2 - $[M(tp)]$ and κ^3 - $[M(tpm)]^+$ ($n = 1, 2, 3$) have similar metal–ligand covalent interactions, the negative charge associated to the tp ligand makes the M - tp bonding stronger.

© 2009 Elsevier B.V. All rights reserved.

1. Introduction

Tris(pyrazol-1-yl)borate anion (hereafter, tp) and tris(pyrazol-1-yl)methane (hereafter, tpm) ligands play a leading role in modern coordination chemistry [1]. In fact, they are able, both in the substituted and unsubstituted forms, to supply an important steric shielding of the metal center serving, at the same time, as reliable spectator ligands. Complexes of the tp -based ligands are known for most of the metals in the periodic table and have applications in diverse and important fields ranging from catalysis to biomedicine, from metal extraction to biomimetic inorganic chemistry [1]. The common coordination geometry for both tp and tpm is the tripodal one¹ (κ^3 -) where the lone pairs of the nitrogen heteroatoms $[N(\bullet)]$ of two pyrazolyl fragments attached to B (tp) or C (tpm) act like the pincers of a scorpion binding the metal centre, while the third pyrazolyl attached to the central atom rotates forward like a scorpion's tail to "sting" the metal. The family of ligands with this coordination

* Corresponding author. Address: Dipartimento di Scienze Chimiche, Università degli Studi di Padova, Via Marzolo 1, 35131 Padova, Italy.

E-mail address: maurizio.casarin@unipd.it (M. Casarin).

¹ tp and tpm may also act as κ^2 -ligands bonded to a single metal (κ^2 -chelating), as κ^1 - κ^2 -ligands bridging two metals or, hardly ever, as κ^1 -ligands likely depending on the steric congestion around the metal center and the number of donor substituents on the central atom X, which may be P and Ga other than B and C (see Refs. [1,2]). tp may also have a " κ^0 " denticity as shown by the Carmona group in $Rh(I)$ and $Rh(III)$ complexes [2a,b].

capability, whose simplest members are tp and tpm , is known as "scorpionates". However, we recently showed [3] that crystal data for both "uncoordinated" tp [2a,b] and free tpm [4] ligands suggest alternative and less evocative coordination modes. In fact, both tp and tpm are characterized by the presence of a single pyrazolyl group with $N(\bullet)$ in *trans* with respect to the B–H (tp)/C–H (tpm) fragments.²

Theoretical work so far devoted to the study of the interaction of tp and tpm ligands with metal ions is rather limited. A few years ago, De Bari and Zimmer [6] carried out a conformational study based on molecular mechanics and structural database analysis of tp and tpm behaving as κ^3 -tripodal ligands. They concluded that "tripodal scorpionate ligands can accommodate a variety of metal sizes by opening up the ligand". More recently, we employed the density functional theory (DFT) to study the electronic structure of $[M(tpm)]^+$ molecular ion conformers ($M = Cu, Ag$) as well as the energetics of their interconversion [3].

In this paper we study the κ^1 -monodentate, κ^2 -chelating, and κ^3 -tripodal conformers of $[M(tp)]$ ($M = Cu, Ag$). Our aim is to investigate the electronic properties and the energetics of the interconversion of the conformers, and to make a comparison with the results previously obtained with the analogous $[M(tpm)]^+$

² The relative position of pyrazolyl fragments in substituted and unsubstituted tp and tpm is strongly influenced by the steric hindrance of substituents possibly present on the ring carbon atoms [5].

complexes [3]. The first section of this contribution is dedicated to the assessment of the conformational properties of the free tp ligand leaving aside any problem concerning optical isomerism, while in the second part we focus on the binding energies and electronic properties of the $[M(tp)]$ conformers, and we finally make a comparison between the $[M(tpm)]^+$ and $[M(tp)]$ bonding schemes.

2. Computational details

All the presented results are based on DFT, and have been obtained by running the Amsterdam Density Functional (ADF) package [7] and adopting the scalar relativistic zeroth-order regular approximation (ZORA) [8]. Generalized gradient corrections have been self-consistently included through the Becke–Perdew formula [9], TZP ZORA basis sets have been adopted for all the atoms [10]; inner cores of Cu (1s2s2p3s3p), Ag (1s2s2p3s3p3d), B (1s), C (1s), and N (1s) atoms were kept frozen throughout the calculations. Geometries for ground- and transition-states (GS and TS, respectively) have been optimized without imposing any symmetry. All TS's have been estimated through the following procedure: (i) a linear transit (LT) calculation has been run by varying a dihedral angle;³ (ii) from the TS guess provided by step (i), a stationary point on the energy surface has been searched; (iii) the adequacy of the TS estimate has been then checked by computing vibrational frequencies at the corresponding geometry and verifying that one of them is imaginary; (iv) the Hessian computed in the third step is employed for the final TS optimization. Binding energies (BE) were analyzed in terms of fragment molecular orbitals (FMO) by applying the Ziegler's extended transition state method (ETS) [11]. According to the ETS scheme,

$$BE = \Delta E_{es} + \Delta E_{pauli} + \Delta E_{int} + \Delta E_{prep} \quad (1)$$

where ΔE_{es} is the pure electrostatic interaction, ΔE_{pauli} is the destabilizing two-orbital-four-electron interaction between the occupied orbitals of the interacting fragments ($\Delta E_{es} + \Delta E_{pauli}$) corresponds to the so called steric interaction (ΔE_{st}) contribution), ΔE_{int} derives from the stabilizing interaction between occupied and empty orbitals of the interacting fragments, and ΔE_{prep} is the energy required to relax the structure of the free fragments to the geometry they assume in the final system. BEs were further corrected by taking into account the basis set superposition error (BSSE) which was estimated by making use of reference energies calculated with “ghost” fragments [12].

One-electron levels are displayed as density of states (hereafter, DOS) by using a 0.25 eV Lorentzian broadening factor. These plots, based on Mulliken's prescription for partitioning the overlap density [13], have the advantage of providing insights into the atomic composition of MOs over a broad range of energy. Finally, information about the localization and the bonding/antibonding character of selected MOs was obtained by using crystal orbital overlap populations (COOP) [14] computed by weighting one-electron energy levels by their basis orbital percentage.

3. Results and discussion

Tp and tpm are potentially tripodal ligands characterized by the presence of three pyrazolyl moieties bonded to a central B and C atom, respectively. The MO structure of both the Hpz free molecule and the $[M(Hpz)]^+$ complexes have been recently described by our group [3]. We briefly resume the main findings in the following. Hpz is planar, fully conjugated, and isoelectronic with the cyclopentadienyl anion, though characterized by a high electronic

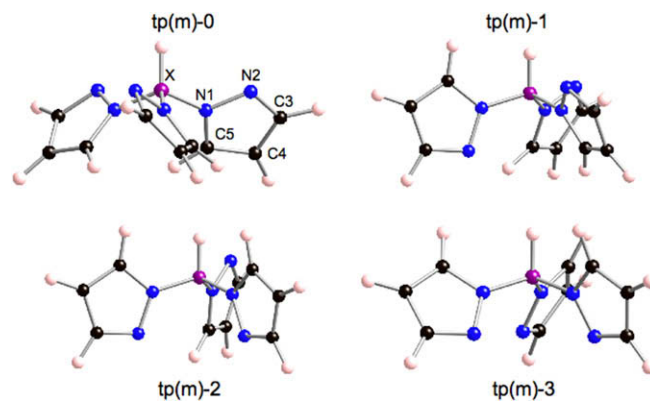


Fig. 1. Schematic representation of possible relative arrangements of the three pyrazolyl fragments in tp (X = B) and tpm (X = C).

Table 1

Relative binding energy contributions (kcal/mol) for tp and tpm free ligands.

	tp-0/(tpm-0)	tp-1/(tpm-1)	tp-2/(tpm-2)	tp-3/(tpm-3)
$\Delta(\Delta E_{pauli})$	-7.86 (-17.51)	-(-)	3.29 (3.18)	6.14 (-1.17)
$\Delta(\Delta E_{el})$	-2.25 (-1.37)	-(-)	-0.87 (-0.42)	-4.99 (-3.76)
$\Delta(\Delta E_{st})$	-10.10 (-18.88)	-(-)	2.42 (2.75)	1.15 (-4.93)
$\Delta(\Delta E_{int})$	10.38 (19.76)	-(-)	-0.89 (-0.25)	5.35 (13.32)

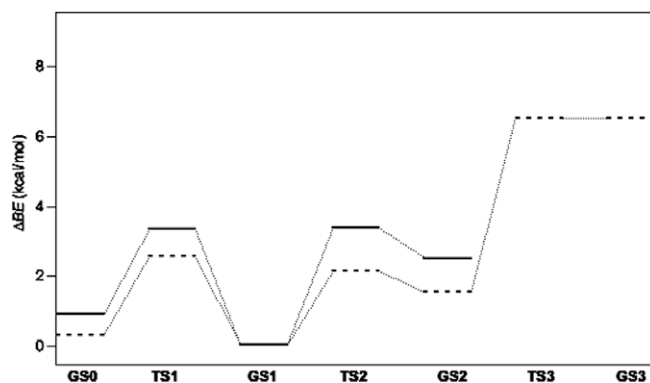


Fig. 2. Relative BE values of GS0, TS1, GS1, TS2, and GS2 for tp (dashed lines) and tpm (solid lines); TS3 and GS3 are limited to tp (see text). The zero energy value corresponds to the GS1 BE.

charge density on N atoms both in the molecular plane and out of it. Its valence manifold includes five π -like MOs and the $N(\bullet)$ lone pair (hereafter, n_N). Among them, the π_1 , π_2 , π_3 ones and n_N are occupied, whereas the π_4 and π_5 MOs are empty. Moreover, π_3 and π_4 correspond to the Hpz HOMO and LUMO, respectively. As a consequence of these peculiarities, each tp/tpm pyrazolyl group may be involved in two competitive metal–ligand bonding mechanisms: a σ -binding implying n_N and a π -binding entailing the π states of the aromatic ring. The DFT results pertaining to σ/π $[M(Hpz)]^+$ complexes revealed the importance of π contributions to the metal–ligand bond in σ - $[M(Hpz)]^+$ molecular ions and the leading role played by the ΔE_{st} term of Eq. (1) in determining the final BE value of σ/π - $[M(Hpz)]^+$ complexes.

3.1. tp conformational properties

Because of its charged nature, the free ligand cannot be characterized by X-ray diffraction. However, it is noteworthy that about 10 years ago Carmona and coworkers [2a,b] synthesized and structurally characterized what they called an isolated

³ A LT calculation implies a linear change of a selected LT parameter from its initial to its final value through a specified number of equidistant steps.

Table 2
Binding energy contributions in kcal/mol for the $[M(tp-n)]$ and $[M(tpm-n)]^+$ conformers.

	$[M(tp-1)]$ ($[M(tpm-1)]^+$)	TS(M)	$[M(tp-2)]$ ($[M(tpm-2)]^+$)	$[M(tp-3)]$ ($[M(tpm-3)]^+$)
${}^{Cu}\Delta E_{Pauli}$	142.49 (129.59)	122.77	160.37 (143.80)	142.47 (131.68)
${}^{Cu}\Delta E_{el}$	-232.29 (-130.46)	-213.24	-261.15 (-157.93)	-262.69 (-161.82)
${}^{Cu}\Delta E_{st}$	-89.80 (-0.87)	-90.47	-100.78 (-14.13)	-120.22 (-30.14)
${}^{Cu}E_{int}$	-103.72 (-97.18)	-95.67	-103.06 (-93.47)	-98.92 (-92.95)
${}^{Cu}\Delta E_{prep}$	8.24 (6.92)		4.55 (4.67)	3.96
${}^{Cu}BSSE$	2.84 (2.79)		2.42 (2.46)	2.71
${}^{Cu}BE$	-182.44 (-88.34)		-196.87 (-100.47)	-212.47
${}^{Ag}\Delta E_{Pauli}$	184.73 (152.24)	152.28	184.57 (160.19)	191.54 (160.37)
${}^{Ag}\Delta E_{el}$	-191.63 (-87.48)	-172.44	-210.22 (-109.92)	-220.52 (-116.45)
${}^{Ag}\Delta E_{st}$	-6.90 (64.76)	-20.16	-25.65 (50.27)	-28.98 (43.92)
${}^{Ag}\Delta E_{int}$	-153.39 (-132.66)	-134.22	-144.32 (-126.87)	-154.67 (-135.32)
${}^{Ag}\Delta E_{prep}$	6.01 (4.50)		4.09 (3.91)	2.14
${}^{Ag}BSSE$	0.66 (0.66)		0.53 (0.52)	0.58
${}^{Ag}BE$	-153.62 (-62.74)		-165.35 (-72.17)	-180.93

hydrotris(pyrazolyl)borate anions having a " κ^0 " coordinative mode. Interestingly, the structure of this κ^0 unsubstituted tp is characterized by a single pyrazolyl group with N(\bullet) in *trans* with respect to the hydrogen of the B-H fragment, similarly to the structural arrangement of the free tpm [5].⁴ In agreement with the labeling scheme adopted in Ref. [3], this conformer has been tagged tp-1, while those corresponding to the κ^2 -chelating and κ^3 -tripodal coordinative modes have been labeled as tp-2 and tp-3, respectively (see Fig. 1). Obviously, the tp-0 conformer is the one with the three N(\bullet) in *cis* with respect to the B-H moiety. Optimized coordinates of tp-0, tp-1, tp-2, tp-3, TS1, TS2, TS3 are reported in Tables S0–S6 of the Supplementary material.

Analogously to tpm-0, the pyrazolyl fragments of the tp-0 optimized structure are symmetry related by a C_3 axis, and assume a propeller-like arrangement. Relative BEs corresponding to tp- n GS as well as to relevant saddle points are reported in Table 1 and displayed in Fig. 2 together BEs of akin tpm conformers. The relative stability order of tp- n conformers ($n = 0-3$) is the same we found for the tpm ones [3], but the energy barriers associated to these interconversion paths (TS1, TS2, and TS3) are systematically lower than those evaluated for tpm (see Fig. 2). This is consistent with NMR data collected at room temperature by the Carmona group for the κ^0 hydrotris(pyrazolyl)borate anions [2a] which indicate a substantial free rotation around the B-N bonds.

A further point worth of note concerns the H-B vibrational frequencies (ν_{BH}) computed for the optimized tp-0, tp-1, and tp-2 structures (2517, 2513, and 2482 cm^{-1} , respectively). These values are all in reasonable agreement with the experimental κ^0 tp ν_{BH} value reported by Paneque et al. [2a] (2474 cm^{-1}). At variance to that, the calculated tp-3 ν_{BH} lies at a significantly lower frequency (2388 cm^{-1}). In this regard, it can be useful to remark that the optimized tp-1 bond lengths and bond angles agree well with structural data reported by Paneque et al. [2a], tp-0, tp-1, and tp-2 H-B bond lengths are very similar (1.201, 1.202, and 1.206 Å, respectively), while the tp-3 H-B internuclear distance (1.218 Å) is longer than that corresponding to the other tp conformers.

In general, theoretical results pertaining to tp- n reproduce those recently published for tpm- n [3]: though common, the κ^3 -tripodal coordinative mode is unlikely to be achieved through a direct interaction of a metal center with the ligand having a tp-3/tpm-3 arrangement. However, at variance to the tpm case, we were able to locate the tp GS3 energy minimum. Consistently with a very flat

⁴ Despite isolated hydrotris(pyrazolyl)borate derivatives may have different conformations, it has to be pointed out that, in these cases [5a,5e], the specific structural arrangement is ruled by steric factors.

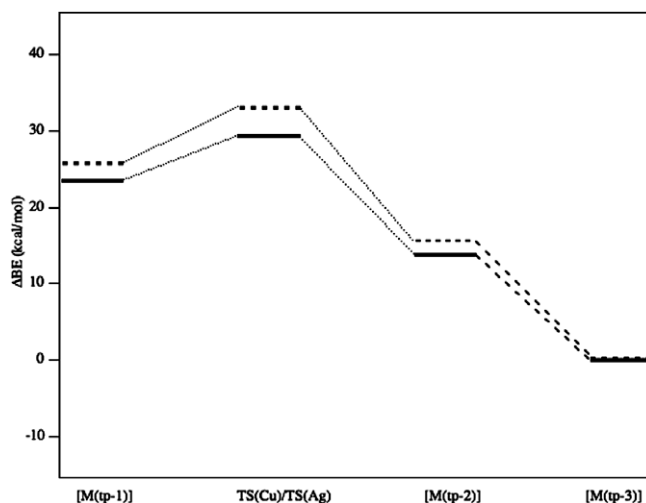


Fig. 3. Relative BE values of $[M(tp-1)]$, TS(M), $[M(tp-2)]$, and $[M(tp-3)]$ ($M = \text{Cu}$ (dashed lines) and Ag (solid lines)). The zero BE value corresponds to the $[M(tp-3)]$ BE. Between $[M(tp-2)]$ and $[M(tp-3)]$ no TS has been found.

potential energy surface in this region, the energy difference between tp TS3 and GS3 is negligible (see Fig. 2).⁵

3.2. $[Cu(tp)]$ and $[Ag(tp)]$ complexes

The structural and electronic properties of tp metal complexes have been the subject of several experimental contributions [1,2,5,6,15]. From these works, it was established that N_3 tripodal ligands such as hydrotris (pyrazolyl)borate anionic ligands or tris(pyrazolyl)methane neutral ligands behave as biomimetic systems. This suggested their use as a modeling tool to investigate the catalytic activity of metal centers in biological systems. However, no study has been so far specifically dedicated to the analysis of the interplay between the metal–ligand interaction and the ligand hapticity.

The strength and the nature of the M(I)–tp bond in $[M(tp-n)]$ ($n = 1, 2,$ and 3) have been obtained through the ETS scheme by considering M(I) and tp as interacting fragments [11]. Optimized coordinates of $[M(tp-n)]$ species and of TS(Cu) and TS(Ag) saddle points corresponding to the $[M(tp-1)] \rightarrow [M(tp-2)]$ conversions

⁵ Vibrational frequencies have been evaluated for both TS3 and GS3 verifying that: (i) one of them is imaginary in the former case; and (ii) they are all positive in the latter one.

are collected in Tables S7–S14. Relative BEs are reported in Table 2 and displayed in Fig. 3.

As far as the relative stability of these species is concerned, a comparison between Figs. 3 and 2 reveals that, as previously found for $[M(\text{tpm}-n)]^+$ molecular ions [3], $[M(\text{tp}-1)]$ is more stable than $[M(\text{tp}-2)]$, i.e. the order is reversed with respect to the free ligand. It is also remarkable that, despite both $[\text{Cu}(\text{tp}-2)]$ and $[\text{Ag}(\text{tp}-2)]$ correspond to local minima, they are so shallow that we were unable to find the saddle point corresponding to the $[M(\text{tp}-2)] \rightarrow [M(\text{tp}-3)]$ conversion. This indicates that, in tune with our previous calculations on $[M(\text{tpm}-n)]^+$ conformers, once the κ^2 -

complex is formed, either from the interaction of $M(I)$ with $\text{tp}-2$ or through the $[M(\text{tp}-1)] \rightarrow [M(\text{tp}-2)]$ conversion, the κ^3 -tripodal species may be readily formed. However, the $[M(\text{tp}-2)] \rightarrow [M(\text{tp}-3)]$ conversion could be hampered by several reasons such as: (i) the coordinative saturation of the metal center by concurrent ligands; (ii) the coordination of the $N(\bullet)$ of the third pyrazolyl group to a different metal center; (iii) steric factors determined by bulky substituents on tp ; (iv) electronic factors favoring specific arrangements [2,16].

Concerning the nature of the metal–ligand interaction, the ETS analysis (see Table 2) indicates that, independently of the coordi-

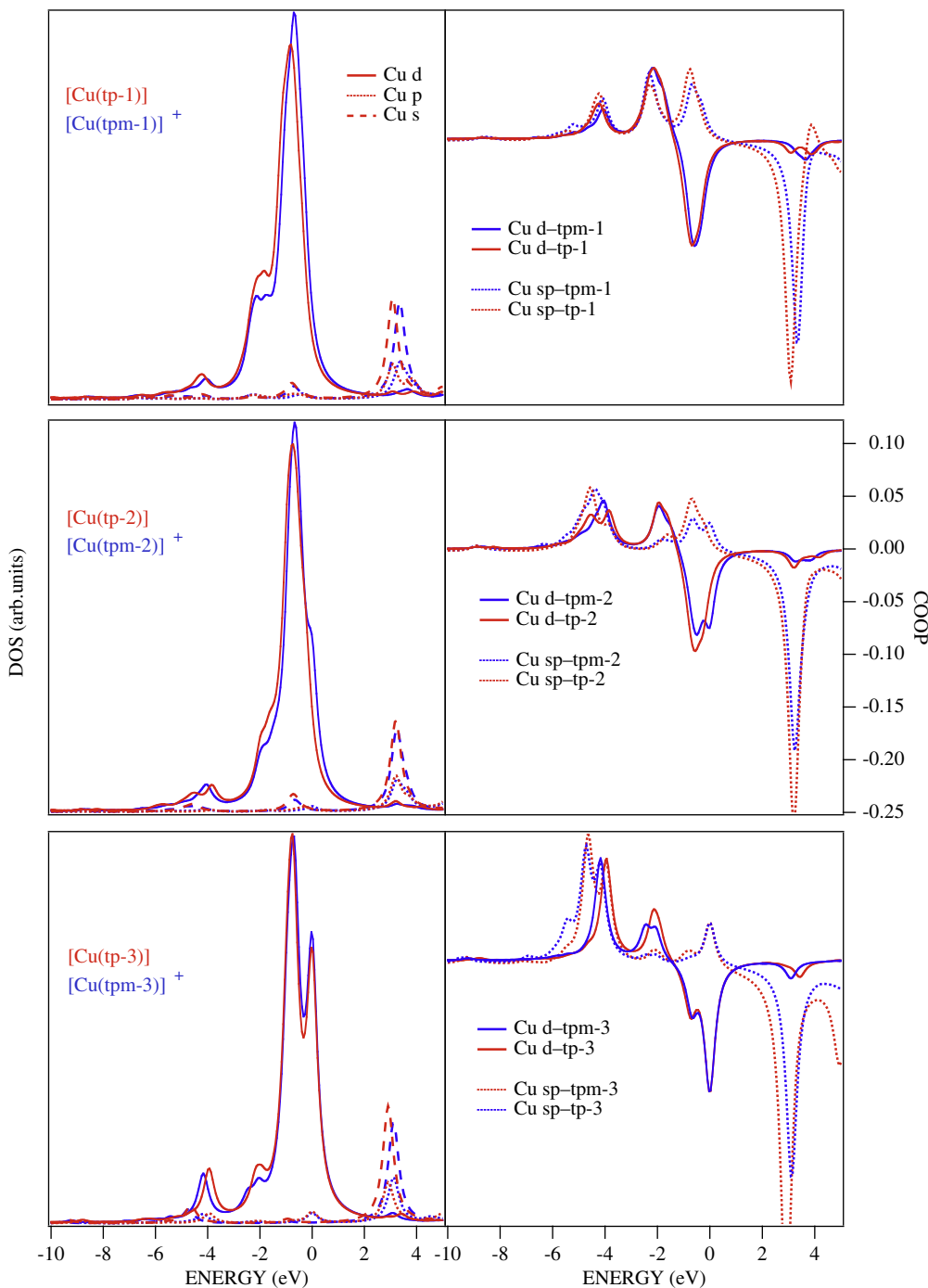


Fig. 4. (Left) d, s and p Cu PDOS of $[\text{Cu}(\text{tp}-n)]^+$ and $[\text{Cu}(\text{tpm}-n)]^+$; (right) Cu–(tp- n) and Cu–(tpm- n) COOP, bonding (antibonding) states correspond to positive (negative) peaks. The zero energy matches the HOMO energy of each species.

native mode, the covalent component of the metal–ligand interaction is quite similar in $[M(tp)]$ and $[M(tpm)]^+$, while the electrostatic interaction between $M(I)$ and the negatively charged tp significantly strengthens the metal–ligand bond on passing from $[M(tpm)]^+$ to $[M(tp)]$. Further insights can be obtained from the inspection of $M(I)$ PDOS and $M(I)$ –ligand COOP curves (see Figs. 4 and 5) coupled to the analysis of the $M(I)$ /ligand Hirshfeld charges [17] (Q^H) in $[M(tp-n)]$ and $[M(tpm-n)]^+$ (Table 3). Though the overall interaction between the $M(I)$ and tp charged fragments is definitely stronger than that between $M(I)$ and the neutral tpm , Figs. 4, 5 and data reported in Table 3 reveal: (i) the close similarity of metal-based s , p , and d PDOS on passing from $[M(tp-n)]$ to $[M(tpm-n)]^+$; (ii) the negligible contribution provided by the $M(I) \rightarrow tp/tpm$ backdonation to the metal–ligand interaction; (iii) the leading role played by the $tp/tpm \rightarrow M(I)$ donation in the metal–ligand bonding.

Structural and electronic differences of a series of κ^3 - $[Cu(tp)]$ and κ^3 - $[Cu(tpm)]^+$ complexes have been recently investigated by Fujisawa et al. [5e] through experimental and DFT studies. One of their main conclusions was that since κ^3 - tpm is a weaker donor than κ^3 - tp , the $Cu(I)$ ion in the κ^3 - tpm complex is electron-poorer, and in consequence less involved in back-donation. In contrast to

Table 3

Q^H values of M , tp , and tpm fragments in $[M(tp-n)]$ and $[M(tpm-n)]^+$ species.

	$[M(tp-1)]$ ($[M(tpm-1)]^+$)	$[M(tp-2)]$ ($[M(tpm-2)]^+$)	$[M(tp-3)]$ ($[M(tpm-3)]^+$)
Q_{Cu}^H	0.75 (0.79)	0.76 (0.78)	0.79 (0.81)
Q_{tp}^H (Q_{tpm}^H)	-0.75 (0.21)	-0.76 (0.22)	-0.79 (0.19)
Q_{tp}^H	0.71 (0.75)	0.77 (0.76)	0.74 (0.77)
Q_{tp}^H (Q_{tpm}^H)	-0.71 (0.25)	-0.77 (0.24)	-0.74 (0.23)

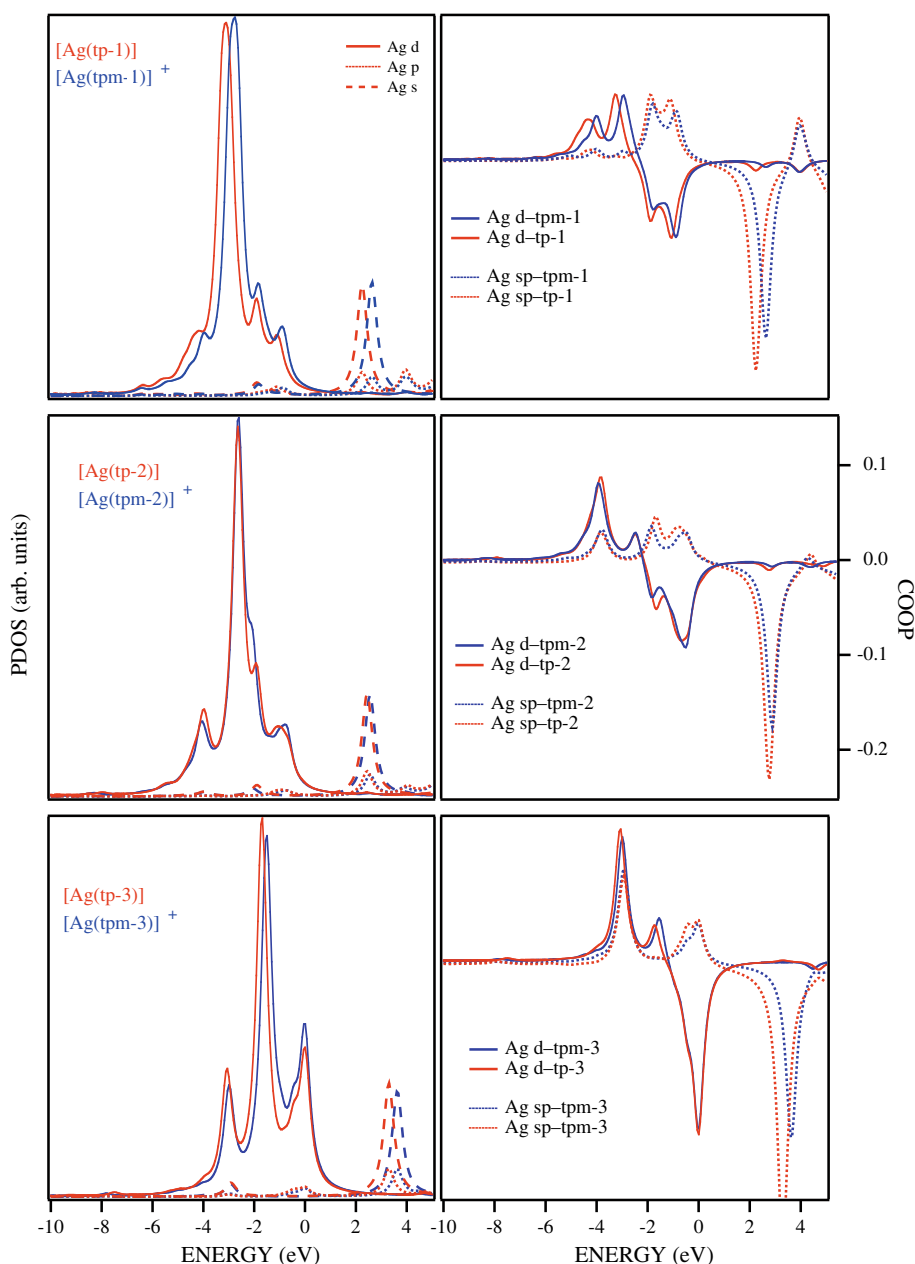


Fig. 5. (Left) d , s and p Ag PDOS of $[Ag(tp-n)]$ and $[Ag(tpm-n)]^+$; (right) Ag – $(tp-n)$ and Ag – $(tpm-n)$ COOP, bonding (antibonding) states correspond to positive (negative) peaks. The zero energy matches the HOMO energy of each species.

Table 4

Binding energy contributions (kcal/mol) to the interaction between M(L) and CO fragment (M = Cu,Ag; L=tp-3, tpm-3).

	M(tp-3)-CO	M(tpm-3)-CO
Cu ΔE_{Pauli}	127.44	109.34
Cu ΔE_{el}	-101.97	-92.23
Cu ΔE_{st}	25.46	17.11
Cu ΔE_{int}	-64.49	-56.14
Cu ΔE_{prep}	3.02	2.64
CuBSSE	0.81	0.96
CuBE	-35.20	-35.43
Q _{M(Ligand)} ^H	0.15	1.10
Q _{CO} ^H	-0.15	-0.10
Ag ΔE_{Pauli}	131.18	112.94
Ag ΔE_{el}	-101.53	-90.52
Ag ΔE_{st}	29.65	22.42
Ag ΔE_{int}	-58.35	-50.46
Ag ΔE_{prep}	0.42	0.01
AgBSSE	0.77	0.70
AgBE	-27.51	-27.33
Q _{M(Ligand)} ^H	0.11	1.05
Q _{CO} ^H	-0.11	-0.05

this conclusion, data reported in Table 3 indicate that the difference between the free tp and tpm charge (-1 and 0, respectively) has negligible effects on the final Q_M^H values, consistently with the rather close ^{Cu} $\Delta E_{\text{int}}(\text{tp-3})$ and ^{Cu} $\Delta E_{\text{int}}(\text{tpm-3})$ values. To clarify this discrepancy, we have carried out calculations also for the [M(tp-3)(CO)] and [M(tpm-3)(CO)]⁺ model complexes. We analyzed the results on the basis of the ETS scheme, considering as interacting fragments [M(tp-3)] and [CO] in one case, and [M(tpm-3)]⁺ and [CO] in the other one. Optimized coordinates of [Cu(tp-3)(CO)] (hereafter, ^{tp}I), [Cu(tpm-3)(CO)]⁺ (^{tpm}I), [Ag(tp-3)(CO)] (^{tp}II), and [Ag(tpm-3)(CO)]⁺ (^{tpm}II) are reported in Tables S15–S18, respectively, while interacting fragments Q^H and corresponding binding energies are collected in Table 4.

As far as the optimized structural parameters are concerned (see Tables S15–S18), both the Cu–CO (1.810 and 1.825 Å in ^{tp}I and ^{tpm}I, respectively) and C–O (1.153 and 1.146 Å in ^{tp}I and ^{tpm}I, respectively) bond lengths (BLs) are in reasonable agreement with experimental and theoretical data reported by Fujisawa et al. [5e]. The same holds for the ^{tp}II Ag–CO and C–O BLs (1.964 and 1.150 Å, respectively) which are quite similar to those experimentally determined by Dias and Jin [18] for the [Ag{HB(3,5-(CF₃)₂Pz₃)}(CO)] complex. No comparison with the ^{tp}II Ag–CO and C–O BLs (1.991 and 1.142 Å, respectively) is possible as crystallographic data pertaining to κ^3 -[Ag(tpm)(CO)]⁺-like species are unavailable.

The inspection of Table 4 results particularly useful to understand the [M(tp-3)]/[M(tpm-3)]-CO bonding interaction. In particular, we point out that carbon monoxide always carries a negative charge, i.e. it is a net electron acceptor; moreover, the absolute value of the charge is larger in the tp-based complexes than in the tpm-based ones. According to that, ν_{CO} (2039, 2090, 2049, 2105 cm⁻¹ in ^{tp}I, ^{tpm}I, ^{tp}II, and ^{tpm}II, respectively)⁶ is systematically red shifted with respect the harmonic theoretical value computed for the free CO (2113 cm⁻¹). Remarkably, the (^{tpm}I – ^{tp}I) $\Delta\nu_{\text{CO}}$ (51 cm⁻¹) exactly reproduces the experimental value reported by Fujisawa et al. [5e]. As a whole, these results confirm the conclusions reported on Ref. [5e]; however, taking advantage of the ETS analysis [11], we find that, despite the [Cu(tpm-3)]⁺ and [Ag(tpm-3)]⁺ positive fragments are weaker electron donor than the neutral [Cu(tp-3)] and [Ag(tp-3)] ones, the ΔE_{B} s between [Cu(tpm-3)(CO)]⁺ and

[Cu(tp-3)(CO)] as well as between [Ag(tpm-3)(CO)]⁺ and [Ag(tp-3)(CO)] are negligible. The reason is that the more negative ^M ΔE_{int} term in the neutral adducts is compensated by the less positive ^M ΔE_{st} contribution in the charged species.

4. Concluding remarks

In this contribution we have presented and discussed the results of a series of first-principle calculations carried out on the free tp ligand and its Cu(I) and Ag(I) complexes. The energetics of conformational transitions has been studied for the free ligand and for its complexes. Moreover, we analyzed the metal–ligand bonding showing that, independently of the coordinative mode, the covalent components are rather similar in M-tp and (M-tpm)⁺. However, the electrostatic interaction between M(I) and the negatively charged tp significantly strengthens the metal–ligand bond on passing from (M-tpm)⁺ to (M-tp). We have also considered the electronic and molecular properties of the adducts [Cu(tp-3)(CO)], [Cu(tpm-3)(CO)]⁺, [Ag(tp-3)(CO)], and [Ag(tpm-3)(CO)]⁺ showing that: (i) CO always behaves as an electron donor; (ii) the charged species [Cu(tpm-3)]⁺ and [Ag(tpm-3)]⁺ are weaker donor than the neutral ones; (iii) [M(tpm-3)(CO)]⁺ and [M(tp-3)(CO)] have, for each metal, the same binding energy.

Acknowledgments

This work was partially supported by the Italian PRIN funding n. 2006038447. The “Laboratorio Interdipartimentale di Chimica Computazionale” (LICC) at the Department of Chemistry of the University of Padova is acknowledged for support of the computer facilities.

Appendix A. Supplementary material

Supplementary data associated with this article can be found, in the online version, at doi:10.1016/j.ica.2009.02.004.

References

- [1] (a) C. Pettinari, R. Pettinari, *Coord. Chem. Rev.* 249 (2005) 525. and references therein reported; (b) C. Pettinari, C. Santini, *Compr. Coord. Chem.* II 1 (2004) 159; (c) S. Trofimenko, *Scorpionates*, The Coordination Chemistry of Polypyrazolylborate Ligands, Imperial College Press, 1999; (d) C. Pettinari, *Scorpionates II: Chelating Borate Ligands*, World Scientific Publishing, New York, 2008; (e) S. Trofimenko, *J. Chem. Ed.* 82 (2005) 1715; (f) S. Murtuza, O.L. Casagrande Jr., R.F. Jordan, *Polym. Mater. Sci. Eng.* 84 (2001) 109; (g) I. Santos, A. Paulo, J.D. Correia, *Top. Curr. Chem.* 252 (2005) 45; (h) T. Kitano, H. Wada, H. Mukai, K. Ueda, Y. Sohrin, *Anal. Sci.* 17 (2001) i1113; (i) A. de la Lande, H. Gérard, V. Moliner, G. Izzet, O. Reinaud, O. Parisel, *J. Biol. Inorg. Chem.* 11 (2006) 593.
- [2] (a) M. Paneque, S. Sirol, M. Trujillo, E. Gutiérrez-Puebla, M.A. Monge, E. Carmona, *Angew. Chem., Int. Ed.* 39 (2000) 218; (b) M. Paneque, S. Sirol, M. Trujillo, E. Carmona, E. Gutiérrez-Puebla, M.A. Monge, C. Ruiz, F. Malbosc, C. Serra-Le Berre, P. Kalck, M. Etienne, J.C. Daran, *Chem. Eur. J.* 7 (2001) 3868; (c) D.D. Ellis, J.C. Jeffery, P.A. Jelliss, J.A. Kautz, F.G.A. Stone, *Inorg. Chem.* 40 (2001) 2041.
- [3] M. Casarin, D. Forrer, F. Garau, L. Pandolfo, C. Pettinari, A. Vittadini, *J. Phys. Chem. A* 112 (2008) 6723.
- [4] C.C. McLauchlan, A.N. Varda, J.R. Giles, *Acta Crystallogr., Sect. E: Struct. Rep.* 60 (2004) o1419.
- [5] (a) H.V.R. Dias, W. Jin, H.-J. Kim, H.-L. Lu, *Inorg. Chem.* 35 (1996) 2317; (b) D.L. Reger, R.F. Semeniuc, M.D. Smith, *Eur. J. Inorg. Chem.* (2003) 3480; (c) J.P. Declercq, M. van Meerssche, *Acta Crystallogr., Sect. C: Cryst. Struct. Commun.* 40 (1984) 40; (d) L.E. Ochando, J. Rius, D. Louer, R.M. Claramunt, C. Lopez, J. Elguero, J.M. Amigo, *Acta Crystallogr., Sect. B: Struct. Sci.* 53 (1997) 939; (e) K. Fujisawa, T. Ono, Y. Ishikawa, N. Amir, Y. Miyashita, K. Okamoto, N. Lehnert, *Inorg. Chem.* 45 (2006) 1698; (f) B.S. Hammes, X. Luo, M.W. Carrano, C.J. Carrano, *Angew. Chem., Int. Ed.* 41 (2002) 3259.

⁶ Experimental ν_{CO} values reported by Fujisawa et al. [5d] for [Cu{HB(3,5-iPr₂pz₃)}(CO)] and [Cu{HC(3,5-iPr₂pz₃)}(CO)](PF₆) are 2056 and 2107 cm⁻¹, respectively. The blue shifted value reported by Dias and Jin [18] for [AgHB(3,5-(CF₃)₂Pz₃)}(CO)] (2162 cm⁻¹) is most probably due to the presence of CF₃ substituents on the pz rings.

- [6] H. De Bari, M. Zimmer, *Inorg. Chem.* 43 (2004) 3344. Database searches and analyses carried out by the authors were done by using the Conquest and Vista programs associated with Cambridge Structural Database13 (CSD) v5.24.
- [7] Amsterdam Density Functional (ADF) version 2007.01 <<http://www.scm.com>>.
- [8] (a) E. van Lenthe, E.J. Baerends, J.G. Snijders, *J. Chem. Phys.* 99 (1993) 4597; (b) E. van Lenthe, E.J. Baerends, J.G. Snijders, *J. Chem. Phys.* 101 (1994) 9783; (c) E. van Lenthe, A.W. Ehlers, E.J. Baerends, J.G. Snijders, *J. Chem. Phys.* 110 (1999) 8543.
- [9] (a) A.D. Becke, *Phys. Rev. A* 38 (1988) 3098; (b) J.P. Perdew, *Phys. Rev. B* 33 (1986) 8822.
- [10] E. van Lenthe, E.J. Baerends, *J. Comput. Chem.* 24 (2003) 1142.
- [11] T. Ziegler, A. Rauk, *Theor. Chim. Acta* 46 (1977) 1.
- [12] A. Rosa, A.W. Ehlers, E.J. Baerends, J.G. Snijders, G. te Velde, *J. Phys. Chem.* 100 (1996) 5690.
- [13] R.S. Mulliken, *J. Chem. Phys.* 23 (1955) 1833.
- [14] R. Hoffmann, *Solids and Surfaces: A Chemist's View of Bonding in Extended Structures*, VCH, New York, 1988.
- [15] (a) L.M. Mirica, X. Ottenwaelder, T.D.P. Stack, *Chem. Rev.* 104 (2004) 1013. and references therein reported; (b) E.A. Lewis, W.B. Tolman, *Chem. Rev.* 194 (2004) 1047; (c) N. Lehnert, U. Cornelissen, F. Neese, T. Ono, Y. Noguchi, K. Okamoto, K. Fujisawa, *Inorg. Chem.* 46 (2007) 3916.
- [16] (a) D.L. Reger, Y. Ding, *Polyhedron* 13 (1994) 869; (b) C. Gemel, R. John, C. Slugovc, K. Mereiter, R. Schmid, K. Kirchner, *J. Chem. Soc., Dalton Trans.* (2000) 2607; (c) J.S. Thompson, R.L. Harlow, J.F. Whitney, *J. Am. Chem. Soc.* 105 (1983) 3522; (d) J.S. Thompson, J.F. Whitney, *Acta Crystallogr., Sect. C: Cryst. Struct. Commun.* 40 (1984) 756; (e) Z. Hu, R.D. Williams, D. Tran, T.G. Spiro, S.M. Gorun, *J. Am. Chem. Soc.* 122 (2000) 3556; (f) E.R. Humphrey, Z. Reeves, J.C. Jeffery, J.A. McCleverty, M.D. Ward, *Polyhedron* 18 (1999) 1335; (g) M. Kujime, S. Hikichi, M. Akita, *Dalton Trans.* (2003) 3506; (h) A.J. Canty, N.J. Minchin, L.M. Engelhardt, B.W. Skelton, A.H. White, *J. Chem. Soc., Dalton Trans.* (1986) 645; (i) A.L. Rheingold, L.M. Liable-Sands, C.L. Incarvito, S. Trofimenko, *J. Chem. Soc., Dalton Trans.* (2002) 2297; (j) A.J. Canty, J.L. Hoare, B.W. Skelton, A.H. White, G. van Koten, *J. Organomet. Chem.* 552 (1998) 23; (k) J. Campora, P. Palma, D. del Rio, J.A. Lopez, E. Alvarez, N.G. Connelly, *Organometallics* 24 (2005) 3624; (l) M. Akita, T. Miyaji, S. Hikichi, Y. Moro-oka, *Chem. Commun.* (1998) 1005; (m) T. Miyaji, M. Kujime, S. Hikichi, Y. Moro-oka, M. Akita, *Inorg. Chem.* 41 (2002) 5286; (n) J.-M. Valk, F. Maassarani, P. van der Sluis, A.L. Spek, J. Boersma, G. van Koten, *Organometallics* 13 (1994) 2320; (o) M. Akita, T. Miyaji, N. Muroga, C. Mock-Knoblauch, W. Adam, S. Hikichi, Y. Moro-oka, *Inorg. Chem.* 39 (2000) 2096; (p) M. Kujime, S. Hikichi, M. Akita, *Organometallics* 20 (2001) 4049; (q) W. Klau, B. Turkowski, H. Wunderlich, *Z. Anorg. Allg. Chem.* 627 (2001) 2397; (r) M. Akita, T. Miyaji, S. Hikichi, Y. Moro-oka, *Chem. Lett.* (1999) 813; (s) A.J. Canty, H. Jin, A.S. Roberts, P.R. Traill, B.W. Skelton, A.H. White, *J. Organomet. Chem.* 489 (1995) 153; (t) P.E. Rush, J.D. Oliver, *Chem. Commun.* (1974) 996; (u) J.D. Oliver, N.C. Rice, *Inorg. Chem.* 15 (1976) 2741; (v) D.D. Wick, K.I. Goldberg, *J. Am. Chem. Soc.* 119 (1997) 10235; (w) S. Reinartz, P.S. White, M. Brookhart, J.L. Templeton, *J. Am. Chem. Soc.* 123 (2001) 12724; (x) S. Reinartz, P.S. White, M. Brookhart, J.L. Templeton, *Organometallics* 19 (2000) 3854; (y) D.L. Reger, J.C. Baxter, L. Lebioda, *Inorg. Chim. Acta* 165 (1989) 201.
- [17] F.L. Hirshfeld, *Theor. Chim. Acta* 44 (1977) 129.
- [18] H.V.R. Dias, W. Jin, *J. Am. Chem. Soc.* 117 (1995) 11381.

New coordination polymers based on the triangular $[\text{Cu}_3(\mu_3\text{-OH})(\mu\text{-pz})_3]^{2+}$ unit and unsaturated carboxylates†

Simone Contaldi,^a Corrado Di Nicola,^b Federica Garau,^{c,d} Yauhen Yu. Karabach,^d Luísa M. D. R. S. Martins,^{d,e} Magda Monari,^{*a} Luciano Pandolfo,^{*c} Claudio Pettinari^{*b} and Armando J. L. Pombeiro^{*d}

Received 5th January 2009, Accepted 3rd April 2009

First published as an Advance Article on the web 18th May 2009

DOI: 10.1039/b823370e

By reacting copper(II) acrylate with pyrazole (Hpz), two trinuclear copper derivatives $[\text{Cu}_3(\mu_3\text{-OH})(\mu\text{-pz})_3(\text{CH}_2=\text{CHCOO})_2(\text{H}_2\text{O})_2(\text{Hpz})]$, **1**, and $[\text{Cu}_3(\mu_3\text{-OH})(\mu\text{-pz})_3(\text{CH}_2=\text{CHCOO})_2(\text{CH}_3\text{OH})]$, **2**, are obtained, in water and methanol respectively, while copper(II) methacrylate affords $[\text{Cu}_3(\mu_3\text{-OH})(\mu\text{-pz})_3(\text{CH}_2=\text{C}(\text{CH}_3)\text{COO})_2]$, **3**, independently from the solvent used. In **1** and **2** two triangular trinuclear units are connected through acrylate bridges forming hexanuclear clusters that, in the case of **2** are further connected through double *syn-syn* carboxylate bridges, generating a 1-D coordination polymer. In the case of **3** a different 1-D coordination polymer is obtained by alternating *syn-syn* and *syn-anti* double carboxylate bridges connecting the trinuclear clusters. In all cases H-bonds contribute both to the stabilization of these arrangements and to the formation of more extended supramolecular networks. Compounds **1–3** are valuable catalysts in the peroxidative oxidation with aqueous H_2O_2 , in MeCN at 25 °C, of cycloalkanes (*i.e.* cyclohexane and cyclopentane) to the corresponding ketones and alcohols (overall yield up to 36%, TON = 36), following a radical mechanism as shown by radical trap experiments, and the effects of various factors are studied. Electrochemical experiments show that the copper(II) centres are reduced to copper(I) and copper(0).

Introduction

In the last decade, the construction of 1-D, 2-D and 3-D Coordination Polymers (CPs) has shown an impressive growth, due not only to the fascinating structural characteristics often found in these compounds, but also to their possible applications as sensors, in catalysis, gas storage, adsorption *etc.*¹ Multidimensional CPs are mainly formed by connecting single metal ions with polynucleating ligands,^{1/2} but often it is possible to identify small aggregates (normally di- tri- or tetra-nuclear metal clusters), the so called Secondary Building Units (SBUs), whose (self)assemblies may generate CPs.²

Trinuclear copper clusters with trigonal symmetry are of interest both in terms of industrial applications and understanding the mechanism of action of copper-containing enzymes.³ As an example, some trinuclear copper(II) triethanolamine derivatives

are highly active and selective catalysts or catalyst precursors for the peroxidative oxidation of cyclohexane, in acetonitrile, to a cyclohexanol and cyclohexanone mixture, by aqueous hydrogen peroxide in acidic medium (liquid biphasic catalysis)⁴ and are also relevant in the studies aiming to discover the role played by copper in multicopper oxidases, such as tree and fungal laccase, ascorbate oxidase, ceruloplasmin, Fe3tp, CotaA and CueO.⁵ Moreover, polynuclear copper complexes have been developed for the efficient and selective 1,6-addition of a nucleophile to the para-methyl group of 2,4,6-trimethylphenol⁶ or for the catalytic decomposition of dimethyldioxirane and cyclic acetone triperoxide.⁷

In the last few years we have developed a procedure to obtain trinuclear triangular copper(II) complexes, containing the $[\text{Cu}_3(\mu_3\text{-OH})(\mu\text{-pz})_3]^{2+}$ core (pz = pyrazolate), by reacting pyrazole (Hpz) with $\text{Cu}(\text{RCOO})_2$ (R = H, CH_3 , CH_2CH_3 , $\text{CH}_2(\text{CH}_2)_2$), in protic solvents (water, alcohols), according to Scheme 1.⁸

These trinuclear clusters self-assemble through carboxylate bridges, often supported by H-bonds, to form hexanuclear systems, 1-, 2- and 3-D CPs, showing, in most cases, interesting molecular and supramolecular features.⁸ Moreover, it was also possible to exchange, partly or completely, the carboxylate ions with: (i) Cl^- ,⁹ (ii) other anions (SO_4^{2-} , ClO_4^- , CF_3COO^- , CF_3SO_3^- , NO_3^-)^{10a} and (iii) neutral dinucleating 4,4'-dipyridine-based ligands^{10b} obtaining, in some cases,^{9,10b} microporous CPs. Finally, most of the above reported compounds are active catalysts (or catalyst precursors) for the peroxidative oxidation of cycloalkanes.^{8e,11}

Here we report the isolation and the structural characterization of three new copper(II) trinuclear triangular derivatives based on unsaturated carboxylates, namely acrylate and methacrylate, which self-assemble in different ways through bridging carboxylates, forming hexanuclear clusters and 1-D CPs, that further

^aDip. di Chimica "G. Ciamician", Università di Bologna, Via Selmi, 2, I-40126, Bologna, Italy. E-mail: magda.monari@unibo.it; Fax: +39 051 2099456; Tel: +39 051 2099559

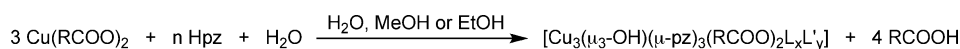
^bDip. di Scienze Chimiche, Università di Camerino, Via S. Agostino, 1, I-62032, Camerino, (MC), Italy. E-mail: claudio.pettinari@unicam.it; Fax: +39 0737 637345; Tel: +39 0737 402234

^cDip. di Scienze Chimiche, Università di Padova, Via Marzolo, 1, I-35131, Padova, Italy. E-mail: luciano.pandolfo@unipd.it; Fax: +39 049 8275161; Tel: +39 049 8275157

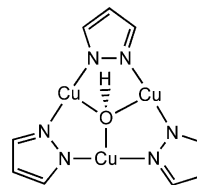
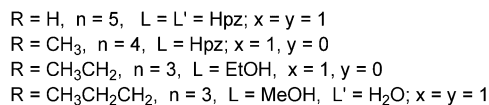
^dCentro de Química Estrutural, Complexo I, Instituto Superior Técnico, TU Lisbon, Av. Rovisco Pais, 1049-001, Lisbon, Portugal. E-mail: pombeiro@ist.utl.pt; Fax: +351 218464455; Tel: +351 218419237

^eDepartamento de Engenharia Química, ISEL, R. Conselheiro Emídio Navarro, 1950-062, Lisbon, Portugal

† Electronic supplementary information (ESI) available: Fig. S1–S15. CCDC reference numbers 715327–715329. For ESI and crystallographic data in CIF or other electronic format see DOI: 10.1039/b823370e



recryst. from H₂O, MeOH or EtOH



Scheme 1

develop into more extended supramolecular networks through H-bonds. The electrochemical properties of these compounds as well as their catalytic behaviour in the peroxidative oxidation of cycloalkanes are also illustrated.

Discussion

The reactions of copper(II) acrylate and methacrylate with Hpz in water or alcohols produce deep blue solutions from which blue crystalline solids are obtained. Actually, the reactions of copper acrylate in water or MeOH yielded compounds **1** and **2**, respectively, while copper methacrylate generated compound **3**, independently from the solvent used. Experimental results indicate that compounds **1–3** have trinuclear triangular structures, analogous to those found when Hpz was reacted with copper(II) saturated carboxylates,^{8,12} *i.e.* the $[\text{Cu}_3(\mu_3\text{-OH})(\mu\text{-pz})_3]^{2+}$ core, whose charge is neutralized by two carboxylates.

In detail, the detection of acrylic and methacrylic acid in the mother liquors of the syntheses of **1–3** is indicative of the occurrence of the protonation of carboxylates by water and pyrazole, thus generating OH[−] and pyrazolate ions that are fundamental constituents of the triangular skeleton, according to Scheme 1.

Solid-state IR spectra of **1–3** are in agreement with the aforementioned identification, showing the presence of carboxylate ions that are differently coordinated to Cu ions and revealing also the presence of other neutral ligands. In particular, taking into account that the carboxylates can coordinate to the metal ions in a bidentate or monodentate fashion, on the basis of Δ criterion [Δ = difference between $\nu_{\text{asym}}(\text{COO})$ and $\nu_{\text{sym}}(\text{COO})$] we can conclude that in **1–3** one or both unsaturated carboxylates adopt bridging mono- or bidentate, coordination modes with Δ values falling around *ca.* 120 cm^{−1},¹³ very close to that found in the precursor copper(II) acrylate and reported for the dinuclear $[\text{Cu}_2(\text{CH}_2=\text{CHCOO})_4(\text{H}_2\text{O})_2]$ cluster.¹⁴ Moreover, the IR spectra of **1–3** always show two signals at *ca.* 1639 cm^{−1} [$\nu(\text{C}=\text{C})$, $\nu(\text{C}=\text{N})$] and 760 cm^{−1} $\delta(\text{CH})_{\text{oop}}$ which correspond to bridging pyrazolate ligands.¹⁵ The presence in **1** of an NH stretching vibration at 3235 cm^{−1} suggests the coordination of Hpz. At a difference with **1** a broad absorption centred at *ca.* 3400 cm^{−1}, due to the H-bonded OH group of coordinated methanol, is observed in **2**, while no NH stretching vibration around 3200 cm^{−1} is present. It has been proposed that the appearance and the structure of conjugated hydrogen bonds depend on the variety of the association forms and on the values of the angles between the donor and the acceptor sites.¹⁶ The NH stretching vibration centred in **1** at 3235 cm^{−1} is typical of systems exhibiting angles of

ca. 120°¹⁷ and this is in accordance with our experimental results (*vide infra*).

Also the ¹H NMR spectra of **1–3** in *d*₃-methanol confirms the presence of pyrazolate moieties. Besides high-field signals due to carboxylate hydrogens, in all spectra two low-field broad signals at *ca.* 37 and 41 ppm, integrating in a 2:1 ratio have been assigned to H⁽³⁾ plus H⁽⁵⁾ and H⁽⁴⁾ pyrazolate hydrogens, respectively, analogously to that found in other copper(II) trinuclear triangular pyrazolate derivatives.^{11,18}

ESI mass spectra suggest the presence of polynuclear assemblies, evidencing signals corresponding to trinuclear and/or hexanuclear copper(II) species.

Λ_{M} values for MeOH solutions of **1–3** fall around 20 $\mu\text{S}/\text{cm}$, analogously to previously reported data on similar derivatives,^{8,11} in the range typical of almost completely non-ionic derivatives.

Room temperature magnetic susceptibilities, with values falling in the range 2.09–2.17 BM, are lower than those expected for three independent copper(II) ions and indicate some kind of exchange coupling, as has been found with strictly related derivatives.^{8,10a,11}

Finally, solid-state reflectance electronic spectra of **1–3**, (Fig. 1a) show similar complex patterns. The spectra are slightly modified in MeOH solutions, where almost identical broad bands centred at 615 nm are observed (Fig. 1b). These spectra, both in solid-state and solution, closely resemble those of related trinuclear triangular derivatives having saturated carboxylates,^{8,11} Cl[−],⁹ SO₄^{2−}, ClO₄[−], CF₃COO[−], CF₃SO₃[−] or NO₃[−]^{10a} as coordinated or uncoordinated anion(s).

For compounds **1–3** the trinuclear triangular arrangement, $[\text{Cu}_3(\mu_3\text{-OH})(\mu\text{-pz})_3]^{2+}$, has been confirmed by single crystal XRD studies and the solid state molecular structures of **1–3** are shown in Fig. 2, while selected bond lengths and angles are reported in Table 1.

Two of the three copper(II) centres are coordinated by one carboxylate ligand and neutral molecules complete the coordination spheres of Cu(3) and Cu(1) in **1** and only Cu(1) in **2**. In all structures the $\mu_3\text{-OH}$ capping ions are placed slightly out of the plane defined by the three Cu(II) centres, with similar O...Cu₃ plane distances [0.483(4) (**1**), 0.424(3) (**2**), and 0.424(2) (**3**)] falling in the range observed in analogous derivatives.^{8,9,10a,18,19}

Besides the molecular structures of **1–3** are clearly very similar to each other, the supramolecular arrangements of the $[\text{Cu}_3(\mu_3\text{-OH})(\mu\text{-pz})_3]^{2+}$ triangles show relevant differences, mainly due to the different coordination modes that carboxylates can adopt. Some of the most frequently observed coordination modes are sketched in Chart 1.

The molecular structure of **1** (Fig. 2a), shows that the two acrylate ions coordinate in different ways, the first one

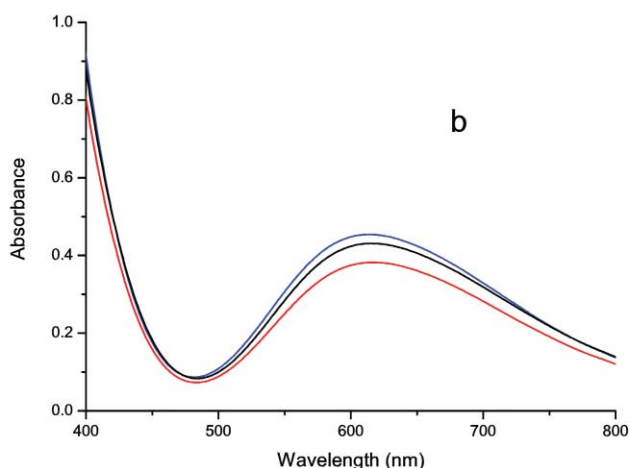
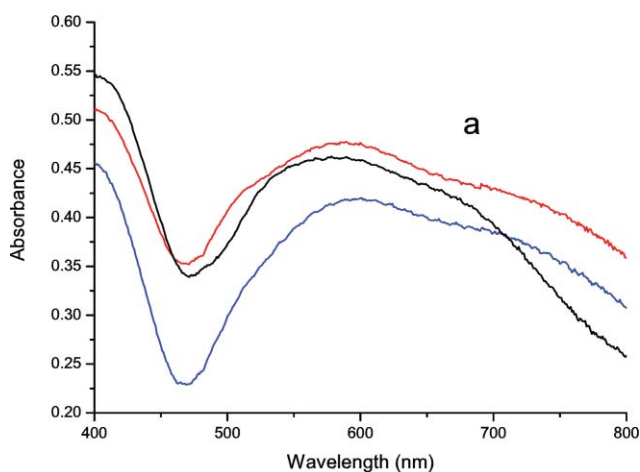


Fig. 1 Solid-state reflectance (a) and MeOH solution (b) electronic spectra of **1** (red), **2** (blue), and **3** (black).

Table 1 Selected bond lengths (Å) and angles (deg) for **1**, **2** and **3**

	1	2	3
Cu(1)–O(1)	2.002(4)	2.007(3)	2.006(2)
Cu(2)–O(1)	1.977(4)	1.991(3)	2.002(2)
Cu(3)–O(1)	1.994(4)	1.976(3)	1.978(1)
Cu(1)–N(1)	1.948(5)	1.944(4)	1.950(2)
Cu(1)–N(6)	1.942(5)	1.947(4)	1.958(2)
Cu(2)–N(2)	1.951(5)	1.943(4)	1.938(2)
Cu(2)–N(3)	1.948(5)	1.938(4)	1.944(2)
Cu(3)–N(4)	1.937(5)	1.944(4)	1.930(2)
Cu(3)–N(5)	1.957(5)	1.933(4)	1.931(2)
Cu(1)–O(2)	1.995(4)	2.005(3)	1.975(2)
Cu(2)–O(4)	1.968(4)		1.953(2)
Cu(3)–O(6w)	2.422(5)		
Cu(3)–N(7)	2.019(5)		
Cu(1)–O(7w)	2.340(6)		
Cu(1)–O(6)		2.344(4)	
Cu(2)–O(4)		1.985(3)	
Cu(3)–O(3) ^a		1.954(3)	
Cu(1)–O(1)–Cu(2)	116.49(19)	116.35(15)	116.26(7)
Cu(1)–O(1)–Cu(3)	110.35(19)	115.56(15)	114.52(7)
Cu(2)–O(1)–Cu(3)	116.07(19)	114.85(14)	116.06(7)

^a Symmetry operation used to generate equivalent atoms: (I) $-x + 1, -y, -z$.

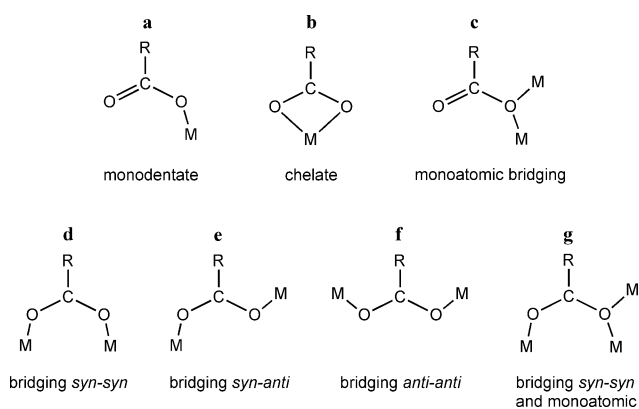


Chart 1

[O(3)C(10)O(2)] asymmetrically chelating Cu(1) (Chart 1b) [O(2)–Cu(1) 1.995(4), O(3)–Cu(1) 2.741(5) Å], while O(4) of the second one [O(4)C(13)O(5)] coordinates in a monoatomic fashion to Cu(2) [O(4)–Cu(2) 1.968(4) Å]. The coordination sphere of Cu(3) comprises also a neutral pyrazole and a water molecule [Cu(3)–N(7) 2.019(5) Å, Cu(3)–O(6w) 2.422(5) Å], while a second water molecule coordinates to Cu(1) [Cu(1)–O(7w) 2.340(6) Å]. A square planar pyramidal coordination geometry is observed around Cu(1), with O(7w) of a water molecule in the axial position, while at Cu(3) the O(6w) occupies the axial position of a slightly distorted square pyramid. Finally, besides O(4), the two nitrogens N(3) and N(2) belonging to two different pyrazolates and the central oxygen O(1)H, Cu(2) is further coordinated by the O(4') atom of the carboxylate pertaining to an adjacent trinuclear unit [Cu(2)–O(4') 2.426(4) Å, symmetry code (I): $-x + 1, -y, -z$], which occupies the axial position of a slightly distorted square pyramid. The inversion centre located midway along the Cu(2)···Cu(2') axis generates an assembly that can be rationalized in terms of centrosymmetric pairs of trinuclear systems joined by O(4) which doubly bridges the Cu(2)···Cu(2') vector [Cu(2)···Cu(2') 3.426(2) Å]. This kind of bridging monoatomic interaction (Chart 1c) generates hexanuclear clusters (Chart 2), an arrangement already observed in the related butyrate derivative, [Cu₃(μ₃-OH)(μ-pz)₃(CH₃(CH₂)₂COO)₂(MeOH)(H₂O)].^{8b}

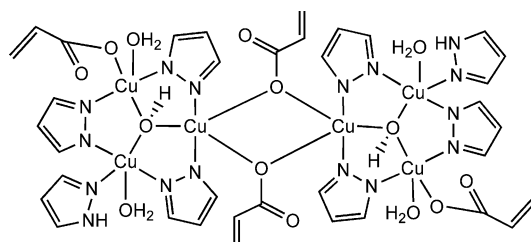


Chart 2

The Cu(2)–O(4') coordination is only the most evident supramolecular interaction present in **1**. Two intramolecular H-bonds involving the hydrogen and oxygen of the water molecule coordinated to Cu(3) are observed as a hydrogen donor with the carboxylate oxygen O(3) [O(3)···O(6w) 2.774(6) Å, O(3)···H(61w)–O(6) 162(6)°], and as a hydrogen acceptor with the NH of

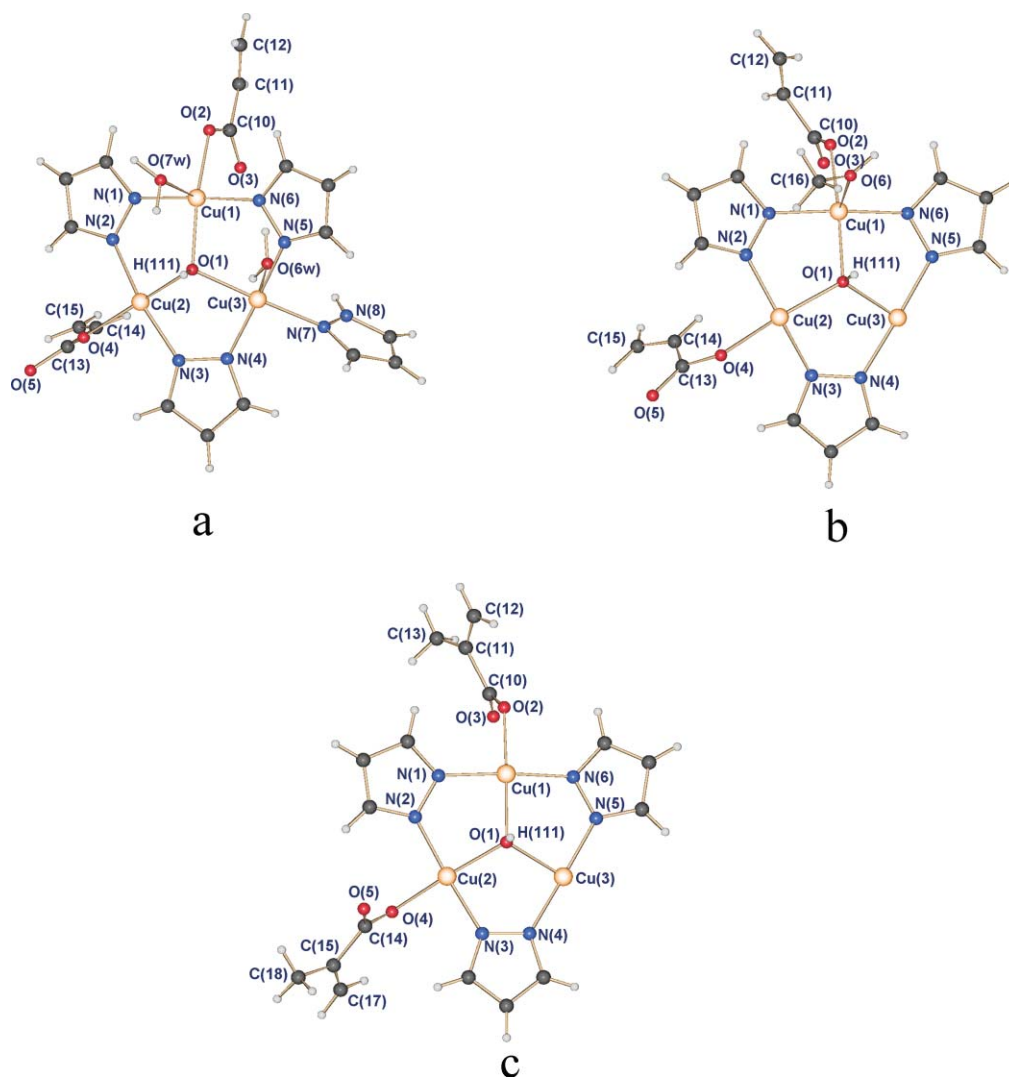


Fig. 2 View of the monomeric units of **1** (a), **2** (b) and **3** (c) with the numbering scheme.

coordinated pyrazole [N(8)⋯O(6w) 2.745(8) Å, N(8)⋯H(8a)–O(6) 130°]. Moreover, two other strong H-bonds, both involving the uncoordinated oxygen of the bridging carboxylate O(5) are present. Particularly, O(5) interacts (*i*) with μ_3 -OH [O(5)⋯O(1') 2.717(6) Å, O(5)⋯H(111')–O(1') 166(6)°] and (*ii*) with a water molecule coordinated to Cu(1) [O(5)⋯O(7w') 2.936(7) Å, O(5)⋯H(71w')–O(7') 167(8)°] of the second trinuclear unit, in both cases reinforcing the hexanuclear clusters (Fig. 3).

The hexanuclear clusters self-assemble generating a 1D supramolecular network running down the crystallographic *a* axis, through intermolecular H-bonds involving O(3) and the water coordinated to Cu(3) ions of two adjacent hexanuclear units [O(3)⋯O(6w'') 2.757(7) Å, O(3)⋯H(6w'')–O(6w'') 166(7)°, symmetry code (II): $-x + 2, -y, -z$], (Fig. 4).

Parallel 1-D networks further self-assemble through a series of H-bonds involving carboxylate O(2) and water coordinated to Cu(1) [O(2)⋯O(7w''') 2.833(7) Å, O(2)⋯H(7w''')–O(7''') 152(8)°, symmetry code (III): $-x + 2, -y + 1, -z$], giving rise to a 2-D supramolecular polymeric network (Fig. 5), similar to that found in the already mentioned butyrate derivative.^{8b}

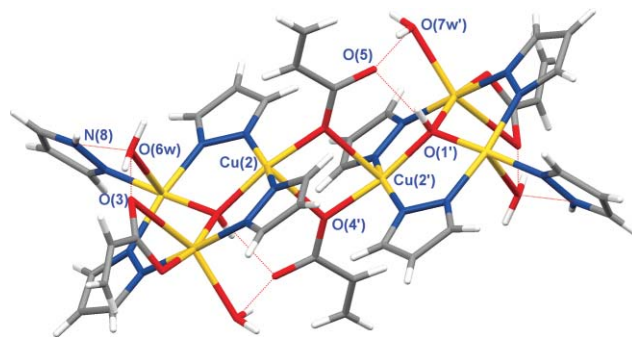


Fig. 3 View of the hexanuclear cluster of **1** generated by an inversion centre located midway along the Cu(2)–Cu(2') vector (symmetry code (I): $-x + 1, -y, -z$). Intramolecular H bonds are represented as red dashed lines.

Moreover, the crystal packing shows also that couples of double bonds of chelating acrylates [C(11)=C(12)] pertaining to adjacent hexanuclear units, lie parallel to each other with a centre-to-centre distance of *ca.* 3.82 Å, a value largely below 4.2 Å, that, according

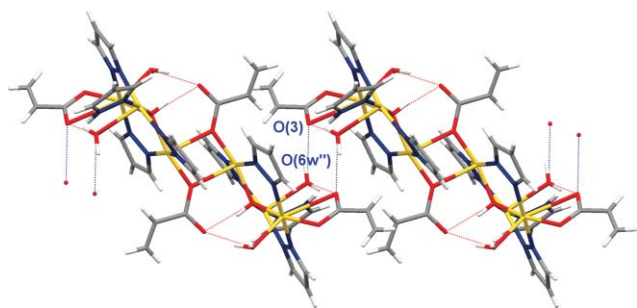


Fig. 4 Arbitrary view of one chain of hexanuclear clusters of **1**, running along the *a* axis, arising by formation of intermolecular H bonds (blue dashed lines) involving one oxygen [O(3)] of chelating carboxylate groups and one hydrogen of the water coordinated to Cu(3) of neighbour hexanuclear dimers. Symmetry code (II): $-x + 2, -y, -z$.

to the Schmidt rule, allows topochemical [2 + 2] cycloaddition in the solid-state.²⁰ Nevertheless, a careful inspection reveals that the above mentioned double bonds are off-set with respect to each other by *ca.* 40°, an arrangement which could hamper the cycloaddition.²¹ The possibility to photochemically induce in **1** a solid-state [2 + 2] cycloaddition, has been ruled out by UV irradiation of a powdered crystalline sample. Even after long exposure (see Experimental section) compound **1** did not react, as revealed by the persistence of the signal due to C=C stretching at 1635 cm⁻¹ after irradiation (see Fig. S2 ESI†).

Finally, a careful inspection of the crystal packing of **1** reveals, the presence of irregular channels running parallel to the crystallographic *b* axis with a very small free opening (*ca.* 1.3 Å, taking into account the vdW radii, see Fig. S1 ESI†).

The solid-state structure of **2** (Fig. 2b) is similar to that of **1**, nevertheless, it is possible to find some important differences. The carboxylates coordinate, both in a monodentate fashion, to Cu(1) [Cu(1)–O(2) 2.005(3) Å] and Cu(2) [Cu(2)–O(4) 1.985(3) Å]. Cu(1) is coordinated also by a MeOH molecule [Cu(1)–O(6) 2.344(4) Å] in the axial position of a slightly distorted square pyramid. In such a way the coordination geometry around Cu(1)

is complete, while the description of the geometries of Cu(2) and Cu(3) is complicated by the coordination of carboxylate oxygens pertaining to other trinuclear units. Analogously to **1**, hexanuclear clusters are formed through a four-membered ring constituted by two acrylates asymmetrically bridging the Cu(2)···Cu(2') vector (Chart 1c) [Cu(2)–O(4') 2.455(3) Å, symmetry code (I): $-x, -y + 2, -z$]. Thus, the coordination geometry around Cu(2) is slightly distorted square pyramidal, with O(4') placed in the axial position and the Cu(2)···Cu(2') distance [3.462(1) Å] almost identical to that of **1**. Also in this case the hexanuclear assembly is further stabilized by symmetric H-bonds involving O(5) and μ₃-OH of the second trinuclear unit [O(5)···O(1') 2.747 Å (5), O(5)···H(111')–O(1') 146(4)°] (Fig. 6).

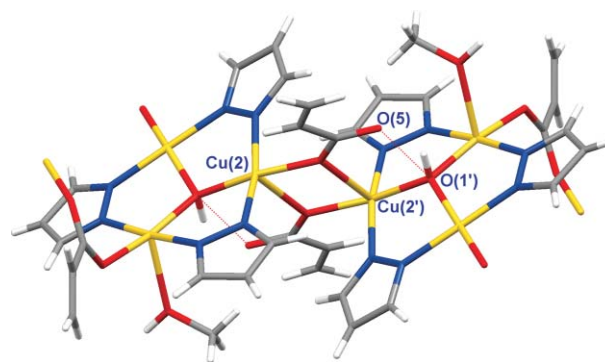


Fig. 6 View of the hexanuclear cluster of **2** generated by an inversion centre located midway along the Cu(2)–Cu(2') vector (symmetry code (I): $-x, -y + 2, -z$). Intramolecular H bonds are represented as red dashed lines.

Cu(3) exhibits a square-planar coordination as the hexanuclear units are linked to each other through two *syn-syn* carboxylate bridges [Cu(3)–O(3'')–C(10'')–O(2'')–Cu(1'') and Cu(3'')–O(3)–C(10)–O(2)–Cu(1), Cu(3'')–O(3) 1.954(3) Å, symmetry code (II): $1 - x, 2 - y, 1 - z$], with the geometry shown in Chart 1d, forming 12-membered rings and, consequently, a 1-D CP (Fig. 7) having

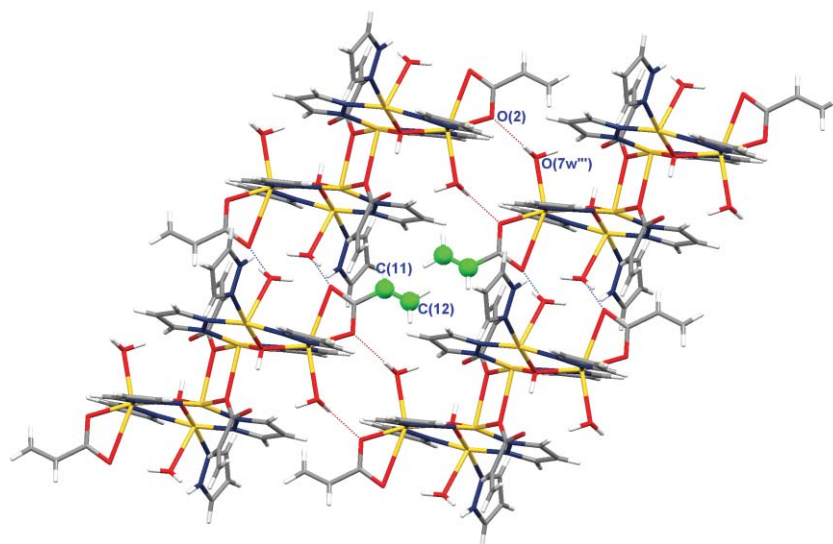


Fig. 5 Crystal packing of **1** showing the 2-D supramolecular network established by intermolecular H bonds. Symmetry code (III): $-x + 2, -y + 1, -z$.

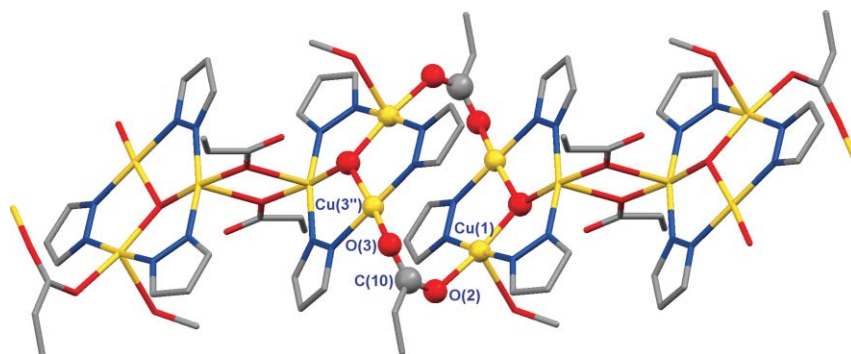


Fig. 7 View of one monodimensional CP (running along the diagonal of the *ac* plane) originated by hexanuclear clusters of **2** that are connected to each other by two *syn-syn* carboxylate bridges forming 12-membered macrocycles (ball and stick style). Hydrogens have been omitted for clarity. Symmetry code (II): $1 - x, 2 - y, 1 - z$.

a supramolecular structure very similar to that found in the propionate derivative $[\text{Cu}_3(\mu_3\text{-OH})(\mu\text{-pz})_3(\text{CH}_3\text{CH}_2\text{COO})_2(\text{EtOH})]$.^{8b}

Parallel 1-D CPs self-assemble generating a 2-D network, through a series of equivalent H-bonds. Actually, O(5) atoms are involved, besides the H-bond with $\mu_3\text{-OH}$, into relevant interactions with OH of coordinated methanol of adjacent 1-D CPs $[\text{O}(5) \cdots \text{O}(6'')] 2.814 \text{ \AA}$, $[\text{O}(5) \cdots \text{H}(61'')\text{-O}(6'')] 167(5)^\circ$, symmetry code (III): $x - 1, y, z$], as depicted in Fig. 8.

Finally, also in the case of **2**, the inspection of the crystal packing reveals the existence of irregular channels running parallel to the crystallographic *c* axis with a very narrow free opening (*ca.* 1.3 Å, taking into account the vdW radii, see Fig. S3 ESI†).

In **3** (Fig. 2c) the two methacrylate ions coordinate, both in a monodentate fashion, to Cu(2) $[\text{Cu}(2)\text{-O}(4) 1.953(2) \text{ \AA}]$ and Cu(1) $[\text{Cu}(1)\text{-O}(2) 1.975(2) \text{ \AA}]$, but, contrarily to **1** and **2**, no solvent or other neutral molecules coordinate to copper(II) ions and the previously observed hexanuclear clusters, obtained through two asymmetric monoatomic oxygen bridges, are absent. Instead, both Cu(2) and Cu(3) have square planar geometry, while Cu(1) shows a square pyramidal environment due to the coordination in an axial position of a carboxylate oxygen $[\text{O}(5'')]$ of another trinuclear unit. Each trinuclear unit shows two relevant

supramolecular interactions, being connected to other two units forming two different sets of 12-membered rings. The first one, similar to that present in compound **2**, involves two *syn-syn* carboxylate bridges (Chart 1d) $[\text{Cu}(3)\text{-O}(3')\text{-C}(10')\text{-O}(2')\text{-Cu}(1')$ and $\text{Cu}(3')\text{-O}(3)\text{-C}(10)\text{-O}(2)\text{-Cu}(1)$, $\text{Cu}(3)\text{-O}(3')$ 1.971(2) Å, symmetry code (I) $-x + 2, -y + 2, -z + 2]$, while in the formation of the second one two *syn-anti* carboxylate bridges are involved (Chart 1e) $[\text{Cu}(1)\text{-O}(5'')\text{-C}(14'')\text{-O}(4'')\text{-Cu}(2'')$ and $\text{Cu}(1'')\text{-O}(5)\text{-C}(14)\text{-O}(4)\text{-Cu}(2)$, $\text{Cu}(1)\text{-O}(5'')$ 2.392(2) Å, symmetry code (II): $-x + 1, -y + 2, -z + 2]$. Thus, the trinuclear units assemble in an unprecedented 1-D CP running along the crystallographic *a* axis (Fig. 9), alternating the two types of 12 membered rings. Only one relevant kind of H-bond is present in the 1-D chain, involving the hydrogen of the capping $\mu_3\text{-OH}$ and one oxygen of the *syn-anti* bridging carboxylate $[\text{O}(5)]$ $[\text{O}(5) \cdots \text{O}(1') 2.747(2) \text{ \AA}$, $\text{O}(5) \cdots \text{H}(111') 2.14(2) \text{ \AA}$, $\text{O}(5) \cdots \text{H}(111') \cdots \text{O}(1') 133(2)^\circ]$ (see Fig. S4 ESI†). In the 1-D CP the trinuclear units are parallel to each other and the distances between the planes defined by Cu(1), Cu(2) and Cu(3) are *ca.* 3.067 and 3.806 Å, as evidenced in Fig. S5 ESI†).

Crystal packing of **3** shows that 1-D polymeric rows are strictly stacked and parallel to each other down the crystallographic *a* axis

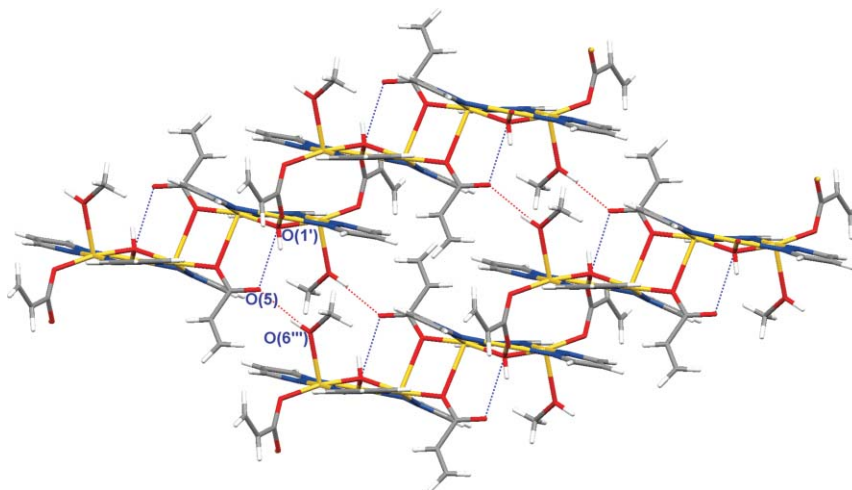


Fig. 8 Crystal packing of **2** showing the 2-D network generated by intermolecular H bonds (red dashed lines) between parallel 1-D CPs. Symmetry code (I): $-x, -y + 2, -z$, (III): $x - 1, y, z$.

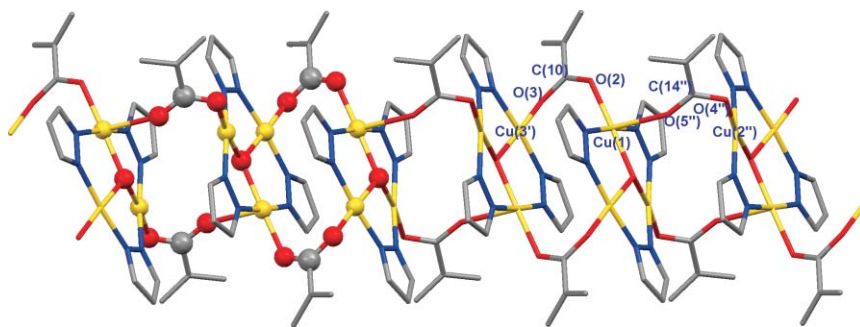


Fig. 9 Crystal packing of **3** showing the polymeric 1-D CP running along the *a* axis generated by trinuclear units of **3** joined together by alternating two *syn-syn* and two *syn-anti* carboxylate bridges forming two types of 12-membered macrocycles (ball and stick style). Hydrogens have been omitted for clarity. Symmetry code (I): $-x + 2, -y + 2, -z + 2$, (II) $-x + 1, -y + 2, -z + 2$.

and evidences the absence of any channel or opening (see Fig. S6 ESI†).

Analogously to the previously reported trinuclear triangular copper(II) derivatives with saturated carboxylates^{8c,11} and SO_4^{2-} , ClO_4^- , CF_3COO^- , CF_3SO_3^- , NO_3^- anions,^{10a} the electrochemical behaviour and the catalytic performances in the peroxidative oxidation of cycloalkanes of compounds **1–3** have been examined.

Electrochemical behaviour of 1–3

The redox properties of **1–3** have been investigated by cyclic voltammetry (CV), at a Pt disc electrode, in a 0.2 M [$^n\text{Bu}_4\text{N}$][BF_4]/DMSO solution, at room temperature.

All the compounds exhibit two single-electron (per metal ion) irreversible reduction waves, assigned to the $\text{Cu}^{\text{II}} \rightarrow \text{Cu}^{\text{I}}$ and $\text{Cu}^{\text{I}} \rightarrow \text{Cu}^0$ reductions, at the reduction peak potential values given in Table 2 ($^{\text{I}}E_{\text{p}}^{\text{red}}$ range from -0.33 to -0.38 V vs. SCE, and $^{\text{II}}E_{\text{p}}^{\text{red}}$ between -1.44 and -1.57 V vs. SCE) (Fig. 10 for complex **3**). A new irreversible anodic wave ($^{\text{I}}E_{\text{p}}^{\text{ox}}$ in the range 0.24 – 0.34 V vs. SCE) is observed upon scan reversal after the first reduction wave (Fig. 10 for complex **3**), corresponding to the oxidation of the Cu^{I} species formed at the first reduction process. No oxidation wave has been detected for any complex by a first anodic sweep without a previous reduction scan, indicating that neither a metal centred nor a ligand centred oxidation is observed.

The three complexes are characterized by the same behaviour in CV, and the shape of their cyclic voltammograms is almost identical to that of other trinuclear triangular copper(II) com-

Table 2 Cyclic voltammetric data^a for complexes **1–3**

Complex ^b	Cathodic waves		Anodic wave ^c
	$^{\text{I}}E_{\text{p}}^{\text{red}}$	$^{\text{II}}E_{\text{p}}^{\text{red}}$	$^{\text{I}}E_{\text{p}}^{\text{ox}}$
1 ^d [$\text{Cu}_3(\text{CH}_2=\text{CHCOO})_2(\text{H}_2\text{O})_2(\text{Hprz})$]	-0.33	-1.44	0.34
2 ^d [$\text{Cu}_3(\text{CH}_2=\text{CHCOO})_2(\text{MeOH})$]	-0.38	-1.50	0.33
3 [$\text{Cu}_3\{\text{CH}_2=\text{C}(\text{CH}_3)\text{COO}\}_2$]	-0.33	-1.57	0.24

^a Potential values in Volt ± 0.02 vs. SCE, in a 0.2 M [$^n\text{Bu}_4\text{N}$][BF_4]/DMSO solution, at a Pt disc working electrode, determined by using the [$\text{Fe}(\eta^5\text{-C}_5\text{H}_5)_2$]^{0/+} redox couple ($E_{1/2}^{\text{ox}} = 0.44$ V vs. SCE) as internal standard at a scan rate of 200 mV s^{-1} . ^b $\text{Cu}_3 = \text{Cu}_3(\mu_3\text{-OH})(\mu\text{-pz})_3$. ^c Only observed upon scan reversal following the corresponding reduction wave I^{red} . ^d A second irreversible anodic wave ($^{\text{II}}E_{\text{p}}^{\text{ox}} = -0.12$ V vs. SCE for **1** and $^{\text{II}}E_{\text{p}}^{\text{ox}} = -0.11$ V vs. SCE for **2**) is formed upon scan reversal after the reduction wave II^{red} .

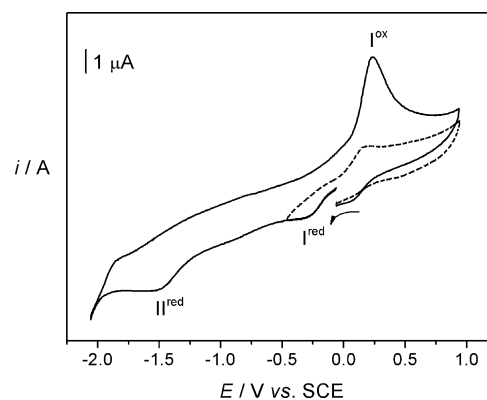


Fig. 10 Cyclic voltammogram of [$\text{Cu}_3(\mu_3\text{-OH})(\mu\text{-pz})_3\{\text{CH}_2=\text{C}(\text{CH}_3)\text{-COO}\}_2$], **3**, in a 0.2 M [$^n\text{Bu}_4\text{N}$][BF_4]/DMSO solution, at a Pt disc working electrode ($d = 0.5$ mm), at a scan rate of 200 mV s^{-1} .

pounds previously studied by us.^{10a,11} It was not necessary to run controlled potential electrolysis experiments to measure the numbers of electrons transferred, since the occurrence of a single-electron reduction per Cu^{II} (or Cu^{I}) atom was confirmed by the similarity of the current functions ($i_{\text{p}} \text{ C}^{-1} \text{ v}^{-1/2}$) of the reduction waves of our complexes with those of other similar trinuclear complexes.^{10a,11} Any of the cathodic waves involves the reduction of the three metal ions, without any detected differentiation. In any case, it is not possible to rule out any metal–metal electronic communication because of the broadness of the reduction waves; these, in fact, can result from the overlap of distinct waves at close but distinct potentials, namely $\text{Cu}^{\text{II}}\text{Cu}^{\text{II}}\text{Cu}^{\text{II}} \rightarrow \text{Cu}^{\text{I}}\text{Cu}^{\text{II}}\text{Cu}^{\text{II}} \rightarrow \text{Cu}^{\text{I}}\text{Cu}^{\text{I}}\text{Cu}^{\text{II}} \rightarrow \text{Cu}^{\text{I}}\text{Cu}^{\text{I}}\text{Cu}^{\text{I}}$. Moreover, cathodically induced Cu–ligand bond cleavage can also occur,²² eventually leading to the split of the triangular trinuclear core upon decoordination of an anionic pyrazolate, carboxylate or hydroxo ligand.

Catalytic peroxidative oxidation of cycloalkanes

The new trinuclear triangular copper(II) complexes behave as catalyst precursors for the mild peroxidative oxidation, with aqueous H_2O_2 in MeCN at 25°C , of cyclohexane and cyclopentane to the corresponding cyclic alcohols and cyclic ketones. Their activities for the cyclohexane oxidation are comparable with those previously observed for other trinuclear triangular copper(II) complexes,^{8c,10} and are shown in Tables 3 and 4. In order to optimize the reaction conditions, the effects of the amounts of

Table 3 Peroxidative oxidation of cyclohexane to cyclohexanol and cyclohexanone catalyzed by compounds 1–3^a. Effect of nitric acid amount

Cat.	<i>n</i> (HNO ₃), mmol	Yield ^b of products, %			A/K ^d	TON ^e
		Alcohol	Ketone	Total ^c		
1	0.05	12.7	8.6	21.3	1.5	21.3
1	0.10	22.9	10.2	33.1	2.2	33.1
1	0.15	25.2	9.8	35.0	2.6	35.0
1	0.20	25.5	10.1	35.6	2.5	35.6
1	0.30	18.8	10.0	28.8	1.9	28.8
2	0.05	8.9	10.0	18.9	0.9	18.9
2	0.10	24.6	10.1	34.7	2.4	34.7
2	0.15	24.3	8.5	32.8	2.9	32.8
2	0.20	24.3	9.7	34.0	2.5	34.0
2	0.30	18.3	10.1	28.4	1.8	28.4
3	0.05	13.8	7.9	21.7	1.7	21.7
3	0.10	25.0	9.9	34.9	2.5	34.9
3	0.15	21.3	10.7	32.0	2.0	32.0
3	0.20	25.7	8.8	34.5	2.9	34.5
3	0.30	18.3	10.2	28.6	1.8	28.6

^a Selected data; reaction conditions: C₆H₁₂ (1 mmol), catalyst precursor (10 μmol), MeCN 4 mL, H₂O₂ (10 mmol, added as an aqueous 30% solution), 6 h reaction time, 25 °C. ^b Moles of product/100 moles of C₆H₁₂, measured upon reduction of ROOH to the alcohol by PPh₃. ^c Cyclohexanol + cyclohexanone. ^d Alcohol (cyclohexanol)/ketone (cyclohexanone) molar ratio, upon reduction of ROOH to the alcohol by PPh₃. ^e Overall TON values (moles of products/mole of catalyst).

Table 4 Peroxidative oxidation of cyclohexane to cyclohexanol and cyclohexanone catalyzed by compounds 1–3^a. Effect of hydrogen peroxide amount

Cat.	<i>n</i> (H ₂ O ₂)/ <i>n</i> (cat)	Yield ^b of products, %			A/K ^d	TON ^e
		Alcohol	Ketone	Total ^c		
1	250	17.3	2.7	20.0	6.0	20.0
1	500	24.3	4.7	29.0	5.2	29.0
1 ^f	500	17.6	10.8	28.4	1.6	28.4
1	750	28.1	6.1	34.2	3.7	34.2
1	1000	22.9	10.2	33.1	2.2	33.1
2	250	18.9	3.5	22.5	5.4	22.5
2	500	25.2	5.3	30.5	4.8	30.5
2 ^f	500	17.1	9.5	26.7	1.8	26.7
2	750	25.8	8.7	34.5	3.0	34.5
2	1000	24.6	10.1	34.7	2.4	34.7
3	250	17.4	1.8	19.2	9.7	19.2
3	500	24.9	3.0	27.9	8.3	27.9
3 ^f	500	18.0	10.9	28.9	1.7	28.9
3	750	27.2	8.0	35.2	3.4	35.2
3	1000	25.0	9.9	34.9	2.5	34.9

^a Selected data; reaction conditions: C₆H₁₂ (1 mmol), catalyst precursor (10 μmol), MeCN 4 mL, HNO₃ (0.10 mmol), H₂O₂ (2.5–10.0 mmol added as an aqueous 30% solution), 6 h reaction time, 25 °C. ^b Moles of product/100 moles of C₆H₁₂, measured upon reduction of ROOH to the alcohol by PPh₃. ^c Cyclohexanol + cyclohexanone. ^d Alcohol (cyclohexanol)/ketone (cyclohexanone) molar ratio, upon reduction of ROOH to the alcohol by PPh₃. ^e Overall TON values (moles of products/mole of catalyst). ^f Reaction performed without addition of PPh₃.

hydrogen peroxide and of acid (nitric acid) were studied, since the catalytic activity is expected^{4,23–31} to depend considerably on such factors.

A maximum overall yield, in a single batch, of 36% was reached for the H₂O₂/catalyst molar ratio of 1000 (*i.e.* 0.01 and 10 mmol of catalyst and hydrogen peroxide, respectively) and the

HNO₃/catalyst molar ratio of 20, with a corresponding turnover number (TON) of 36 moles of products per mole of catalyst under the same conditions. Simple salts of copper(II), such as copper(II) acrylate and copper(II) methacrylate, exhibit much lower catalytic activities under similar reaction conditions, leading to a total yield of oxidation products of 3.3% and 4.3% respectively. No oxidation products are obtained in the absence of the metal catalyst.

The reaction is believed^{4,23–25} to proceed *via* cyclohexylhydroperoxide (CyOOH), and cyclohexanol is the main final product, upon reduction of this organoperoxide by PPh₃ prior to the gas chromatographic (GC) analysis according to a method developed by Shul'pin.³² The highest values of cyclohexanol-to-cyclohexanone molar ratio (A/K) of *ca.* 6, 5 and 10 for complexes 1–3, respectively, were obtained for the H₂O₂/catalyst molar ratio of 250 and the HNO₃/catalyst molar ratio of 10.

The involvement of CyOOH is substantiated by the marked increase of the amount of cyclohexanone and decrease of the cyclohexanol amount, when the GC analysis of the final reaction mixture is performed without addition of PPh₃ (experiments marked with [f] in Table 4). The decomposition of CyOOH to the alcohol and ketone in the GC injector and/or chromatographic column is then the main source of those products.

Amount of acid

The presence of acid is essential for the formation of the alcohol and ketone, as we have shown earlier^{8c,11} for other trinuclear triangular copper complexes which do not exhibit catalytic activity in the absence of nitric acid. Moreover, the peroxidative oxidations of cycloalkanes catalyzed by multinuclear copper(II) triethanolamine complexes^{4,23,27,31} and some other systems such as half sandwich scorpionate complexes of vanadium, iron and copper,^{28,29} a heterometallic iron(III)–copper(II)–cobalt(III) complex,³³ and heteronuclear iron(III)–chromium(III) hydroxo complexes,³⁴ proceed in acidic medium. The acid can play a multiple role, by creating unsaturation at the metal upon ligand protonation, stabilizing peroxo species and hampering the decomposition of hydrogen peroxide.

The overall yield of cyclic alcohol and cyclic ketone increases with the HNO₃/catalyst molar ratio up to *ca.* 10–20 (Table 3, Fig. 11), but a further increase of this ratio results in a slight yield drop. For example, for the catalyst precursor 1, the increase of the HNO₃/catalyst molar ratio from 5 to 20 leads to a promotion of the overall products yield from 21 to 36%. Such a dependence was followed by other copper(II) based systems.^{8c,23,31} The A/K molar ratio behaves similarly and reaches maxima of *ca.* 2.6–3, for the acid-to-catalyst molar ratio of 15–20.

Amount of hydrogen peroxide

The overall yield is also enhanced by the increase in H₂O₂ amount, *e.g.* from *ca.* 20% to *ca.* 35% for H₂O₂/catalyst molar ratios of 250 and 750, respectively (Table 4, Fig. 12). In contrast the A/K molar ratio correspondingly diminishes from *ca.* 6 (complexes 1 and 2) or *ca.* 10 (complex 3) to *ca.* 2, mainly due to the enhanced formation of the ketone. This behaviour is also typical for copper(II) trinuclear triangular compounds previously studied by us,^{8c,11} for mono- and multinuclear copper(II) triethanolamine based compounds^{4,31} and for some hexanuclear iron systems.³⁵

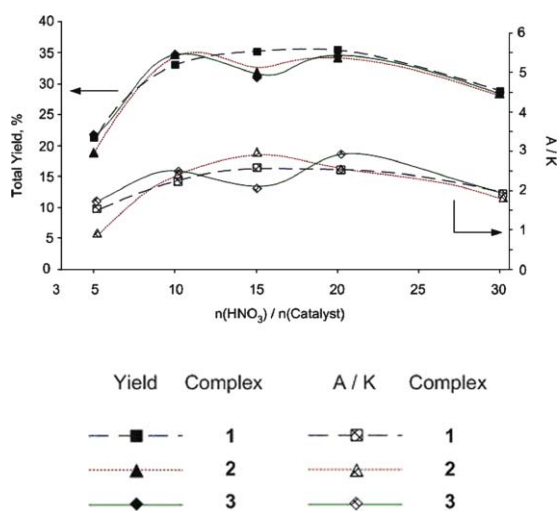


Fig. 11 Effect of the HNO_3 /catalyst molar ratio on the overall yield and A/K molar ratio.

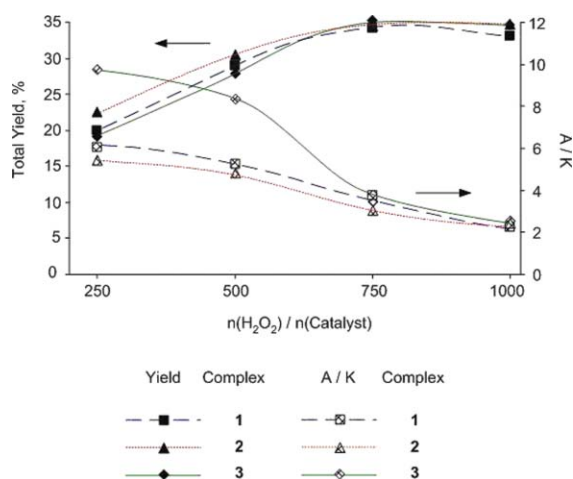


Fig. 12 Effect of the H_2O_2 /catalyst molar ratio on the overall yield and A/K molar ratio.

Such a trend could suggest that, for high peroxide-to-catalyst molar ratios, the alcohol could be an intermediate in the oxidation to the ketone. However, by using cyclohexanol as the substrate, only small conversions (5–7%, see Table 5) to the ketone were obtained. Moreover, the changes of conversion into the ketone (upon

Table 5 Peroxidative oxidation of cyclohexanol catalyzed by compound 1–3^a

Catalyst	$n(\text{H}_2\text{O}_2)/n(\text{catalyst})$	Yield ^b of ketone, %
1	500	5.9
1	1000	4.7
2	500	7.1
2	1000	5.9
3	500	5.8
3	1000	6.6

^a Selected data; reaction conditions: $\text{C}_6\text{H}_{11}\text{OH}$ (1 mmol), catalyst precursor (10 μmol), MeCN 4 mL, HNO_3 (0.10 mmol), H_2O_2 (5.0–10.0 mmol added as an aqueous 30% solution), 6 h reaction time, 25 °C. ^b Moles of ketone/100 moles of $\text{C}_6\text{H}_{11}\text{OH}$.

varying the H_2O_2 /catalyst molar ratio from 500 to 1000) are minor (they lie within $\pm 1\%$) and could not account for the pronounced yield rise of cyclohexanone derived from the alkane. Therefore, the decrease of the A/K ratio for high H_2O_2 /catalyst molar ratios conceivably results from the promotion of metal assisted decomposition of cyclohexyl hydroperoxide to the ketone.^{11,36}

Effect of radical traps

In order to get a further insight into the mechanism of the reaction, the effects of radical traps (Table 6) were studied. The tests proved that the reaction mainly proceeds *via* radical mechanisms involving both carbon-centred radicals and oxygen-centred radicals in view of the dramatic fall of the catalytic activity in the presence of these types of radical traps. In fact, the addition to the reaction mixture of CBrCl_3 (a carbon radical trap^{37a}) essentially suppressed the formation of the products (the overall yield dropped by 99%) and cyclohexyl bromide was formed in the reaction mixture, thus showing that the cyclohexyl radical was generated and trapped. Moreover, the addition of 2,6-di-*tert*-butyl-4-methylphenol (BHT, a carbon and oxygen radical trap^{37b,37c}) or Ph_2NH (oxygen radical trap^{37a}) resulted in high yield drops of 71 and 66%, respectively.

Cyclopentane oxidation

The complexes 1–3 also act as catalyst precursors for the peroxidative oxidation of cyclopentane to the corresponding cyclic alcohol and cyclic ketone (cyclopentanol and cyclopentanone, respectively), under similar conditions to those used in the oxidation of cyclohexane. However, the product yields, TONs and A/K molar ratios (maxima of *ca.* 30%, *ca.* 30 and *ca.* 4, respectively; Table 7) are slightly lower than those observed for the cyclohexane oxidation.

Conclusions

The reactions of Hpz with copper(II) acrylate and methacrylate yield triangular trinuclear copper(II) derivatives having in common the $[\text{Cu}_3(\mu_3\text{-OH})(\mu\text{-pz})_3]^{2+}$ core. The acrylate species 1 and 2 connect through carboxylate bridges forming hexanuclear clusters that, when the reaction has been carried out in methanol, (compound 2) are further linked to each other through double *syn-syn* carboxylate bridges thus generating a monodimensional CP. The trinuclear triangular clusters based on methacrylate, 3, self-assemble through 12-membered rings forming an unprecedented 1-D CP by alternating *syn-syn* and *syn-anti* double carboxylate bridges. In spite of their parallel alignment and a centre-to-centre distance of *ca.* 3.82 Å, double bonds of chelating acrylates belonging to adjacent hexanuclear units of solid compound 1 do not undergo topochemical [2 + 2] cycloaddition by UV irradiation, very likely due to their off-set that does not allow a valid overlapping between the respective p_z orbitals.

All three compounds exhibit, by cyclic voltammetry, irreversible $\text{Cu}^{\text{II}} \rightarrow \text{Cu}^{\text{I}}$ and $\text{Cu}^{\text{I}} \rightarrow \text{Cu}^0$ reduction waves that conceivably involve the reduction of the three metal ions, without any detected differentiation. Nevertheless, it is not possible to exclude either any metal–metal electronic communication because of the broadness of the reduction waves, or any cathodically induced Cu–ligand bond cleavage.

Table 6 Peroxidative oxidation of cyclohexane to cyclohexanol and cyclohexanone catalyzed by compound **3**^c. Effects of radical traps

<i>n</i> (trap)/ <i>n</i> (C ₆ H ₁₂)	Trap ^b	Yield ^c , %			A/K ^e	TON ^f	Yield drop with trap ^g , %
		Alcohol	Ketone	Total ^d			
2.5	CBrCl ₃	0.3	0.0	0.3	—	0.3	99
2.5	BHT ^h	5.8	2.2	8.0	2.6	8.0	71
2.5	Ph ₂ NH	5.2	4.4	9.6	1.2	9.6	66
0	No trap	24.9	3.0	27.9	8.3	27.9	—

^a Selected data; reaction conditions: C₆H₁₂ (1 mmol), catalyst precursor (10 μmol), MeCN 4 mL, HNO₃ (0.10 mmol), H₂O₂ (5 mmol, added as an aqueous 30% solution), 6 h reaction time, 25 °C. ^b Radical trap (2.5 mmol). ^c 100 × Moles of product/moles of C₆H₁₂, measured upon reduction of ROOH to the alcohol by PPh₃. ^d Cyclohexanol + cyclohexanone. ^e Alcohol (cyclohexanol)/ketone (cyclohexanone) molar ratio, upon reduction of ROOH to the alcohol by PPh₃. ^f Overall TON (moles of products/mole of catalyst). ^g (1–total yield with radical trap/total yield without radical trap) × 100. ^h BHT = 2,6-di-tert-butyl-4-methylphenol.

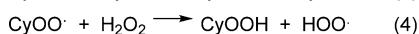
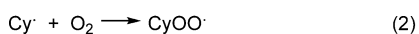
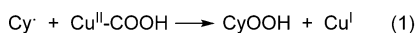
Table 7 Peroxidative oxidation of cyclopentane to cyclopentanol and cyclopentanone catalyzed by compounds **1–3**^a

Cat.	<i>n</i> (H ₂ O ₂)/ <i>n</i> (cat)	Yield ^b of products, %			A/K ^d	TON ^e
		Alcohol	Ketone	Total ^c		
1	500	20.4	6.2	26.6	3.3	26.6
2	500	20.3	5.5	25.8	3.7	25.8
3	500	22.2	7.4	29.6	3.0	29.6

^a Selected data; reaction conditions: C₅H₁₀ (1 mmol), catalyst precursor (10 μmol), MeCN 4 mL, HNO₃ (0.10 mmol), H₂O₂ (5 mmol added as an aqueous 30% solution), 6 h reaction time, 25 °C. ^b 100 × Moles of product/moles of C₅H₁₀, measured upon reduction of ROOH to the alcohol by PPh₃. ^c Cyclopentanol + cyclopentanone. ^d Alcohol (cyclopentanol)/ketone (cyclopentanone) molar ratio, upon reduction of ROOH to the alcohol by PPh₃. ^e Overall TON values (moles of products/mole of catalyst).

Compounds **1–3** exhibit high catalytic activities towards cycloalkanes oxidations with H₂O₂, which are comparable with those of related copper(II) systems,^{8e,11} of some multicopper(II) triethanolamine complexes,²⁷ in particular a copper(II) tetranuclear cluster,⁴ and are higher than those observed for half-sandwich scorpionate tris(pyrazolyl)methane complexes of copper, iron or vanadium.²⁸ Cyclohexyl hydroperoxide (CyOOH) appears to be a relevant intermediate towards cyclohexanol (A) and cyclohexanone (K), and its further reduction by PPh₃ to cyclohexanol leads to the increase of the A/K molar ratio. This ratio decreases at high hydrogen peroxide-to-catalyst molar ratios due to the enhanced formation of the ketone, but this fact is not due to overoxidation of cyclohexanol to the ketone.

The catalytic reaction proceeds *via* a radical mechanism as shown by radical trap experiments. Metal-assisted decomposition of H₂O₂ leads to the hydroxyl radical³⁸ which, on reaction with cyclohexane, forms the cyclohexyl radical (Cy[•]). The formation of CyOOH possibly results (Scheme 2) from reaction of Cy[•] with a metal-hydroperoxo species or with O₂ to give, in the

**Scheme 2** Possible routes to CyOOH.

latter case, the cyclohexylperoxyl radical (CyOO[•]) which, upon H-abstraction *e.g.* from cyclohexane or H₂O₂, would form the cyclohexyl hydroperoxide.^{25,26,35–40} Further metal-assisted decomposition of CyOOH can lead to the final products,^{28,29,32,38a,41–42} while the pyrazole and carboxylate ligands can promote proton-transfer steps involving H₂O₂, oxo and/or peroxo species, as is believed^{32,38a,43,44} to occur for V-catalyst bearing N,O-ligands.

Experimental

Material and methods

All reaction and manipulations were carried out in the air. Copper(II) acrylate and methacrylate were prepared according to a slightly modified general procedure.⁴⁵ All other chemicals, were purchased from Aldrich and used without further purification. Elemental analyses (C, H, N) were performed with a Fisons Instruments 1108 CHNS-O Elemental Analyser. IR spectra were recorded from 4000 to 400 cm⁻¹ with a Perkin-Elmer System 2000 FT-IR instrument. Positive electrospray mass spectra were obtained with a Series 1100 MSI detector HP spectrometer, using MeOH as mobile phase. Solutions for electrospray ionization mass spectrometry (ESI-MS) were prepared using reagent grade methanol and/or acetonitrile and obtained data (masses and intensities) were compared to those calculated by using the IsoPro isotopic abundance simulator.⁴⁶ Peaks containing copper(II) ions are identified as the centres of isotopic clusters. The magnetic susceptibilities were measured at room temperature (22 °C) by the Gouy method, with a Sherwood Scientific Magnetic Balance MSB-Auto, using HgCo(NCS)₄ as calibrant and corrected for diamagnetism with the appropriate Pascal constants. The magnetic moments (in BM) were calculated from the equation $\mu_{\text{eff}} = 2.84 (\chi_{\text{m}}^{\text{corr}} T)^{1/2}$. The electrical conductances of methanol solutions were measured with a Crison CDTM 522 conductimeter at room temperature. Reflectance solid-state and solution UV-vis spectra were recorded on a Perkin Elmer Lambda 19 UV-vis-NIR and on a Perkin Elmer Lambda 25 UV-vis spectrophotometer, respectively. ¹H NMR spectra were obtained with a Bruker Avance 300 instrument. Acrylic and methacrylic acids, developed in the reactions with Hpz, were detected by GC analyses carried out on a Thermo Electron Trace DSQ instrument equipped with a 30 m, 0.25 mm, 0.25 μm Thermo TR 5MS column. Plots of IR, (S7–S9) ¹H NMR (S10–S12) and ESI Mass (S13–S15) spectra of compounds **1–3** are included in the ESI.†

Syntheses

Copper acrylate, $\text{Cu}(\text{CH}_2=\text{CHCOO})_2$. Basic copper(II) carbonate (16.1 g, 72.8 mmol) was suspended in 30 mL of acrylic acid and stirred at r.t. After 1 h acetone (20 mL) was added and the mixture was stirred overnight, obtaining a green-blue solid that was filtered off and then extracted with acetone (Soxhlet). The obtained solution was cooled at 0 °C yielding a green-blue solid that was filtered off, washed with cold acetone and dried under vacuum. Yield 16.74 g, 81.4 mmol, 56%, based on starting basic copper carbonate. Elem. Anal. Calcd for $\text{C}_6\text{H}_6\text{CuO}_4$: C, 35.04; H, 2.94. Found: C, 35.26; H = 2.87. IR (KBr, cm^{-1}): 1641, 1567, 1496, 1427, 1361, 1285, 1276, 1064, 985, 969, 914, 822, 687.

Copper methacrylate $\text{Cu}(\text{CH}_2=\text{C}(\text{CH}_3)\text{COO})_2 \cdot 2\text{H}_2\text{O}$. Basic copper(II) carbonate (9.73 g, 44.02 mmol) was suspended in 30 mL of methacrylic acid and stirred at r.t. After 30 min 10 mL of acetone were added and the mixture was stirred overnight. The solid was filtered off and washed with acetone until the solution was colourless. The dark green solution was left to evaporate in the air obtaining green crystals that were filtered off, washed with cold acetone and dried under vacuum. Yield 17.57 g, 65.1 mmol, 74%, based on starting basic copper carbonate. Elem. Anal. Calcd for $\text{C}_8\text{H}_{14}\text{CuO}_6$: C, 35.62; H, 5.23. Found: C, 35.97; H = 5.54. IR (KBr, cm^{-1}): 2980, 2963, 2929, 1678, 1647, 1584, 1554, 1498, 1456, 1411, 1393, 1372, 1299, 1240, 1222, 1202, 1006, 934, 915, 855, 826.

$[\text{Cu}_3(\mu_3\text{-OH})(\mu\text{-pz})_3(\text{CH}_2=\text{CHCOO})_2(\text{H}_2\text{O})_2(\text{Hpz})]$, **1.** To a solution of 918 mg of copper(II) acrylate (4.46 mmol) in 50 mL of water 410 mg of Hpz (6.03 mmol) dissolved in 15 mL of water was added under stirring. The obtained deep blue solution was stirred for 1 h and then left to slowly evaporate in the air. Dark blue crystals were obtained after a week, separated from mother liquors, washed with 5 mL of cold water and dried under vacuum. Yield 610 mg, 0.93 mmol, 63%. In mother liquors the presence of acrylic acid was ascertained.

1 M.p. 250 °C (dec). Elem. Anal. Calcd for $\text{C}_{18}\text{H}_{24}\text{Cu}_3\text{N}_8\text{O}_7$: C, 33.00; H, 3.69; N, 17.11. Found: C, 33.35; H, 3.22; N, 17.06. IR (KBr, cm^{-1}): 3358, 3236, 3115, 1635, 1535, 1416, 1380, 1346, 1278, 1181, 1060, 965, 900, 829, 761, 749, 679. ESI-MS (+) (MeOH, MeCN) (higher peaks, m/z ; relative abundance, %) 529.8 (50) $[\text{Cu}_3(\text{OH})(\text{C}_3\text{H}_3\text{N}_2)_3(\text{CH}_2\text{CHCOO})(\text{CH}_3\text{OH})(\text{H}_2\text{O})]^+$, 654.8 (42) Higher peak of a complex cluster likely due to the superimposition of more than one signal: a value at 656.6 (signal also present) corresponds to $[\text{Cu}_3(\text{OH})(\text{C}_3\text{H}_3\text{N}_2)_3(\text{CH}_2\text{CHCOO})_2(\text{CH}_3\text{OH})_2(\text{CH}_3\text{CN}) + \text{H}]^+$, 1058.7 (100) $[\text{Cu}_6(\text{OH})_3(\text{C}_3\text{H}_3\text{N}_2)_6(\text{CH}_2\text{CHCOO})_2(\text{CH}_3\text{OH})_2(\text{H}_2\text{O})]^+$. μ_{eff} (295 K) = 2.175 BM. Λ_{M} (MeOH, 1×10^{-3} M) = 19.4 $\mu\text{S cm}^{-1}$. UV-vis spectra: $\lambda_{\text{max}}/\text{nm}$ (reflectance): 589; $\lambda_{\text{max}}/\text{nm}$ (MeOH solution 1.92×10^{-3} M) 616 ($\epsilon = 199$). $^1\text{H NMR}$ (CD_3OD , 298 K) δ (ppm) 37.26 (2H), 40.82 (1H).

$[\text{Cu}_3(\mu_3\text{-OH})(\mu\text{-pz})_3(\text{CH}_2=\text{CHCOO})_2(\text{MeOH})]$, **2.** To a solution of 1.07 g of copper(II) acrylate (5.22 mmol) in 30 mL of MeOH 430 mg of Hpz (6.32 mmol) dissolved in 10 mL of MeOH was added under stirring. The deep blue solution was stirred for 30 min and then left to slowly evaporate in air. After a week the solution was reduced to ca. 5 mL and formed dark blue crystals

that were collected, washed with 2 mL of cold MeOH and dried under vacuum. Yield 522 mg, 0.90 mmol, 51%. In mother liquors the presence of acrylic acid was ascertained.

2: M.p. 185–188 °C (dec). Elem. Anal. Calcd for $\text{C}_{16}\text{H}_{20}\text{Cu}_3\text{N}_6\text{O}_6$: C, 32.96; H, 3.46; N, 14.42. Found: C, 32.80; H, 3.26; N, 14.37. IR (KBr, cm^{-1}): 3427, 3137, 1638, 1547, 1429, 1380, 1366, 1278, 1178, 1061, 966, 900, 828, 764, 678, 625, 48. ESI-MS (+) (MeOH, MeCN) (higher peaks, m/z ; relative abundance, %) 531.8 (40) Higher peak of a complex signal likely due to two, partly superimposed clusters, at 529.8 $\{[\text{Cu}_3(\text{OH})(\text{C}_3\text{H}_3\text{N}_2)_3(\text{CH}_2\text{CHCOO})(\text{CH}_3\text{OH})(\text{H}_2\text{O})]^+\}$ and 533.8 $\{[\text{Cu}_3(\text{OH})(\text{C}_3\text{H}_3\text{N}_2)_3(\text{CH}_2\text{CHCOO})(\text{H}_2\text{O})_3]^+\}$, 654.8 (35) Higher peak of a complex cluster likely due to the superimposition of more than one signal: a value at 656.6 (signal also present) corresponds to $[\text{Cu}_3(\text{OH})(\text{C}_3\text{H}_3\text{N}_2)_3(\text{CH}_2\text{CHCOO})_2(\text{CH}_3\text{OH})_2(\text{CH}_3\text{CN}) + \text{H}]^+$, 1022.7 (40) $[\text{Cu}_6(\text{OH})_4(\text{C}_3\text{H}_3\text{N}_2)_5(\text{CH}_2\text{CHCOO})_2(\text{MeOH})_3]^+$, 1058.7 (100) $[\text{Cu}_6(\text{OH})_3(\text{C}_3\text{H}_3\text{N}_2)_6(\text{CH}_2\text{CHCOO})_2(\text{CH}_3\text{OH})_2(\text{H}_2\text{O})]^+$. μ_{eff} (295 K) = 2.143 BM. Λ_{M} (MeOH, 1×10^{-3} M) = 22.5 $\mu\text{S cm}^{-1}$. UV-vis spectra: $\lambda_{\text{max}}/\text{nm}$ (reflectance): 601; $\lambda_{\text{max}}/\text{nm}$ (MeOH solution 2.44×10^{-3} M) 615 ($\epsilon = 186$). $^1\text{H NMR}$ (CD_3OD , 298 K) δ (ppm) 37.71 (2H), 40.80 (1H).

$[\text{Cu}_3(\mu_3\text{-OH})(\mu\text{-pz})_3\{\text{CH}_2=\text{C}(\text{CH}_3)\text{COO}\}_2]$, **3.** Copper(II) methacrylate (619 mg, 2.29 mmol) partly dissolved in 80 mL of a 3:1 $\text{H}_2\text{O}/\text{EtOH}$ mixture was treated under vigorous stirring with 212 mg of Hpz (3.11 mmol) dissolved in 30 mL of H_2O yielding a deep blue solution from which a light blue solid formed after ca. 1 min. The solid was filtered off, washed with 20 mL of water in four portions and dried under vacuum. Yield 312 mg, 0.54 mmol, 71%. In a week ca. 10 mg of crystals, suitable for a single crystal XRD determination, were collected from mother liquors, in which the presence of methacrylic acid was also ascertained. The XRPD spectrum of the first precipitate compare very well with the calculated one from single crystal XRD determination. By carrying out the reaction in MeOH a deep blue solution is obtained, from which, by evaporation, well formed crystals of **3** separated in a lower yield (ca. 45%).

3: M.p. 250 °C (dec). Elem. Anal. Calcd for $\text{C}_{17}\text{H}_{20}\text{Cu}_3\text{N}_6\text{O}_5$: C, 35.26; H, 3.48; N, 14.51. Found: C, 35.37; H, 3.32; N, 14.42. IR (KBr, cm^{-1}): 3417, 3142, 2948, 1640, 1563, 1535, 1390, 1415, 1383, 1281, 1239, 1180, 1069, 934, 830, 785, 762, 628, 463. ESI-MS (+) (MeOH, MeCN) (higher peaks, m/z ; relative abundance, %) 543.8 (23) $[\text{Cu}_3(\text{OH})(\text{C}_3\text{H}_3\text{N}_2)_3(\text{CH}_2\text{CCH}_3\text{COO})(\text{CH}_3\text{OH})(\text{H}_2\text{O})]^+$ 561.9 (37) $[\text{Cu}_3(\text{OH})(\text{C}_3\text{H}_3\text{N}_2)_3(\text{CH}_2\text{CCH}_3\text{COO})(\text{CH}_3\text{OH})(\text{H}_2\text{O})_2]^+$, 668.8 (45), Higher peak of a complex cluster likely due to the superimposition of more than one signal: a value at 670.8 (signal also present) corresponds to $[\text{Cu}_3(\text{OH})(\text{C}_3\text{H}_3\text{N}_2)_3(\text{CH}_2\text{CCH}_3\text{COO})_2(\text{CH}_3\text{OH})(\text{CH}_3\text{CN})(\text{H}_2\text{O}) + \text{H}]^+$ 1064.7 (45) $[\text{Cu}_6(\text{OH})_3(\text{C}_3\text{H}_3\text{N}_2)_7(\text{CH}_2\text{CCH}_3\text{COO})(\text{H}_2\text{O})_2(\text{MeCN})]$, 1100.8 (100) $[\text{Cu}_6(\text{OH})_3(\text{C}_3\text{H}_3\text{N}_2)_7(\text{CH}_2\text{CCH}_3\text{COO})(\text{H}_2\text{O})_4(\text{MeCN})]$. μ_{eff} (295 K) = 2.095 BM. Λ_{M} (MeOH, 1×10^{-3} M) = 16.3 $\mu\text{S cm}^{-1}$. UV-vis spectra: $\lambda_{\text{max}}/\text{nm}$ (reflectance): 583; $\lambda_{\text{max}}/\text{nm}$ (MeOH solution 2.11×10^{-3} M): 615 ($\epsilon = 204$). $^1\text{H NMR}$ (CD_3OD , 298 K) δ (ppm) 37.47 (2H), 40.72 (1H).

Photochemical experiments

In photochemical experiments a sample of compound **1** was finely ground using a mortar and pestle and placed between two quartz

windows. Continuous irradiation (1–4 h) was performed with a light source housing (Oriol instruments) equipped with a 500 W Hg–Xe arc lamp, power supply (200–500 W), F/1.5 UV grade fused silica condenser to collect the radiation from the emitting source, a 5 cm path length liquid (water) filter with fused silica windows to absorb IR radiation, and a secondary focusing lens. In one case, a glass cut-off filter ($l > 300$ nm) was also used. FT-IR (KBr) spectra were collected before and after irradiation experiments using a Nicolet 5700 FT-IR instrument.

Electrochemical studies

The electrochemical experiments were performed on an EG&G PAR 273A potentiostat/galvanostat connected to a computer through a GPIB interface. Cyclic voltammograms (CV) were obtained in 0.2 M solutions of $[\text{Bu}_4\text{N}][\text{BF}_4]$ in DMSO, at a platinum disc working electrode ($d = 0.5$ mm) and at 25 °C. A silver-wire and a Pt wire were employed as pseudo-reference electrode and counter-electrode, respectively. The electrochemical experiments were performed under a N_2 atmosphere at room temperature. The potentials of the complexes were measured by CV in the presence of ferrocene as the internal standard, and the redox potential values are normally quoted relative to the SCE by using the $[\text{Fe}(\eta^5\text{-C}_6\text{H}_5)_2]^{0/+}$ redox couple ($E_{1/2}^{\text{ox}} = 0.44$ V vs. SCE)⁴⁷ in a 0.2 M $[\text{Bu}_4\text{N}][\text{BF}_4]$ /DMSO solution.

Catalytic activity studies

To the reaction flask with the catalyst precursor (10 μmol) were added 4 mL of acetonitrile (MeCN), 0.05–0.3 mmol (typically 0.1 mmol) of HNO_3 , 1.0 mmol of C_6H_{12} (or 1.0 mmol of C_5H_{10}) and 2.5–10.0 mmol H_2O_2 (30% in H_2O), in this order. The reaction

mixture was stirred for 6 h at room temperature (*ca.* 25 °C) and under air at atmospheric pressure. Cycloheptanone (90 μL) was then added as internal standard, diethyl ether (typically 9.0 mL to extract the substrate and the organic products of the reaction mixture) and PPh_3 (0.5 g, to reduce the organo-hydroperoxides if formed, according to a method developed by Shul'pin³²). The resulting mixture was stirred for a few minutes and then a sample taken from the organic phase was analyzed by GC using a FISON Instruments GC 8000 series gas chromatograph with a DB WAX fused silica capillary column (30 m \times 0.25 mm \times 0.25 μm) and the Jasco-Borwin v.1.50 software. The GC analyses of the aqueous phase showed the presence of only traces (less than 0.05%) of oxidation products.

Crystallographic data collection and structure determination

The X-ray intensity data for 1–3 were measured on a Bruker Apex II CCD diffractometer. Cell dimensions and the orientation matrix were initially determined from a least-squares refinement on reflections measured in three sets of 20 exposures, collected in three different ω regions, and eventually refined against all data. A full sphere of reciprocal space was scanned by 0.3° ω steps. The software SMART⁴⁸ was used for collecting frames of data, indexing reflections and determination of lattice parameters. The collected frames were then processed for integration by the SAINT program,⁴⁸ and an empirical absorption correction was applied using SADABS.⁴⁹ The structures were solved by direct methods (SIR 97)⁵⁰ and subsequent Fourier syntheses and refined by full-matrix least-squares on F^2 (SHELXTL),⁵¹ using anisotropic thermal parameters for all non-hydrogen atoms. In the three structures all hydrogen atoms were located in difference Fourier maps and treated as riding atoms in geometrically idealized

Table 8 Crystal data and structure refinement for 1, 2 and 3

Compound	1	2	3
Formula	$\text{C}_{18}\text{H}_{24}\text{Cu}_3\text{N}_8\text{O}_7$	$\text{C}_{16}\text{H}_{20}\text{Cu}_3\text{N}_6\text{O}_6$	$\text{C}_{17}\text{H}_{20}\text{Cu}_3\text{N}_6\text{O}_5$
Fw	655.07	583.00	579.01
T , K	298(2)	273(2)	298(2)
λ , Å	0.71073	0.71073	0.71073
Crystal symmetry	Triclinic	Monoclinic	Monoclinic
Space group	$P\bar{1}$	$P2_1/c$	$P2_1/c$
a , Å	11.4780(19)	10.982(2)	10.0069(5)
b , Å	11.8535(19)	20.322(4)	11.7324(6)
c , Å	12.389(2)	10.4061(19)	17.9975(8)
α , °	117.338(2)	90	90
β , °	92.502(3)	113.891(3)	95.366(1)
γ , °	115.928(2)	90	90
Cell volume, Å ³	1282.0(4)	2123.4(7)	2103.74(18)
Z	2	4	4
D_c , Mg m ⁻³	1.697	1.824	1.828
μ (Mo-K α), mm ⁻¹	2.519	3.023	3.048
$F(000)$	662	1172	1164
Crystal size/mm	0.15 \times 0.20 \times 0.25	0.15 \times 0.20 \times 0.28	0.18 \times 0.20 \times 0.25
θ limits, °	1.94–23.36	2.00–26.45	2.07–27.50
Reflections collected	7874 ($\leq h, \leq k, \leq l$)	16594 ($\leq h, \leq k, \leq l$)	17658 ($\leq h, \leq k, \leq l$)
Unique obs. Reflect. [$F_o > 4\sigma(F_o)$]	3684 [$R(\text{int}) = 0.0507$]	4369 [$R(\text{int}) = 0.0772$]	4798 [$R(\text{int}) = 0.0259$]
Goodness-of-fit-on F^2	0.954	0.936	1.076
R_1 ($F > 4\sigma(F)$) ^a	0.0416	0.0435	0.0255
wR_2 (F^2 , all data) ^b	0.1046	0.1157	0.0697
Largest diff. peak and hole, e Å ⁻³	0.419 and -0.409	0.843 and -0.471	0.299 and -0.276

^a $R_1 = \sum \|F_o\| - |F_c| / \sum \|F_o\|$. ^b $wR_2 = [\sum w(F_o^2 - F_c^2)^2 / \sum w(F_o^2)^2]^{1/2}$ where $w = 1/[\sigma^2(F_o^2) + (aP)^2 + bP]$ where $P = (F_o^2 + F_c^2)/3$.

positions, except the hydroxy and the acrylate hydrogens (the latter only in **2**), and refined with $U_{\text{iso}}(\text{H})$ values set equal to $1.2 U_{\text{eq}}(\text{C})$ or $1.5 U_{\text{iso}}(\text{C}-\text{Me})$. Crystal data and details of the data collection for all structures are reported in Table 8. Molecular graphics were generated using Mercury 1.4.2⁵² and Schakal⁵³ programs. Colour codes for all molecular graphics: yellow (Cu), blue (N), red (O), grey (C), white (H).

Acknowledgements

This work was supported by the Italian PRIN fund no. 2006038447 and by the Foundation for Science and Technology (programme POCI 2010, FEDER funded), Portugal. M. M. wishes to thank the University of Bologna for financial support. F. G. acknowledges a grant of the "Aldo Gini" Foundation to support a research period at Lisbon. The authors are indebted to Dr M. Bonchio and Dr M. Carraro (ITC-CNR and Chemical Sciences Dept. of Padova University) for the photochemical experiments and to Mr Andrea Boaretto (Chemical Sciences Dept. of Padova University) for running the GC spectra for the identification of carboxylic acids.

References

- (a) O. M. Yaghi, H. Li, C. Davis, D. Richardson and T. L. Groy, *Acc. Chem. Res.*, 1998, **31**, 474; (b) M. Eddaoudi, H. Li and O. M. Yaghi, *J. Am. Chem. Soc.*, 2000, **122**, 1391; (c) M. D. Ward, J. A. McCleverty and J. C. Jeffery, *Coord. Chem. Rev.*, 2001, **222**, 251; (d) B. Moulton and M. J. Zaworotko, *Chem. Rev.*, 2001, **101**, 1629; (e) M. Eddaoudi, J. Kim, N. Rosi, D. Vodak, J. Wachter, M. O'Keeffe and O. M. Yaghi, *Science*, 2002, **295**, 469; (f) C. Janiak, *Dalton Trans.*, 2003, 2781; (g) S. L. James, *Chem. Soc. Rev.*, 2003, **32**, 276; (h) S. Kitagawa, R. Kitaura and S.-I. Noro, *Angew. Chem., Int. Ed.*, 2004, **43**, 2334; (i) R. Matsuda, R. Kitaura, S. Kitagawa, Y. Kubota, T. C. Kobayashi, S. Horike and M. Takata, *J. Am. Chem. Soc.*, 2004, **126**, 14063; (j) Y. Kubota, M. Takata, R. Matsuda, R. Kitaura, S. Kitagawa, K. Kato, M. Sakata and T. C. Kobayashi, *Angew. Chem., Int. Ed.*, 2005, **44**, 920; (k) S. Kitagawa and K. Uemura, *Chem. Soc. Rev.*, 2005, **34**, 109; (l) J. L. C. Rowsell and O. M. Yaghi, *Angew. Chem., Int. Ed.*, 2005, **44**, 4670; (m) N. W. Ockwig, O. Delgado-Friedrichs, M. O'Keeffe and O. M. Yaghi, *Acc. Chem. Res.*, 2005, **38**, 176; (n) H. Hofmeier and U. S. Shubert, *Chem. Commun.*, 2005, 2423; (o) B. Chen, C. Liang, J. Yang, D. S. Contreras, Y. L. Clancy, E. B. Lobkovsky, O. M. Yaghi and S. Dai, *Angew. Chem., Int. Ed.*, 2006, **45**, 1390; (p) U. Mueller, M. Shubert, F. Teich, H. Puetter, K. Schierle-Arndt and J. Pastré, *J. Mater. Chem.*, 2006, **16**, 626; (q) C. Serre, C. Mellot-Draznieks, S. Surblé, N. Audebrand, Y. Filinchuk and G. Férey, *Science*, 2007, **315**, 1828.
- (a) M. Eddaoudi, D. B. Moler, H. Li, B. Chen, T. M. Reineke, M. O'Keeffe and O. M. Yaghi, *Acc. Chem. Res.*, 2001, **34**, 319; (b) B. Chen, F. R. Fronczek and A. W. Maverick, *Inorg. Chem.*, 2004, **43**, 8209; (c) H. K. Chae, D. Y. Siberio-Pérez, J. Kim, M. Eddaoudi, A. J. Matzger, M. O'Keeffe and O. M. Yaghi, *Nature*, 2004, **427**, 523; (d) R. Murugavel, M. G. Walawalkar, M. Dan, H. W. Roesky and C. N. R. Rao, *Acc. Chem. Res.*, 2004, **37**, 763; (e) Q.-R. Fang, G.-S. Zhu, M. Xue, J.-Y. Sun, S.-L. Qiu and R.-R. Xu, *Angew. Chem., Int. Ed.*, 2005, **44**, 3845; (f) W. Ouellette, M. H. Yu, C. J. O. Connor, D. Hagrman and J. Zubietta, *Angew. Chem., Int. Ed.*, 2006, **45**, 3497; (g) B. Ding, L. Yi, P. Cheng, D.-Z. Liao and S.-P. Yan, *Inorg. Chem.*, 2006, **45**, 5799.
- (a) M. Shimizu, Y. Watanabe, H. Orita, T. Hayakawa and K. Takehira, *Bull. Chem. Soc. Jpn.*, 1993, **66**, 251; (b) P. Gamez, P. G. Aubel, W. L. Driessen and J. Reedijk, *Chem. Soc. Rev.*, 2001, **30**, 376; (c) A. Granata, E. Monzani and L. Casella, *JBIC, J. Biol. Inorg. Chem.*, 2004, **9**, 903.
- A. M. Kirillov, M. N. Kopylovich, M. V. Kirillova, E. Y. Karabach, M. Haukka, M. F. C. Guedes da Silva and A. J. L. Pombeiro, *Adv. Synth. Catal.*, 2006, **348**, 159.
- (a) E. J. Solomon, U. M. Sundaram and T. E. Machonkin, *Chem. Rev.*, 1996, **96**, 2563; (b) E. J. Solomon, P. Chen, M. Metz, S. K. Lee and A. E. Palmer, *Angew. Chem., Int. Ed.*, 2001, **40**, 4570.
- C. Boldron, Ş. Özalp-Yaman, P. Gamez, D. M. Tooke, A. L. Spek and J. Reedijk, *Dalton Trans.*, 2005, 3535.
- M. Zaręba, M. Legięd, B. Sanecka, J. Sobczak, M. Hojniak and S. Wołowicz, *J. Mol. Catal. A: Chem.*, 2006, **248**, 144.
- (a) M. Casarin, C. Corvaja, C. Di Nicola, D. Falcomer, L. Franco, M. Monari, L. Pandolfo, C. Pettinari, F. Piccinelli and P. Tagliatesta, *Inorg. Chem.*, 2004, **43**, 5865; (b) M. Casarin, C. Corvaja, C. Di Nicola, D. Falcomer, L. Franco, M. Monari, L. Pandolfo, C. Pettinari and F. Piccinelli, *Inorg. Chem.*, 2005, **44**, 6265; (c) C. Di Nicola, E. Yu. Karabach, A. M. Kirillov, M. Monari, L. Pandolfo, C. Pettinari and A. J. L. Pombeiro, *Inorg. Chem.*, 2007, **46**, 221.
- M. Casarin, A. Cingolani, C. Di Nicola, D. Falcomer, M. Monari, L. Pandolfo and C. Pettinari, *Cryst. Growth Des.*, 2007, **7**, 676.
- (a) C. Di Nicola, F. Garau, M. Monari, L. Pandolfo, C. Pettinari and A. J. L. Pombeiro, *Proceedings of 4th EuChemMS Conference on Nitrogen Ligands*, Garmisch-Partenkirchen, Germany August 24–28, 2008, P79, pp. 165; (b) C. Di Nicola, F. Garau, M. F. C. Guedes da Silva, J. Ngoune, L. Pandolfo, C. Pettinari and A. J. L. Pombeiro, *Proceedings of 4th EuChemMS Conference on Nitrogen Ligands*, Garmisch-Partenkirchen, Germany August 24–28, 2008, SL8, p. 52.
- C. Di Nicola, F. Garau, Y. Yu. Karabach, L. M. D. R. S. Martins, M. Monari, L. Pandolfo, C. Pettinari and A. J. L. Pombeiro, *Eur. J. Inorg. Chem.*, 2009, 666.
- In the reactions of Hpz with copper(II) valerate, 2-methylbutyrate, hexanoate and heptanoate, we were unable to obtain XRD suitable crystals, but the trinuclear triangular arrangement was inferred on the basis of other characterizations, as ESI MS, magnetic susceptibility, NMR, IR, and UV-vis spectra, (see ref. 11).
- G. J. Catterick and P. Thornton, *Adv. Inorg. Chem. Radiochem.*, 1977, **20**, 291.
- Y. Y. Wang, Q. Shi, Q.-Z. Shi, Y.-C. Gao and Z.-Y. Zhou, *Polyhedron*, 1999, **18**, 2009.
- E. Pretsch, T. Clerc, J. Seibl and W. Simon, *Tables of Determination of Organic Compounds. ¹³C NMR, ¹H NMR, IR, MS, UV/Vis*, Chemical Laboratory Practice, Springer-Verlag, Berlin, Germany, 1989.
- J. P. Castaneda, G. S. Denisov, S. Y. Kucherov, V. M. Schreiber and A. V. Shurukina, *J. Mol. Struct.*, 2003, **660**, 25.
- (a) T. N. Wassermann, C. A. Rice, A. Suhm and D. Luckhaus, *J. Chem. Phys.*, 2007, **127**, 234309; (b) H. T. Flakus and A. Machelska, *Spectrochim. Acta, Part A*, 2002, **58**, 553; (c) C. A. Rice, N. Borho and M. A. Suhm, *Z. Phys. Chem.*, 2005, **219**, 379.
- (a) P. A. Angaridis, P. Baran, R. Boča, F. Cervantes-Lee, W. Haase, G. Mezei, R. G. Raptis and R. Werner, *Inorg. Chem.*, 2002, **41**, 2219; (b) G. Mezei, M. Rivera-Carrillo and R. G. Raptis, *Inorg. Chim. Acta*, 2004, **357**, 3721.
- (a) F. Hulsbergen, R. W. M. ten Hoedt, G. C. Verschoor, J. Reedijk and A. L. Spek, *J. Chem. Soc., Dalton Trans.*, 1983, 539; (b) M. Angaroni, G. A. Ardizzoia, T. Beringhelli, G. La Monica, D. Gatteschi, N. Masciocchi and M. Moret, *J. Chem. Soc., Dalton Trans.*, 1990, 3305; (c) K. Sakai, Y. Yamada, T. Tsubomura, M. Yabuki and M. Yamaguchi, *Inorg. Chem.*, 1996, **35**, 542; (d) S. Ferrer, J. G. Haasnoot, J. Reedijk, E. Muller, M. Biagini Cingi, M. Lanfranchi, A. M. Manotti Lanfredi and J. Ribas, *Inorg. Chem.*, 2000, **39**, 1859; (e) S. Ferrer, F. Lloret, I. Bertomeu, G. Alzueta, J. Borrás, S. Garcia-Granda, M. Liu-Gonzales and J. G. Haasnoot, *Inorg. Chem.*, 2002, **41**, 5821; (f) R. Boča, L'. Dihán, G. Mezei, T. Ortiz-Pérez, R. G. Raptis and J. Telsler, *Inorg. Chem.*, 2003, **42**, 5801; (g) G. Mezei and R. G. Raptis, *Inorg. Chim. Acta*, 2004, **357**, 3279.
- G. M. J. Schmidt, *Pure Appl. Chem.*, 1971, **27**, 647.
- The authors are indebted with one of the referees for the suggestion to check this point..
- (a) E. Reisner, V. B. Arion, M. F. C. Guedes da Silva, R. Lichtenecker, A. Eichinger, B. K. Keppler, V. Yu. Kukushkin and A. J. L. Pombeiro, *Inorg. Chem.*, 2004, **43**, 7083; (b) E. Reisner, V. B. Arion, B. K. Keppler and A. J. L. Pombeiro, *Inorg. Chim. Acta*, 2008, **361**, 1569; (c) *Trends in Molecular Electrochemistry*, ed. A. J. L. Pombeiro and C. Amatore, Marcel Dekker/FontisMedia, New York, USA, 2004; (d) P. Zanello, *Inorganic Electrochemistry*, Royal Society of Chemistry, Cambridge, 2003.
- A. M. Kirillov, M. N. Kopylovich, M. V. Kirillova, M. Haukka, M. F. C. Guedes da Silva and A. J. L. Pombeiro, *Angew. Chem., Int. Ed.*, 2005, **44**, 4345.
- M. V. Kirillova, A. M. Kirillov, P. M. Reis, J. A. L. Silva, J. J. R. Fraústo da Silva and A. J. L. Pombeiro, *J. Catal.*, 2007, **248**, 130, and references therein.

- 25 M. V. Kirillova, A. M. Kirillov, M. F. C. Guedes da Silva and A. J. L. Pombeiro, *Eur. J. Inorg. Chem.*, 2008, 3423.
- 26 A. M. Kirillov, M. Haukka, M. F. C. Guedes da Silva and A. J. L. Pombeiro, *Eur. J. Inorg. Chem.*, 2005, 2071.
- 27 Y. Y. Karabach, A. M. Kirillov, M. F. C. Guedes da Silva, M. N. Kopylovich and A. J. L. Pombeiro, *Cryst. Growth Des.*, 2006, 6, 2200.
- 28 T. F. S. Silva, E. C. B. Alegria, L. M. D. R. S. Martins and A. J. L. Pombeiro, *Adv. Synth. Catal.*, 2008, 350, 706.
- 29 E. C. B. Alegria, M. V. Kirillova, L. M. D. R. S. Martins and A. J. L. Pombeiro, *Appl. Catal., A*, 2007, 317, 43.
- 30 (a) G. S. Mishra and A. J. L. Pombeiro, *J. Mol. Catal. A: Chem.*, 2005, 239, 96; (b) G. S. Mishra and A. J. L. Pombeiro, *Appl. Catal., A*, 2006, 304, 185; (c) G. S. Mishra, J. J. R. Fraústo da Silva and A. J. L. Pombeiro, *J. Mol. Catal. A: Chem.*, 2007, 265, 59; (d) G. S. Mishra, E. C. B. Alegria, L. M. D. R. S. Martins, J. J. R. Fraústo da Silva and A. J. L. Pombeiro, *J. Mol. Catal. A: Chem.*, 2008, 285, 92.
- 31 Y. Y. Karabach, A. M. Kirillov, M. Haukka, M. N. Kopylovich and A. J. L. Pombeiro, *J. Inorg. Biochem.*, 2008, 102, 1190.
- 32 (a) G. B. Shul'pin, *J. Mol. Catal. A: Chem.*, 2002, 189, 39; (b) G. B. Shul'pin, *C. R. Chim.*, 2003, 6, 163.
- 33 D. S. Nesterov, V. N. Kokozay, V. V. Dyakononko, O. V. Shishkin, J. Jezierska, A. Ozarowski, A. M. Kirillov, M. N. Kopylovich and A. J. L. Pombeiro, *Chem. Commun.*, 2006, 4605.
- 34 M. N. Kopylovich, A. M. Kirillov, A. K. Baev and A. J. L. Pombeiro, *J. Mol. Catal. A: Chem.*, 2003, 206, 163.
- 35 G. Trettenhahn, M. Nagl, N. Neuwirth, V. B. Arion, W. Jary, P. P. Chlauer and W. Schmid, *Angew. Chem., Int. Ed.*, 2006, 45, 2794.
- 36 A. Maldotti, A. Molinari, G. Varani, M. Lenarda, L. Storaro, F. Bigi, R. Maggi, A. Mazzacani and G. Sartori, *J. Catal.*, 2002, 209, 210.
- 37 (a) L. M. Slaughter, J. P. Collman, T. A. Eberspacher and J. I. Brauman, *Inorg. Chem.*, 2004, 43, 5198; (b) I. N. Moiseeva, A. E. Gekhman, V. V. Minin, G. M. Larin, M. E. Bashtanov, A. A. Krasnovskii and I. I. Moiseev, *Kinet. Catal.*, 2000, 41, 170; (c) J. M. Mattalia, B. Vacher, A. Samat and M. Chanon, *J. Am. Chem. Soc.*, 1992, 114, 4111.
- 38 (a) G. B. Shul'pin, Y. N. Kozlov, G. V. Nizova, G. Süß-Fink, S. Stanislas, A. Kitaygorodskiy and V. S. Kulikova, *J. Chem. Soc. Perkin Trans.*, 2001, 2, 1351; (b) G. B. Shul'pin, *J. Mol. Catal. A: Chem.*, 2005, 227, 247; (c) Y. N. Kozlov, V. B. Romakh, A. Kitaygorodskiy, P. Buglyó, G. Süß-Fink and G. B. Shul'pin, *J. Phys. Chem. A*, 2007, 111, 7736; (d) M. Kuznetsov and A. J. L. Pombeiro, *Inorg. Chem.*, 2009, 48, 307.
- 39 (a) M. Costas, M. P. Mehn, M. P. Jensen and L. Que, Jr., *Chem. Rev.*, 2004, 104, 939; (b) M. Costas, K. Chen and L. Que, Jr., *Coord. Chem. Rev.*, 2000, 517, 200; (c) G. Roelfes, M. Lubben, R. Hage, L. Que, Jr. and B. L. Feringa, *Chem.–Eur. J.*, 2000, 6, 2152.
- 40 T. Hogan and A. Sen, *J. Am. Chem. Soc.*, 1997, 119, 2642.
- 41 (a) G. B. Shul'pin in *Transition Metals for Organic Synthesis*, eds. M. Beller and C. Bolm, 2nd edn, vol. 2. Wiley-VCH, New York, 2004, p. 215; (b) G. B. Shul'pin, *Organic Reactions Catalyzed by Metal Complexes*, Nauka, Moscow, 1988.
- 42 (a) G. V. Nizova, B. Krebs, G. Süß-Fink, S. Schindler, L. Westerheide, L. G. Cuervo and G. B. Shul'pin, *Tetrahedron*, 2002, 58, 9231; (b) G. Süß-Fink, L. Gonzalez and G. B. Shul'pin, *Appl. Catal. A: Gen.*, 2001, 217, 111; (c) G. B. Shul'pin and G. Süß-Fink, *J. Chem. Soc., Perkin Trans.*, 1995, 2, 1459; (d) M. Kodera, H. Shimakoshi and K. Kano, *Chem. Commun.*, 1996, 1737; (e) H.-J. Schneider and W. Müller, *J. Org. Chem.*, 1985, 50, 4609; (f) G. B. Shul'pin, H. Stoeckli-Evans, D. Mandelli, Y. N. Kozlov, A. T. Vallina, C. B. Woitiski, R. S. Jimenez and W. A. Carvalho, *J. Mol. Catal. A: Chem.*, 2004, 219, 255.
- 43 G. B. Shul'pin, J. Gradinaru and Y. N. Kozlov, *Org. Biomol. Chem.*, 2003, 1, 3611.
- 44 P. M. Reis, J. A. L. Silva, A. F. Palavra, J. J. R. F. da Silva, T. Kitamura, Y. Fujiwara and A. J. L. Pombeiro, *Angew. Chem., Int. Ed.*, 2003, 42, 821.
- 45 R. L. Martin and H. Waterman, *J. Chem. Soc.*, 1957, 2545.
- 46 M. W. Senko, *IsoPro Isotopic Abundance Simulator*, v. 2.1: National High Magnetic Field Laboratory, Los Alamos National Laboratory, Los Alamos, NM, 1994.
- 47 A. J. L. Pombeiro, M. F. C. Guedes da Silva and M. A. N. D. A. Lemos, *Coord. Chem. Rev.*, 2001, 219-221, 53.
- 48 *SMART & SAINT Software Reference Manuals*, version 5.051 (Windows NT Version), Bruker Analytical X-ray Instruments Inc., Madison, WI, 1998.
- 49 G. M. Sheldrick, *SADABS, program for empirical absorption correction*, University of Göttingen, Germany, 1996.
- 50 A. Altomare, M. C. Burla, M. Cavalli, G. L. Casciarano, C. Giacovazzo, A. Guagliardi, A. G. Moliterni, G. Polidori and R. Spagna, *J. Appl. Crystallogr.*, 1999, 32, 115.
- 51 G. M. Sheldrick, *SHELXTLplus (Windows NT Version) Structure Determination Package*, Version 5.1, Bruker Analytical X-ray Instruments Inc., Madison, WI, USA, 1998.
- 52 C. F. Macrae, P. R. Edgington, P. McCabe, E. Pidcock, G. P. Shields, R. Taylor, M. Towler and J. van de Streek, Mercury: visualization and analysis of crystal structures, *J. Appl. Crystallogr.*, 2006, 39, 453.
- 53 E. Keller, *SCHAKAL A Computer Program for the Graphic Representation of Molecular and Crystallographic Models*, Institute for Crystallography of the University of Freiburg, Freiburg (Germany), 1999.

Trinuclear Triangular Copper(II) Clusters – Synthesis, Electrochemical Studies and Catalytic Peroxidative Oxidation of Cycloalkanes

Corrado Di Nicola,^[a] Federica Garau,^[b,c] Yauhen Y. Karabach,^[c]
Luísa M. D. R. S. Martins,^[c,d] Magda Monari,^[e] Luciano Pandolfo,^{*,[b]} Claudio Pettinari,^{*,[a]}
and Armando J. L. Pombeiro^{*,[c]}

Keywords: Cluster compounds / Copper / Oxidation / Electrochemistry / Copper(II) trinuclear complexes / Catalytic peroxidative oxidation

The reactions of Cu^{II} carboxylates (valerate, 2-methylbutyrate, hexanoate, heptanoate) with pyrazole (Hpz) in EtOH or EtOH/water solutions easily afford the triangular trinuclear copper derivatives [Cu₃(μ₃-OH)(μ-pz)₃(RCOO)₂(L)_x] [R = CH₃(CH₂)₃, L = H₂O, x = 1 for **5**; R = CH₃CH₂CH(CH₃), L = EtOH, x = 2 for **6**; R = CH₃(CH₂)₄, L = EtOH, x = 1 for **7**; R = CH₃(CH₂)₅, L = EtOH, x = 1 for **8**] as it has been previously found for R = H, L = Hpz, x = 2, (**1**); R = CH₃, L = Hpz, x = 1, (**2**); R = CH₃CH₂, L = EtOH, x = 1, (**3**) and [Cu₃(μ₃-OH)(μ-pz)₃-(CH₃(CH₂)₂COO)₂(MeOH)(H₂O)], (**4**). The trinuclear structure common to **5–8** has been assigned on the basis of magnetic susceptibility studies, ESI MS, IR and UV/Vis spectroscopy as well as ¹H NMR measurements. The room temp. magnetic susceptibilities of **5–8** almost correspond to the presence of a single unpaired electron for each trinuclear unit. The IR spectra exhibit signals due to the bridging μ₃-OH in accordance with what was observed in the spectra of **1–4**. Solid-state and MeOH solution UV/Vis spectra show the

same features previously reported for **1–4** and ¹H NMR spectra of **1–8** show almost identical low field signals that can be assigned to pz⁻ hydrogens. A detailed investigation of the supramolecular structures of **1** and **4** and the single-crystal X-ray study of the polymeric *paddlewheel* Cu(2-methylbutyrate)₂, **A**, are also reported. Electrochemical experiments show that in **1–8** the Cu^{II} ions can be reduced, in distinct steps, to Cu^I and Cu⁰. All the complexes act as catalysts or catalyst precursors for the efficient peroxidative oxidation, by aqueous hydrogen peroxide in acetonitrile and at room temp., of cycloalkanes RH (cyclohexane and cyclopentane) to the corresponding cyclic alcohols and ketones, with overall yields of up to 34 % and TONs up to 42. Radical pathways involving the formation of alkyl hydroperoxides (ROOH) are involved.

(© Wiley-VCH Verlag GmbH & Co. KGaA, 69451 Weinheim, Germany, 2009)

Introduction

Oligonuclear transition metal complexes have drawn a significant amount of attention due to their magnetic properties, redox characteristics and relevance in numerous catalytic industrial and biological processes.^[1] The strong interest in di-, tri- and polynuclear copper(II) complexes mainly

stems from the fact that copper has been recognised as a fundamental element in biological systems. As an example, copper species are present in numerous enzymes that selectively catalyse various oxidation reactions,^[1g–l,2] including those performed by the still poorly characterised particulate methane monooxygenase (pMMO) present in methanotrophs, in which a Cu cluster catalyses alkane hydroxylation and alkene epoxidation.^[2c,f,g] Moreover, trinuclear arrays of copper(II) have been indicated as the essential functional units in numerous multicopper blue oxidases such as laccase and ascorbate oxidases.^[3]

In past years we have successfully synthesised di-, tri-, tetra- and polynuclear triethanolamine copper(II) complexes,^[4] as well as trinuclear triangular copper(II) complexes with carboxylate ligands^[5] and shown^[4,5c] that they can act as remarkably active and selective catalysts or catalyst precursors for peroxidative oxidation of cycloalkanes to the corresponding alcohols and ketones.

Continuing our studies on these compounds, we have synthesised and characterised four new trinuclear triangular Cu^{II} compounds, [Cu₃(μ₃-OH)(μ-pz)₃(RCOO)₂L_x] [pz = pyr-

[a] Dipartimento di Scienze Chimiche, Università di Camerino, Via S. Agostino, 1, 62032 Camerino (MC), Italy
Fax: +39-0737-637345

E-mail: claudio.pettinari@unicam.it

[b] Dipartimento di Scienze Chimiche, Università di Padova, Via Marzolo, 1, 35131 Padova, Italy
E-mail: luciano.pandolfo@unipd.it

[c] Centro de Química Estrutural, Complexo I, Instituto Superior Técnico, TU Lisbon, Av. Rovisco Pais, 1049-001 Lisbon, Portugal
E-mail: pombeiro@ist.utl.pt

[d] Departamento de Engenharia Química, ISEL, R. Conselheiro Emídio Navarro, 1950-062 Lisbon, Portugal

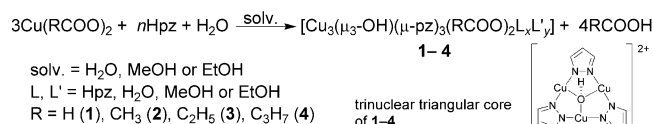
[e] Dipartimento di Chimica “G. Ciamician”, Università di Bologna, Via Selmi, 2, 40126 Bologna, Italy

Supporting information for this article is available on the WWW under <http://www.eurjic.org> or from the author.

azolate; L = EtOH, H₂O; R = CH₃(CH₂)₃ (valerate), CH₃CH₂CH(CH₃) (2-methylbutyrate), CH₃(CH₂)₄ (hexanoate), CH₃(CH₂)₅ (heptanoate)]. For these compounds, as well as for the related previously reported derivatives with R = H (formate),^[5b] CH₃ (acetate)^[5a] or CH₃(CH₂)₂ (butyrate),^[5b] we report the catalytic properties for the peroxidative oxidation of cycloalkanes. Moreover, the electrochemical behaviour of such compounds and of an analogous derivative with R = CH₃CH₂ (propionate) is presented. Finally, the crystal structure of Cu(2-methylbutyrate)₂ and the supramolecular H-bonding features of trinuclear triangular derivatives [with R = H and CH₃(CH₂)₂] are briefly outlined.

Results and Discussion

Recently, we established a synthetic procedure for obtaining trinuclear triangular copper(II) derivatives simply by treating Cu^{II} carboxylates with Hpz in the presence of water, according to the reaction reported in Scheme 1.^[5]



Scheme 1. General procedure for the synthesis of trinuclear copper complexes [Cu₃(μ₃-OH)(μ-pz)₃(RCOO)₂L_xL'_y].

The single-crystal X-ray diffraction molecular structures of compounds 1–4^[5] indicated the formation of a trinuclear triangular core [Cu₃(μ₃-OH)(μ-pz)₃]²⁺, the three Cu^{II} ions also being coordinated by two carboxylate groups, neutral azoles and/or solvent molecules.^[6]

Moreover, these trinuclear triangular clusters act as secondary building units (SBUs) forming 1D (3) or 2D (1, 2) metal organic frameworks (MOFs) or a hexanuclear cluster (4) through bridging carboxylates. Since a deep examination of other relevant supramolecular interactions, such as H-bonds, was in some cases explicitly omitted,^[5a,5b] we have hereby taken opportunity to briefly describe these features which are involved in the supramolecular assembly of 1 and 4.^[7]

In [Cu₃(μ₃-OH)(μ-pz)₃(HCOO)₂(Hpz)₂·H₂O (1), the most relevant supramolecular interactions are due to formate bridges generating a “fishing net” 2D MOF^[5b] but a relevant role is also played by H-bonds which involve the crystallisation water molecules, the two formate groups and the μ₃-OH unit (see Figure S1). In particular, each crystallisation water molecule behaves as an H donor in two strong H-bonds, the first one with μ₃-OH [O(1w)···O(1) 2.710(4) Å, O(1w)···H(1)–O(1) 163(5)°] from the complex in the same asymmetric unit, while the second one is with the

uncoordinated carboxylate oxygen [O(5')] of another trinuclear unit [O(5')···O(1w) 2.780(5) Å, O(5')···H(1w)–O(1w) 130(4)°; symmetry code: (I) –x, y – 0.5, –z + 1]. Moreover, compound 1 forms two relatively strong intermolecular H-bonds between: i) the pyrazolic hydrogen bound to N(10) and the coordinated oxygen [O(4')] of the formate group belonging to the adjacent trinuclear unit [O(4')···N(10) 2.828(4) Å, O(4')···H(10N)–N(10) 168°] and ii) the pyrazolic hydrogen H(8N) of the second terminally bound pyrazole and a formate oxygen O(2'') of a third trinuclear unit [O(2'')···N(8) 2.677(4) Å, O(2'')···H(8N)–N(8) 167°; symmetry code: (II) x + 1, y, z]. In both cases the 2D MOFs generated through formate bridges are reinforced.

In compound 4 the most striking structural feature is the presence, in contrast to 1, of hexanuclear units located around inversion centres and generated by two monodentate carboxylate bridges (see Scheme S1 in the Supporting Information).^[5b] Two intramolecular H-bonds can also be detected, those involving the carboxylate oxygen O(3) with the proton of the central μ₃-OH group [O(3)···O(1) 2.763(4) Å, O(3)···H–O(1) 162(4)°] and two interactions involving the carboxylate O(5) with the hydrogen of coordinated methanol [O(5)···O(6) 2.815(4) Å, O(5)···H(61)–O(6) 171(6)°] (see Figure S2a). O(5) is also engaged in an intermolecular H-bond with the coordinated water of another hexanuclear unit [O(5)···O(7'') 2.694(4) Å, O(5)···H(8w'')–O(7'') 166(5)°; symmetry code: (II) –x + 1, –y + 1, –z] thus generating a 1D supramolecular network running along the *ab* diagonal (see Figure S2b). Moreover, the carboxylate oxygens O(3) pertaining to these parallel networks are also involved in another series of intermolecular H-bonds with coordinated water molecules of neighbouring units [O(3)···O(7'') 2.947(4) Å, O(3)···H(7w'')–O(7'') 151(5)°; symmetry code: (III) x, y + 1, z] with formation of a 2D supramolecular network (see Figure S3).

Continuing our studies, we examined the reactions of Hpz with other Cu^{II} carboxylates, namely valerate, 2-methylbutyrate, hexanoate and heptanoate. Incidentally, in the course of the synthesis of copper(II) 2-methylbutyrate, A, we isolated well formed crystals of this compound. A single-crystal X-ray diffraction study showed that compound A has the typical paddlewheel structure which behaves as a secondary building unit (SBU) to form a 1D MOF in a manner similar to what can be observed in other copper(II) carboxylates.^[8]

The molecular structure of A,^[9] which is based on a crystallographic inversion centre located midway along the Cu–Cu vector, is shown in Figure 1. The paddlewheel motif of A is generated by two different types of carboxylate anions almost symmetrically bridging two copper(II) ions. The Cu(1)–O bond lengths are very similar, falling in the range 1.927–1.966(3) Å with the exception of the Cu(1')–O(4) distance which is slightly longer [2.004(3) Å]. In addition, O(4) is also coordinated to the copper Cu(1'') of another paddlewheel unit [O(4)–Cu(1'') 2.216(2) Å] thus generating a 1D MOF running down the crystallographic *a* axis (see Figure S4). Finally, the Cu(1)···Cu(1') separation in the carboxylate bridged complex is 2.5820(8) Å [symmetry code (I):

$-x + 1, -y, -z]$ which is substantially shorter than the inter-paddlewheel distance $[\text{Cu}(1)\cdots\text{Cu}(1'')] 3.2438(8) \text{ \AA}$, symmetry code (II): $-x, -y, -z]$.

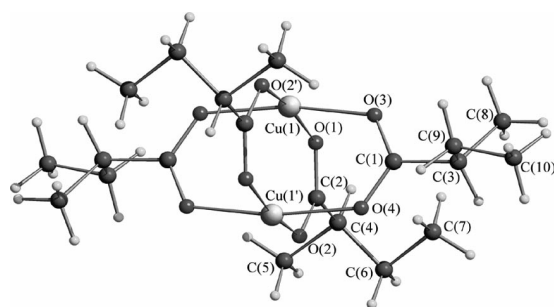


Figure 1. Molecular structure of **A** showing the typical paddlewheel arrangement. Relevant bond lengths [Å]: Cu(1)–O(1) 1.937, Cu(1)–O(2) 1.927, Cu(1)–O(3) 1.966, Cu(1')–O(4) 2.004(3), Cu(1)⋯Cu(1'') 2.5820(8).

The reaction of Hpz with Cu^{II} valerate, 2-methylbutyrate, hexanoate or heptanoate yielded compounds **5–8**, respectively. Unfortunately, we were unable to obtain crystals suitable for X-ray diffraction but we inferred their structures from analytical and spectroscopic data all of which suggest that they have the same trinuclear triangular $[\text{Cu}_3(\mu_3\text{-OH})(\mu\text{-pz})_3]^{2+}$ core sketched in Scheme 1.

First of all, the formation in each synthesis of the corresponding carboxylic acid (see Experimental Section) indicates that the carboxylates have deprotonated water and Hpz generating OH^- and pz^- ions which build up the Cu^{II} trinuclear triangular core.

IR spectra are in accordance with the proposed structure for **5–8**. The IR spectra of **5**, **7** and **8** in fact show two strong bands corresponding to $\nu_{\text{asym}}(\text{COO})$ (ca 1570 cm^{-1}) and $\nu_{\text{s}}(\text{COO})$ (1430 cm^{-1}). The Δ values [$\nu_{\text{asym}}(\text{COO}) - \nu_{\text{s}}(\text{COO})$] are in agreement with a nearly symmetric bridging bidentate coordination for the carboxylates, analogous to that found in derivative **4**.^[5b] On the other hand, the spectrum of **6** is very similar to that of derivative **3**:^[5b] two sets of absorptions of very different intensities, due to carboxylates, are actually present. Both sets exhibit a Δ value of ca. 120 cm^{-1} and could be assigned to methylbutyrate symmetrically bridging two Cu^{II} centres in a mono- or bidentate fashion.^[16] The IR spectra of **5–8** always show a signal at ca. 750 cm^{-1} [$\delta(\text{CH})_{\text{oop}}$] which corresponds to bridging pyrazolate ligands.^[17] No absorption assignable to $\nu(\text{N-H})$ could be observed. Besides the expected band over 3000 cm^{-1} , due to $\nu(\text{C-H})$ of the pyrazolate,^[18] a broad absorption between $3300\text{--}2800 \text{ cm}^{-1}$, most likely due to hydrogen-bonded OH from alcohol or water, is present. Very small absorptions, sometimes found at ca. 1715 cm^{-1} , are due to traces of RCOOH formed during the synthesis.

^1H NMR measurements carried out on CD_3OD solutions of **1–8** show, besides relatively high-field signals due to carboxylate hydrogens, two low-field broad peaks at ca. 37 ppm (δ_1) and ca. 41 ppm (δ_2), integrating in a 2:1 ratio.

These can be assigned to the two equivalent H(3) and H(5) (δ_1) and H(4) (δ_2) pyrazolate hydrogens as already reported for some similar Cu^{II} trinuclear triangular derivatives.^[19]

The room temperature magnetic susceptibilities of compounds **5–8** are consistent with the proposed trinuclear arrangement. The observed μ values, ranging between 2.45 and 2.73 BM, although a little bit larger than those found for **1–4**,^[5a,5b] are too low for three independent Cu^{II} ions, suggesting some kind of exchange coupling in these cases as well.

ESI MS data further support the presence, in **5–8**, of the $[\text{Cu}_3(\mu_3\text{-OH})(\mu\text{-pz})_3]^{2+}$ core with positive charges balanced by two carboxylate ions. In detail, most relevant signals (Table 1) can be attributed to trinuclear and hexanuclear moieties, analogous to what was previously observed for compounds **1–4**.^[5] Even though the ESI MS data are not an exhaustive proof of the presence, in the solid-state, of trinuclear or hexanuclear Cu^{II} clusters,^[20] they certainly strongly suggest this feature, particularly if we take into account that peaks attributable to mononuclear Cu^{II} species are generally not observed (see Figures S5–S8).

Table 1. Most relevant signals in the ESI mass spectra of compounds **5–8**.

	Signal ^[a]	Rel. ab. ^[b]	Assignment ^[c]
5	684.8	63	$[\text{Cu}_3(\text{OH})(\text{pz})_3(\text{RCOO})_2(\text{MeOH})(\text{S})] + \text{H}^+$
	1112.8	100	$[\text{Cu}_6(\text{OH})_4(\text{pz})_6(\text{RCOO})(\text{MeOH})_3]^+$
	1148.8	96	$[\text{Cu}_6(\text{OH})_4(\text{pz})_6(\text{RCOO})(\text{H}_2\text{O})_2(\text{MeOH})_3]^+$
6	752.7	16	$[\text{Cu}_3(\text{OH})(\text{pz})_3(\text{RCOO})_2(\text{H}_2\text{O})_2(\text{MeOH})_2(\text{S})] + \text{H}^+$
	1112.6	40	$[\text{Cu}_6(\text{OH})_4(\text{pz})_6(\text{RCOO})(\text{MeOH})_3]^+$
	1148.5	100	$[\text{Cu}_6(\text{OH})_4(\text{pz})_6(\text{RCOO})(\text{H}_2\text{O})_2(\text{MeOH})_3]^+$
7	698.8	52	$[\text{Cu}_3(\text{OH})(\text{pz})_3(\text{RCOO})_2(\text{H}_2\text{O})(\text{S})] + \text{H}^+$
	1154.8	83	$[\text{Cu}_6(\text{OH})_3(\text{pz})_6(\text{RCOO})_2(\text{H}_2\text{O})_3]^+$
	1190.8	100	$[\text{Cu}_6(\text{OH})_3(\text{pz})_6(\text{RCOO})_2(\text{H}_2\text{O})_4]^+$
8	619.9	25	$[\text{Cu}_3(\text{OH})(\text{pz})_3(\text{RCOO})(\text{MeOH})_2(\text{H}_2\text{O})]^+$
	1196.8	35	$[\text{Cu}_6(\text{OH})_3(\text{C}_3\text{H}_3\text{N}_2)_6(\text{RCOO})_2(\text{H}_2\text{O})_4(\text{MeOH})]^+$
	1232.8	100	$[\text{Cu}_6(\text{OH})_3(\text{C}_3\text{H}_3\text{N}_2)_6(\text{RCOO})_2(\text{H}_2\text{O})_6(\text{MeOH})]^+$

[a] Values corresponding to the higher signals of the isotopic clusters. All isotopic clusters fit satisfactorily with calculated ones.^[21]

[b] Relative abundance of the higher signal of the isotopic cluster.
[c] S = MeCN; R = $\text{CH}_3(\text{CH}_2)_3$, (**5**), $\text{CH}_3\text{CH}_2\text{CH}(\text{CH}_3)$, (**6**), $\text{CH}_3(\text{CH}_2)_4$, (**7**), $\text{CH}_3(\text{CH}_2)_5$, (**8**).

Finally, the trinuclear triangular structure of **5–8** is supported by their solid-state reflectance and MeOH solution electronic spectra (400–800 nm) (Figure 2).

The solid-state spectra of **5–8** (Figure 2a) show almost identical patterns. In detail, besides two shoulders around 520 and 720 nm, they display a complex absorption band where two maxima positioned at ca. 610 and 650 nm are evident. These spectroscopic patterns are only slightly different in MeOH solutions (Figure 2b) and the two low energy maxima observed in the solid-state mediate into broad asymmetric signals centred around 620–625 nm. The observed patterns are almost identical to those shown by **1–4**^[5] and other closely related species with Cl^- ,^[22] SO_4^{2-} , ClO_4^- , CF_3COO^- , CF_3SO_3^- and NO_3^- counter anions^[23] and trinuclear triangular structures ascertained by single-crystal X-ray determinations. Moreover, these patterns differ greatly from the UV/Vis spectra of MeOH solutions of the mononuclear species $\text{Cu}(\text{Hpz})_4(\text{X})_2$ ($\text{X} = \text{Cl}^-$, NO_3^- ,

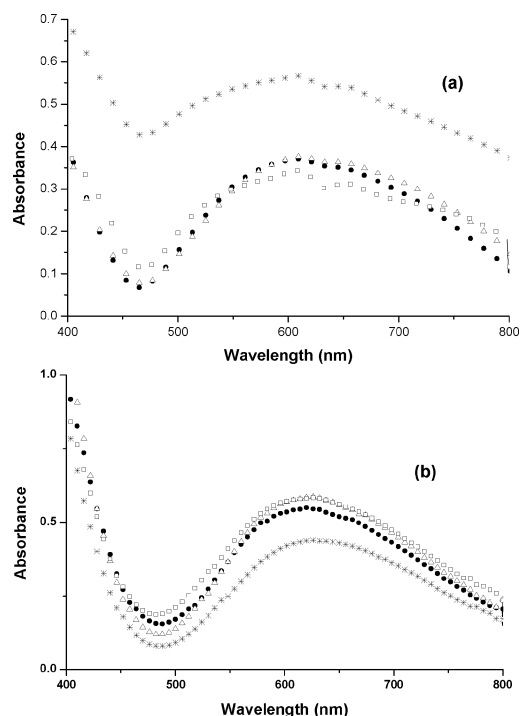


Figure 2. Solid-state reflectance (a) and MeOH solution (b) electronic spectra of **5** (squares), **6** (stars), **7** (solid circles) and **8** (triangles).

H_2PO_4^- , ClO_4^- , CF_3COO^- , CF_3SO_3^- ; $\text{X}_2 = \text{SO}_4^{2-}$), which exhibit a characteristic broad signal in the range 710–720 nm.^[22,23]

Electrochemical Behaviour of 1–8

The redox properties of compounds **1–8** have been investigated by cyclic voltammetry using a Pt electrode in a 0.2 M $[\text{nBu}_4\text{N}][\text{BF}_4]/\text{DMSO}$ solution at 25 °C. All compounds exhibit similar voltammograms, showing two single-electron (per metal atom) irreversible reduction waves, (Figure 3 shows the voltammogram of **2**) assigned to the $\text{Cu}^{\text{II}} \rightarrow \text{Cu}^{\text{I}}$ (wave I) and $\text{Cu}^{\text{I}} \rightarrow \text{Cu}^0$ (wave II) reductions, at the reduction peak potential values given in Table 2 ($^{\text{I}}E_{\text{p}}^{\text{red}}$ in the range from –0.38 to –0.45 V vs. SCE and $^{\text{II}}E_{\text{p}}^{\text{red}}$ between –1.31 and –1.52 V vs. SCE). In addition, a new irreversible oxidation wave (wave *a*) in the range 0.2–0.5 V vs. SCE (Table 2, Figure 3) can be observed upon scan reversal following the first reduction wave. It corresponds to the oxidation of the Cu^{I} species formed at the first reduction process.

The occurrence of a single-electron reduction per Cu^{II} (or Cu^{I}) ion was confirmed by exhaustive controlled potential electrolysis (CPE) at a potential slightly more cathodic to that of the peak potential of wave I (or II). This corresponds to a charge consumption of 3 F mol^{–1} of complex. The reduced Cu^{I} compounds appear to be stable in the solvent/electrolyte medium along the CPE and the corresponding $\text{Cu}^{\text{I/III}}$ oxidation (wave *a*) and $\text{Cu}^{\text{I/0}}$ reduction (wave II) can be observed at the end of the electrolysis

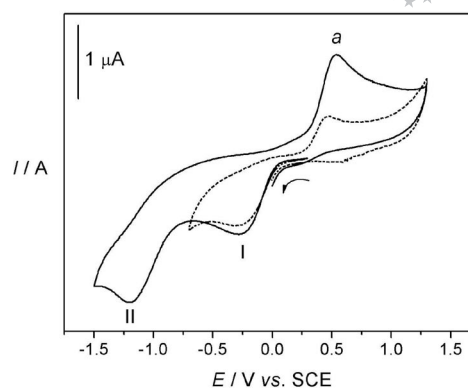


Figure 3. Cyclic voltammogram of $[\text{Cu}_3(\mu_3\text{-OH})(\mu\text{-pz})_3(\text{CH}_3\text{COO})_2(\text{Hpz})]$, **2**, in a 0.2 M $[\text{nBu}_4\text{N}][\text{BF}_4]/\text{DMSO}$ solution ($c = 2.41 \text{ mM}$), at a Pt disk working electrode ($d = 0.5 \text{ mm}$) at 200 mV s^{-1} .

Table 2. Cyclic voltammetric data^[a] for complexes **1–8**.

Complex	Cathodic waves		Anodic wave ^[b]
	$^{\text{I}}E_{\text{p}}^{\text{red}}$	$^{\text{II}}E_{\text{p}}^{\text{red}}$	E_{p}^{ox}
1	–0.40	–1.40	0.28
2	–0.44	–1.31	0.19
3	–0.38	–1.42	0.35
4	–0.38	–1.51	0.33
5	–0.45	–1.44	0.47
6 ^[c]	–0.45	–1.49	0.28
7 ^[c]	–0.45	–1.44	0.54
8	–0.42	–1.52	0.39

[a] Potential values in volts ± 0.02 vs. SCE in a 0.2 M $[\text{nBu}_4\text{N}][\text{BF}_4]/\text{DMSO}$ solution with a Pt disk working electrode, determined by using the $[\text{Fe}(\eta^5\text{-C}_5\text{H}_5)_2]^{0/+}$ redox couple ($E_{1/2}^{\text{ox}} = 0.44 \text{ V}$ vs. SCE) as internal standard and a scan rate of 200 mV s^{-1} . [b] Anodic wave (*a*) generated upon scan reversal following the first reduction wave. [c] An oxidation wave at $E_{\text{p}}^{\text{ox}} = -0.10 \text{ V}$ is generated upon scan reversal following the second reduction wave.

(Table 2). The CPE performed at the second reduction wave leads to the deposition of metallic copper which can be clearly observed by its sharp oxidation (with desorption) wave at $E_{\text{p}}^{\text{ox}} = -0.11 \text{ V}$, as shown in Figure 4 for compound **2**.

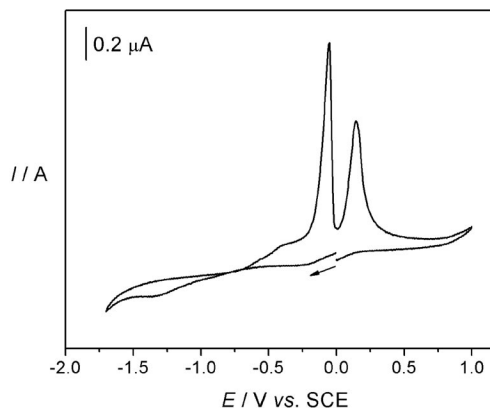


Figure 4. Cyclic voltammogram after CPE at the reduction wave II of $[\text{Cu}_3(\mu_3\text{-OH})(\mu\text{-pz})_3(\text{CH}_3\text{COO})_2(\text{Hpz})]$, **2**, in a 0.2 M $[\text{nBu}_4\text{N}][\text{BF}_4]/\text{DMSO}$ solution with a Pt disk working electrode ($d = 0.5 \text{ mm}$) at 20 mV s^{-1} .

No oxidation wave has been detected for any of the complexes by a first anodic sweep without a previous reduction scan, indicating that neither a metal centred nor a ligand centred oxidation occurs. Since any of the cathodic waves involve the reduction of the three metal atoms without differentiation of distinct waves at different potentials, no metal–metal electronic communication was detected. Nevertheless, the occurrence of such an interaction, to a limited extent, cannot be ruled out in view of the considerable broadness of the reduction waves which can result from the overlap of other waves at close but distinct reduction potentials, corresponding to the sequential metal reductions, i.e. $\text{Cu}^{\text{II}}\text{Cu}^{\text{II}}\text{Cu}^{\text{II}} \rightarrow \text{Cu}^{\text{I}}\text{Cu}^{\text{II}}\text{Cu}^{\text{II}} \rightarrow \text{Cu}^{\text{I}}\text{Cu}^{\text{I}}\text{Cu}^{\text{II}} \rightarrow \text{Cu}^{\text{I}}\text{Cu}^{\text{I}}\text{Cu}^{\text{I}}$ for wave I and, similarly, for the further reductions to Cu^0 at wave II. The values of the reduction potentials of our complexes could reflect the electron-donor character of their ligands but the narrow range and the broadness of the waves prevent reliable comparisons.

All the above indicated characterisations made us fully confident of the trinuclear triangular nature of compounds **5–8**. We therefore tested them (as well as compounds **1**, **2** and **4**) as catalysts for the peroxidative oxidation of cycloalkanes in order to compare their behaviour with that shown by compound **3**.^[5c]

Catalytic Peroxidative Oxidation of Cycloalkanes (Compounds **1**, **2** and **4–8**)

All the new trinuclear triangular copper(II) complexes behave as catalysts or catalyst precursors for the mild peroxidative oxidation of cyclohexane and cyclopentane with aqueous H_2O_2 , at room temperature and atmospheric pressure, to the corresponding cyclic alcohols (i.e. cyclohexanol or cyclopentanol) and cyclic ketones (i.e. cyclohexanone or cyclopentanone). The reactions were carried out in a liquid biphasic ($\text{MeCN}/\text{H}_2\text{O}$) medium in the presence of nitric acid. The activity and selectivity depend on a variety of factors such as the relative amounts of the reagents and solvent which can be varied for the optimisation of the reaction conditions as we have reported^[4b,24–28] for other alkane functionalisation catalytic systems. Moreover, the addition of nitric acid to the reaction mixture strongly enhances the activity as reported^[29–31] for other metal catalysts with N,O ligands, since it can activate the catalyst by promoting unsaturation of the metal centre upon ligand protonation, stabilises peroxo intermediate species^[4a] and prevents the decomposition of hydrogen peroxide. According to our previous observations,^[5c] the maximum activity for the trinuclear copper(II) complexes was reached for the acid-to-catalyst and H_2O_2 -to-catalyst molar ratios of ca. 10:1 and ca. 500–1000, respectively, values that were chosen as typical for the experiments. An increase in the temperature leads to a yield drop (Table 3, entry 18), probably due to the decomposition of hydrogen peroxide.

The use of such catalysts precursors led, in a single batch, to overall yields (based on the cycloalkane) of up to 34% and turnover numbers (TONs) of up to 42 mol of products

per mol of catalyst (see Tables 3, 4, and 5 and Figures 5, 6, and 7). Simple salts of copper(II), such as basic copper(II) carbonate and copper(II) 2-methylbutyrate, exhibit much lower catalytic activities under similar reaction conditions (Tables 3, entries 19, 20 and 5, entries 7, 8). Only traces of cycloalkane oxidation products are obtained in the absence of the copper(II) catalyst.

Table 3. Peroxidative oxidation of cyclohexane to cyclohexanol and cyclohexanone catalysed by compounds **1–8**.^[a]

Entry	Cat ^[b]	$n(\text{H}_2\text{O}_2)/n(\text{Cat})$	% Yield ^[c] of products			A/K ^[e]	TON ^[f]
			alcohol	ketone	total ^[d]		
1	1	500	26.5	4.9	31.4	5.6	31.4
2	2	500	26.4	4.6	31.0	5.9	31.0
3	3 ^[g]	500	23.0	2.6	25.6	9.1	25.6
4	4	500	23.8	4.3	28.1	5.6	28.1
5	5	500	23.3	3.3	26.6	7.1	26.6
6	6	1000	25.2	6.4	31.6	4.0	31.6
7	7	1000	25.2	6.8	32.0	3.7	32.0
8	8	1000	24.1	6.1	30.2	4.0	30.2
9	1	250	23.9	3.1	27.1	7.7	27.1
10	1	750	26.3	7.9	34.2	3.3	34.2
11	1	1000	23.4	9.0	32.4	2.6	32.4
12	4	250	20.2	2.8	23.0	7.1	23.0
13	4	750	25.0	8.2	33.2	7.1	23.0
14	4	1000	19.8	9.7	29.5	2.0	29.5
15	5	250	21.2	3.6	24.8	5.9	24.8
16	5	750	24.7	8.2	32.9	3.0	32.9
17	5	1000	21.2	11.4	32.6	1.9	32.6
18 ^[h]	1	1000	5.5	7.2	12.7	0.8	12.7
19	^[i]	1000	8.0	8.0	16.0	1.0	16.0
20	^[j]	1000	–	7.9	7.9	–	7.9

[a] Selected data; reaction conditions: C_6H_{12} (1 mmol), catalyst precursor (10 μmol), MeCN (4 mL), HNO_3 (0.10 mmol), H_2O_2 (2.5–10 mmol, added as a 30% aqueous solution), 6 h reaction time, room temperature. [b] Cat = catalyst. [c] Mol of product/100 mol of C_6H_{12} , measured upon reduction of ROOH to the alcohol by PPh_3 . [d] Cyclohexanol + cyclohexanone. [e] Alcohol (cyclohexanol)/ketone (cyclohexanone) molar ratio, upon reduction of ROOH to the alcohol by PPh_3 . [f] Overall TON values (mol of products/mol of catalyst). [g] Included^[5c] for comparative purposes. [h] At 50 °C. [i] $\text{CuCO}_3 \cdot \text{Cu}(\text{OH})_2$ as catalyst, for comparative purposes. [j] $\text{Cu}\{\text{CH}_3\text{CH}_2\text{CH}(\text{CH}_3)\text{COO}\}_2$ as catalyst, for comparative purposes.

The complexes **1**, **2** and **4**, in the peroxidative oxidation of cyclohexane under the same reaction conditions (Table 3, entries 1–5), exhibit similar catalytic activities which are slightly higher than those of **5** or **3** (the latter has already been investigated^[5c] and is included for comparative purposes).

An increase in the peroxide-to-catalyst molar ratio results in a yield increase, e.g., for complexes **1**, **4** and **5**, from 24–27 to 33–34% on changing that ratio from 250 to 750 (H_2O_2 amount increase from 2.5 to 7.5 mmol) whereupon the maximum yields are reached (Figure 5). A further rise of the oxidant amount (up to 10 mmol) does not lead to a better yield.

The relative amounts of the products are also dependent on the hydrogen peroxide amount. In fact, although for the H_2O_2 /catalyst molar ratio in the 250–500 range the cyclohexanol-to-cyclohexanone molar ratio (A/K) remains grossly invariant (close to 6–8 for catalysts **1**, **4** and **5**)

Table 4. Effect of the catalyst amount in the peroxidative oxidation of cyclohexane catalysed by compound **4**.^[a]

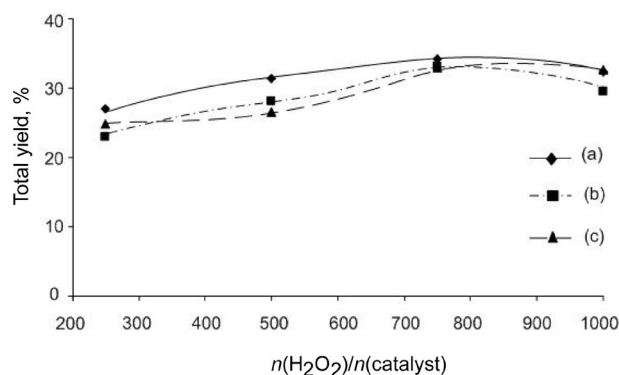
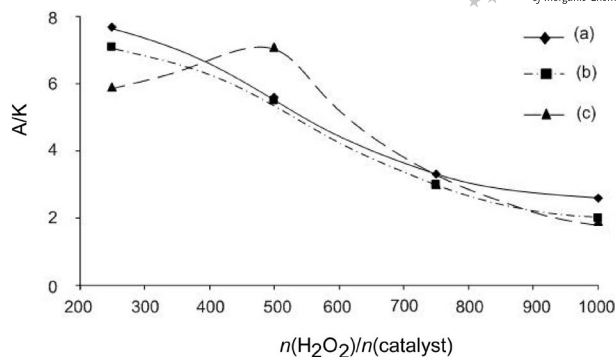
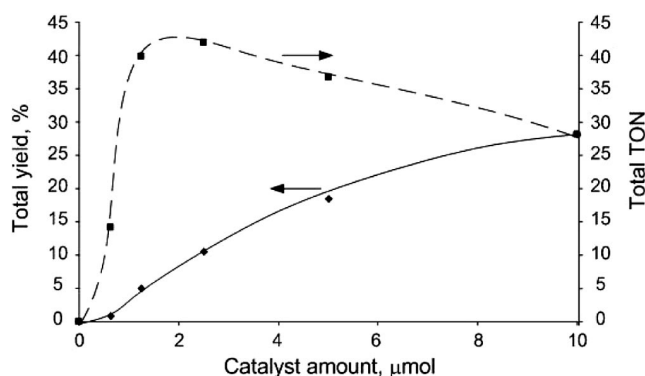
Entry	Catalyst amount μmol	% Yield ^[b] of products			A/K ^[d]	Overall TON ^[e]
		alcohol	ketone	total ^[c]		
1	0.0	0.1	0.0	0.1	—	—
2	0.63	0.9	0.0	0.9	—	14.1
3	1.25	4.5	0.5	5.0	9.1	39.8
4	2.50	9.6	0.9	10.5	11	41.9
5	5.0	16.7	1.7	18.4	10	36.8
6	10.0	23.8	4.3	28.1	5.6	28.1

[a] Selected data; reaction conditions: C_6H_{12} (1 mmol), MeCN 4 mL, HNO_3 (0.10 mmol), H_2O_2 (5 mmol, added as a 30% aqueous solution), 6 h reaction time, room temperature. [b] Mol of product/100 mol of C_6H_{12} , measured upon reduction of ROOH to the alcohol by PPh_3 . [c] Cyclohexanol + cyclohexanone. [d] Alcohol (cyclohexanol)/ketone (cyclohexanone) molar ratio, upon reduction of ROOH to the alcohol by PPh_3 . [e] Overall TON values (mol of products/mol of catalyst).

Table 5. Peroxidative oxidation of cyclopentane to cyclopentanol and cyclopentanone catalysed by compounds **1–5**.^[a]

Entry	Cat ^[b]	$n(\text{H}_2\text{O}_2)/n(\text{Cat})$	% Yield ^[c] of products			A/K ^[e]	TON ^[f]
			alcohol	ketone	total ^[d]		
1	—	500	0.0	0.0	—	—	
2	1	500	16.5	9.4	25.9	1.8	25.9
3	2	500	22.2	7.8	30.0	2.9	30.0
4	3 ^[g]	500	22.6	8.4	31.0	2.7	31.0
5	4	500	18.5	11.1	29.6	1.7	29.6
6	5	500	21.6	9.8	31.4	2.2	31.4
7	^[h]	1000	6.9	8.9	15.8	0.8	15.8
8	^[i]	1000	3.3	5.1	8.4	0.8	8.4

[a] Selected data; reaction conditions: C_5H_{10} (1 mmol), catalyst precursor (10 μmol), MeCN 4 mL, HNO_3 (0.10 mmol), H_2O_2 (5 or 10 mmol, added as an aqueous 30% solution), 6 h reaction time, room temperature. [b] Cat = Catalyst. [c] Mol of product/100 mol of C_5H_{10} , measured upon reduction of ROOH to the alcohol by PPh_3 . [d] Cyclopentanol + cyclopentanone. [e] Alcohol (cyclopentanol)/ketone (cyclopentanone) molar ratio, upon reduction of ROOH to the alcohol by PPh_3 . [f] Overall TON values (mols of products/mol of catalyst). [g] Included^[5c] for comparative purposes. [h] $\text{CuCO}_3 \cdot \text{Cu}(\text{OH})_2$ as catalyst, for comparative purposes. [i] $\text{Cu}\{\text{CH}_3\text{CH}_2\text{CH}(\text{CH}_3)\text{COO}\}_2$ as catalyst, for comparative purposes.

Figure 5. Effect of the peroxide-to-catalyst molar ratio on the overall yield of cyclohexanol and cyclohexanone in the cyclohexane oxidation catalysed by **1** (a), **4** (b) or **5** (c).Figure 6. Effect of the peroxide-to-catalyst molar ratio on the cyclohexanol-to-cyclohexanone molar ratio (A/K), in the cyclohexane oxidation catalysed by **1** (a), **4** (b) or **5** (c).Figure 7. Effect of the amount of catalyst **4** on the total yield and turnover number (TON).

(Figure 6), a further increase of the oxidant amount leads to higher yields of cyclohexanone with rough preservation of the cyclohexanol yields (Table 3) [e.g. A/K decreases from 7.1 to 1.9 and K/A increases correspondingly from 0.14 to 0.54 in the case of catalyst **5**, for the $\text{H}_2\text{O}_2/\text{catalyst}$ molar ratio change from 500 to 1000]. Hence, the growth of the overall yield with $n(\text{H}_2\text{O}_2)/n(\text{catalyst})$ (250–750 range) is essentially due to the enhanced formation of cyclohexanone for higher oxidant amounts.

The catalyst amount also plays a role and, as expected, its increase leads to a yield enhancement (Table 4, Figure 7), e.g., from 0.9% to 28% for the respective amounts of 0.63 and 10 μmol of catalyst **4** (which correspond to a substrate/catalyst molar ratio decrease from 1.59×10^3 to 100, respectively). On the other hand, a decrease of the catalyst amount below the typical value of 10 μmol results in enhancements of the overall TON from 28 up to 42 and of the A/K ratio from 5.6 up to 11 (Table 4, Figure 7, for catalyst **4**), the maximum TON corresponding to the catalyst amount of 2.5 μmol (substrate/catalyst molar ratio of 400) (entry 4). A further decrease of the amount of catalyst (below ca. 2 μmol , Figure 7) leads to lower TON values.

Our complexes also behave as efficient catalysts or catalyst precursors for the peroxidative oxidation of cyclopentane to cyclopentanol and cyclopentanone, leading to over-

all yields and TONs (Table 5) that are comparable to those observed in the case of cyclohexane oxidation under similar experimental conditions. Typical yields and TONs of ca. 30% and ca. 30, respectively, have been achieved for catalysts 2–5 with 1 being slightly less active. A significant reduction of the relative amount of the alcohol is observed in the cyclopentane oxidation (typical A/K values in the 2–3 range, Table 5) in comparison with the case of cyclohexane (typical A/K values, under identical experimental conditions, within the 6–9 range, Table 3).

The high overall yields (up to 34% in a single batch, in the case of cyclohexane oxidation) achieved with our catalysts (including 3, already studied previously^[5c]) are comparable with those obtained by other valuable catalysts based on multicopper triethanolamine complexes^[4] or on iron(III)–chromium(III) hydroxides,^[32] a bit lower than that (up to 45%) of a heterotrimetallic Fe/Cu/Co complex with a *N,O*-coordination environment^[33a] and are markedly higher than those with half-sandwich scorpionate tripyrazolymethane complexes of copper, iron or vanadium^[27a] as well as some pyrazole and trispyrazolymethane rhenium complexes.^[27b] They are also better than that reported very recently^[27c] for a dipicolinate-Cu/Na coordination polymer (which, however, has the advantages of being water soluble and operating in the absence of acid) and those shown by other Cu catalytic systems,^[33b–33d] namely with salen, acetonitrile or phthalocyanine ligands.

Although the detailed mechanisms of the reactions are unknown, we believe they proceed by means of a radical pathway involving both C- and O-centred radicals since, as observed in other cases,^[4b,5c,28a,28c,28d] the oxidations of the cycloalkanes are essentially suppressed in the presence of radical trapping agents such as bromotrichloromethane, diphenylamine and 2,6-di-*tert*-butyl-4-methylphenol (BHT).

The formation of the ketone does not appear to proceed significantly by oxidation of the alcohol, since by using cyclohexanol as the substrate, instead of the cycloalkane, only very low conversions (2–4%) of cyclohexanol to cyclohexanone were detected (for the H₂O₂/catalyst molar ratio in the 500–1000 range). Hence, the fall in the A/K ratio for high values of the H₂O₂/catalyst molar ratio cannot be explained by further oxidation of cyclohexanol (CyOH) to cyclohexanone but may be accounted for by metal-assisted decomposition of cyclohexyl hydroperoxide (CyOOH) to the ketone.^[28c]

The involvement of CyOOH in the process is indicated by the marked increase of the amount of CyOH (by ca. 70–50%, for the conditions indicated by entries 1 and 11 in Table 3) with the corresponding decrease in the amount of the cycloketone upon treatment of the final reaction solution with an excess of PPh₃ prior to the GC analysis (see Exp. Sect.), following the method reported by Shul'pin.^[34] Reduction of CyOOH by PPh₃ gives CyOH (with formation of phosphane oxide), thus eliminating the decomposition of CyOOH to both CyOH and the cycloketone in the gas chromatograph. The method^[34] also allows the estimation of the amount of CyOOH present at the end of the reaction. This organohydroperoxide is then the main product

(e.g. 67% or 47% of the total of all products, for the conditions indicated by entry 1 or 11, respectively, in Table 3).

The reduction in the amount of CyOOH still present at the end of the reaction, upon increasing the H₂O₂/catalyst molar ratio, suggests that the higher concentrations of H₂O₂ favour the decomposition of CyOOH to the products during the reaction.

The formation of the cycloalkyl hydroperoxide (ROOH) can result from the reaction of a metal-peroxo intermediate, e.g. bearing a Cu^{II}-OOH type moiety, with the organoradical R[•] to form ROOH (and Cu^I).^[27a,35,36] The organohydroperoxide ROOH can undergo metal-assisted homolytic decomposition to alkoxy (RO[•], upon O–O bond cleavage) and alkylperoxy (ROO[•], upon O–H bond rupture) radicals from which the final oxygenates can be formed,^[34a,27a,37,38] i.e. cycloalcohol (ROH) upon H-abstraction from the alkane (RH) by RO[•] or upon decomposition of ROO[•] to both ROH and the cycloketone. In addition, the pyrazole and carboxylate ligands of our catalysts can be involved in proton-transfer steps, e.g., among H₂O₂, oxo and/or peroxo species, as suggested^[33c,34a,38b,39] for some V-catalysts with *N,O*-ligands.

Conclusions

The reactions of Hpz with some copper(II) carboxylates (namely valerate, 2-methylbutyrate, hexanoate and heptanoate) yield Cu^{II} derivatives 5–8 the structures of which, in the absence of XRD data, were inferred on the basis of physico-chemical measurements (magnetic susceptibility, ESI MS, IR and UV/Vis spectroscopy and ¹H NMR spectroscopy). In all cases, the triangular trinuclear skeleton [Cu₃(μ₃-OH)(μ-pz)₃]²⁺ is present, analogous to compounds 1–4.^[5] The compounds 1–8 exhibit, by cyclic voltammetry, irreversible Cu^{II} → Cu^I and Cu^I → Cu⁰ reduction waves which did not clearly reflect any electronic communication between the metals.

All the compounds 1, 2 and 4–8 behave as catalyst precursors for the efficient peroxidative oxidation of cycloalkanes by aqueous hydrogen peroxide, in acetonitrile at room temperature, similar to the previously reported compound 3. Cyclo-alcohols and -ketones are the products of oxidation obtained in markedly high yields, by formation of the corresponding cycloalkyl hydrogen peroxide intermediates (ROOH), following radical mechanisms which were substantiated by radical trap experiments.

Experimental Section

Materials and Methods: All reaction and manipulations were carried out in air. Excluding formate and acetate (Aldrich), copper(II) carboxylates were prepared according to previously reported procedures^[40] that were slightly modified. Trinuclear triangular Cu^{II} derivatives of the type [Cu₃(μ₃-OH)(μ-pz)₃(RCOO)₂L_x] with R = H, [Cu₃(μ₃-OH)(μ-pz)₃(HCOO)₂(Hpz)₂] (1)^[5b] R = CH₃, [Cu₃(μ₃-OH)(μ-pz)₃(CH₃COO)₂(Hpz)] (2)^[5a] R = CH₃CH₂, [Cu₃(μ₃-OH)(μ-pz)₃(CH₃CH₂COO)₂(EtOH)] (3)^[5b] and R = CH₃(CH₂)₂, [Cu₃(μ₃-

OH)(μ -pz)₃(CH₃(CH₂)₂COO)₂(MeOH)(H₂O)] (**4**)^[5b] were synthesised as previously reported. All other chemicals were purchased from Aldrich and used without further purification. Elemental analyses (C,H,N) were performed with a Fisons Instruments 1108 CHNS-O Elemental Analyser. IR spectra were recorded from 4000 to 100 cm⁻¹ with a Perkin-Elmer System 2000 FTIR instrument. Positive electrospray mass spectra were obtained with a Series 1100 MSI detector HP spectrometer by using MeOH as mobile phase. Solutions for electrospray ionisation mass spectrometry (ESI-MS) were prepared using reagent grade methanol and acetonitrile and the obtained data (masses and intensities) were compared with those calculated by using the IsoPro isotopic abundance simulator.^[21] Peaks containing copper(II) ions were identified as the centres of isotopic clusters. The magnetic susceptibilities were measured at room temperature (20–28 °C) by the Gouy method with a Sherwood Scientific Magnetic Balance MSB-Auto, using HgCo(NCS)₄ as a calibrating agent and data were corrected for diamagnetism with the appropriate Pascal constants. The magnetic moments (in BM) were calculated from the equation $\mu_{\text{eff}} = 2.84 (X_{\text{m}}^{\text{corr}} T)^{1/2}$. Reflectance solid-state and MeOH solution UV/Vis spectra were recorded on a Varian Cary 5E spectrophotometer, equipped with a device for reflectance measurements. ¹H NMR spectra were obtained with a Bruker Avance 300 instrument. Valeric, 2-methylbutyric, hexanoic and heptanoic acids, formed in the reactions of corresponding copper(II) carboxylates with Hpz, were detected by GC analyses carried out on a Thermo Electron Trace DSQ instrument equipped with a 30 m × 0.25 mm, 0.25 μ Thermo TR 5MS column.

Syntheses

Basic Copper(II) Carbonate: To a water solution (ca. 100 mL) of copper(II) sulfate pentahydrate (10 g) (40 mmol) was added a water solution (75 mL) of K₂CO₃ (5.54 g, 40 mmol) whilst stirring in 1 mL portions. The resultant light-blue basic copper carbonate [CuCO₃·Cu(OH)₂] was filtered off and washed with water until SO₄²⁻ ions were completely eliminated. Wet CuCO₃·Cu(OH)₂ was used to prepare some copper(II) carboxylates.

Copper(II) Valerate: To a valeric acid (12 mL, 11.27 g, 110 mmol) solution in water (400 mL) was added the freshly prepared wet CuCO₃·Cu(OH)₂ in small portions, leading to the formation of a green solid. The suspension was stirred for 48 h and the solid filtered off, washed with water and dried under vacuum in the presence of solid KOH. Yield 6.25 g, 24 mmol, 60%, based on starting copper(II) sulfate. C₁₀H₁₈CuO₄ (265.79): calcd. C 45.19, H 6.83; found C 44.61, H 6.85. IR (KBr): $\tilde{\nu} = 1589$ (s), 1449 (m), 1433 [m v(COO)] cm⁻¹.

Copper(II) 2-Methylbutyrate, A: The synthesis was carried out as for copper(II) valerate. Yield 60%, based on starting copper(II) sulfate. Recrystallisation from hot EtOH yielded crystals suitable for single crystal XRD determination. C₁₀H₁₈CuO₄ (265.79): calcd. C 45.19, H 6.83; found C 45.19, H 6.85. IR (KBr): $\tilde{\nu} = 1589$ (s), 1467 (m), 1422 [s v(COO)] cm⁻¹.

Copper(II) Hexanoate: Commercial basic copper(II) carbonate (1.91 g, 8.5 mmol) was suspended in a little excess of hexanoic acid (5 mL, 4.64 g, 40 mmol). The green suspension was stirred overnight, filtered and washed with cold acetone to remove the excess hexanoic acid. The solid was dried under vacuum and extracted with acetone (Soxlet). The resultant solution was concentrated under vacuum, yielding a green solid that was filtered off, washed with cold acetone and dried under vacuum. Yield 3.0 g, 9.3 mmol, 57%, based on basic copper carbonate. C₁₂H₂₂CuO₄ (293.85): calcd. C 49.05, H 7.55; found C 49.42, H 7.86. IR (KBr): $\tilde{\nu} = 1590$ (s), 1417 [m v(COO)] cm⁻¹.

Copper(II) Heptanoate: The synthesis was carried out as for copper(II) hexanoate. Yield 63%, based on basic copper carbonate. C₁₄H₂₆CuO₄ (321.90): calcd. C 52.24, H 8.14; found C 52.46, H 8.05. IR (KBr): $\tilde{\nu} = 1596$ (s), 1433 (m), 1417 [m v(COO)] cm⁻¹.

[Cu₃(μ -OH)(μ -pz)₃(CH₃(CH₂)₃COO)₂(H₂O)] (5**):** To a solution of copper(II) valerate (500 mg, 1.88 mmol) dissolved in EtOH (50 mL), was added Hpz (140 mg, 2.08 mmol) dissolved in EtOH (10 mL) and H₂O (1 mL). The solution immediately turned deep blue and was stirred overnight to give a blue solid that was filtered off, washed with ethanol and dried under vacuum. Yield 350 mg, 0.57 mmol, 89%. The presence of valeric acid was ascertained in the mother liquor.

5: M.p. above 200 °C. C₁₉H₃₀Cu₃N₆O₆ (629.12): calcd. C 36.27, H 4.81, N 13.36; found C 36.87, H 4.13, N 13.22. IR (KBr): $\tilde{\nu} = 1570$ (s), 1540 [s v(COO)], 1444 (m), 1398 [m v(COO)], 2101 (w) cm⁻¹. MS (ESI+, MeOH, MeCN): *m/z* (%) = 684.8 (68) [Cu₃(OH)(pz)₃(C₄H₉COO)₂(MeOH)(MeCN)]+H⁺; 1076.7 (23) [Cu₆(OH)₄(pz)₆(C₄H₉COO)₂(MeOH)₅]⁺+Na⁺; 1112.8 (100) [Cu₆(OH)₄(pz)₆(C₄H₉COO)(MeOH)₅]⁺ 1148.8 (96) [Cu₆(OH)₄(pz)₆(C₄H₉COO)(H₂O)₂(MeOH)₅]⁺. μ_{eff} (295 K) = 2.58 BM. λ_{max} /nm (reflectance): 607, 651. λ_{max} /nm (MeOH solution): 626 ($\epsilon = 191$). ¹H NMR (CD₃OD, 298 K): $\delta = 37.78$ (2 H), 40.88 (1 H) ppm.

[Cu₃(μ -OH)(μ -pz)₃(CH₃CH₂CH(CH₃)COO)₂(EtOH)₂] (6**):** To a solution of copper(II) 2-methylbutyrate (550 mg, 2.06 mmol) in EtOH (30 mL) was added Hpz (150 mg, 2.19 mmol) dissolved in EtOH (10 mL). The deep blue solution was stirred overnight and then evaporated to dryness under vacuum. Collected vapours revealed the presence of 2-methylbutyric acid. The deep blue solid was washed with hexane to remove the 2-methylbutyric acid and dried under vacuum. Yield 420 mg, 0.597 mmol, 87%.

6: M.p. above 200 °C. C₂₃H₄₀Cu₃N₆O₇ (703.24): calcd. C 39.28, H 5.73, N 11.9; found C 38.71, H 5.29, N 11.48. IR (Nujol): $\tilde{\nu} = 1584$ (s), 1548 [s v(COO)], 1465 (s), 1420 [s v(COO)] cm⁻¹. MS (ESI+, MeOH, MeCN): *m/z* (%) = 591.8 (13) [Cu₃(OH)(pz)₃(C₄H₉COO)(MeOH)₂(H₂O)]⁺; 625.8 (20) [Cu₃(pz)₃(C₄H₉COO)₂(MeOH)]⁺; 752.7 (16) [Cu₃(OH)(pz)₃(C₄H₉COO)₂(H₂O)₂(MeOH)₂(MeCN)]+H⁺; 1076.6 (10) [Cu₆(OH)₄(pz)₆(C₄H₉COO)₂+Na⁺; 1112.6 (40) Cu₆(OH)₄(pz)₆(C₄H₉COO)(MeOH)₅]⁺; 1148.5 (100) [Cu₆(OH)₄(pz)₆(C₄H₉COO)(H₂O)₂(MeOH)₅]⁺, 1182.4 (19) [Cu₆(OH)₃(pz)₆(C₄H₉COO)₂(H₂O)(MeOH)₄]⁺. μ_{eff} (295 K) = 2.45 BM. λ_{max} /nm (reflectance): 609, 647, 551 (shoulder). λ_{max} /nm (MeOH solution): 626 ($\epsilon = 179$). ¹H NMR (CD₃OD, 298 K): $\delta = 37.77$ (2 H), 40.87 (1 H) ppm.

[Cu₃(μ -OH)(μ -pz)₃(CH₃(CH₂)₄COO)₂(EtOH)] (7**):** To a solution of copper(II) hexanoate (530 mg, 1.81 mmol) in EtOH (20 mL) was added Hpz (130 mg, 1.84 mmol) dissolved in EtOH (5 mL). The deep blue solution was stirred overnight and then evaporated to dryness under vacuum. Collected vapours revealed the presence of hexanoic acid. The blue solid obtained was washed with cyclohexane to eliminate hexanoic acid and dried under vacuum. Yield 400 mg, 0.58 mmol, 96%.

7: M.p. 195–198 °C (dec., blue colour turns to grey). C₂₃H₃₈Cu₃N₆O₆ (685.22): calcd. C 40.31, H 5.59, N 12.26; found C 40.00, H 4.96, N 12.92. IR (Nujol): $\tilde{\nu} = 1569$ (s), 1542 [s v(COO)], 1430 (m), 1398 [w v(COO)], 2096 (w) cm⁻¹. MS (ESI+, MeOH, MeCN): *m/z* (%) = 536 (15) [Cu₃(OH)₂(pz)₃(H₂O)(EtOH)₂]⁺; 698.8 (52) [Cu₃(OH)(pz)₃(C₅H₁₁COO)₂(H₂O)(MeCN)]+H⁺; 748.8 (14) [Cu₃(OH)(pz)₃(C₅H₁₁COO)₂(H₂O)₂(MeOH)(MeCN)]+H⁺; 1118.8 (17) [Cu₆(OH)₃(pz)₆(C₅H₁₁COO)₂(H₂O)₃]⁺; 1154.8 (83) [Cu₆(OH)₃(pz)₆(C₅H₁₁COO)₂(H₂O)₅]⁺; 1190.8 (100) [Cu₆(OH)₃(pz)₆(C₅H₁₁COO)₂(H₂O)₇]⁺; 1238.8 (10) [Cu₆(OH)₃(pz)₅(C₅H₁₁COO)₃

(H₂O)₇)⁺. μ_{eff} (295 K) = 2.73 BM. λ_{max} (reflectance): 611 nm, 645 nm (shoulder). $\lambda_{\text{max}}/\text{nm}$ (MeOH solution): 621 (ϵ = 181). ¹H NMR (CD₃OD, 298 K): δ = 37.74 (2 H), 40.89 (1 H) ppm.

[Cu₃(μ_3 -OH)(μ -pz)₃(CH₃(CH₂)₅COO)₂(EtOH)] (8): To a solution of copper(II) heptanoate (540 mg, 1.68 mmol) dissolved in EtOH (50 mL) was added Hpz (120 mg, 1.70 mmol) dissolved in EtOH (10 mL). The deep blue solution was stirred for 3 h and then the addition of ca. 80 mL of water produced the precipitation of a clear-blue solid that was filtered off, washed with water and dried under vacuum. Yield 370 mg, 0.52 mmol, 92%. Heptanoic acid was detected in the mother liquor.

8: M.p. 190–195 °C (dec., blue colour fades). C₂₅H₄₂Cu₃N₆O₆ (713.28): calcd. C 42.10, H 5.94, N 11.78; found C 42.05, H 5.47, N 11.96. IR (Nujol): $\tilde{\nu}$ = 1569 (s), 1539 [s ν (COO)], 1456 (w), 1430 [m ν (COO)], 2095 (w) cm⁻¹. MS (ESI+, MeOH, MeCN): *m/z* (%) = 588 (12) [Cu₃(OH)(pz)₃(C₆H₁₃COO)(MeOH)(H₂O)]⁺; 619.9 (25) [Cu₃(OH)(pz)₃(C₆H₁₃COO)(MeOH)₂(H₂O)]⁺; 650 (10) [Cu₃(pz)₃(C₆H₁₃COO)₂]⁺; 682 (15) [Cu₃(pz)₃(C₆H₁₃COO)₂MeOH]⁺; 712.8 (50) [Cu₃(OH)(pz)₄(Hpz)(MeOH)₄(MeCN)]⁺; 1196.8 (35) Cu₆(OH)₃(C₃H₃N₂)₆(C₆H₁₃COO)₂(H₂O)₄(CH₃OH); 1232.8 (100) Cu₆(OH)₃(C₃H₃N₂)₆(C₆H₁₃COO)₂(H₂O)₆(CH₃OH); 1294.8 (18) [Cu₆(OH)₂(pz)₆(C₆H₁₃COO)₃(H₂O)₅]⁺. μ_{eff} (295 K) = 2.56 BM. λ_{max} (reflectance): 611 nm, 643 nm. $\lambda_{\text{max}}/\text{nm}$ (MeOH solution): 626 (ϵ = 191). ¹H NMR (CD₃OD, 298 K): δ = 37.76 (2 H), 40.83 (1 H) ppm.

¹H NMR Spectroscopic Data of 1–4

¹H NMR spectra of compounds 1–4 were recorded at 298 K from CD₃OD solutions.

[Cu₃(μ_3 -OH)(μ -pz)₃(HCOO)₂(HPz)₂] (1): δ = 36.71 (2H), 41.09 (1 H) ppm.

[Cu₃(μ_3 -OH)(μ -pz)₃(CH₃COO)₂(HPz)] (2): δ = 37.48 (2H), 40.94 (1 H) ppm.

[Cu₃(μ_3 -OH)(μ -pz)₃(CH₃CH₂COO)₂(EtOH)] (3): δ = 37.84 (2H), 40.82 (1 H) ppm.

[Cu₃(μ_3 -OH)(μ -pz)₃(CH₃(CH₂)₂COO)₂(MeOH)(H₂O)] (4): δ = 37.77 (2H), 40.82 (1 H) ppm.

Electrochemical Studies: The electrochemical experiments were performed on an EG&G PAR 273A potentiostat/galvanostat connected to a personal computer through a GPIB interface. Cyclic voltammograms were obtained in 0.2 M [*n*Bu₄N][BF₄]/DMSO at a platinum disc working electrode (*d* = 0.5 mm) and at 25 °C. Controlled-potential electrolyses (CPE) were carried out in electrolyte solutions with the above-mentioned composition in a three-electrode H-type cell. The compartments were separated by a sintered glass frit and equipped with platinum gauze working and counter electrodes. For both CV and CPE experiments, a Luggin capillary connected to a silver wire pseudo-reference electrode was used to control the working electrode potential and a Pt wire was employed as the counter-electrode for the CV cell. The CPE experiments were monitored regularly by cyclic voltammetry, thus assuring no significant potential drift occurred along the electrolyses. The redox potentials of the complexes were measured by CV in the presence of ferrocene as the internal standard and their values are quoted relative to the SCE by using the [Fe(η^5 -C₅H₅)₂]^{0/+} redox couple (*E*_{1/2}^{ox} = 0.44 V vs. SCE^[41]).

Catalytic Activity Studies: The reaction mixtures were prepared as follows: to 0.63–10.0 μmol (typically 10.0 μmol) of catalyst precursor contained in the reaction flask were added MeCN (4 mL), HNO₃ (0.1 mmol), C₆H₁₂ (or C₅H₁₀, 1.0 mmol) and H₂O₂ (30% in H₂O, 2.5–10.0 mmol), in that order. The reaction mixture was stirred for 6 h at room temperature (ca. 25 °C) and atmospheric

pressure, thereafter cycloheptanone (as internal standard, 90 μL), diethyl ether (to extract the substrate and the products from the reaction mixture, typically 9.0 mL) and PPh₃ (0.5 g, to reduce the organohydroperoxides, if formed, according to a method developed by Shul'pin^[34]) were added. The resultant mixture was stirred for 15 min and then a sample taken from the organic phase was analysed by GC using a FISIONS Instruments GC 8000 series gas chromatograph with a DB WAX fused silica capillary column and the Jasco-Borwin v.1.50 software. The GC analyses of the aqueous phase showed the presence of only traces (less than 0.05%) of oxidation products.

Supporting Information (see also the footnote on the first page of this article): Structures of 1, 4, copper(II) butyrate; ESI-MS spectra and XRPD patterns for 5, 6, 7, 8.

Acknowledgments

This work was supported by the Italian Programma di Ricerca di Rilevante Interesse Nazionale (PRIN) (fund number 2006038447) and by the Portuguese Fundação para a Ciência e a Tecnologia (FCT), and Federación Española de Enfermedades Raras (FEDER), POCI 2010 programme. M. M. wishes to thank the University of Bologna for financial support. F. G. thanks the “Aldo Gini” Foundation (Padova) for a grant to support a research period at Lisbon. The authors are indebted with Mr. Andrea Boaretto for the execution of GM spectra for the identification of carboxylic acids.

- [1] a) G. La Monica, G. A. Ardizzoia, *Prog. Inorg. Chem.* **1997**, *46*, 151–238; b) D. E. Fenton, *Advances in Inorganic and Bioinorganic Mechanisms* (Ed.: A. G. Sykes), Academic Press, London, **1983**, vol. 2; c) S. Ménage, S. E. Vitols, P. Bergerat, E. Codjovi, O. Kahn, J.-J. Girerd, M. Guillot, X. Solans, T. Calvet, *Inorg. Chem.* **1991**, *30*, 2666–2671; d) *Magnetic Molecular Materials* (Eds.: D. Gatteschi, O. Kahn, J. S. Miller, F. Palacio); NATO ASI Series 198; Kluwer Academic Publishers, Dordrecht, The Netherlands, **1991**; e) D. E. Fenton, H. Okawa, *J. Chem. Soc., Dalton Trans.* **1993**, 1349–1357; f) M. Thomann, O. Kahn, J. Guilhem, F. Varret, *Inorg. Chem.* **1994**, *33*, 6029–6037; g) E. I. Solomon, U. M. Sundaram, T. E. Machonkin, *Chem. Rev.* **1996**, *96*, 2563–2605; h) W. Kaim, J. Rall, *Angew. Chem. Int. Ed. Engl.* **1996**, *35*, 43–60; i) R. H. Holm, P. Kennepohl, E. I. Solomon, *Chem. Rev.* **1996**, *96*, 2239–2314; j) A. P. Sadimenko, S. S. Basson, *Coord. Chem. Rev.* **1996**, *147*, 247–297; k) O. Kahn, *Chem. Phys. Lett.* **1997**, *265*, 109; l) O. Roubeau, J. M. A. Gómez, E. Balskus, J. J. A. Kolnar, J. G. Haasnoot, J. Reedijk, *New J. Chem.* **2001**, *25*, 144–150.
- [2] a) J. P. Klinman, *Chem. Rev.* **1996**, *96*, 2541–2562; b) A. P. Cole, D. E. Root, P. Mukherjee, E. I. Solomon, T. D. P. Stack, *Science* **1996**, *273*, 1848–1850; c) S. J. Elliot, M. Zhu, L. Tso, H.-H. T. Nguyen, J. H.-K. Yip, S. I. Chan, *J. Am. Chem. Soc.* **1997**, *119*, 9949–9955; d) J. J. R. Fraústo da Silva, R. J. P. Williams, *The Biological Chemistry of the Elements*, Oxford University Press, Oxford, **2001**; e) S. Itoh in *Comprehensive Coordination Chemistry*, vol. 8 (Eds.: J. A. McCleverty, T. J. Meyer, L. Que, W. B. Tolman), 2nd ed., Elsevier, Dordrecht, **2003**, chap. 8.15, pp. 369–393; f) D. H. Lee in *Comprehensive Coordination Chemistry*, vol. 8 (Eds.: J. A. McCleverty, T. J. Meyer, L. Que, W. B. Tolman), 2nd ed., Elsevier, Dordrecht, **2003**, chap. 8.17, pp. 437–457; g) M. Ayala, E. Torres, *Appl. Catal. A* **2004**, *272*, 1–13; h) R. L. Lieberman, A. C. Rosenzweig, *Crit. Rev. Biochem. Mol. Biol.* **2004**, *39*, 147–164; i) R. L. Lieberman, A. C. Rosenzweig, *Nature* **2005**, *434*, 177–182; j) J. Yoon, E. I. Solomon, *Inorg. Chem.* **2005**, *44*, 8076–8086.

- [3] R. Huber, *Angew. Chem. Int. Ed. Engl.* **1989**, *28*, 848–869.
- [4] a) A. M. Kirillov, M. N. Kopylovich, M. V. Kirillova, M. Haukka, M. F. C. Guedes da Silva, A. J. L. Pombeiro, *Angew. Chem. Int. Ed.* **2005**, *44*, 4345–4349; b) A. M. Kirillov, M. N. Kopylovich, M. V. Kirillova, Y. Y. Karabach, M. Haukka, M. F. C. Guedes da Silva, A. J. L. Pombeiro, *Adv. Synth. Catal.* **2006**, *348*, 159–174.
- [5] a) M. Casarin, C. Corvaja, C. Di Nicola, D. Falcomer, L. Franco, M. Monari, L. Pandolfo, C. Pettinari, F. Piccinelli, P. Tagliatesta, *Inorg. Chem.* **2004**, *43*, 5865–5876; b) M. Casarin, C. Corvaja, C. Di Nicola, D. Falcomer, L. Franco, M. Monari, L. Pandolfo, C. Pettinari, F. Piccinelli, *Inorg. Chem.* **2005**, *44*, 6265–6276; c) C. Di Nicola, Y. Y. Karabach, A. M. Kirillov, M. Monari, L. Pandolfo, C. Pettinari, A. J. L. Pombeiro, *Inorg. Chem.* **2007**, *46*, 221–230.
- [6] We also obtained the analogous pivalate derivative $[\text{Cu}_3(\mu_3\text{-OH})(\mu\text{-pz})_3(\text{Me}_3\text{CCOO})_2\{(\text{Me}_3\text{CCOOH})\}]$, whose synthesis, through a different procedure, as well as its SCXRD crystal structure has been recently reported, see J.-H. Zhou, Z. Liu, Y.-Z. Li, Y. Song, X.-T. Chen, X.-Z. You, *J. Coord. Chem.* **2006**, *59*, 147–153.
- [7] H-bonds concerning data and figures reported in the Supporting Information have been obtained by using the CIF files supplied as Supporting Information in refs. 5b (compounds **1** and **4**) and 5a (compound **2**). To these CIF files are also referred the atom labels used here.
- [8] The Cambridge Structural Database contains 667 crystal structures where the $[\text{Cu}_2(\text{RCOO})_4]$ paddlewheel moiety is present but only 19 of them refer to polymeric unsubstituted copper(II) carboxylates.
- [9] Crystal data for $\text{C}_{20}\text{H}_{36}\text{Cu}_2\text{O}_4$, **A**: triclinic, space group $P\bar{1}$ (No. 2), $a = 5.1829(6)$, $b = 11.1982(13)$, $c = 11.8865(14)$ Å, $\alpha = 65.631(2)^\circ$, $\beta = 88.023(2)^\circ$, $\gamma = 88.948(2)^\circ$, $V = 628.04(13)$ Å³, $Z = 1$, R (R_w) [$I > 2\sigma(I)$] = 0.0448 (0.1388). The X-ray intensity data for **A** were recorded on a Bruker SMART Apex II CCD area detector diffractometer [$\lambda = 0.71073$ Å, $T = 293(2)$ K]. Cell dimensions and the orientation matrix were initially determined from a least-squares refinement on reflections measured in three sets of 20 exposures, collected in three different ω regions and eventually refined against all data. For all crystals, a full sphere of reciprocal space was scanned in 0.3° ω steps. The software SMART^[10] was used for collecting frames of data, indexing reflections and determining lattice parameters. The collected frames were then processed for integration by the SAINT program^[10] and an empirical absorption correction was applied using SADABS.^[11] The structure was solved by direct methods (SIR 97)^[12] and subsequent Fourier syntheses and refined by full-matrix least-squares on F^2 (SHELXTL)^[13] using anisotropic thermal parameters for all non-hydrogen atoms. Some disorder in the carboxylate chains was detected and, in particular, in one of the chains there was a disorder between the methyl and ethyl chains bound at C(3) and a second position for the methyl [bound to C(9) and alternative to C(10)]. Therefore the site occupation factors of the methyls were refined yielding 0.54 for C(10), 0.26 for C(81) and 0.19 for C(91), respectively. All hydrogen atoms were added in calculated positions, included in the final stage of refinement with isotropic thermal parameters, $U(\text{H}) = 1.2 U_{\text{eq}}(\text{C})$ [$U(\text{H}) = 1.5 U_{\text{eq}}(\text{C}-\text{Me})$] and allowed to ride on their carrier carbons. Molecular graphics were generated using Mercury^[14] and Schakal^[15] software. CCDC-697289 contains the supplementary crystallographic data for this paper. These data can be obtained free of charge from The Cambridge Crystallographic Data Centre via www.ccdc.cam.ac.uk/data_request/cif.
- [10] SMART & SAINT Software Reference Manuals, version 5.051 (Windows NT Version), Bruker Analytical X-ray Instruments Inc., Madison, WI, 1998.
- [11] G. M. Sheldrick, *SADABS, program for empirical absorption correction*, University of Göttingen, Germany, 1996.
- [12] A. Altomare, M. C. Burla, M. Cavalli, G. L. Casciaro, C. Giacovazzo, A. Guagliardi, A. G. G. Moliterni, G. Polidori, R. Spagna, *J. Appl. Crystallogr.* **1999**, *32*, 115–119.
- [13] G. M. Sheldrick, SHELXTLplus (Windows NT Version) Structure Determination Package, Version 5.1, Bruker Analytical X-ray Instruments Inc., Madison, WI, USA, 1998.
- [14] Mercury: Visualisation and Analysis of Crystal Structures: C. F. Macrae, P. R. Edgington, P. McCabe, E. Pidcock, G. P. Shields, R. Taylor, M. Towler, J. van de Streek, *J. Appl. Crystallogr.* **2006**, *39*, 453–457.
- [15] E. Keller, SCHAKAL A Computer Program for the Graphic Representation of Molecular and Crystallographic Models, Institute for Crystallography of the University of Freiburg, Freiburg (Germany), 1997.
- [16] G. B. Deacon, R. J. Phillips, *Coord. Chem. Rev.* **1980**, *33*, 227–250.
- [17] E. Pretsch, T. Clerc, J. Seibl, W. Simon, *Tables of Determination of Organic Compounds. ¹³C NMR, ¹H NMR, IR, MS, UV/Vis*, Chemical Laboratory Practice, Springer-Verlag, Berlin, Germany, 1989.
- [18] a) J. G. A. Luijten, G. J. M. Van der Kerk, *Recl. Trav. Chim. Pays-Bas* **1963**, *82*, 1181–1188; b) J. G. Vos, W. L. Groeneveld, *Inorg. Chim. Acta* **1977**, *24*, 123–126; c) H. Okkersen, W. L. Groeneveld, J. Reedijk, *Recl. Trav. Chim. Pays-Bas* **1973**, *92*, 945–953.
- [19] a) G. Mezei, M. Rivera-Carrillo, R. G. Raptus, *Inorg. Chim. Acta* **2004**, *357*, 3721–3732; b) P. A. Angaridis, P. Baran, R. Boča, F. Cervantes-Lee, W. Haase, G. Mezei, R. G. Raptis, R. Werner, *Inorg. Chem.* **2002**, *41*, 2219–2228.
- [20] It is well known that in ESI MS conditions aggregation phenomena, leading to oligomeric species, may occur. See, as an example a) M. Fujita, F. Ibukuro, H. Hagihara, K. Ogura, *Nature* **1994**, *367*, 720–723; b) R. Colton, A. D'Agostino, J. C. Traeger, *Mass Spectrom. Rev.* **1995**, *14*, 79–106; c) C. E. C. A. Hop, R. Bakhtiar, *J. Chem. Educ.* **1996**, *73*, A162, A164–169; d) L. S. Bonnington, R. K. Coll, E. J. Gray, J. I. Flett, W. Henderson, *Inorg. Chim. Acta* **1999**, *299*, 213–221; e) A. Cingolani, Effendy, M. Pelli, C. Pettinari, C. Santini, B. W. Skelton, A. H. White, *Inorg. Chem.* **2002**, *41*, 6633–6645.
- [21] M. W. Senko, *IsoPro Isotopic Abundance Simulator*, v. 2.1, National High Magnetic Field Laboratory, Los Alamos National Laboratory, Los Alamos, NM, 1994.
- [22] M. Casarin, A. Cingolani, C. Di Nicola, D. Falcomer, M. Monari, L. Pandolfo, C. Pettinari, *Cryst. Growth Des.* **2007**, *4*, 676–685.
- [23] C. Di Nicola, F. Garau, M. Monari, L. Pandolfo, C. Pettinari, *Proceedings of VIII Congresso Nazionale di Chimica Supramolecolare*, Trieste (Italy), Sept. 19–22, 2007, P53.
- [24] a) M. V. Kirillova, A. M. Kirillov, P. M. Reis, J. A. L. Silva, J. J. R. Fraústo da Silva, A. J. L. Pombeiro, *J. Catal.* **2007**, *248*, 130–136, and references cited therein; b) M. V. Kirillova, M. L. Kuznetsov, P. M. Reis, J. A. L. Silva, J. J. R. Fraústo da Silva, A. J. L. Pombeiro, *J. Am. Chem. Soc.* **2007**, *129*, 10531–10545; c) M. V. Kirillova, M. L. Kuznetsov, J. A. L. Silva, M. F. C. Guedes da Silva, J. J. R. Fraústo da Silva, A. J. L. Pombeiro, *Chem. Eur. J.* **2008**, *14*, 1828–1842.
- [25] A. M. Kirillov, M. Haukka, M. F. C. Guedes da Silva, A. J. L. Pombeiro, *Eur. J. Inorg. Chem.* **2005**, 2071–2080.
- [26] Y. Y. Karabach, A. M. Kirillov, M. F. C. Guedes da Silva, M. N. Kopylovich, A. J. L. Pombeiro, *Cryst. Growth Des.* **2006**, *6*, 2200–2203.
- [27] a) T. F. S. Silva, E. C. B. Alegria, L. R. Martins, A. J. L. Pombeiro, *Adv. Synth. Catal.* **2008**, *350*, 706–716; b) E. C. B. Alegria, M. V. Kirillova, L. R. Martins, A. J. L. Pombeiro, *Appl. Catal. A: Gen.* **2007**, *317*, 43–52; c) M. V. Kirillova, A. M. Kirillov, M. F. C. Guedes da Silva, A. J. L. Pombeiro, *Eur. J. Inorg. Chem.* **2008**, 3423–3427.
- [28] a) G. S. Mishra, A. J. L. Pombeiro, *J. Mol. Catal. A* **2005**, *239*, 96–102; b) G. S. Mishra, A. J. L. Pombeiro, *Appl. Catal. A: Gen.* **2006**, *304*, 185–194; c) G. S. Mishra, J. J. R. Fraú-

- sto da Silva, A. J. L. Pombeiro, *J. Mol. Catal. A* **2007**, *265*, 59–69; d) G. S. Mishra, E. C. B. Alegria, L. R. Martins, J. J. R. Fraústo da Silva, A. J. L. Pombeiro, *J. Mol. Catal. A: Chem.* in press.
- [29] P. M. Reis, J. A. L. Silva, J. J. R. Fraústo da Silva, A. J. L. Pombeiro, *Chem. Commun.* **2000**, 1845–1846.
- [30] P. M. Reis, J. A. L. Silva, J. J. R. Fraústo da Silva, A. J. L. Pombeiro, *J. Mol. Catal. A* **2004**, *224*, 189–195.
- [31] Y. Y. Karabach, A. M. Kirillov, M. Haukka, M. N. Kopylovich, A. J. L. Pombeiro, *J. Inorg. Biochem.* **2008**, *102*, 1190–1194.
- [32] M. N. Kopylovich, A. M. Kirillov, A. K. Baev, A. J. L. Pombeiro, *J. Mol. Catal. A* **2003**, *206*, 163–178.
- [33] a) D. S. Nesterov, V. N. Kokozay, V. V. Dyakonenco, O. V. Shishkin, J. Jezierska, A. Ozarowski, A. M. Kirillov, M. N. Kopylovich, A. J. L. Pombeiro, *Chem. Commun.* **2006**, 4605–4607; b) S. Velusamy, T. Punniyamurthy, *Tetrahedron Lett.* **2003**, *44*, 8955–8957; c) G. B. Shul'pin, J. Gradinaru, Y. N. Kozlov, *Org. Biomol. Chem.* **2003**, *1*, 3611–3617; d) R. Raja, P. Ratnasamy, *Catal. Lett.* **1997**, *48*, 1–10.
- [34] a) G. B. Shul'pin, *J. Mol. Catal. A* **2002**, *189*, 39–66; b) G. B. Shul'pin, *C. R. Chim.* **2003**, *6*, 163–178.
- [35] a) M. Costas, M. P. Mehn, M. P. Jensen, L. Que Jr., *Chem. Rev.* **2004**, *104*, 939–986; b) M. Costas, K. Chen, L. Que Jr., *Coord. Chem. Rev.* **2000**, *200–20*, 517–544; c) G. Roelfes, M. Lubben, R. Hage, L. Que Jr., B. L. Feringa, *Chem. Eur. J.* **2000**, *6*, 2152–2159.
- [36] T. Hogan, A. Sen, *J. Am. Chem. Soc.* **1997**, *119*, 2642–2646.
- [37] a) G. B. Shul'pin in *Transition Metals for Organic Synthesis* (Eds.: M. Beller, C. Bolm), 2nd edn., vol. 2, Wiley-VCH, New York, **2004**, p. 215; b) G. B. Shul'pin, *Organic Reactions Catalyzed by Metal Complexes*, Nauka, Moscow, **1988**.
- [38] a) G. V. Nizova, B. Krebs, G. Süss-Fink, S. Schindler, L. Westerbeide, L. G. Cuervo, G. B. Shul'pin, *Tetrahedron* **2002**, *58*, 9231–9237; b) G. B. Shul'pin, Y. N. Kozlov, G. V. Nizova, G. Süss-Fink, S. Stanislas, A. Kitaygorodskiy, V. S. Kulikova, *J. Chem. Soc., Perkin Trans. 2* **2001**, *2*, 1351–1371; c) G. Süss-Fink, L. Gonzalez, G. B. Shul'pin, *Appl. Catal. A: Gen.* **2001**, *217*, 111–117; d) G. B. Shul'pin, G. Süss-Fink, *J. Chem. Soc., Perkin Trans. 2* **1995**, *2*, 1459–1463; e) M. Koderer, H. Shimakoshi, K. Kano, *Chem. Commun.* **1996**, 1737–1738; f) H.-J. Schneider, W. Müller, *J. Org. Chem.* **1985**, *50*, 4609–4615; g) G. B. Shul'pin, H. Stoeckli-Evans, D. Mandelli, Y. N. Kozlov, A. T. Vallina, C. B. Woitiski, R. S. Jimenez, W. A. Carvalho, *J. Mol. Catal. A* **2004**, *219*, 255–264.
- [39] P. M. Reis, J. A. L. Silva, A. F. Palavra, J. J. R. Fraústo da Silva, T. Kitamura, Y. Fujiwara, A. J. L. Pombeiro, *Angew. Chem. Int. Ed.* **2003**, *42*, 821–823.
- [40] R. L. Martin, H. Waterman, *J. Chem. Soc.* **1957**, 2545–2551.
- [41] A. J. L. Pombeiro, M. F. C. Guedes da Silva, M. A. N. D. A. Lemos, *Coord. Chem. Rev.* **2001**, *219–221*, 53–80.

Received: August 21, 2008

Published Online: January 13, 2009

